ALIGNMENT OF LINES IN SPACE

(With particular reference to laser-fibre coupling)

BY

JOHN A. OPONO-MOYAHI-OKELLO

BSc(Hons) Mechanical Engineering (Lanchester)
AMIMechEng

A Doctoral Thesis

Submitted in partial fulfilment of the requirements for the award of the degree of Doctor of Philosophy of the Loughborough University of Technology

1987

ABSTRACT

The object of this work (featuring the study of alignment of lines in space) is to produce a novel system for automatic production of optoelectronic components. It begins by reviewing the different components associated with optical fibre transmission and examines the existing laser-fibre coupling methods. The manual alignment technique adopted by STC to align a laser beam with a monomode optical fibre is then presented.

The various interpretations of alignment are explored. The results obtained from the analysis determine the type of manipulator required for laser to optical fibre coupling. The central axis of a divergent beam emitted by a semi-conductor laser diode is manipulated for alignment with the axis of the fibre. Such an alignment places stringent displacement tolerance and accuracy demands on the manipulator.

To construct a manipulator, actuators need to be coupled together. The coupling methods are studied and presented. Prior to this study, commercially available actuators are surveyed leading to the selection of the Oriel Encoder Mike actuator. This actuator exhibits some inherent control problems but meets the laser-fibre coupling accuracy demands. Various types of couplings are also examined based on the expansion of the Kelvin coupling for the construction of a four degree of freedom manipulator. A computational algorithm analogous to that used to solve two plane balancing problems is sucessfully tested on this manipulator for alignment of a conventional He-Ne laser beam with the centres of two transparent screens. This algorithm requires linearity for its success. For this reason and for purposes of completeness, spatial displacement characteristics of the manipulator are analysed and confirmed experimentally.

This work ends with the construction and testing of a program based on a hill climbing technique for the control of a three degree of freedom (Oriel Encoder Mike) manipulator to align a laser beam emitted by a semi-conductor laser diode with a monomode optical fibre.

A C K N O W L E D G E M E N T S

I would like to express my gratitude to the following people for making this work possible:

Mr. T. H. Davies, my supervisor, for his guidance, advice and encouragement.

Dr. R. V. Vitols, my co-supervisor, for introducing the research work from STC and his help to obtain part of the alignment components.

Prof. G. Wray, my Director of Research, for his co-operation both administratively and helping to obtain the alignment test components from STC.

Mr. A. Slade for his assistance in helping to build the electronic control units and travelling for long distances to Torquay on more than one occasion in order to secure the alignment test components.

Mr. R. Ludlam and his workshop staff for helping to manufacture the necessary test pieces whenever they were required.

Overseas Research Studentship Award for their financial assistance at the time I most needed it.

Mr. K. Topley for the photographs.

Mrs. Janet Smith for typing Chapter 7 and other corrections that needed expertise.

And finally, to all those without whose help, this work could have been completed in less than half the time.

C O N T E N T S

NOMENCLATURE

c — Total number of constraints in a coupling or manipulator (section 5.3)

d_{31}(c/N) — Transverse piezoelectric constant of PVDF or PZT (Table 4.3.2)

f — Total number of degrees of freedom of a manipulator or coupling (f = 6 - c) (section 5.3)

g — Amplifier gain (section 8.2.6)

ℓ_d(mm) — Distance between the origin of reference frame and the point of intersection of common perpendicular with a fixed line (Fig.3.2)

x_ℓ(mm) — Alignment tolerance in the X-axis (Table 2.3.5)

x,y,z(mm) — Laser-fibre misalignment in the X,Y,Z axes respectively (Fig.2.2.4)

Y_{GP}, Y_{Gt}(mm) — Experimental and theoretical displacement of point G in the Y-axis (Table 7.4.3)

y_r(mm) — Alignment tolerance in the Y-axis (Table 2.3.5)

z(mm) — Alignment tolerance in the Z-axis (Table 2.3.5)

V(mm) — Laser beam spot displacement before and after manipulator feet adjustment (Table 6.9.1(I))

VRTH(volts) — Thermistor voltage (Fig.8.2.6)

$\{V_\ell^{cp}\}$ — Local column velocity vector of a manipulator coupling (cp = a,b,c,d,e,f,g and h Chapter 7 and accompanying appendices)

$\{V^{cp}\}$ — Column vector of coupling velocity referred to global frame (Chapter 7 and accompanying appendices)

γ(deg.) — Angular displacement of laser spot on target screens before and after manipulator feet adjustment (Table 6.9.1(I))

θ(deg.) — Angular alignment tolerance (Table 2.3.5)

θ(deg.) — Angle between local and global frames (Figs.7.1.1(c) and 7.1.2(c) etc.)

$\phi / \mu m$ — Diameters of fibre core and cladding (Table 2.3.5)

ABBREVIATIONS

Cylindric.	Cylindrical lens (Table 2.3.5)
Fs	Full scale (Section 8.2.11)
Hem. Lens	Hemispherical lens (Table 2.3.5)
LHS (L.H.S)	Left Hand Side (Table 6.9.1(I))
LR	Spring loaded lever mechanism (Fig.8.2.9)
MASS.	Massachussetts (Appendix B)
RHS(R.H.S)	Right Hand Side (Table 6.9.1(I))
Selfoc	Selfoc lens (Table 2.3.5)
S.M.F	Single Mode Fibre (Table 2.3.5)
mW	milliwatts (section 2.1.4)
nm	nanometer (section 2.1.4)
ns	nanosecond (section 2.1.4)
µm	microns
DAC	Digital to Analogue Converter (Section 8.2.11)

LABELS USED

A,B,C,D,E,F,G and H Couplings (Figs.7.1.1(a),(b) and 7.1.2(a),(b))

B1	Tripod (Fig.5.6.1(b))
B2	Base of Kelvin coupling (Fig.5.6.1(b))
C1,C2	Capacitors (Fig.8.2.9)
D1	Diode (Fig.8.2.9)
E1	Tripod (Fig.5.6.1(a))
E2	Base of Kelvin coupling (Fig.5.6.1(a))
FB	Beads (Fig.8.2.9)
L1,L2	Inductors (Fig.8.2.9)
M1,M2	Plane mirrors (Fig.8.2.3(a))
O	Centre of surface of manipulator (Fig.7.1.1(a))
RV1,RV2	Variable resistors (Fig.8.2.6)
Sh	Hemispherical foot of tripod (Figs.5.6.1(a),(b))

CHAPTER 1

INTRODUCTION

Optical fibres have been increasingly used in communication systems because of their inherently high bandwidth and low attenuation, immunity from electromagnetic frequencies and freedom from noise and pick up. In the U.K, optical fibre communication has been restricted to trunk networks because its high costs (compared to copper cables) makes it economically viable only when the data traffic density is high (Wilkinson [1]). In 1984, a company called Mercury planned a 440 mile figure-of-eight network round the U.K linking London, Birmingham, Manchester, Leeds, Liverpool and Bristol [4]. The constructon of this 1300 nm single-mode fibre (described in Chapter 2) communication system network transmitting data at the rate of 1400 Mbits/s commenced in 1985 and has now been completed (Ball et al [2], [1]). British Telecom expects 50% of its U.K trunk transmission network to be optical fibre by 1988 [1].

In Japan, as of beginning of 1985, optical fibre cables totalling 7000 km have been installed for commercial communication(Kimura [3]). This system is based on a 1300 nm carrier and achieves data rate transfer of up to several Gbits/s with repeater (described in Chaper 2) spacing exceeding 100 km [3]). No information on the exact data rate transfer is given.

USA is known[1, 4] to be the world leader in fibre optics technology, production and applications. However, it has not been possible to obtain the total length of optic fibre so far laid or the greatest bandwidth achieved.

The major components of optical fibre communication are the laser diode, optical fibre and the laser detector. The light signal emitted by the laser diode is launched into the fibre and propagates through it by means of total internal reflection. The signal is then detected at the far end of the fibre. An optical fibre is a dielectric waveguide that consists of the inner core with high refractive index and the outer layer (with lower refractive index) called the cladding. Depending on the size of the core diameters, fibres are classified as single- or multi-modes. The alignment of semiconductor

laser diode with a single mode fibre is, however, more difficult to perform than with the latter because multimode fibre core diameters are much larger than single mode fibre core diameters.

Semiconductor lasers are suitable for optical communication because they produce coherent laser radiation. This means that the output radiation is highly monochromatic and the laser light beam is very directional (Keiser [5]). Laser action is the result of three processes namely photon absorption, spontaneous emission and stimulated emission. Absorption takes place when an electron normally at ground state absorbs an impinging photon and gets excited to a higher energy level. Since this electron is unstable at this state, it will either drop down to the ground state by itself or be induced by an external stimulation (incident photon). A photon of energy is released in both cases and if it corresponds to the former, the emission is spontaneous which is of random phase appearing as a gaussian output (laser output power versus wavelength) otherwise stimulated [5]. The latter is in phase with the incident photon producing a coherent radiation. This laser emission can be modulated for both analog and digital data transmission [5].

Laser-fibre coupling presents a major problem in optical fibre communication. Several approaches to the problem of laser-fibre coupling featuring different techniques have been reported together with their accompanying efficiencies. Sunak and Zampronio [6] report laser/fibre transfer efficiencies of 10% to 18% for plane ended multimode fibres (butt-joints), Saruwatari and Nawata [7] report 25% efficiency using plane ended single mode fibres. The latter is relatively more efficient because single mode fibres are several times smaller in size. The same authors used a selfoc lens (defined in Chapter 2) configuration and achieved 22% efficiency. Timmerman [8] on the other hand achieved 80% efficiency when he incorporated hemispherical or tapered hemispherical or cylindrical lenses. Lastly, by incorporating a cylindrical lens together with a rotationally symmetric lens, Ashton et al [9] report efficiency of 50%. No efficiency figures were quoted for use of single cylindrical lens configurations described by others to enhance laser-fibre coupling.

STC is a U.K based company employing 47,000 people [10]. In 1966, STC laboratory was the first to come up with a proposal that glass fibres

can be used to transmit laser signals (Bacon [11]). Although there is an indication of its involvement with semiconductor lasers since 1970 [2], it is not clear when STC actually started manufacturing them. Recently, STC set up a project to produce a novel system for automatic alignment of optoelectronic components.

The problem of laser-fibre alignment clearly involves the concept of alignment of two lines in space. This is because the central axis of the laser beam can be regarded as one straight line in space while the axis of the fibre is the other. A straight line can be defined as an infinitely continuous line for which the distance between any two selected points along it is least. The concept of general line representation in space, line transformations and the mathematical description of a straight line as an essential prerequisite to the derivation of this transformation are summarised by Rooney [12]. This highlights the fact that a line has four degrees of freedom of location and orientation compared to three for a point. Thus, the alignment of lines in space is a four degree of freedom problem. Another type of line is the line segment. It is defined as that part of an infinite straight line which is bound by (or terminates at) two points. Alignment of line segments requires one more degree of freedom compared to that of infinitely continuous straight lines because line segments have finite lengths. Alignment of lines can alternatively be called superposition of lines. Alignment can be extended to cover superposition of spatial congruent figures but this is irrelevant to this work.

A mathematical description of the misalignment of lines is the first step towards solving the problem of their alignment. Bottema [13] studied the screw displacements needed to displace rigid bodies in space, superpose misaligned line segments and lines respectively (see Appendix A) and concluded that:

(i) the screw required to move a body from one position to another in space is unique provided that the rotation angle, the translation distance and the screw axis are fully determined.

(ii) there are altogether oo^1 screw displacements transforming a row of points on one line segment into a congruent row on the other.

(iii) there are ∞^2 complete screw displacements required to align two skew lines.

A literature search on alignment conducted in the course of this research revealed no reported work by others on alignment by method of kinematics apart from Bottema's. Alignment ,however, features quite prominently in other areas like machinery alignment, circuit alignment and so on.

Inorder to obtain an automatic method for optical fibre/laser alignment using the concepts of spatial line alignment, it is necessary to use some mechanical device to position and orientate the objects relative to each other. A manipulator is the most appropriate device because its function is to reach a set of desired points in space with the end effector in prescribed orientations. That is, from the view point of kinematics, a manipulator is essentially a positioning device.

Manipulators may be classified into two major categories according to their basic design. These are the serial and parallel manipulators. A serial manipulator has actuators connected in series along a more or less anthropomorphic arm, each actuator being at or associated with a single degree of freedom joint. This type of manipulator accumulates errors from shoulder out to end-effector. Such manipulators suffer from lack of rigidity and are subject to load dependent errors. A parallel manipulator on the other hand, has actuators connected in parallel and again each actuator has one degree of freedom. Even if each actuator on its own has more than one degree of freedom, this is usually always reduced to one in the overal manipulator configuration. This type of actuation is characterised by rigidity and lightness and because actuator error is not cumulative, greater precision is likely to be attained.

The control of manipulators has been extensively studied and generalised by the use of transformations relating coordinate frames attached to the various arm segments, the end-effector and the manipulated object. That is, to control a manipulator, it is necessary to understand the relationships between the objects, and betweenthe objects and manipulator. A method used by Paul [14] to describe manipulators with respect to these relationships is the

homogeneous transformations. These transformations which consist primarily of translation and rotation were first employed by Denavit and Hartenberg [15] to describe linkages.

The use of an articulated mechanical system (eg manipulator) is related to its behaviour in the task space (Coiffet [16]). This space can be represented by a set of cartesian coordinates bound to the body of a manipulator. If the structural parameters are given, the coordinates and the velocities of the different points of the articulated system as well as the orientation and velocity of displacement of the various sets of coordinate axes linked to the body in space can be obtained [16]. As in homogeneous transformations, the results of such an analysis help to predict the position of end effector in space which can in turn be linked to the positions of objects to be aligned and thus their alignment. This problem is tackled by considering a complete chain of articulated segments and performing vector translations and rotations [16].

Apart from vector and homogeneous transformations, others like screw calculus, tensor analysis and combinations of these have also been described by people like Rooney [17], Duffy [18] and so on. Since all these methods aim at determining the equations that relate the parameters of motion in joints and that of the trajectory plus the orientation of the end-effector, it is pointless to try and report all of them here. However, manipulators are commonly described in terms of the Denavit-Hartenberg parameters (Gupta [19]). Examples of such applications have been described by other authors notably Litvin and Parenti Castelli [20], Lee [21] and Pieper and Roth [22] who have presented closed-loop manipulator solutions along these lines. The solutions to those equations are not unique because the manipulator links can form various configurations when the manipulator executes the given trajectory.

This is a multi-disciplinary research work putting together different technologies with a view to solve the alignment problem. The ultimate objective is to produce a novel patentable system for automatic production of optoelectronic components.

REFERENCES

1. M. Wilkinson
"Filling in the missing links"
The Engineer vol.264, May 1987.

2. P.R. Ball, P. Wells and J.P. Hincliffe
"Optical fibre transmission systems in telecommunications"
GEC Review vol.2, No.2, 1986.

3. T. Kimura
"Fibre optic transmission systems -status and trend in Japan"
IEEE Journal on selected Areas in Communication, USA vol. SAC-4, No.4, 1986.

4. "Fibre Optics in the U.K and USA"
The Financial Times Business Information (Key Issue Briefs)
(The Financial Times Media Intelligence Unit Jan. 1984).
Edited by Rosemary Flem-Ath
Published by the Financial Times Business Information Ltd.

5. G. Keiser
"Optical Fiber Communications", McGraw-Hill Inc.1983. (p.20-21).

6. H.R.D. Sunak and M.A. Zampronio
"Launching light from semiconductor lasers into plane-ended multimode optical fibres", Applied Optics 1983, vol.22, No.15, p.2337.

7. M. Saruwatari and K. Nawata
"Semiconductor Laser to Single Mode fiber Coupler", Applied Optics, 1979, vol.18, No.11, p.1847.

8. C. C. Timmerman
"Highly Efficient Coupling from GaAlAs Lasers into Optical Fibers", Applied Optics 1976, vol.15, No.10, p.2432.

9. J.E.U. Ashton, R.M. Gibb and B.A. Eales
"New generation semiconductor CW laser packages with full hermiticity, integral power monitoring and direct fibre optic launching". Microelectronics Journal vol.12, No.3, 1981. p.14-18.

10. Key British enterprises (KBE)
The Top 20,000 British Companies
Published by Dun and Bradstreet Ltd vol.2 (N-Z), 1986 (section 1.1096).

11. K. Bacon
"Fibre Optics: 120 years - Telecommunications"
Journal of Engineering vol.226, Jan. 1986.

12. J. Rooney
"A comparison of representations of general spatial screw displacement", Environment and Planning B, vol.5, 1978 (p.45-88).

13. O. Bottema
"On a set of displacements in space", Contributed by the Design Engineering Division for representation at the Mechanisms Conference, San Francisco, California, USA. Oct. 8-12, 1972 of the ASME. Paper No.72 - Mech - 19. Transactions of the ASME. Journal of Engineering for Industry (p.1-4).

14. R. P. Paul
"Robot Manipulators: Mathematics, Programming and Control". Cambridge: MIT Press 1981.

15. J. Denavit and R.S. Hartenberg
"A kinematic notation for lower pair mechanisms based on matrices". ASME Journal of Applied Mechanics vol.22, 1955 (p.215-221).

16. P. Coiffet
"Modelling and Control", Robot Technology vol.1. Englewood Cliffs, N.J.: Prentice Hall 1983.

17. J. Rooney
"On obtaining the Velocity Motor of any link in a general N-link spatial manipulator". The Institution of Mechanical Engineers 1975 (p.1083-1087).

18. J. Duffy
"Analysis of mechanisms and robot manipulators", Wiley 1980.

19. K.C. Gupta
"Kinematic Analysis of Manipulators Using the Zero Reference Position Description". Edited by J.M. McCarthy. Cambridge: MIT Press 1987.

20. F.L. Litvin and V. Parenti Castelli
"Robot's Manipulator: stimulation and identification of the configurations, execution of prescribed trajectories". Proc. of the IEEE. International Conference on Robotics, 1984 (p.34-44).

21. C.S.G Lee
"Robot arm kinematics, dynamics and control". Computer vol.15, 1982 (p.62-80).

22. D.L. Pieper and B. Roth
"The kinematics of manipulators under computer control". Proc. 2nd IFToMM Int. Congress on Theory of Machines and Mechanisms vol.2, 1969 (p.168-169).

CHAPTER 2

OPTICAL FIBRE TRANSMISSION

CHAPTER OVERVIEW

Although the bulk of this work is centred on the study of mechanical laser/fibre or fibre/fibre alignment, it is first necessary to understand the functions and characteristics of the associated components as well as the difficulties involved in getting them to couple the minimum acceptable power level. A review of such components is therefore presented in section 2.1 while a theoretical analysis of the laser field distributions and the laser/fibre coupling efficiency are discussed in section 2.2.

The angular and lateral misalignment problems and the different methods of launching the laser beam into optical fibres are presented in section 2.3. The difficulties associated with the physical set up of each method and consequently their effects on the final alignment results are also discussed.

The literature survey of the presently available alignment experimental results are presented in section 2.3.5 while the problems associated with the manual laser/fibre coupling process currently employed by STC are discussed in section 2.4. A brief account of a proposed basic sequence of operation intended for a semi-skilled operator conducting the laser/fibre alignment process and the alignment specifications are then presented in section 2.5.

2.0 INTRODUCTION

Optical fibre conveyancing is superior to its wire cable counterpart in many ways. Firstly, light signals are transmitted in form of photons. This means that high electric or magnetic fields can not affect the transmission because the photons are not charged. Shielding signal bearing fibres cuts off leakage flux which in turn eliminates interference.

By means of electromagnetic pick up loop, wire cable transmission can be easily tapped. In contrast, there is no easy way of picking up information transmitted optically along the fibres for illicit use.

The propagation of light waves through optical fibres is accompanied by large bandwidths (i.e. information carrying capacity). This bandwidth varies inversely only as the first power of the fibre optic cable length while in conventional wire cables, it varies inversely as the square of the wire length [1]. For this reason, optical fibre carrying capacity is exceedingly higher than the wire cable carrying capacity.

Optical fibres are more resistant to flexure, impact and crush than conventional wire cables of the same size subjected to similar abuses. For the same amount of information capacity, optical fibres are lighter in weight and tolerate severe environmental conditions better than wire cables.

Saruwatari and Nawata [2] state that the transmission loss of optical fibres has been reduced to 0.5 dB per km. It is therefore clear that a viable long distance transmission system using single-mode fibres is feasible. However, non-uniformity and inhomogeneity of fibres can cause signal dispersion along the fibre. Wolf [3] states that in graded index fibres where the refractive index varies hyperbolically as the radial distance from the centre of the fibre, it is practically difficult to achieve the required profile. So, some other methods of reducing losses need to be devised.

Morris [4] states that fibre optical conveyance can be used to transfer both analog or digital data, although ideally, it is best for digital data by just switching ON and OFF according to the data 1 and 0 state respectively. Keiser [5] states that the power of an optical pulse launched into an optical fibre is distributed over all (or most) of the modes (defined in 2.1.1) of the fibre. Each of the modes that can propagate in a multimode fibre, travels at a different velocity. Data voltage pulses are converted into optical pulses by driving an electrical current pulse through a light emitted diode (LED) as shown in Figure 2. This radiates light pulses into the

fibre. This signal propagates through the fibre and is picked up by a photodiode at the opposite end.

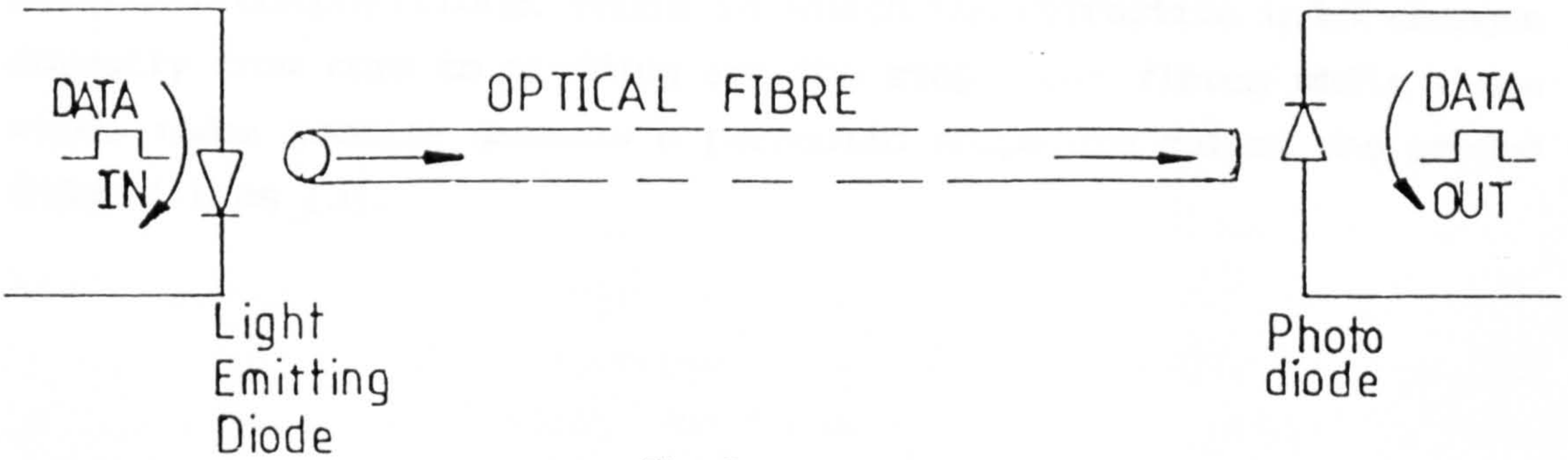

Fig.2

2.1 REVIEW OF FIBRE OPTICS TRANSMISSION COMPONENTS

The major components of the optical fibre communication system are the laser emitter, optical fibre and the laser detector. Coupled to an optical fibre at a spacing of 2 to 6 km for purposes of long haul transmission, are the repeaters. These are receivers and transmitters connected back to back [4]. Apart from converting optical signals to electrical signals by way of light detection, they also amplify the signals and then reconvert them to optical signals for further propagation along the fibre.

2.1.1 Optical Fibres

An optical fibre is a dielectric waveguide that consists of a pure glass fibre core surrounded by a concentrated layer called the cladding. Allan [6] states that the cladding has a lower refractive index than the core so that a light generated at one end of the fibre propagates along the fibre by total internal reflection principles with minimum loss. The angle of the light signal as it enters the fibre is important to the propagation success.

The cladding is covered by a protective material normally made of

silica to strengthen the fibre. The outer jacket is made of plastic and the whole fibre diameter is between 2 to 4mm as given in [3] and shown below.

There are two major types of optical fibres whose attenuation and signal dispersion characteristics depend entirely on their core material compositions. Those in which the refractive index changes abruptly from core to cladding are the step index fibres while those whose index profile assumes a parabolic shape are called the graded index fibres [3].

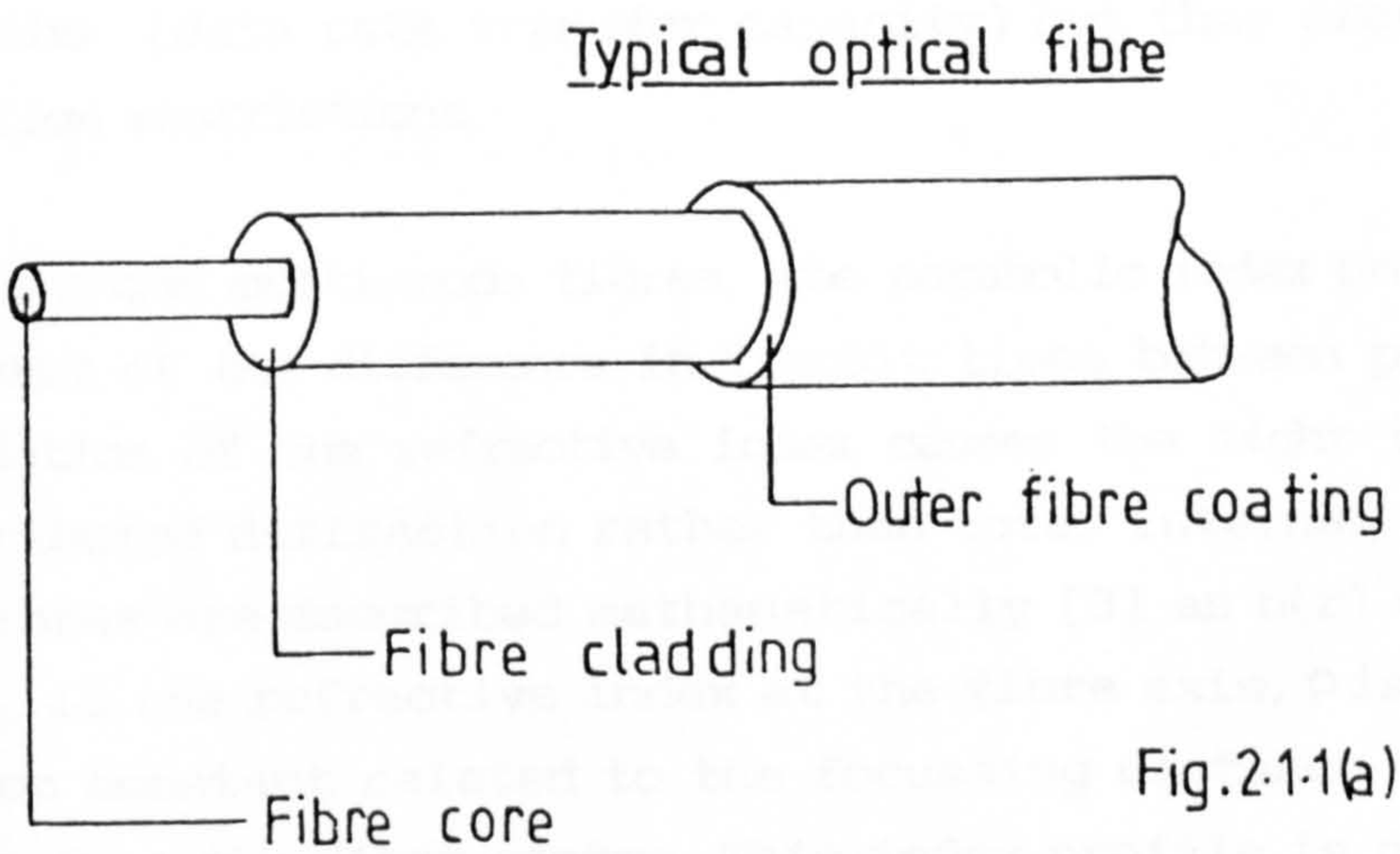

Fig.2.1.1(a)

The two classes can be further distinguished depending on whether they can support single or multi- modes. The single-mode fibres support only one mode of propagation while the multi-mode fibres support hundreds [3]. Modes of a waveguide are defined [5] as a set of guided electromagnetic waves. These guided modes are sometimes referred to as bound or trapped modes [5]. Each guided mode is a pattern of electric and magnetic field lines that is repeated along the fibre at intervals equal to its own wavelength. Only a certain discrete number of modes are capable of propagating along the fibre.

In step index multimode fibres, a small index difference ($\Delta=1-n_2/n_1$) of 1% or less is quoted [3] where n_1 is the core index and n_2 the

cladding index. Since different partial rays propagate at different angles and therefore follow different paths, they exhibit different transit times giving rise to a limited bandwidth of the fibre. Ashton et al [7] states that for an interface between two media of different refractive indices, the transmission $T = 4n_o n_1/(n_1 + n_o)^2$ where n_1 and n_o are the refractive indices of core and air respectively. The transmission loss is defined [7] as $10\log_{10}(1/T)$ dB.

In step index single-mode fibres, the core diameter ($2a_1$) is so small that essentially only one axial partial ray can propagate. Mathematically, the critical fibre core radius is expressed [3] as $a_1 = (1.202/\pi)(\lambda/n_1(2\Delta)^{1/2})$ where λ = wavelength of propagated light and $\Delta = 1-n_2/n_1$. These fibres are most attractive for achieving large bandwidths (data rate transfer capacity) but they present severe fabrication restrictions.

In graded index multi-mode fibres, the parabolic index profile solves the problem of the difference in transit times between partial rays. The gradation of the refractive index causes the light to be guided by distributed diffraction rather than total internal reflection. These fibres are described mathematically [3] as $n(r) = n_o \mathrm{sech}(\rho r)$ where n_o is the refractive index at the fibre axis, ρ is the radial variation constant related to the focussing distance and r is the distance from the fibre centre. This index profile is difficult to achieve in practice and probably explains why it is extremely difficult to produce single-mode graded index fibres.

These fibres are shown in Figure 2.1.1(b) with typical core diameters ranging from 1 to 5 μm for monomode step-index, 30 to 100 μm for multi-mode step index and 20 to 50 μm for multi-mode graded index fibres as given in [3].

A measure of information capacity of an optical fibre is given [5] by the bandwidth-distance product in MHz.km. For a step-index fibre this is limited by the various signal distortion effects to about 20 MHz.km while in graded-index fibres it can be as high as 2.5 GHz.km. Single-mode fibres, however, can have capacities well in excess of this [5].

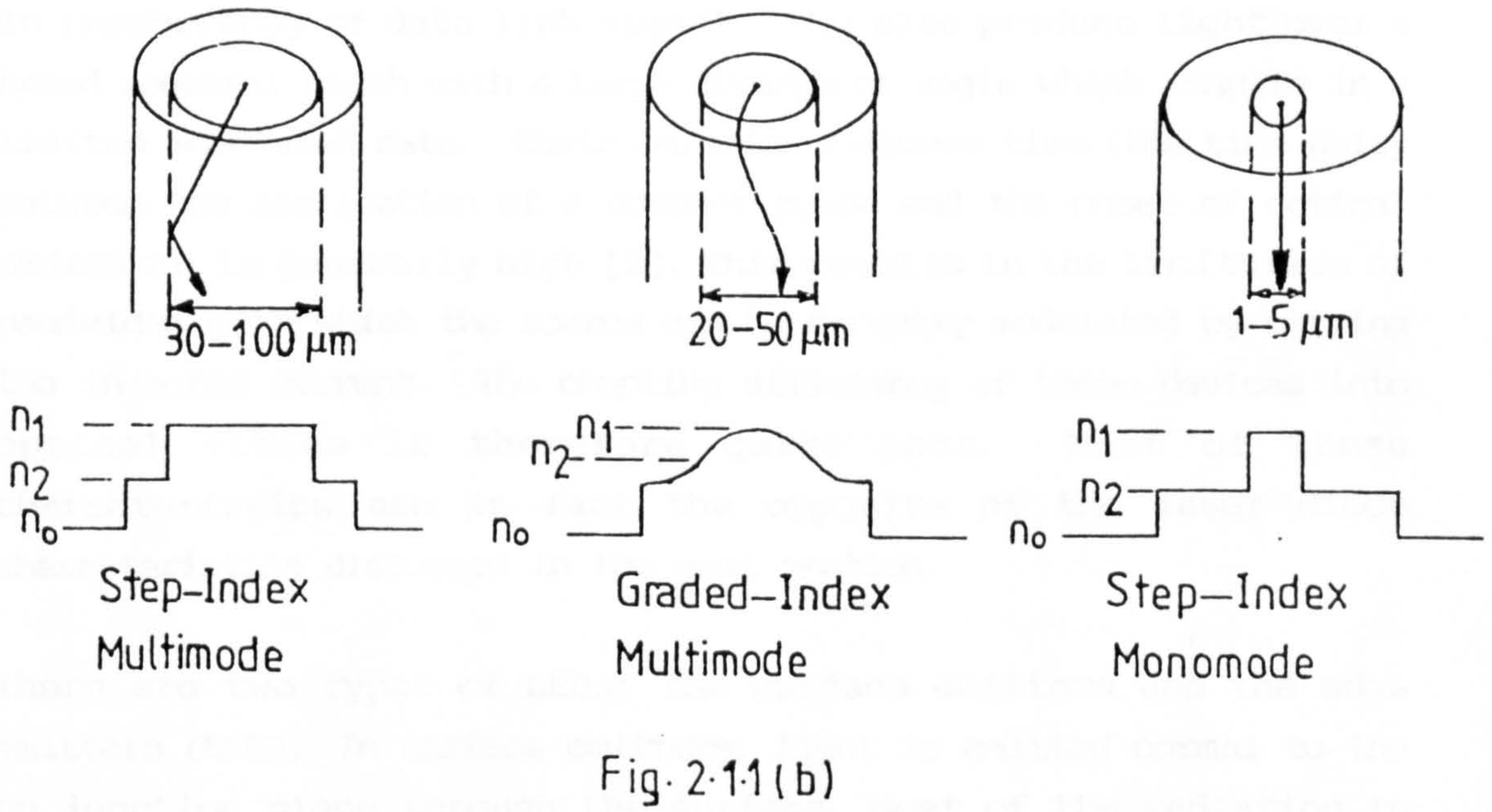

Fig. 2·1·1 (b)

2.1.2 Light Emitters

Semiconductor lasers and the light emitting diodes (LED) are the only two forms of light sources utilised for optical data transmission. Davies et al [8] state the reasons for this as the only sources that can be directly modulated at the high bit rates required with such low drive and high output power. The laser is used for the wideband long haul communication systems while LEDs are used for short and medium range narrow band systems. This is because lower output power, lower frequency response and broader spectrum are not the limiting factors in short and medium range systems and more importantly, the LEDs drive and control circuitry is simpler to construct.

These two sources are characterised by high speed, efficiency and reliability and these qualities are highly suited to optical fibre

communication.

2.1.3 Light Emitting Diodes (LED)

In general, light intensity produced by LEDs bears a direct relationship to the current magnitude flowing through them resulting in incoherency of data link signal. They also produce light over a broad spectral width with a large divergence angle which results in a limited modulated rate. Their emission response time (the time delay between the application of a current pulse and the onset of optical emission) is generally high [5]. This results in the limitation of bandwidth with which the source can be directly modulated by varying the injected current. The coupling efficiency of these devices into optical fibres is therefore quite poor. Most of these characteristics are in fact the opposite of the laser diode characteristics discussed in the next section.

There are two types of LEDs: the surface emitters and the edge emitters (ELED). In surface emitters, light is emitted normal to the pn junction plane through the surface. Most of the radiation is absorbed in the substrate and the emission is Lambertian (wide-angled) [8]. That is, the source is equally bright when viewed from any direction [5].

In edge emitters, light is emitted in the plane of the junction thus little absorption takes place. Its emission is directional when stripe geometry is used [8]. This structure offers better external quantum efficiencies and far more efficient and easier coupling to optical fibres. While internal quantum efficiency is known [5] to be ill defined (vary from 0.6 to 0.7 at room temperatures) for laser diodes, external quantum efficiency is defined [5] as the number of photons emitted per radiative electron-hole pair recombination above threshold. It is reported [8] to use the same geometry as the stripe laser minus laser action. It is characterised by ease of operation and low noise, with output power, launch efficiency and modulation rates approaching those of the laser. The ELED therefore has a much longer range and better bandwidth performance than the surface emitters. It is suited to digital and analog links of medium data

capacity and range.

There are two versions of GaAs/GaAlAs ELED operating at 850 nm wavelength. ELEDs performance makes it suited to demanding communication systems such as cable TV links. A description of the two versions and comments on the current trials of a broadband optical fibre link carrying high quality TV programs on a cable network operated by British Telecom are presented in [8].

2.1.4 Laser Diodes

In contrast to LEDs, the injection laser diode (ILD) is a threshold device which emits signal only if the current through it is above a limiting value. It is reported [4] that the threshold level of an injection laser diode is usually about 100 mA and they reach maximum emission of light at about 120 mA. ILD signals are coherent and ideal for ON/OFF data transmission with extremely high speeds. They produce narrow light bands which are highly directed and confined resulting in higher modulation rates and better coupling efficiency.

Currently, most laser diodes being investigated and used for optical communication purposes are multi-layered heterojunction structured optical devices. A typical stripe geometry SiO_2 insulated laser illustrated by Selway et al [9] is shown in Figure 2.1.4(a). The junction structure is a conventional double heterostructure with $Ga_xAl_{1-x}As$ passive layers containing nearly 35% Al and an active region with nearly 5% Al [9]. According to these authors, the latter quantity minimises the strain in the active layer caused by thermal expansion mismatch between the GaAs substrate and the $Ga_xAl_{1-x}As$ passive layers. A detailed analysis of the major aspects of laser diodes are carried out by the same authors, [3] and [8] and can also be found in books covering laser light sources for optical fibre communications.

The relationship between the laser output power versus the diode drive current is illustrated in Figure 2.1.4(b). This is a purely theoretical representation but in practice, kinks usually appear in the curve. It is reported [9] that these were experimentally proved

to be associated with a sideways displacement of the light filament and that the near and far -field patterns change in the vicinity of the kinks. Several practical methods have, however, been developed to avoid the kinks [9].

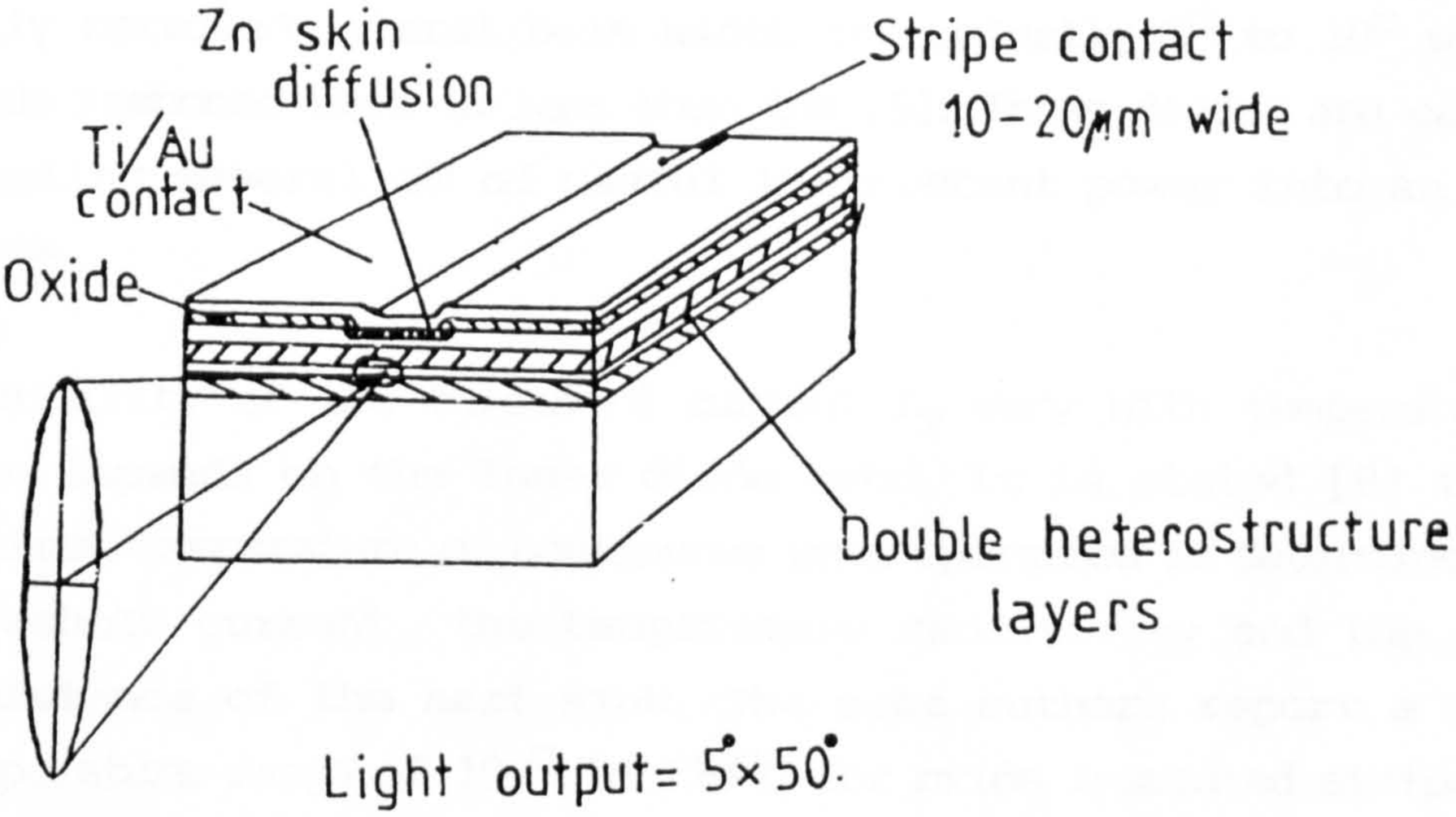

Light output= 5°× 50°.

SiO_2 Insulated stripe geometry laser

Fig. 2·1·4 (a)

Laser light output versus drive current.

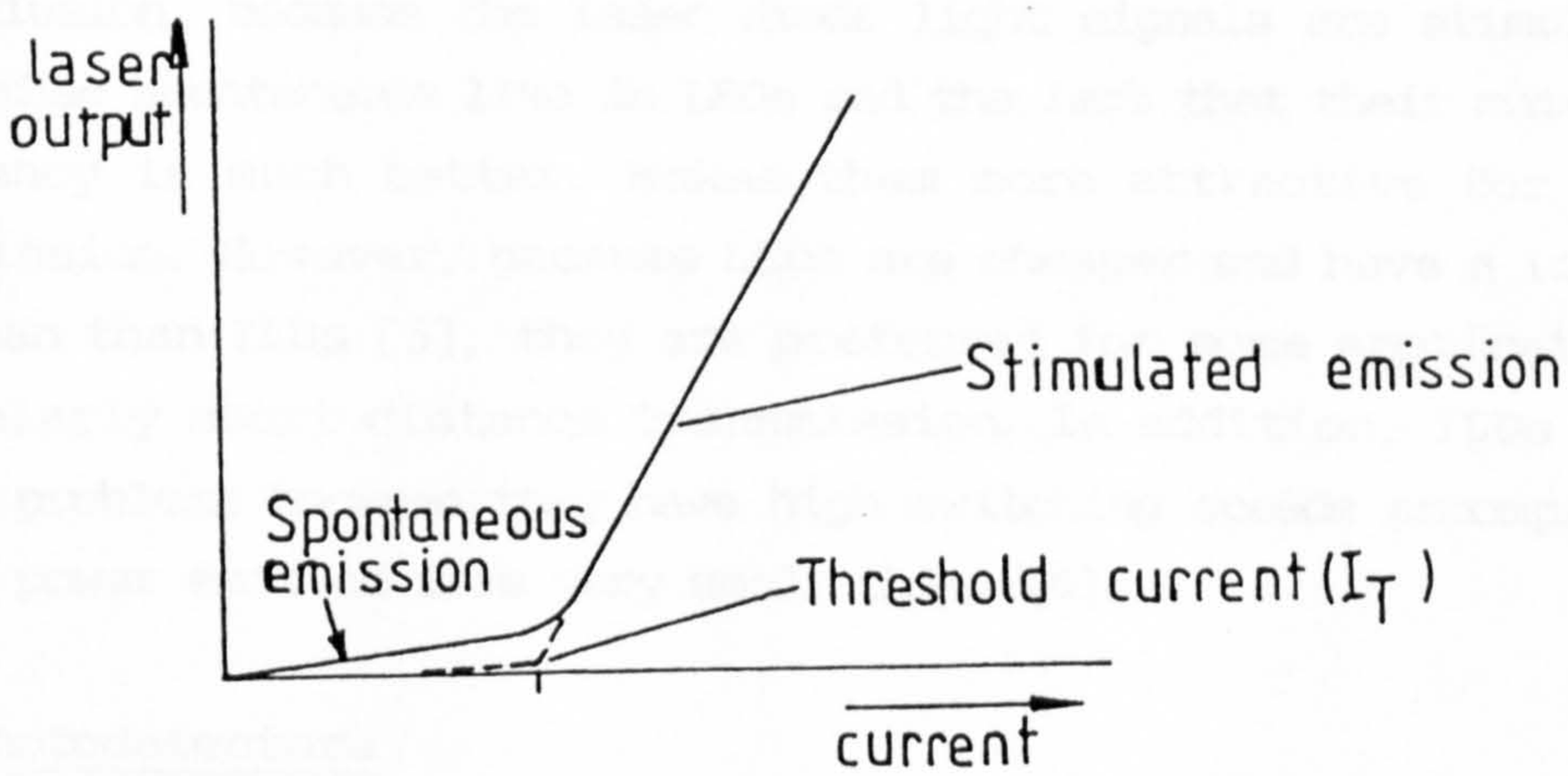

Fig. 2·1·4 (b)

At low diode currents, only spontaneous emission is obtained. This

emission has both a broad spectral range and lateral beam width similar to LED emission. A stimulated power output or emission sharply shoots out as soon as the threshold current I_T is reached. On approaching this point, the spectral range and the beam width will both narrow down. The final spectral width is approximately 1nm and fully narrowed lateral beam width is nominally 5^{o} to 10^{o} while the diode response time is less than 1ns [5]. These diodes are capable of coupling several mW of useful luminescent power into an optical fibre.

Sensitivity of the threshold current I_T vary with temperatures and also depends on the laser diode used. It is stated [8] that the maximum temperature of continuous wave operation is determined by the threshold current, the temperature sensitivity and the thermal resistance of the heat sink. The same authors report a maximum temperature range of 100^{o} to 120^{o}C for oxide insulated stripe GaAlAs lasers and 50^{o} to 60^{o}C for GaInAsP devices although advanced structures can operate at temperatures of 30^{o} to 40^{o}C higher.

The two principal methods used to vary the optical output from laser diodes are pulse modulation used for digital systems and amplitude modulation used for analog data transmission [5].

In conclusion, because the laser diode light signals are stimulated rather than spontaneous like in LEDs and the fact that their matching efficiency is much better, makes them more attractive for data transmission. However, because LEDs are cheaper and have a longer life span than ILDs [5], they are preferred for some applications particularly short distance transmission. In addition, ILDs have cooling problems because they have high switching speeds accompanied by high power emitted from very small chips [4].

2.1.5 Photodetectors

In any optical alignment system, the optical fibre is terminated with a detector in the form of either photoemitting diodes or avalanche photodiodes both of which are sensitive to light. This detection is a way of interpreting the information contained in an optical fibre. As

the luminescent power falls on the surface of a photodiode, the electric current magnitude flowing through them changes. The diodes then convert the light input signals to variations of electrical currents [5]. These current variations are amplified and reshaped before generating them back to voltage data pulses. In order to achieve this, the photodiodes must be permanently biased by a current that flows through them. The current variations are generally small for photodiodes and so they operate with a specially designed high impedance low noise preamplifier which is sensitive to small current changes [5].

The photodetectors used for this type of application must meet very high performance requirements because the optical signal arriving at the end of a long optical fibre is generally weakened, distorted or simply degenerated. The vital features include good sensitivity in the emission wavelength range of the optical source being used and a fast response speed [5]. It should have long operative life and be compatible with the physical dimensions of the optical fibre.

Normally, the avalanche photodiodes are preferred for the detection of low optical power signals. Detailed reviews of photodetectors can be found in [3, 8 and 9] and other books on optical communication. While it is critical to observe the alignment tolerance of a laser beam to a monomode or multi-mode optical fibre, the positioning tolerance of the photodetectors are not so important [8].

2.2 ANALYSIS OF LASER DIODE - OPTICAL FIBRE COUPLING

It is established [2] that single-mode optical fibres are more efficient to use in the 1.3 μm wavelength region since silica fibres exhibit both low loss and zero dispersion near this wavelength. According to these authors repeater spacing is limited by the amount of light launched into the optical fibre rather than fibre dispersion. In order to achieve a proper single-mode fibre communication systems therefore, a rigid connection with high coupling efficiency is the answer.

In this section, the coupling efficiency and the alignment tolerance

between a laser diode and a single-mode fibre are described. The butt-joint configuration alignment of laser diode to single-mode fibre has been chosen for this design study because it offers the worst alignment conditions. This is known [2] to be due to the following factors: (a) the core diameter of a single-mode fibre is only about a tenth (5 to 10μm) of that of a multimode fibre, (b) the laser diode has a large beam divergence angle (40^{o} to 60^{o}) perpendicular to the junction plane and (c) the alignment tolerance of the laser relative to the fibre axis is as small as 1 μm.

2.2.1 The Gaussian Beam Approximation

Kogelnik and Li [10] reviewed the fundamental properties of laser beams and showed that the beam emitted by a semiconductor laser diode is not uniform in intensity (power per unit area) over its cross-sectional area. It has a Gaussian distribution similar in form to the random error frequency distribution curve. Its specified diameter (2w) is the beam width at which the intensity has fallen to $1/e^2$ of its peak value (Figure 2.2.1(a)).

It is shown [10] that the measure of the decrease of the field amplitude E with the distance z, from the axis is given by $w^2(z) = w_o^2[1+(\lambda z/ w_o^2)^2]$. The intensity distribution is Gaussian in every beam cross-section but the width of the intensity profile changes along the axis. This Gaussian beam contracts to a minimum diameter of $2w_o$ at the beam waist (Figure 2.2.1(b)) where phase front is plane. z is measured from this point in order to simplify the expansion laws [2, 10].

Sunak and Zampronio [11] reported the dimension of the lasing slit to be much smaller than the core diameters of the fibres. This means that the launching efficiency is hardly affected in the laser near field but seriously reduced in the far-field by the much larger beam divergence angles compared to the maximum fibre acceptance angles. It is therefore important to first study the laser far-field radiation patterns before attempting to construct a suitable laser/fibre coupling procedure that achieves acceptable launch efficiency. They found the experimental curves of these far-field patterns to be

slightly narrower than a Gaussian fitted to the $1/e^2$ x maximum intensity points. These are shown in Figures 2.2.1(c) and (d). Coupled with the work of these authors, two sample far-field patterns (supplied by STC) are shown in Figures 2.2.1(e) and (f). The far-field patterns of the beam both perpendicular (x-axis) and parallel (y-axis) to the junction plane are approximately Gaussian.

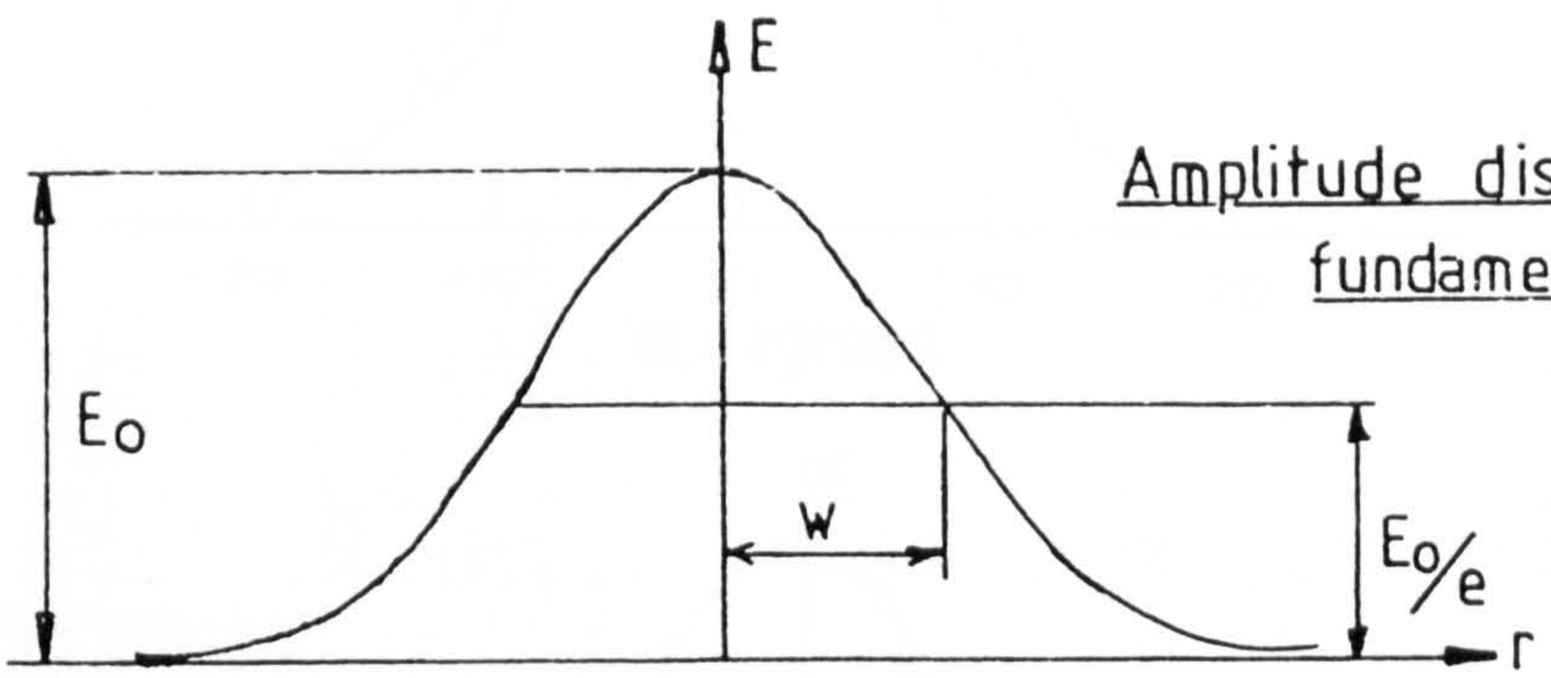

Amplitude distribution of the fundamental beam.

Fig.2·2·1(a)

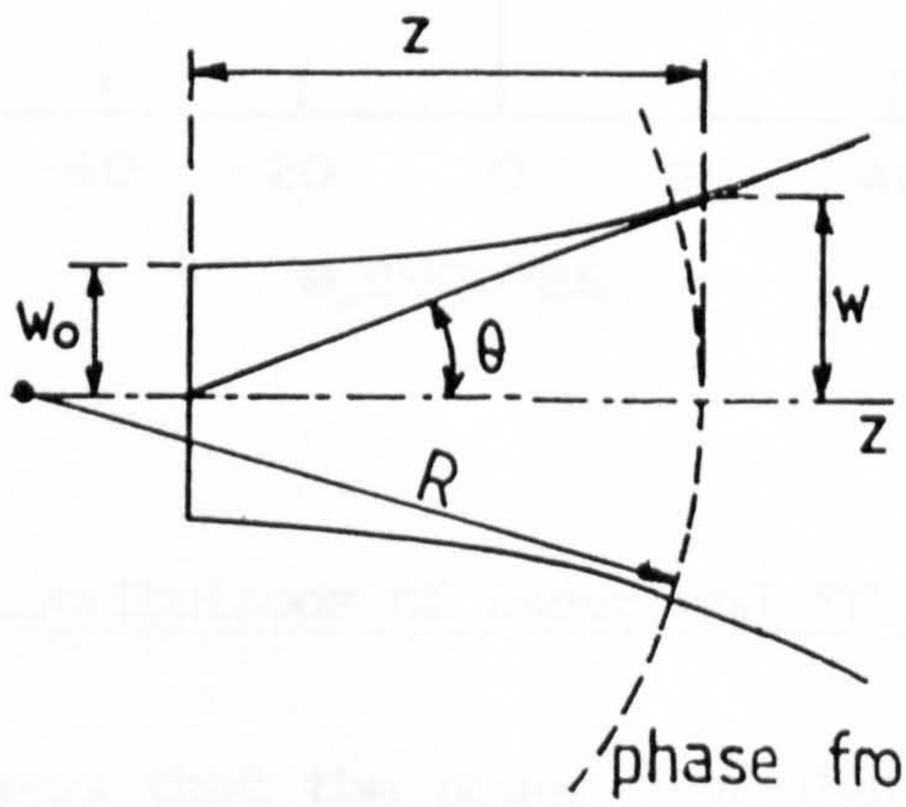

Contour of a Gaussian beam.

Fig.2·2·1(b)

Far-field intensity distributions L of laser beam emitted by a laser diode and a fitted Gaussian distribution G.

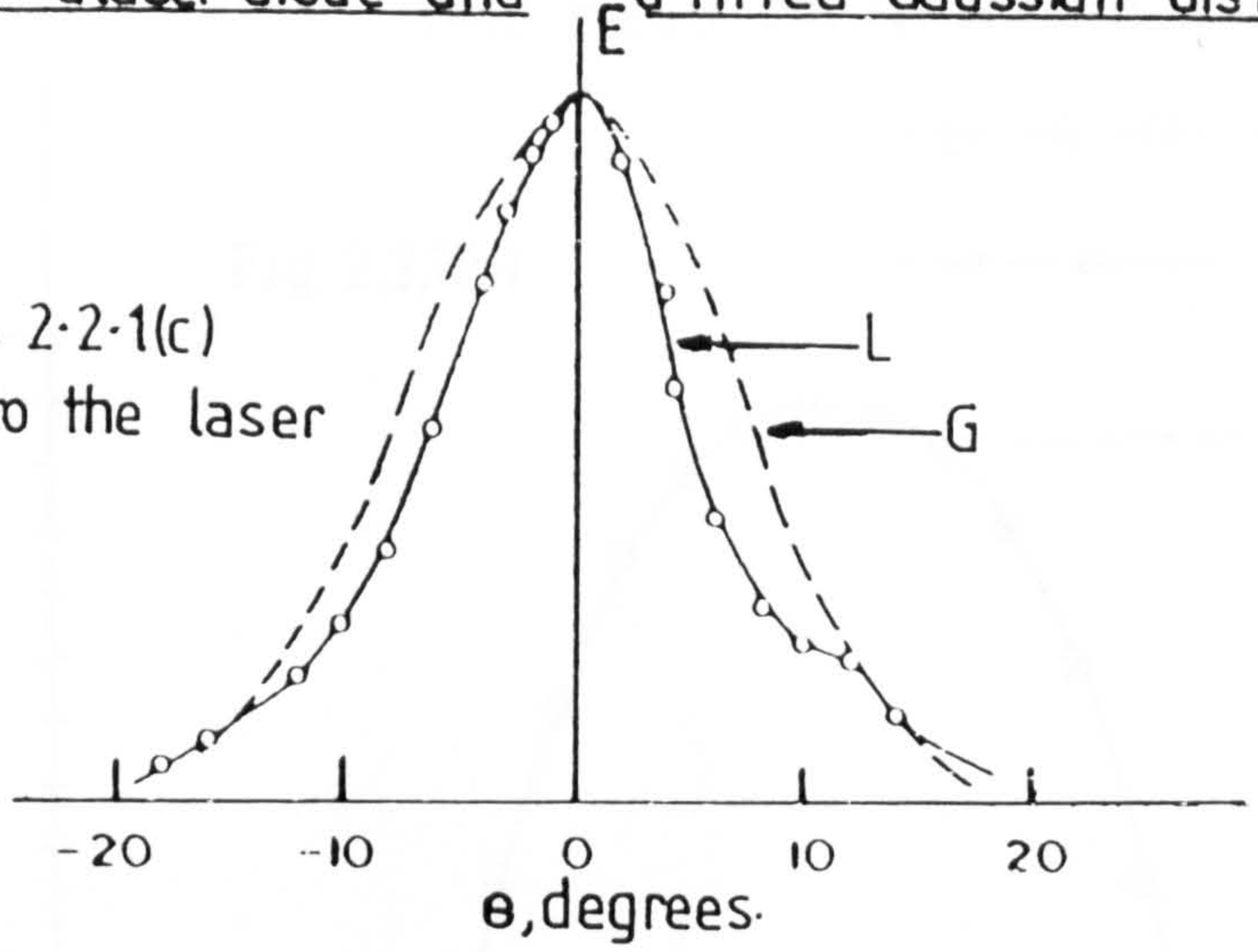

Fig. 2·2·1(c)
Parallel to the laser stripe.

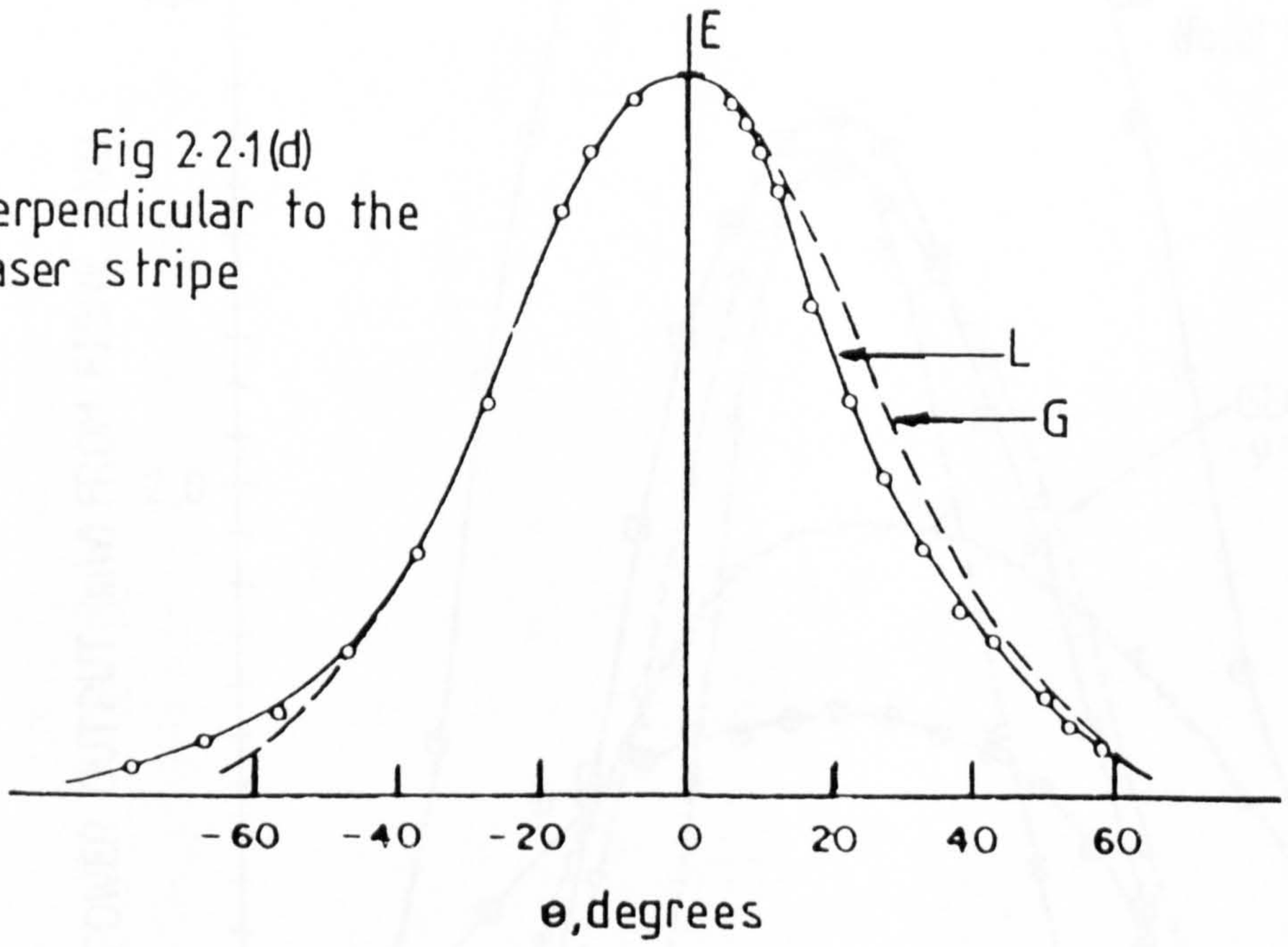

Fig 2·2·1(d)
Perpendicular to the laser stripe

2.2.2 Field Distributions of Laser and Fibre

Nicia [12] states that the power distribution in a single-mode step index fibre can be approximated by a Gaussian shape to within 1% error as long as the normalised frequency V of the fibre is in the range of 1.9 to 2.4. Since this condition is true for a practical single-mode fibre, the characteristics of the field leaving the fibre

FAR-FIELD PATTERN IN X-AXIS

Fig, 2,2,1(e)

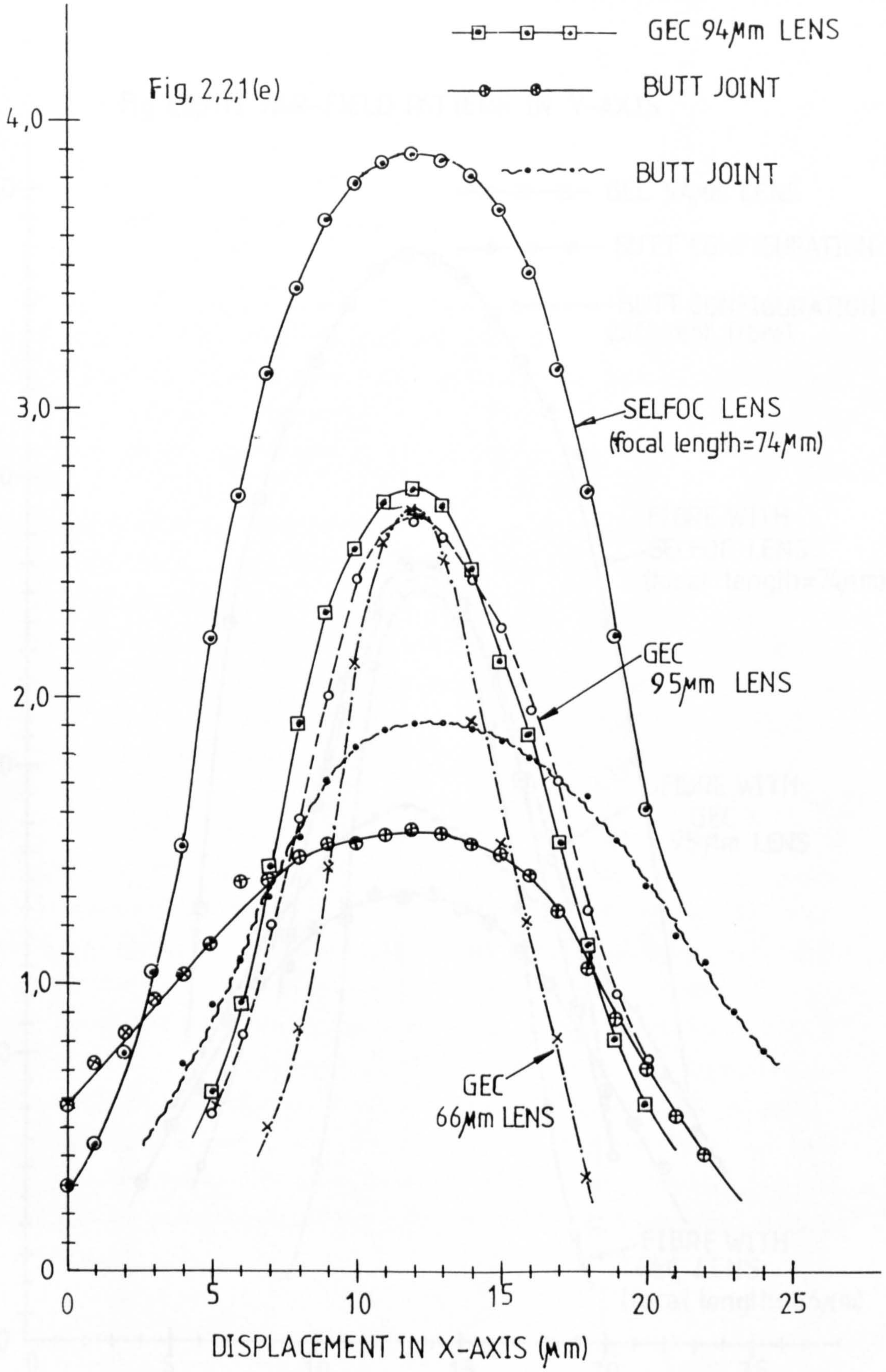

Fig,2,2,1.(f) FAR-FIELD PATTERN IN Y-AXIS

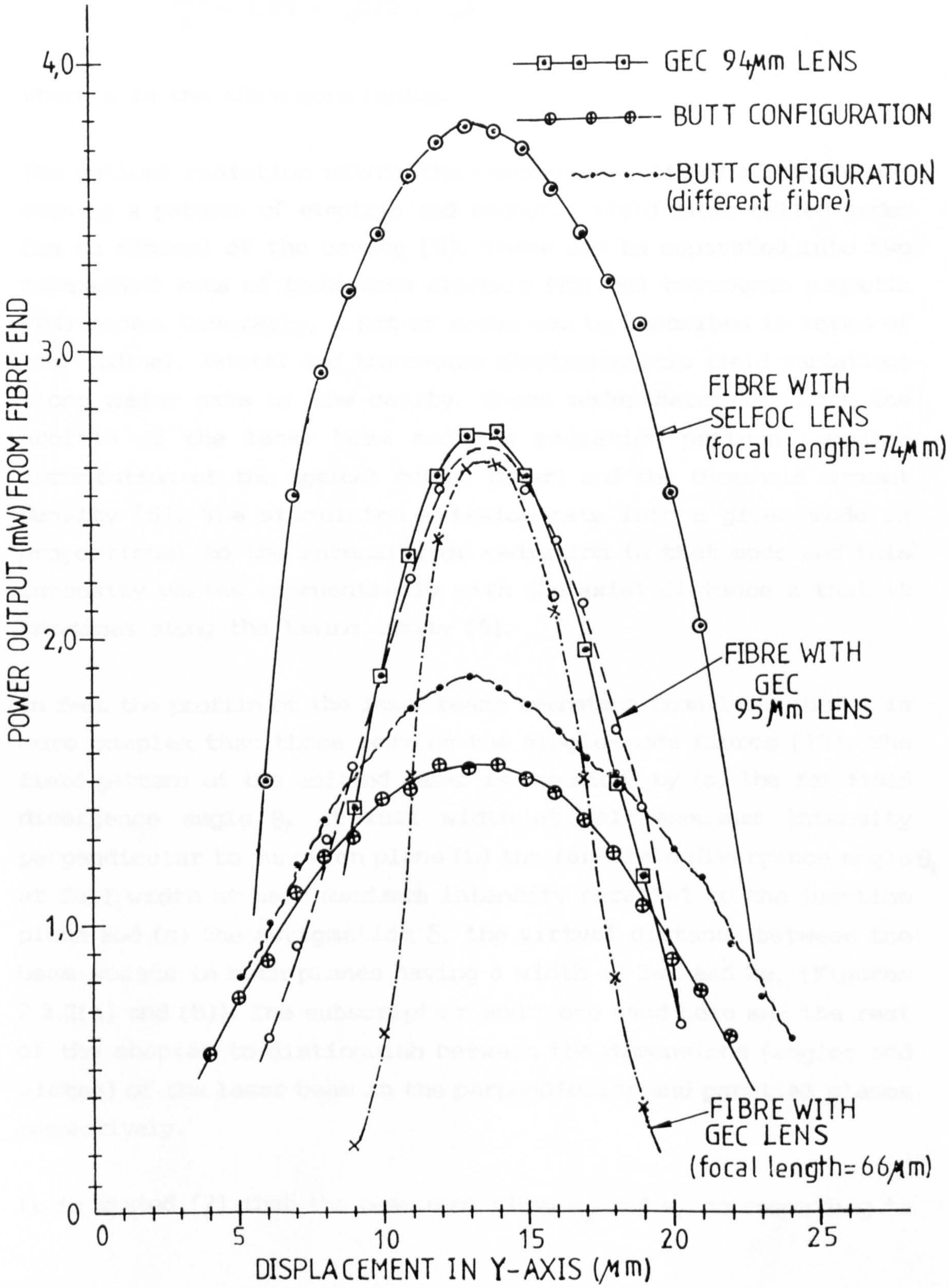

end can be estimated sufficiently accurately by a Gaussian approximation. Marcuse [13] gives the beam spot size w_o for step index fibres (its only characterised geometrical parameter at e^{-1} amplitude [12]) as

$$\frac{w_o}{a} = 0.65 + \frac{1.619}{V^{3/2}} + \frac{2.879}{V^6}$$

where a is the fibre core radius.

The optical radiation within the resonance cavity of a laser diode sets up a pattern of electric and magnetic field lines called modes (as in fibres) of the cavity [5]. These can be separated into two independent sets of transverse electric (TE) and transverse magnetic (TM) modes. Generally, a set of modes can be described in terms of longitudinal, lateral and transverse electromagnetic field variations along major axes of the cavity. These modes determine both the profile of the laser beam and its radiation pattern (angular distribution of the optical output power) and the threshold current density [5]. The stimulated emission rate into a given mode is proportional to the intensity of radiation in that mode and this intensity varies exponentially with the axial distance z that it traverses along the lasing cavity [5].

In fact the profile of the laser beams emanating from laser diodes is more complex than those leaving the single-mode fibres [12]. The field pattern of the emitted laser is described by (a) the far-field divergence angle θ_r at full width at half maximum intensity perpendicular to junction plane (b) the far-field divergence angle θ_l at full width at half maximum intensity parallel to the junction plane and (c) the astigmatism δ, the virtual distance between the beam waists in both planes having a width of $2w_r$ and $2w_l$. (Figures 2.2.2(a) and (b)). The subscripts r and l are used here and the rest of the chapter to distinguish between the dimensions (angles and widths) of the laser beam in the perpendicular and parallel planes respectively.

It is stated [2] that the beam spot sizes w_r and w_l corresponding to

the two planes are related to the far-field divergence angles θ_r and θ_l respectively by $w_r=\lambda/\pi\theta_r$ and $w_l = \lambda/\pi\theta_l$. Steenwijk [14], however, expresses the two beam spot sizes slightly differently as $w_l = \lambda_o(2\ln 2)^{\frac{1}{2}}/2\pi \tan(\theta_l/2)$ and $w_r = \lambda_o(2\ln 2)^{1/2}/2\pi\tan(\theta_r/2)$ where λ_o is the free space wavelength of light and λ is the wavelength of the light under investigation.

Radiation pattern of a laser diode

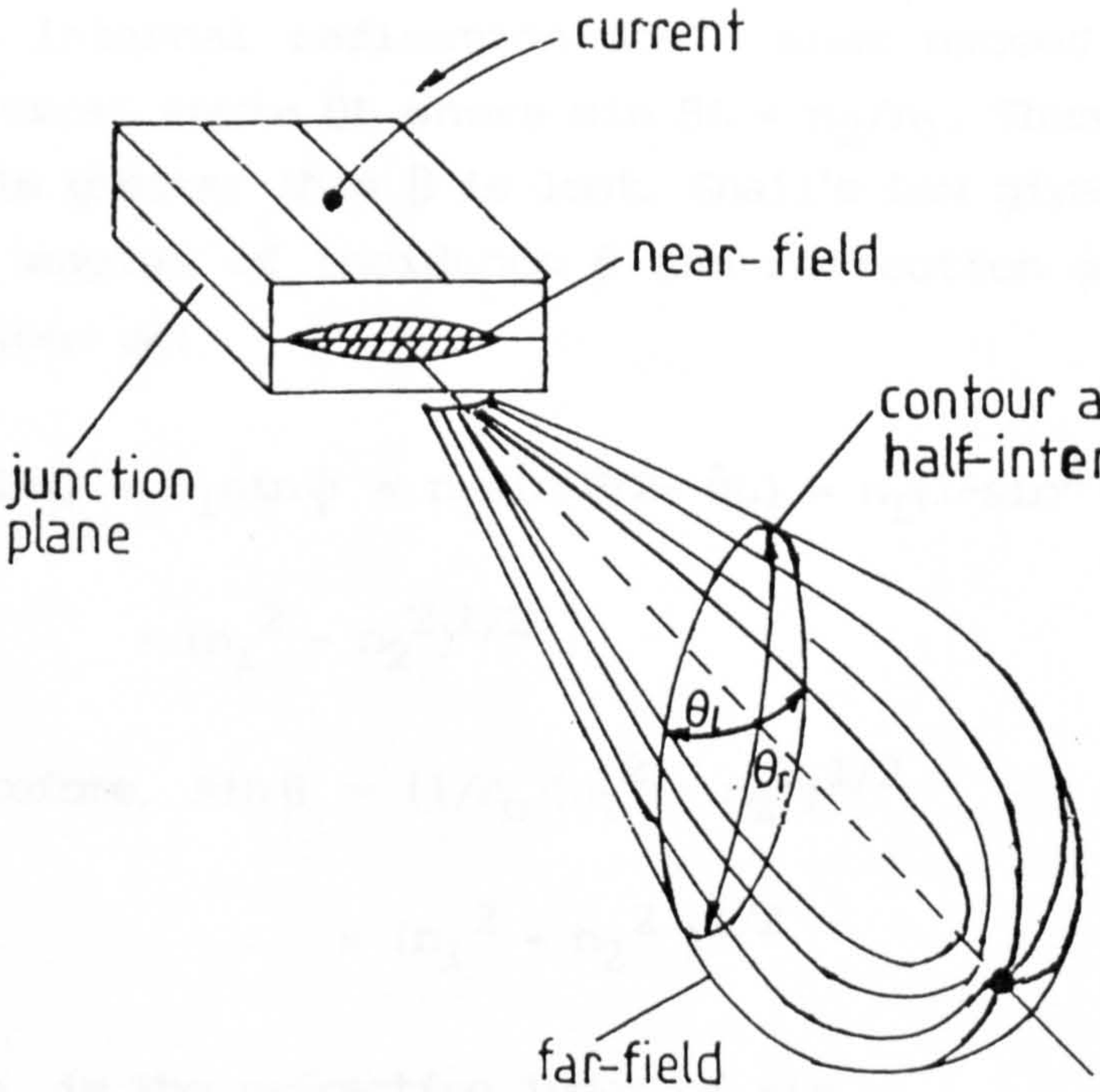

Fig,2,2,2 (a)

θ_l and θ_r are the far-field angles parallel and perpendicular to the junction plane.

Contours of a laser beam parallel and perpendicular to the junction plane.

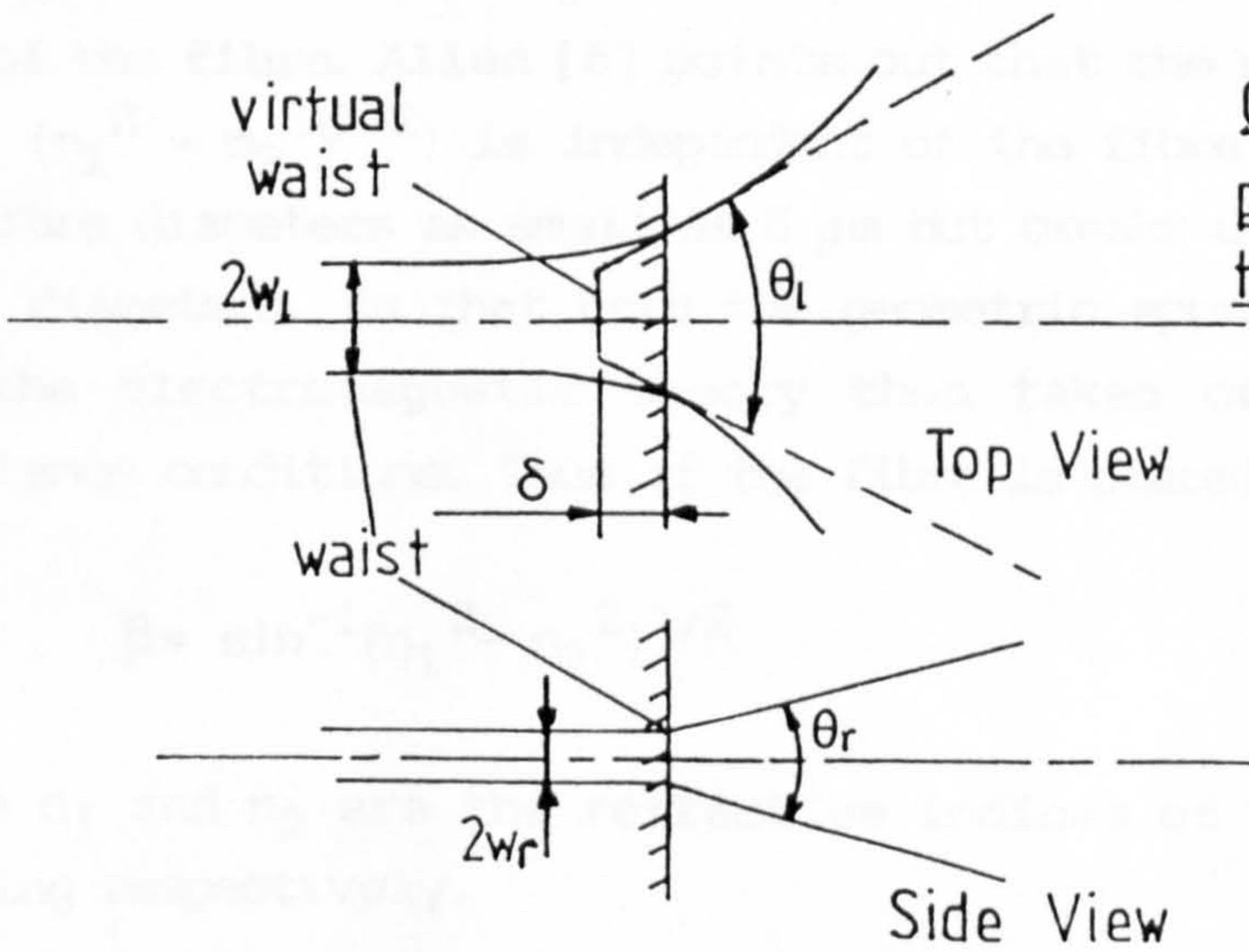

Fig,2,2,2(b)

2.2.3 Laser-Fibre Coupling Efficiency

A divergent laser beam cannot be transmitted efficiently along an optical fibre unless the divergent angle of the beam emanating from the semiconductor laser diode is less than or equal to the acceptance angle of the fibre. The laser beam is propagated along the fibre by total internal reflection principles.

Considering Figure 2.2.3(a), if efficient transmission is to occur, the internal reflection angle must exceed the the limiting or critical angle θL where $\sin \theta L = n_2/n_1$. Thus a ray entering at an angle greater than β is lost. Snell's Law gives the relation between the angles of incidence β and refraction ψ via the refractive indices as:

$$n_o \sin\beta = n_1 \sin\psi = n_1 \sin(\pi/2 - \theta L) = n_1(1-\sin^2 \theta L)^{1/2}$$

$$= (n_1^2 - n_2^2)^{1/2} \qquad (1)$$

Therefore, $\sin\beta = (1/n_o)(n_1^2 - n_2^2)^{1/2}$

$$= (n_1^2 - n_2^2)^{1/2} \qquad (2)$$

if n_o is the refractive index of air.

The right hand side of equation (2) is called the numerical aperture (NA) of the fibre. Allan [6] points out that the numerical aperture ($NA = (n_1^2 - n_2^2)^{1/2}$) is independent of the fibre diameter and holds for fibre diameters as small as 5 μm but breaks down for any smaller fibre diameters. In that case the geometric approach is invalidated and the electromagnetic theory then takes over to supply the acceptance conditions. Thus if the fibre is placed in air,

$$\beta = \sin^{-1}(n_1^2 - n_2^2)^{1/2} \qquad (3)$$

where n_1 and n_2 are the refractive indices of the fibre core and cladding respectively.

Light transmission through optical fibre

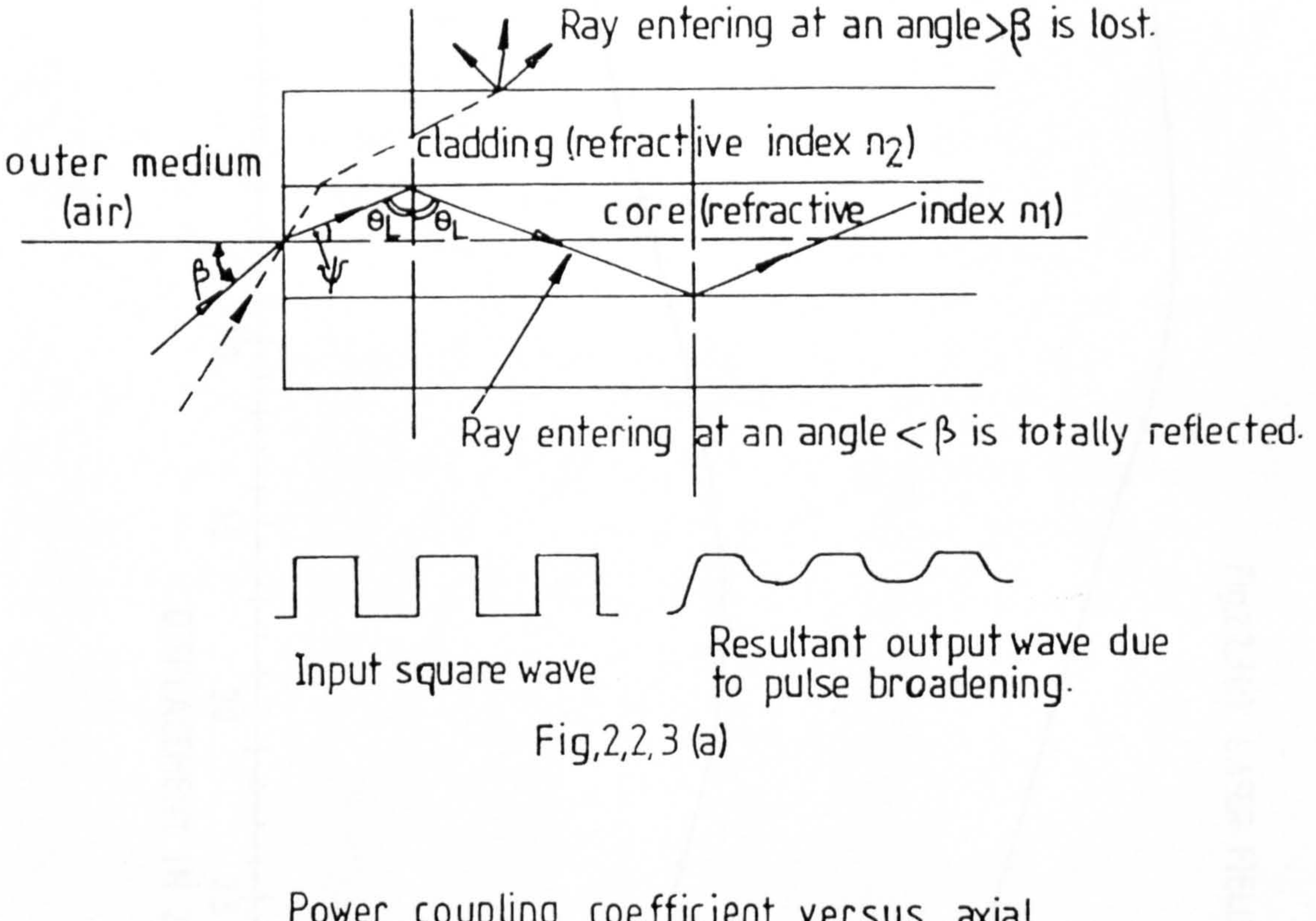

Fig, 2, 2, 3 (a)

Power coupling coefficient versus axial separation between laser diode and single-mode fibre.

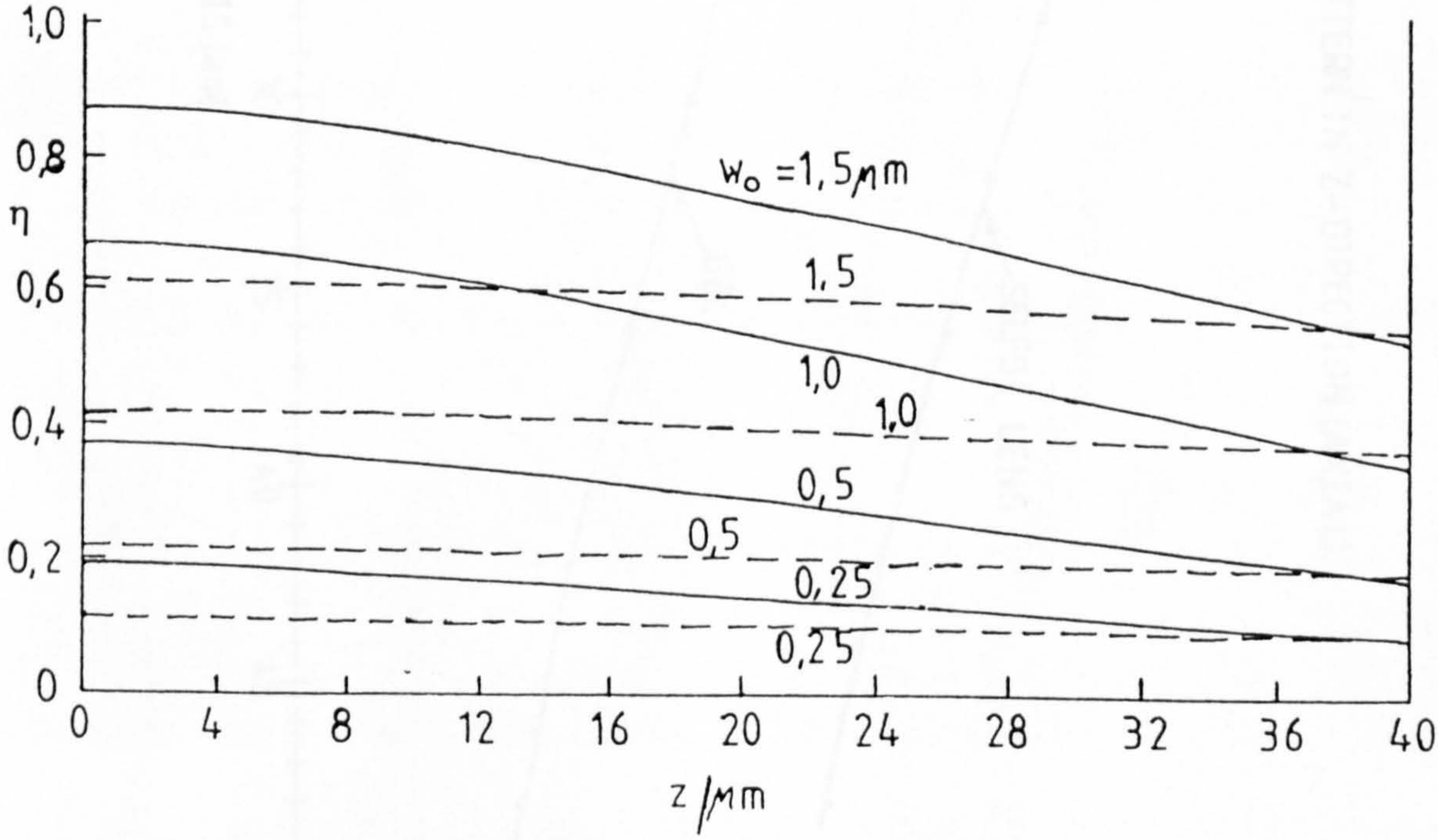

Fig. 2·2·3 (b)

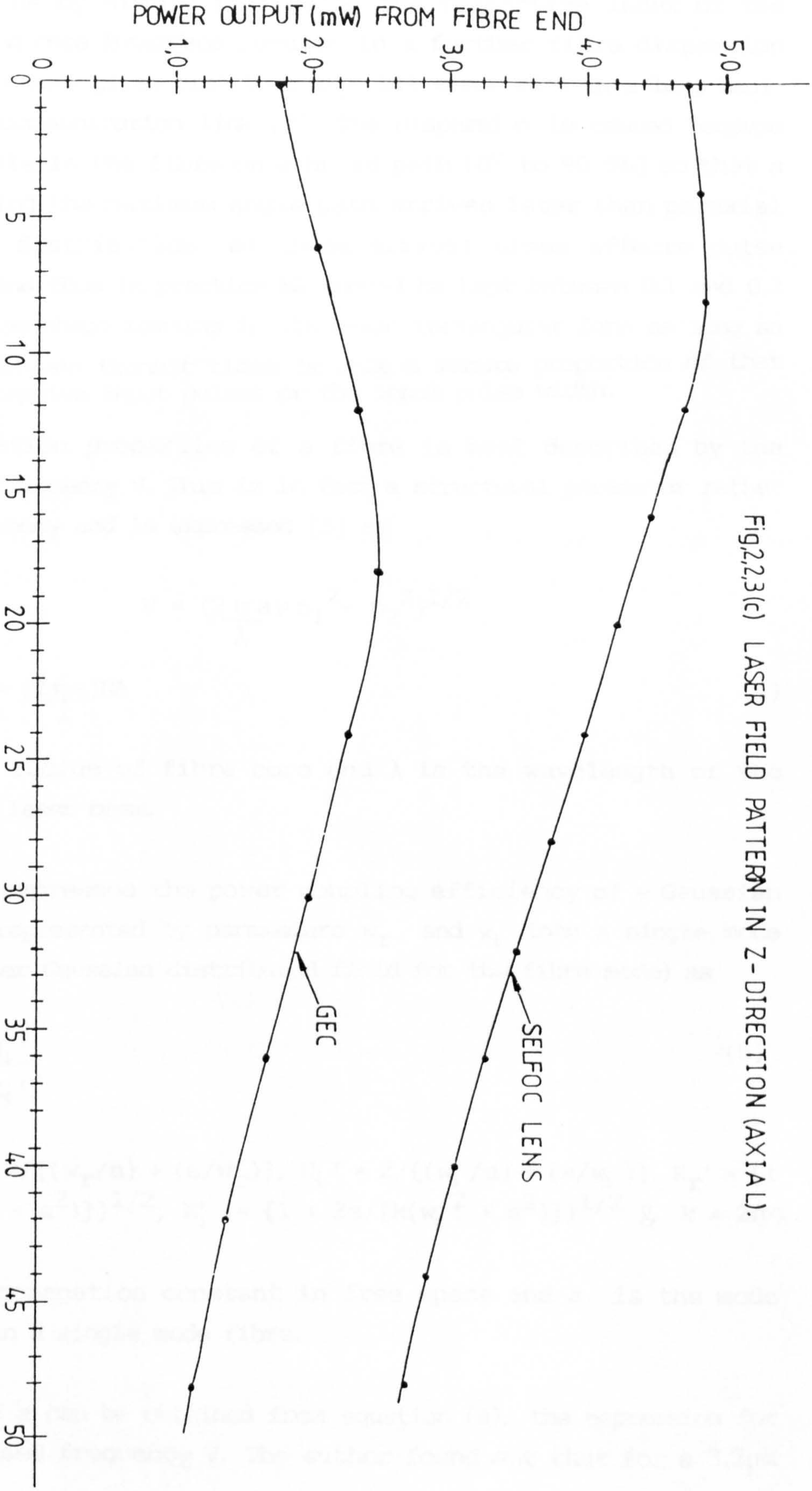

Fig,2,2,3(c) LASER FIELD PATTERN IN Z-DIRECTION (AXIAL).

Increasing NA by simply increasing the refractive index of the step/cladding core interface results in a further fibre dispersion [7]. This in turn gives rise to a high bit error rate in a long haul, high speed communication link [7]. The dispersion is caused because light travels in the fibre on a broad path (0^{o} to 90-θL) so that a ray following the maximum angle path arrives later than paraxial light. The distribution of these arrival times affects pulse broadening and thus in practice NA should be kept between 0.1 and 0.2 [7]. The pulse shape remains in its basic rectangular form as long as the delay between transit times is only a minute proportion of that between successive input pulses or the input pulse width.

The propagation properties of a fibre is best described by the normalised frequency V. This is in fact a structural parameter rather than a frequency and is expressed [3] as

$$V = \left(\frac{2\pi a}{\lambda}\right)(n_1^2 - n_2^2)^{1/2}$$

or
$$V = \left(\frac{2\pi a}{\lambda}\right)NA \qquad (4)$$

where a = radius of fibre core and λ is the wavelength of the transmitted laser beam.

Cohen [15] expresses the power coupling efficiency of a Gaussian laser beam represented by parameters w_r and w_l into a single mode fibre (another Gaussian distributed field for the fibre mode) as

$$\eta = \frac{W_r'}{K_r'} \cdot \frac{W_l'}{K_l'} \qquad (5)$$

where $W_r' = 2/\{(w_r/a) + (a/w_r)\}$, $W_l' = 2/\{(w_l/a) + (a/w_l)\}$, $K_r' = \{1 + 2z/[k(w_r^2 + a^2)]\}^{1/2}$, $K_l' = \{1 + 2z/[k(w_l^2 + a^2)]\}^{1/2}$ & $k = 2\pi/\lambda$.

k is the propagation constant in free space and a is the mode radius within a single mode fibre.

The value of a can be obtained from equation (4), the expression for the normalised frequency V. The author found out that for a 3.2μm

single mode DeBell Richardson fibre 79% of the power was transmitted within the core and for a 3.7μm single mode Corning fibre only 57% of the power was transmitted within the core. A one-dimensional form of equation (5) ($w_l = w_r = w_o$) was then plotted [15] against the axial separation z between two optical fibres (3.2 μm-solid curves and 3.7μm-dashed curves) and lasers parameterized by w_o (radius of beam waist parallel or perpendicular to the junction plane). These are presented in Figure 2.2.3(b) where the coefficient η gradually tilts off in the laser far field because of the increasing mismatch between the beam and the fibre diameters. These theoretical results compare quite favourably with the experimental results of Figure 2.2.3(c) produced by STC.These were obtained by measuring the power received by an optical fibre as it was being gradually moved away from the laser source in the axial direction. Weidel [16] reported that the slow rise in the experimental curves up to $z <= 10\mu m$, is due to oscillations caused by small optical feedback into the laser from the input end of the fibre. This optical feedback is a result of optical reflections.

Laser beam emanating from a laser aperture and injected into the core of an optical fibre.

α_y = beam divergence angle

$z \simeq d/2 / (\tan(\theta))$

θ = fibre acceptance angle.

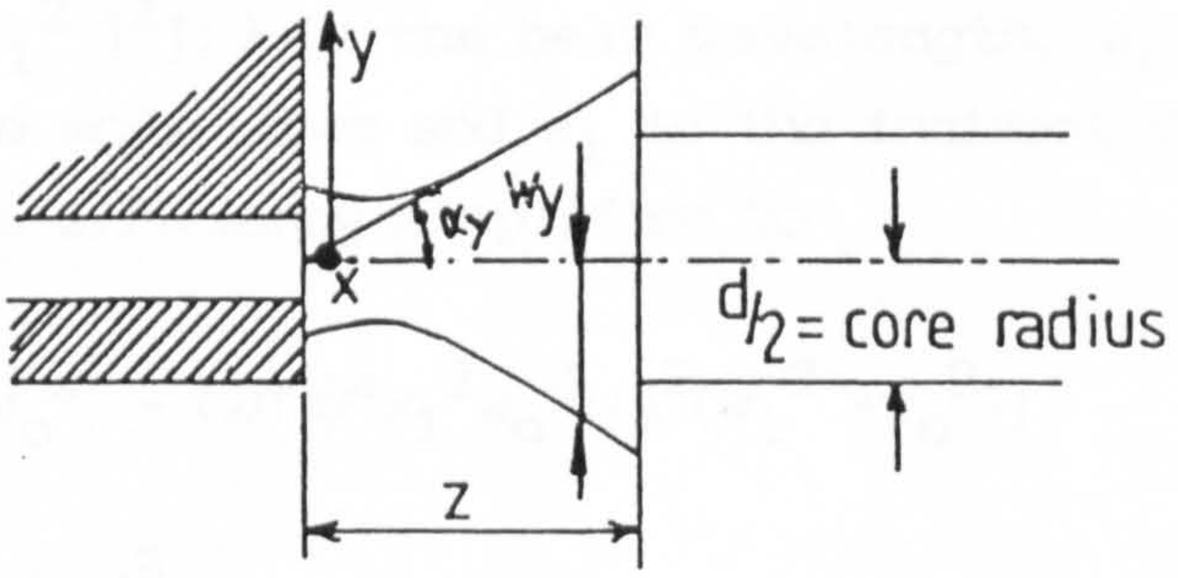

Fig. 2·2·3 (d)

It is also shown [15] that a multimode fibre begins losing additional light when the fibre is separated from the laser by more than a

critical distance $z = d/2\tan\theta$ (Figure 2.2.3(d)). This is the point at which rays normally within the fibre's acceptance core hit the cladding and get reflected away from fibre core having diameter d.

Some very close theoretical and experimental results were obtained [16, 15]. The latter, for example, had z(theoretical) = 24 μm, z(experimental) = 19μm for a 10μm core diameter fibre and z(theoretical) = 46μm, z(experimental) = 45 μm for a 20μm core diameter fibre. Angular misalignments can, however, greatly affect these results.

2.2.4 Angular and Lateral Misalignment

Equation (5) (2.2.3) formulated in [15] does not take account of the lateral and angular misalignments x and ψ respectively (Figure 2.2.4). Kogelnik [17] shows that the coupling efficiency between two Gaussian beams is given by

$$\eta = k \exp\{-k[x^2/2\,(1/w_1^2+1/w_o^2) + \pi\psi^2(w_1^2(z) + w_o^2)/2\lambda^2 - x\psi z/w_1^2]\} \qquad (6)$$

where $k = 4w_1^2w_o^2/[(w_1^2 + w_o^2)^2 + \lambda^2z^2/\pi^2]$;

$w_1^2(z) = w_1^2[1 + (\lambda z/\pi w_1^2)^2]$; λ is the beam wavelength, w_o is the beam spot size of single mode fibre and w_1 is the incident Gaussian beam waist. If z = 0, the efficiency simplifies to

$$\eta_o = k_o\exp\{-2x^2/(w_1^2 + w_o^2) - (2\pi\psi^2w_1^2w_o^2)/\lambda^2(w_1^2 + w_o^2)\} \qquad (7)$$

where $k_o = 4/(w_o/w_1 + w_1/w_o)^2$.

The excess losses caused by the angular(ψ) and lateral(x) misalignments are inseparable as long as the beam waist is located some distance away from the fibre end. However, these losses become independent of each other if the beam waist is located just at the fibre end as shown by equations (6) and (7) of this section.

The laser beam emerging from the semiconductor laser diode has an elliptical cross-section. Thus, the beam spot sizes perpendicular and parallel to the junction plane (w_r and w_l) respectively not only differ quite markedly from each other ($w_r \neq w_l$), but also from the characteristic spot size w_o of the fibre. The coupling efficiency between an elliptical laser beam and a single mode fibre set in a butt configuration can therefore be calculated from the modified equations (6) and (7) above. This efficiency is also expressed [2] as the product of $[\eta_o(w_1^l, w_o)]^{1/2}$ and $[\eta_o(w_1{}^r, w_o)]^{1/2}$ where the former corresponds to the coupling efficiency between one-dimensional Gaussian beams whose spot sizes are w_1^l and w_o and the latter to efficiency between spot sizes $w_1{}^r$ and w_o.

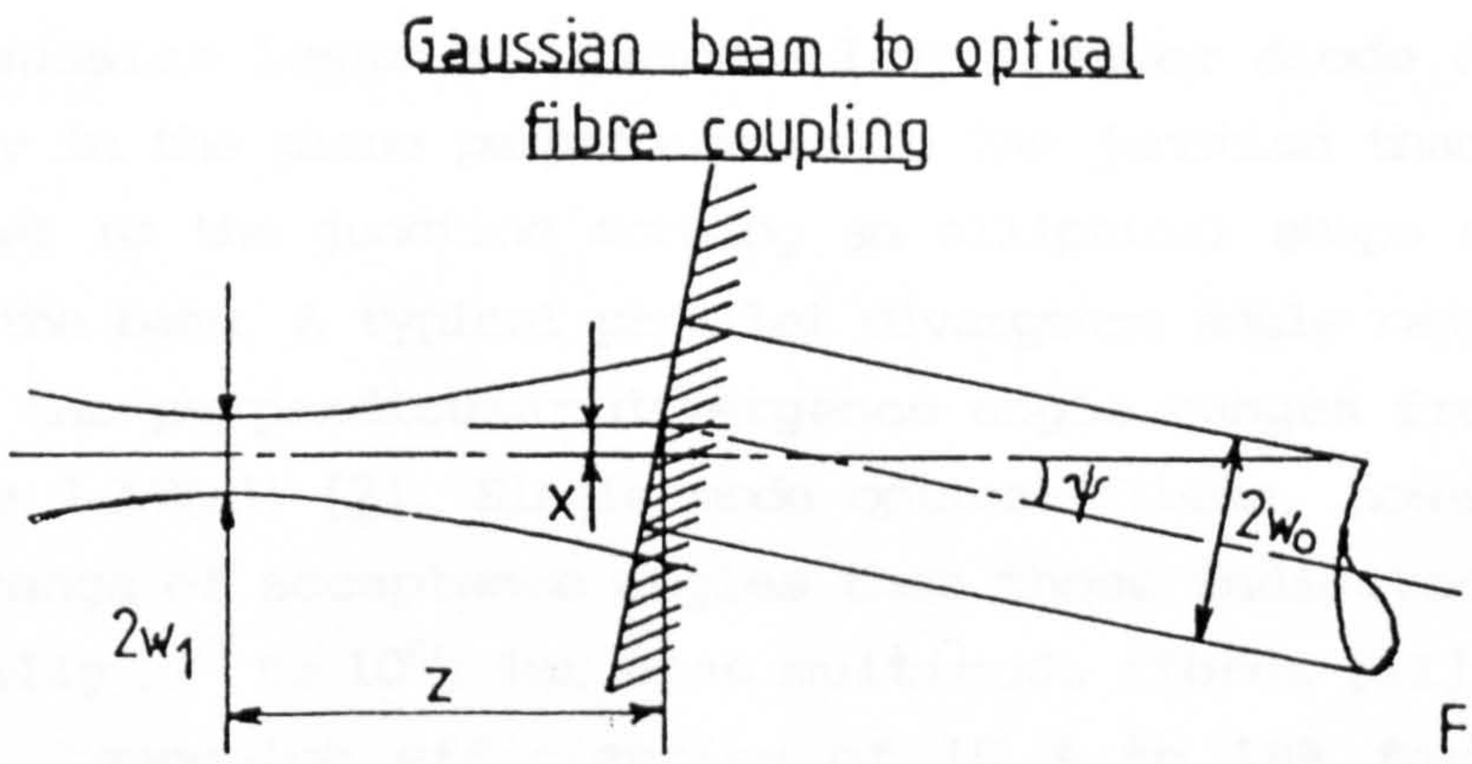

Fig.2·2·4

The present literature on the alignment techniques of optical fibres and semiconductor laser diodes does not give a theoretical method of calculating the tolerances in any particular axis taking account of all the misalignments (x, y, z and ψ). In an attempt to investigate the variations between angular(ψ) and lateral(x) misalignments when the incident beam waist is located at the fibre end, it was discovered [2] that as the incident beam spot size increases, the lateral alignment tolerance also increases but the angular alignment tolerance decreases and vice-versa. However, this is only true for rotationally symmetric beams. In a butt-joint configuration, the angular alignment tolerance perpendicular to the junction plane of an

elliptical beam is larger than that parallel to the junction plane whereas the lateral alignment tolerances are of the same order and independent of misalignment directions [2].

2.3 DIFFERENT METHODS OF COUPLING LASERS TO OPTICAL FIBRES

Efficient launching of laser beams from semiconductor laser diodes into optical fibres is very important in loss limited high capacity communications systems for maximum repeater separation. Any suitable methods that can achieve acceptably high laser/fibre coupling efficiencies would therefore go along way to maximise separation distances between repeaters and improve the quality of optical communication links.

The Gaussian laser beam emitted by a laser diode diverges more rapidly in the plane perpendicular to the junction than to the plane parallel to the junction forming an elliptical shape at any section along the beam. A typical parallel divergence angle range is 2^{o} to 5^{o} while the perpendicular divergence angle ranges from 15^{o} to 30^{o} (Figure 2.2.2(a)) [2]. Single mode optical fibres, however, have far less range of acceptance angles than those indicated above. It is typically (2^{o} to 10^{o}) for some multimode fibres [11]. The authors report launching efficiencies of 10 % to 18% for plane ended multimode fibres (butt joints). Timmerman [18] reports that when microlenses (hemispherical or tapered hemispherical or cylindrical) are incorporated, efficiencies as high as 80% are known to be achievable.

Quite a few laser diode to single mode fibre coupling experimental results obtained by different methods have already been reported. These include a simple butt joint, a selfoc-lens, a cylindrical lens placed at the input end of a fibre, a micro-lens fabricated at the fibre end and a combination of a cylindrical and a selfoc lens. A selfoc lens is a cylindrical lens with graded index of refraction which decreases as the square of the radial distance from the optical axis [19]. Due to this parabolic index of refraction, the selfoc lens performs the same optical functions as the standard spherical (rotationally symmetrical) lenses with the added feature that the end

NOTE: (See p.29, parag.3, line 4)

In this work, the words launching and coupling efficiency are used interchangeably to mean the proportion of laser light emitted by a laser diode that can be coupled into an optical fibre.

surfaces are flat. As shown in Figure 2.3.2, it converges the divergent non-linear laser beam to a point on the optical axis. A cylindrical lens on the other hand, has a uniform index of refraction and because of its shape, it focuses rays of light to a line rather than a point. When it is rotated, the focal line also changes its orientation. This implies that cylindical lenses are rotationally asymmetrical.

These configurations are summarised in the accompanying sub-sections below. Owing to the differences in the laser diodes and optical fibres used, the coupling efficiencies of these methods can not be directly compared.

2.3.1 The Butt-Joint Configuration

In this set up, the spacing between a laser diode and a single mode fibre must be as small as possible. Results of the experimentation conducted in [2] revealed that a spacing of 10 μm was achievable resulting in a maximum launching efficiency of -6.2 dB or 25%. The lateral alignment tolerances were found to be far more sensitive than the axial alignment tolerances. They were found to be about ±1.4μm and ±1.6 μm along directions perpendicular and parallel to the junction plane respectively.

Although this configuration (Fig.2.3.1) is simplest in fabricating laser-diode coupler arrangement, the coupling efficiency is limited to a small value because of the mismatch between the laser diode pattern and the power distribution in the single-mode fibre.

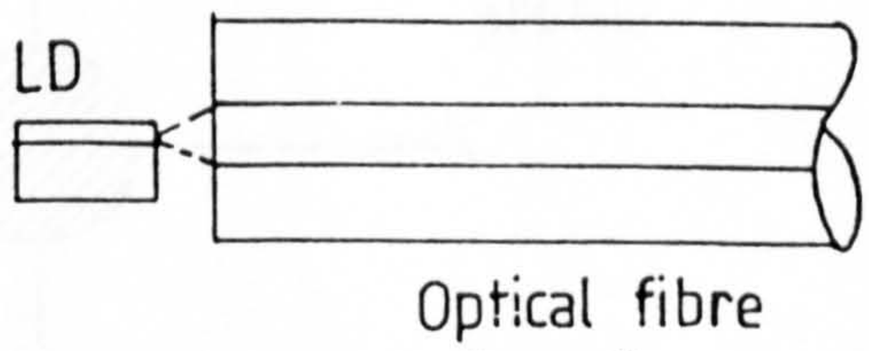

Fig,2,3,1 Butt joint configuration.
LD ≡ laser diode

2.3.2 Selfoc Lens Configuration

The coupling efficiency achieved by this method cannot be improved over the butt-joint efficiency because of the rotational symmetry of the selfoc lens which is incapable of transforming the asymmetrical laser beam into a rotationally symmetric form [2]. An experiment was conducted [2] in which three selfoc lenses with diameters of 1.25 mm, 1.5mm and 2.0mm were examined. The lens lengths were set to 1/4 pitch of the undulation period and the maximum launching efficiency achieved with the 1.5mm diameter lens was -6.5dB or 22%. One pitch corresponds [19] to the lens length for one cycle of cyclic move of the ray in the lens. The coupling efficiencies of the other lenses were found to be 3dB or 4% worse. While the axial spacing tolerance was found to be five times larger (50 μm within 1-dB loss) than that obtained for the butt-joint, the lateral tolerances were nearly the same as those of the butt-joint. A typical coupling arrangement utilising a selfoc lens is illustrated in Figure 2.3.2.

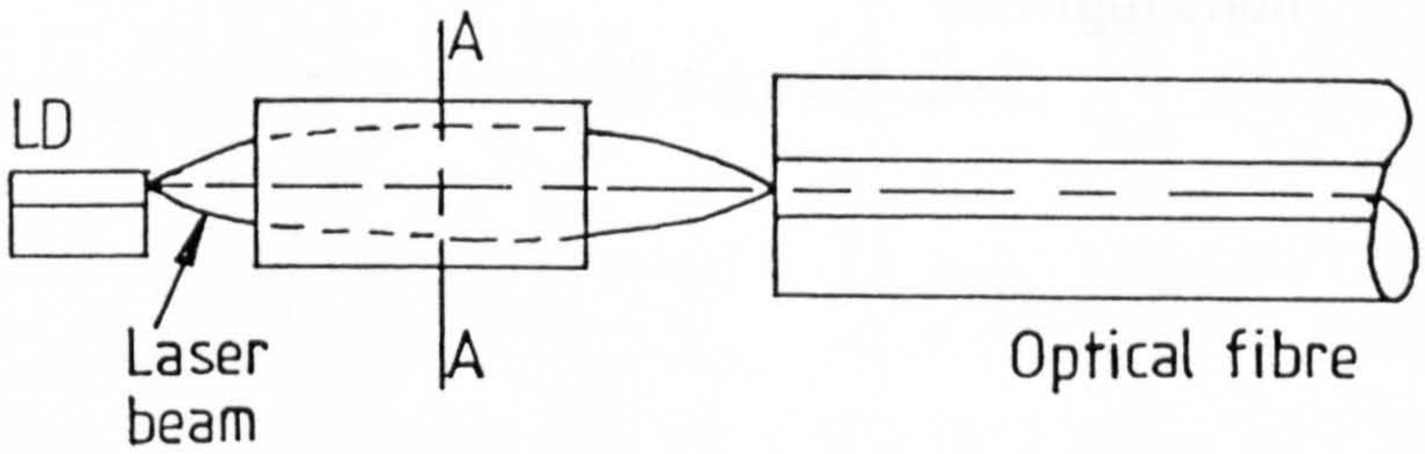

Fig,2,3,2 Selfoc lens configuration
LD≡ Laser diode

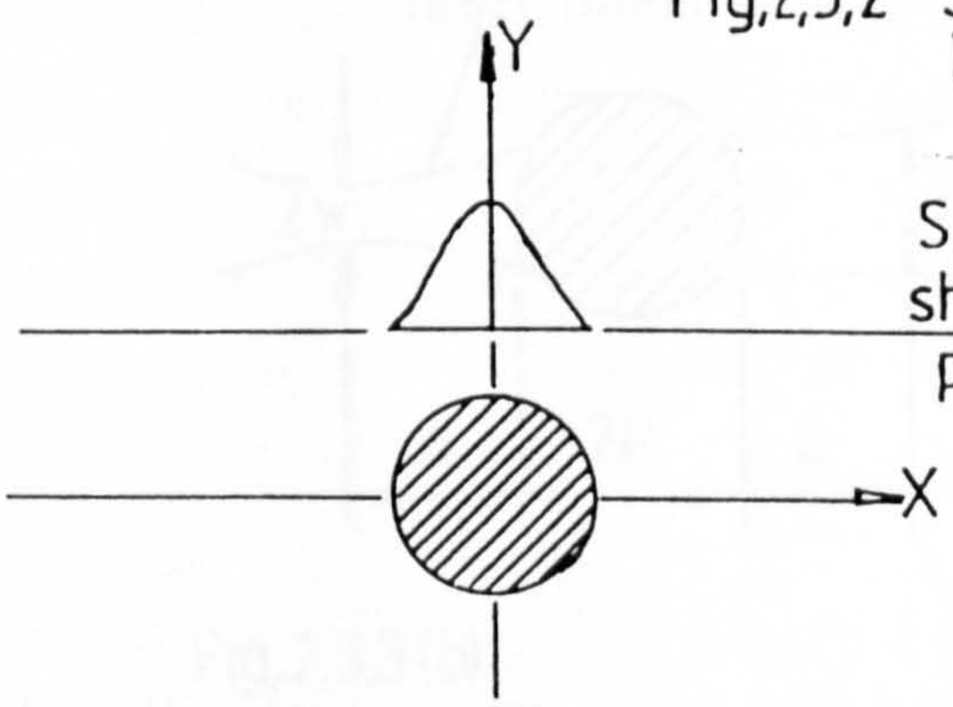

Section A-A of the lens showing parabolic index profile.

2.3.3 Cylindrical Lens Method

A number of investigations using this coupling method have already been carried out. Since photoetching entails a complicated process of fabricating a lens and directly forming it at the fibre end, an experiment was conducted [2] in which the laser diode, lens and fibre were independently mounted on separate manipulators. This is shown schematically in Figure 2.3.3 (a). Borosilicate glass cylindrical lenses of radii 11 μm, 8.35 μm, 7.3 μm and 6.25μm were used. The greatest coupling efficiency is reported [2] to have been obtained with the smallest lens ensuring that the separations between lens and laser diode and between lens and fibre were minimised.

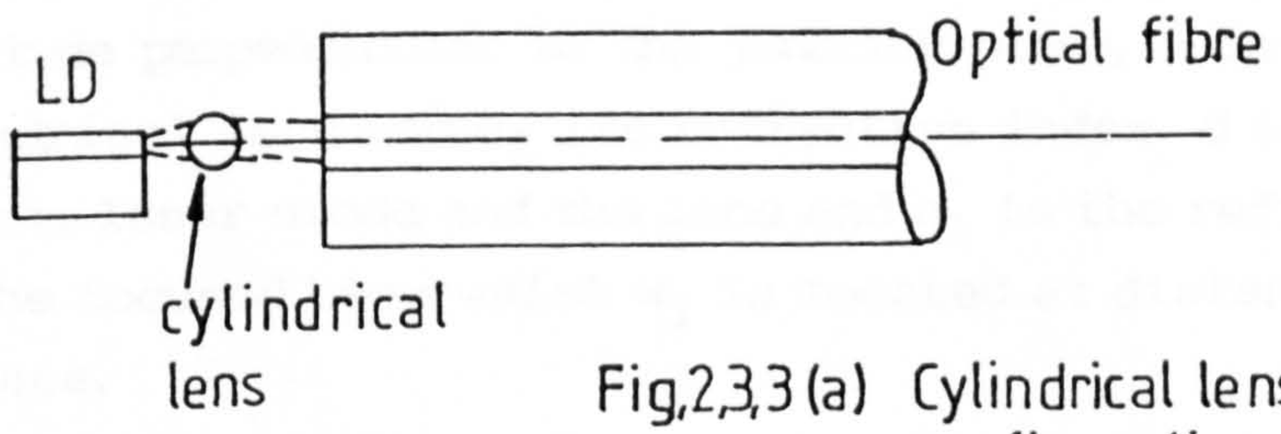

Fig,2,3,3 (a) Cylindrical lens configuration.

LD ≡ Laser diode

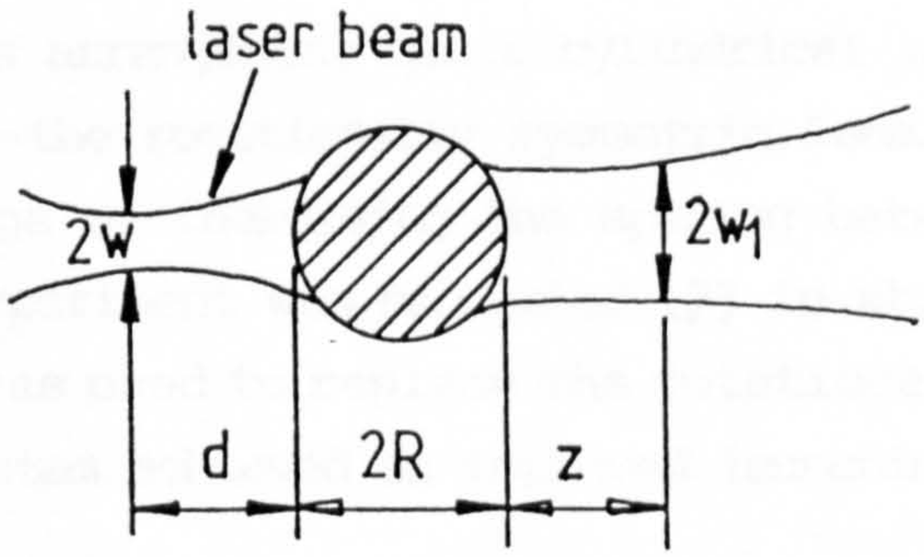

Fig,2,3,3 (b)

Gaussian beam transformation by cylindrical lens

The lateral misalignment tolerances required to keep the excess loss to within 1-dB were found [2] to be ±1.4 μm and ±1.8 μm for a 6.25 μm and 11 μm radius lenses respectively. These tolerances are quite comparable to those for the butt-joint. It was also realised [2] that coupling through a cylindrical lens is more tolerant of axial separation than the butt-joint method.

Thus the application of a cylindrical lens for laser to fibre coupling not only improves the coupling efficiency but also the tolerances for lateral and axial misalignments. Above all, it appears that a lens with a small radius can focus the laser beam to a smaller spot than a lens with a larger radius. Figure 2.3.3 (b) shows an illustration of a Gaussian beam transformation by a cylindrical lens given in [2]. w is the emitting spot size of the laser diode at the e^{-1} amplitude perpendicular to the junction plane, R is the radius of the cylindrical lens and n_2 its refractive index. d is the spacing between the laser diode and the lens and n_1 is the refractive index of air. The focused beam waist w_1 is located at distance z from the lens surface.

2.3.4 Cylindrical and Rotationally Symmetric Lens Method

As already noted (2.3.2), a rotationally symmetric lens has not got the capability of transforming an elliptical laser beam into a rotationally symmetric beam. In anticipating a higher coupling efficiency, this arrangement has a cylindrical lens placed between a laser diode and the rotationally symmetric lens. This configuration has the advantage of increasing the spacing between the laser diode and fibre. An experiment was conducted [2] in which a selfoc lens of 1.5 mm radius was used to replace the rotationally symmetric lens. The combined system achieved an improved launching efficiency of 40%.

In general, these coupling methods (2.3.1-2.3.4) allow for very small positioning tolerances of components. Although the selfoc lens arrangement has a relatively large spacing between the selfoc lens and the single mode fibre, it couples a very small amount of power into the monomode fibre [2]. Its coupling efficency can hardly be

improved over the butt joint configuration [2]. The rest of the configurations present obvious handling and positional problems which are incompatible with large scale production. This is because two or three manipulators would be needed to handle the fibre, lens and laser diode separately within a confined space.

To avoid the above problems, the fibre end is modified into a hemispherical form. This is done by fusing a bead of glass directly to the fibre end, controlled etching of the fibre or melting the fibre tip to form a bead [7]. The techniques produce a prealigned lens/fibre that can be inserted into a modular package. In general a hemispherically fused end doubles the effective NA of the fibre axis [7]. This increases the launch efficiency considerably as well as laser/fibre alignment sensitivity. An offset of 10 μm for example, produces a fall in launch power of 50% [7]. This type of fibre is used in this thesis to align a laser beam with a monomode optical fibre.

The majority of suppliers such as STC, normally sell these products already assembled with a generally short length of optical fibre (1m or less). A typical STC arrangement already assembled in an optimum position is shown in Figure 2.4. This short fibre length is called a "pigtail" or "flylead".

2.3.5 Summary of Reported Experimental Alignment Results

A number of extensive alignment investigations have been carried out in order to reduce the coupling power loss. A close survey of the available literature yielded the results of various experiments presented in table 2.3.5 below.

Since the object of this thesis is to produce a general purpose semi-automated alignment system capable of obtaining the optimum efficiency for any coupling method, it is best to base it on the worst available tolerances. These can be obtained from table below. These tolerances will only take account of any misalignments on the axes for which they are quoted.

It is recommended by STC (the supplier of the laser diode and monomode fibre used) that the axial separation between the laser diode face and the fibre input end must not be less than 40 μm. This prevents the fibre from knocking and consequently damaging the laser diode emitting face. The program constructed in chapter 9 for the automatic alignment of the components is intended to combine the effects of misalignments in (a) the x, y and z-axes for a purely translational 3-axis manipulator and (b) all the three translational axes and two rotary axes (ψ_x and ψ_y) that is, for a 5-axis manipulator. The tolerances listed below could be useful in checking the validity of the results obtained by the use of the program to control the relevant manipulator.

TABLE 2.3.5: A Survey of Experimental Alignment Results.

REFS.	OPTICAL FIBRE DIMENSIONS		COUPLING METHOD	ALIGNMENT TOLERANCES			
	CORE ϕ/μm	CLADDING ϕ/ μm		P_i TO Jn. PLANE x_i/μm	P_r TO Jn. PLANE y_r/μm	ANGULAR θ/deg.	AXIAL z/μm
2	5.3	70	Butt-J't	1.4	1.6	-	7
2	5.3	70	Selfoc	1.2	1.6	-	50
2	5.3	70	Cylindr. (ϕ44μm)	1.8	1.8	-	26
2	5.3	70	Cylindr. (ϕ25μm)	1.4	1.4	-	22
11	61	127	Butt-J't	-	-	4°	-
11	42	120	Butt-J't	-	-	2.5°	-
20	9.9	125.5	Butt-J't	3.1	3.2	-	18.8
20	9.9	125.5	Hem. Lens on S.M.F	1.4	1.5	-	8.0
20	9.9	125.5	Tapered Hem. Lens on S.M.F	1.3	3.0	-	17.0
13	8.3	-	Butt-J't	-	-	0.9°	-
21	8.0	-	Hem. Lens on S.M.F (ϕ17 μm)	1.5	1.4	-	8.0

P_r, P_l , Jn. and J't in table 2.3.5 stand for perpendicular, parallel, junction and joint respectively.

2.4 CURRENT MANUAL COUPLING PROCESS

In this section, a typical coupling procedure of "pigtails" to laser diodes carried out in STC workshop at Paignton is described. This manual coupling process is currently done by hand under a microscope. The output end of an optical fibre is connected to a laser detector which measures the amount of laser intensity launched and transmitted through the fibre.

The coupling module (Figure 2.4) is mounted into a pair of clamps (or heat sink) under a microscope. The semiconductor laser diode that emits the beam is already premounted in position inside the module (sub-mount) and a power line connected to it so that it can be fired or activated during alignment. The operator threads the brass strengthened input end of the fibre through the hole inside the epidermic tube and then into a saddle which rests on the submount platform (Figure 2.4). The laser is then fired and by simply observing through the microscope, the operator carefully moves the fibre in front of the laser diode ensuring that an estimated axial gap of approximately 40 μm between the laser diode and the fibre input end is not traversed. The desired fibre position at which more than a set minimum value of laser intensity is recorded by the detector is obtained by trial and error. The fibre is then soldered (to the epidermic tube) in this position while being held steady as the solder sets.

When the unit has cooled down, it is removed and checked for efficiency degradation because the fibre tends to be pulled out of position as the solder sets and solidifies. This checking procedure takes place under a second microscope where the soldered fibre tip is physically tweaked into some other position in an effort to pick up a higher level of laser intensity. This procedure compensates for the possible pulling effect of the solder during the solidification process which tends to move the fibre away from the alignment

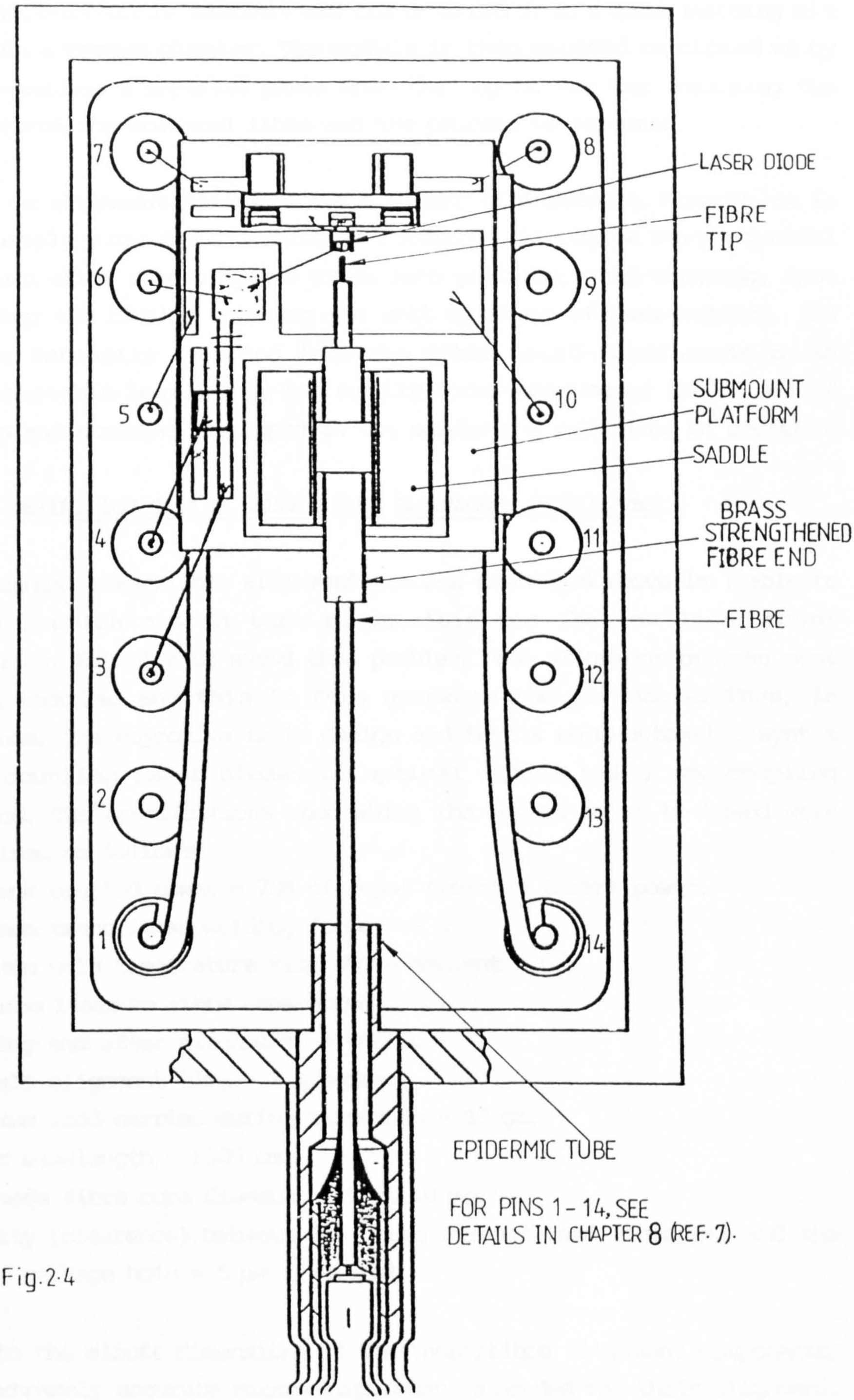

Fig. 2·4

Laser diode to optical fibre coupling

position. The saddle is then spot welded on to the platform. The assembled unit is removed and transferred into a seam welding kit inside a vacuum chamber. The module is then encased or closed up by seam-welding a separate plate onto the top of the box enclosing the laser and the soldered fibre and the process is repeated.

Such an alignment procedure has a number of drawbacks. Firstly, it is extremely slow and inaccurate. Secondly, it can be very wasteful because after soldering the fibre into position, then tweaking, spot welding and finally encasing the unit by means of seam-welding, the laser intensity launched into the fibre could deteriorate to an unacceptable level. This can easily occur because of the effect of creep and stresses developed as the solder and weld sets in position.

2.5 DEFINITION OF THE LASER-FIBRE ALIGNMENT OBJECTIVES

The manual laser/fibre alignment process described above is liable to errors which are in turn responsible for the low laser power coupling. In order to avoid this problem, the alignment process must be automated and this in turn quickens the procedure. Thus, in essence, the objective is to design and test a semi-automatic system for coupling laser diodes to optical fibres using any coupling method. The specifcations upon which the design is to be based were outlined as follows:

Minimum coupled power = 70% of input (emitted laser) power.
Maximum transmitted welding force = 2 N.
Maximum weld temperature rise above ambient = $6^{o}C$.
Minimum laser to fibre separation
(during and after alignment) = 40 μm.
Overall alignment time = 3 minutes.
Maximum load carried during alignment = 40 gm.
Laser wavelength = 1300 nm.
Monomode fibre core diameter = 5 to 10 μm.
Ovality (clearence) between the brass strengthened fibre tip and the laser package hole = 5 μm (± 2.5μm).

Due to the minute dimensions of the laser/fibre alignment components, an extremely accurate micromanipulator is needed for their alignment.

The results of a survey of microactuators presented in Chapter 4 for purposes of locating such a positioner, is entirely based on the first six specifications. These were outlined right at the onset of this research. However, the last two specifications were given after the survey, selection and purchase of the manipulator. Since this research only looks at the hard and software alignment procedures, the welding specifications (force and temperature rise) play no role.

The following sequence of the alignment system operation is proposed:

1. the operator mounts the module which contains premounted laser diode onto the surface of the manipulator;

2. the laser diode is then fired or activated using a manual switch (constant current source of 125 mA);

3. the operator connects the output end of the fibre to a detector which is in turn connected to a desk top computer;

4. the operator then threads or places the fibre into the epidermic tube inside the module and then has it gripped into a stationary position;

5. the program is then run and the manipulator optimises the position of the laser diode (premounted inside the module in front of the fibre) using feedback readings obtained by the detector and fed to the computer;

6. when the optimum position for that particular arrangement (butt joint or other) is reached, the manipulator automatically comes to a stop;

7. a separate robot is then used to solder and spot weld the fibre in the optimised position;

8. the module is then encased by means of seam welding as soon as the solder has cooled down;

9. lastly, the grippers release the fibre and the manipulator moves out of the vacuum chamber and the operator removes the fully assembled unit.

It is, however, envisaged that the last three steps can not be accomplished in this particular exercise but can be implemented at a later stage. In addition, a further investigation into the effects of creep and stresses developed after soldering and welding will also need to be carried out if later deterioration in the coupled laser power level has to be avoided.

This system should be capable of speeding up the assembly process and significantly increase both the quality of the product and its reliability. Above all, it should not require a highly skilled worker to operate it.

* * * * * * *

REFERENCES

1. Hewlett-Packard Applications Engineering Staff.
"Optoelectronics/Fiber Optics Applications Manual."
Second Edition, McGraw-Hill, 1981 (pp.10.1-10.3).

2. M. Saruwatari and K. Nawata.
"Semiconductor Laser to Single-mode fiber Coupler", Applied Optics, 1979, vol.18, No.11, p.1847.

3. H.F. Wolf.
"Handbook of Fiber Optics (Theory and Applications)", Edited by H.F. Wolf. First published by Garland TTPM, 1979, (USA). Published by Granada Publishing, 1981, (UK). p.5,49-58.

4. D.J. Morris.
"Communication for Command and Control Systems", International Series on Systems and Control, vol.5, Pergamon Press, 1983, p.252-256, 259.

5. G. Keiser.
"Optical Fiber Communications", McGraw-Hill Inc.1983. p.20-21, 26-28, 59-60, 87, 97-100, 119.

6. W.B. Allan.
"Fiber Optics". Engineering Design Guides. Published for the Design Council, the British Standards Institutions and the Council of Engineering Institutions. Oxford University Press. Edited by P.W. Watts, 1980. p.1-4.

7. J.E.U. Ashton, R.M. Gibb and B.A. Eales.
"New generation semiconductor CW laser packages with full hermiticity, integral power monitoring and direct fibre optic launching". Microelectronics Journal vol.12, NO.3, 1981. p.14-18.

8. I.G.A. Davies, A.R. Goodwin, P.A. Kirby and R.F. Murison.
"Optical Fiber Technology, Semiconductor Light Sources", Electrical Communication, 1981, vol.56, No.4, p.338.

9. "Optical Fibre Communication Systems", Edited by C.P. Sandbank. John Wiley and Sons, 1980. (Chapter 7. P.R. Selway, A.R. Goodwin and P.A. Kirby, "Semiconductor Laser Light Sources for Optical Fibre Communications"), p.156-171.

10. H.W. Kogelnik and T. Li.
"Laser beams and resonators", Applied Optics, 1966, vol.5, No.10, p.1550-.

11. H.R.D. Sunak and M.A. Zampronio.
"Launching Light from Semiconductor Lasers into plane-ended Multimode Optical Fibres", Applied Optics, 1983, vol.22, No.15, p.2337.

12. A. Nicia.
"Loss Analysis of Laser-fiber Coupling and the Fiber combiner, and its Application to Wavelength Division Multiplexing", Applied Optics, 1982, vol.21, No.23, p.4280.

13. D. Marcuse.
"Loss Analysis of Single-Mode Fiber Splices", The Bell System Technical Journal, 1977, vol.56, No.5, p.703.

14. J.A. Van Steenwijk.
"Correct Relation between the Impulse Response of GRIN fibers and the Excitation by a Laser diode", Applied Optics, 1983, vol. 22, No.23, p.3864.

15. L.G. Cohen.
"Power Coupling from GaAs Injection Lasers into Optical Fibers", The Bell System Technical Journal,1972, vol.51, p.573.

16. E. Weidel.
"Light Coupling problems for GaAs Laser-Multimode Fibre Coupling", Optical and Quantum Electronics,1976,vol.8, p.301-7.

17. H.W. Kogelnik.
"Coupling and Conversion Coefficients for Optical Modes", Microwave Research Institute Symposia Series, vol.14, Edited by J. Fox. Polytechnic Press, Brooklyn, 1964, p.333.

18. C.C. Timmermann.
"Highly Efficient Light Coupling from GaAlAs Lasers into Optical Fibers", Applied Optics, 1976, vol.15, No.10, p.2432.

19. "Optical Fiber Applications of the Selfoc Micro Lens."
Nippon Sheet Glass - Brussells. Personal Communication.

20. M. Saruwatari and T. Sugie.
"Efficient Laser diode to Single-Mode Fiber Coupling using a combination of two lenses in confocal condition", IEEE Journal of Quantum Electronics, 1981, vol. QE-17, No.6, p.1021.

21. Y. Murakami, J. Yamada, J. Sakai and T. Kimura.
"Microlens Tipped on a Single-Mode Fiber end for InGaAsP Laser Coupling improvement", Electronics Letters, 1980, vol.16, No.9, p.321.

CHAPTER 3

ALIGNMENT OF LINES

CHAPTER OVERVIEW

In this chapter, the various interpretations of the word alignment are explored. This is done by considering the alignment of points (3.1), lines (3.2), line segments (3.3) and the superposition of two congruent figures (3.4) in two ways: (a) from first principles and (b) by screw displacements. The latter is summarised in Appendix A. While the screw method investigates all the different screw displacements for each alignment (3.1 - 3.4), the former specifies the degrees of freedom involved and thus the manipulator required to correct the misalignment. The results of both methods (summarised in 3.5) aims at drawing the attention of engineers to the application of screws as well as the role of manipulators in alignment.

3.0 INTRODUCTION

Evidently, efforts in carrying out alignment has been in existence for a long time. Harrison [1] gives two very early examples as the Nazca lines on an arid plateau in Peru and the 'Alignments' at Menec in Brittany. The former is said [1] to comprise of a series of straight-edged geometrical shapes and straight lines formed by removing loose surface rock; spread over a distance of 50 km. The latter comprise [1] of twelve impressive parallel rows of granite blocks almost 1 km long. Their purpose is not only intriguing but the techniques used for their construction can be challenging even to the present day engineers [1]. The same applies to the Egyptian pyramids built nearly five thousand years ago.

The purposes of alignment are numerous and varied depending upon the discipline involved. Current literature reveals that physicists, photo-optical and electronic engineers and researchers in other fields have produced a large amount of alignment results. For purposes of this thesis, the discussions are confined to laser-fibre coupling (chapter 2) and partly machinery alignment. The former and others like circuit alignments are classified under optical alignment.

This is because circuit alignment is almost wholy dependent on the use of light as described by Fehrenbach [2]. On the contrary, methods employed in machinery alignment may be completely divorced from optical alignment as described by Mitchell [3]. A few other alignment examples ([9] to [13]) are also cited. These and many others not mentioned serve little or no purpose here but simply gives an idea of the extent to which alignment is studied.

Essentially, laser-fibre coupling as well as machinery alignment can be reduced to the alignment of lines in space. The central axis of a laser beam is one line in space while the axis of the fibre is the other. Similarly, in machinery alignment involving the alignment of two coupled shafts or a machine string, the central axes of the shafts represent two lines in space. It follows that the analysis of alignment of lines in space could provide ready solutions to the above problems. It is for this reason that alignment is investigated in this chapter.

Figure 3 illustrates a typical shaft to shaft misalignments. Angular misalignments Θy and Θz about Y and Z -axes respectively require correction. Θx has no effect on the misalignments of shaft axes except for torque and can therefore be disregarded. Other significant misalignments are the linear displacements along the X, Y and Z-axes. They are referred to as axial (X-axis) and transverse (Y and Z-axes) misalignments respectively. As in laser/fibre coupling, there are five independent variables (2.2.4) that require correction. It is stated [3] that the objective of alignment is to have two coupled shafts in perfect coincidence under operating conditions. Due to large temperature differences from ambient to operating conditions, twisting or uneven settling of the support structure and other factors that influence the position of one machine relative to the coupled one, it is difficult to achieve this objective. To solve this problem, couplings which accommodate changes in operating alignment as well as slight offsets due to tolerances in both the measurement and alignment procedures and also absorb for short periods, the offsets applied to compensate for thermal growth are employed [3]. Methods used for accurately aligning shafts and a machine string are relegated to [3] and Murray [4].

Fig,3 Types of shaft misalignment.

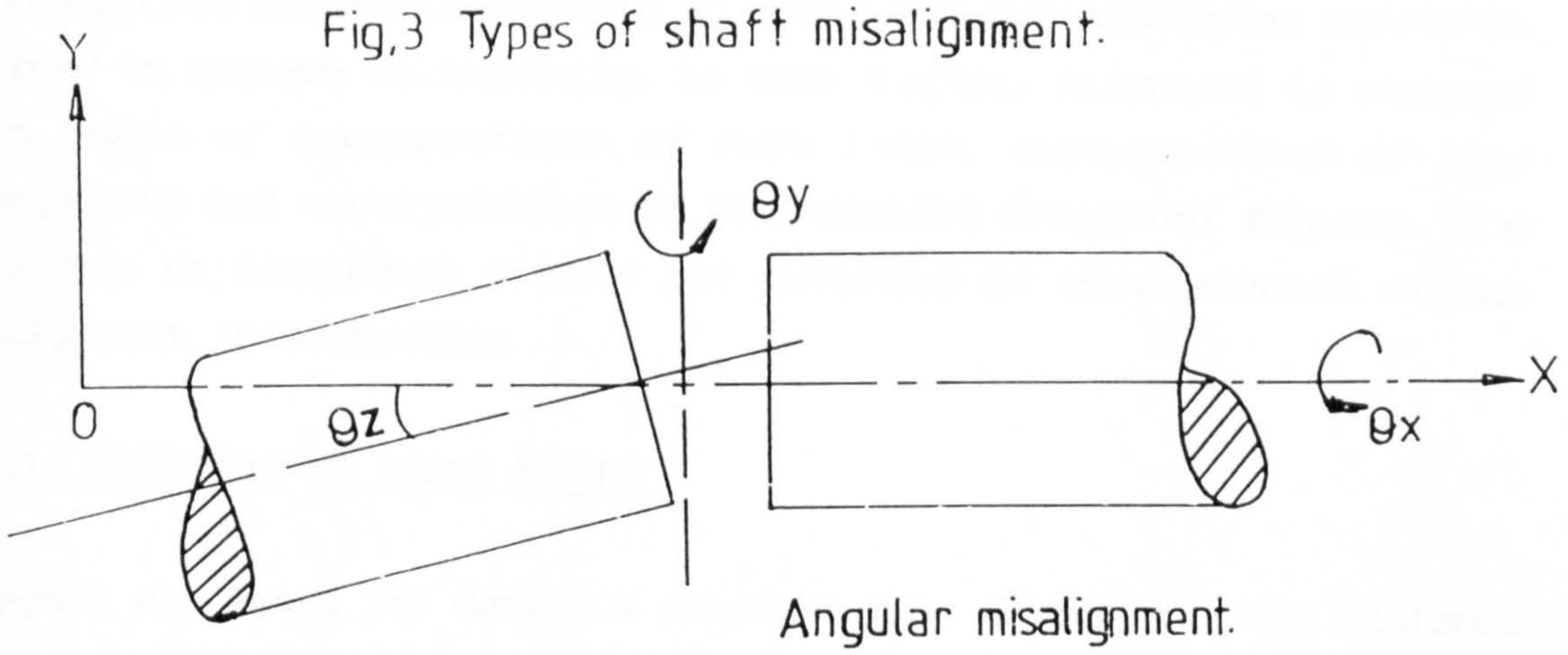

Angular misalignment.

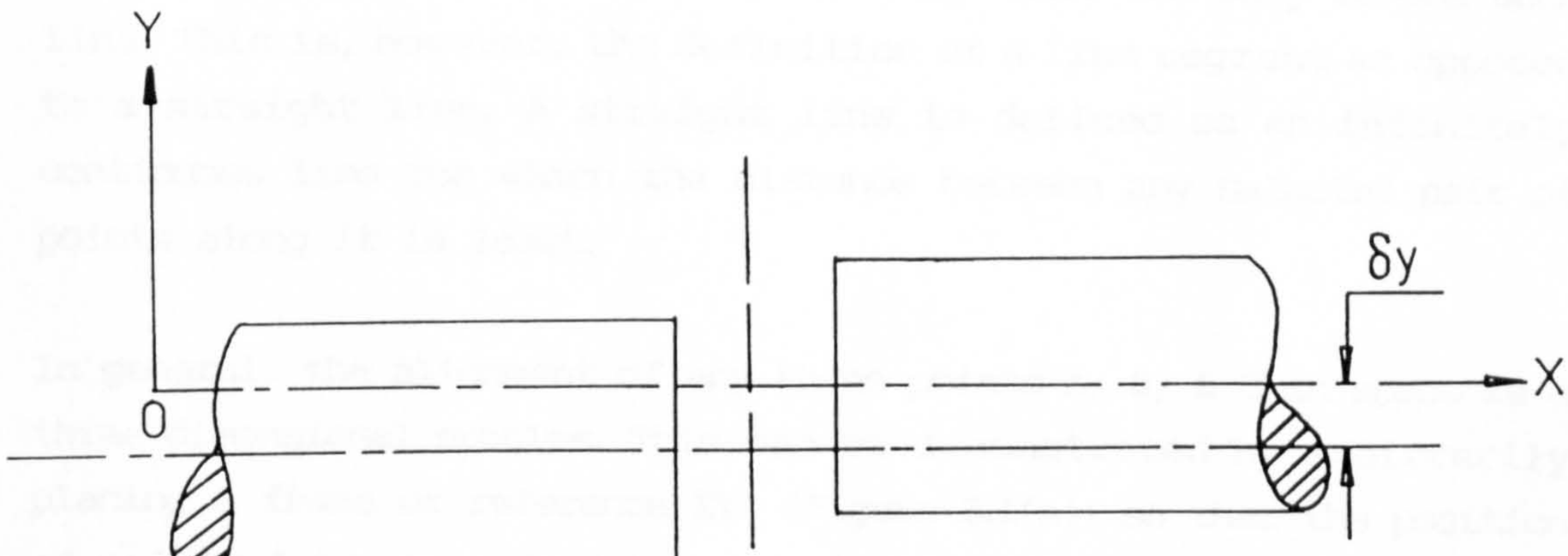

Transverse misalignment

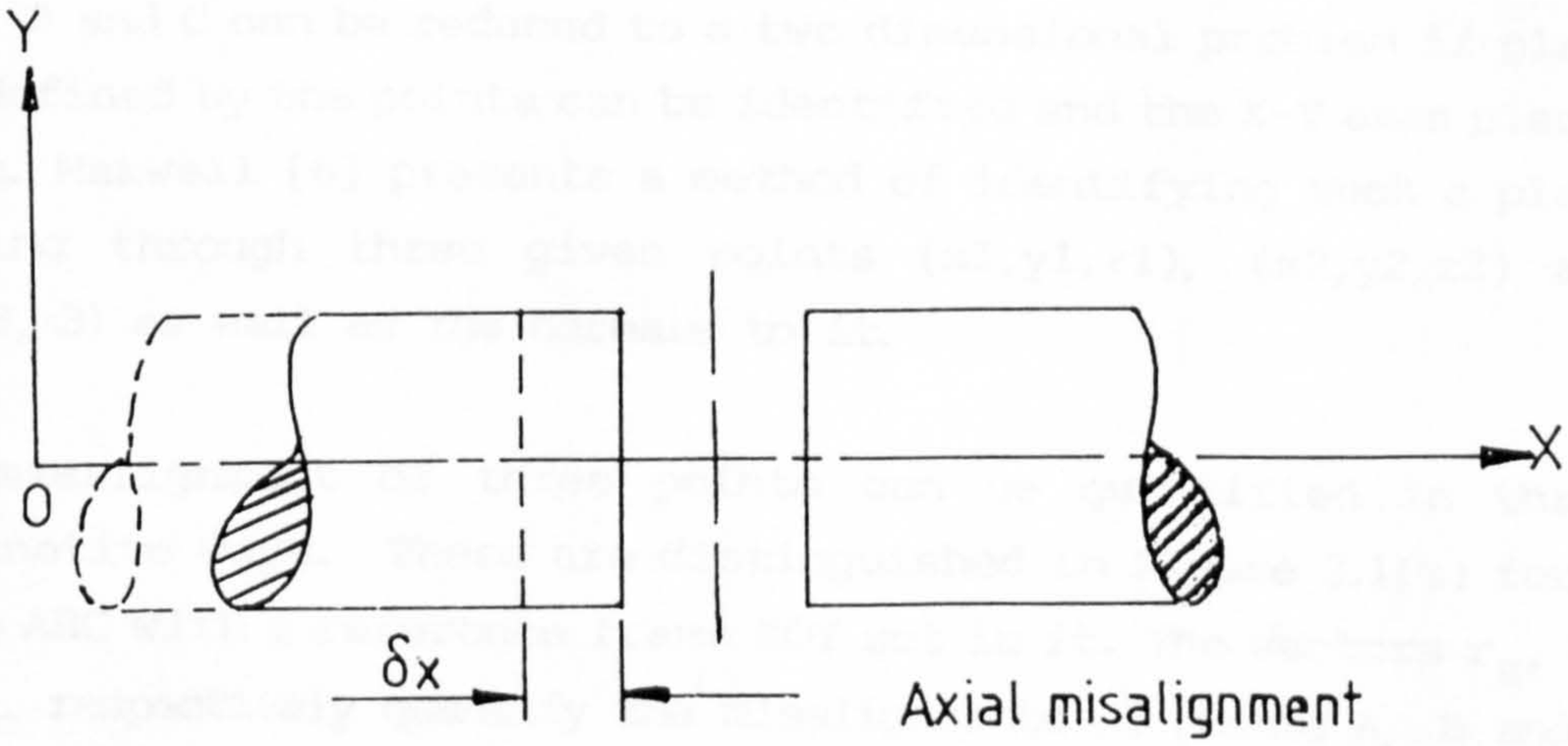

Axial misalignment

Alignment is described [1] as the measurement of a departure of a series of points . . . . . from a straight line which

may have any attitude. This is a quantification of misalignment which is only part of a complete definition of alignment. Alignment is the corrective process necessary to collocate non-collinear points in order to achieve collinearity. In this chapter, alignment is analysed in terms of superposition of skew lines, superposition of line segments and superposition of two spatial congruent figures. The latter is discussed simply for purposes of completeness of the alignment investigation.

3.1 ALIGNMENT OF THREE POINTS

Dagnal and Pearn [5] define a straight line as the shortest distance between two given points A and B and that there can only be one such line. This is, however, the definition of a line segment as opposed to a straight line. A straight line is defined as an infinitely continuous line for which the distance between any selected pair of points along it is least.

In general, the alignment of any three points A, B, & C in space is a three dimensional problem. This can be demonstrated by arbitrarily placing a frame of reference XYZ (Figure 3.1(a)) so that the position of points A (x_a,y_a,z_a), B (x_b,y_b,z_b) and C (x_c,y_c,z_c) are described by three dimenional vectors R_a,R_b and R_c respectively. The alignment of A, B and C can be reduced to a two dimensional problem if plane ABC defined by the points can be identified and the X-Y axes placed in it. Maxwell [6] presents a method of identifying such a plane passing through three given points (x1,y1,z1), (x2,y2,z2) and (x3,y3,z3) as well as the normals to it.

The misalignment of three points can be quantified in three alternative ways. These are distinguished in Figure 3.1(b) for a plane ABC with a reference frame XOY set in it. The vectors r_a, r_b and r_c respectively quantify the misalignments of points A, B and C from the other two. In this case the vectors are coplanar but in general they are three dimensional. The process of collocating any of the displaced points requires a two-degree of freedom manipulator. This is because two variables (displacements and angles) are required to specify the misalignments of the displaced point. That is, A is

moved to A' so that the required straight line is A'BC or similarly B to B' or C to C'. Vector $\mathbf{r}_a$ is any one of oo^1 pencil of lines among oo^2 passing through A and similarly for $\mathbf{r}_b$ and $\mathbf{r}_c$.

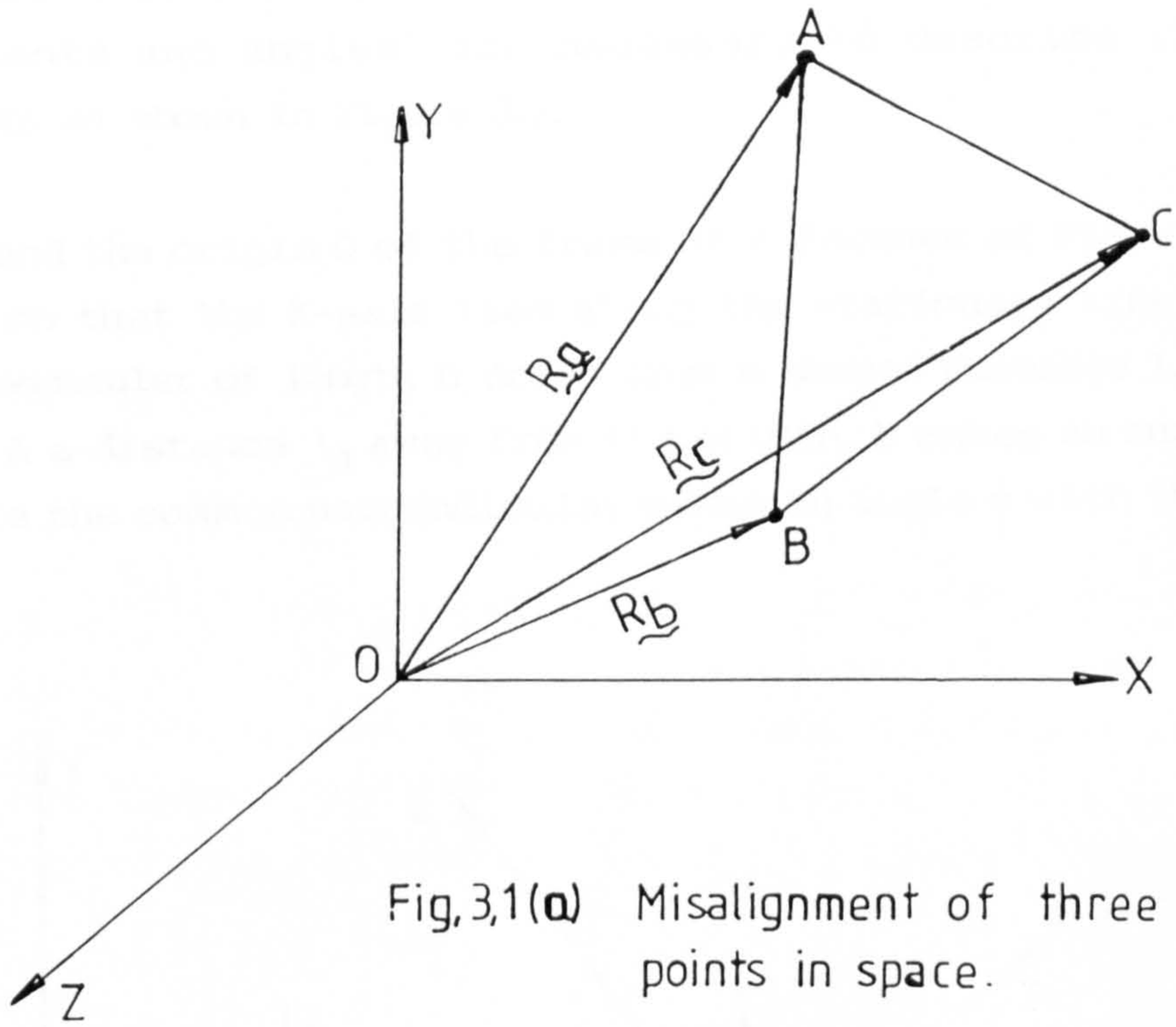

Fig, 3,1(a) Misalignment of three points in space.

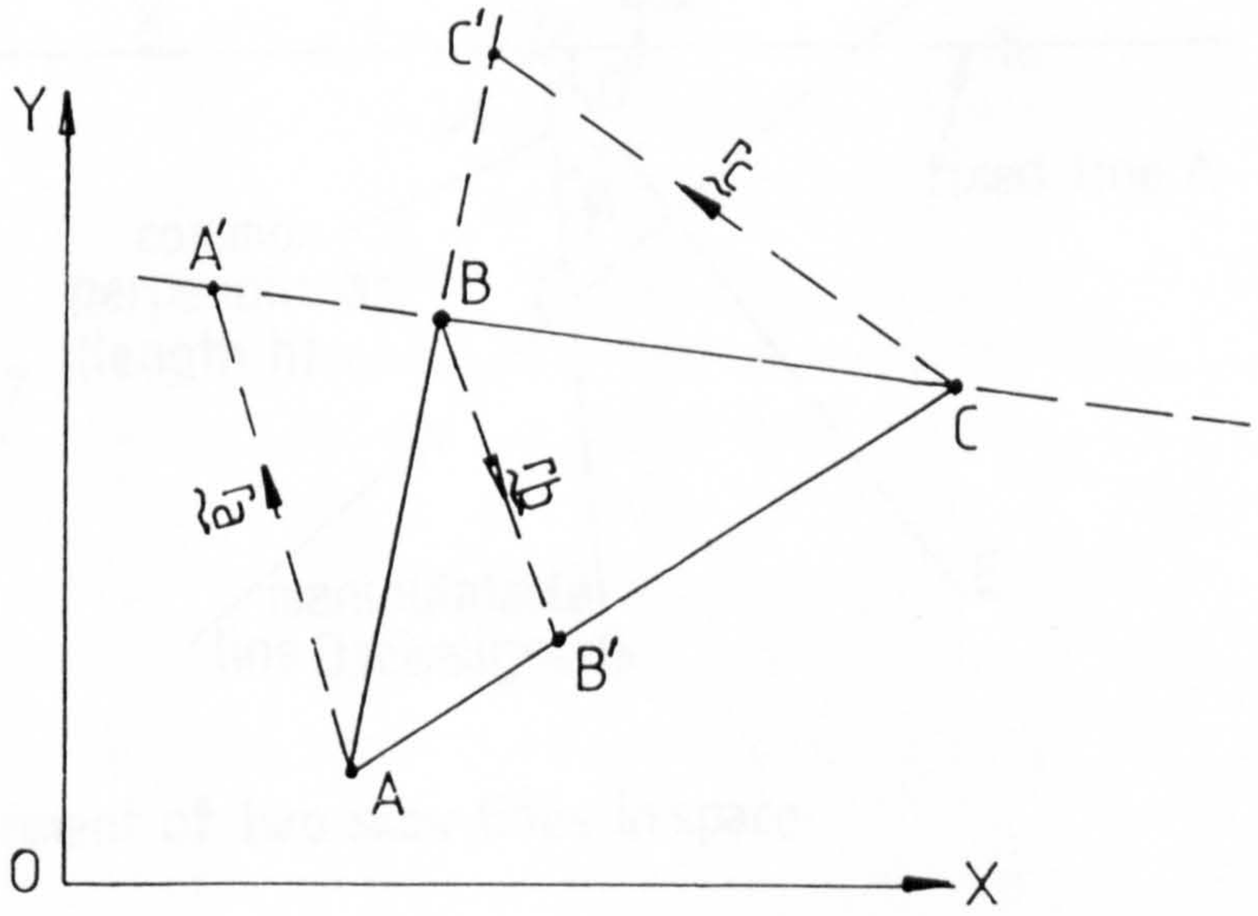

Fig,3,1(b) Alignment of points.

3.2 ALIGNMENT OF SKEW LINES IN SPACE

Two lines that do not intersect and are not parallel are said to be skew. Unlike the alignment of three points (3.1), alignment of two skew lines is more difficult because it requires four degrees of freedom. This is because four independent quantities or variables (displacements and angles) are necessary to describe their misalignments as shown in Figure 3.2.

The Y-axis and the origin O of the frame of reference of Figure 3.2 are chosen so that the X-axis lies along the stationary line A. A common perpendicular of length h drawn from a skewed moveable line D intersects A a distance l_d away from the origin. D makes an angle θ with A while the common perpendicular makes an angle ϕ with the Z-axis.

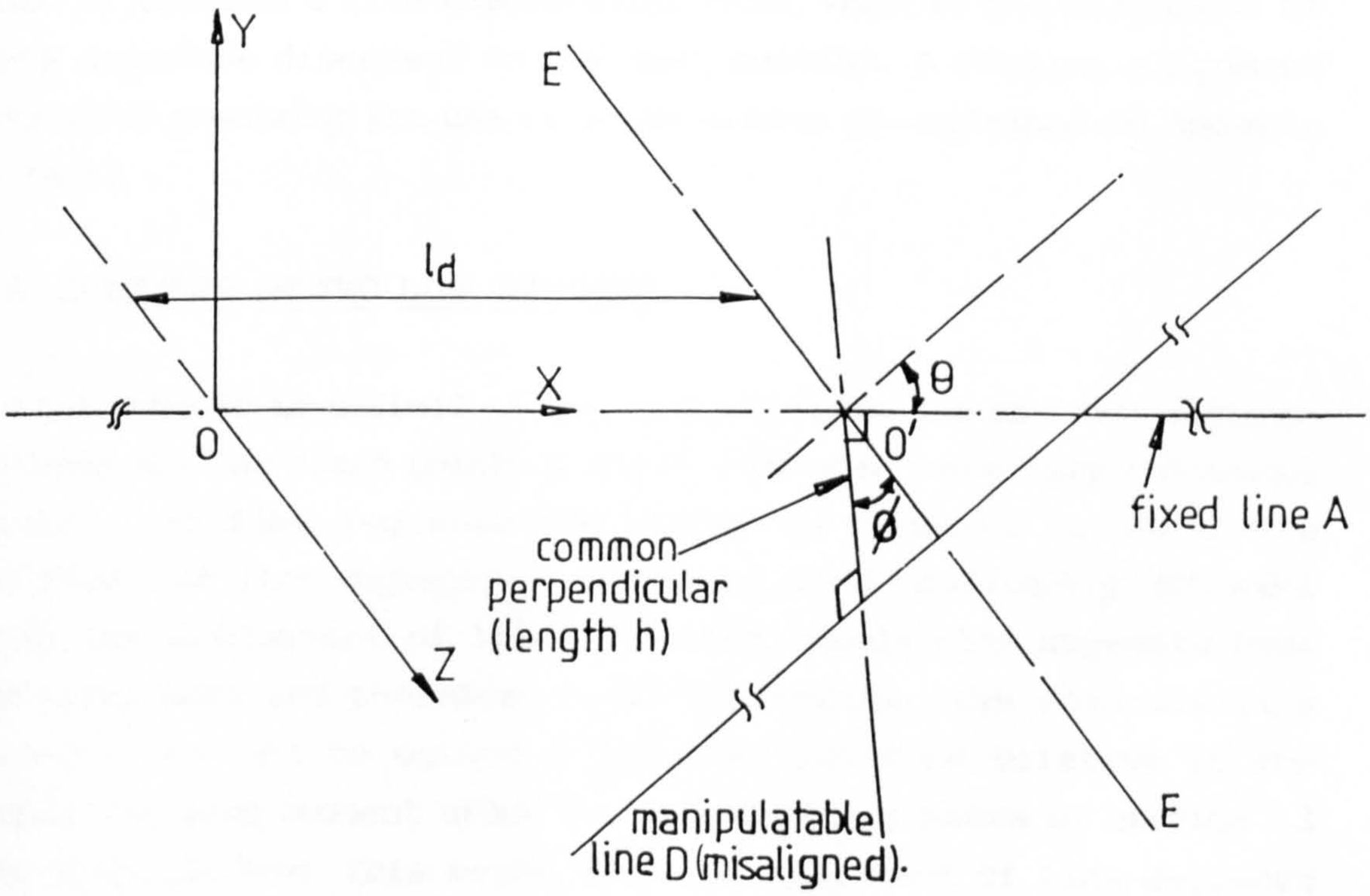

Fig,3,2 Alignment of two skew lines in space.

The alignment of these two lines can be achieved in a number of different ways by changing the order by which each of the four

quantities is reduced to zero. The sequence of such an operation is, however, irrelevant to the final result. It is envisaged that one such sequence through which alignment can be achieved is to translate D in the Y-direction (negatively if D is above A) until a point P_D on it intersects a point P_A on A. Let the new position of D be D'. This translation accounts for one dimension. D' is then rotated about a line EE' drawn through P_A parallel to the Z-axis so that it occupies the same plane as A (X-Z plane). Let this position be D''. This rotation gives the second dimension while the choice of EE' is a third dimension. Finally, D'' is rotated about a line drawn through the point of intersection of A & D" parallel to the Y-axis to bring it into alignment with A. This is a fourth dimension.

In this alignment procedure, the intersection of a point on D with another point on A is completely arbitrary. If it is conducted such that a given point on D coincides with another specifed point on A, then it becomes a five dimensional task. This is the alignment of line segments discussed in the next section. A similar alignment procedure involving the use of screw motion is explained in Appendix A (A.4).

3.3 ALIGNMENT OF TWO LINE SEGMENTS

A line segment is defined as the line which has the shortest distance between any two fixed points A and B. Like two infinitely continuous lines, two line segments can either be coplanar or skew. The alignment of line segments is therefore not significantly different from the alignmment of lines. However, since line segments have definite ends and therefore definite lengths, the moveable line segment has got to occupy a specific position relative to the stationary line segment after the alignment procedures of section 3.2 are accomplished. This means that the alignment of line segments whether coplanar or skew has one more dimension compared to the corresponding alignment procedures of lines (3.2).

Let A1B1 be a fixed line segment lying along the X-axis and A2B2 a moveable line segment lying along line D (Fig.3.2). For these line segments to be aligned, the procedures for aligning lines (3.2) are

repeated provided that care is taken to ensure that A2B2 intersects A1B1 when it is translated along the Y or Z-axis. This places A2B2 anywhere along the X-axis. If it is required that A2 should coincide with A1 or B1, then a further movement of A2B2 along the X-axis is necessary. If the line segments are equal in length, then the corrective action needed to transform one on to the other such that A1 coincides with A2 and B1 with B2 is known as superposition. If one is longer than the other, then the normal process of transforming one to the other is conducted such that a row of points on one is moved to coincide with a congruent row on the other (A.2 - Appendix A).

3.4 SUPERPOSITION OF TWO CONGRUENT SPATIAL FIGURES

After the completion of alignment of lines or line segments, the final orientations or attitudes of the bodies that contain them are irrelevant to the problem. Such orientations are only important when the superposition of spatial congruent figures are considered.

It has been shown (3.1 to 3.3) that the alignment of three points, skew lines and line segments are respectively 3-(reducible to 2-), 4- and 5-dimensional and therefore requires the corresponding number of degree of freedom manipulators to align them. In a similar progression, and in an attempt to analyse the various interpretations of the word alignment, it is shown here that the superposition of two congruent spatial figures is a 6-dimensional problem. This is because it requires six independent quantities (angles and distances) to describe their misalignment.

In Figure 3.4, two congruent spatial figures ABC and PQR are shown. ABC is fixed in space with A and C located on a fixed or stationary line parallel to the Z-axis such that AB is parallel to the X-axis. PQR, a moveable figure, occupies a completely different plane in space such that PR and AC are two line segments located on the corresponding infinite lines whose common perpendicular of length du is parallel to the Y-axis.

Since PQR is a moveable figure in space, the coordinates of P, Q and R can be arbitrarily defined by a total of nine different variables

as $P(x_p,y_p,z_p)$, $Q(x_q,y_q,z_q)$ and $R(x_r,y_r,z_r)$. Since PQ, QR, and RP are line segments in space, their corresponding equations can be set out as follows:

$$\{(x_p-x_q)^2+ (y_p-y_q)^2+ (z_p-z_q)^2\}^{1/2} = k1 \quad \ldots\ldots\ldots\ldots(1).$$

$$\{(x_q-x_r)^2+ (y_q-y_r)^2+ (z_q-z_r)^2\}^{1/2} = k2 \quad \ldots\ldots\ldots\ldots(2).$$

$$\{(x_r-x_p)^2+ (y_r-y_p)^2+ (z_r-z_p)^2\}^{1/2} = k3 \quad \ldots\ldots\ldots\ldots(3).$$

where k1, k2 and k3 are the respective line segment lengths. Three equations are therefore obtained but with nine independent variables. Since a line is completely defined by only four independent variables, it means that three variables must be dropped to leave six. This proves that the procedure of superposing PQR on to ABC is 6-dimensional requiring a six degree-of-freedom manipulator.

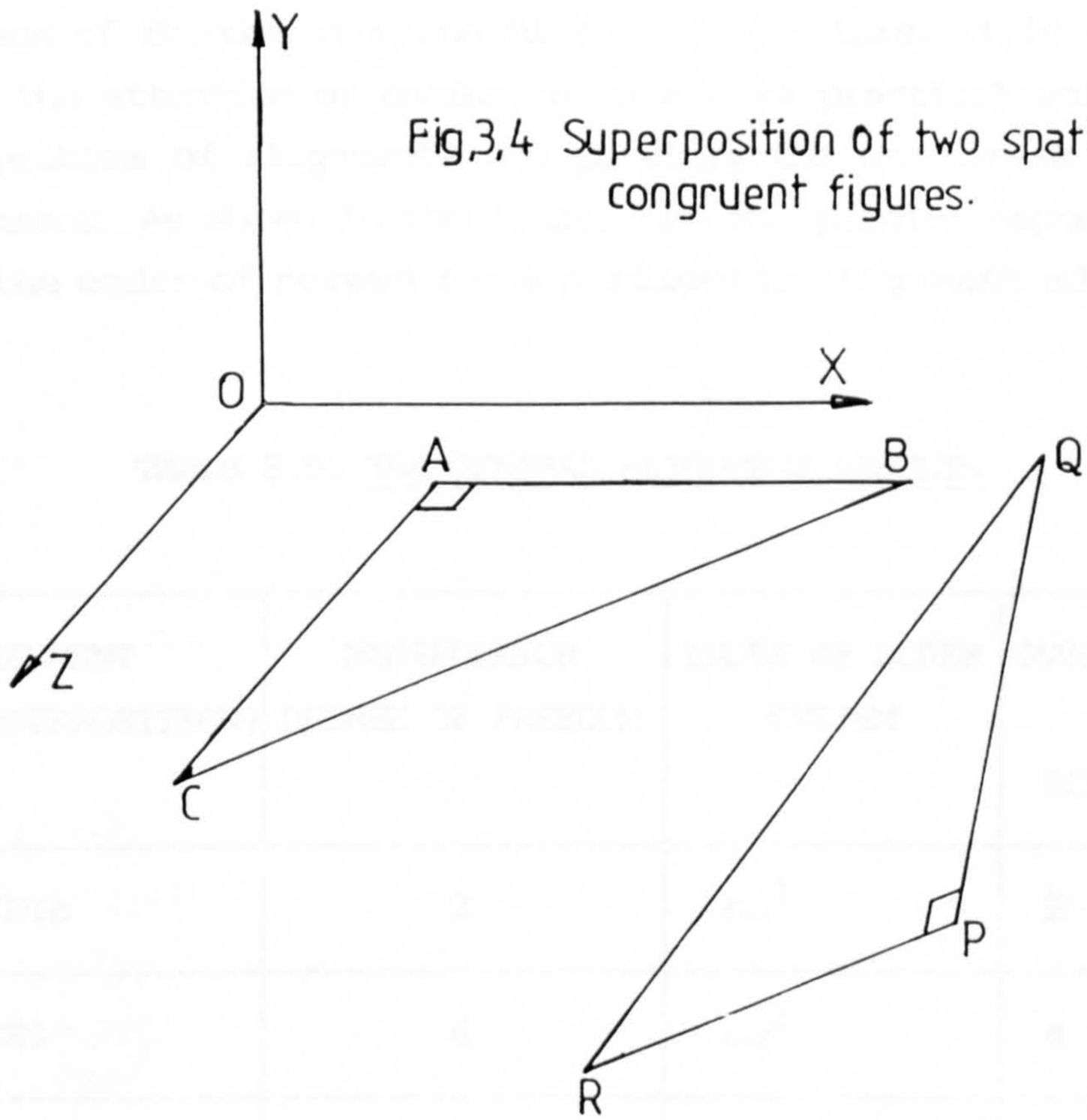

Fig,3,4 Superposition of two spatial congruent figures.

3.5 SUMMARY OF ALIGNMENT METHODS

Roth [7] defines a screw displacement as a rotation of a body about a given axis s_{ij} and a translation d_{ij} along the same axis. i and j being the initial and final positions respectively. That is, the position of a body can be transformed into a second position by a screw displacement. For the displacement of a rigid body in which the rotation angle γ_{ij}, the translation distance d_{ij} and the screw axis s_{ij} are fully determined, the screw is unique. This fact was established by others and restated by Bottema [8]. This method was utilised [8] to solve the alignment problems (3.2 - 3.4) the results of which are presented in Appendix A.

The results of Appendix A and those discussed above are summarised in table 3.5 below. While Appendix A investigates the different screw systems involved in each alignment, the alignment discussions presented in this Chapter lead to a recognition of the number of degrees of freedom required of the manipulators. It is also meant to draw the attention of engineers to a more practical solution to the the problem of alignments and possibly the usefulness of screws in alignment. As shown in the table, the manipulator degree of freedom and the order of screws for a particular alignment adds up to six.

TABLE 3.5: THE GENERAL ALIGNMENT RESULTS

ALIGNMENT (SUPERPOSITION)	MANIPULATOR DEGREE OF FREEDOM	INDEX OF SCREW ·· SYSTEM	MANIP. FREEDOM + SCREW ORDER
POINTS	2	∞^4	2 + 4 = 6
LINES	4	∞^2	4 + 2 = 6
LINE SEGMENTS	5	∞^1	5 + 1 = 6
RIGID BODIES	6	∞^0	6 + 0 = 6

REFERENCES.

1. "Optical transducers and techniques in Engineering Measurements", Edited by A.R. Luxmore. Applied Science publishers Ltd, 1983. (Chapter 4. P.W. Harrison, "Alignment Techniques", p.109).

2. P.A. Fehrenbach.
"Optical alignment of dual-in-line components for assembly." Intelligent Robots: 3rd International Conference on Robot Vision and Sensory Controls. Proceedings of the Society of Photo-Optical Engineers (SPIE) - Vol.449, (p.609-615) 1983.

3. J.S. Mitchell.
"An introduction to Machinery Analysis and Monitoring".
PennWell publishers (p.262-265), 1981.

4. M.G. Murray, Jr.
"Out of room? Use minimum Machinery Alignment." Hydrocarbon Processing Vol.58 (p.112-114), 1979.

5. R.H. Dagnall and B.S. Pearn.
"Optical Alignment. (A guide to techniques based upon the use of the Rank Taylor Hobson Microalignment Telescope and its Acessories)". Hutchinson. First published , 1967.

6. E.A. Maxwell
"Coordinate geometry with vectors and tensors". Oxford University Press 1958 (p.20-27).

7. B. Roth.
"On the Screw Axis and Other special lines associated with spatial displacements of a rigid body." Journal of Engineering for Industry. Transactions of the ASME (p.102), 1967.

8. O. Bottema.
"On a set of displacements in space". Contributed by the Design Engineering Division for presentation at the Mechanisms

Conference, San Francisco, California. USA. Oct.8-12, 1972 of the ASME. Paper No.72-Mech - 19. Transactions of the ASME. Journal of Engineering for Industry (p.1-4).

9. E.J. Zuiderwijk.
"Alignment of randomly distributed objects."
Nature vol.295, 1982 (p.577-578).

10. R.M. Schectman, L.J. Curtis and H.G. Berry.
"Alignment, Orientation and the beam - Foil Interaction."
International Conference on Coherence and Collision. London 1978. (Plennnum Publishers 1980, p.387-393).

11. J. Davis, W.J. Tango and R.J. Thompson.
"Interferometric alignment of optical surfaces and rotational axes." Applied Optics vol.21, No.16, 1982 (p.2867-2868).

12. B.A. Buck, R.L. Siddon and G.K. Svensson.
"Beam alignment device for matching fields."
International Journal of Radiation Oncology (Biology, Physics) vol. 11, 1985 (p.1039-1043).

13. R.E. Hopkins.
"Optical element mounting and alignment techniques."
Society of the Photo-Optical and Instrumentation Engineers vol. 531, 1985 (p.187-195).

CHAPTER 4

SURVEY OF MICROACTUATORS

CHAPTER OVERVIEW

This chapter presents the results of a survey of commercially available micropositioners. The differences between microactuators, micropositioners and micromanipulators are made clear in section 4.1 by defining each of these terms. The reasons for conducting this survey are stated in the introduction.

Some specifications (not given in Chapter 2) which outline the lateral, axial, and angular tolerances based on the presently available literature are also presented in the introduction.

A brief survey of bimetals is presented in sections 4.2 to 4.2.1 followed by a detailed survey of piezoelectric actuators presented in sections 4.3 up to 4.3.13. This includes looking at their properties, problems associated with their construction and briefly commenting on the presently available micromanipulators constructed out of them.

The survey of electric motor actuation is presented in Appendix B. The reasons for selecting the Oriel Encoder Mike micrometers as the most appropriate actuator for use in this thesis are also discussed in the Appendix. The survey ends in section 4.5 with a brief discussion of fluid actuators comprising of pneumatic and hydraulic actuators.

4.0 INTRODUCTION

A literature review of the various optical fibre transmission components and their associated coupling problems have been discussed (2.1) followed by the analysis of alignment of lines (chapter 3) with a view of linking them for a possible solution to the coupling problems outlined. A selection procedure to obtain a suitable actuator for the construction of an appropriate manipulator aimed at achieving this is presented. This procedure can only be carried out

after the alignment tolerances to be accommodated by the actuator are specified.

Since the object of this research work is to produce a general purpose semi-automated micro-alignment system capable of obtaining the optimum launch efficiency for any coupling method (2.3.1-2.3.4), it is important to base the specifications on the worst available established practical tolerances. These are partly obtained from a literature survey of the presently available alignment results already discussed (2.3.5) and partly from STC the supplier of the semiconductor laser diode and the monomode optical fibre to be experimented up on.

The results from the literature survey of Chapter 2 produced the following selected tolerances:

Lateral alignment tolerance = 1.2 μm.
Axial alignment tolerance = 7.0 μm.
Angular alignment tolerance = 0.9^{o}.

These specifications will only account for misalignment tolerances for particular coupling configurations (methods) and the axes for which they are quoted.

However, the optical fibre provided by STC for experimental purposes has a converging lens of 35 μm in diameter and focal length of 80 μm permanently inserted into its input face. In order to avoid contact between this lens and the laser diode face, which could result in the damage of both, STC recommends a minimum separation axial distance of 40μm between this lens and the laser diode face and that the maximum load (weight of laser diode package) to be tested is 40 gm (2.5). It is also envisaged that the maximum overall distance to be covered by an actuator along any axis during the laser fibre alignment can not exceed 6 mm. As it was later discovered (2.5), for laser/fibre alignment, the largest distance traversed by any actuator can not in general exceed 100 μm.

4.1 ACTUATORS FOR ALIGNMENT

An actuator may be defined as a coupling which contains an element that provides power and motion. If the optical misalignment problems involving minute tolerances of the order discussed above are to be solved by an automated means as suggested in the specifications, then a very precise actuator whose response is least affected by applied electrical signal as well as temperature must be utilised. It is necessary to highlight the concise definitions and discussions of the associated terms like stability, repeatabilty, resolution, hysteresis etc, before delving fully into the discussions of these actuators. These in turn help foster a good understanding of the properties and capabilities of some of the actuators to be discussed.

Definitions

1. The mechanical accuracy is defined as the difference between a theoretical and a real dimensional value. In micropositioning, the dimension measured is the difference between two successive positions of the same object. In a measuring instrument, accuracy is the instrument's ability to record the true value of the measured variable whereas in a controlling instrument it is its ability to establish the desired value of the variable being controlled.

2. Hysteresis is defined as the difference in the absolute position of the moving portion of a stage after travelling in one direction and then reversing to return by the opposite way. It would appear to be backlash but in fact is a change in the equilibrium position created by an inversion of the direction of friction force.

Dario and De Rossi [1] define hysteresis as the difference in the value of a physical parameter (such as an electric charge) according to whether a phenomenon on which it depends (such as a force) is increasing or decreasing.

3. Repeatability is defined as the consistency in the quality of a measurement system. It is by far the most important factor in such a system. If the same value of the measured variable is reproduced many times under the same environmental conditions and origin of reference, then the instrument is said to have a high degree of repeatability.

4. Sensitivity is the ability of a positioner to respond to motion command. That is, the smallest change in the input signal that will cause a change in its displacement position. In a measuring instrument, it is the size of the deflection produced by the instrument for a given change in the measured variable. Jones [2] states that sensitivity is used to denote the smallest change in the value of the variable being measured to which the instrument will respond. The largest change in the measured variable to which the instrument does not respond is called the dead zone [2].

5. Resolution is the smallest movement attainable in an actuator. A micropositioner which is driven by a stepper motor can be said to provide a resolution of 1 step. This single step can be equivalent to a linearly resolved distance of say 1 micron. A micropositioner driven by Oriel Encoder Mikes, for example, has a resolution of 0.02 microns.

6. The limit of resolution is defined as the threshold at which the positioner's motion will correspond to the value of the command signal.

7. A microactuator is defined as a movement reduction element providing a unidirectional motion.

8. A micropositioner is defined as a movement reduction instrument providing translational movement in 2-dimensions. It comprises of two microactuators assembled together to give the two translation motions.

9. A micromanipulator is a movement reduction instrument providing

translational motion in 3-dimensions. It consists of three actuators assembled together so that each actuator is directly associated with a translation motion in a particular direction.

It must be realised that 5-degree of freedom micromanipulators with three translational axes and two rotary axes or some other combinations including 4-degrees of freedom are also available.

4.1.1 Drift

Drift of an instrument is defined [2] as a gradual shift of its calibration over a period of time. It is directly related to the repeatability of a measuring system. The higher the degree of repeatability, the less is its tendency to drift. The causes of drift are dependent on the operating system. It may occur in thermocouples owing to changes in the metals as a result of contamination. It occurs in flowmeters because of wear of the differential pressure producing element and may occur in hydraulic systems because of leakage due to wear and tear.

4.1.2 Stability of a Positioner

The stability of a system is its ability to maintain its performance characteristics under different environmental conditions over a period of time. The stability of a positioner or any other system is dependent on the interaction of various factors or constraints normally considered an elastic equilibrium phenomena.

Although in a stable environment the position repeatabilty is considered ideal, a small amount of drift can not be ruled out. This drift is caused by factors of unequal importance namely wear and tear, variation in lubricant thickness with contact pressure and thermal equilibrium with particular reference to sporadic localised heating.

4.1.3 Creep

Olsen [3] summarises creep as the time dependent strain that occurs

at elevated temperatures when a material is subjected to stress for a prolonged period of time.

In piezoelectric actuators when a step voltage is applied, the actuator executes a step displacement which tends to increase over a period of time. This phenomena takes place at a specific voltage range for a given piezoelectric actuator and can lead to fracture at even higher voltages. This is also known as creep.

Unless otherwise stated, the word MICRO will be detached from actuation (actuators), positioning (positioners), and manipulation (manipulators) but implied in further discussions because it appears quite frequently in the Chapter.

In an attempt to find a suitable micro-actuator, a survey of four major types of conventional actuators is now launched. These comprise the bimetallic, piezoelectric, electric motor and fluid actuators respectively. Electromagnetic actuators are dismissed because of their poor response to hysteresis problems.

4.2 BIMETALLIC THERMAL ACTUATORS

A bimetallic strip consists of two permanently bonded layers of dissimilar metals with different coefficients of thermal expansion. On applying heat, the metal with a higher coefficient of thermal expansion will tend to move away from its counterpart. This results in the bending of the entire strip because of the bonding between the two metals. Baker et al [4] state that depending thus entirely on the elastic property, this type of element is not suited to high precision.

The bending action of these elements has for a long time been utilised for actuating automatic recorders, telemetering devices and controls. Such selections are made on the basis of (a) the simplicity and (b) the relatively low cost of the bimetallic operated units.

Although nothing tangible has been reported in the presently available literature about the role of bimetallic actuators in

manipulation, Umetani [5] reports that thermal expansion type manipulators employing elongation properties of materials by heating are in operation.

4.2.1 Range of Maximum Sensitivity and the Response of Bimetals

The American Gas Association [6] reports that although a specific bimetal is normally recommended for use at a particular temperature range, it does not necessarily maintain the same deflection over the entire range.

It might in fact be desirable to use some bimetals over the maximum sensitivity range for some particular applications. If this happens to be important, it means that successful operations can only be carried out if the temperature of the thermal bimetallic element remains within its range of maximum sensitivity.

In addition, due to heat inertia, the deflection of bimetallic strips is not proportional to the rate of heat flow (i.e. electrical power $P = I^2R$, where I = current and R = resistance). On the contrary, the deflection is proportional to the temperature. That is, temperature lags behind the heat flow through the strips. Likewise, the strips are slow to cool down.

In conclusion, bimetallic strips are dismissed for a possible application in this thesis on the grounds that their response are generally too slow. In addition, it is confirmed [4] that depending on the elastic property of bimetals, they are unsuitable for high precision work.

4.3 PIEZOELECTRIC ACTUATORS

Piezoelectric materials have only been recently introduced in the construction of manipulators. The majority of cases have been carried out at experimental stage by people like Spanner and Marth [7] and Umetani and Suzuki [8] aimed at solving problems associated with microcircuit assembly, cellular biological research and bacterial culture. As far as the present literature suggests, nobody has so far

successfully utilised block piezoelectric translators by themselves for laser/fibre or fibre/fibre alignment.

There is, however, no doubt that these materials are indeed promising for such alignment tasks. This belief is shared by Spanner and Marth [7] who successfully incorporated a fine adjustment x-y-z piezoelectric block translators on top of a coarse mechanical x-y-z stage for laser/fibre alignment. Quite recently (Octber 1986), two companies (Centronic Sales-Croydon and Photon Control-Cambridge) claimed to have produced similar alignment manipulators with uniaxial resolution of 0.1 μm. It was therefore not only found necessary to investigate the major drawbacks of this material in micropositioning but also to study its properties, areas of current application and evaluate its future potential for micro-alignment.

4.3.1 Piezoelectricity in Ceramics and Polymeric PVDF

Piezoelectricity, discovered by Jacques and Pierre Curie in the 1880's, is defined by Vernitron [9] as the capability of certain particular class of materials to change their dimensions when subjected to an electric field or conversely produce an electric signal when mechanically deformed. It is therefore sometimes called pressure electricity. Pyroelectric materials on the other hand develop an electric charge from a thermal change but according to Bloomfield et al [10] inverse pyroelectricity is of minor importance.

Only 20 out of the normal 32 classes of crystals known to the crystallographer exhibit piezoelectricity but 10 out of the 20 exhibit both piezo- and pyroelectricity [10]. The only linkage between the 20 groups being the absence of a centre of symmetry.

The two major groups of piezoelectric materials currently in commercial use are the ceramics and polymer films. However, the very first piezoelectric materials ever known to scientists were naturally occurring Rochelle salt and quartz. More recently, ceramics that have improved piezoelectric activity have been synthesized. The advantage of ceramics over polymers in the energy conversion from one form to another, lies in its greater rigidity [11,12]. These brittle

materials are, however, hard to make in the thin large sections that are common place for polymer films [13]. Their applications can be classified [10] as either generator (mechanical vibration transformed into an electrical signal) or motor (electrical signal transformed into a mechanical force). Thus these two materials are more complementary than competitive as confirmed by their comparison given below.

4.3.2 Piezoelectric Polymers Versus Ceramics

Of all the ceramic and polymeric materials so far investigated, the action of lead zirconate titanate (PZT) and polyvinylidene fluoride (PVDF or PVF_2) have been found by Corey and Hudspeth [11] and Toda [13] respectively to have higher piezoelectric activity than any other piezoelectric materials in the two respective groups. These materials differ from each other in many respects. Most of the typical properties of PVDF which sharply contrast with those of the ceramic PZT are summarised in table 4.3.2 below.

TABLE 4.3.2: Comparison of PVDF and PZT materials

No.	DESCRIPTION	PVDF or PVF_2 POLYMER	PZT CERAMIC	REFERENCES
1	Approximate minimum obtainable thickness for the same length.	6 to 7 μm	Unknown but max. thickness is 0.25 mm	13,p.127
2	Induction of electric field for same applied voltage.	High	Low	13,p.127
3	Maximum safe voltage applied (without degradation)	300 kv/cm	3 kv/cm	13,p.127 18,p.14-46

4	Maximum mechanical power output per unit volume	Five times larger than for PZT	One-fifth of that of PVDF	13,p.127 18,p.14-46
5	Density	$1.78 gmcm^{-3}$	$7.5 gmcm^{-3}$	18,p.14-38
6	Piezoelectric constant, d_{31}	$21 \times 10^{-12} c/N$	$-274 \times 10^{-12} c/N$	18,p.14-38
7	Relative dielectric constant	12	3400	18,p.14-38
8	Max. strain produced by application of max. safe voltage	10^{-4}	10^{-5}	18,p.14-46
9	Force produced as a result of the application of electric field	Low but accompanied with large displacement of PVDF	High but accompanied with small displacement of PZT	9,13,17& 11
10	Flexibility, softness and ruggedness	Very flexible, soft and pliable	Quite brittle	19 for PVDF and 9,11,12 for PZT
11	Maximum safe service temperature before depolarisation	$80^{o}C$	$200^{o}C$	19,13 for PVDF and 12,p.251 for PZT

4.3.3 Fabrication of Piezoelectric PVDF and PZT Actuators

The PVDF and PZT can both be fabricated into various shapes. Although PZT is rigid, Vernitron [9] has devised some special techniques of fabricating it into a cylindrical form. However, due to PVDF

pliability, Dameron and Linvill [14] were able to fabricate a cylinder out of it with ease.

Metalised Polymer Monomorph showing directions of polarisation and accentuation when a voltage is applied to the electrodes.

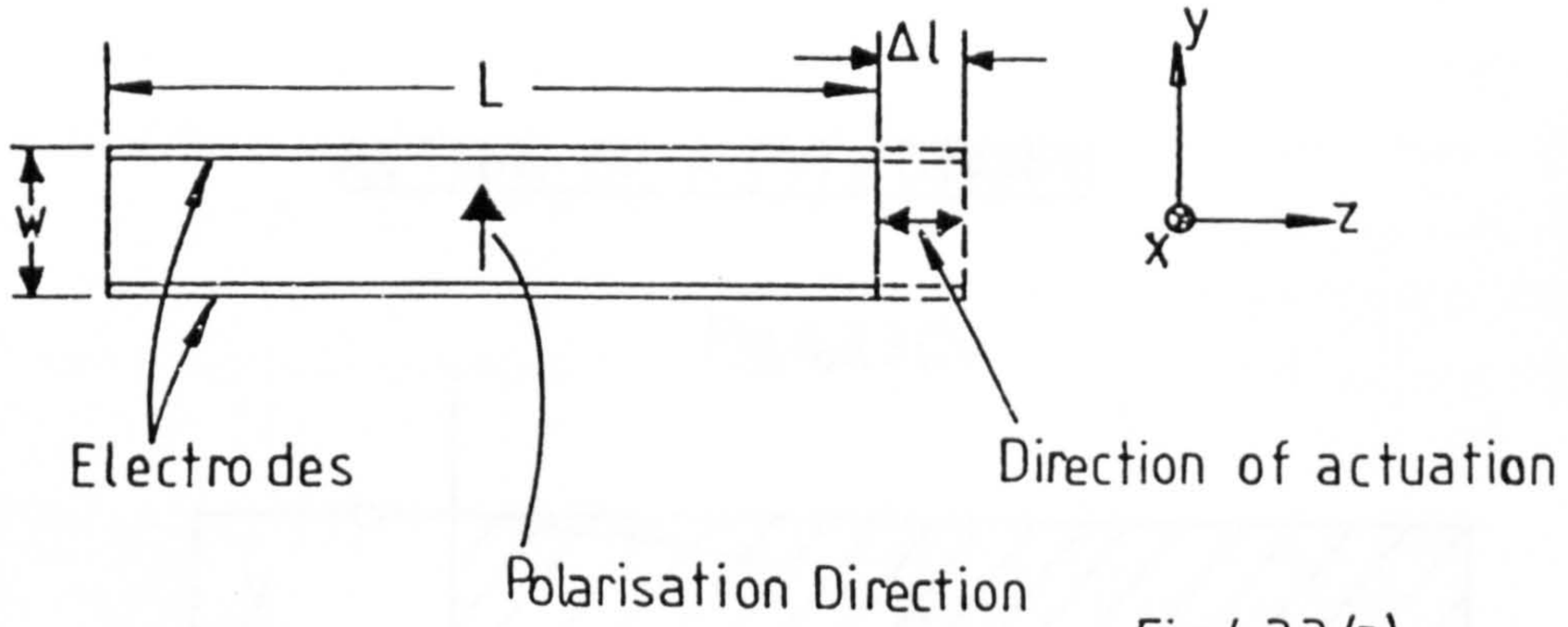

Fig,4,3,3 (a)

L = Length
w = Width
Δl = Actuation due to applied voltage

The basic unit of either material is called a monomorph. When two or more monomorphs (usually an even number) are glued together, they form a bimorph. On application of an electric field, a monomorph executes a linear displacement (expands) but contracts with reverse polarity (Fig.4.3.3(a)). By contrast, a bimorph bends as shown in Figure 4.3.3(b) and the direction similarly changes with reverse polarity. Toda [13] reveals that while the bending displacement of a bimorph is proportional to the reciprocal of the total number of unit layers (monomorphs), the force due to bending is proportional to the square of the same number of layers. This bending displacement is a result of having differing relationships between the polarisation directions and the electric field for each layer. The design analysis of conventional bimorph structures carried out a long time ago by Thurston [15] and others has been superseded by the modern design analysis of the mechanical output of (a) a multi-layer bimorph device composed of a central non-piezoelectric layer, (b) a multi-layer

bimorph device composed of various membrane thicknesses and (c) a single layer device with interdigitated electrodes fabricated by Toda [16]. It is stated [13] that the length of a bimorph is limited by gravity sagging at the far end of the bimorph if its major surface is horizontal. This is because gravity sagging is proportional to the fourth power of the bimorph length [13].

ACTION OF A PVF_2 BIMORPH

Fig, 4,3,3 (b)

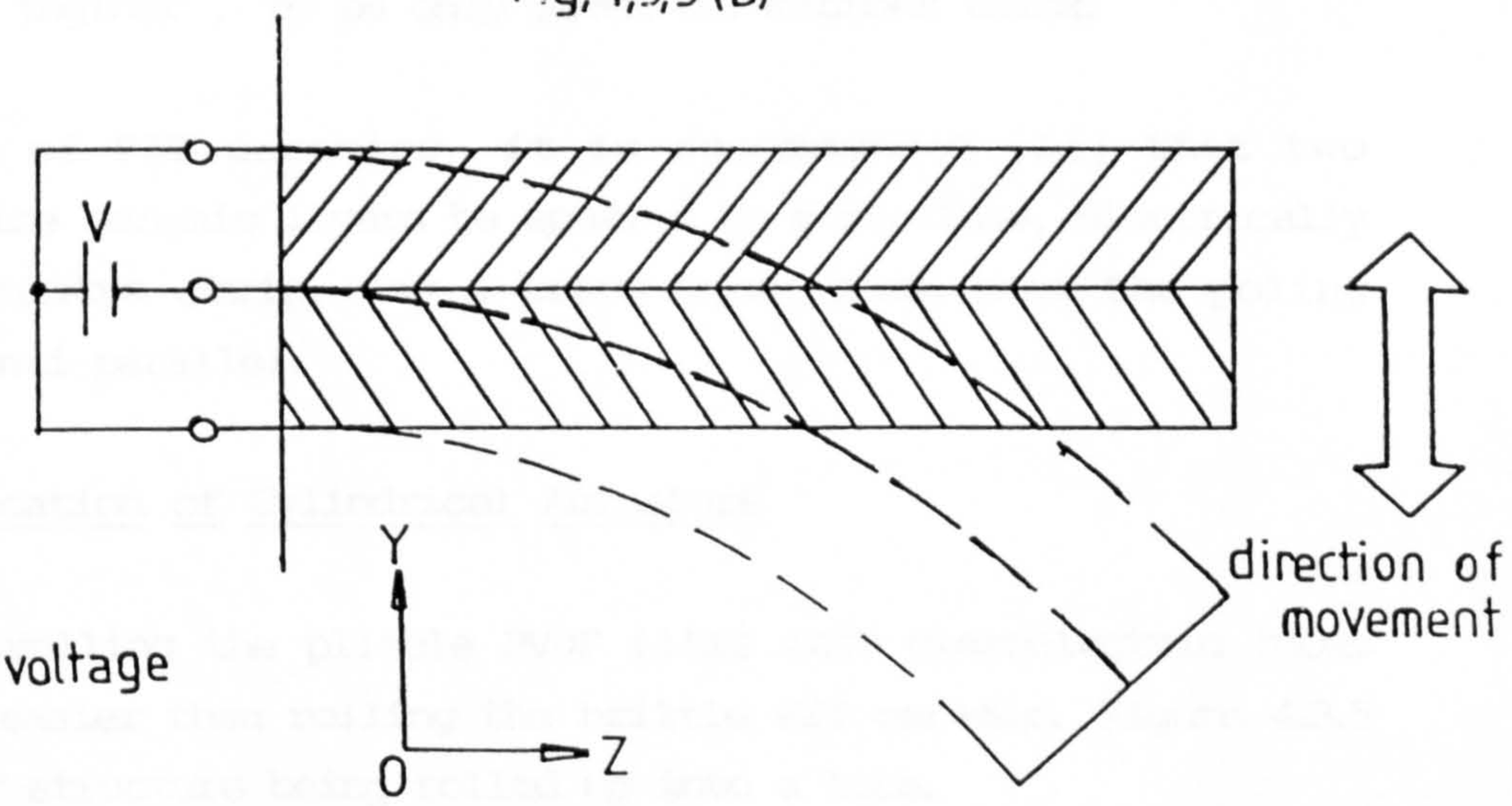

4.3.4 Fabrication of Bimorphs

The PZT and PVDF bimorphs are fabricated in a similar manner. Most PVDF films used for this purpose normally range from 5 to 9μm in thickness [10, 17] while PZT layers can each be up to 0.25mm thick [18,13,11].

The PVDF films and PZT layers are normally bound together by means of epoxy resin [17,11]. It is necessary to minimise the thickness of the epoxy layers since they are not normally actively useful in the device action. Liquid epoxy resin becomes solid after mixing with a

hardener [17].

In this technique, epoxy resin and the hardener are separately coated on the surfaces to be bound and almost completely wiped off. So, a very thin layer covers each surface and does not harden during the coating and wiping off process. The surfaces are then contacted by fingers to give a tight bond.

The thickness of the epoxy layer can be estimated from the difference in the thickness of a given number of epoxied layers and the same number of non-epoxied layers (piezoelectric matrial). Each epoxy layer was estimated [17] in the case of ten 9-micron thick PVDF layers bound togther , to be only about 0.3 microns thick.

In the case of PZT ceramics, it is recommended [11] that two polycrystalline ceramic layers be epoxied to a flexible, electrically conductive centre strip, say a brass vane, such that the poling fields are anti-parallel.

4.3.5 Fabrication of Cylindrical Actuators

The task of rolling the pliable PVDF films into piezoelectric tubes is normally easier than rolling the brittle PZT ceramic. Figure 4.3.5 shows a PVDF structure being rolled up into a tube.

Dameron and Linvill [14] criticises the technique of winding PVDF films on a mechanical rig. This is because the films tend to develop folds and wrinkles which form as the film is being rolled and propagate as it is wound further.

A hand method in which the cylinder is rolled tightly between the fingers by applying a force transferred tangentially to the sheets is preferred. In such a method, the application of methanol to the PVDF layers in order to increase friction by means of surface tension so that the cylinder winds down properly without slipping is recommended [14]. In the process of winding, the epoxy resin and hardener are separately coated to the surfaces to be bound and almost completely wiped off before binding the sheets together.

In the case of PZT ceramic tubes, Vernitron [9] has a number of different variations. Electrodes may, for example, cover the cylindrical surfaces with polarisation in the thickness direction. In another, the electrodes may cover the ends of the tube with polarisation in the lengthwise direction and thirdly, the tube is cut lengthwise into an even number of curved plates. Electrodes are then applied to the cut edges. The individual plates are then polarised and the cylinder is finally assembled.

Hollow cylinder formed from a sheet of PVF_2.

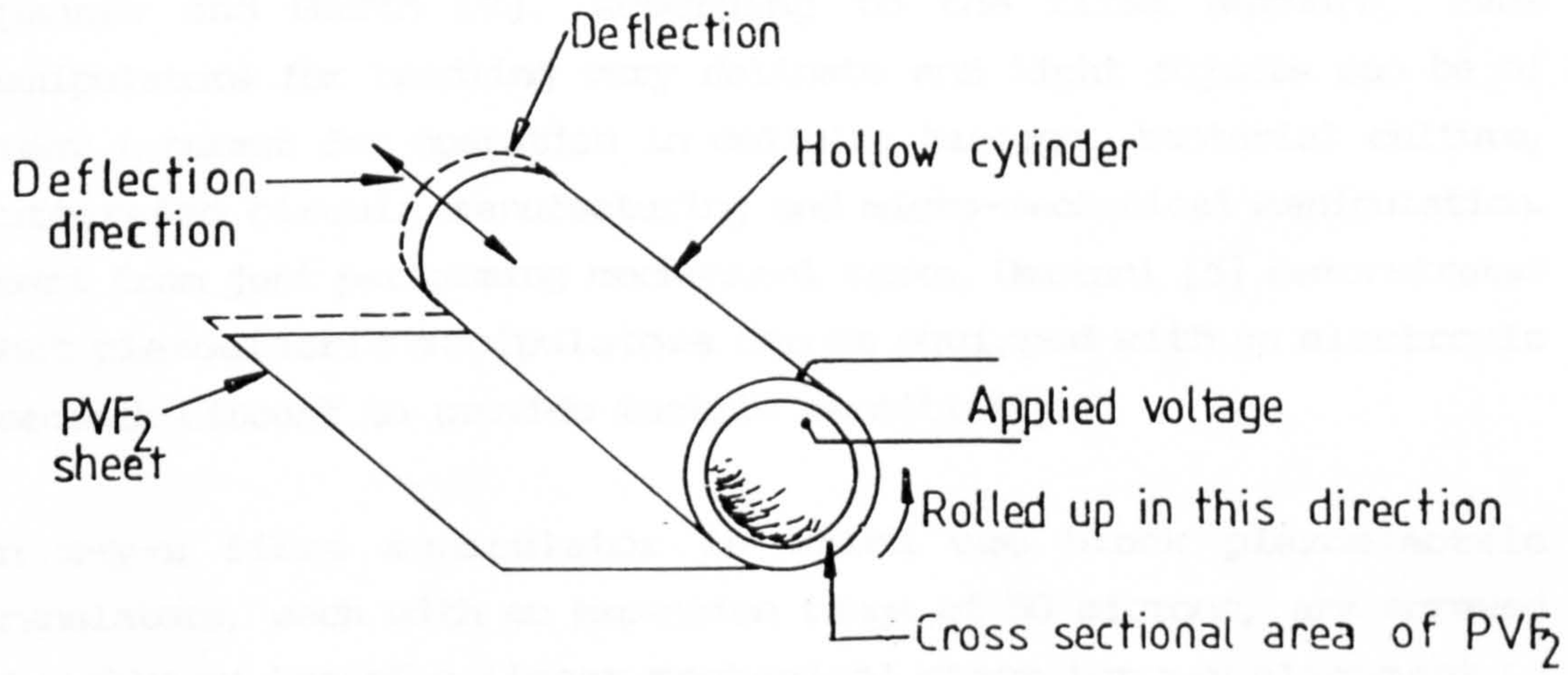

Fig. 4, 3, 5

4.3.6 Action of Cylindrical Actuators

The hollow cylinder fabricated either by hand or a mechanical jig is operated in a length extender mode along the film stretch direction. Hengstenberg [12] mathematically describes the change in length ΔL when an electric field is applied across the tube wall as $\Delta L = (LxVxd_{13})/w$ where L = length of tube, V = applied voltage, w = wall thickness and d_{13} is the transverse piezoelectric constant of the tube material. The tube expands ($\Delta L>0$) if the electrical field is positive on the inner face of the tube and contracts ($\Delta L<0$) with reverse polarity.

It is stated [14] that when the tube is operated below its resonant frequency where the strain is considered uniform along the length, then the deflection ΔL versus applied electric field is proportional to the length of the tube. Since the stiffness of the tube is proportional to the cross-sectional area of PVDF used [14], it can be varied by the number of turns wound round to form the tube.

4.3.7 Application of Piezoelectric Actuators in Micropositioning

The feasibility of piezoelectric PVDF in manipulation has been demonstrated by Umetani and Suzuki [8] and also to a large extent by spanner and Marth [7]. According to the first authors, PVDF manipulators for handling very delicate and light objects can be of great interest for operation in cellular biology, bacterial culture, integrated circuit manufacturing and micro-mechanical manipulation. Apart from just performing mechanical tasks, Umetani [5] demonstrated that piezoelecric manipulators can be equipped with an electronic feedback circuit to provide tactile sensitivity.

An x-y-z fibre manipulator in which two block piezoelectric translators, each with an expansion range of 50 microns, are screwed directly on top of a linear mechanical stage for x-y alignment is also described [7]. This linear stage, driven by a high resolution stepper motor, takes care of alignment in the fibre axis.

It has been found [11] that because the apparent centre of rotation of a probe attached to a cantilever mounted bimorph is at the centre of the bimorph, many plausible arrangements of bimorphs fail to produce motions along orthogonal axes. Workable solutions [11] for PZT bimorphs, involve the use of struts to transfer the displacement in a parallelogram arrangement or mounting configurations other than the cantilever. The authors discovered a Pi- configuration which is much stiffer compared to the strutted parallelogram arrangement. It is pointed out [11] that the Pi configuration is sufficiently rigid, low in drift and therefore suited to holding microelectrodes for cell impalement. It is also believed [11] that depending upon microscopic visibility, an electrode tip may be readily positioned to within a few tenths of a micron.

The device can be used [11] for mechanical stimulation of cells, microdisection, and positioning of microelectrodes to impale cells. The attenuation in the control electronics brings all sensitivities of the device to 0.5 microns per volt although the individual sensitivities along the z(probe), y(vertical) and x(horizontal) axes were found to be 0.56 microns/V, 1.25 microns/V and 2.0 microns/V respectively [11].

Hengstenberg [12] developed a piezoelectric jolter which consists of a small piezoceramic tube attached to a micromanipulator and carries a microelectrode at its front end. Precise steps measured in nanometres per volt were linearly achieved with this tube up to a maximum excursion of 2 microns at 450 volts D.C.

It is reported [12] that interneurons of the visual system of a blow fly were impaled with the device attached to a hydraulic microdrive. In addition, it was possible to penetrate and stain fibres as small as 1 micron in diameter buried more than 100 microns deep in neuropil.

4.3.8 The Drawbacks of Piezoelectric Actuators to Micromanipulation

Although piezoelectric actuators are envisaged suitable for microalignment, they have some drawbacks arising from the physics of their operation. Some of these are due to the improper construction of the actuators while the rest are mainly the result of applied electric potential and their control.

Some of the major drawbacks of these materials have been summarised [7] as follows:

(a) The piezoelectric effect is non-linear at high electric field. This results in an S-shaped curve of strain dependence versus applied electric field.
(b) The piezoelectric effect in artificially poled ceramic depends on time in certain voltage ranges. At high electric fields, an additional polarisation occurs and the piezoelectric translator

changes its expansion by a small amount even if the applied high voltage is constant. This creeping depends logarithmically on time and has a value of 1% to 2% during each order of magnitude increase in time.

(c) The achievable length variation is up to 1 or 2 thousandths of the piezoelectric ceramic length. The expansion of piezoelectric translators, including lever amplification, is limited to about 1mm because of size limitations and stability considerations.

However, other drawbacks have also been considered and presented in sections 4.3.9 to 4.3.12.

4.3.9 Problems Associated with Construction of Piezoelectric Actuators

Piezoelectric tubes formed by a rolling process, normally develop problems. The winding process that forms the tubes usually produces small creases in the film which causes small cracks in the electrodes. These cracks are known [14] to electrically isolate portions of the film preventing all or portions of the film from being excited. The damaged films and electrodes are prone to quick failure due to high current densities and weaker electrodes. This is aggravated by thermal expansion of PVF_2 and the conductive epoxy causing micro-cracks to form in the electrodes both of which give rise to favourable propagation failure sites.

The use of thicker PVDF films (say 30 microns) is recommended [14] because they have less number of flaws and usually give fewer winding and cracking problems. They, however, need larger voltages in order to produce the required electric strengths.

The construction of bimorphs can also develop similar problems if (a) the layers are not properly pressed down onto each other resulting in the formation of wrinkles and (b) there are cracks or flaws in the individual layers. These problems are more common in PVDF than ceramics.

4.3.10 Resonance of Piezoelectric Actuators

Due to the elastic compliance and mass of a bimorph, it has to display mechanical resonance. Mechanical failure can occur if a bimorph is driven undamped and unloaded at the resonant frequency. It is known [11] that the large flexion that occurs can cause a strain failure. The mechanical damping is usually low giving significance to the resonant behaviour.

When the driving voltage is of a frequency near the resonant frequency, the motion of the bimorph will greatly accentuate that component of the driving voltage. The response of the bimorph to a step in the driving voltage has been given [14] as a graphic example. The step has a continuous frequency spectrum including the resonant frequency and so the bimorph "rings" following the STEP. Although other waveforms like the triangle waves contain smaller high frequency components, the ringing can still be significant.

It was found [11] that for a combined effective mass and compliance of a PZT-5H cantilevered bimorph, the resonant frequency $f_r = K_r/l^2$ where $K_r = 0.2$ Hzm^2 and l is the length of the cantilever. This problem can only be solved by either (a) constructing a circuit to counteract the resonance or (b) devising alternative means of mounting the bimorph [11].

4.3.11 Creep

It is stated [11] that following a step displacement, the PZT-5H bimorph's displacement continues to increase over a period of milliseconds to seconds to a value 15% larger than the initial displacement. This is called creep. At high electric fields an additional polarization of artificially poled ceramics occurs and the piezoelectric translator changes its expansion by a small amount, even if the applied voltage is constant [7]. This creeping depends logarithmically on time and has a value of about 1% to 2% during each order of magnitude increase in time [7]. None of these authors specify the creep time scale of these materials.

It is recognised [7] that there are two distinct types of creep. One is intrinsic to the bimorph and the other is attributable to its coupling to probes and holders.

Since creep and resonance inevitably contribute to the malfunction of the bimorph, they have to be reduced or eliminated. One method of reducing creep is by a mechanical preload but can only be eliminated [7] with a separate linear sensor operating in a closed loop circuit.

4.3.12 Problems Associated with Control of Piezoelectric Actuators

In order to construct a proper control of piezoelectric actuators, Syrinx [20] recommends the use of a power supply with a very good regulator and a large reservoir. This is because an electric signal applied to such an actuator usually decays after sometime and if improperly topped up, the actuator droops.

The impedance representing the mechanical system in a resonant device may become a resistance of relatively low value at resonance [9]. This is shunted by static capacitance. Shunt static capacitance is known [9] to be undesirable whether the device is designed for operation at resonance or for broad band below resonance operation. In electrically driven devices, it shunts the driving amplifier or other signal source requiring that the source be capable of supplying extra current.

The problem of control is made more complex by the fact that it is designed to look after both creep and resonance. The general solution for resonance is given [11] as being the removal of high frequency components from the driving voltage. This is effected by filtering or otherwise shaping the waveform if ringing is found to be significant above certain frequencies. The time course of the slow displacement like that of other viscoelastic relaxations, is not a simple linear or exponential relationship, but is adequately fitted by a sum of exponential decays with time constants nearly an order of magnitude apart [11]. The authors also state that shaping the driving signal to correct for such a creep requires compensation for each of the terms.

4.3.13 Conclusion

In general, the major limitations of the usefulness of piezoelectric actuators in micromanipulation are their slow speeds, high applied voltages that give very small change in length and the costly electronics to go with it.

Although Spanner and Marth [7] (and the claim put forward by the two companies (4.3)) strongly suggest that the positioning of monomode fibres will undoubtedly be an important future application of piezoelectric actuators, evidence from the investigations carried out on the subject still defies it. Effective reduction in hysteresis, creep, the cost of electronics to go with it, the time of operation and possibly the cost of manufacture are mandatory if these materials are to be used for precise positioning of optical fibres. Thus despite their attractive properties, piezoelctric actuators are still envisaged generally unsuitable.

4.4 ELECTRIC MOTOR ACTUATION

Mechanical manipulators have been more successful compared to other designs because they have no major inherent design limitations, more easily manufactured and consequently less expensive. This is because the manufacture of actuators (translators) used for assembling these manipulators is based up on known technology and there is high demand for them. There are currently a variety of commercially available motorised mechanical micropositioners produced by various manufacturers. Although their load capacity, accuracy, speed, repeatability and other properties already discussed vary a great deal, they are either motorised by DC or stepper motors both of which are geared down and converted to linear motion.

A few actuators thought to be representative of the type required for the alignment work are discussed in Appendix B. The reasons for picking Oriel Encoder Mike actuator for this work are outlined in that Appendix. To maintain consistency, the sequence of sub-section numbering (4.4.1 - 4.4.4) is continued in the Appendix and the references given there are presented at the end of this chapter.

4.5 FLUID ACTUATORS

Generally, mechanical micromanipulators or actuators are more successful because they have far less inherent design limitations. Thus, in addition to those already discussed, a brief survey of the non-mechanical ones like hydraulic and pneumatic actuators are also discussed in this section.

4.5.1 Pneumatic Actuators

It is stated [11] that while pneumatic and hydraulic manipulators give exellent control for manipulation in up to three dimensions, they can not be driven at high frequencies. In addition, they are usually bulky and quite expensive.

Pneumatic manipulators in particular, have two major limitations. Firstly, air volume changes due to variation in ambient temperature , result in spurious output movement. Secondly, because of air compressibility, the output movement does not correspond directly with the input movement and so there is a tendency for it to lag behind and then overshoot. This is most evident in situations where the output has to exert a force.

4.5.2 Hydraulic Actuators

In hydraulic micromanipulators, movement reduction is obtained in the same way as in pneumatic design except that liquid is used instead of air. There are severe practical difficulties involved both in excluding air bubbles and making good low-friction piston seals. Thus both of these micromanipulator types would not be of any great value in this exercise since their deficiencies will generally affect their accuracies and tolerances.

4.5.3 Conclusion

The overall literature analysis presented in this Chapter, strongly suggests that there are no better actuators presently suited to

laser-fibre alignment than the Oriel Encoder Mikes. Although relatively slow, its tolerance and accuracy and other notably supeior features it possesses, greatly favour it for use in this microalignment work.

The other actuators that could be seriously considered after the Encoder Mikes, are the Stepper Mikes (except for its price and size) and piezoelectric actuators in that order.

* * * *

REFERENCES.

1. P. Dario and D. De Rossi.
"Tactile Sensors and the gripping challenge", IEEE Spectrum. August 1985 (p.46-).

2. E.B. Jones.
"Measurement of pressue level, flow and temperature." Instrument Technology Vol.1. Butterworths 1965 (p.ix).

3. G.A. Olsen.
"Elements of Mechanics of Materials."
Prentice Hall 1982 (p. 84-85).

4. H.D. Baker, E.A. Ryder and N.H. Baker.
"Temperature Measurement in Engineering", John Wiley and Sons Inc., vol.1, 1953 (p.16). Second printing March, 1963.

5. Y. Umetani.
"Principle of a piezoelectric micromanipulator with tactile sensibility", Proceedings of the 8th International Symposium on Industrial Robots (ISIR), vol.1, 1978 (p.406-13).

6. American Gas Association Testing Laboratories.
"A study of Bimetallic Thermal Elements", Research Bulletin No.42 (Sponsored by Committee on Domestic Gas Research, F.M. Banks, Chairman). First published, 1947.(p.2,16-19).

7. K. Spanner and H. Marth.
"Precise positioning with piezoelectric translators (Direct Electrical to Mechanical Conversion yields Effective Micropositioning)", Lasers and Applications. August 1983 (p.61-63).

8. Y. Umetani and H. Suzuki.
"Piezoelectric micromanipulator in multi-degrees of freedom with tactile sensibility", Proceedings of the 10th International Symposium on Industrial Robots (ISIR), 1980 (p.571-79).

9. Vernitron Piezoelectric Division, Bedford, Ohio (USA).
"Piezoelectric Technology (Data for Designers) Catalogue", 1983 (p.1,4,7,10,13,17).

10. P.E. Bloomfield, R.A. Ferren, P.F. Radice, H. Stefanou, and O.S. Sprout.
"Piezo- and Pyroelectricity in Poly(Vinylidene Fluoride)", Naval Research Review, vol.31, 1978 (p.1-15).

11. D.P. Corey and A.J. Hudspeth.
"Mechanical Stimulation and Micromanipulation with Piezoelectric Bimorph Elements", Journal of Neuroscience Methods, vol.3, 1980 (p.183-202).

12. R. Hengstenberg.
"A piezoelectric device to aid penetration of small nerve fibres with micro-electrodes", Journal of Neuroscience Methods, vol.4, 1981 (p.249-255).

13. M. Toda.
"Voltage-induced large amplitude bending device - PVF2 bimorph - its properties and applications", Ferroelectrics, vol.32, 1981 (p.127-133). Gordon and Breach, Science Publishers, Inc.

14. D.H. Dameron and J.G. Linvill.
"Cylindrical PVF2 Electromechanical Transducers", Sensors and Actuators, vol.2, 1981/82 (p.73-84).

15. E.G. Thurston.
"The theoretical sensitivity of three types of rectangular bimorph transducers",Journal of Acoustics Society of America, vol.25, 1953 (p.870).

16. M. Toda.
"Design of Piezoelectric Polymer Motional Devices with various Structures", The Transactions of the IECE of Japan, vol.E-61, No.7, July 1978 (p.513-18).

17. M. Toda and S. Osaka.
"Electromotional device using PVF2 Multilayer Bimorph", The Transactions of the IECE of Japan, vol.E-61, No.7, July 1978 (p.507-512).

18. P.Dario, C. Domenici, R.Bardelli,D. De Rossi and P.C. Pinotti.
"Piezoelectric Polymers: New Sensor Materials for Robotic Applications", 13th International Symposium on Industrial Robots and Robots 7. Conference Proceedings, vol.2, April 17 - 21, 1983, Chicago - USA.(p.14-34).

19. G.M. Sessler.
"Piezoelectricity in Polyvinylidene Fluoride", Journal of Acoustics Society of America, Vol.70, No.6, Dec.1981(p.1596-1608)

20. Syrinx Precision Instruments Limited.
(Manufacturer of PVDF Polymer-Edinburg, U.K.)
Personal Communication.

21. Ealing Corporation, Mass.-USA.
"(Ealing Optics Catalog,1981)".

22. Microcontrole Evry, Cedex - France.
"(Microcontrole Catalog 1985-86)".

23. Oriel Corporation, Conneticut-USA.
"(Oriel Motorized Precision Motion Devices With Position Read Out Catalog and personal communication)".

24. Newport Corporation, California, USA.
"(Newport Corporation Catalog 1983-84 and The New Product Supplement Catalog 1985)".

25. McLennan Servo Supplies Ltd, Surrey - England.
"Digitran Stepper Motor Drive TM 164C Catalog".

26. Unimatic Engineers Ltd.
"Stepping Motors - Sigma Motion Control Catalog", Printed in USA, 1984.

CHAPTER 5

COUPLINGS AND THE CONSTRUCTION OF MANIPULATORS

CHAPTER OVERVIEW

Manipulators are required for different purposes. In this chapter, they are examined for the purpose of alignment. This is tackled by looking at different types of couplings (actuators) inorder to gang them together to form the required manipulator. That is, manipulators need actuators to be coupled together either in series or parallel as discussed in section 5.1. In section 5.7, a three-legged parallel coupling called the Kelvin Coupling (Figure 5.6.1(a)) is analysed for a possible transformation into a four degree of freedom manipulator for this alignment.

The Kelvin coupling consists of two parts. One of them (a tripod) has three vertical legs that make contacts with a second surface (5.6.1). These legs are close to each other and this makes it difficult to introduce a fourth leg let alone incorporating actuators. This in turn leads to difficulties in manipulation. Inorder to overcome these difficulties, a variant of the same coupling is formed (5.7) by moving the legs further apart and introducing a fourth leg. This variant is then later (chapter 6) transformed into a manipulator by incorporating actuators in all the four legs for purposes of alignment. The need for a four degree of freedom manipulator is explained by the fact that two misaligned lines in space require four independent variables to define fully their misalignment (3.2).

A general discussion of couplings including series and parallel couplings is also presented. For purposes of completeness of the discussion on couplings, a distinction is also made between form and force closures.

5.0 INTRODUCTION

The launching of a non-linear laser beam into a mono- or multimode optical fibre needs a manipulator. The basic unit required for the construction of a manipulator is called an actuator. An actuator may

be defined (4.1) as a coupling that provides unidirectional motion. They are normally coupled together either in series or parallel to form the respective manipulators (series or parallel). Series coupling is structurally the simplest of the two. In an attempt to build a manipulator with actuators in parallel, it is necessary to first examine suitable couplings to see how they can be modified to accomodate the actuators. In this chapter, a distinction is made between series and parallel couplings as well as between form and force closures.

5.1 MANIPULATORS

As already described (section 4.1), a manipulator consists of three or more actuators coupled together such that each actuator executes motion in or about a particular direction. This means that its overall number of degrees of freedom may be 3, 4, 5 or 6 depending on the purpose for which the manipulator is required. The particular number of degrees of freedom mentioned above can either be all linear or mixed with rotation by incorporating the appropriate actuators.

The actuators are assembled either in series or parallel giving rise to a series or parallel manipulator respectively. These two types of manipulators have advantages and disadvantages over each other. Discussions of these two types of manipulators including their advantages and disadvantages are relegated to chapter 6 to leave room for couplings here.

Since the object of this chapter is to seek a manipulator for the alignment of lines in space, it is appropriate to point out the reason for the need of one with four degrees of freedom. This can be explained by referring to the discussions of the alignment of two skew lines in space (section 3.2). In that section, it is established that four independent variables are required to fully describe the misalignment of two skew lines. This implies that a four degree of freedom manipulator is required to correct the misalignment. Either a series or parallel manipulator can be used but the latter has advantage over the former because generally, it accumulates less errors during manipulation.

5.2 COUPLINGS

The term coupling is used to describe any means by which a wrench can be trasmitted from one body to another. Phillips [1] quotes others who describe a wrench in terms of a dual vector quantity comprising of (a) a resultant force upon the whole body acting along a given axis and (b) a couple acting parallel with the force and applicable at every point within the body. This statement is only partly correct as confirmed by Hunt [2] who describes a wrench as a force-couple combination associated with a particular line called the wrench axis or screw axis. The combination consists of a resultant force upon the whole body acting along the wrench axis but the resultant couple acts at a specified point parallel to the same axis.

Couplings are introduced with different objectives in mind. Some of the objectives will simply be mentioned in this section. As already stated, couplings are discussed here with the aim of building a manipulator for alignment. In their most general form, they include fluid (hydraulic), flexible, elastic, gravitational and contact couplings. A contact coupling, can be described as a connected network of bodies, of which two are the only members in contact with bodies that do not belong to the network. If it comprises of only two bodies, this coupling is described as simple and the contacting elements are referred to [2] as a kinematic pair. Others with more than two bodies (Hooke's joint or ball and roller bearings for example) are compound.

Broersma [3] explains that the primary role of couplings is to permit certain machine elements either to be manufactured in separate parts to a higher degree of accuracy or to be heat treated separately to a more uniform quality. Generally, they are used for both purposes and in addition [3] to obtain increased freedom of movement of machine parts relative to each other. Thus inorder to provide for dynamic freedom of the machine parts relative to each other, the flexible, fluid or electromagnetic couplings are employed. These couplings yield the possibilty of dampening certain types of vibrations (for example, torsional and turbine blade vibrations) or impact loads

(say, propeller loads) propagated from one point of a propulsion unit to another [3]. That is, they provide compliance. Contact couplings on the other hand, serve to increase quasi-static freedom of relative movement between parts. It is stated [3] that such a coupling can be used to absorb misalignment between a prime mover and a marine gear due to changes in their relative position created by thermal expansion. This change depends on speed and power conditions. The expansion occurs slowly enough to enable the acceleration effects to be assumed negligible during the expansion process. Such a process is known [3] as quasi-static. Another example of a contact coupling is an involute tooth type coupling found between steam or gas turbine and the first reduction pinion of a gear. This is described [3] as fine toothed coupling.

Trylinski [4], however, narrows down the use of couplings to the connection of shafts and that they can be divided into flexible and rigid types. While flexible couplings provide elastic connection of shafts, allow for some misalignment and damp shocks and vibrations, rigid couplings provide either for complete rigdity or just in the direction of rotation. Those that provide rigidity in the direction of rotation may be sub-divided into (a) expansion couplings where the shaft has freedom of axial movement; (b) slip couplings if the shaft axes can shift while remaining parallel to each other; and (c) universal joint couplings where the angle formed by the joined shafts can vary [4].

Rigid couplings have severe limitations. Stewart [5] states that if one of the coupled shafts is supported in more than one bearing, then unless the shaft system itself is flexible, considerable loading and wear will develop at the bearings and in the shaft due to small amounts of misalignments. The solution [5] is to employ a common housing for the two shafts and to ensure that the tolerances and accuracy of fitting are such as to achieve the necessary precise alignment.

Sinclair [6] who deeply studied hydraulic couplings points out that fluid couplings are essentially of the two element type having only a primary and secondary member without any intermediate guide vane or reaction member

such as is necessary to obtain torque conversion. The torque at the output shaft being equal to the torque at the input shaft under all conditions of speed, filling and slip.

5.3 FORM AND FORCE CLOSURES

Since this chapter is largely dedicated to the discussions of the different types of couplings, there is need to give some space to form and force closures for purposes of completeness. These are the two major methods of locking couplings together. A distinction between them will help to clarify the methods by which couplings interact together.

The movement of a rigid body in space can be constrained (fully or partially) by making contacts with fixed surfaces. Lakshminarayana [7] states that if such a contact is maintained by virtue of the action of certain forces, then it is called force closure. When contact is maintained without reference to the applied forces, then it is called form closure [7].

It might appear rather premature to talk about the Kelvin coupling at this stage but the use of gravity and spring force to close two bodies is well illustrated by this coupling. The coupling is introduced in the summary and it is hoped that this will suffice for it to be used here to illustrate force closure. Otherwise full details can be found in section 5.6.1.

Normaly, the elements of this coupling (Figure 5.6.1(a)) are closed by the force of gravity. Pollard [8] and Furse [9] explain that whenever gravity can not be utilised to maintain contacts, spring force applied at one or more points may be used. In the Kelvin coupling, separation of the elements can be avoided by this method. It is important that none of these springs should define a position for the body on which they act but to apply unidirectional force only [9]. That is, the direction of the applied forces must be determined correctly. This is called force closure.

Figure 5.3(a) illustrates another application of force closure in

which A can be adjusted relative to a fixed plate B. Rod A1 has a V-groove at its free end and is fixed to A while A2 has a sphere at its free end and is screwed to A. B also carries two rods B1 and B2 both fixed to it. B1 has a hemispherical end which interacts with the V-groove of A1 while the trihedral hollow of B2 interacts with A2. The result is five constraints leaving A to rotate about a single axis that joins the centres of the two spheres B1 and A2. Inorder to fix A relative to B, screw M is arranged to contact a prolongation of A. The two bodies are then locked together by two springs K. Rotation of M will then make A rotate about the given axis (Figure 5.3(a)). This approach was employed [8] to adjust the slit of a large spectograph.

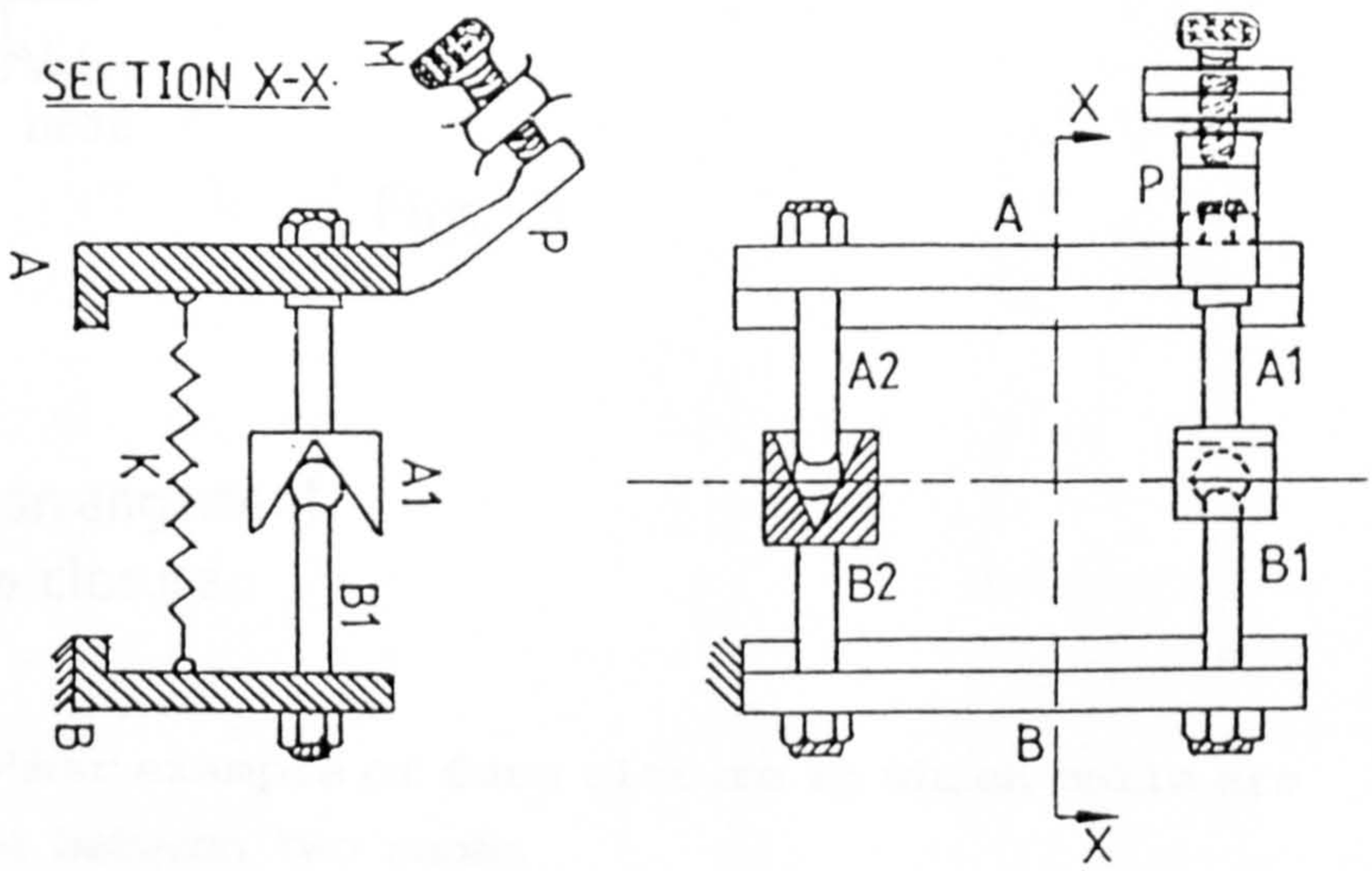

Fig, 5,3 (a) Bodies A and B are locked in a force closure arrangement by two springs K

Another example of a force closure is a cam and tappet mechanism shown in Figure 5.3(b). As the cam rotates, the spring K1 pushes upwards to close the valve.

Figure 5.3(c) illutrates a simple example of form closure. It is a cam mechanism in which the curve is made in form of a slot forming two equidistant curves c1 and c2. The roller R is unable to roll simultaneously on both surfaces thus clearence is required between the roller and the two surfaces. There are a number of other examples of cam mechanisms that illustrate form closure.

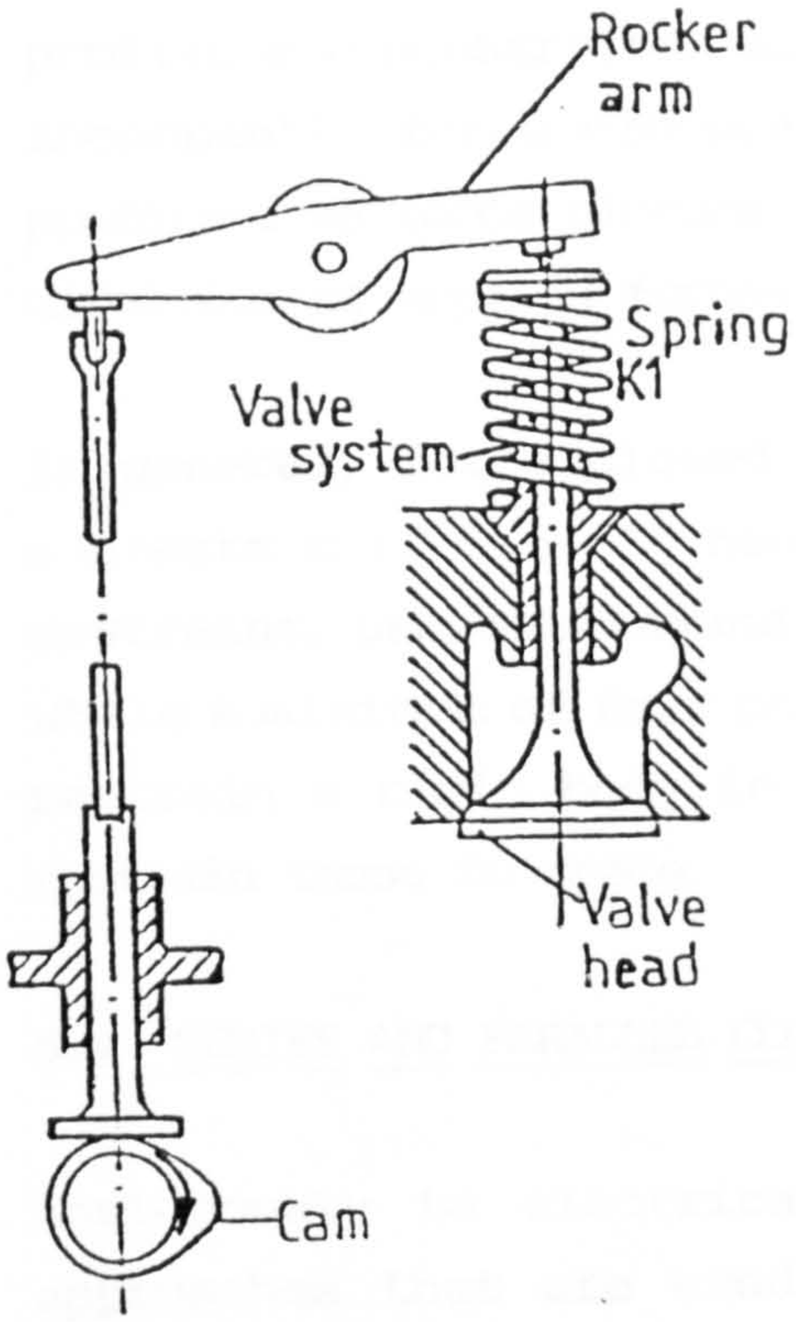

(b) Cam and tappet arrangement illustrating force closure.

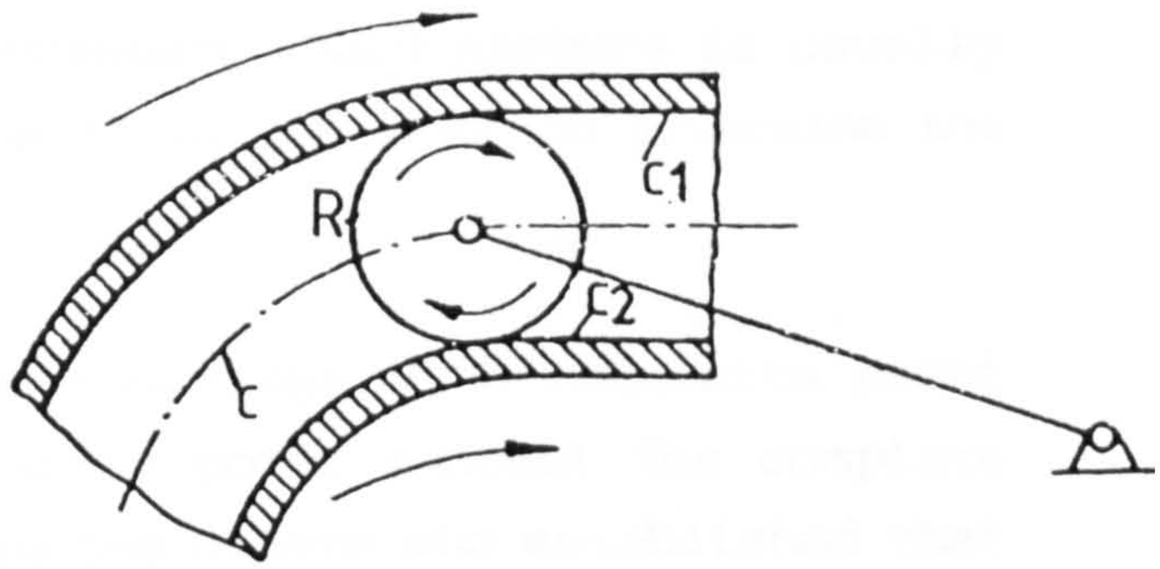

(c) Cam mechanism

Figs, 5,3

Figure 5.3(d) is another example of form closure in which balls are trapped inside a cage between two races.

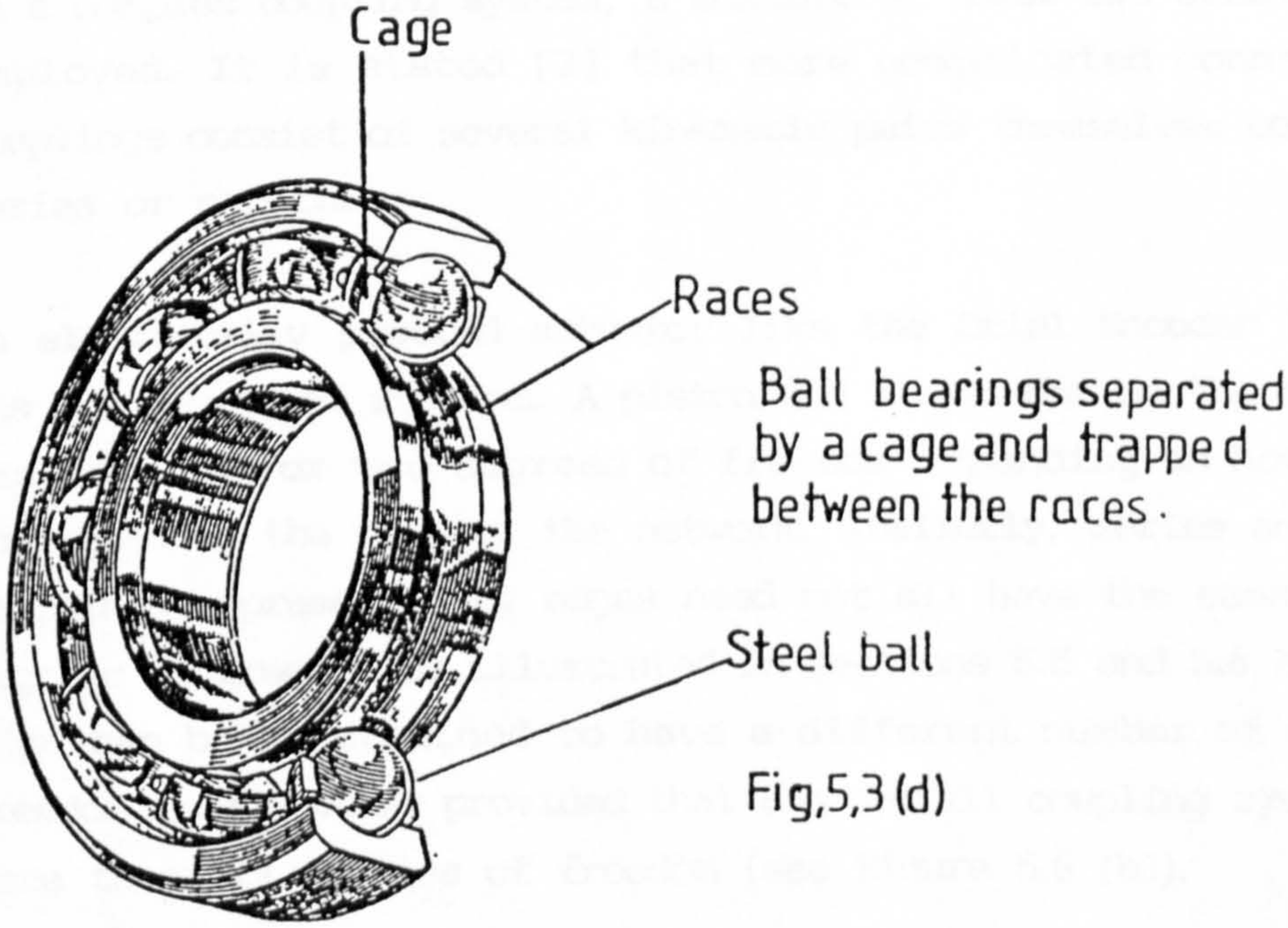

Fig, 5,3 (d)

Lower pairs where an element completely contains another within its profile are constrained and closure is complete. If restraint is incomplete, force closure is necessary. Form closure is usually preferred to force closure because it is difficult to determine the direction of applied forces.

In general, force closed higher couplings with requisite point contacts c (f = 6-c), need an extra point contact for complete restraint. Laksminarayana [7] quotes others who established that while a minimum of four point contacts are required to completely restrain a rigid body in planar motion, seven are necessary to restrain those in space.

5.4 SERIES AND PARALLEL COUPLINGS

Analogously to electrical network circuits, the two extreme approaches that are used for coupling bodies together may be described as the series and parallel arrangements. While the series arrangement consists of couplings joined end to end and therefore forming a single chain (zero loop), the parallel coupling method forms independent loops or circuits. A distinction between these two couplings is made in sections 5.5 and 5.6 below.

In a complex coupling system, a mixture of these two arrangements is employed. It is stated [2] that more complicated connections or couplings consist of several kinematic pairs themselves connected in series or parallel.

An electrically powered actuator like the Oriel Encoder Mike (4.4), has one degree of freedom. A piston and a cylinder on the other hand, can have one or two degrees of freedom depending on how they are connected to the rest of the network. Similarly, series and parallel couplings represented by edges need not all have the same number of degrees of freedom as illustrated in sections 5.5 and 5.6 below. Each edge can be constrained to have a different number of degrees of freedom from another provided that the overall coupling system has no more than six degrees of freedom (see Figure 5.6 (b)).

NOTE: (See p.87, parag.2)

This is because in a serial manipulator, each actuator is carried by the Other actuators below it on the arm. Therefore errors due to encoder inaccuracies and other system control effects (eg steady state errors) are cumulative.

5.5 SERIES COUPLINGS

In general, the series coupling arrangement is represented graphically as in Figure 5.5. These couplings are connected end to end and in turn connect body A to B. The bodies are represented by vertices none of which needs to be fixed. This arrangement allows six degrees of freedom because there are six edges each representing a single degree of freedom (f = 1).

Since this chapter deals largely with the development of a parallel manipulator for the alignment of lines, little needs to be said about series couplings. It is therefore considered appropriate to terminate further discussion of series couplings here.

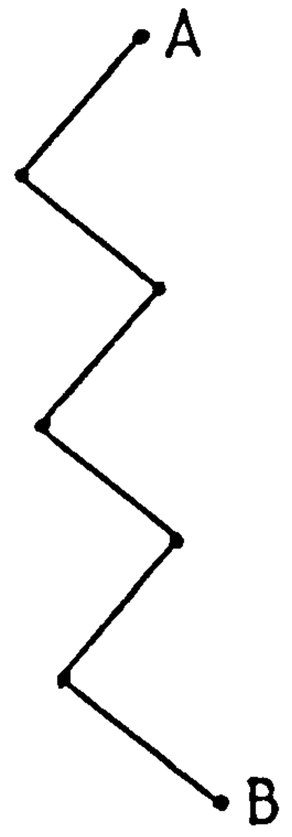

Fig 5,5 Graphical representation of a series coupling.

5.6 PARALLEL COUPLINGS

The parallel coupling arrangement of Figure 5.6(a) is a graphical representation drawn with each edge independently connecting body A to B. This results in the formation of a loop between any two edges. This coupling arrangement has six edges connecting A to B but only five independent loops are formed. It allows zero degrees of freedom but each of the six edges represents five degrees of freedom (f = 5).

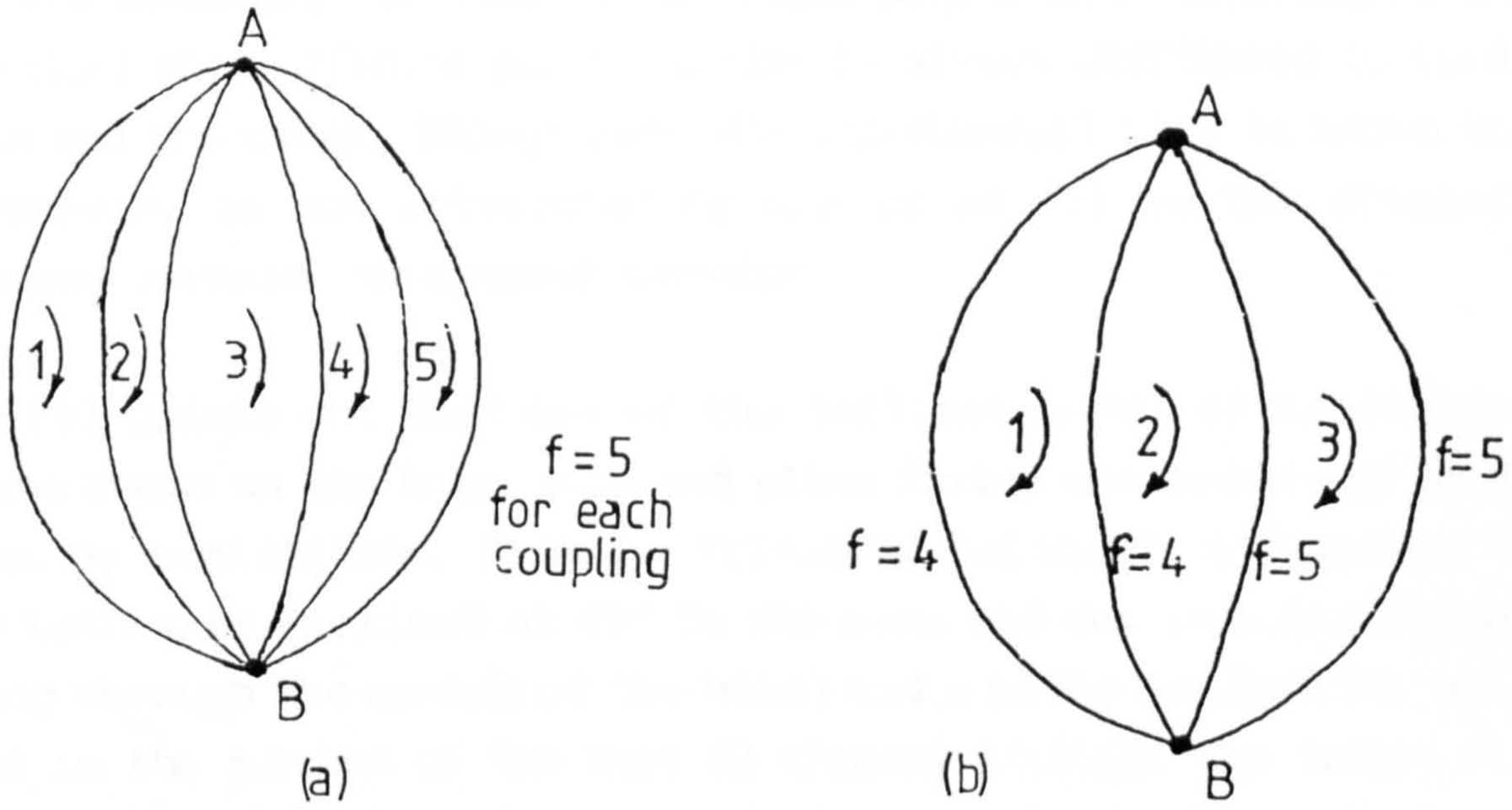

Fig.5,6 Graphical representation of parallel couplings.

There is an upper limit on the number of independent circuits associated with a graphical representation of a parallel coupling. Figure 5.6(a) is one such example in which each of the six edges of the graphical representation of a zero degree of freedom coupling has one constraint. That is, if an actuator is introduced into the coupling represented by each edge, the resulting manipulator acquires six degrees of freedom. Since the object of this study is to produce a four degree of freedom manipulator for alignment purposes (5.1), four independent paths from A to B need to be created. This is an intermediate parallel arrangement (Figure 5.6 (b)) in which two edges are each associated with two constraints (f = 4) while each of the remaining pair has one constraint (f = 5). A coupling that matches this type of arrangement could be modified to achieve the required manipulator.

This leads to the discussion of the Kelvin coupling presented below (5.6.1). As stated earlier, this is a parallel coupling in which three vertical legs of one component interacts and makes contact with a second surface. The contacts being maintained by gravity.

5.6.1 The Kelvin Coupling

There are evidently two methods of supporting bodies (instruments in particular) in a definite position. One is always attributed to Lord Kelvin and the other, though according to Maxwell [10] is known to Lord Kelvin, is not attributed by him or as far as the present literature reveals, to a named inventor.

Furse [9] points out that one of the earliest forms of kinematic fixtures known as the hole, slot and plane fixing was devised by Lord Kelvin. By implication, it has a trihedral hollow T, a V-groove G (with both axes inclined at 45^{o} to the base and cut in a direction passing through the centre of the hole) and a plane surface Ps, all formed in the surface of the base E2 (Figure 5.6.1(a)). The tripod E1 has three hemispherical feet one of which rests in the trihedral hollow T and produces three point contacts, a second one interacts with G and makes two point contacts while the third rests on the plane surface Ps making a single point contact. Overall, six point contacts are made between the hemispherical feet and the base E2 such that E1 is fully constrained and kept in place with respect to E2. Ps and T substitute S and H as originally used by Lord Kelvin to avoid confusing them with the universal representation of the spherical joint and the screw pair respectively.

It is stated [10] that in his design, Lord Kelvin chose to arrange the tripod E1 to have three hemispherical feet of unequal lengths. The longest foot was made to interact with T making three point contacts, the second longest interacted with G producing two point contacts and the shortest rested on Ps making a single point contact. There is no advantage of this over the tripod with equal leg lengths because all the forces still pass through the legs and so, there is no bending. In fact, that method presents more design problems because it has to cater for the appropriate dimensions of G and T to accomodate the different leg lengths so that E1 is levelled with respect to E2. This point was seized by later designers who made all legs equal.

The second method to which even Maxwell [10] does not attach a name,

consists of three similar V-grooves G formed on the surface of B2 (Figure 5.6.1(b)). The directions of these V-grooves meet in a single point preferably at an angle of 120^{o}. It is not essential that the grooves meet at this angle but it is preferred because of symmetry and also ensures well conditioning [11]. Another possibility is that the three V-grooves could be engraved on B2 so that the three lines (p,q,r) of intersection of their planes meet each other at different points a,b,c shown (exagerated) in Figure 5.6.1(c). The tripod B1 with three equal hemispherical feet, each of which interacts with G and makes two point contacts, is fully constrained and kept in place with respect to B2.

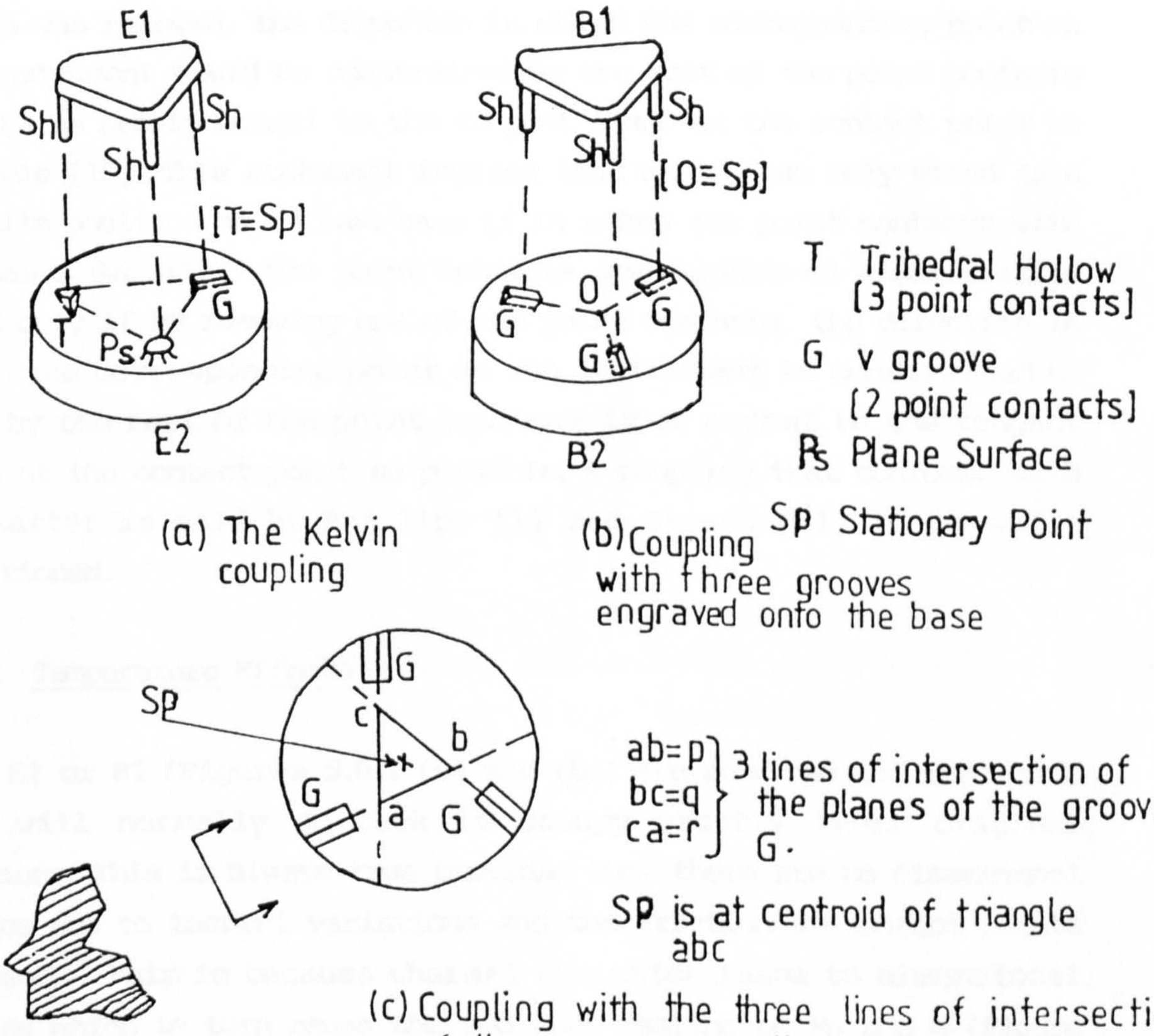

Fig, 5,6,1

In Lord Kelvin's method where the tripod has three unequal feet, it is impossible to place any but the correct foot into the hole without detecting the mistake. However, it is mechanically difficult to produce T and normally a conical hollow is used but this is kinematically unsound unless the mating foot is machined away to provide three point contacts [9]. It is stated [12] that a trihedral hollow is preferred to a conical hollow because it is simply constructed by pressing a trihedral punch into soft brass which is less costly to produce than drilling a conical hollow. Above all, it ensures that proper contacts are made. Other methods of constructing the trihedral hollow are discussed in section 5.6.3.

For an instrument to stand in a definite position on a fixed base, it must have six point contacts arranged such that if one of the contact points was removed, the direction in which the corresponding point on the instrument would be constrained by the rest of the point contacts must be as nearly normal to the tangent plane at the contact point as possible [10]. This statement implies that a body can only stand in a definite position on a fixed base if it makes six point contacts with the base. Secondly, the point contacts are considered kinematically sound only if by removing one of the point contacts, the direction in which the corresponding point on the instrument is constrained to move by the rest of the point contacts is as normal to the tangent plane at the contact point as possible. A coupling that conforms with the latter is said by Phillips [1] and Steeds [11] to be well-conditioned.

5.6.2 Temperature Effects

When E1 or B1 (Figures 5.6.1 (a) and (b)) are removed and replaced, they will normally go back to occupy exactly their original positions. This is always true provided that there are no dimensional changes due to thermal variations and the friction at contact points are small. This is because thermal variation leads to dimensional changes which in turn cause the two feet resting on Ps and G (Figure 5.6.1(a)) to slide on the plane surface Ps and along the V-groove G respectively. The third foot ,however, remains seated in T. If the frictional forces at Ps and G are small, then the resulting strains

will be negligible [2]. The stationary point (Sp), which is a point on the base of the couplings that does not move with respect to the feet, is therefore left at the third foot position in T [10].

In Figure 5.6.1(b), however, thermal changes will cause all the three feet to slide outwards in their V-locations and if friction is small, the strain will be negligible. Consequently, the centre of the tripod B1 remains unchanged with respect to the centre of the base B2 [10]. This means that the centre of the tripod B1 lies on the same vertical axis as the stationary point (Sp) located at O on the surface of B2.

This type of coupling is not only suited to the design of instruments where the vertical axis of the tripod needs to retain its position relative to the base regardless of thermal changes but also ensures that the tripod resumes its original position precisely in the event of a displacement. Symmetry is also maintained in this coupling.

In Figure 5.6.1 (c), when there is a relative expansion of the tripod with respect to the base, the tripod experiences a small rotation. This is because the feet are constrained to slide in directions other than 120^{o} to each other.

5.6.3 Methods of forming a trihedral hollow

As stated in section 5.6.1, one major problem with the Kelvin coupling is the production of the trihedral hollow T. Two simple methods of producing T which have been successfully used are outlined in [9]. The first consists of three inclined surfaces at one end of a cylindrical rod or block. An angled cutter, usually 45^{o} is then used to make three successive cuts across the diameter of the rod or block; rotating it through 120^{o} for each cut. This is shown in Figure 5.6.3(a).

The second method (Figure 5.6.3(b)) consists of three balls pressed into a hole or ring to give three contact points with a hemispherical foot. The size of the hole (ring) may be calculated [9] from $D = d(1 + \sec 30^{o})$ where D is the diameter of the hole and d the diameter of the balls.

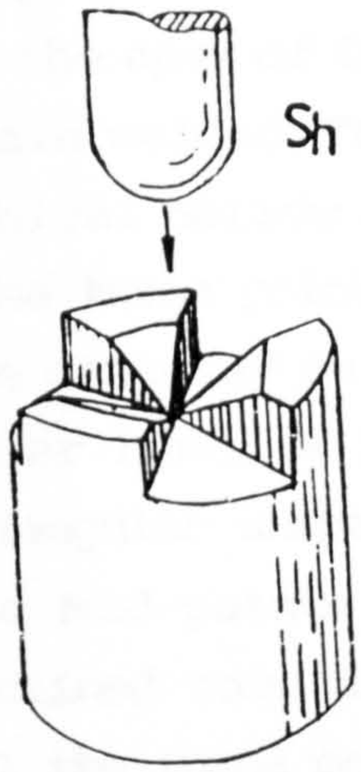

(a) Three inclined surfaces forming a trihedral hollow

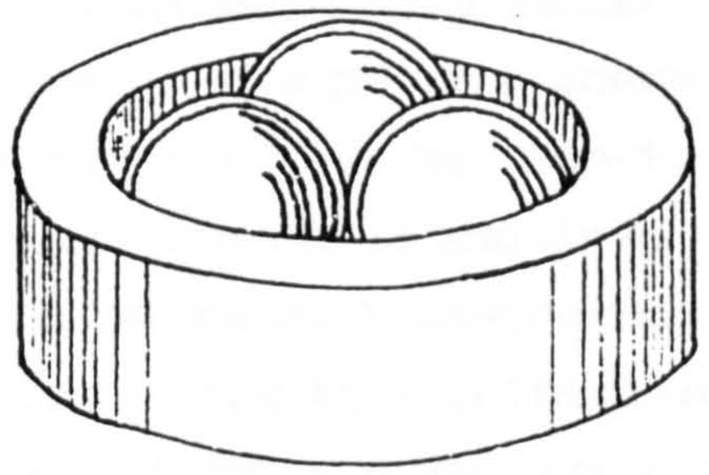

(b) Balls that provide three point contacts

Fig,5,6,3

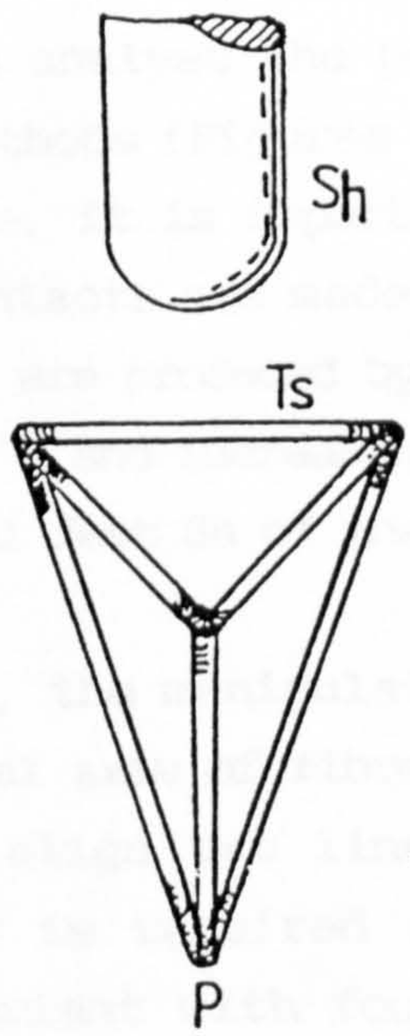

Fig,5,6,3(c) Fused Cylindrical rods forming a trihedral hollow.

Apart from these two and a third in which a conical hollow is used to replace T, Figure 5.6.3(c) shows yet another method which consists of three cylindrical rods welded together into an equilateral triangular shape Ts. Three other rods are in turn symmetrically welded onto each of the apex of Ts and all three converge at a point P where they are again welded. The trihedral structure can then be inserted in to a conical hollow and welded in postion. The three inclined rods then make three point contacts with an interacting hemispherical foot in the same way as the trihedral hollow of the Kelvin Coupling. On the other hand, a larger hemispherical foot resting on the welded triangular shaped rods Ts makes a single point contact with each of the mid-points of the sides of the triangle. In that case, the inclined rods do not support the interacting hemispherical foot. In all the three methods discussed above, the three common normals meet at a single point inside the sphere.

5.7 VARIATION ON THE KELVIN AND 3-GROOVED COUPLING PRINCIPLES

The review of the different types of couplings reveals that the Kelvin coupling is suitable for modification to achieve the required manipulator. As a start to this construction, it is necessary to examine and analyse the possible variants arising from the two coupling methods (Figures 5.6.1 (a) and (b)). In order to carry out such analysis, it is important to first understand the various ways by which contacts are made between the two bodies. This is because the variants are produced by splitting up the trihedral hollow T and the V-groove G and increasing the corresponding number of interacting hemispherical feet Sh of the tripod.

Essentially, the manipulator is needed for aligning two lines in space (central axis of fibre with the central axis of a laser beam). Inorder to align two lines in space, a four degree of freedom manipulator is required as already discussed (3.2 and 5.1). A coupling variant with four feet is therefore sought inorder to produce this manipulator. For purposes of completeness, coupling variants with five and six feet are also briefly mentioned.

NOTE: (See p.95, parag. 3, line 11)

Fig.5.7(d) (p.96) is a special case where feet A1 and A2 lie in the same plane as the 90^{o} v-groove. If A1 and A2 lie in a different plane, then the normal forces will be skew.

In both couplings (Figures 5.6.1 (a) and (b)), not only must the bodies be properly constrained but the contacts between them should be well conditioned. It is stated [11] that the force exerted between the surfaces of an ill conditioned contact is always greater than that in a well conditioned one.

In the Kelvin coupling, the three ways of contacting surfaces are between a sphere Sh and a plane surface Ps, a sphere Sh and a V-groove G and a sphere Sh and a trihedral hollow T. These will be referred to here and the rest of the chapter as the ShPs, ShG and ShT -configurations respectively. In the ShPs-configuration, the common normal passes through the centre of the sphere. In ShG, the two common normals intersect at the centre of the sphere and similarly for ShT where the three normal forces also intersect at the centre of the sphere. Configuration ShG is shown in Figures 5.7(a), (b) and (c) while ShT is shown in Figure 5.7 (e). Configuration ShPs is illustrated by Figure 5.7(d) where contacts are made between the plane surfaces and each of the hemispherical feet.

However, overturning configuration ShG (as in Figure 5.7(c)) and indeed the other two configurations does not affect the normal forces provided that the two bodies in question can support each other's weight. They still intersect at the centre of the sphere as in ShG and ShT and pass through the hemispherical foot as in ShPs. That is, the set up in each of the three configurations is interchangeable. An inversion of these three configurations produces the same results. That is, the plane surface, the V-groove and the trihedral hollow can be replaced by short hemispherical projections or stumps while they are transferred on to the contacting surfaces of the corresponding hemispherical feet. It is shown (Figure 5.7(d)) that by having two hemispherical feet A1 and A2 resting on an enlarged V-groove instead of one as in Figure 5.7(a), the common normals N1 and N2 can still be made to intersect at a single point. This is a general case where lengths of the feet are unequal. The feet can also be chosen to have equal lengths without affecting the kinematical soundness of the supports. If such changes are to be effected on the V-grooves and trihedral hollow of Figures 5.6.1(a) and (b), then the final orientations of the resultant planes must be maintained in relation

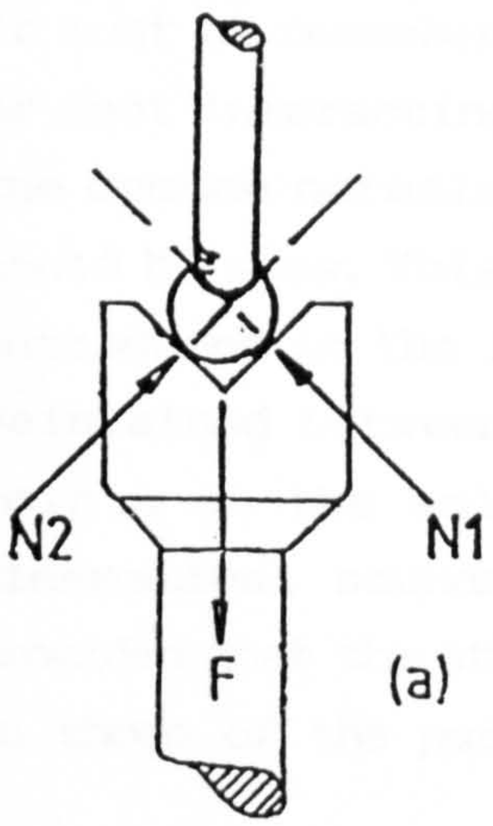

(a)

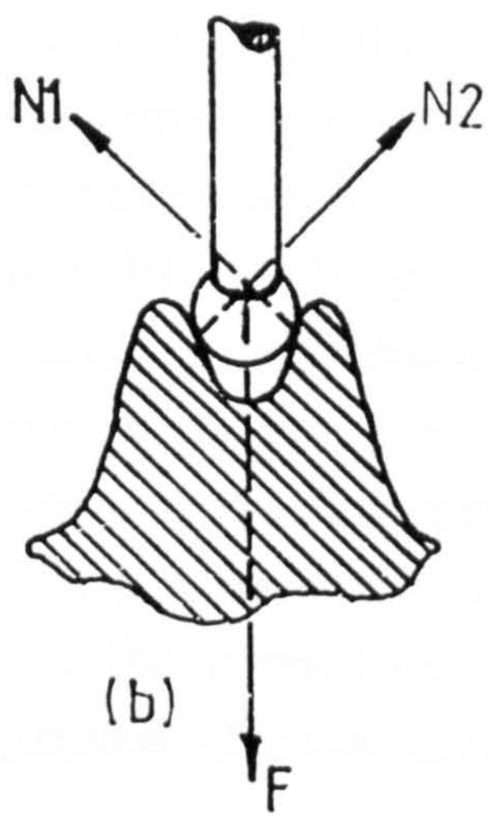

(b)

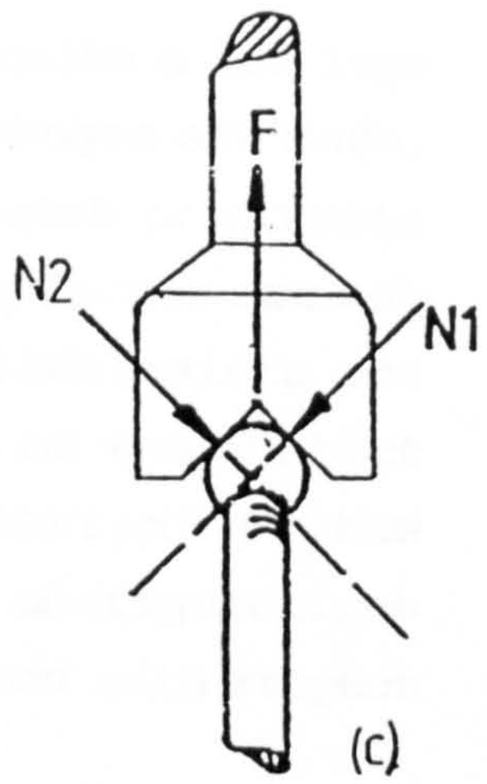

(c)

Figs, 5,7

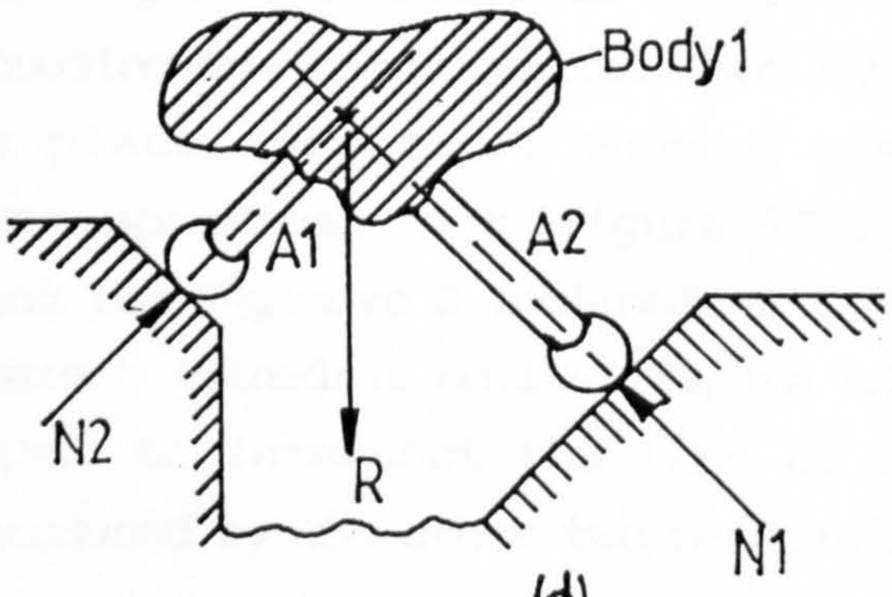

(d)

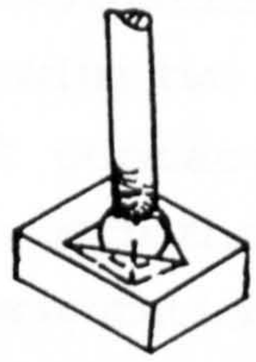

Fig,5,7 (e) Hemispherical foot interacting with the trihedral hollow.

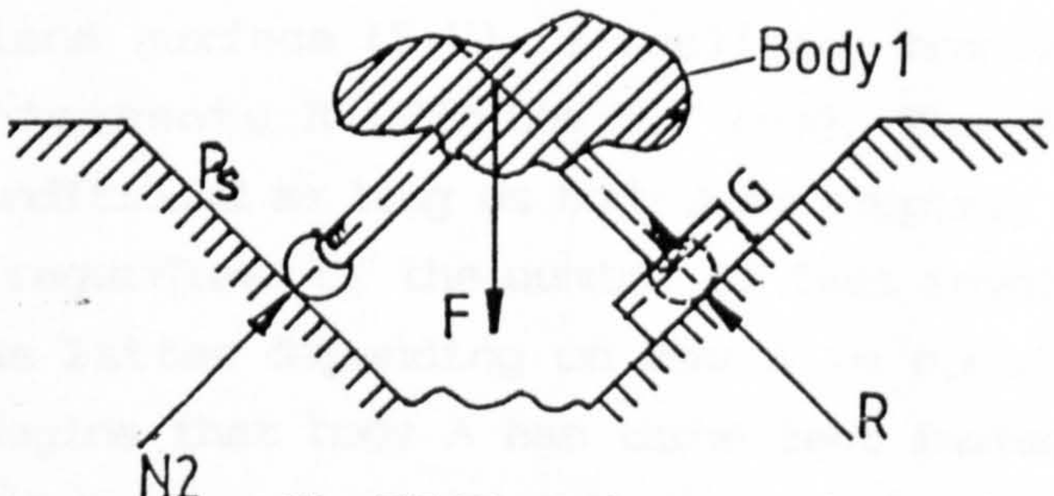

Fig,5,7 (f) A support configuration derived from (e) above.

Figs. 5,7 (b) to (d) above show support configurations derived from the V-groove configuration of Fig. 5,7(a).

to those of the parent V-grooves or trihedral hollow in the two couplings. This ensures well-conditioning.

It must be remembered that even though there may be quite a few legs or feet interacting with a second body after the changes are made, the common normals for a particular expanded V-groove or grooves could be skew. This is acceptable as long as bending forces are not introduced in the legs of body 1 and the correct constraints are maintained between the bodies. Also, the heights of the contact points on the enlarged (new) planes are unimportant to the kinematical soundness of the resultant support configurations provided that the attitudes of the planes are maintained with respect to those of the parent V-grooves (Figure 5.7(d)).

In the ShT-configuration (Figure 5.7(e)), the three contact normals intersect inside the sphere. The three point contacts in such a configuration could be regarded as a combination of a V-groove G housing one hemispherical foot and thus making two point contacts and a plane surface Ps making one point contact with a second hemispherical foot (Figure 5.7(f)). With both the plane surface Ps and the V-groove G inclined at the same orientations as those of the parent trihedral hollow (Figure 5.7(e)), the contact normal N2 can be made to intersect the line of action of the resultant force R produced by the other two normals in the V-groove. However, if the V-groove as well as the plane surface (X-X) are horizontal (Figure 5.7(g)), then the contact normal N2 will meet R at infinty. If the plane surface (Y-Y) is inclined, however, the contact normal N2 intersects R (Figure 5.7 (g)). The former is regarded well-conditioned as long as body A is properly constrained with respect to B regardless of the number of feet involved. This is also true for the latter depending on how A is constrained with respect to B. Imagine that body A has three feet instead of two as ilustrated and that B has two parallel V-grooves (drawn as in Figure 5.7(g) with the second groove hidden) such that two feet interact with the grooves and the third rests on a plane surface leaving one degree of freedom. It is pointed out [11] that the contact made with the plane horizontal surface X-X is well-conditioned while that made with Y-Y is ill-conditioned. This is because the common tangent plane X-X at

the contact point Px is perpendicular to the direction in which Px would move if the surface X-X were removed but in the latter, the tangent plane Y-Y is at an acute angle to the direction of motion of the equivalent point Py.

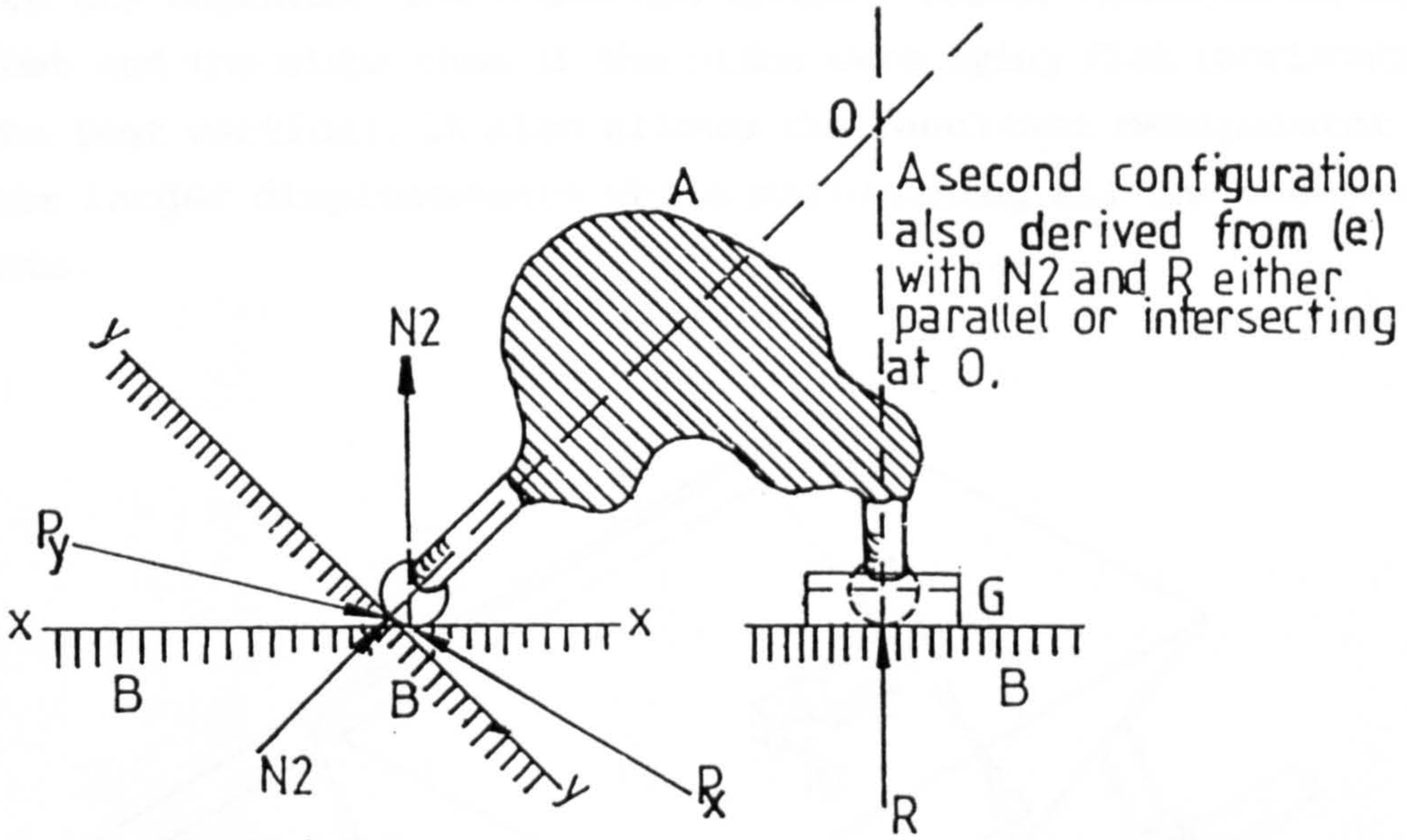

Fig.5.7 (g)

The trihedral hollow can still be further split up so that the three planes are inclined at the same orientations as the corresponding parent planes each making contact with a hemispherical foot. It does not matter whether or not all the three common normals or just two intersect provided that the two bodies are properly constrained and all the contacts are well-conditioned irrespective of the number of feet involved.

Several possible alternative support configurations can be derived from the different contact cases already examined. Figure 5.7(h) is just one of many support configurations derived from the Kelvin coupling. It is produced by splitting up the trihedral hollow T of the Kelvin coupling (Figure 5.6.1(a)) to form a plane surface Tp and a V-groove Tg. The original V-groove G and the plane surface Ps being left unchanged. The new and old V-grooves Tg and G are closer to each other than they are from the new and old plane surfaces Tp and Ps.

The original tripod is replaced by a triangular prism (body A) whose hemispherical feet Sh interact with the V-grooves and the plane surfaces. Shapes do not affect the kinematical soundness of this coupling as long as the contacts are well conditioned. The original flat base is changed in to two inclined slabs 1 and 2 on to which the grooves are engraved. These changes enhance better contacts between the feet and the slabs than if the slabs were lying flat (horizontal) and the feet vertical. It also allows the resultant manipulator to execute larger displacements while maintaining all the necessary contacts.

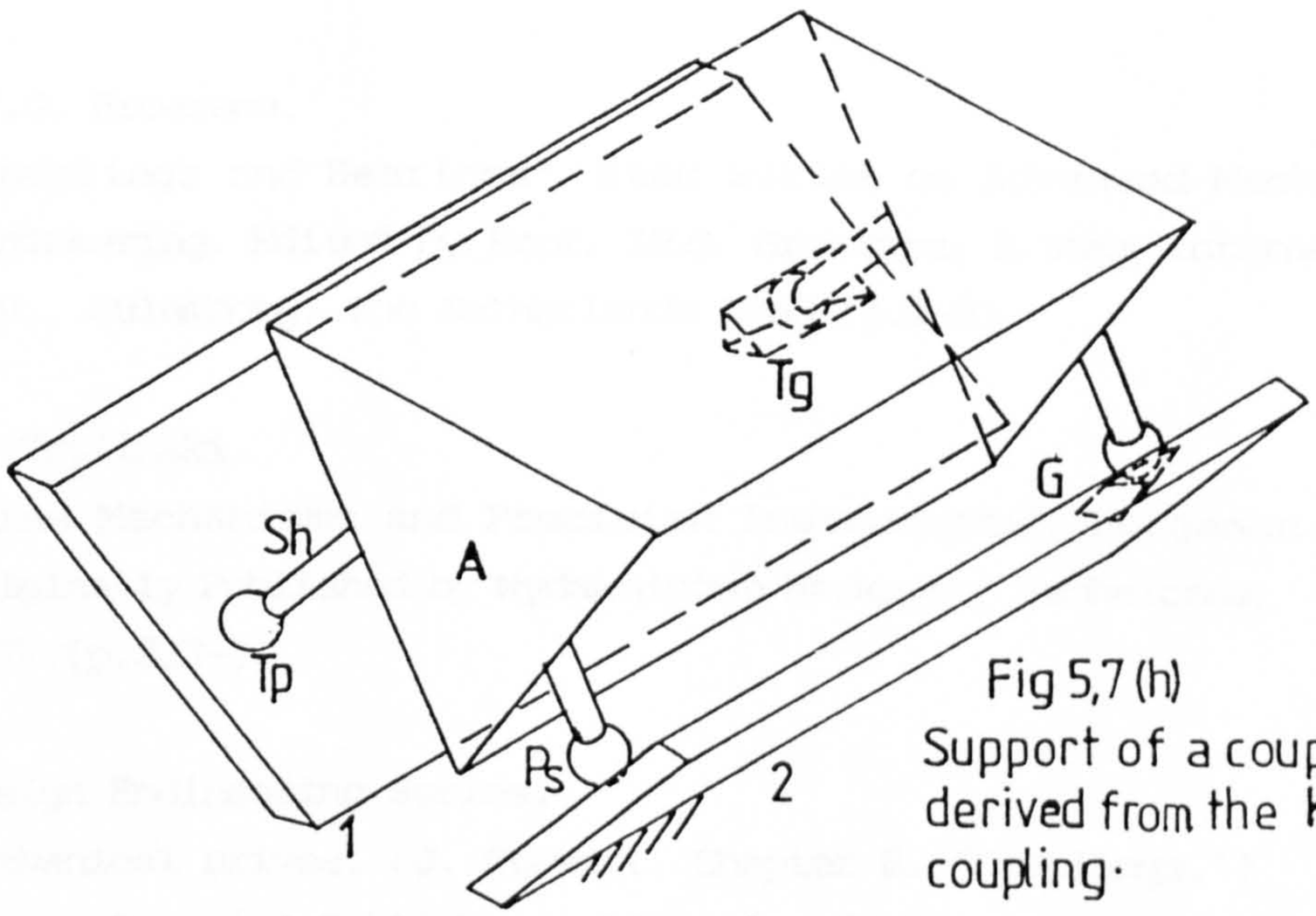

Fig 5,7 (h)
Support of a coupling derived from the Kelvin coupling.

The new and original V-grooves Tg and G can each be further split in turn increasing the number of feet of body A to five and six respectively.

REFERENCES.

1. J. Phillips.
"Freedom in Machinery (Introducing Screw Theory)", vol.I. Cambridge University Press 1984. (p.2,90,109,110).

2. K.H. Hunt.
"Kinematic Geometry of Mechanisms". Clarendon Press, 1978. Oxford. The Oxford Engineering Science Series. General Editors L.C. Woods, W.H. Wittrick. A.L. Cullen. (p.5-6).

3. IR.G. Broersma.
"Couplings and Bearings". Stam Series on Advanced Mechanical Engineering. Edited by Prof. IR.G. Broersma. H.Stam International N.V., Culemborg. The Netherlands 1968 (p.1-3).

4. W. Trylinski.
"Fine Mechanisms and Precision Instruments". Pergamon Press. Originally Published by Wydawnictwa Naukowo - Techniczne, Warsaw 1971.(p.333-).

5. Design Engineering Series.
Mechanical Drives. (J. Stewart. Chapter 8. "Couplings.")
Morgan-Grampian Publishers, 1970. (pp.77-96).

6. Harold Sinclair.
"Recent developments in hydraulic couplings, Proceedings of the Institution of Mechanical Engineers, 1935, vol.130. (p.75).

7. K. Lakshminarayana.
"Mechanics of form closure."
Transactions of the American Society of Mechanical Engineers, 1978. Paper No. 78-DET-32 (p.2-8).

8. A.F.C Pollard.
"Kinematic Design in Engineering". The twentieth Thomas Hawksley

Lecture. Institution of Mechanical Engineers (U.K), Nov.1933 (p. 156,184).

9. J.E. Furse.
"Kinematic design of fine mechanisms in instruments". Journal of Physics and Scientific Instruments (Instrument Science and Technology) 1981, vol.14 (p.264-271).

10. James Clerk Maxwell.
"The Scientific papers of James Clerk Maxwell", Edited by W.D. Niven Dover, 1965. Originally published by Cambridge University Press 1890. vol.II (p.507-508).

11. W. Steeds.
"Mechanism and the kinematics of machines". First published by Longmans and Green 1940.(p.52).

12. A.F.C Pollard.
"The kinematical design of couplings in instrument mechanisms". First published by Hilger and Watts Ltd. 1929. London.(p.31-52).

CHAPTER 6

MANIPULATORS AND THE EXPERIMENTAL LASER/SCREEN ALIGNMENT

CHAPTER OVERVIEW

In the last two chapters, couplings and actuators were discussed. Inorder to produce a manipulator, the two concepts must be amalgamated. In this chapter, a four degree of freedom manipulator is sought for alignment of lines. The reasons for selecting four degrees of freedom are already discussed (3.2 & 5.1).

Initially, the Kelvin manipulator derived from the Kelvin coupling is discussed (6.2). Its discussion bears no real tangible practical purpose but serves to illustrate the difference between series and parallel manipulators. The modification is then extended to achieve the required manipulator (6.3). The manipulator without a computation procedure can not solve the problem of alignment. The analogy between two plane balancing and the alignment of lines is therefore examined (6.5) in an attempt to adapt the balancing procedure for use in conducting tests to align a laser beam with a line in two ways namely manipulating (a) the line and (b) the laser.

In addition, a distinction is made between series and parallel manipulators by giving specific examples of manipulator arrangements. The manipulators are reviewed from literature based on robotics.

6.0 INTRODUCTION

Fichter and McDowell [1] state that manipulators and robots are becoming ever more ubiquitous because they are used to perform monotonous and hazardous tasks. Nearly all robot arms in use today are essentially similar to human or animal limbs [1]. A description of an anthropomorphic arrangement in which Hunt [2] closely relates the shortening of a linear actuator across a "hinge" with the contraction of a muscle arising from one bone and insering in an adjacent one across a hinge confirms this claim. The authors [1,2] describe robot arms (manipulators) based on the open and closed kinematic chains and give a detailed account of the advantages and

disadvantages of both types.

The application of manipulators in industry is not only confined to monotonous and hazardous tasks. They have been increasingly introduced to the manufacture and alignment of communications components as well as the manipulation of microscopic bodies in bacterial culture (4.3.7).

An established method of alignment of lines in space would provide ready solution for alignment of the central axis of a non-linear laser beam with an optical fibre (3.2). This is because the two procedures are essentially the same. In search for a suitable means of manipulating a line inorder to align it with another, a start is made by describing the design and construction of a four degree of freedom manipulator based on the Kelvin Coupling. The modification of the Kelvin coupling for incorporation of actuators to achieve this manipulator follows directly from the previous chapter (5.7).

6.1 SERIES AND PARALLEL MANIPULATORS

The word manipulator or micro-manipulator and the associated terms are fully discussed in chapter 4. As in couplings, manipulators can also have either series or parallel structural arrangements. In this section, the difference between series and parallel manipulators is illutrated by discussing specific manipulator arrangements.

A method of manipulating an end-effector (table) in planar motion with all three actuated connecting chains fully in parallel with one another is shown in Figure 6.1(b). This arrangement, described in [2], is the antithesis of a simple in series actuation of a three axis motorised manipulator shown in Figure 6.1(a). In the latter, Mx, My and Mz are motorised actuators each stacked on top of another (series) such that the motion of Mz affects the positions of Mx and My and Mx in turn affects My but My affects none of them. It is stated [2] that most robot-arms (whether for industrial robots or other manipulators) have their actuators connected in series along a more or less 'anthropomorphic' arm , each actuator being at or associated with a single degree of freedom joint in the arm.

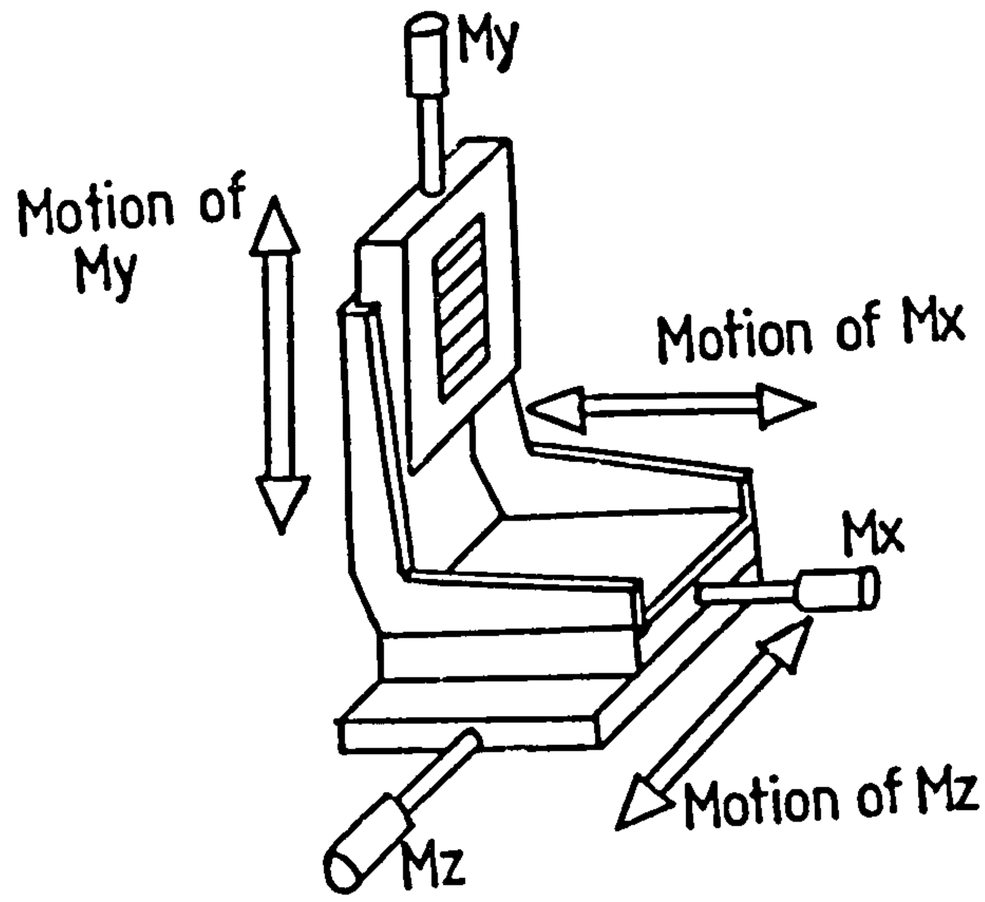

Fig 6,1(a) Motorised Series Manipulator.

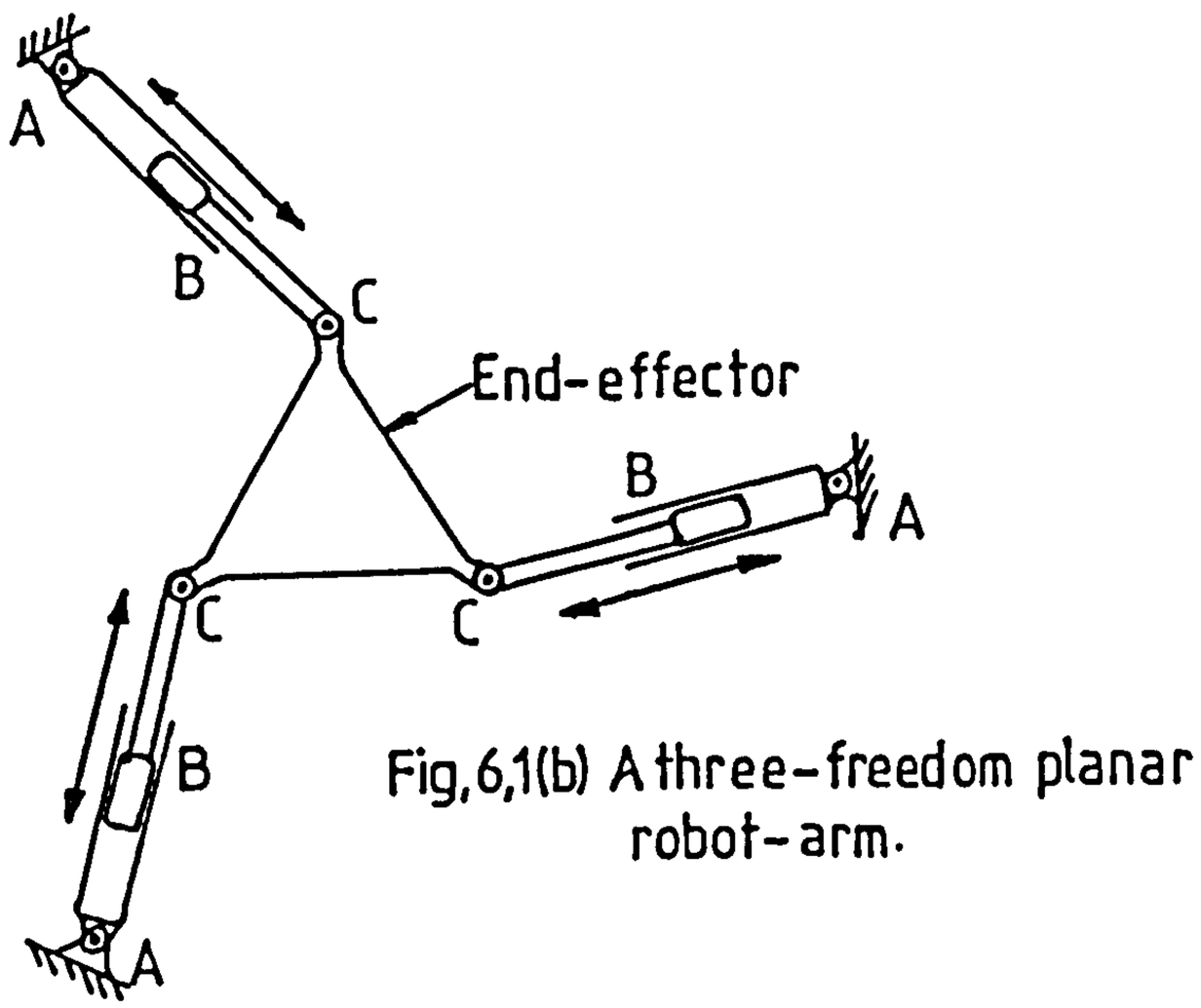

Fig,6,1(b) A three-freedom planar robot-arm.

A series-actuated arm is known [2] to accumulate errors from shoulder out to end-effector. It is stated [2] that such arms often suffer from lack of rigidity and in the absence of sophisticated computer control techniques, are subject to load-dependent error. Ofcourse, series-jointed links can be stiffened but this increases the arm-mass to be moved thus making greater demands on the actuator-system. With

in parallel actuation, there are prospects of an arm having both greater rigidity and lightness [2]. Since actuator error is not cumulative, greater precision is likely to be attained without excessive control complication.

Another in-parallel arrangement of actuators which is fully analysed by Stewart [3] and recited in a slightly different form in [1] is illustrated in Figure 6.1(c). It is described [1] as an octahedron with two opposite rigid faces; the base and the platform. The other six faces are open and the six edges that outline these faces are linear actuators. With the base fixed, the platform has six degrees of freedom. The freedom can be worked out from the mobility equation expressed [2] as $F = 6(n-1) - \sum_{i=0}^{g} u_i$ ..... 6.1. where n is the number of jointed members, g is the number of working joints between the n bodies, u_i is the number of constraints of the i^{th} joint and F is the number of degrees of freedom of the manipulator. The solution is shown below the graphical network representation of the Stewart Platform (Figure 6.1(d)).

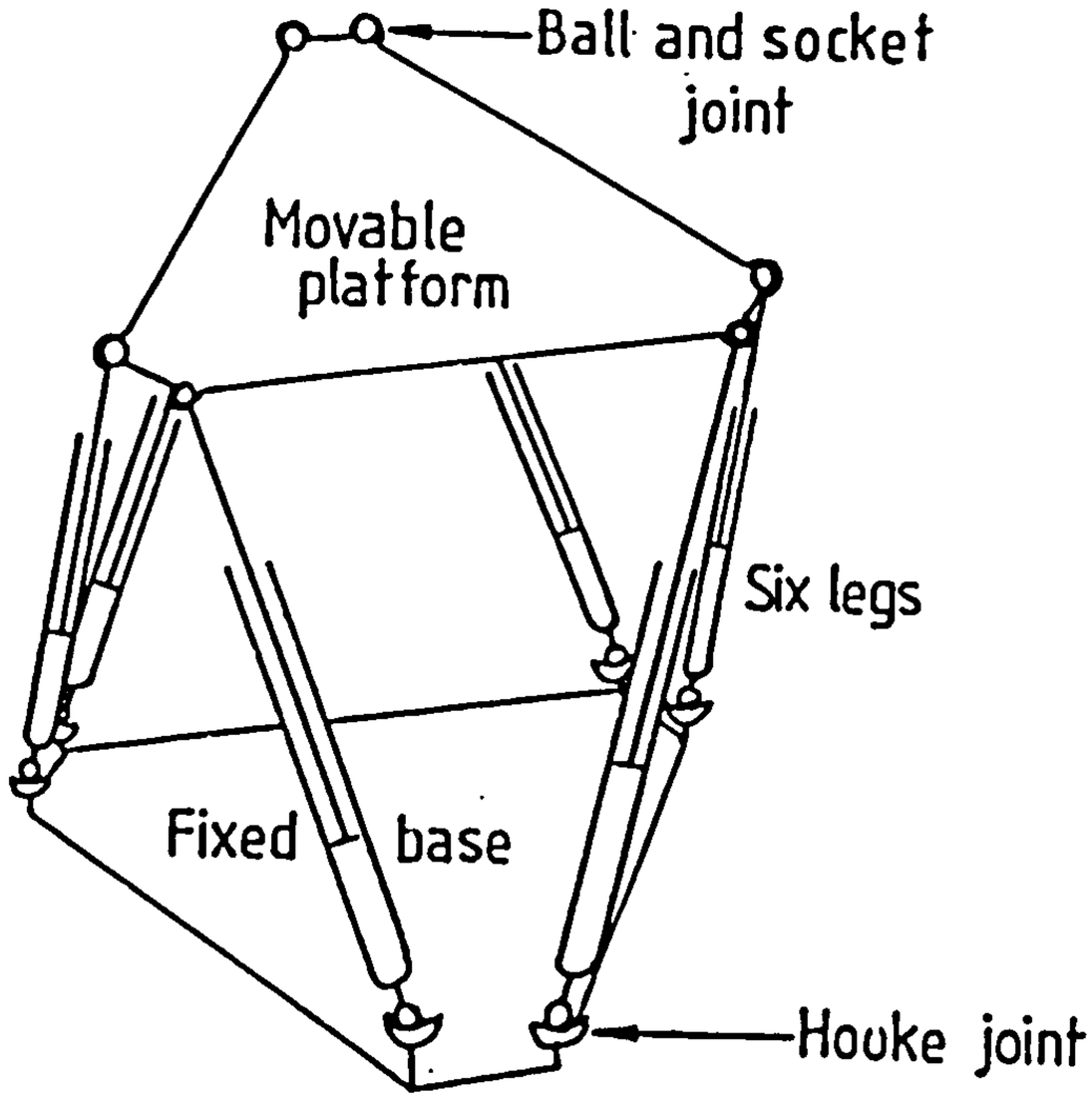

Fig,6,1(c) Stewart Platform based on an octahedron

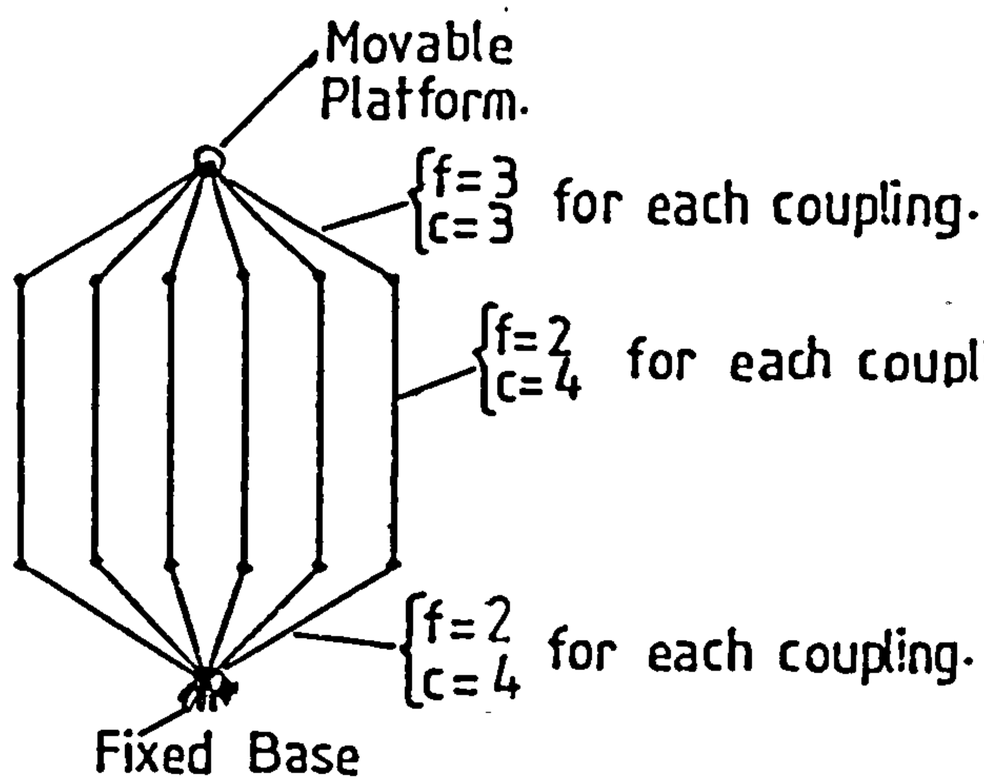

Fig,6,1(d) Graphical Representation of the Stewart Platform.

Freedom of the Stewart Platform is given by the mobility equation (Section 6.1):

$$F = 6(n-1) - \sum_{i=0}^{g} U_i$$

n = 14 and total number of constraints, C or $(U_i \to g)$ = (6x4) + (6x4) + (6x3)

$$\therefore \quad F = 6 \times 13 - (18+2\times24) = \underline{12}$$

But each piston has one degree of freedom to rotate about the ball joint to cylindrical joint axis. Thus freedom = 12 - (6x1) = 6.

6.2 THE KELVIN MANIPULATOR

If the table is overturned so that the base E2 of Figure 5.6.1(a) (Kelvin Coupling) is now uppermost and the tripod E1 is the base, then the number of contacts made between E1 and E2 are still the same and nothing else changes. An inversion also produces the same results. That means the trihedral hollow T, the V-groove G and the plane surface Ps on the surface of E2 are replaced by short hemispherical projections (stumps) while they get transferred onto the contacting surfaces of the corresponding hemisperical feet of E1.

The introduction of a linear actuator into each of the three couplings of the overturned Kelvin coupling ensures a small motion manipulation of the end-effector E2. This is a three degree of freedom manipulator shown in Figure 6.2(a). The number of degrees of freedom is obtained from the mobility equation as before and this is shown in Figure 6.2(b) (-the graphical representation of the manipulator). Each of the three actuators must have a small displacement otherwise the contacts between the spheres and the trihedral T and the groove G could be lost rendering this configuration kinematically unsound. Since the actuators execute small displacements, the rotary motion of the manipulator is correspondingly minimised.

All the three actuated couplings of this manipulator are in parallel with one another. Like the manipulator of Figure 6.1(b), this arrangement is the antithesis of the simple in series actuation such as that shown in Figure 6.1(a). Roth [4] states that manipulators are usually formed by an open loop chain of binary links where every link has one degree of freedom relative to one of its neighbours. Due to lack of rigidity of such manipulators and the accumulation of errors from shoulder out to end-effector[1], parallel manipulators might present a better alternative.

A manipulator along the lines of Figure 6.2(a) will be referred to as the "Kelvin Manipulator" because it is derived from the Kelvin Coupling. It is probably more appropriate to call it the Kelvin micro-manipulator because of the minute amount of actuation executed. A similar procedure of overturning the table and introducing actuators can also be applied to the coupling of Figure 5.6.1(b). The result is again three actuated couplings in parallel with one another. Such a manipulator as well as that of Figure 6.2(a) has three degrees of freedom.

The advantages and disadvantages of the parallel versus series manipulators are discussed in [1,2]. Some of these are re-cited in section 6.1.

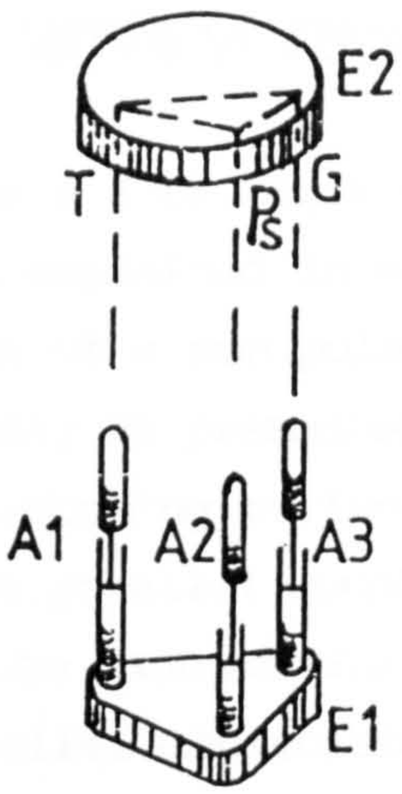

"The Kelvin manipulator"

Fig,6,2(a) The Kelvin coupling of fig,5, 6,1(a) overturned and actuators A1, A2 and A3 introduced.

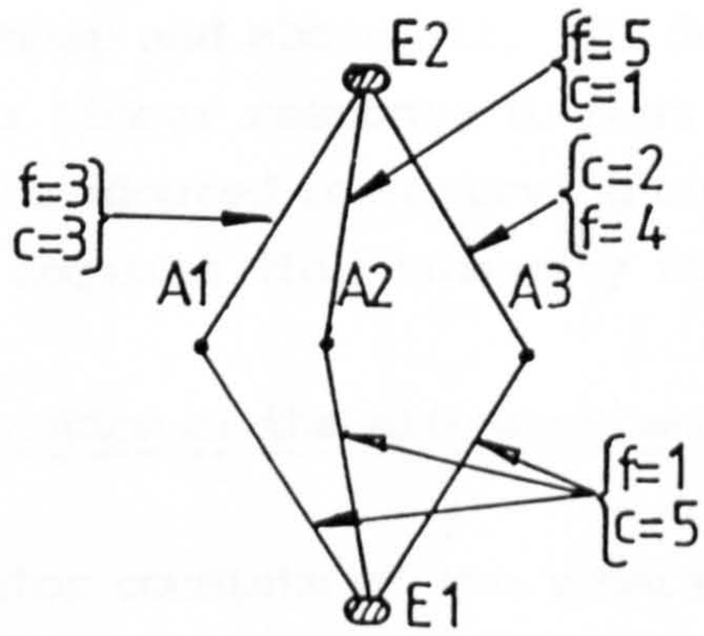

Fig,6,2 (b) Graphical representation of the Kelvin coupling.

Freedom of the Kelvin manipulator is expressed (Section 6.1) by:

$$F = 6(n-1) - \sum_{i=0}^{g} U_i \quad \text{as before}$$

n = 5 and total number of constraints, C or $(U_i \rightarrow g)$ = 3 + 1 +2 + (3x5)

$\therefore$ Freedom = 6 x 4 - (6+15) = 3

6.3 A FOUR DEGREE OF FREEDOM MANIPULATOR FOR ALIGNMENT OF LINES

The need for a four degree of freedom manipulator for the alignment of lines is explained in section 5.1. In this section, the design and construction of a manipulator to demonstrate the alignment of lines experimentally is presented. The manipulator is derived directly from the Kelvin coupling variant of Figure 5.7(h) which has been modified to have four parallel couplings. This is achieved by incorporating an actuator into each of the four feet. The result is a four degree of freedom parallel manipulator.

This alignment can also be achieved by a four degree of freedom series manipulator as long as a suitable method for conducting tests can be improvised. A parallel manipulator is chosen here beacause its design is selected for simplicity. For this reason, it can be constructed locally without the need for special skills. It is therefore cheap and above all, its design and construction (6.3.1) allows for a linear response to feet adjustments. As will be seen, the procedure adopted for carrying out the alignment tests on this manipulator requires this linearity for its success.

6.3.1 Construction of the alignment manipulator

The manipulator consists of two separate parts. One is a 90^{o} V-shaped perspex body P (Figure 6.3.1(a) -simply referred to hereafter as P) and the other is a steel base (Figure 6.3.1 (b)) on to which four 45^{o} angled stands T are firmly mounted. The stands in turn carry threaded bolts (A',B',C' and D') with steel ball bearings glued on to their tips so that two lines drawn through the axes of a pair of feet (A' and B' or C' and D') form a right angle (view V-V, Fig.6.3.1(b)). These ball bearings ensure that single and two point contacts are made with a plane surface and a V-groove respectively.

P is 300 mm long by 80 mm and 7 mm thick and has a series of equally spaced V-grooves G (each about 1.5 mm wide by 4 mm deep) milled inside it. It is supported on the four feet so that A' and B' on plane 1 each makes two point contacts with it via a pair of smaller

PLAN AND END VIEWS OF PERSPEX HOLDING SCREENS

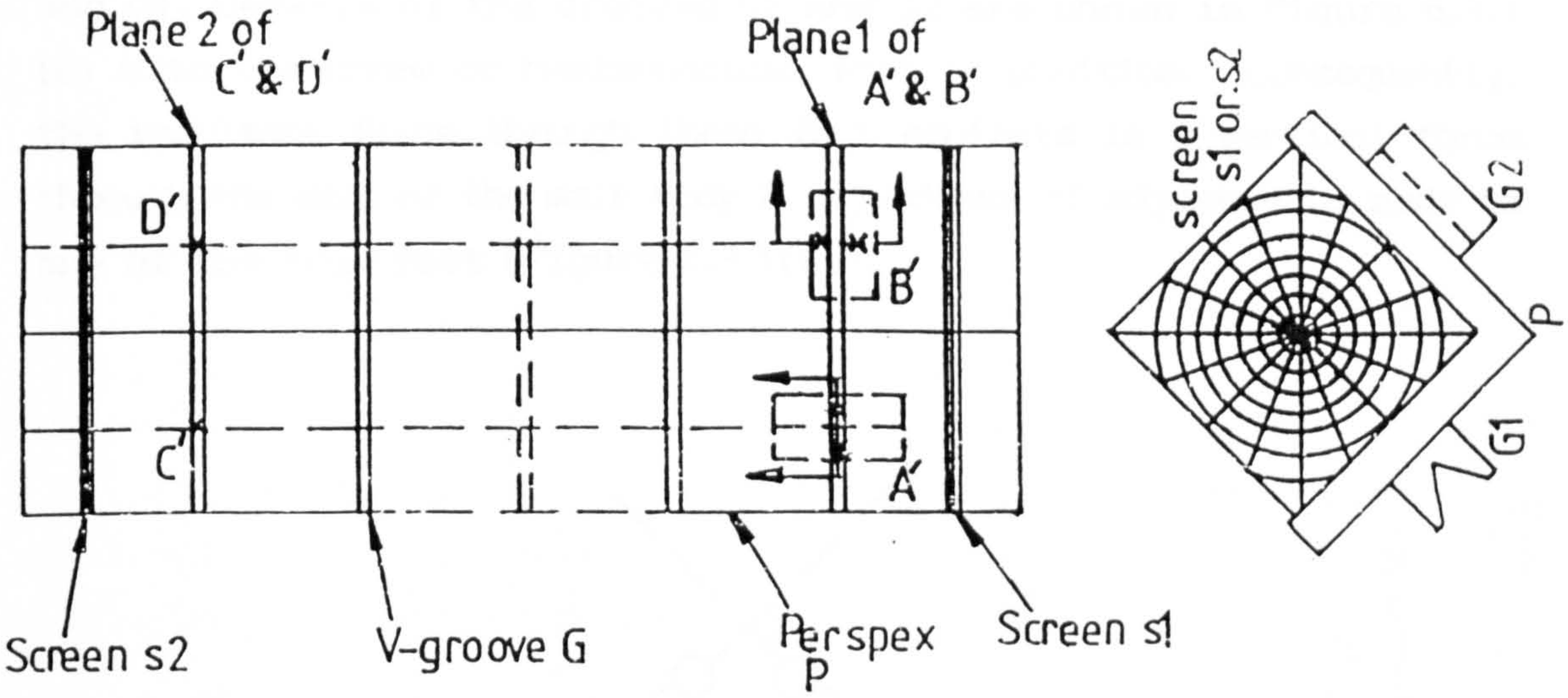

Four hemispherical feet A', B', C'& D' support and make contacts with P. A'& B' each makes two point contacts while C' & D' each makes one point contact.

Smaller grooves G1 & G2 screwed to P accomodate A' & B'.

Fig, 6,3,1(a)

Stands T holding the feet which in turn support the V-shaped perspex body P in (a) above.

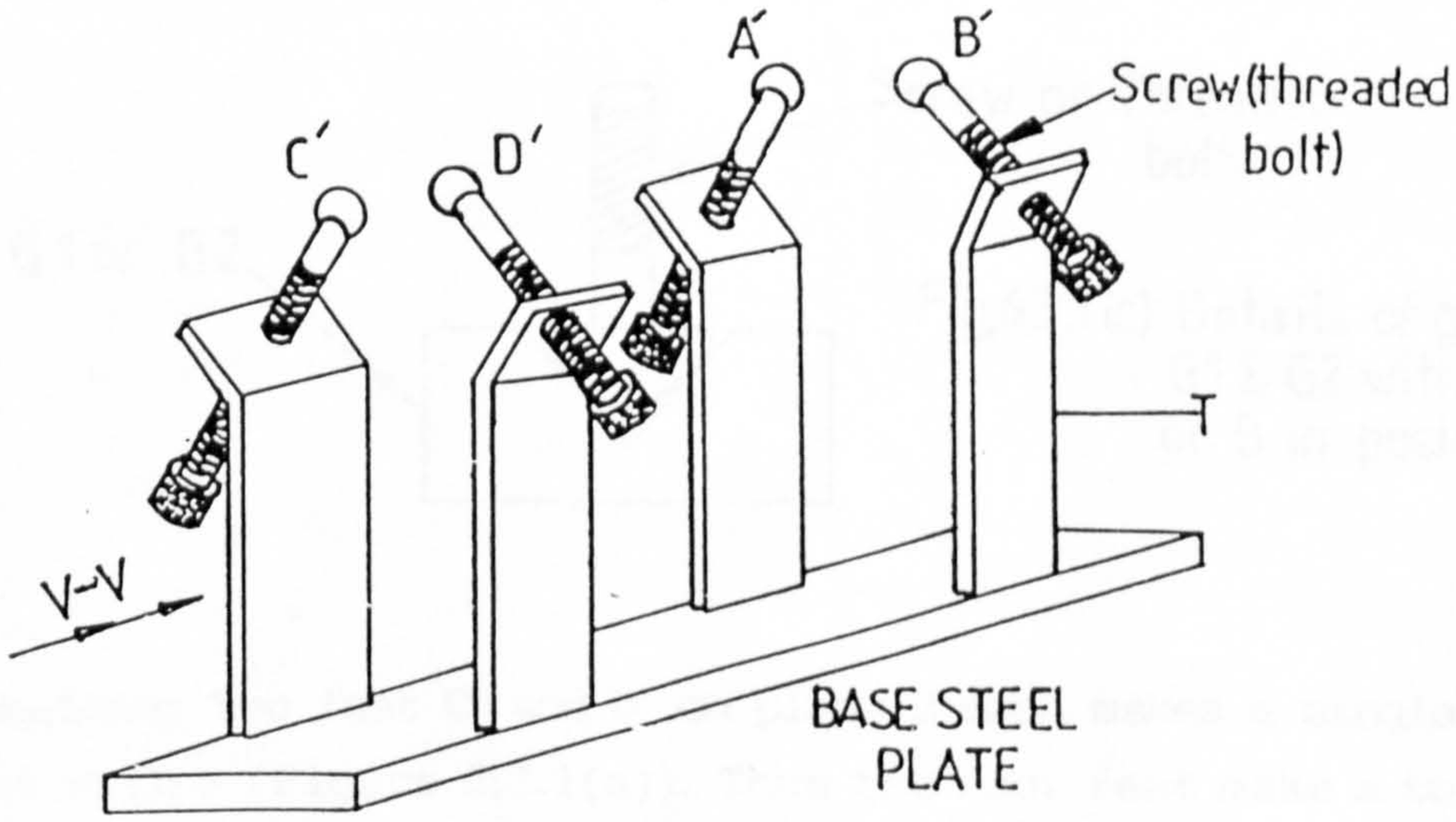

Fig, 6,3,1 (b)

V-grooved perspex G1 and G2 both fixed onto it (Figure 6.3.1(a)). G1 whose axis is parallel to that of P, accommodates A' while the second foot B' sits in G2 whose axis is perpendicular to both the axes of P and G1. Details of the grooves G1 and G2 are shown in Figure 6.3.1 (c) with the screw or hemispherical foot in position. Consequently, the resultant force through these four contacts is a vertical force through the axis of the main body P regardless of adjustments made to any of the four feet (Figure 6.3.1(a)).

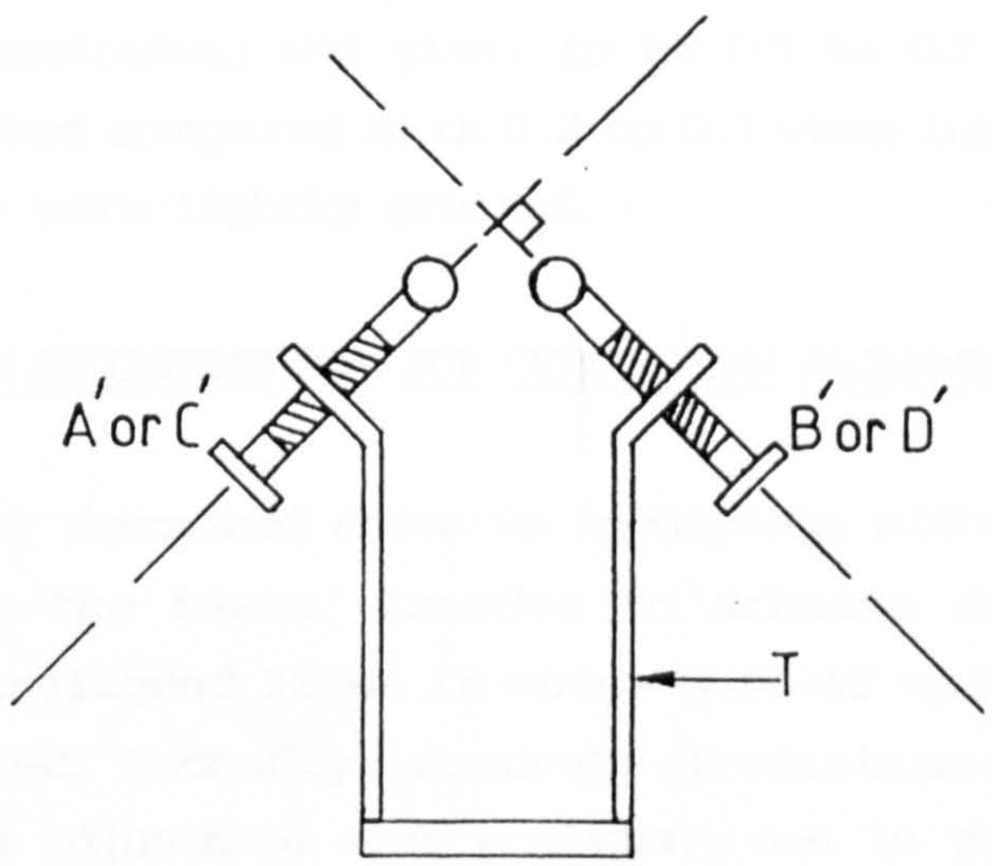

End view V–V of Fig. 6.3.1 (b).

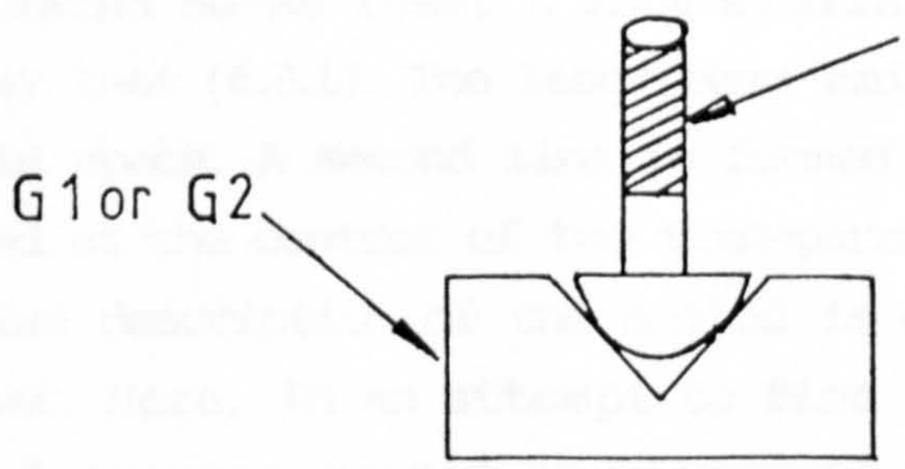

Fig. 6.3.1 (c) Details of grooves G1 & G2 with foot A or B in position.

The remaining two feet C' and D' on plane 2 each makes a single point contact with P (Figure 6.3.1(a)). Thus the four feet make a total of six point contacts with P. P can be removed and replaced but all six contacts are maintained at the same locations as long as no foot is

adjusted. The distance between planes 1 and 2 can not be altered, which means that all point contacts are generally fixed unless affected by secondary motion. This is an erratic forward motion of P caused by a combination of the fairly large backlash and any non-linear behaviour of the feet.

In order to reduce friction between the ball bearings and the perspex surface where contacts are made, glass was glued onto the appropriate locations including the inclined planes of the grooves G1 and G2. Bowden and Tabor [5] found the coefficient of static friction between metal (steel inclusive) and glass to be 0.5 to 0.7 when the surfaces are unlubricated compared with 0.2 to 0.3 when lubricated. Thus the glass surfaces were lightly greased.

6.4 THE NEED (REQUIREMENTS) FOR CONDUCTING ALIGNMENT TESTS

The manipulator described above is incomplete without a proper means of conducting the tests. Inorder to achieve completeness, two physically misaligned lines in space both of which are adjustable must be created. Secondly, accurate prediction of the arbitrary changes of the adjustable line position due to feet adjustments is necessary for a successful general alignment procedure. This requires an algorithm and a means of measuring the position changes.

As revealed later, the first problem is solved by mounting a fixed collimated He-Ne laser L in a similar way to P supported on four similar feet (6.3.1). The laser beam emitted by L then represents one line in space. A second line is formed by two circular target points located at the centres of two transparent screens mounted inside P. A detailed description of the method is given towards the end of this Chapter. Here, in an attempt to find a suitable algorithm, a two plane balancing procedure pioneered by Thearle [6] is investigated for a possible adaptation for use in this alignment. This leads to the discussion of the balancing analogy presented below.

6.5 ANALOGY BETWEEN TWO PLANE BALANCING AND ALIGNMENT OF LINES

The investigation of a vectorial alignment method based on two plane

balancing of stiff rotors for alignment of lines forms the basis of the discussions that follow. The problem of two plane balancing of stiff rotors was solved [6] by assuming that vibration amplitudes are proportional to the forces that cause them. This asssumption is valid only if damping as well as speed of rotation remain constant for all tests conducted [6].

To ascertain the existence of analogy between two plane balancing and the alignment of lines, the balancing procedure is first described. Thomson [7] states that a rotor is unbalanced if its shaft is violently rocked about the bearings during rotation. This is due to unbalanced rotor-mass on both planes. Generally, such a rotor is balanced by fastening the appropriate corrective weight on to each rotor plane [7].

The determination of size and location of the two balance weights only needs three test runs conducted at the same speed [7,8]. The vibration levels V and phase angles Y produced by the unbalanced masses are then measured at both bearings for each test run. Test 1 is carried out without attaching weights to the rotor planes. Test 2 is conducted at the same speed with a reasonably sized mass M1 firmly attached to plane 1 at some angular location. M1 is then removed and another mass M2 of similar size is attached to plane 2 . Test 3 is then conducted at the same speed as before.

The object of this exercise is to produce two simultaneous vector equations with two unkowns [8]. The solutions to these equations correspond to vibration vectors with equal magnitudes but opposite phase angles to those produced by the required balance masses on planes 1 and 2 respectively [8]. The balance masses are then obtained by multiplying each vibration level with the corresponding trial mass. Details of the equations and the reasons for conducting three tests are given in [7,8].

The balancing equations were reproduced [8] and stored in a magnetic tape in form of a program for general purpose two plane balancing. By keying the tape into an HP67 calculator [8] and entering values of displacements, angles and trial masses into the calculator in the

correct order [8], the required balance masses are produced.

Let two transparent target screens be mounted inside P (6.4) (which is in turn supported on four feet A',B',C',D'- Fig.6.3.1(a)) so that one of them occupies the same plane as A' & B' and the second one shares the same plane with C' & D'. These planes are analogous to the rotor planes described in the last paragraph. Thus the amount of adjustment made to the feet is analogous to the forces or added mass to the corresponding rotor planes while the change in body position and consequently the laser spot position represents the vibration amplitudes. The validity of this particular analogy depends entirely on the linearity of the manipulator. That is, the amount of manipulator adjustment must be proportional to the change in laser spot positions. This is because, as already stated, the concept of two plane balancing is based fundamentally [6] on the assumption that vibration amplitudes are proportional to the forces causing them. In the alignment manipulator (6.3), this can be achieved by making small adjustments to the feet which in turn causes small changes in body position. To ensure that this is achieved, the existence of linearity in the alignment manipulator must be verified. Since the verification involves measurements, the method of measurement first needs to be described.

6.6 METHOD OF MEASUREMENT

It is argued (6.4) that the alignment manipulator is incomplete without an algorithm and a means of measurements. Since the arguments presented (6.5) suggest the existence of analogy between two plane balancing and alignment of lines, it needs to be proven. A practial proof can be carried out if a suitable method of measurement is obtained. This leads to further discussion of the screens already mentioned in 6.4.

Two transparent glass screens S (Figure 6.6) each about 1.4mm thick cut so as to fit into grooves G (Figure 6.3.1(a)), were etched with radial and circular lines at equal intervals for two reasons. Firstly, their centres form a second moveable line (6.4). Secondly, they provide a means of reading the polar coordinates of a fine

impinging He-Ne laser beam representing the other line in space. This enables measurements of laser spot positions to be made for use as entry data into the balancing program [8]. Each screen can also be individually moved from one groove to the other thus allowing their planes to be varied.

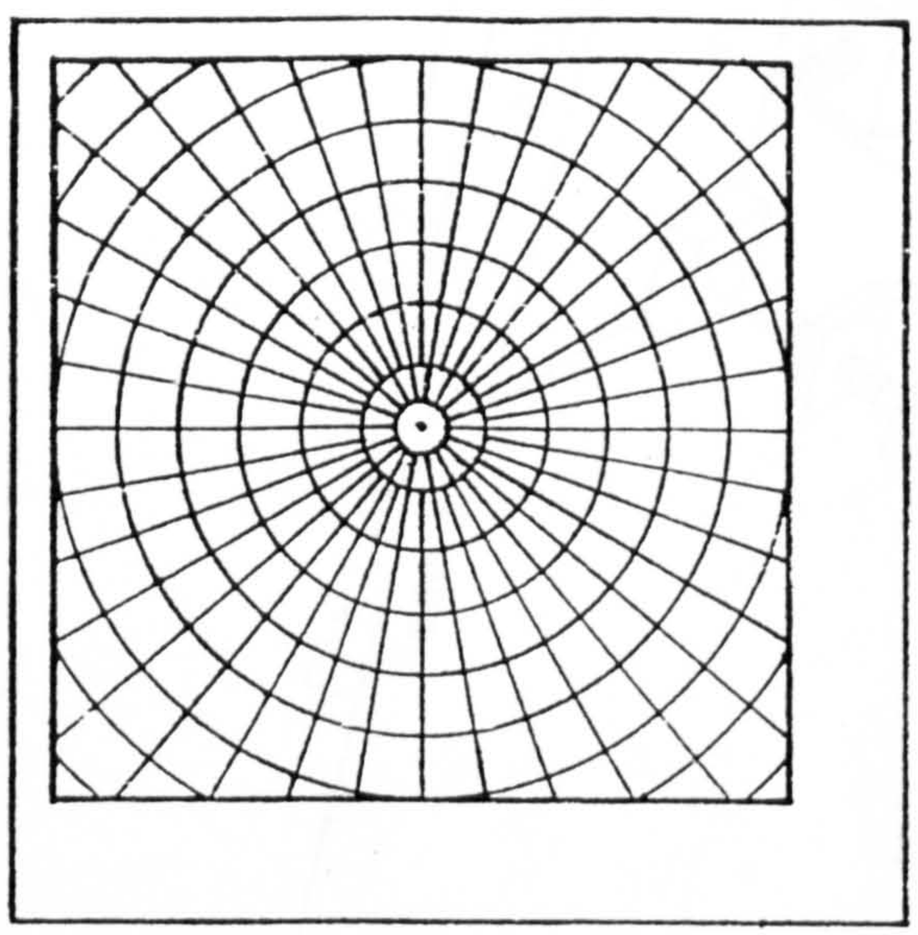

Fig,6,6 Etched glass screen, S (10° every 5mm radius).

6.7 SIGN CONVENTION

A suitable convention which must be consistent with that used for reading the position of weights attached to unbalanced rotors is now sought for reading the polar coordinates of the impinging laser beam. Figure 6.7(a) shows the alignment set up in which a collimated He-Ne laser beam b impinges on two etched glass screens S1 and S2. It is finally blocked by a steel plate R which simply provides a stop. The two screens are held in separate slots inside a perspex body P2 supported by A',B',C',D' (6.3.1) while the laser L is held inside a similar perspex body P1 supported by A,B,C,D. Both manipulators are fixed on to a steel base (Fig.6.7 (a)).

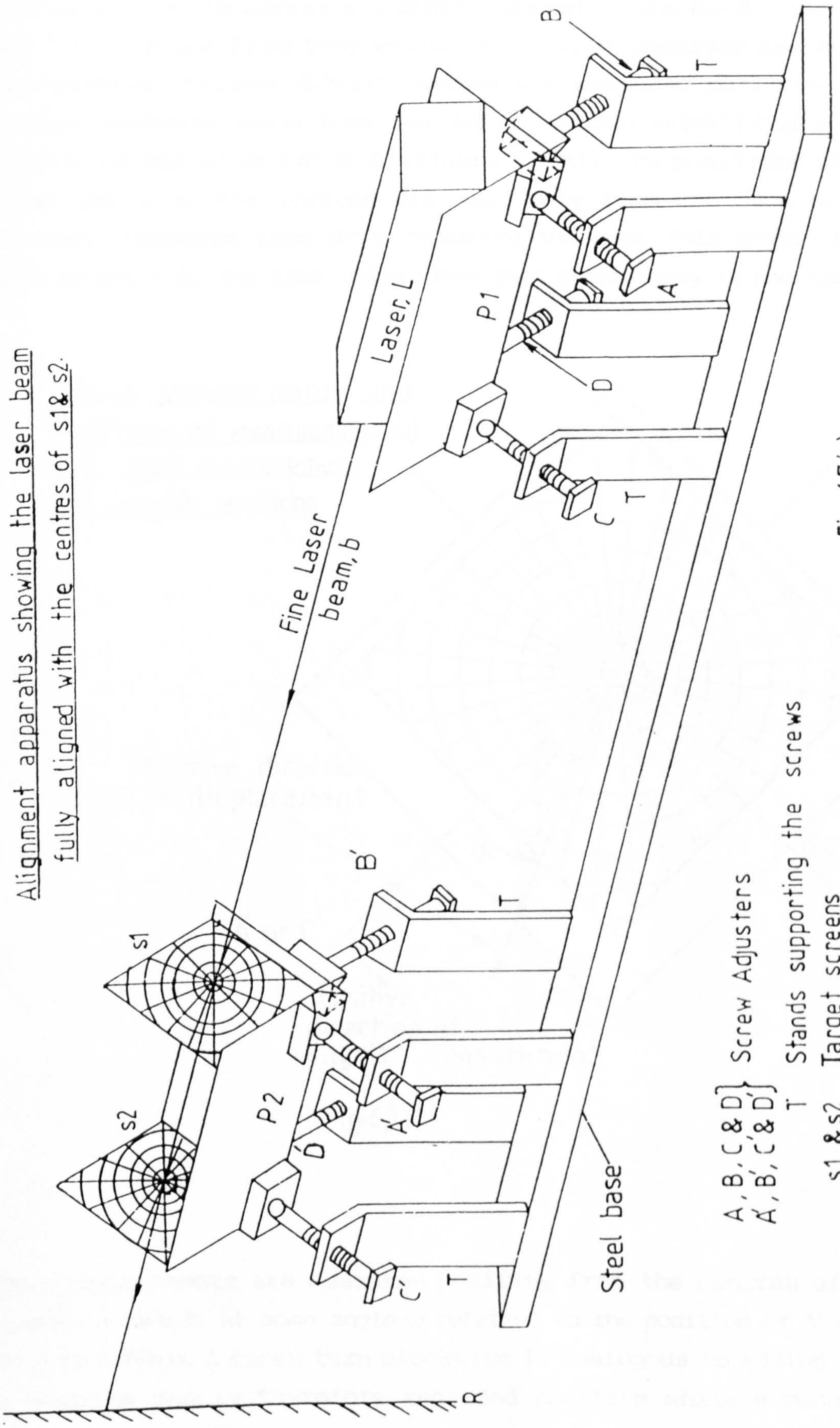
Alignment apparatus showing the laser beam fully aligned with the centres of s1& s2.
A, B, C & D} Screw Adjusters
A', B', C'& D'}
T Stands supporting the screens
s1 & s2 Target screens
P Perspex holding the screens and laser
Steel base
Laser, L
Fine Laser beam, b
P1
P2
s1
s2
A
B
C
D
A'
B'
C'
D'
T
R

Fig, 6,7(a)

The balancing planes of P2 (holding the screens) where it makes contacts with the screws are distinguished as the R.H.S. (plane 1) and L.H.S. (plane 2) as they would appear to an observer facing the manipulator (Figures 6.7(a)). Angles are measured positive in a counter-clockwise sense from the datum position established by the postion of the screws A' or C' (Figure 6.7(b)). The positions of the laser spots on the screens are read only from one face of the screens; preferably from those receiving the beam. This avoids laser penetration into the eyes and ensures that consistency is maintained.

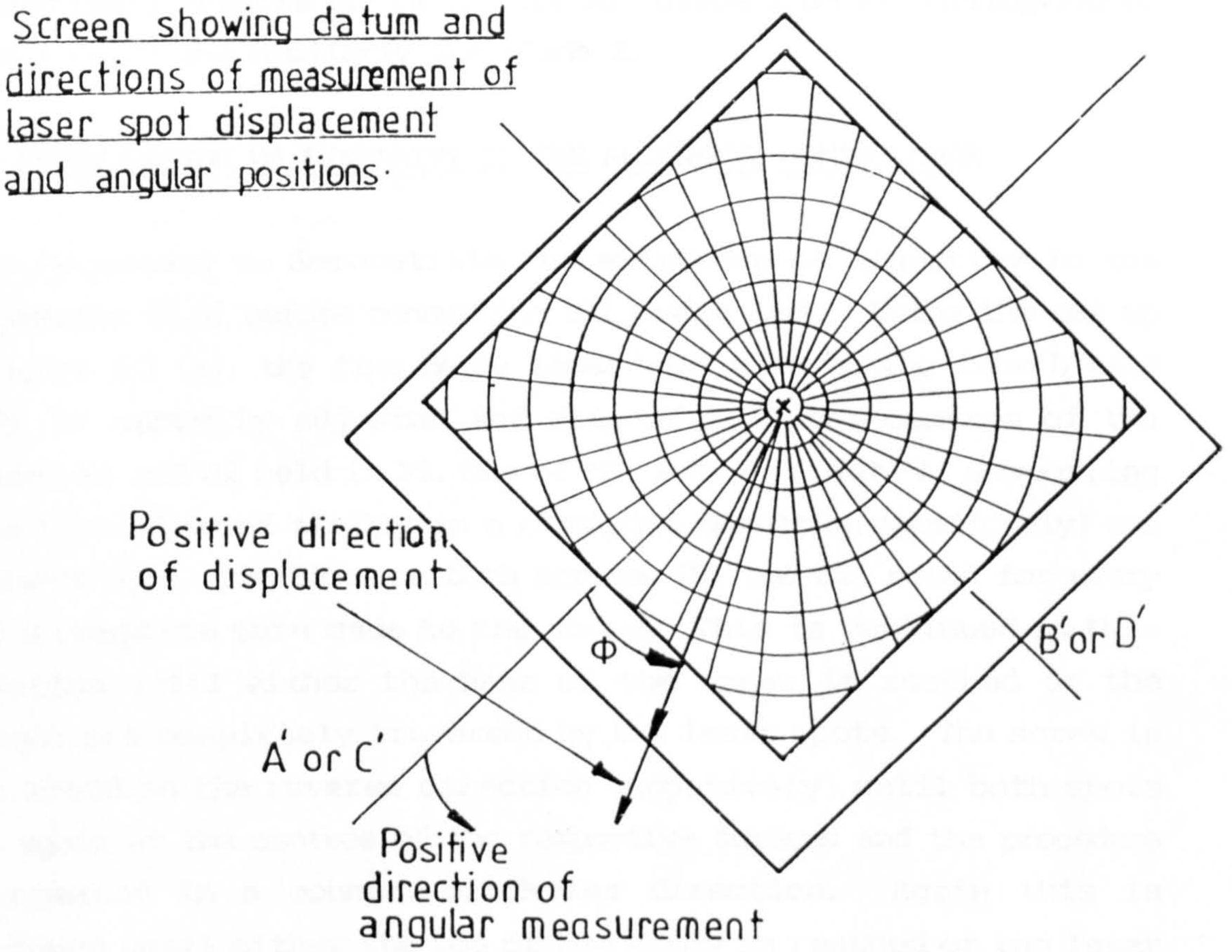

Fig.6,7(b)

The displacements are measured positive from the centres of the screens outwards at some angle ϕ relative to the position of A' or C' (Figure 6.7(b)). A screw turn clockwise is analogous to adding mass to a plane and is therefore regarded positive while a counter-

clockwise turn is analogous to removal of mass from that plane and is therefore regarded negative. After conversion of the screw turns into linear displacements using specified screw pitch values, they are then keyed into the HP67 calculator [8] as negative or positive values depending up on the direction of screw turning.

The same procedure applies to the adjustment of the laser while the screens are left stationary. In this case, the R.H.S. (plane 1) containing screws A and B and the L.H.S. (plane 2) containing screws C and D supporting the laser, correspond to the screens S1 and S2 respectively (Figure 6.7 (a)). That is, plane 1 on P1 correspond to plane 1 on P2 and similarly for plane 2.

6.8 VERIFICATION OF LINEARITY IN THE ALIGNMENT MANIPULATOR

It is necessary to demonstrate the existence of linearity in the manipulator (6.5) before conducting alignment tests. Using the set up in Figure 6.7 (a), the fine He-Ne laser beam b emanating from L held in P1 is manually adjusted and aligned with the centres of the screens S1 and S2 held in P2. One of the screws (feet) A' supporting P2 is then adjusted firstly in a clockwise direction (positively) and the laser spot positions on both screens (S1 and S2) noted for every half a complete turn made to the screw. This is continued in this direction until either the base of the screw is reached or the screens are completely traversed by the laser spots. The screw is then wound in the reverse direction (negatively) until both spots fall again at the centres of the respective screens and the procedure is repeated in a counter-clockwise direction. Again this is continued until either the top of the screw is reached or the laser spots completely traverse the screens. The spots are again returned to the centres of the screens by srewing A' clockwise. The same cycle is then repeated for each of the remaining three feet (screws) B', C' and D' in turn.

The results of these experiments are presented graphically in Figures 6.8 (a) and (b). In Figure 6.8(a), the laser beam paths on both screens S1 and S2 are traced by adjusting screws (feet) A' and B'. It can be seen that the traces produced by A' on both screens are only

Effect of feet (A' & B') adjustments on laser beam paths on screens s1 & s2 (see fig. 6,7(a)).

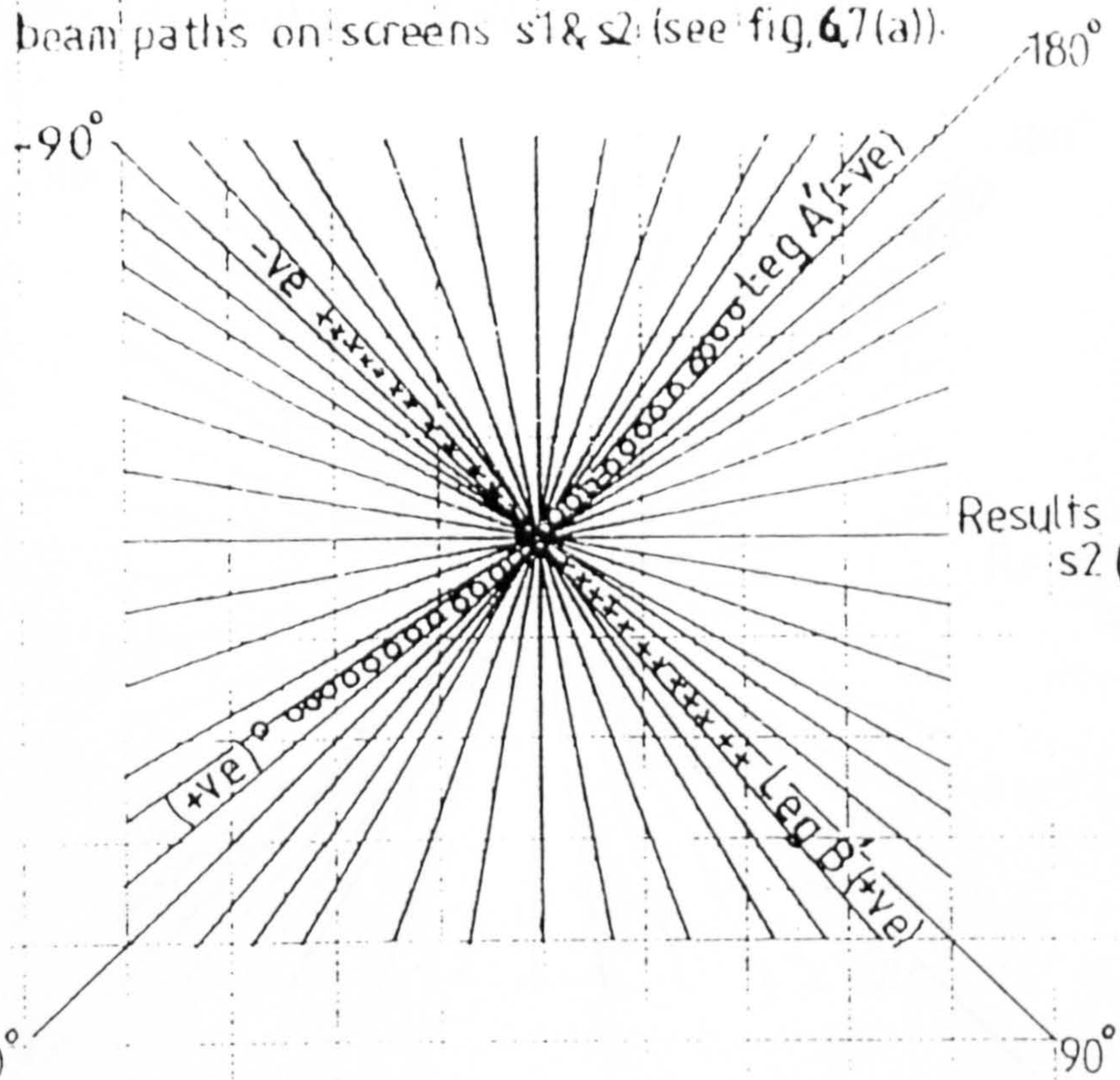

Results for screen s2 (fig. 6,7(a))

FIG. 6,8(a)

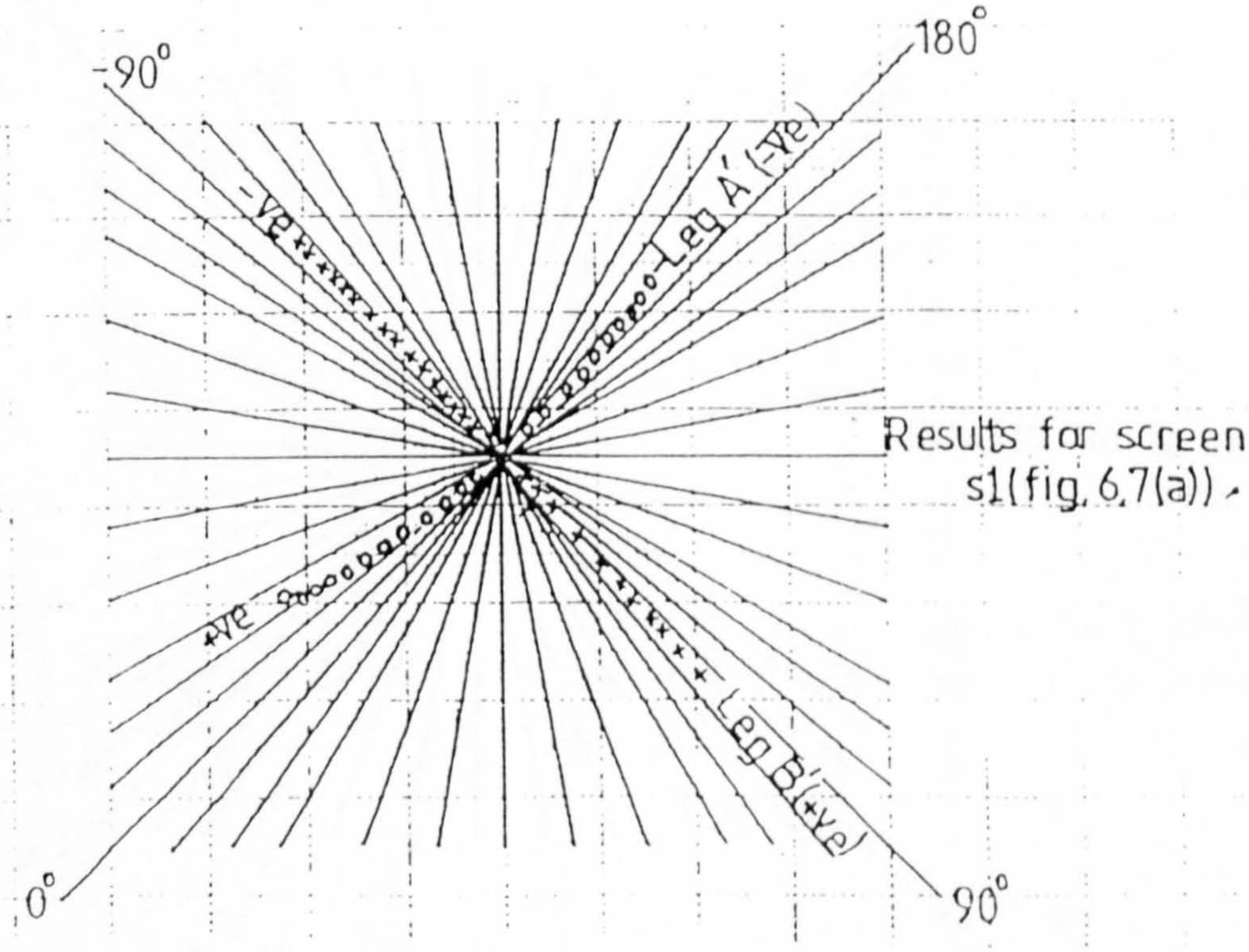

Results for screen s1 (fig. 6,7(a)).

Effect of feet (C' & D') adjustments on laser beam paths on screens s1 & s2 (see fig, 6,7(a))

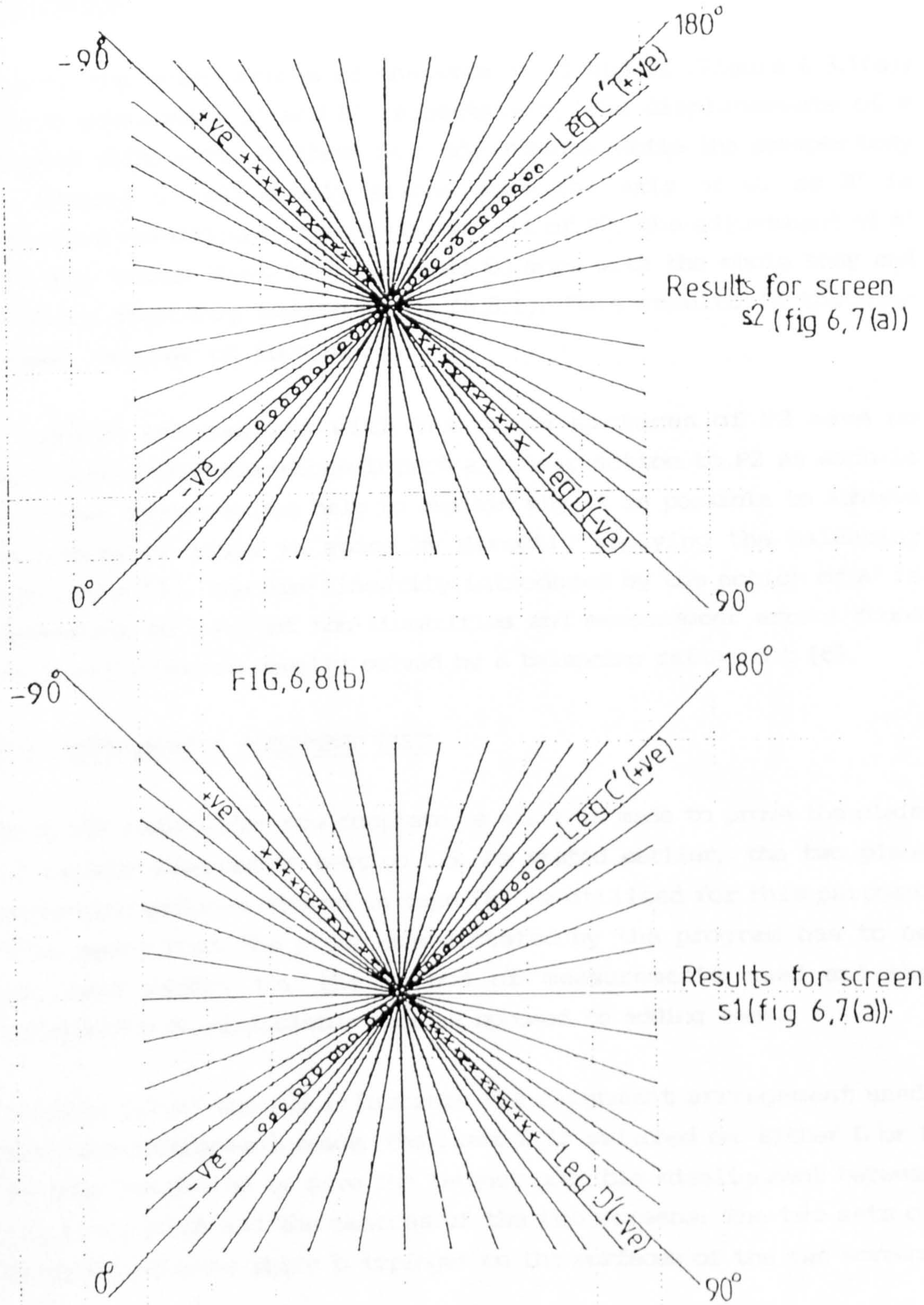

Results for screen s2 (fig 6,7(a))

FIG,6,8(b)

Results for screen s1(fig 6,7(a)).

linear up to 5 mm radius from the centres of the screens but becomes increasingly non-linear outside this range. However, the traces produced by B' are completely linear and the same applies to those produced by adjusting C' and D' (Figure 6.8 (b)).

Conclusion.

Due to the orientations of the axes of G1 and G2 (Figure 6.3.1(a)) which accomodate A' and B' respectively, the displacements of P respond differently to these feet adjustments. While the perspex body P2 (Figure 6.7(a)) simply slides down the axis of G2 as B' is adjusted resulting in the position tilt of P2, the adjustment of A' not only brings about tilt but tends to move with the whole body and imparts secondary motion to P2 (6.3.1). This results in the non-linear response of foot A'.

C' and D' interacting with the plane surfaces of P2 have no restriction and therefore impart a linear action to P2 as each is adjusted. These results help to explain why it is possible to achieve alignment of lines in space by directly applying the balancing algorithm [8]. The non-linearity introduced by the action of A' is equivalent to inherent non-linearities and measurement errors found in rotary machines usually solved by a balancing refinement [6].

6.9 EXPERIMENTAL ALIGNMENT TESTS

With the manipulator now complete, a start is made to prove the claim of analogy advanced in section 6.5. As stated earlier, the two plane balancing program stored in tape [8] is utilised for this purpose. This means that the procedure dictated by the program has to be followed except for the method of measurements used and the adjustments of manipulator feet as opposed to adding mass.

Figures 6.7(a) and 6.9 illustrate the alignment arrangement used. With the arrangement ready, the laser L is switched on. Either L or P is then readjusted to give the largest possible misalignment between the laser beam and the centres of the two screens. The two sets of polar coordinates where b impinges on the surfaces of the two screens

S1 and S2 (Fig.6.9) are read and recorded in row 1 of table 6.9.1(I) below. A given number of screw turns n (clockwise or anti-clockwise) are then made to one of the two R.H.S. feet (A' or B' on plane 1) leaving the laser stationary. A new set of readings of the polar coordinates where the spots get shifted on S1 and S2 (Figure 6.9) are again read and recorded in row 2 of table 6.9.1(I). This adjustment is removed by screwing the same foot n times in the reverse sense. The two beam spots on S1 and S2 are then checked to ensure that they fall back to their original positions. Finally, a new adjustment is made to one of the two L.H.S. feet (C' or D' on plane 2) say m times clockwise or anti-clockwise and a third set of readings on S1 and S2 noted. These are recorded in row 3 of the same table and the adjustment is removed as before followed by a check in spot positions to ensure that they return to the original misalignment as measured by the first set of polar coordinates. These are recorded in row 4.

Alignment apparatus showing laser beam, b misaligned with the centres c1 & c2 of screens s1 & s2.

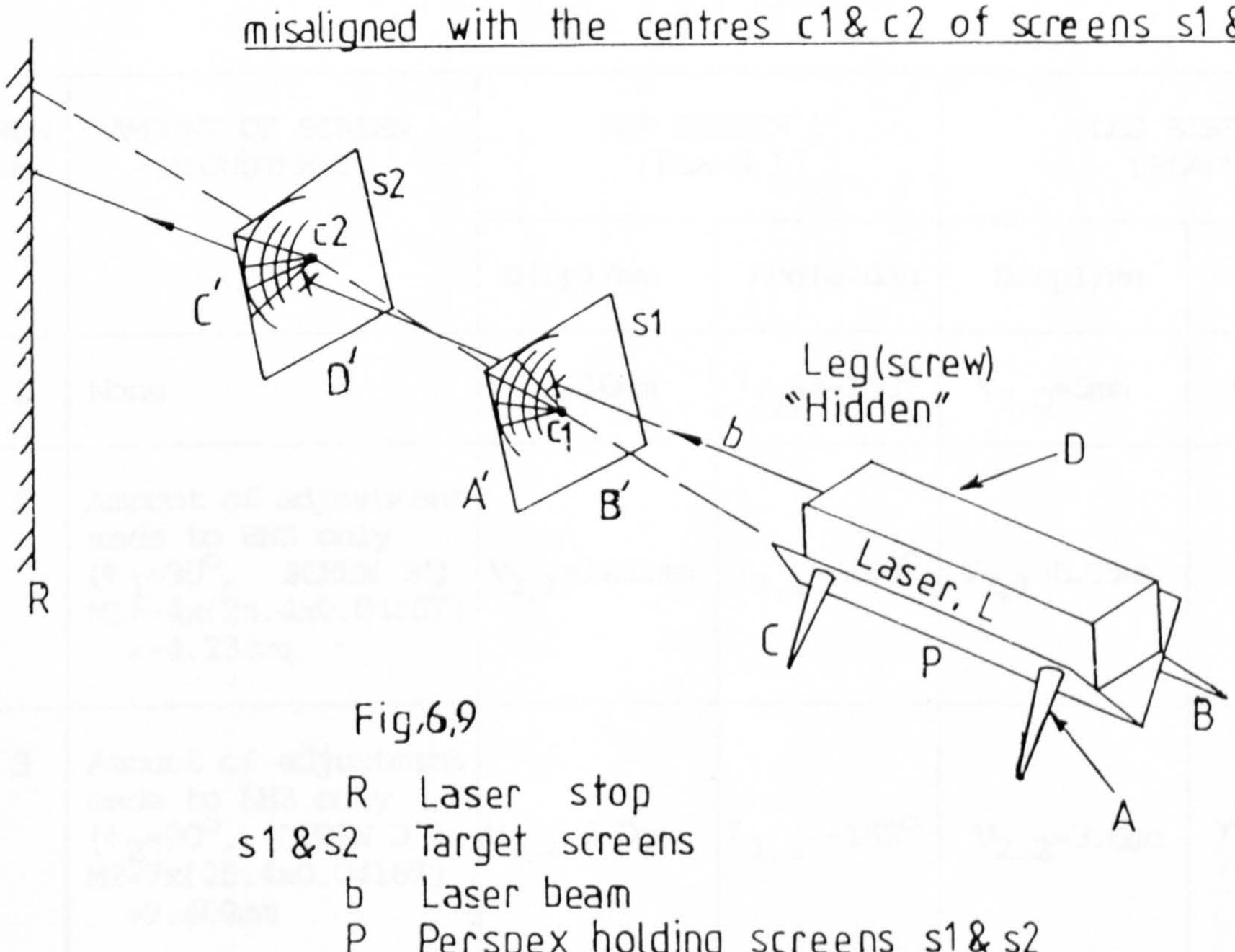

Fig,6,9

R Laser stop
s1 & s2 Target screens
b Laser beam
P Perspex holding screens s1 & s2 and laser, L
A, B, C & D } Screw Adjusters
A', B', C' & D' } (Those supporting the screens are not shown)
c1 & c2 Centres of s1 & s2 respectively (a line drawn through these two points forms a second skew line in space)

These results are then keyed into the HP67 programmable calculator with a copy of B and K magnetic program card WW9002 [8] to obtain the necessary adjustments (as opposed to balance masses) required. The procedure of keying these results is given in [8]. Table 6.9.1(I) presents one set of experimental results. When the adjustments obtained from the calculator are made, the beam should then pass through the centres C1 and C2 of screens S1 and S2 respectively (Figure 6.7(a)). Conversely, the screens can be left stationary while body P1 holding L (Figure 6.9) is adjusted.

6.9.1 Presentation of Results - Screen Adjustments.

Table 6.9.1(I) below shows the results produced by adjusting screens placed in slots 280mm apart leaving the laser stationary. Each screen is 10mm outside planes 1 and 2 of the pair of feet A' & B' and C' & D' respectively (Figure 6.3.1 (a)).

Results of adjusting screens
Table 6.9.1 (I)

RUN No	AMOUNT OF SCREEN ADJUSTMENT	RHS SCREEN 1 (PLANE 1)		LHS SCREEN 2 (PLANE 2)	
		Displ/mm	Angle/deg	Displ/mm	Angle/deg
1	None	$V_{1,0}$=10mm	$\gamma_{1,0}$=-150°	$V_{2,0}$=5mm	$\gamma_{2,0}$=-70°
2	Amount of adjustment made to RHS only (ϕ_1=90°, SCREW B') M1=-4x(25.4x0.04167) =-4.234mm	$V_{1,1}$=12.5mm	$\gamma_{1,1}$=-134°	$V_{2,1}$=5.5mm	$\gamma_{2,1}$=-70°
3	Amount of adjustment made to LHS only (ϕ_2=90°, SCREW D') M2=7x(25.4x0.04167) =7.409mm	$V_{1,2}$=8.0mm	$\gamma_{1,2}$=-152°	$V_{2,2}$=3.0mm	$\gamma_{2,2}$=40°
4	None (recheck on first run)	$V_{1,0}$=10mm	$\gamma_{1,0}$=-150°	$V_{2,0}$=5.0mm	$\gamma_{2,0}$=-70°

Pitch of screws = 0.04167".

These results are then keyed into the HP67 programmable calculator with a copy of B and K magnetic program card WW9002 [8] to obtain the necessary adjustments (as opposed to balance masses) required. The procedure of keying these results is given in [8]. Table 6.9.1(I) presents one set of experimental results. When the adjustments obtained from the calculator are made, the beam should then pass through the centres C1 and C2 of screens S1 and S2 respectively (Figure 6.7(a)). Conversely, the screens can be left stationary while body P1 holding L (Figure 6.9) is adjusted.

6.9.1 Presentation of Results - Screen Adjustments.

Table 6.9.1(I) below shows the results produced by adjusting screens placed in slots 280mm apart leaving the laser stationary. Each screen is 10mm outside planes 1 and 2 of the pair of feet A' & B' and C' & D' respectively (Figure 6.3.1 (a)).

Results of adjusting screens
Table 6.9.1 (I)

RUN No	AMOUNT OF SCREEN ADJUSTMENT	RHS SCREEN 1 (PLANE 1)		LHS SCREEN 2 (PLANE 2)	
		Displ/mm	Angle/deg	Displ/mm	Angle/deg
1	None	$V_{1,0}$=10mm	$\gamma_{1,0}$=-150°	$V_{2,0}$=5mm	$\gamma_{2,0}$=-70°
2	Amount of adjustment made to RHS only (ϕ_1=90°, SCREW B') M1=-4x(25.4x0.04167) =-4.234mm	$V_{1,1}$=12.5mm	$\gamma_{1,1}$=-134°	$V_{2,1}$=5.5mm	$\gamma_{2,1}$=-70°
3	Amount of adjustment made to LHS only (ϕ_2=90°, SCREW D') M2=7x(25.4x0.04167) =7.409mm	$V_{1,2}$=8.0mm	$\gamma_{1,2}$=-152°	$V_{2,2}$=3.0mm	$\gamma_{2,2}$=40°
4	None (recheck on first run)	$V_{1,0}$=10mm	$\gamma_{1,0}$=-150°	$V_{2,0}$=5.0mm	$\gamma_{2,0}$=-70°

Pitch of screws = 0.04167".

RESOLVING RESULTANT VECTORS AFTER COMPUTATION OF RESULTS

(Hewlett-Packard HP-67 (15 seconds)).

Table 6.9.1 (II) - Position of Laser Spot

LEG ADJUSTMENT (DISPLACEMENT/MM)	SCREEN S1	SCREEN S2
None	10mm @ -150^{o}	5mm @ -70^{o}
Leg B' (-4 Turns) = -4.324mm	12.5mm @ -134^{o}	5.5mm @ -70^{o}
Leg D' (+7 Turns) = 7.41mm	8.0mm @ -152^{o}	3.0mm @ 40^{o}

↓

COMPUTE

(HEWLETT PACKARD HP-67 ONLY 15 SECONDS)

↓

PLANE	ADJUSTMENT/MM
Legs A' and B'	-9.62mm @ (90^{o}+113.89^{o})
Legs C' and D'	5.19mm @ (90^{o}+37.96^{o})

↓

FINAL ADJUSTMENT COMPONENTS

	LINEAR LEG DISPLACEMENT/MM	EQUIVALENT No. OF TURNS
A'	8.795	8.31
B'	3.896	3.68
C'	3.192	3.02
D'	4.092	3.87

↓

DIVISION OF COMPUTED VECTORS
INTO FINAL ADJUSTMENT COMPONENTS.

RHS (LEGS A' AND B')	LHS (LEGS C' AND D')
PLANE 1	PLANE 2
R=-9,62 mm Φ=203,89°	R = 5,19mm Φ=127,96°

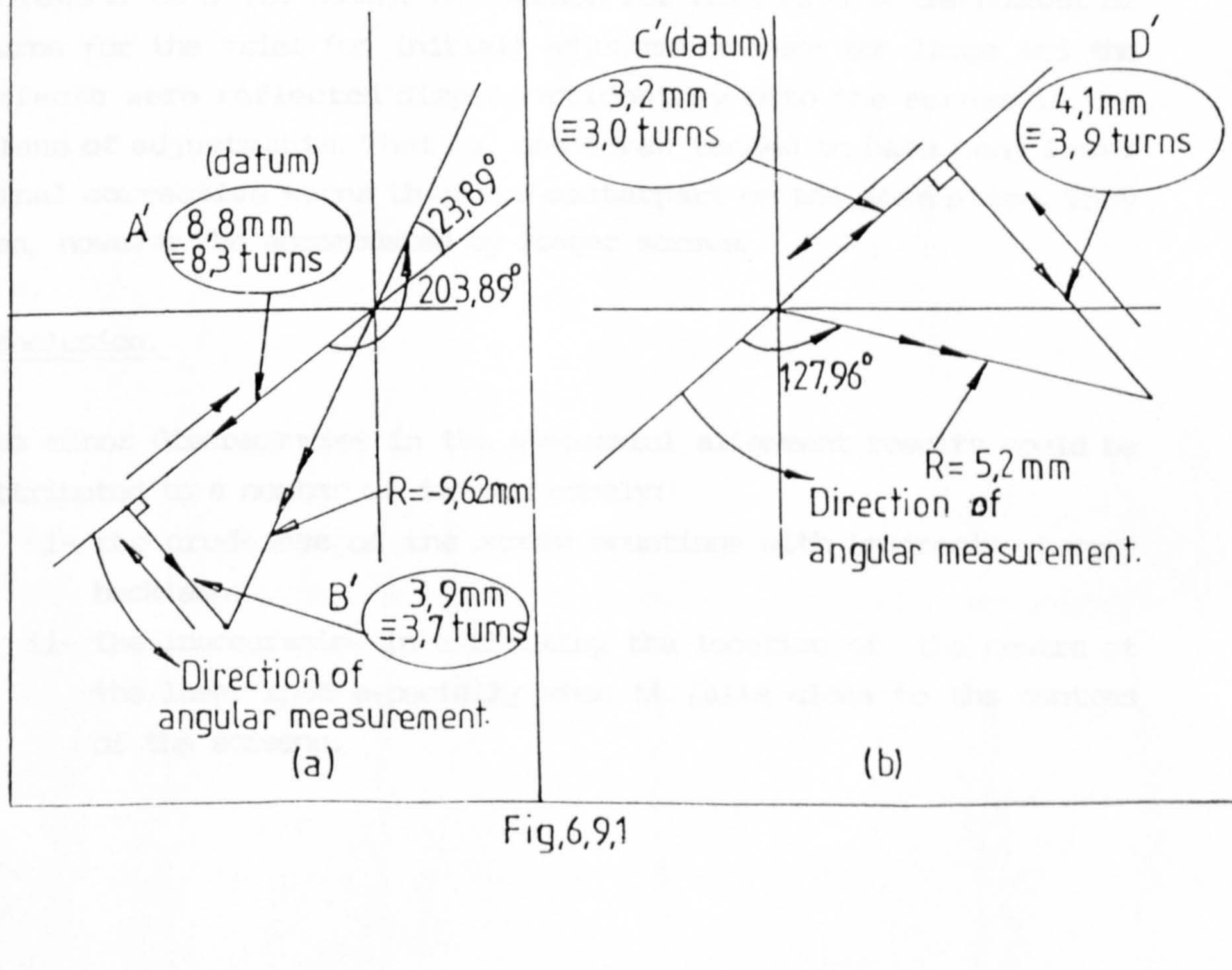

Fig,6,9,1

RESULTS AND COMMENTS

After the appropriate adjustments (Figures 6.9.1(a) and (b)) were made to the four screws, the laser spot on the R.H.S. (plane 1) fell approximately 0.5mm away from the centre of the screen S1 at an angle of approximately $+30^{o}$. The spot on the L.H.S.(plane 2) fell exactly at the centre of the screen S2.

The outside arrows in the two triangles of Figures 6.9.1 (a) and (b) show the directions and the number of turns that an individual screw needs to be adjusted for alignment. The directions of screw adjustments indicated by these arrows are opposite to those worked out by calculations. A possible explanation for this is that the planes of adjustment of the screws supporting the screens are outside those supporting the laser.

In addition to the above experiment, many similar ones were also conducted with different number of screw turns. The majority achieved reasonably good alignment results. In certain exceptional cases, the final number of screw turns obtained from the computer results were either too large to be accomodated on some screw lengths or the perspex body holding the screens simply moved out of contacts with screws A' or B' (or both). The reason for this is that the number of turns for the trial (or initial) adjustments were too large and the effects were reflected disproportionately onto the screws in the plane of adjustments. That is, one screw tended to have many fewer final corrective turns than its couterpart on the same plane. They can, however, be accomodated by longer screws.

Conclusion.

The minor discrepancies in the successful alignment results could be attributed to a number of factors namely:

i- the crudeness of the screw mountings with imminently large backlash.

ii- the inaccuracies in estimating the location of the centre of the laser spot especially when it falls close to the centres of the screens.

iii- the glass screens never fitted squarely into the slots because the screens were inaccurately cut out.

Apart from these minor discrepancies and the loss of contacts caused by large initial trial screw turns, alignment by screen adjustments were successful and thus proves the existence of analogy between balancing and alignment.

6.9.2 Adjustment of the laser.

Since alignment by laser adjustment follows exactly the same procedure as in 6.9.1 above, it is pointless to try and present results obtained by this method. As in screen adjustments and for similar reasons, the outside arrows in triangles obtained by this method (similar to those in Figures 6.9.1(a) and (b)) give directions of final adjustments.

In all the experimental attempts conducted using this method, the problem of inadequate screw lengths sometimes involving two srews (one from each plane) were encountered when making the final adjustments. This problem persisted even when the screens were moved closer to the laser source. This suggests the existence of an optical lever. Longer screws, likely to accomodate the relatively large number of turns, and longer V-grooves to avoid loss of contacts are suggested.

* * * * * * * * * * * * *

REFERENCES

1. E.F. Fichter and E.D. McDowell.
"A novel Design for a robot arm", Presented at the International Technology Conference ASME Century 2. Emerging Technology Conference V1. San Francisco, California, Aug. 12-15, 1980. Published in 1980 by ASME, New York. (p.250-256).

2. K.H. Hunt.
"Structural Kinematics of in-parallel-actuated robot-arms", Transactions of the American Society of Mechanical Engineers, 1983 ,vol. 105, (Journal of Mechanisms, Transmissions and Automation in Design p.705-712).

3. D. Stewart.
"A platform with six degrees of freedom", Proceedings of the Institution of Mechanical Engineers ,1965, vol.180, Part 1 (p.371-378).

4. B. Roth.
"Robots", Applied Mechanics Reviews, vol.31, No.11, Nov.1978 (p.1511-1519).

5. F.P. Bowden and D. Tabor.
"The friction and lubrication of solids". Part I. Clarendon Press 1950. (p.9, 11, 327).

6. E.L. Thearle.
"Dynamic Balancing of Rotating Machinery in the Field", Transactions of the American Society of Mechanical Engineers, 1934 ,vol.56. (p.745-753).

7. W.T. Thomson.
"Vibration Theory and Applications", George Allen and Unwin. Published 1966. (p.86-89).

8. J. Vaughan.
"Static and dynamic balancing". Operation manual and application notes. Bruel and Kjaer. Naerum-Denmark. (p.1-11).

CHAPTER 7

SMALL DISPLACEMENT ANALYSIS OF 3- AND 4-DEGREE OF FREEDOM MANIPULATORS

CHAPTER OVERVIEW

In Chapter 6, alignment of lines in space has been successfully demonstrated by means of a 4-degree of freedom manipulator of unknown displacement characteristics whose construction is based on the Kelvin Coupling. This chapter examines the potential of such a manipulator in laser/fibre alignment by first analysing its displacement characteristics theoretically. Establishment of the characteristics leads to better prediction of the variation of laser diode position either on or outside the manipulator with respect to actuator displacements. These displacements are responsible for laser-fibre misalignments and can therefore be directly linked to the laser efficiency equations (2.2.4). In this respect, a vectorial technique devised by Davies [2] is applied to analyse the spatial displacements of 3- and 4- degree of freedom manipulators (7.1.1 and 7.1.2) respectively. Results obtained from the latter are checked intuitively (7.2.1), experimentally (7.4) and by computation (7.5). This technique is unique because it does not only involve the normal vector transformations (used for transferring quantities from one frame to another) but it also brings in the application of Kirchhoff's Laws [3]. The derivations of some of the essential transformation matrices applied in this method are presented in Appendix B.

The study of both spatial and planar small motions of bodies can be pursued as a matter of general interest. In this chapter, the study is specifically linked to the analysis of manipulators in order to try and solve the problems of mechanical misalignments between a laser beam and an optical fibre. In Section 7.3, the relationship between the displacements of a selected point of interest on a 4-degree of freedom manipulator and the laser/fibre coupling efficiency is derived. All the three mechanical misalignment tolerances which must be greatly minimised in order to obtain an acceptable coupling efficiency, are taken into account in that analysis. Although this analysis is deemed successful, the discussions and conclusions

presented in section 7.4.4 highlight the major reasons for dismissing these results for direct application to the practical laser/fibre alignment.

7.0 INTRODUCTION

Successful launching of the non-linear laser beam emanating from the face of a semiconductor laser diode into a monomode or multi-mode optical fibre depends largely upon the effects of mechanical alignment tolerances to the input coupling loss. Barnoski [1] states that in the design and development of the practical laser source to fibre coupling, not only is it important to realise the expected magnitude of the coupling coefficient but also the effects of the mechanical tolerances. There are three basic types of mechanical tolerances that contribute to the coupling loss. These are (a) the lateral misalignment tolerance, (b) the longitudinal misalignment tolerance and (c) the angular misalignment tolerance between the laser diode and the input face of the fibre. Due to the non-linearity of the beam, it has been discovered [1] that the lateral misalignment tolerance has the most severe effects on the coupling efficiency followed by the longitudinal misalignment and lastly the angular misalignment tolerance in that order.

Evidence of the imposition of severe lateral misalignment tolerance is presented [1] in Figure 7(a) where the increase in input coupling loss is plotted as a function of radial displacement of the centre of a Corning low-loss step index (NA = 0.14) fibre and the centre of a 50μm diameter surface emitting LED manufactured by Plessey. The plot shows that the input coupling is highly sensitive to lateral misalignment.

The effects on the input coupling loss of the other two remaining mechanical tolerances (longitudinal and angular misalignments) are shown plotted [1] in Figures 7(b) and (c) respectively. As can be seen, the input coupling is relatively insensitive to both the longitudinal fibre-to-LED (source) separation and the angular misalignment of the axis of the source to that of the fibre. These plots show that if the fibre and LED are separated by a distance of 150 μm, the increase in coupling loss is approximately 0.9 dB while an angular shift of the fibre axis with respect to the LED surface of

Increase in input coupling loss versus
lateral displacement

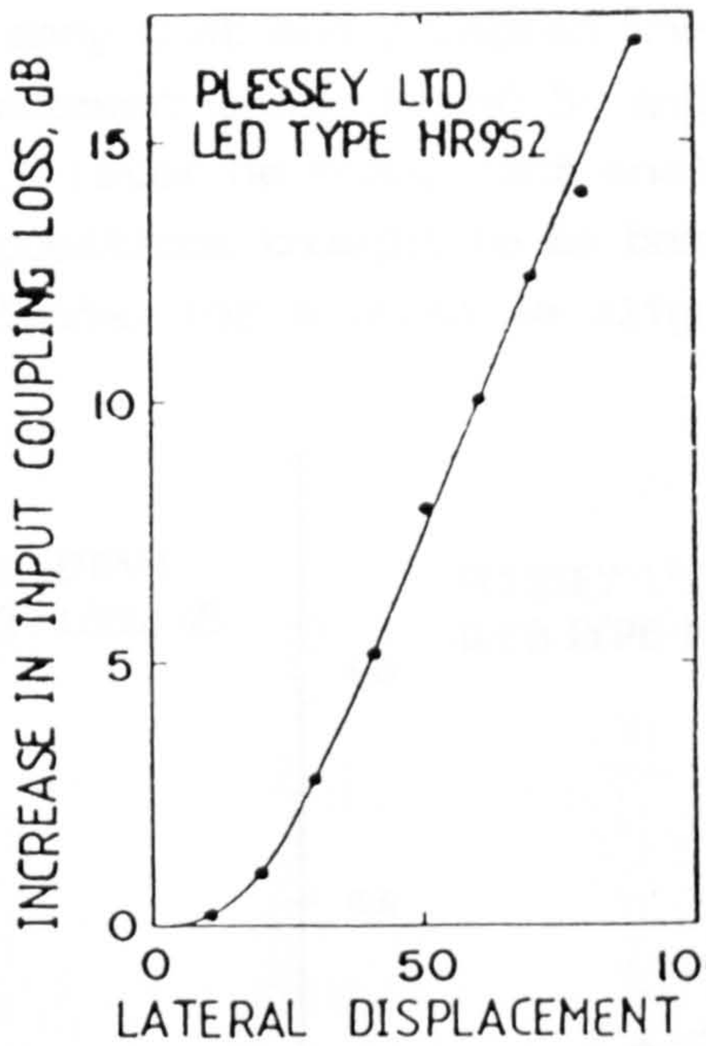

Fig,7 (a)

Increase in input coupling loss versus
longitudinal LED-to-fiber separation.

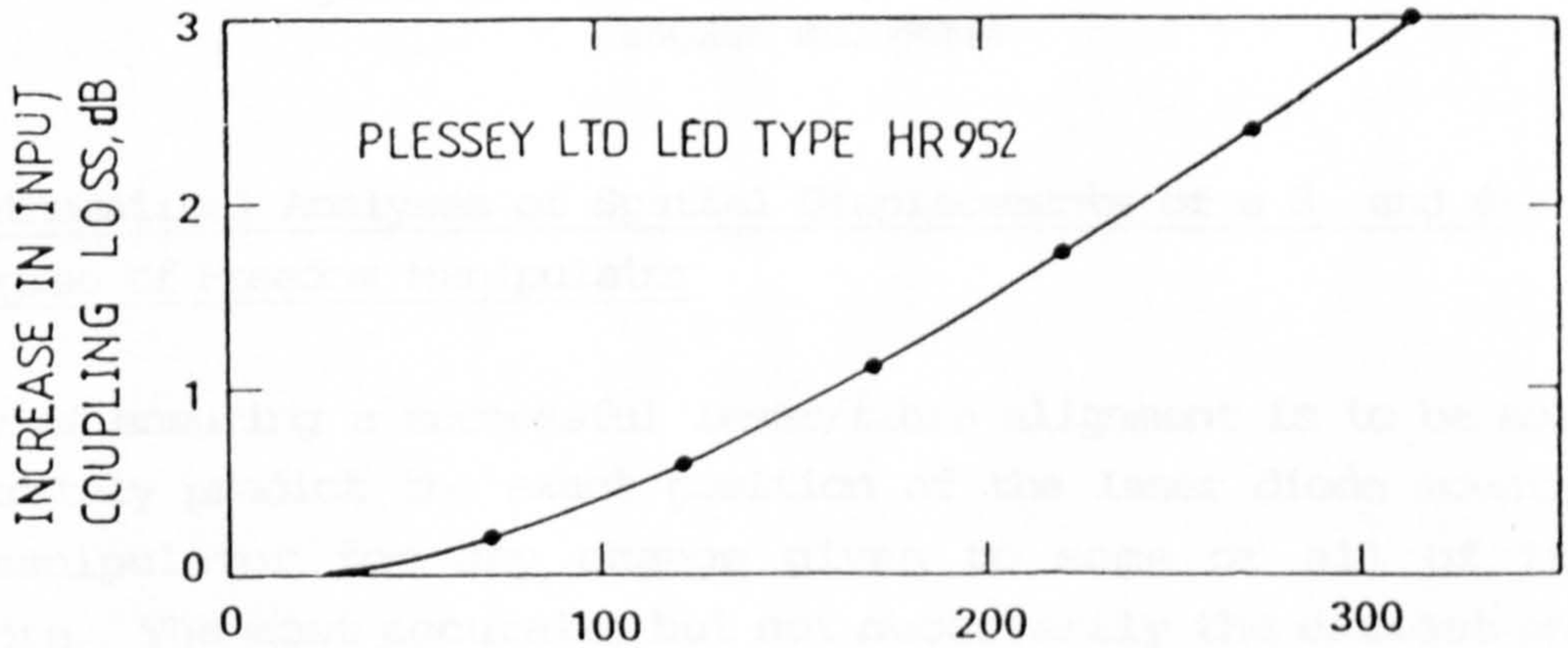

Fig,7 (b)

10^{o} produces a loss increase of only approximately 0.25 dB.

Barnoski [1] also found out that the severity of these mechanical alignment tolerances are not only restricted to input couplers using single strands but are equally sensitive in bundle couplers. It is the differing effects of these three types of alignment tolerances (particularly the effects of lateral misalignments) on the laser-fibre coupling efficiency that has prompted the investigation of the study of small displacement analysis of 3- and 4-degree of freedom manipulators. As will later be seen, such analyses are targeted on the displacements of positions thought to be best suited for mounting semiconductor laser diodes for a possible alignment with stationary optical fibres.

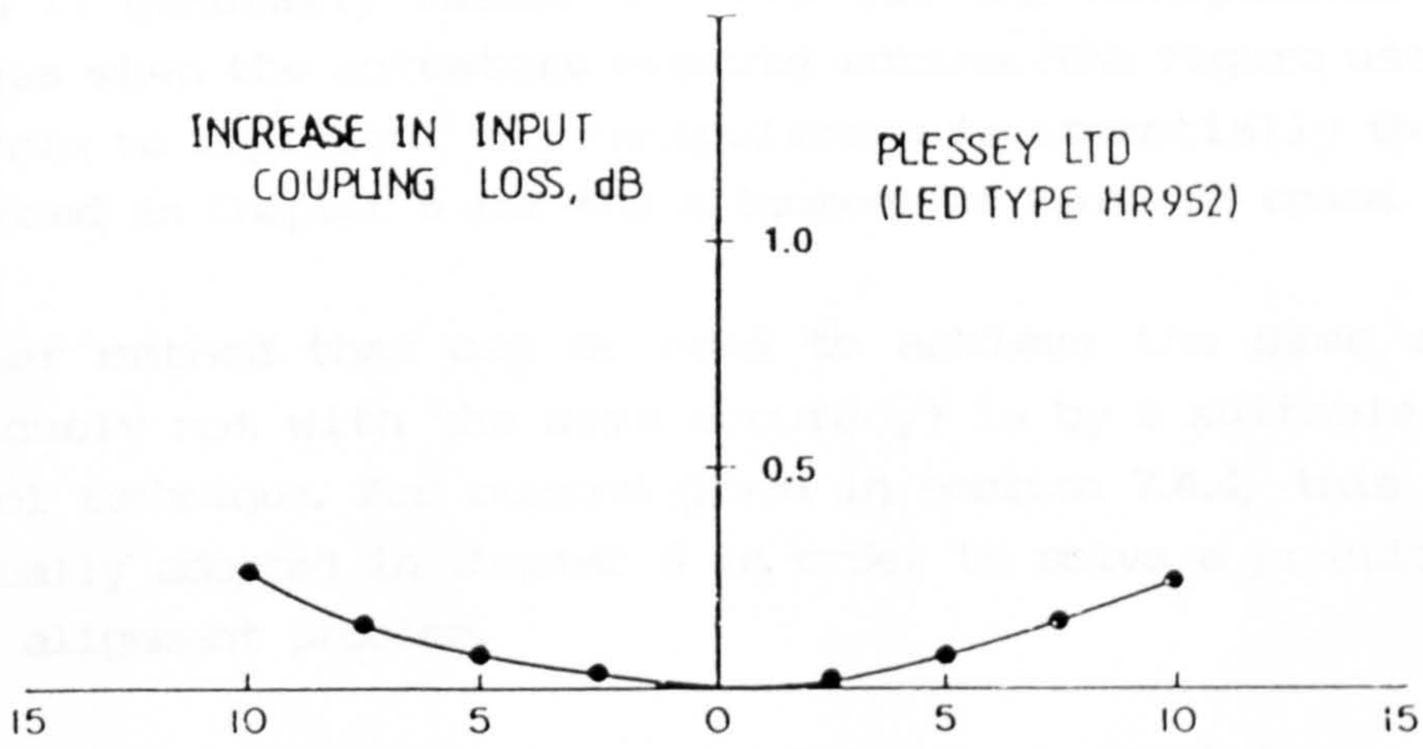

Fig.7 (c) Increase in input coupling loss versus angular misalignment.

7.1 Mathematical Analyses of Spatial Displacements of a 3- and 4-Degree of Freedom Manipulator

One way of ensuring a successful laser/fibre alignment is to be able to accurately predict the exact position of the laser diode mounted on a manipulator for any change given to some or all of its actuators. The most accurate, but not necessarily the easiest and only way of accomplishing this, is by formulating a mathematical expression that correctly describes the path prescribed by the point of interest when the manipulator changes position. In Sections 7.1.1 and 7.1.2, method I which utilises a tensor technique [2] is used to

produce analytical results for the 3- and 4-degree of freedom manipulators respectively.

This technique, however, is only useful in determining the characteristics of a manipulator with any number of degrees of freedom as long as the actual size of adjustments to the feet are known (7.1.2). It cannot be used to solve the laser/fibre misalignment problems at this stage because of both the practical and analytical problems associated with the process (as later seen in 7.4.4).

The two manipulators analysed here are symmetrical. This symmetry makes it generally easier to work out the manipulator position changes when the actuators execute motion. The figure used in this analysis to represent the manipulators is essentially the same as that used in Chapter 6 for the alignment of lines in space.

Another method that can be used to achieve the same alignment (obviously not with the same accuracy) is by a suitable adaptive control technique. For reasons given in section 7.4.4, this method is eventually adopted in Chapter 9 in order to solve a practical laser-fibre alignment problem.

7.1.1 The analysis of a 3-degree of freedom manipulator (Method I)

The analysis of the small displacements of point O located on the surface of this manipulator (Figure 7.1.1(a)) is presented in stages as outlined below.

1. Selection of the position of global frame with origin at O on the surface of body 3 is given in Figure 7.1.1(a).

2. Setting of local frames and the corresponding velocity components.

   i) Coupling A:(Fig.7.1.1(c))

This coupling has four degrees of freedom and hence four velocity components.The local frame is set (at O^a) parallel to the global

SUPPORT OF A3-DEGREE OF FREEDOM MANIPULATOR
(A,D & E EACH MAKES TWO POINTS CONTACTS)

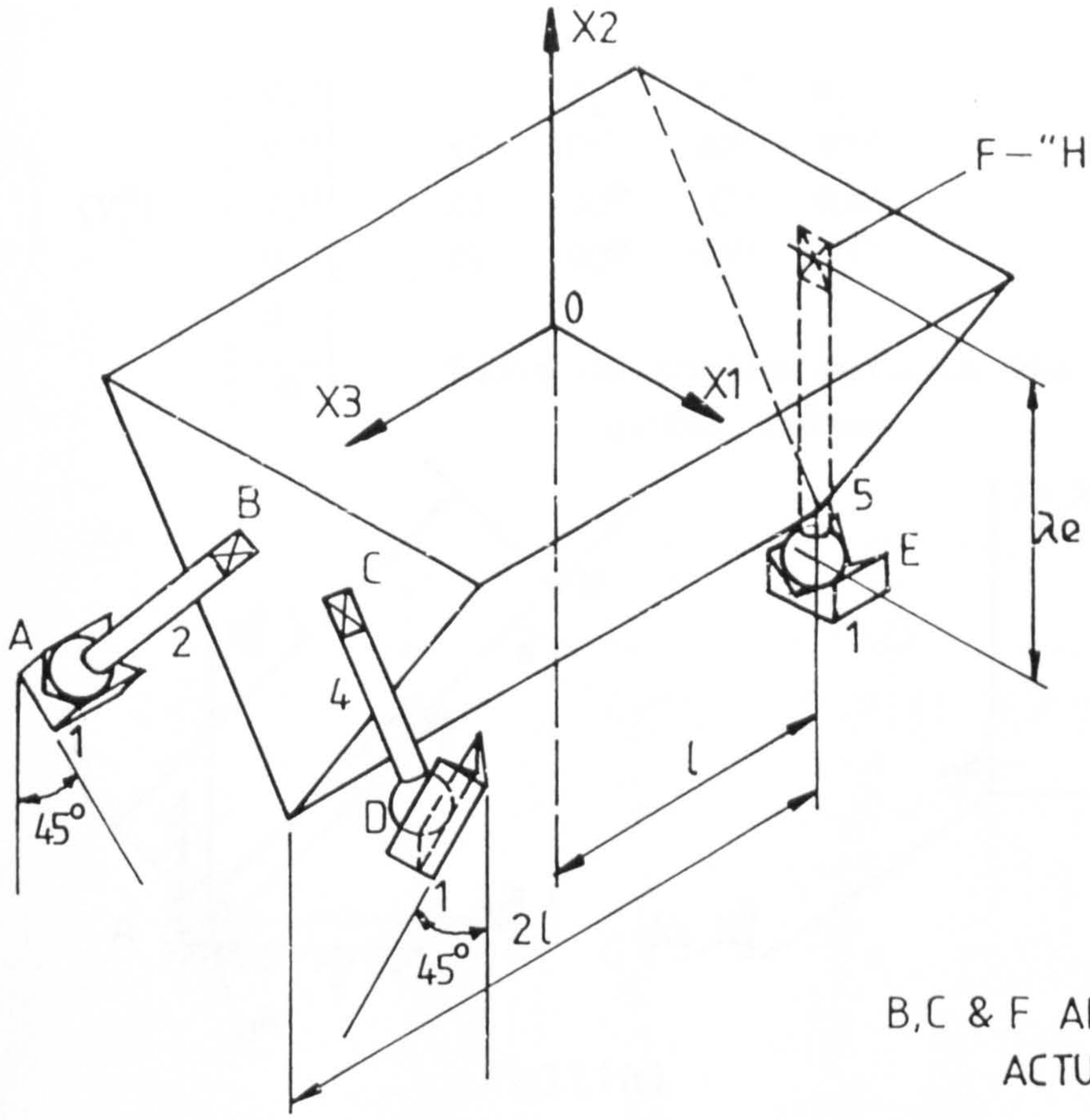

B,C & F ARE LINEAR ACTUATORS

Fig. 7,1,1 (a)

CONSTRAINT GRAPH FOR THE ABOVE MANIPULATOR

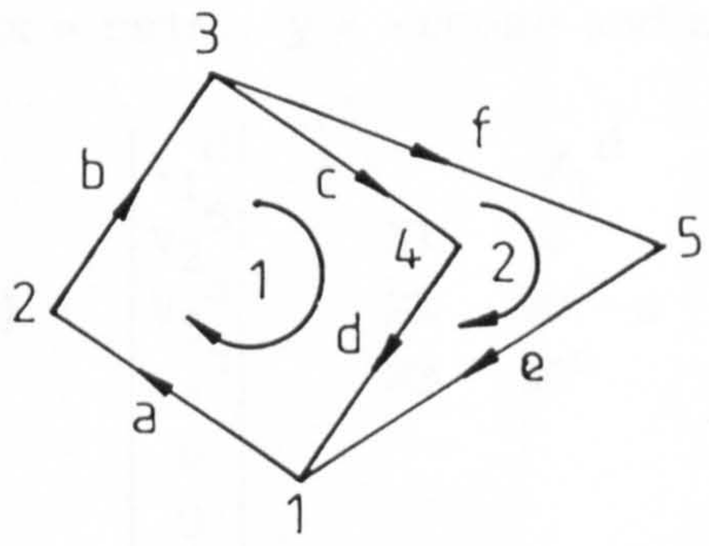

Fig. 7,1,1 (b)

frame so that only translation is necessary. The position of O^a with respect to the global frame is given by $x = -r\sin\theta$, $y = -r\cos\theta$ and $z = \ell$.

$$\{V_\ell^a\} = \begin{Bmatrix} V_1{}^a \\ V_2{}^a \\ V_3{}^a \\ 0 \\ 0 \\ V_6{}^a \end{Bmatrix}$$

	$X_1{}^a$	$X_2{}^a$	$X_3{}^a$
X1	0^o	90^o	90^o
X2	90^o	0^o	90^o
X3	90^o	90^o	0^o

Table of angles between the local and global frames.

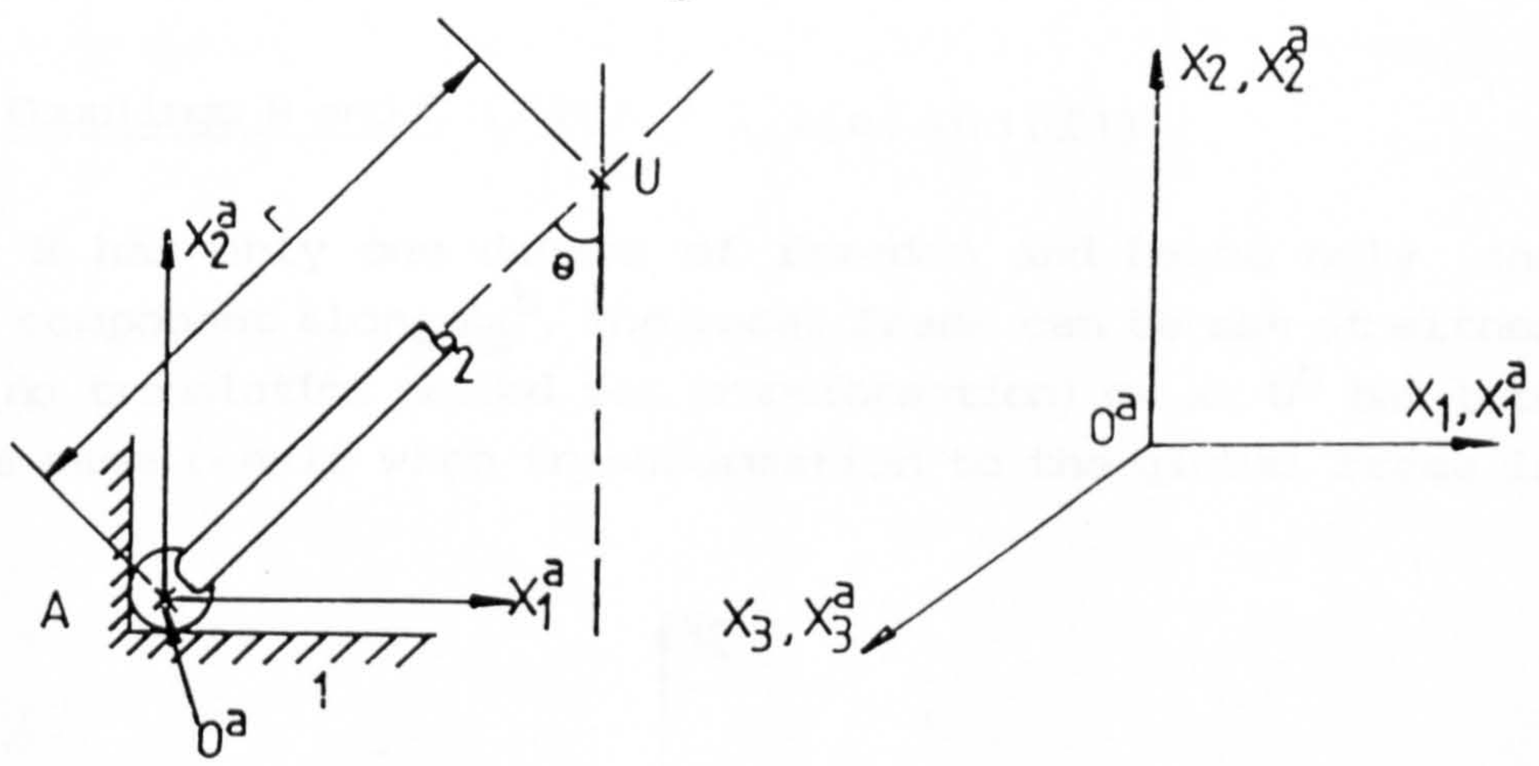

Fig.7.1.1(c)

ii) Coupling D:(Fig.7.1.1(d))

With four degrees of freedom, D has four velocity components. $X_2{}^d$ is set along body 4 (leg) and $X_1{}^d$ parallel to the groove G which forms part of body 1. The position of O^d with respect to the global frame is given as $x = r\sin\theta$, $y = -r\cos\theta$ and $z = \ell$.

$$\{V_\ell^d\} = \begin{Bmatrix} V_1{}^d \\ V_2{}^d \\ V_3{}^d \\ V_4{}^d \\ 0 \\ 0 \end{Bmatrix}$$

	$X_1{}^d$	$X_2{}^d$	$X_3{}^d$
X1	θ	$90^o+\theta$	90^o
X2	$90^o-\theta$	θ	90^o
X3	90^o	90^o	0^o

Table of angles between the local and global frames.

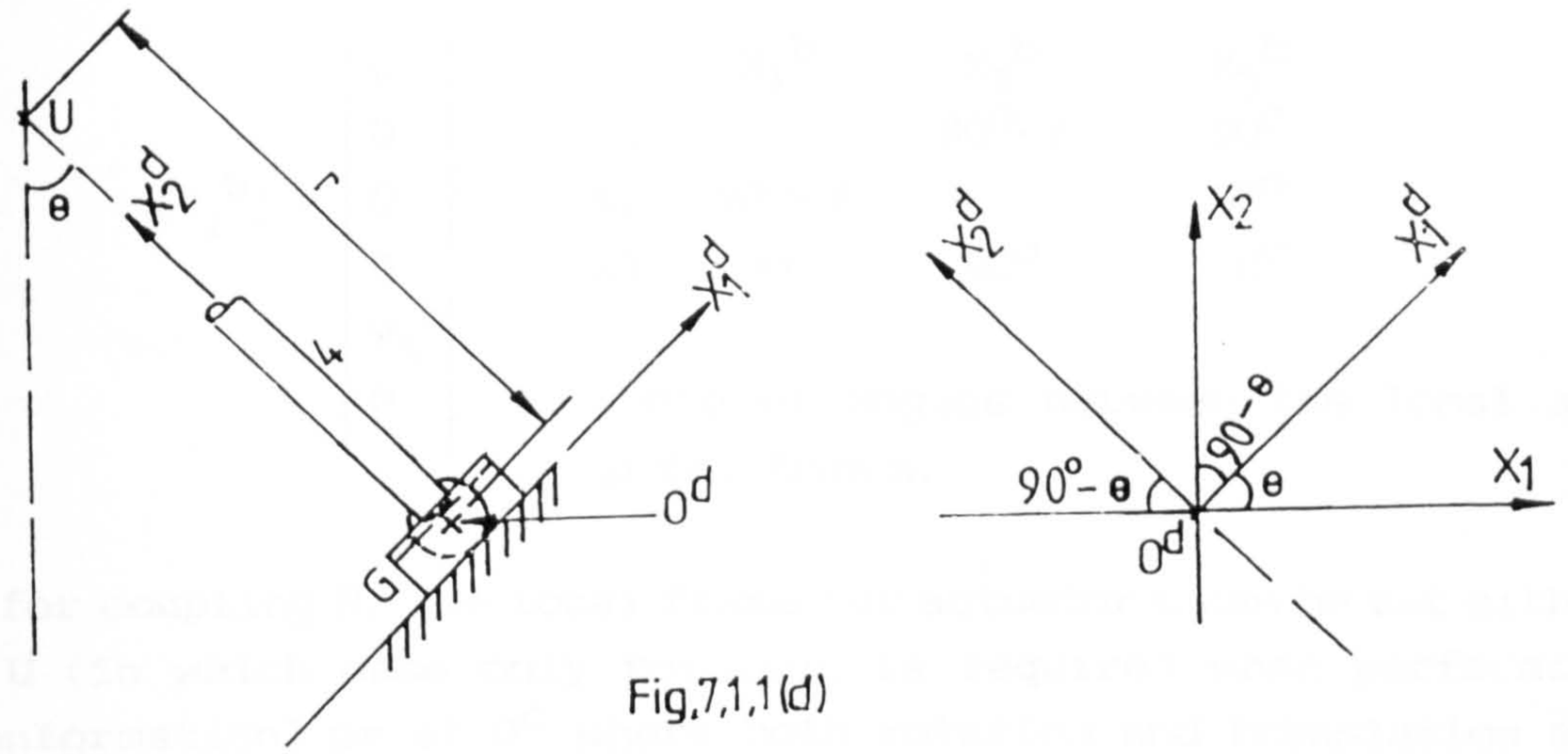

Fig.7.1.1(d)

iii) Couplings B and C:(Figs.7.1.1(e)and(f))

Actuator B has only one degree of freedom and hence only one velocity component along X_2^b. The local frame can be set at either point U (no translation needed for transformation) or at 0^b but both yield the same result when transformation to the global frame is effected.

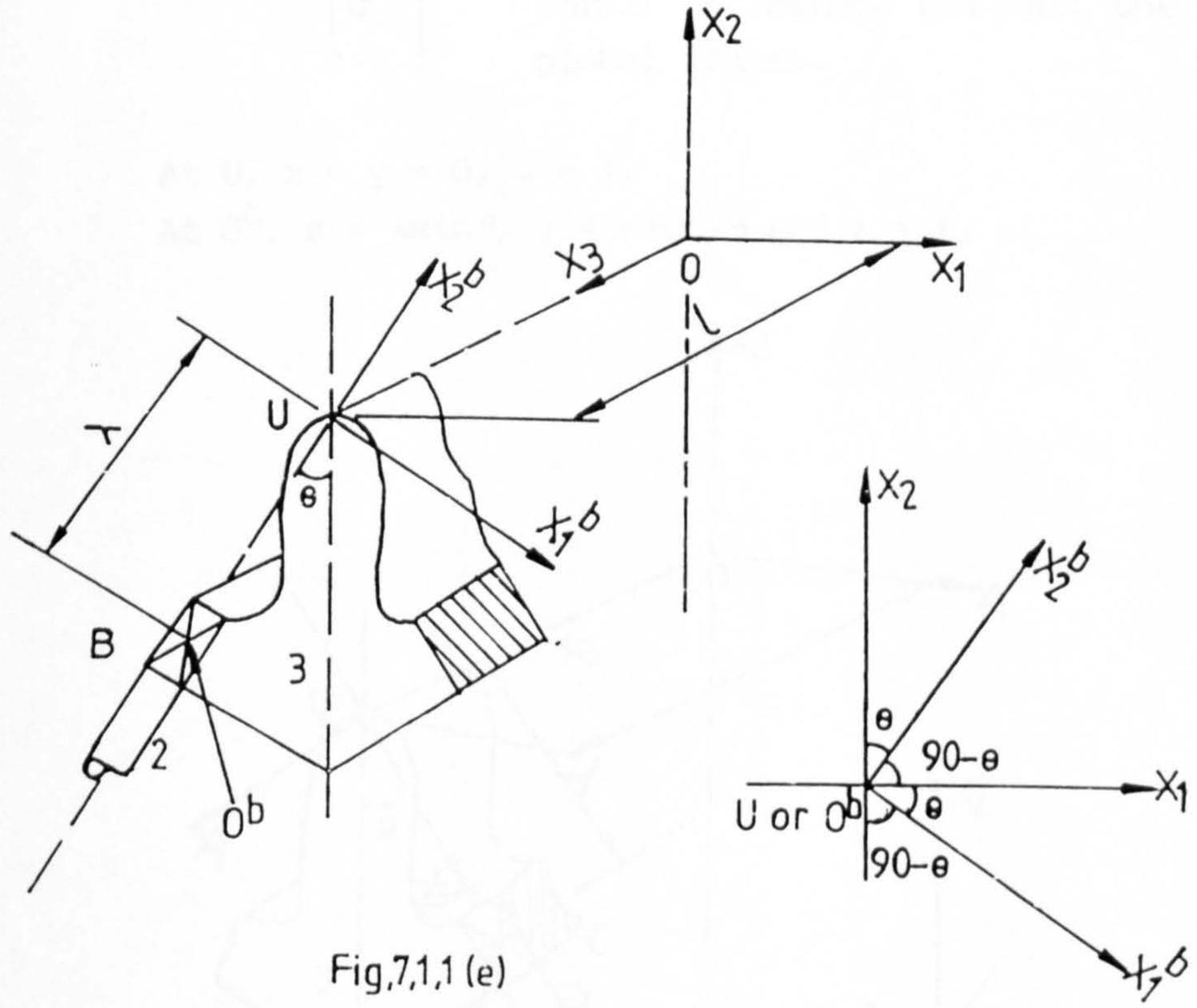

Fig.7.1.1 (e)

At U, $x = y = 0$, $z = \ell$

At 0^b, $x = -\lambda\sin\theta$, $y = -\lambda\cos\theta$, $z = \ell$.

$$\{V_\ell{}^b\} = \begin{Bmatrix} 0 \\ 0 \\ 0 \\ 0 \\ V_5{}^b \\ 0 \end{Bmatrix}$$

	$X_1{}^b$	$X_2{}^b$	$X_3{}^b$
X1	θ	$90^o - \theta$	90^o
X2	$90^o + \theta$	θ	90^o
X3	90^o	90^o	0^o

Table of angles between the local and global frames.

As for coupling B, the local frame for actuator C can be set either at U (in which case only rotation is required when performing tranformation) or at 0^C where both rotation and translation are required when transforming to the global frame but the same result is obtained for either method used.

$$\{V_\ell{}^C\} = \begin{Bmatrix} 0 \\ 0 \\ 0 \\ 0 \\ V_5{}^C \\ 0 \end{Bmatrix}$$

	$X_1{}^C$	$X_2{}^C$	$X_3{}^C$
X1	$180^o - \theta$	$90^o - \theta$	90^o
X2	$90^o + \theta$	$180^o - \theta$	90^o
X3	90^o	90^o	0^o

Table of angles between the local and global frames.

At U, $x = y = 0$, $z = \ell$.

At 0^C, $x = \lambda \sin\theta$, $y = -\lambda\cos\theta$ and $z = \ell$.

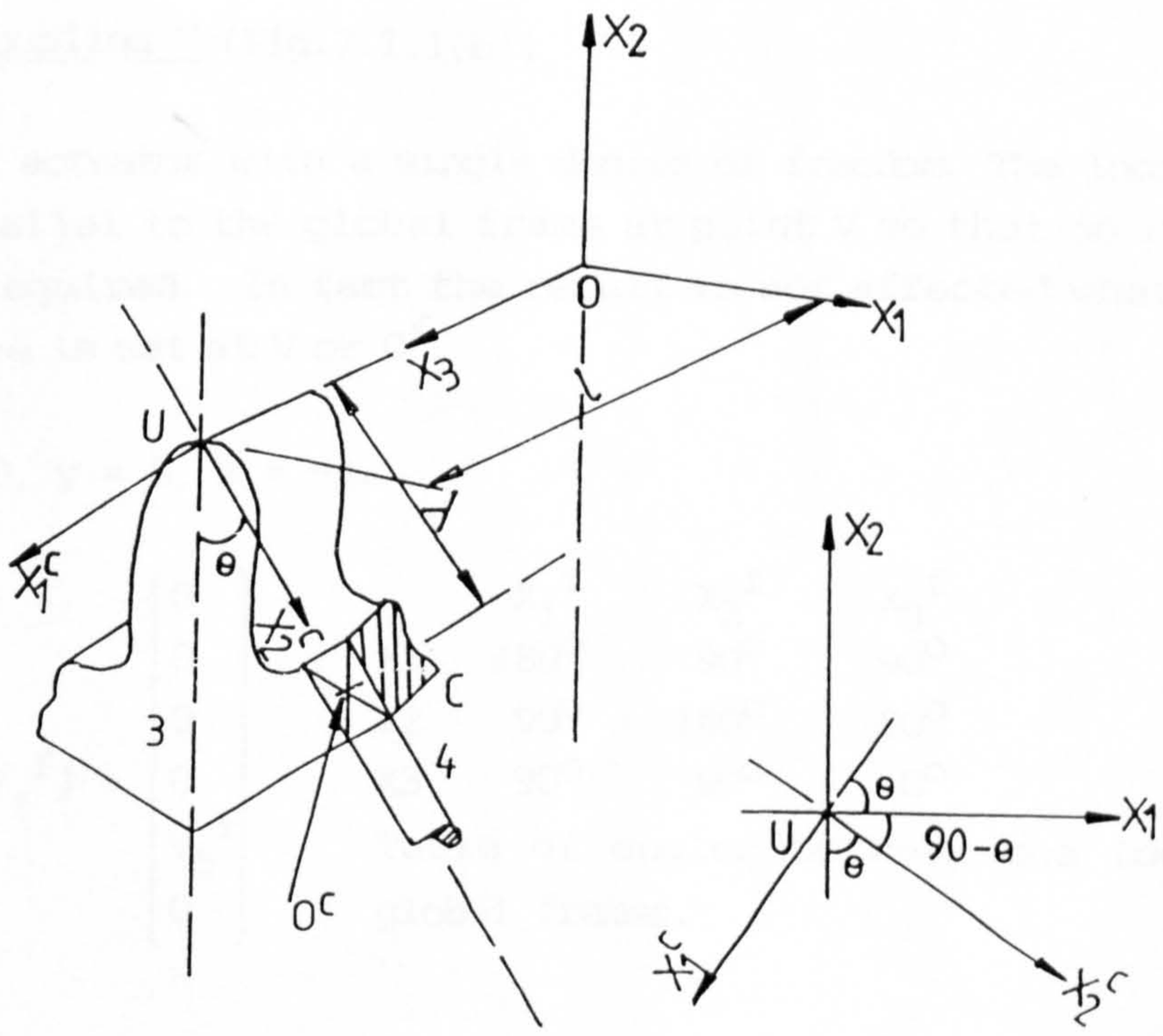

Fig. 7.1.1 (f)

iv) Coupling E:(Fig.7.1.1(g))

This coupling has four degrees of freedom and therefore four velocity components. The local frame is set such that X_2^e and X_1^e are parallel to the respective planes of the groove body 1. That is, the position of 0^e with respect to the global frame is x = 0, y = $-\lambda e$ and z = $-\ell$.

$$\{V_\ell{}^e\} = \begin{Bmatrix} V_1{}^e \\ V_2{}^e \\ V_3{}^e \\ 0 \\ 0 \\ V_6{}^e \end{Bmatrix}$$

	X_1^e	X_2^e	X_3^e
X1	θ	$90^o+\theta$	90^o
X2	$90^o-\theta$	θ	90^o
X3	90^o	90^o	0^o

Table of angles between the local and global frames.

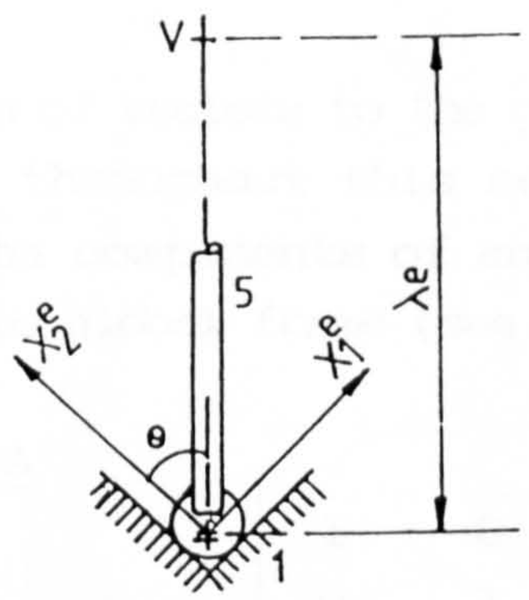

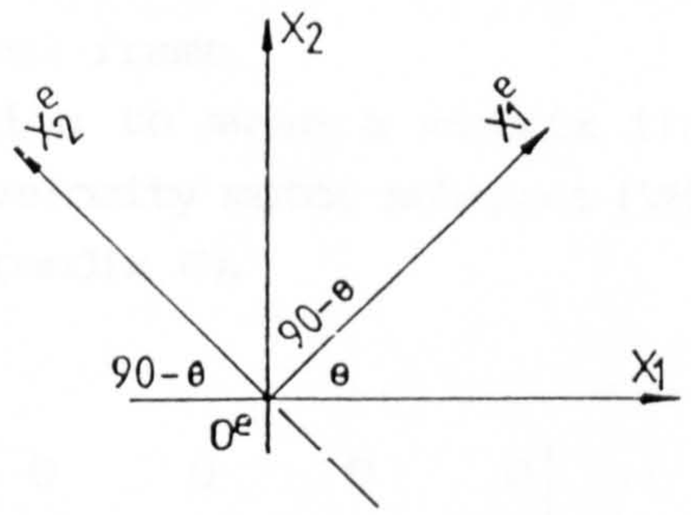

Fig.7.1.1(g)

v) Coupling F:(Fig.7.1.1(h))

This is an actuator with a single degree of freedom. The local frame is set parallel to the global frame at point V so that no rotation would be required. In fact the result is not affected whether the local frame is set at V or 0^f.

At V, x = 0, y = 0, z = $-\ell$.

$$\{V_\ell{}^f\} = \begin{Bmatrix} 0 \\ 0 \\ 0 \\ 0 \\ V_5{}^f \\ 0 \end{Bmatrix}$$

	X_1^f	X_2^f	X_3^f
X1	180^o	90^o	90^o
X2	90^o	180^o	90^o
X3	90^o	90^o	0^o

Table of angles between the local and global frames.

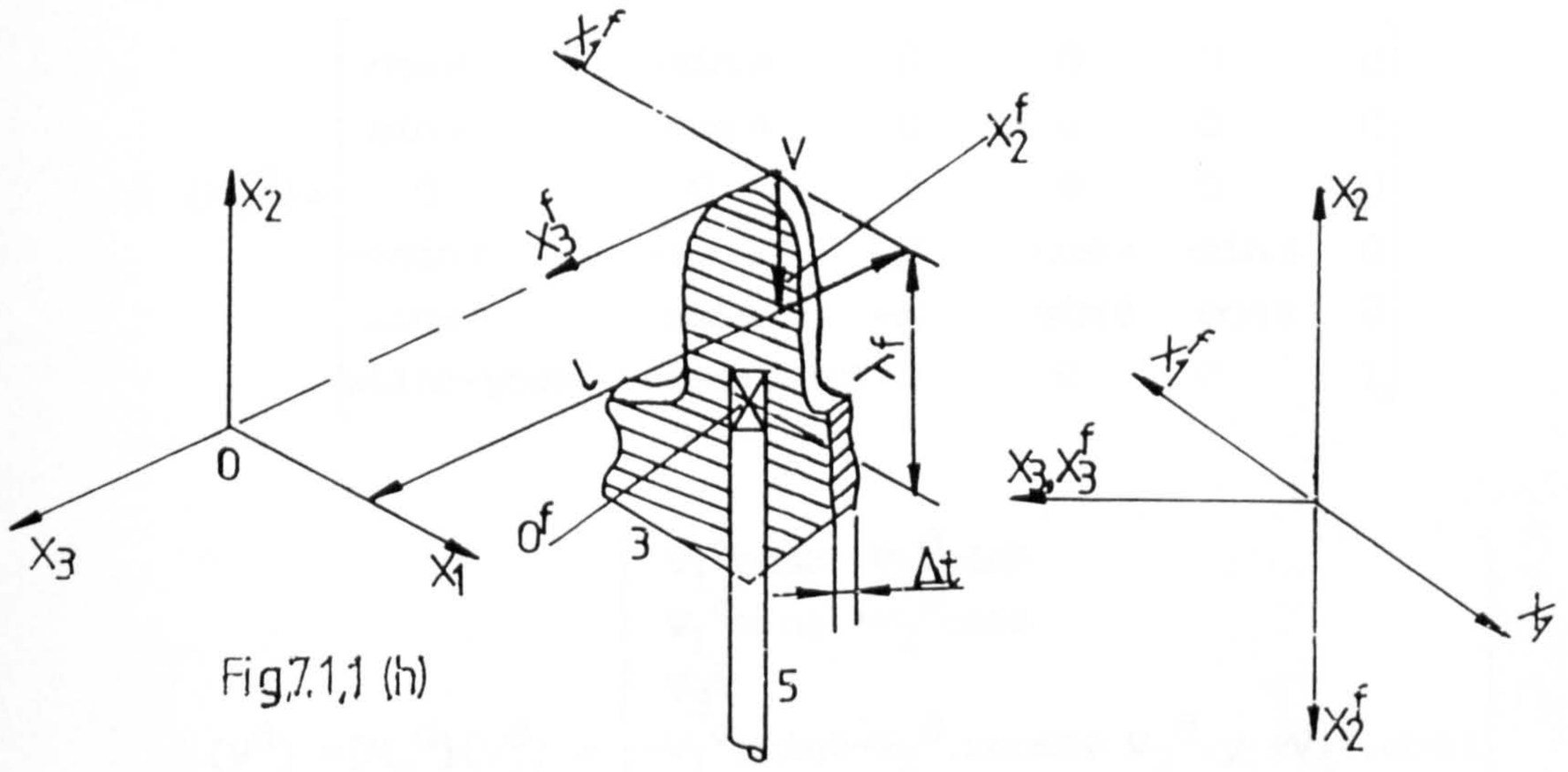

Fig 7.1.1 (h)

3. Transformation of vectors to the global frame.

$[M_v]$ is used throughout this section to mean a matrix that transforms the components of any velocity motor subspace (VMS) from a local to global frame (see Appendix C).

i) Coupling A

$$[M_v{}^a] = \begin{bmatrix} 1 & 0 & 0 & 0 & 0 & 0 \\ 0 & 1 & 0 & 0 & 0 & 0 \\ 0 & 0 & 1 & 0 & 0 & 0 \\ 0 & -\ell & -r\cos\theta & 1 & 0 & 0 \\ \ell & 0 & r\sin\theta & 0 & 1 & 0 \\ r\cos\theta & -r\sin\theta & 0 & 0 & 0 & 1 \end{bmatrix}$$

$$\text{But } \{V^a\} = [M_v{}^a]\ \{V_\ell{}^a\} = \begin{bmatrix} V_1{}^a \\ V_2{}^a \\ V_3{}^a \\ -(\ell V_2{}^a + V_3{}^a . r\cos\theta) \\ \ell V_1{}^a + V_3{}^a . r\sin\theta \\ V_1{}^a\, r\cos\theta - V_2{}^a\, r\sin\theta + V_6{}^a \end{bmatrix}$$

ii) Coupling D

$$[M_v^d] = \begin{bmatrix} \cos\theta & -\sin\theta & 0 & 0 & 0 & 0 \\ \sin\theta & \cos\theta & 0 & 0 & 0 & 0 \\ 0 & 0 & 1 & 0 & 0 & 0 \\ -z\sin\theta & -z\cos\theta & y & \cos\theta & -\sin\theta & 0 \\ z\cos\theta & -z\sin\theta & -x & \sin\theta & \cos\theta & 0 \\ x\sin\theta - y\cos\theta & x\cos\theta + y\sin\theta & 0 & 0 & 0 & 1 \end{bmatrix}$$

$$\therefore \{V^d\} = [M_v^d]\{V_\ell^d\} = \begin{bmatrix} V_1^d\cos\theta - V_2^d\sin\theta \\ V_1^d\sin\theta + V_2^d\cos\theta \\ V_3^d \\ -V_1^d z\sin\theta - V_2^d.z\cos\theta + V_3^d.y + V_4^d.\cos\theta \\ V_1^d.z\cos\theta - V_2^d.z\sin\theta - V_3^d.x + V_4^d.\sin\theta \\ V_1^d(x\sin\theta - y\cos\theta) + V_2^d(x\cos\theta + y\sin\theta) \end{bmatrix}$$

But $x = r\sin\theta$, $y = -r\cos\theta$, $z = \ell$.

$$\therefore \{V^d\} = \begin{bmatrix} V_1^d\cos\theta - V_2^d\sin\theta \\ V_1^d\sin\theta + V_2^d\cos\theta \\ V_3^d \\ -\ell(V_1^d\sin\theta + V_2^d\cos\theta) - V_3^d.r\cos\theta + V_4^d.\cos\theta \\ \ell\,(V_1^d\cos\theta - V_2^d\sin\theta) - V_3^d.r\sin\theta + V_4^d\sin\theta \\ V_1^d.r \end{bmatrix}$$

iii) Coupling B

Since the local frame is chosen to be at U (Figure 7.1.1(e)), only rotation is required.

$$\therefore [M_v^b] = \begin{bmatrix} \cos\theta & \sin\theta & 0 & 0 & 0 & 0 \\ -\sin\theta & \cos\theta & 0 & 0 & 0 & 0 \\ 0 & 0 & 1 & 0 & 0 & 0 \\ \ell\sin\theta & -\ell\cos\theta & 0 & \cos\theta & \sin\theta & 0 \\ \ell\cos\theta & \ell\sin\theta & 0 & -\sin\theta & \cos\theta & 0 \\ 0 & 0 & 0 & 0 & 0 & 1 \end{bmatrix}$$

$$\{V^b\} = [M_V{}^b]\{V_\ell{}^b\} = \begin{bmatrix} 0 \\ 0 \\ 0 \\ V_5{}^b \sin\theta \\ V_5{}^b \cos\theta \\ 0 \end{bmatrix}$$

iv) Coupling C

Since local frame is again chosen to be at U (Figure 7.1.1(f)), only rotation is required.

$$[M_V{}^C] = \begin{bmatrix} -\cos\theta & \sin\theta & 0 & 0 & 0 & 0 \\ -\sin\theta & -\cos\theta & 0 & 0 & 0 & 0 \\ 0 & 0 & 1 & 0 & 0 & 0 \\ \ell\sin\theta & \ell\cos\theta & 0 & -\cos\theta & \sin\theta & 0 \\ -\ell\cos\theta & \ell\sin\theta & 0 & -\sin\theta & -\cos\theta & 0 \\ 0 & 0 & 0 & 0 & 0 & 1 \end{bmatrix}$$

$$\{V^C\} = [M_V{}^C]\{V_\ell^C\} = \begin{bmatrix} 0 \\ 0 \\ 0 \\ V_5{}^C \sin\theta \\ -V_5{}^C \cos\theta \\ 0 \end{bmatrix}$$

v) Coupling E

$$[M_V{}^e] = \begin{bmatrix} \cos\theta & -\sin\theta & 0 & 0 & 0 & 0 \\ \sin\theta & \cos\theta & 0 & 0 & 0 & 0 \\ 0 & 0 & 1 & 0 & 0 & 0 \\ \ell\sin\theta & \ell\cos\theta & -\lambda_e & \cos\theta & -\sin\theta & 0 \\ -\ell\cos\theta & \ell\sin\theta & 0 & \sin\theta & \cos\theta & 0 \\ \lambda_e\cos\theta & -\lambda_e\sin\theta & 0 & 0 & 0 & 1 \end{bmatrix}$$

$$\{V^e\} = [M_V{}^e]\{V_\ell{}^e\} = \begin{bmatrix} V_1{}^e\cos\theta - V_2{}^e\sin\theta \\ V_1{}^e\sin\theta + V_2{}^e\cos\theta \\ V_3{}^e \\ \ell(V_1{}^e\sin\theta + V_2{}^e\cos\theta) - V_3{}^e.\lambda_e \\ \ell(-V_1{}^e\cos\theta + V_2{}^e\sin\theta) \\ \lambda_e(V_1{}^e\cos\theta - V_2{}^e\sin\theta) + V_6{}^e \end{bmatrix}$$

vi) Coupling F

$$[M_V{}^f] = \begin{bmatrix} -1 & 0 & 0 & 0 & 0 & 0 \\ 0 & -1 & 0 & 0 & 0 & 0 \\ 0 & 0 & 1 & 0 & 0 & 0 \\ 0 & \ell & 0 & -1 & 0 & 0 \\ -\ell & 0 & 0 & 0 & -1 & 0 \\ 0 & 0 & 0 & 0 & 0 & 1 \end{bmatrix}$$

$$\therefore \{V^f\} = [M_V{}^f]\{V_\ell{}^f\} = \begin{bmatrix} 0 \\ 0 \\ 0 \\ 0 \\ -V_5{}^f \\ 0 \end{bmatrix}$$

4. Now apply Kirchhoff's circulation law [3] to the two circuits of Figure 7.1.1(b):

a) Thus for Circuit 1 (involving couplings A, B, C and D),

$$\{V^a\} + \{V^b\} + \{V^c\} + \{V^d\} = \{0\}$$

$$\begin{bmatrix} 1 & c\theta & 0 & -s\theta & 0 & 0 & 0 & 0 & 0 & 0 \\ 0 & s\theta & 1 & c\theta & 0 & 0 & 0 & 0 & 0 & 0 \\ 0 & 0 & 0 & 0 & 1 & 1 & 0 & 0 & 0 & 0 \\ 0 & -\ell s\theta & -\ell & -\ell c\theta & -rc\theta & -rc\theta & c\theta & s\theta & s\theta & 0 \\ \ell & \ell c\theta & 0 & -\ell s\theta & rs\theta & -rs\theta & s\theta & c\theta & -c\theta & 0 \\ rc\theta & r & -rs\theta & 0 & 0 & 0 & 0 & 0 & 0 & 1 \end{bmatrix} \begin{bmatrix} V_1{}^a \\ V_1{}^d \\ V_2{}^a \\ V_2{}^d \\ V_3{}^a \\ V_3{}^d \\ V_4{}^d \\ V_5{}^b \\ V_5{}^c \\ V_6{}^a \end{bmatrix} = \{0\}.$$

Note that $c\theta$ and $s\theta$ stand for $\cos\theta$ and $\sin\theta$ respectively. But $\theta = 45^{o}$ and so the constant matrix becomes

$$\begin{bmatrix} 1 & 1/\sqrt{2} & 0 & -1/\sqrt{2} & 0 & 0 & 0 & 0 & 0 & 0 \\ 0 & 1/\sqrt{2} & 1 & 1/\sqrt{2} & 0 & 0 & 0 & 0 & 0 & 0 \\ 0 & 0 & 0 & 0 & 1 & 1 & 0 & 0 & 0 & 0 \\ 0 & -\ell/\sqrt{2} & -\ell & -\ell/\sqrt{2} & -r/\sqrt{2} & -r\sqrt{/2} & 1/\sqrt{2} & 1/\sqrt{2} & 1/\sqrt{2} & 0 \\ \ell & \ell/\sqrt{2} & 0 & -\ell/\sqrt{2} & r/\sqrt{2} & -r/\sqrt{2} & 1/\sqrt{2} & 1/\sqrt{2} & -1/\sqrt{2} & 0 \\ r/\sqrt{2} & r & -r/\sqrt{2} & 0 & 0 & 0 & 0 & 0 & 0 & 1 \end{bmatrix}$$

or

$$\begin{bmatrix} \sqrt{2} & 1 & 0 & -1 & 0 & 0 & 0 & 0 & 0 & 0 \\ 0 & 1 & \sqrt{2} & 1 & 0 & 0 & 0 & 0 & 0 & 0 \\ 0 & 0 & 0 & 0 & 1 & 1 & 0 & 0 & 0 & 0 \\ 0 & -\ell & -\ell\sqrt{2} & -\ell & -r & -r & 1 & 1 & 1 & 0 \\ \ell\sqrt{2} & \ell & 0 & -\ell & r & -r & 1 & 1 & -1 & 0 \\ r/\sqrt{2} & r & -r/\sqrt{2} & 0 & 0 & 0 & 0 & 0 & 0 & 1 \end{bmatrix}$$

or

$$\begin{bmatrix} 1/\sqrt{2} & 0 & -1/\sqrt{2} & -1 & 0 & 0 & 0 & 0 & 0 & 0 \\ 1/\sqrt{2} & 1 & 1/\sqrt{2} & 0 & 0 & 0 & 0 & 0 & 0 & 0 \\ 0 & 0 & 0 & 0 & 1 & 1 & 0 & 0 & 0 & 0 \\ -\ell/\sqrt{2} & -\ell & -\ell/\sqrt{2} & 0 & -r & 0 & 0 & 0 & 1 & 0 \\ \ell/\sqrt{2} & 0 & -\ell/\sqrt{2} & -\ell & 0 & -r & 1 & 1 & 0 & 0 \\ r/\sqrt{2} & r & -r/\sqrt{2} & 0 & 0 & 0 & 0 & 0 & 0 & 1 \end{bmatrix}$$

Hence,

i) $V_1^{a}/\sqrt{2} - V_2^{a}/\sqrt{2} - V_2^{d} = 0$

ii) $V_1^{a}/\sqrt{2} + V_1^{d} + V_2^{a}/\sqrt{2} = 0$

iii) $V_3^{a} + V_3^{d} = 0$

iv) $-\ell V_1^{a}/\sqrt{2} - \ell V_1^{d} - \ell V_2^{a}/\sqrt{2} - r.V_3^{a} + V_5^{c} = 0$

v) $\ell\, V_1^a/\sqrt{2} - \ell V_2^a/\sqrt{2} - \ell V_2^d - r.V_3^d + V_4^d + V_5^b = 0$

vi) $r\, V_1^a/\sqrt{2} + r.V_1^d - r\, V_2^a/\sqrt{2} + V_6^a = 0$

b) For Circuit 2 (involving couplings C, D, E, F),

$$\{V^f\} + \{V^e\} - \{V^c\} - \{V^d\} = \{0\}$$

$$\begin{bmatrix} -c\theta & c\theta & s\theta & -s\theta & 0 & 0 & 0 & 0 & 0 & 0 \\ -s\theta & s\theta & -c\theta & c\theta & 0 & 0 & 0 & 0 & 0 & 0 \\ 0 & 0 & 0 & 0 & -1 & 1 & 0 & 0 & 0 & 0 \\ \ell s\theta & \ell s\theta & \ell c\theta & \ell c\theta & rc\theta & -\lambda_e & -c\theta & -s\theta & 0 & 0 \\ -\ell c\theta & -\ell c\theta & \ell s\theta & \ell s\theta & rs\theta & 0 & -s\theta & c\theta & -1 & 0 \\ -r & \lambda_e c\theta & 0 & -\lambda_e s\theta & 0 & 0 & 0 & 0 & 0 & 1 \end{bmatrix} \begin{bmatrix} V_1^d \\ V_1^e \\ V_2^d \\ V_2^e \\ V_3^d \\ V_3^e \\ V_4^d \\ V_5^c \\ V_5^f \\ V_6^e \end{bmatrix} = \{0\}.$$

Again $c\theta$ and $s\theta$ stand for $\cos\theta$ and $\sin\theta$ respectively and $\theta = 45^o$, so the constant matrix becomes:

$$\begin{bmatrix} -1/\sqrt{2} & 1/\sqrt{2} & 1/\sqrt{2} & -1/\sqrt{2} & 0 & 0 & 0 & 0 & 0 & 0 \\ -1/\sqrt{2} & 1/\sqrt{2} & -1/\sqrt{2} & 1/\sqrt{2} & 0 & 0 & 0 & 0 & 0 & 0 \\ 0 & 0 & 0 & 0 & -1 & 1 & 0 & 0 & 0 & 0 \\ \ell/\sqrt{2} & \ell/\sqrt{2} & \ell/\sqrt{2} & \ell/\sqrt{2} & r/\sqrt{2} & -\lambda_e & -1/\sqrt{2} & -1/\sqrt{2} & 0 & 0 \\ -\ell/\sqrt{2} & -\ell/\sqrt{2} & \ell/\sqrt{2} & \ell/\sqrt{2} & r/\sqrt{2} & 0 & -1/\sqrt{2} & 1/\sqrt{2} & -1 & 0 \\ -r & \lambda_e/\sqrt{2} & 0 & -\lambda_e/\sqrt{2} & 0 & 0 & 0 & 0 & 0 & 1 \end{bmatrix}$$

or

$$\begin{bmatrix} -1 & 1 & 1 & -1 & 0 & 0 & 0 & 0 & 0 & 0 \\ -1 & 1 & -1 & 1 & 0 & 0 & 0 & 0 & 0 & 0 \\ 0 & 0 & 0 & 0 & -1 & 1 & 0 & 0 & 0 & 0 \\ \ell & \ell & \ell & \ell & r & -\lambda_e\sqrt{2} & -1 & -1 & 0 & 0 \\ -\ell & -\ell & \ell & \ell & r & 0 & -1 & 1 & -\sqrt{2} & 0 \\ -r & \lambda_e/\sqrt{2} & 0 & -\lambda_e/\sqrt{2} & 0 & 0 & 0 & 0 & 0 & 1 \end{bmatrix}$$

or

$$\begin{bmatrix} 0 & 0 & 1 & -1 & 0 & 0 & 0 & 0 & 0 & 0 \\ -1 & 1 & 0 & 0 & 0 & 0 & 0 & 0 & 0 & 0 \\ 0 & 0 & 0 & 0 & -1 & 1 & 0 & 0 & 0 & 0 \\ \ell & \ell & 0 & 0 & 0 & -\lambda_e/\sqrt{2} & 0 & -1 & 1/\sqrt{2} & 0 \\ 0 & 0 & \ell & \ell & r & -\lambda_e/\sqrt{2} & -1 & 0 & -1/\sqrt{2} & 0 \\ -r & \lambda_e/\sqrt{2} & 0 & -\lambda_e/\sqrt{2} & 0 & 0 & 0 & 0 & 0 & 1 \end{bmatrix}$$

Hence,

i) $V_2^d = V_2^e$

ii) $V_1^e = V_1^d$

iii) $V_3^d = V_3^e$

iv) $\ell V_1^d + \ell V_1^e - V_3^e \lambda_e/\sqrt{2} = 0$

v) $\ell . V_2^d + \ell V_2^e + r V_3^d - V_3^e \lambda_e/\sqrt{2} = 0$

vi) $-r . V_1^d + V_1^e . \lambda_e/\sqrt{2} - V_2^e . \lambda_e/\sqrt{2} + V_6^e = 0$

5. Final solutions of the spatial analysis

The detailed procedure of working out the final solutions is relegated to Appendix D to avoid labouring a relatively minor point in the main pages further than its importance justifies. The final solutions are presented here because they are thought to be more important than merely showing the manipulation of numbers.

Since the displacements are very small, the velocities V_5^b, V_5^c and V_5^f can be replaced by displacements ε^b, ε^c and ε^f. Now, since this is an analysis of a 3-degree of freedom manipulator, the corresponding motion or displacements of point O in body 3 can be obtained from the results of $\{V^a\} + \{V^b\}$ (Appendix D) as

(a) $x_1 = \frac{1+\sqrt{2}}{\sqrt{2}} \varepsilon^b + \frac{(\beta r - \sqrt{2}.\lambda_e)}{2\sqrt{2}.r} \varepsilon^c$ in the X_1-direction

Equations 7.1.1(b) $x_2 = \frac{(\varepsilon^b + \varepsilon^c + \varepsilon^f)}{2\sqrt{2}}$ in the X_2-direction

(c) $x_3 = \frac{(\lambda_e - r\sqrt{2})}{2\sqrt{2}\ell} \varepsilon^c$ in the X_3-direction

These solutions are made easier by selecting $\theta = 45^{o}$ and the solutions of the angular displacements are ignored because this is a 3-degree of freedom manipulator.

7.1.2 Solutions of the analysis of a 4-degree of freedom manipulator (Method I)

The detailed analysis of a 4-degree of freedom manipulator follows exactly the same trend as that of the 3-degree of freedom manipulator. In order to avoid labouring essentially the same points here, therefore, the details are relegated to Appendix E. In this section, however, only the final solutions to the 18 equations (of the three circuits) derived in Appendix E by the application of Kirchoff's Laws [3] are presented.

Selection of a path from body 1 to 3 and summation of velocity vectors:

$$\{V^a\} + \{V^b\} = \begin{bmatrix} \{(V_5^g - V_5^b + V_5^f - V_5^c)/2\ell\}.1/\sqrt{2} \\ \{(V_5^f - V_5^c - V_5^g + V_5^b)/2\ell\}.1/\sqrt{2} \\ V_5^f/r \\ \frac{\ell/\sqrt{2}}{2\ell} \quad (V_5^g - V_5^b - V_5^f + V_5^c) - \frac{V_5^f}{\sqrt{2}} + \frac{V_5^f - V_5^c}{\sqrt{2}} + V_5^b/\sqrt{2} \\ \frac{\ell/\sqrt{2}}{2\ell} \quad (V_5^g - V_5^b + V_5^f - V_5^c) + \frac{V_5^f}{\sqrt{2}} - \frac{(V_5^f - V_5^c}{\sqrt{2}} + V_5^b/\sqrt{2} \\ \frac{r}{2\ell} \quad (V_5^g - V_5^b) + (V_5^b - V_5^g - V_5^c + V_5^f)\ r/2\ell \end{bmatrix}$$

$$= \begin{bmatrix} \{(V_5^f + V_5^g) - (V_5^b + V_5^c)\}/2\sqrt{2}\ell \\ \{(V_5^f - V_5^g) + (V_5^b - V_5^c)\}/2\sqrt{2}\ell \\ V_5^f/r \\ \{(V_5^g - V_5^f) + (V_5^b - V_5^c)\}/2\sqrt{2} \\ \{(V_5^g + V_5^f) + (V_5^b + V_5^c)\}/2\sqrt{2} \\ (V_5^f - V_5^c)r/2\ell \end{bmatrix}$$

Since the displacements are very small, the velocities V_5^b, V_5^c, V_5^f and V_5^g can be replaced by the displacements ε_5^b, ε_5^c, ε_5^f and ε_5^g respectively. Since this is an analysis of a 4-degree of freedom manipulator, the solutions must include at least one angular rotation as well as three linear displacements. This is because it would be a waste to use a four degree of freedom manipulator for the manipulation of a point - a task that only requires a three-degree of freedom manipulator as already demonstrated in Section 7.1.1.

So, if rotations about the X_1- and X_2-axes are considered negligible, then the solutions to this analysis are obtained from the results of $\{V^a\} + \{V^b\}$ shown above as:

(a) $x_1 = \frac{1}{2\sqrt{2}}(\varepsilon^g - \varepsilon^f + \varepsilon^b - \varepsilon^c)$ in the X_1-direction

(b) $x_2 = \frac{1}{2\sqrt{2}}(\varepsilon^f + \varepsilon^g + \varepsilon^b + \varepsilon^c)$ in the X_2-direction

Equations 7.1.2

(c) $x_3 = (\varepsilon^f - \varepsilon^c)\ r/2\ell$ in the X_3-direction

(d) $\theta_3 = \varepsilon^f/r$ (rotation about X_3-axis)

Again these solutions are made easier by selecting $\theta = 45^o$.

In general, this tensor technique (Method I) gives results of the form $\{\delta\} = [M]\{\Delta\}$ where $\{\Delta\}$ are the known displacements of a manipulator feet (actuators), [M] is a characteristic matrix of a manipulator that depends on geometry and $\{\delta\}$ is a column vector of three angular (velocities or) rotations about the X_1-, X_2- and X_3-axes and three linear (velocities or) displacements in the X_1- ,X_2- and X_3-directions. It is a very useful technique because the characteristics [M] of any manipulator with any number of degrees of freedom can be obtained once the actual size actuator-adjustments are known.

It cannot, however, be used to solve the laser/fibre misalignment problems because of the practical difficulties involved (Section 7.4.4) and above all the analysis of a 4-degree of freedom

manipulator tackled here gives the results of the small displacements of a point (position of laser diode 0) - a task already solved by the analysis of the 3-degree of freedom manipulator. Section 7.4.4 gives the conditions that need to be fulfilled before this method can be effectively applied to answer the misalignment problems.

7.2 MATHEMATICAL FORMULATION OF THE DISPLACEMENTS OF THE 4-DEGREE OF FREEDOM MANIPULATOR (METHOD II)

The first method which has been applied to the geometrical studies of the displacements of the 3- and 4-degree of freedom manipulators (Section 7.1) makes use of a vectorial transformation. This section, however, presents a second approach which is totally intuitive and in general simpler than the first but only valid for this particular manipulator. It is however more difficult to solve similar problems intuitively for more complicated manipulators. As this is not a general method, it is felt that its illustration on a 4-degree of freedom manipulator is not only representative but sufficient for purposes of comparison with Method I. There is therefore no need for repeating the procedure for a 3-degree of freedom manipulator.

7.2.1 The Intuitive Analysis of a 4-Degree of Freedom Manipulator

In this method, like in the preceding cases of the general vector approach, point G (Figure 7.2.1(a)) located symmetrically on the surface of the manipulator is considered the best position for placing a laser diode. It is this point whose displacements are of major interest in this section.

The apparatus used in this analysis is adopted directly from Figure 6.3.1(a) (Chapter 6). The only exception is that the laser L has been replaced here (Figure 7.2.1(a)) by the solid triangular perspex body P while the feet A, B, C and D are drawn without stands T because they are unnecessary for purposes of this analysis.

Assuming that Figure 7.2.1(a) shows the initial (datum) position of body P, then the positions of G can be worked out in terms of the amount of displacements of feet A and B as follows (Fig. 7.2.1(b)):

i) Initial positions of A', B' and G_1, measured with respect to frame 2

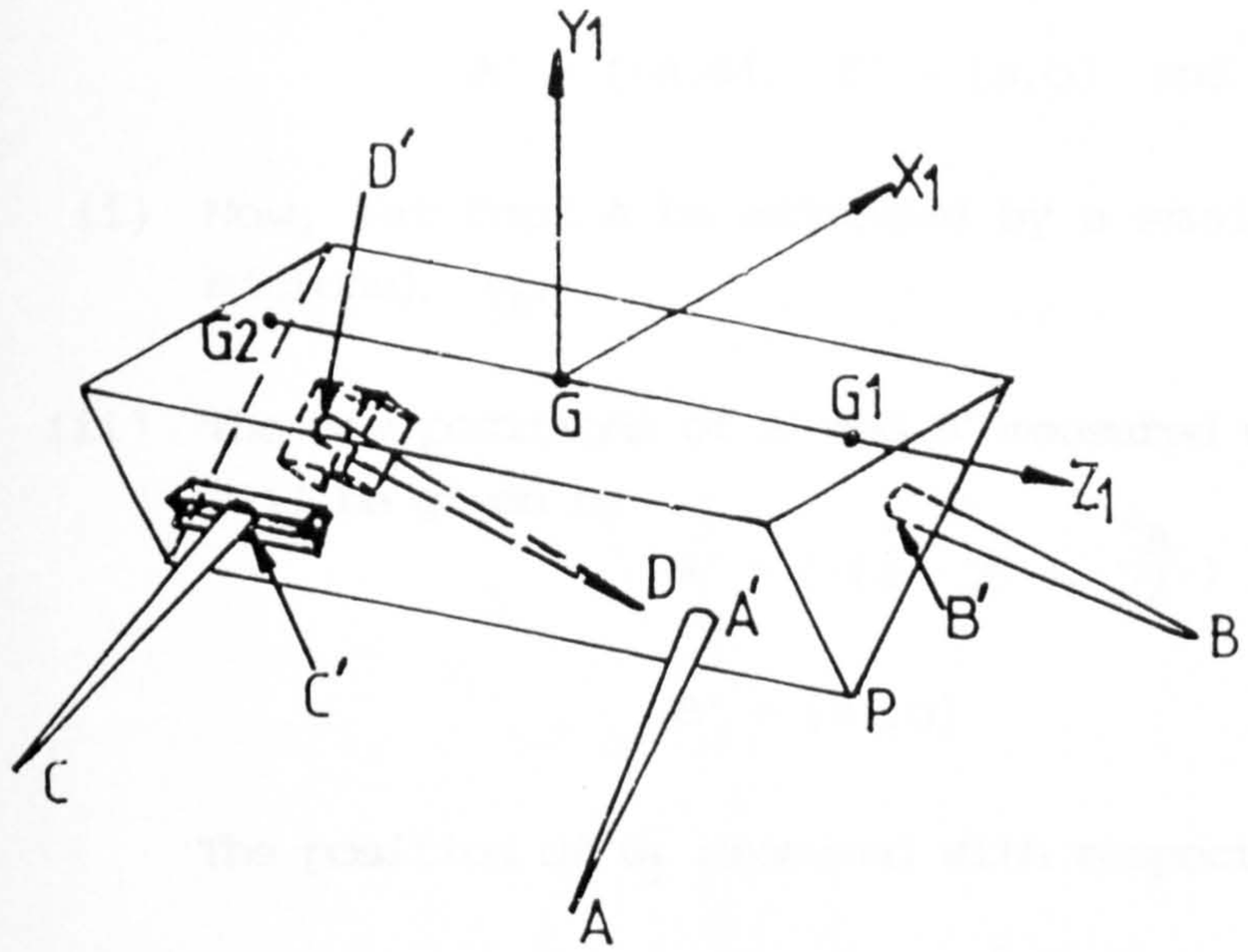

Fig,7,2,1 (a) SUPPORT OF A 4 DEGREE OF FREEDOM MANIPULATOR

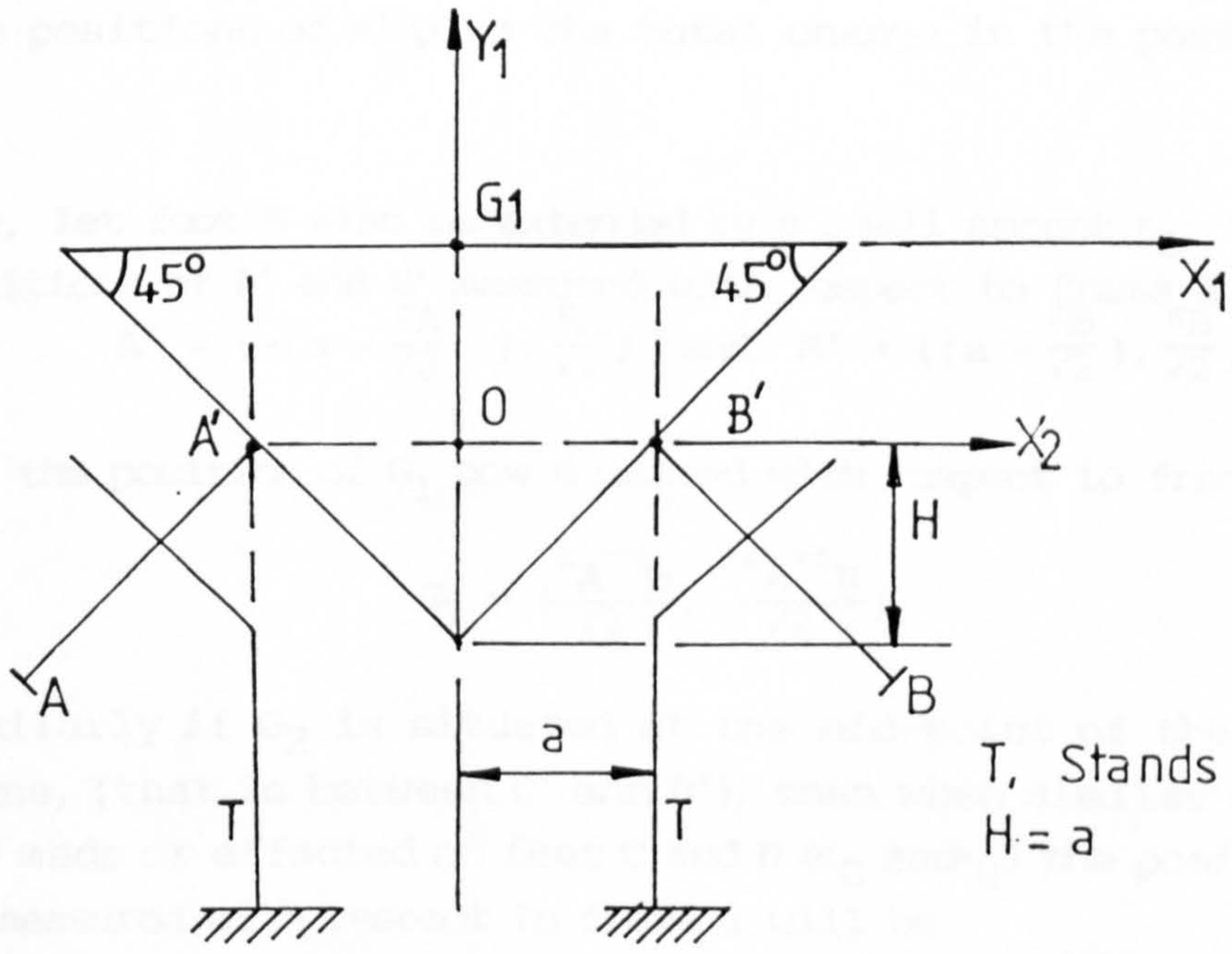

Fig,7,2,1(b) Hemispherical feet A, B supporting plane 1 of body P.

$$A' = (-a,o), \quad B' = (a,o) \quad \text{and} \quad G_1 = (o,a)$$

ii) Now, let foot A be extended by a small amount (measured in microns), ε_A.

iii) The new positions of A' and B' measured with respect to frame 2 will be given by

$$A' = (-(a - \frac{\varepsilon_A}{\sqrt{2}}), \frac{\varepsilon_A}{\sqrt{2}}) \text{ and}$$

$$B' = (a',o)$$

The position of G_1 measured with respect to frame 1 is given by

$$G_1 = (\frac{\varepsilon_A}{\sqrt{2}}, \frac{\varepsilon_A}{\sqrt{2}})$$

That is, the position of G_1 is defined by the total change in the positions of A' plus the total change in the position of B'.

iv) Now, let foot B also be extended by a small amount ε_B, then the positions of A' and B' measured with respect to frame 2 will be

$$A' = (-(a - \frac{\varepsilon_A}{\sqrt{2}}), \frac{\varepsilon_A}{\sqrt{2}}) \quad \text{and} \quad B' = ((a - \frac{\varepsilon_B}{\sqrt{2}}), \frac{\varepsilon_B}{\sqrt{2}})$$

But the position of G_1 now measured with respect to frame 1 is

$$G_1 = (\frac{\varepsilon_A - \varepsilon_B}{\sqrt{2}}, \frac{\varepsilon_A + \varepsilon_B}{\sqrt{2}}) \qquad [A]$$

Similarly if G_2 is situated at the mid-point of the second plane, (that is between C' and D'), then when similar changes are made or effected on feet C and D (ε_C and ε_D) the position of G_2 measured with respect to frame 1 will be

$$(\frac{\varepsilon_C - \varepsilon_D}{\sqrt{2}}, \frac{\varepsilon_C + \varepsilon_D}{\sqrt{2}}) \qquad [B]$$

v) To obtain the coordinates of G with respect to frame 1, it is then a matter of getting the coordinates of the mid-point of the line joining G_1 to G_2. Thus, the position of G measured with respect to frame 1 is:

$$\left(\frac{\varepsilon_A + \varepsilon_C - \varepsilon_B - \varepsilon_D}{2\sqrt{2}},\ \frac{\varepsilon_A + \varepsilon_B + \varepsilon_C + \varepsilon_D}{2\sqrt{2}}\right) \qquad [C]$$

Thus $x_G = \frac{\varepsilon_A+\varepsilon_C-\varepsilon_B-\varepsilon_D}{2\sqrt{2}}$ and $Y_G = \frac{\varepsilon_A+\varepsilon_B+\varepsilon_C+\varepsilon_D}{2\sqrt{2}}$

These final equations are consistent with equations 7.1.2(a) and (b) respectively.

Confirmation of Angular displacements θ_1, θ_2 and θ_3.

Angular rotation θ_1 about the X_1-axis is given by the difference in the Y_1 and Z_1-coordinates of G1 and G2 (Fig.7.2.1(c)).

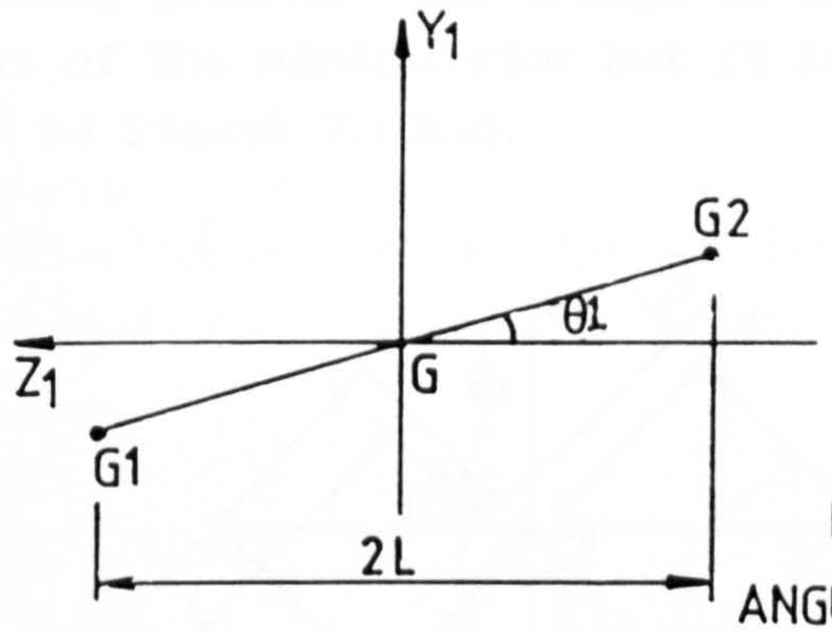

Fig.7.2.1(c)
ANGULAR ROTATION OF G1G2
(Fig.7.2.1(a)) ABOUT X1-AXIS.

$\theta_1 = (Y_{G2}-Y_{G1})/2\iota$ assuming negligible change in the Z1-coordinates of G1 and G2 after adjustment of manipulator.

But $Y_{G1} = (\varepsilon_A + \varepsilon_B)/\sqrt{2}$ and $Y_{G2} = (\varepsilon_C + \varepsilon_D)/\sqrt{2}$ (Eqns. 7.2.1 [A] & [B]).

i.e. $\theta_1 = \{(\varepsilon_C + \varepsilon_D) - (\varepsilon_A + \varepsilon_B)\}/2\sqrt{2}\,\iota$

Similarly, θ_2 about the Y_1-axis is given by the difference in X_1- and Z_1-coordinates of G1 and G2 (Fig.7.2.1(d)). $\theta_2 = (x_{G1}-x_{G2})/2\iota$ assuming negligible change in Z1-coordinates of G1 and G2 after adjustment of manipulator.

But $x_{G1} = (\varepsilon_A - \varepsilon_B)/\sqrt{2}$ and $x_{G2} = \varepsilon_C - \varepsilon_D$ (Eqns.7.2.1 [A] & [B]).

i.e. $\theta_2 = \{(\varepsilon_A - \varepsilon_B) + (\varepsilon_D - \varepsilon_C)\}/2\sqrt{2}\,\iota$ [E].

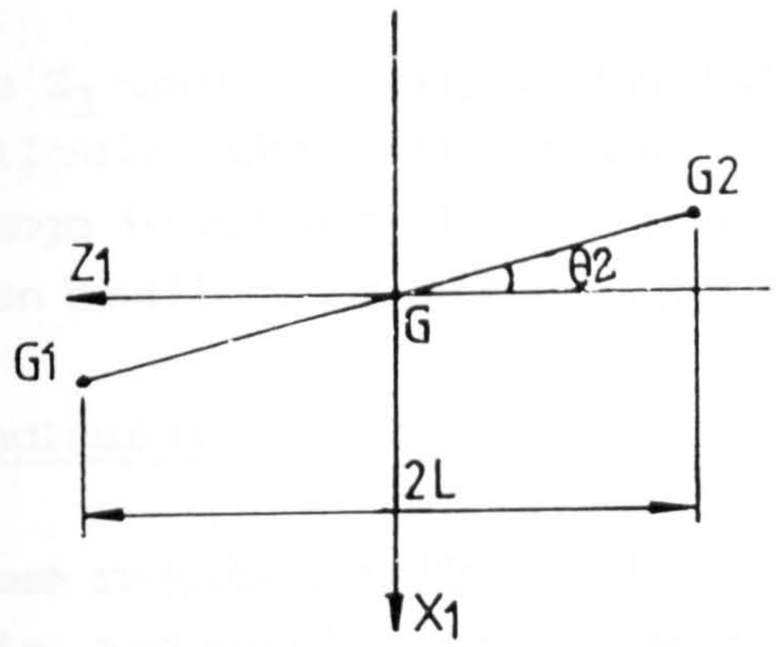

Fig.7.2.1(d)
ROTATION OF G1G2 (Fig.7.2.1(a))
ABOUT Y1-AXIS

Figure 7.2.1(e) represents plane 2 of Fig.7.2.1(a) with a slight difference in that the actuator positions are swopped with their corresponding grooves. This change is immaterial to the kinematical soundness of the manipulator but it is made inorder to relate it directly to Figure 7.1.2(a).

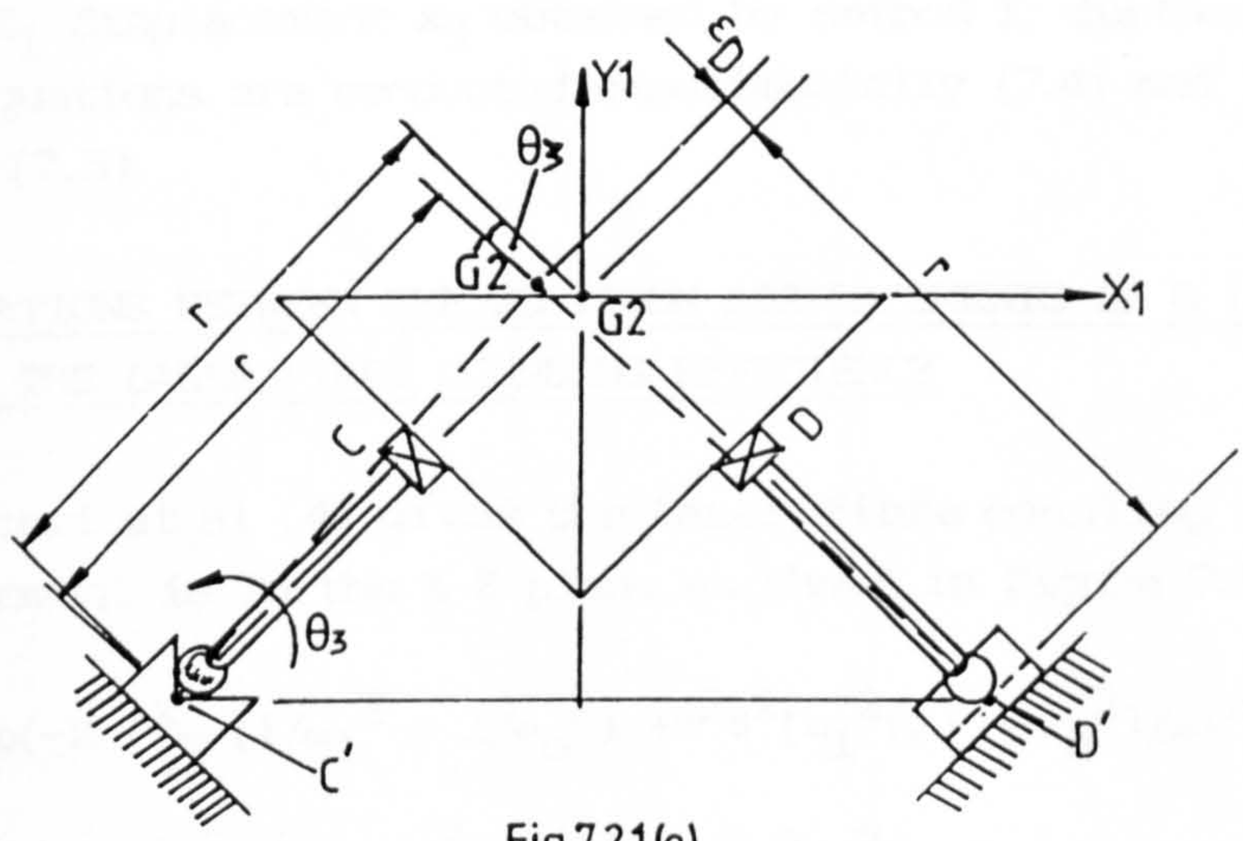

Fig.7.2.1(e)
PLANE 2 (Fig.7.2.1(a)) WITH THE GROOVE POSITIONS REVERSED
(SHOWING THE EFFECT OF EXTENDING ACTUATOR D BY ε_D)

When actuator C is extended, point contacts D' represented by a single point (Fig.7.2.1(e)) for simplicity, slides UP along the groove. A' and B' (Fig.7.2.1(a) with point contacts swopped) slide slightly forwards and the whole body tilts about the X_1-axis rather than the Z_1-axis. Similarly, when A or B is extended, both A' and B' slide upwards while C'(also represented by one point) and D' rotate about line C'D'. Thus, the overall rotation is about the X_1-axis again.

When D is extended, A', B', and C' all rotate about lines parallel to

the Z_1-axis. Consequently, tilting takes place about the Z_1-axis following the dashed triangle (C'D'G2') of Fig.7.2.1(e). Since the change in actuator length ε_D is very small, the change in angle θ_3 is even smaller. Thus from Fig. 7.2.1(e), $\tan \theta_3 = \theta_3 = \varepsilon_D/r$.

Conclusion

These results for linear displacements x_1 along X_1-axis, x_2 along Y_1-axis, and angular displacements θ_1, θ_2, and θ_3 are consistent with those obtained below section 7.1.2 provided that velocities V_5 are replaced by displacements ε_5 and the difference in lettering Figs. 7.1.2(a) and 7.2.1(a) are noted. The results confirm theoretically that the methods as well as the results are valid. It was, however, found intuitively difficult to validate the linear displacement in the Z_1-direction. For this reason and for purposes of satisfying the linear Z_1 displacement x_3 obtained by method I, further validation of these equations are conducted experimentally (7.4) and by computation method (7.5).

7.3 RELATIONS BETWEEN THE POSITION DISPLACEMENTS OF G (FIGURE 7.2.1(a)) AND THE LASER/FIBRE COUPLING EFFICIENCY

Saruwatari et al [4] gives the laser/fibre coupling efficiency (if misalignment is in the X-Z plane as shown in Figure 7.3) as:

$$\eta = K \exp(-K \{\frac{x^2}{2} (1/\omega_1^2 + 1/\omega_o^2) + \pi^2\theta^2[\omega_1^2(z) + \omega_o^2]/2\lambda^2 - x\theta z/\omega_1^2\}) \quad (a)$$

where $K = 4\omega_1^2 \omega_o^2 /[(\omega_1^2 + \omega_0^2)^2 + \lambda^2 z^2/\pi^2]$,

$$\omega_1^2(z) = \omega_1^2[1 + (\lambda z/\pi\omega_1^2)^2]$$

λ = wavelength of the laser, ω_0 = fibre core radius and
ω_1 = laser beam neck radius (that is at z = 0).

The same expression is also used to represent the coupling efficiency when misalignment takes place in the Y-Z plane except that x - the lateral misalignment, and θ - the angular misalignment in the X-Z plane, are replaced by the corresponding lateral and angular misalignments y and ϕ in the Y-Z plane.

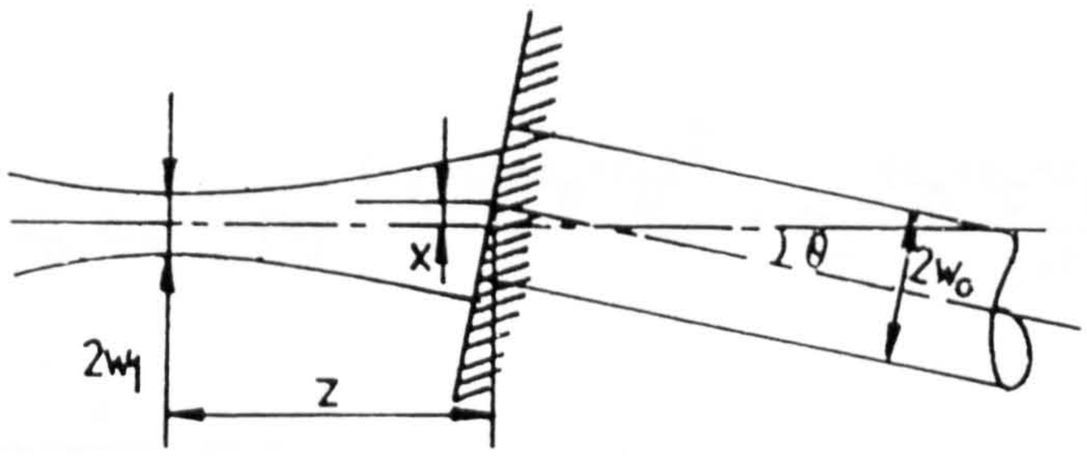

Fig.7,3 Gaussian Laser Beam
to optical fibre coupling.

If however, the input end of the optical fibre lies at the beam waist (neck), then z = 0. In that case the above equations reduce [4] to

$$\eta_o = k_o \exp\{-2x^2/(\omega_1^2+\omega_o^2)-2\pi^2\theta^2\omega_1^2\omega_0^2/[\lambda^2(\omega^2+\omega^2)]\} \qquad (b)$$

where $k_o = 4/(\omega_o/\omega_1 + \omega_1^2/\omega_o)^2$

In the x-z and y-z efficiency relationship analyses that follow, the support configuration of plane 1 (Figure 7.2.1(b)) which is the same as that of plane 2 is assumed to represent the datum support position of body P (Figure 7.2.1(a)). In addition, the laser diode is placed close to the origin G (Figure 7.2.1(a)) such that (a) its emitted beam is propagated along the Z_1 axis; (b) the beam waist is located at the origin G and (c) a stationary receiving optical fibre lying along the Z_1-axis has its input end also located at G. This implies that z is fixed at zero. Bearing in mind these conditions, the x-z and y-z efficiency relationships can now be presented.

i) Analysis of misalignment in the X-Z plane

For very small displacements of the point G (Figure 7.2.1(a)) the angular displacement $\theta = x_G/\ell$. Now,

$$x_G = \frac{(\varepsilon_A + \varepsilon_C - \varepsilon_B - \varepsilon_D)}{2\sqrt{2}}$$

from equation 7.2.1 [C].

$$\therefore \theta = \frac{(\varepsilon_A + \varepsilon_C - \varepsilon_B - \varepsilon_D)}{2\sqrt{2}\ell} \text{ (rads)}$$

Substituting for θ into the efficiency equation 7.3(b) for the X-Z

plane,

$$\eta_o = k_o \exp - \{k_1 \frac{(\varepsilon_A+\varepsilon_C-\varepsilon_B-\varepsilon_D)^2}{8} + k_2 \frac{(\varepsilon_A+\varepsilon_C-\varepsilon_B-\varepsilon_D)^2}{8\ell^2}\}$$

where $k_1 = \frac{2}{(\omega_1^2 + \omega_0^2)}$

$$k_2 = \frac{2\pi^2\omega_1^2\omega_0^2}{\lambda^2(\omega_1^2\omega_0^2)} \quad \text{and } k_o = \frac{4}{(\omega_0/\omega_1+\omega_1/\omega_0)^2}$$

ii) Analysis of misalignment in the Y-Z plane

Similarly, for very small displacements of the point G (Figure 7.2.1(a)) the angular displacement $\phi = y_G/\ell$. But

$$Y_G = (\varepsilon_A + \varepsilon_B + \varepsilon_C + \varepsilon_D)/2\sqrt{2}$$

from equation 7.2.1 [C]

$$\therefore \phi = (\varepsilon_A + \varepsilon_B + \varepsilon_C + \varepsilon_D)/2\sqrt{2}\ell$$

Now, substituting for ϕ into the coupling efficiency equation 7.3(b) for the Y-Z plane,

$$\eta_o = k_o e^{-\{k_1 \frac{(\varepsilon_A+\varepsilon_B+\varepsilon_C+\varepsilon_D)^2}{8} + k_2 \frac{(\varepsilon_A+\varepsilon_B+\varepsilon_C+\varepsilon_D)^2}{8\ell^2}\}}$$

where $k_1 = 2/(\omega_1^2+\omega_0^2)$, $k_2 = \frac{2\pi^2\omega_1^2\omega_0^2}{\lambda^2(\omega_1^2+\omega_0^2)}$ and $k_o = 4/(\omega_0/\omega_1 + \omega_1/\omega_0)^2$.

In both the coupling efficiency expressions of the X-Z and Y-Z planes, maximum efficiency is obtained when the exponential expression is unity. That is $\eta_o = k_o.1$. So, from the X-Z and Y-Z planes

$$\frac{k_1}{8}(\varepsilon_A+\varepsilon_C-\varepsilon_B-\varepsilon_D)^2 = \frac{k_2}{8\ell^2}(\varepsilon_A+\varepsilon_C-\varepsilon_B-\varepsilon_D)^2 = 0$$

and $$\frac{k_1}{8}(\varepsilon_A+\varepsilon_B+\varepsilon_C+\varepsilon_D)^2 = \frac{k_2}{8\ell^2}(\varepsilon_A+\varepsilon_B+\varepsilon_C+\varepsilon_D)^2 = 0$$

Hence $\varepsilon_A+\varepsilon_C-\varepsilon_B-\varepsilon_D = 0$ and $\varepsilon_A+\varepsilon_B+\varepsilon_C+\varepsilon_D = 0$.

From these two equations, $\varepsilon_B = -\varepsilon_D$ and $\varepsilon_A = -\varepsilon_C$. (c)

The experimental results of Figures 6.8(a) and (b) (Chapter 6) obtained by adjusting feet A, B, C and D clockwise (positive) and anticlockwise (negative) clearly support these results.

7.4 VALIDATION OF THE MATHEMATICAL MODEL DERIVED IN SECTIONS 7.1 AND 7.2

In order to ensure that the equations derived for the displacement of the position of a laser diode mounted on the manipulator are correct, some experimental tests need to be carried out.

Although the general vector method (applied in Section 7.1) seems to hold for a manipulator of any number of degrees of freedom, a 4-degree of freedom manipulator has been selected for this experiment. This is because it is much simpler to construct and carry out such a verification on this manipulator.

7.4.1 Construction of Apparatus for Verification of the Mathematical Model

A similar apparatus used for the alignment of lines in space (Chapter 6) is adopted for this experiment. A right angled solid V-shaped perspex body P (Figure 7.4.2) with a rectangular top surface 360 mm by 113 mm and two equal but opposite right angled isosceles triangular faces is supported on four hemispherical lengthwise adjustable feet in the same way as the laser L (Figure 6.3(a)). These hemispherical feet are threaded screws or bolts with steel ball bearings glued onto their tips. To avoid repetitions, see sections 6.3 and 6.3.1 of Chapter 6.

The apparatus is, however, redrawn here (Figure 7.4.2) with a clock gauge spindle pressing against the top surface so that the change in position of the central point G can be measured once A, B, C and D are adjusted. This body P is supported symmetrically on four feet so that the two planes of support coinciding with the axes of a pair of feet A and B and C and D respectively are 60 mm from the respective ends while G is 180 mm from either end.

7.4.2 Experimental Test Procedure Using the Apparatus of Figure 7.4.2

The flat rectangular surface of the perspex body P supported in Figure 7.4.2 is first levelled by adjusting the four feet appropriately and then checking it by means of a spirit level and the clock gauge Y to ensure that it is levelled. The dial gauge is mounted on stand M such that its position can be varied by loosening and then retightening the support screw W. The stand M itself has a magnetic base which firmly grips the surface of a flat steel table.

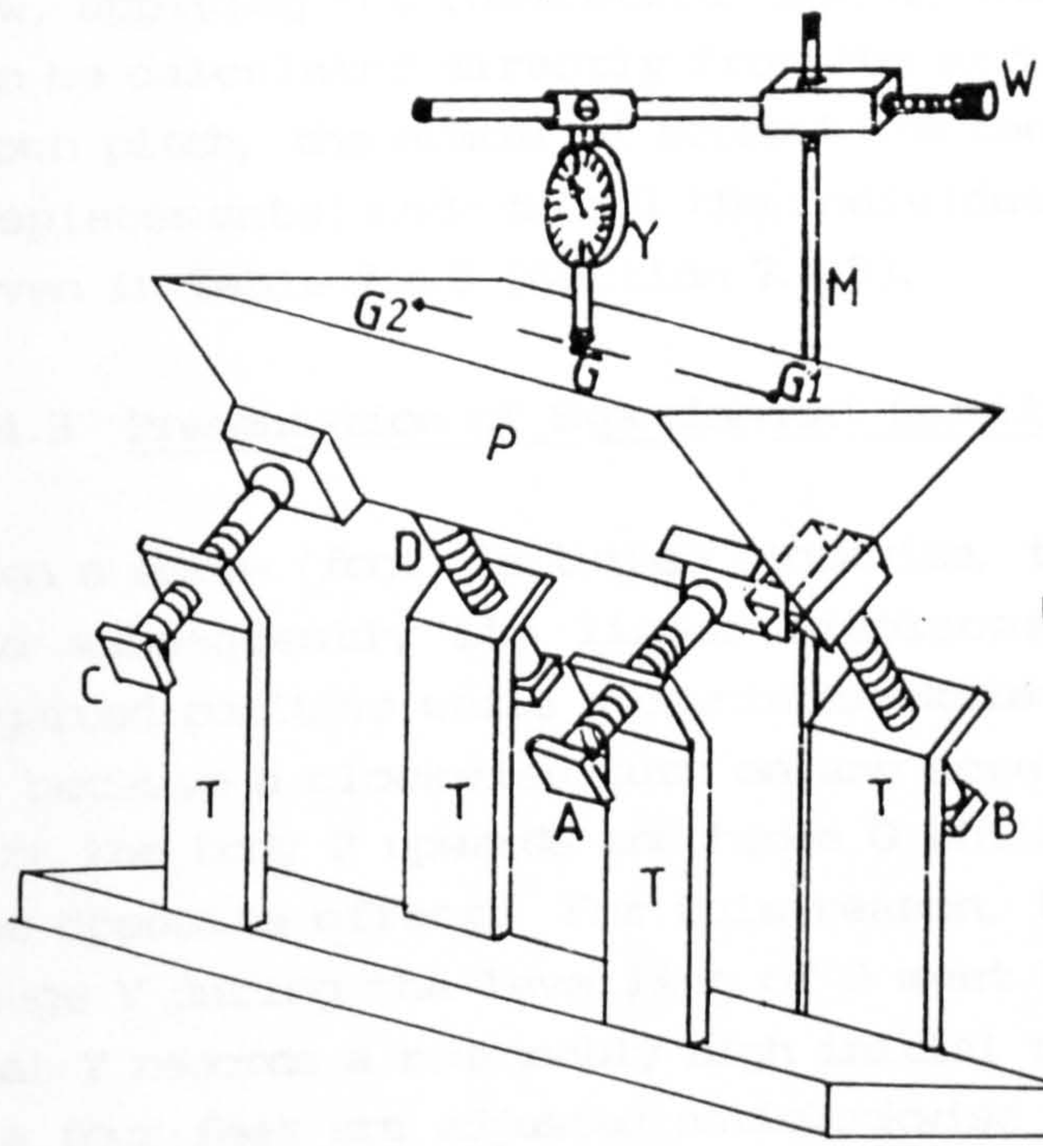

Fig.7.4.2 Support of the solid perspex body P showing the spindle position of dial gauge Y.

A and B Hemispherical screws interacting with V-grooves.
C and D Hemispherical screws interacting with plane surfaces.

With the whole arrangement placed on a steel table and the surface of P levelled, a known number of turns n (preferably small) clockwise or anticlockwise are made to each of the four feet (n does not have to be the same for every foot). The reading on the clock gauge Y mounted directly on top of G will change from the initial value

measured when P is levelled to some other value. The difference between the initial and final readings on the gauge is then the experimental value of the overall change in the position displacement of G due to the changes made to the feet. The gauge is then moved to positions G1 and G2 and the corresponding readings noted. Again, the difference between the initial gauge reading and those in the final positions of G1 and G2 respectively give the corresponding changes in the positions of G1 and G2.

Now, applying the theoretical model, the values of y_{G1}, y_{G2} and y_G can be calculated directly from the amount of adjustments (with a known pitch, the number of screw turns can be transformed into linear displacements) made to all the individual screws. The results are given in Table 7.4.3 (Section 7.4.3).

7.4.3 Presentation of Experimental Results

When a screw (foot) is turned clockwise, the number of turns recorded and subsequently its linear displacment (after conversion) is regarded positive while a counterclockwise turning is negative. This is because a clockwise turn on any screw (foot) has a tendency to lift the body P upwards and hence G while an anticlockwise turn has the opposite effect. For this reason, the initial setting of the gauge Y during the levelling of P must be conducted in such a way that Y records a reasonably high initial reading. In that case, when the four feet are adjusted anticlockwise and the level of G falls, a final reading (lower than the initial gauge reading) can still be recorded. Thus the amount of fall in G can be found and hence the experimental value of y_G.

Example of theoretical evaluation

In order to illustrate the theoretical evaluation of the y-displacements of G1, G2 and G, case 1 of the results presented in Table 7.4.3 is analysed. Such an evaluation is effected directly from equations 7.1.2(b) or 7.2.1 [A] to [C] as follows:

$$y_{Gt1} = \frac{\varepsilon_A+\varepsilon_B}{\sqrt{2}}, \quad y_{Gt2} = \frac{\varepsilon_C+\varepsilon_D}{\sqrt{2}} \text{ and } y_{Gt} = \frac{\varepsilon_A+\varepsilon_B+\varepsilon_C+\varepsilon_D}{2\sqrt{2}}$$

TABLE 7.4.3: EXPERIMENTAL VERSUS THEORETICAL RESULTS IN VERIFYING THE MATHEMATICAL MODEL

CASE	SCREW NO	SCREW ADJUSTMENT		EXPERIMENTAL RESULTS/mm			THEORETICAL RESULTS/mm			% DIFF OF EXP OVER THEORY		
		No. of Screw Turns (n)	Equivalent Linear Displacement (ε/mm)	y_{GP_1}	y_{GP_2}	y_{GP}	y_{Gt_1}	y_{Gt_2}	y_{Gt}	$\frac{\Delta y_{G1}}{y_{Gt_1}} \times 100$	$\frac{\Delta y_{G2}}{y_{Gt_2}} \times 100$	$\frac{\Delta y_{G}}{y_{Gt}} \times 100$
1	A B C D	2 5 1 4	$\varepsilon_A = 2.117$ $\varepsilon_B = 5.292$ $\varepsilon_C = 1.0584$ $\varepsilon_D = 4.234$	5.20	3.73	4.51	5.239	3.742	4.49	0.744	0.32	0.423
2	A B C D	-1 -2 3 4	$\varepsilon_A = -1.0584$ $\varepsilon_B = -2.117$ $\varepsilon_C = 3.175$ $\varepsilon_D = 4.234$	-2.33	5.30	1.52	-2.245	5.239	1.497	-3.8	1.16	1.54
3	A B C D	4 3 -2 -1	$\varepsilon_A = 4.234$ $\varepsilon_B = 3.175$ $\varepsilon_C = -2.117$ $\varepsilon_D = -1.0584$	5.21	-2.30	1.52	5.239	-2.245	1.497	0.55	2.45	1.51
4	A B C D	-5 1 -4 -4	$\varepsilon_A = -5.292$ $\varepsilon_B = 1.0584$ $\varepsilon_C = -4.232$ $\varepsilon_D = -4.232$	-3.11	-5.94	-4.43	-2.994	-5.99	-4.49	3.87	0.802	1.34

But ε_A = 2.117 mm, ε_B = 5.292 mm, ε_C = 1.0584 mm and ε_D = 4.234 mm.

$$Y_{Gt1} = \frac{2.117+5.292}{\sqrt{2}} = 5.239 \text{ mm}, \quad Y_{Gt2} = \frac{1.0584+4.234}{\sqrt{2}} = 3.742 \text{ mm}$$

and $Y_{Gt} = \frac{2.117+5.292+1.058+4.234}{2\sqrt{2}} = 4.491$ mm as shown in Table 7.4.3.

It should be noted that the pitch of the screws used = 0.04167". So, for n screw turns clockwise, the linear displacement = (n x 0.04167 x 25.4) mm. This value is then substituted into the theoretical formulae (equations 7.2.1[A] to [C]) as a positive figure otherwise negative for a counterclockwise turn.

7.4.4 Comments and Conclusion

The experimental procedure discussed above was conducted to find the position changes of G, G1 and G2 only in the y-direction. This does not mean that it is impossible to obtain the displacements of these points in the x and z directions, but it was found to be practically difficult. However, sixteen different experiments conducted, produced relatively accurate results for the y-displacements depending on the amounts of adjustments given to each of the four feet. The larger the amounts of adjustments, the less accurate the results are. Four samples of the results given above compare very favourably with theoretical results despite the crudeness of the apparatus.

So, although the displacements in the x- and z-directions have not been confirmed experimentally, the theoretical confirmation by the two methods already discussed in this chapter and the partial displacement validation in the y-direction are sufficient to verify this model. Thus the general vector approach (Method I) which is applicable to any manipulator is very useful.

However, it is envisaged that this model cannot be utilised at this stage for a laser/fibre alignment. This is because even if the displacements can be directly linked with the coupling efficiency as in Section 7.3 there are still many practical problems associated with establishing the laser diode datum position in relation to the fibre input face for such minute displacements. In addition, the coupling efficiency equations (7.3 (i) & (ii)) obtained as a function

of the linear screw displacements (ε_A, ε_B, ε_C and ε_D) does not produce independent results for ε_A, ε_B, ε_C and ε_D in terms of ω_o and ω_1 when maximised or minimised. It is therefore difficult to implement the idea in reality and more work needs to be done towards solving the equation if the concept is to be utilised.

Ideally, a 5-degree of freedom manipulator is most appropriate for laser/fibre alignment because it takes into account all the alignment tolerances. It is, however, envisaged that a 3-degree of freedom manipulator is the best manipulator for experimental laser/fibre alignment. This is because firstly angular and longitudinal misalignments are not very sensitive to laser/fibre alignment [1]. Secondly, it is more economical to use a 3-degree of freedom manipulator and more importantly, very much easier to program it for the purpose of such an alignment.

Thus due to the difficulties already discussed, it is felt that the use of a suitable adaptive control technique in conjunction with an accurate 3-degree of freedom manipulator (say Oriel Encoder Mike) will achieve a satisfactory alignment result. Such an algorithm, devised for the programming of a 3- and 5-degree of freedom manipulator and believed to be a better alternative to the model derived in this section is presented in Chapter 9.

7.5 COMPUTATION METHOD

An attempt to evaluate the linear x_3-displacement by the intuitive method yielded a completely different result from that produced by Method I. It was also found to be practically difficult to measure it by experimental method.

Thus, since it is not possible to check the results of Method I either intuitively or experimentally, a NAG FORTRAN subroutine (F04AAF) available on the University main frame computer was used to calculate all the linear and angular displacements. Generally, the routine can be used to solve linear equations of the form $A\underset{\sim}{X} = B$ where A is an array of coefficients of column vector $\underset{\sim}{X}$ and B the array (or column) of constants. In this respect, the three sets of circuit equations derived in sections 4(a), (b) and (c) (of Appendix D) were all assembled in terms of the actuator velocities V^b_5, V^c_5,

TABLE 7.5(I): ASSEMBLED CIRCUIT EQUATIONS OF THE 4 DOF MANIPULATOR

$$
\begin{bmatrix}
1 & 0 & 0 & 0 & 0 & -1 & 0 & 0 & 0 & 0 & 0 & 0 & 0 & 0 & 0 & 0 & 0 & 0 \\
0 & 1 & 0 & 0 & 1 & 0 & 0 & 0 & 0 & 0 & 0 & 0 & 0 & 0 & 0 & 0 & 0 & 0 \\
0 & 0 & 0 & 0 & 0 & 0 & 0 & 0 & 1 & 1 & 0 & 0 & 0 & 0 & 0 & 0 & 0 & 0 \\
0 & -2 & 0 & 0 & -2 & 0 & 0 & 0 & -\sqrt{2} & 0 & 0 & 0 & 1 & 0 & 0 & 0 & 0 & 0 \\
2 & 0 & 0 & 0 & 0 & -2 & 0 & 0 & 0 & -\sqrt{2} & 0 & 0 & 0 & 1 & 0 & 0 & 0 & 0 \\
\sqrt{2} & \sqrt{2} & 0 & 0 & 0 & 0 & 0 & 0 & 0 & 0 & 0 & 0 & 0 & 0 & 1 & 1 & 0 & 0 \\
0 & -1 & 1 & 0 & 0 & 0 & 0 & 0 & 0 & 0 & 0 & 0 & 0 & 0 & 0 & 0 & 0 & 0 \\
0 & 0 & 0 & 0 & 0 & 1 & -1 & 0 & 0 & 0 & 0 & 0 & 0 & 0 & 0 & 0 & 0 & 0 \\
0 & 0 & 0 & 0 & 0 & 0 & 0 & 0 & 0 & -1 & 1 & 0 & 0 & 0 & 0 & 0 & 0 & 0 \\
0 & 0 & 0 & 0 & 0 & 2 & 2 & 0 & 0 & \sqrt{2} & -\sqrt{2} & 0 & 0 & -1 & 1 & 0 & 0 & 0 \\
0 & 2 & 2 & 0 & 0 & 0 & 0 & 0 & 0 & 0 & 0 & 0 & 0 & 0 & 0 & 0 & 0 & 0 \\
0 & -\sqrt{2} & \sqrt{2} & 0 & 0 & 0 & 0 & 0 & 0 & 0 & 0 & 0 & 0 & 0 & 0 & -1 & 0 & 0 \\
0 & 0 & -1 & .707 & 0 & 0 & 0 & .707 & 0 & 0 & 0 & 0 & 0 & 0 & 0 & 0 & 0 & 0 \\
0 & 0 & 0 & .707 & 0 & 0 & 1 & -.707 & 0 & 0 & 0 & 0 & 0 & 0 & 0 & 0 & 0 & 0 \\
0 & 0 & 0 & 0 & 0 & 0 & 0 & 0 & 0 & 0 & -1 & 1 & 0 & 0 & 0 & 0 & 0 & 0 \\
0 & 0 & 0 & -\sqrt{2} & 0 & 0 & -2 & \sqrt{2} & 0 & 0 & \sqrt{2} & 0 & 0 & 0 & -1 & 0 & 0 & 0 \\
0 & 0 & -2 & \sqrt{2} & 0 & 0 & 0 & \sqrt{2} & 0 & 0 & 0 & -\sqrt{2} & 0 & 0 & 0 & 0 & 0 & 0 \\
0 & 0 & -\sqrt{2} & 1 & 0 & 0 & 0 & -1 & 0 & 0 & 0 & 0 & 0 & 0 & 0 & 0 & 0 & 1
\end{bmatrix}
\begin{bmatrix}
V_{1_d}^{a} \\ V_{1_e} \\ V_{1_h} \\ V_{1_a}^{a} \\ V_{2_d}^{d} \\ V_{2_e} \\ V_{2_h} \\ V_{2_a} \\ V_{3_d} \\ V_{3_e} \\ V_{3_h} \\ V_{3_a} \\ V_{4_d} \\ V_{4_e} \\ V_{4_a} \\ V_{6_d} \\ V_{6_h} \\ V_{6}
\end{bmatrix}
\begin{bmatrix}
0 & 0 & 0 & 0 \\
0 & 0 & 0 & 0 \\
0 & 0 & 0 & 0 \\
0 & -1 & 0 & 0 \\
-1 & 0 & 0 & 0 \\
0 & 0 & 0 & 0 \\
0 & 0 & 0 & 0 \\
0 & 0 & 0 & 0 \\
0 & 0 & 0 & 0 \\
0 & 0 & 0 & 0 \\
0 & 1 & -1 & 0 \\
0 & 0 & 0 & 0 \\
0 & 0 & 0 & 0 \\
0 & 0 & 0 & 0 \\
0 & 0 & 0 & 0 \\
0 & 0 & 0 & 1 \\
0 & 0 & 1 & 0 \\
0 & 0 & 0 & 0
\end{bmatrix}
\begin{bmatrix}
V_{5}^{b} \\ V_{5_c} \\ V_{5_f} \\ V_{5_g}
\end{bmatrix}
$$

V^f_5 and V^g_5 in the form $A\underset{\sim}{X} = B\underset{\sim}{V}$. This is shown in matrix form in table 7.5(I) where A is a 18x18 coefficient matrix of the unknown local velocities $\underset{\sim}{X}$ and B is a 4x18 matrix coefficient of the four actuator velocities $\underset{\sim}{V}$. Choosing $\iota(=2)$ and $r(\simeq\sqrt{2})$ arbitrarily and then substituting into the circuit equations of Appendix D gives the necessary data (table 7.5 (I)) for entry into the program.

By entering the data into the F04AAF column by column starting from matrix A and then running the program, the final results were obtained in terms of the primary variables (the 4 actuator velocities) as shown in table 7.5(II). From sections 3(i) and (ii) of Appendix E and section 7.1.2,

$$\{V^a\} + \{V^b\} = \begin{bmatrix} V^a_1\cos\theta + V^a_2\sin\theta \\ V^a_2\cos\theta - V^a_1\sin\theta \\ V^a_3 \\ \iota(V^a_1\sin\theta - V^a_2\cos\theta) - V^a_3.r\cos\theta + V^a_4\cos\theta + V^b_5\sin\theta \\ \iota(V^a_1\cos\theta + V^a_2\sin\theta) + V^a_3.r\sin\theta - V^a_4\sin\theta + V^b_5\cos\theta \\ r.V^a_1 + V^a_6 \end{bmatrix}$$

TABLE 7,5 (II): COMPUTED RESULTS FROM INPUT DATA OF TABLE 7,5(I).

$$\{V\} = \begin{bmatrix} -0.25 & -0.00 & 0.00 & 0.25 \\ 0.00 & 0.25 & -0.25 & 0.00 \\ 0.00 & 0.25 & -0.25 & 0.00 \\ 0.18 & 0.18 & -0.18 & -0.18 \\ 0.00 & -0.25 & 0.25 & 0.00 \\ -0.25 & 0.00 & 0.00 & 0.25 \\ -0.25 & 0.00 & 0.00 & 0.25 \\ -0.18 & 0.18 & -0.18 & 0.18 \\ 0.00 & 0.00 & 0.71 & 0.00 \\ 0.00 & 0.00 & -0.71 & 0.00 \\ 0.00 & 0.00 & -0.71 & 0.00 \\ 0.00 & -1.00 & 1.00 & 0.00 \\ -1.00 & 0.00 & -1.00 & 0.00 \\ 0.00 & 0.00 & -1.00 & -1.00 \\ 0.35 & -0.35 & 0.35 & -0.35 \\ 0.00 & 0.00 & 0.00 & 0.00 \\ -0.35 & 0.35 & -0.35 & 0.35 \end{bmatrix} \begin{bmatrix} V^b_5 \\ V^c_5 \\ V^f_5 \\ V^g_5 \end{bmatrix}$$

Vector {V} represents all the local velocities in table 7,5(I).

Table 7.5(II) gives a computer output of values of all the local velocities that appear in Table 7.5(I). A check was made by substituting values of the local velocities (7.5(II)) into the above equations and the results were found to be consistent with those obtained in Section 7.1.2. Since only the linear x_3 displacement needs to be checked and because the substitution procedure (from Table 7.5(II) into above equations) is simple, the rest will be left to the reader.

Thus, from the above equations, $x_3 = r.V_1^a + V_6^a$

From Table 7.5(II),

$$V_1^a = (V_5^g - V_5^b)/4 \text{ and}$$
$$V_6^a = 0.35(V_5^b - V_5^c + V_5^f - V_5^g)$$

That is, $x_3 = 0.35(V_5^f - V_5^c)$ which confirms the results of section 7.1.2.

* * * * *

REFERENCES

1. M. K. Barnoski.
"Fundamentals of Optical Fibre Communications", Edited by M K Barnoski. Academic Press Inc, 1976, London. (Chapter 3. M K Barnoski, "Coupling Components for Optical Fibre Waveguides"). (pp 98-101).

2. T. H. Davies.
"Transformations for Motors and the Dual Subspaces Characteristic of Contact Couplings". A report presented at the Department of Mechanical Engineering, Loughborough University of Technology, July 1984 (p 3-7, 13).

3. T. H. Davies.
"Kirchhoff's Circulation Law Applied to Multi-Loop Kinematic Chains", Mechanism and Machine Theory, Vol 16, 1981 (p 171-183).

4. M. Saruwatari and K. Nawata.
"Semiconductor Laser to Single-Mode Fibre Coupler", Applied Optics Vol 18, No 11, 1979 (p 1848).

CHAPTER 8

DESIGN OF LASER ALIGNMENT CONTROL CIRCUIT

CHAPTER OVERVIEW

The fast growth of the optical fibre market has been accelerated by the need for better communications (2.0). The fibre assembly requires repetitive handling of a number of components such as injection and detection terminations, connectors, couplers etc. Such assembly process is still very frequently handled manually (2.4) which limits the coupling efficiency.

This chapter examines individual design circuit components with the aim of constructing an overall control circuit for use in automatic laser-fibre alignment. This type of alignment needs a suitable type of control. A description of an open loop control deemed suitable for this purpose is presented in section 8.1. The Oriel Encoder Mike (4.4.3) drive circuit designed for purposes of their control is then presented in section 8.2.1 followed by a general description of shaft encoders and an experimental proof of the selected motor accuracy. The detector circuit is summarised in section 8.2.4 followed by a description of the peltier drive cicuit, a gripper for the optical fibre and the laser protection cicuit respectively. Also given in section 8.2.10, is an account of the different types of computers available on the market and the reasons for selecting a Transam micro-computer.

Interfacing the individual components to the MPU namely the motor and encoder circuits is examined in section 8.3 and the accompanying subsections. Finally, this is followed by a summary of the power supply circuit which channels the appropriate signal levels to the different parts of the overall control system.

8.0 Introduction.

In general, successful automated optimisation of laser-fibre alignment requires a transverse alignment accuracy of the order of laser wavelength or even better. This is because the dimensions of the monomode fibre core diameters and laser beams are of the order of a few microns (Chapter 2). Apart from resolution, factors like

backlash, repeatabilty, and control circuit efficiency, ease of programming and safety power handling also play an important part. The majority of these in turn depend on the type of actuators used (Chapter 4). With the advent of automated microalignment work (lasers, circuits and bacterial culture (4.3.7)), progress has been made in producing better actuators and the corresponding alignment control systems such as described by Edye et al [1] and others which are mentioned in Chapter 9.

In this Chapter, an attempt is made to select the appropriate components to build an electronic control circuit system for automating the search for optimum laser-fibre alignment. This includes selection of the type of control used and the discussion of the fibre gripper which must be set manually each time a fibre is gripped. Some circuits already designed by STC are simply adopted and produced here to avoid wasting time and a possible design repetition.

8.1 The Control System.

The Oriel Encoder Mike actuator (4.4.3) has operating variables like load, torque (friction and inertia) and possibly amplifier gains because it is a dynamic system. It is therefore necessary to select a suitable system of control to compensate for variations in these parameters. In open loop control, the output follows the desired function provided that all such system parameters are constant. As outlined by Electrocraft [2], any change in load, amplifier gain or any other system variable causes a deviation from the desired value. Closed loop control, however, has the capability of compensating for such variations. Ideally, this type of control would be preferred for this kind of work.

Using the Oriel Encoder Mike together with its dedicated controller results in an initial overshoot of 15μm (4.4.3). As outlined in Chapter 2 (2.5), this choice was based on the initial research specifications. The updated specifications, however, indicates that this overshoot conflicts with the maximum clearence of 5μm between the outer diameter of the optical fibre and the hole through which it is threaded into the laser box for alignment. Due to lack of time and expertise in the Department, a suitable controller could not be

designed to overcome this problem. For this reason and those outlined in sections 8.2.3 and 8.3.1, an open loop control system is chosen. Fig. 8.1 shows a typical control circuit applied to the laser-fibre alignment system. Thus further discussions of closed loop control with respect to this work will be terminated but must be considered for similar problems provided that the controller is compatible. For example, the system discussed in [1] utilises closed loop control for laser-fibre alignment. Details of both types of control applied to D.C. motors are given in [2].

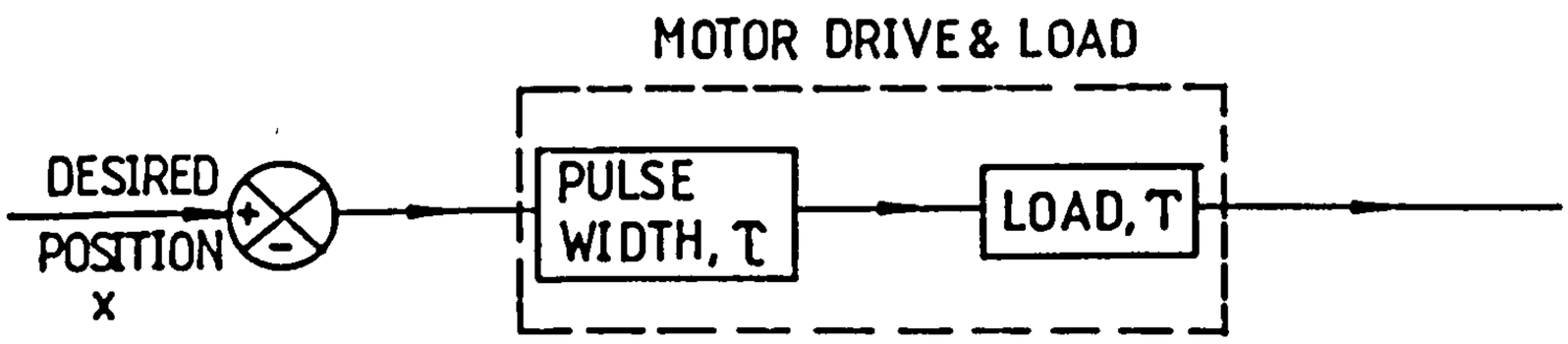

Fig, 8,1 OPEN LOOP CONTROL
OF D·C MOTORS

8.2 Components of the Control Circuit

The block diagram of the layout of electronic control circuit is shown in Fig. 8.2. Each circuit consists of a Hex Buffer driver, an Opto-isolator, a Relay, a D.C motor with an optical encoder attached to it, a Multiplexer and a Microcomputer. A detector whose function is to couple the laser beam from the fibre to the microcomputer also forms part of the circuit. The decision to incorporate the various components into the circuit was based partly on availability but more importantly on their suitabilty to the functioning of the circuit.

Discussion of the individual components are presented in the sections below. Since new products frequently replace older ones, it is necessary to update relevant information on these components. Some of the product sources are given in Chapter 4 but lasers, detectors and optical fibres were provided by STC. Other common components like opto-isolators, relays, buffer drivers etc. were obtained from local dealers. Table 8.2 shows details of their costs. An overall estimate can be reached if the cost of the microcomputer is included.

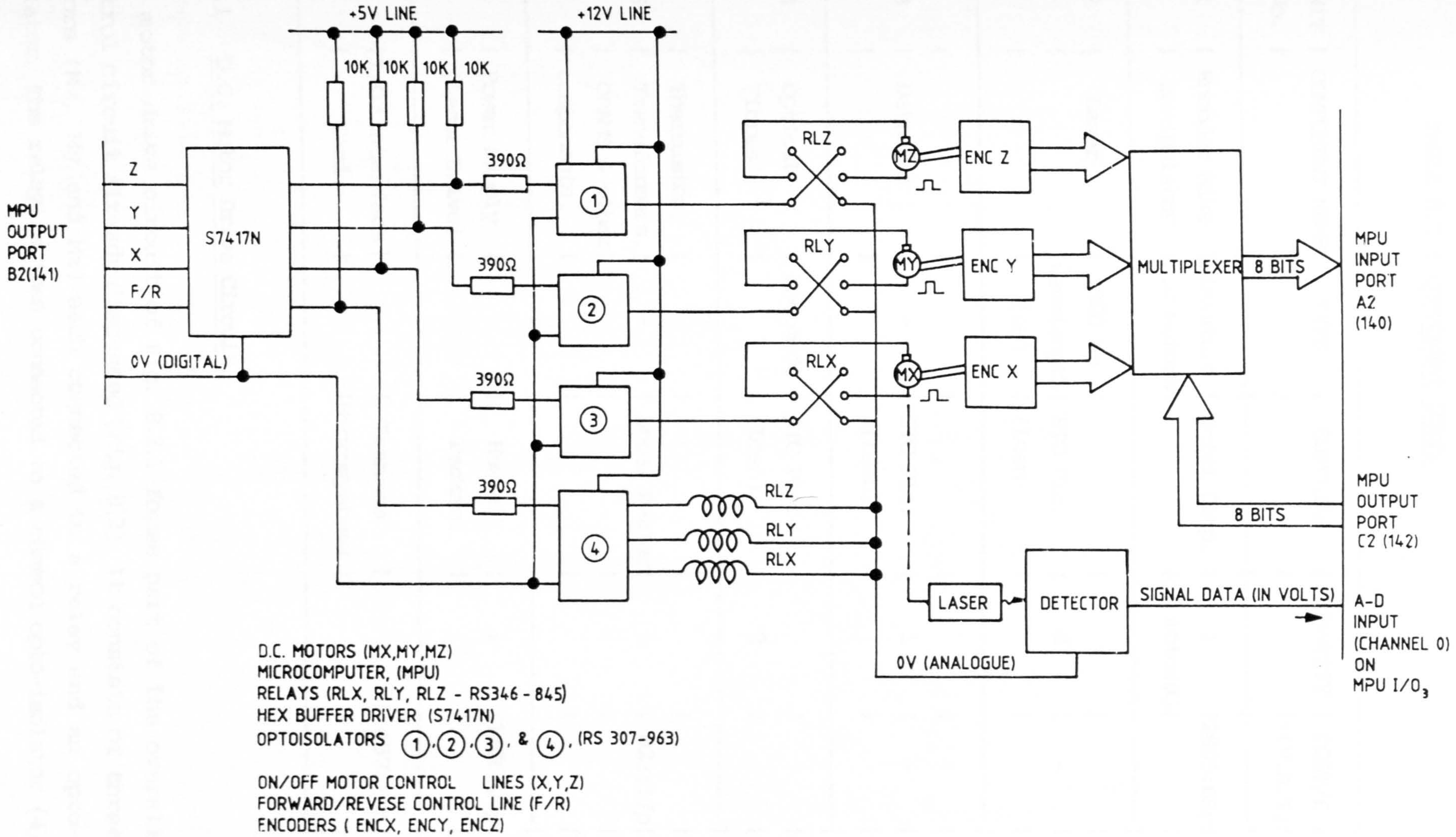

D.C. MOTORS (MX,MY,MZ)
MICROCOMPUTER, (MPU)
RELAYS (RLX, RLY, RLZ - RS346 - 845)
HEX BUFFER DRIVER (S7417N)
OPTOISOLATORS (1), (2), (3), & (4), (RS 307-963)

ON/OFF MOTOR CONTROL LINES (X,Y,Z)
FORWARD/REVESE CONTROL LINE (F/R)
ENCODERS (ENCX, ENCY, ENCZ)

FIG. 8.2 ALIGNMENT CONTROL CIRCUIT (GENERAL LAYOUT)

TABLE 8.2 : COMPONENT COSTS

UNIT No.	COMPONENT NAME	TYPE	SUPPLIER	QUANTITY	COST/£ +(V.A.T)
1	Encoder Mike manipulator	Miniature D.C Motors	Oriel Corp.	1 (3 motors)	2805:68p
2	Laser	1300 nm wavelength (cw)	STC Plc. (Loan)	4	-
3	Detector	-	STC Plc. (Loan)	1	-
4	Optical Fibres	Monomode	STC Plc. (Loan)	2	-
5	Thermistor, Transformers, OPAMS & other components.	-	Local Dealer	-	823:17p
6	Power Supply (Laser Drive)	-	Hewlett Packard	1	1486:95p
7	I/O3 Interface Card	-	Transam Microsystems	1	457:70p

8.2.1 D.C. Motor Drive Circuit.

The motor drive circuit of Fig. 8.2.1 forms part of the overall control circuit already discussed (Fig. 8.2). It consists of three motors (Mx, My and Mz) each connected to a relay and an opto-isolator. The relay is then connected to a common opto-isolator (4)

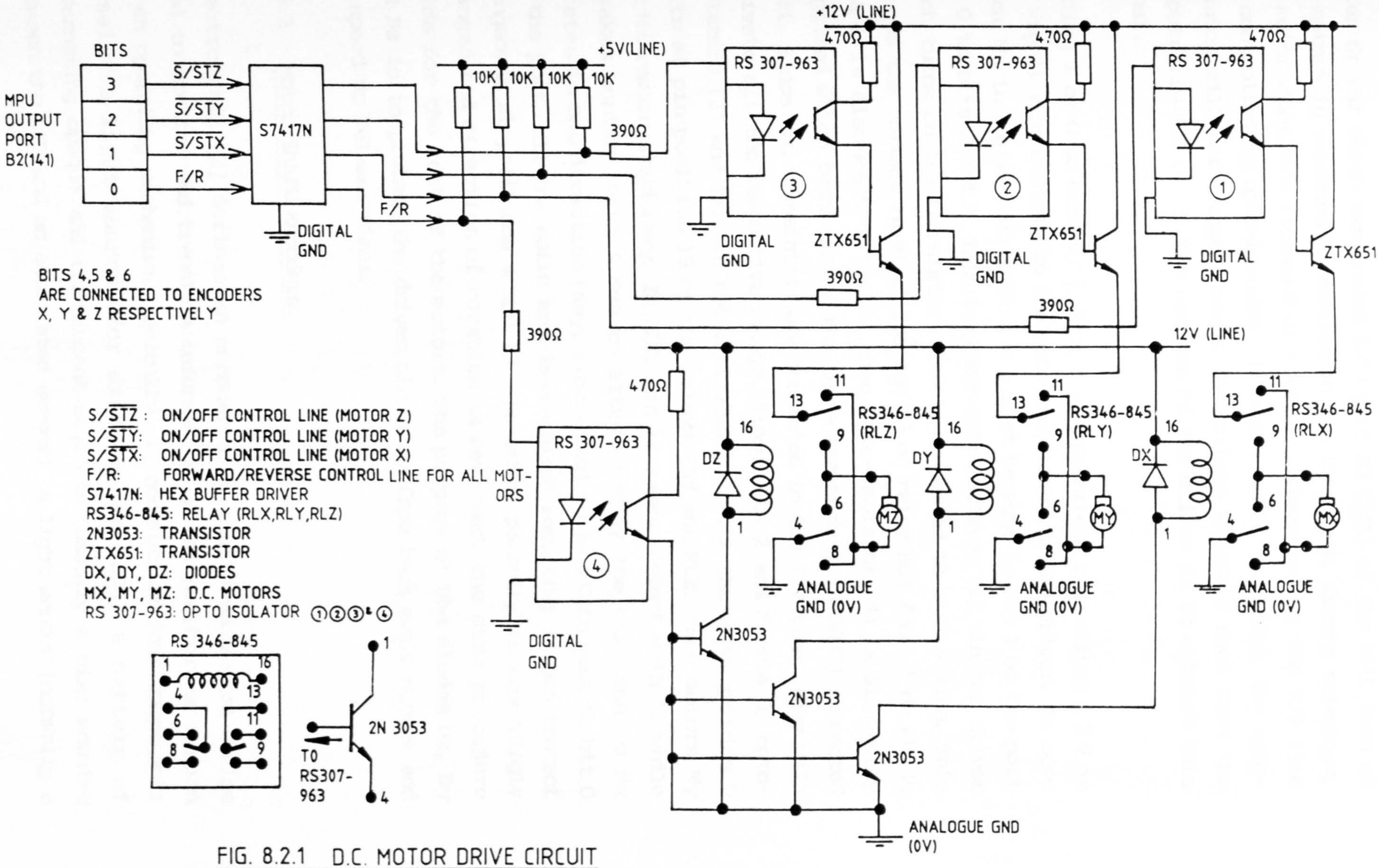

FIG. 8.2.1 D.C. MOTOR DRIVE CIRCUIT

via a transistor. The opto-isolators are in turn connected to a Hex Buffer driver which terminates into port B2 (141) of the MPU. Each of the motors is selected or deselected via this port. During selection, the motor direction (forward or reverse) determined by the F/R line and controlled by opto-isolator (4) must also be specified. The opto-isolator will not trigger unless the voltage signal V sent from the computer is 2.4 <V< 5. The purpose of the driver is to enhance this signal.

Sending 1 or 0 to bits 0, 1, 2 or 3 is equivalent to sending a 5 V or 0 V signal respectively to the opto-isolators via the driver. To move motor Mx in a given direction, a 1 must be sent to bit 1 of the port and 0 to bits 2 and 3. This triggers opto-isolator (1) via the driver which turns on the transistor (ZTX651) connected to a 12 V line. This changes the voltage level at position 13 of relay RLX from 0 to +12 V. If a 1 is also sent to bit 0, then opto-isolator (4) is similarly triggered which turns on all the three transistors (2N3053) connected to it. Since the transistors are connected to the 12V line, they will activate all the respective relays. Since bits 2 and 3 have 0, opto-isolators (2) and (3) are not activated and will therefore provide 0 volts at pin position 13 of the relays RLY and RLZ. Thus motors My and Mz remain stationary. In RLX, pin 11 makes contact with 13 while 8 makes contact with 4 due to attraction by the coil and so Mx rotates in one direction (say, clockwise). When a 0 is sent to bit 0 on the port, all the coils are de-energised resulting in pin contact changeover at positions 4 and 13. The motor polarity is accordingly changed and direction of rotation is reversed. The same procedure holds for the rest of the motors. The purpose of the diodes Dx, Dy and Dz is to protect the driver circuitry from back e.m.f surges and to speed up release times.

8.2.2 Motor Shaft Encoders.

Electrocraft [2] defines an encoder as an electromechanical device used to monitor and translate information on the position or motion of an operating mechanism. Basically, it consists of four components namely: a light source (for example, an LED), a pattern of alternating opaque and translucent segments (usually a disc mounted between the LED and an associated sensor), a light sensor (normally a

phototransistor) and a conditioning circuitry such as may be required to convert sensor output to properly formatted information for interface. To achieve increased resolution, the LED is collimated and a mask is added between the disc and the sensor [2]. In such applications light is transmitted to the sensor only when the translucent segments of both are in alignment.

Encoders are either linear or rotary. The former obtains direct digital information of the position or velocity of an arm moving along a linear axis while the latter senses position or movements of rotary devices. The latter is preferred and can either be incremental or absolute in its encoding function. Although both absolute and incremental encoders are used for control of industrial robots and NC machines, the latter is preferred for speed control while the former is best for position control [2]. This is because the absolute encoder mechanism for reading and maintaining memory of shaft position is superior to that of the incremental encoder. The former reads and maintains memory of the shaft position information within the encoder system itself. Such information is not erased or changed whether or not the encoder is powered down. However, the latter maintains memory of position in an external digital counter which can be lost when the incremental encoder is powered down. The absolute encoder is therefore better in this respect but an assessment of the two encoders by Udoakang [3] reveals that the choice between them normally lies in the cost trade-offs. Details of their construction and functioning procedure can be obtained from manufacturers like Litton (U.K) [4] and other books on encoders.

In Oriel Encoder Mikes, a pair of LEDs and phototransistor detectors are used with a shutter to generate square signals in synchronisation with motor operation. The shutter has ten equally spaced openings which produces ten quadrature cycles per motor revolution. One complete revolution of the motor being equivalent to 1 μm of linear displacement (4.4.3). Thus each cycle represents 0.1 μm of motion. Signals obtained from the Encoder Mike encoders by driving the motor using a program constructed in chapter 9 are shown in Figs.8.2.2(a) and (b). Fewer signals are recorded when the motor is driven for a short period of time as shown in Fig. 8.2.2(b) where the motor has moved approximately 0.1μm compared to 1μm in (a).

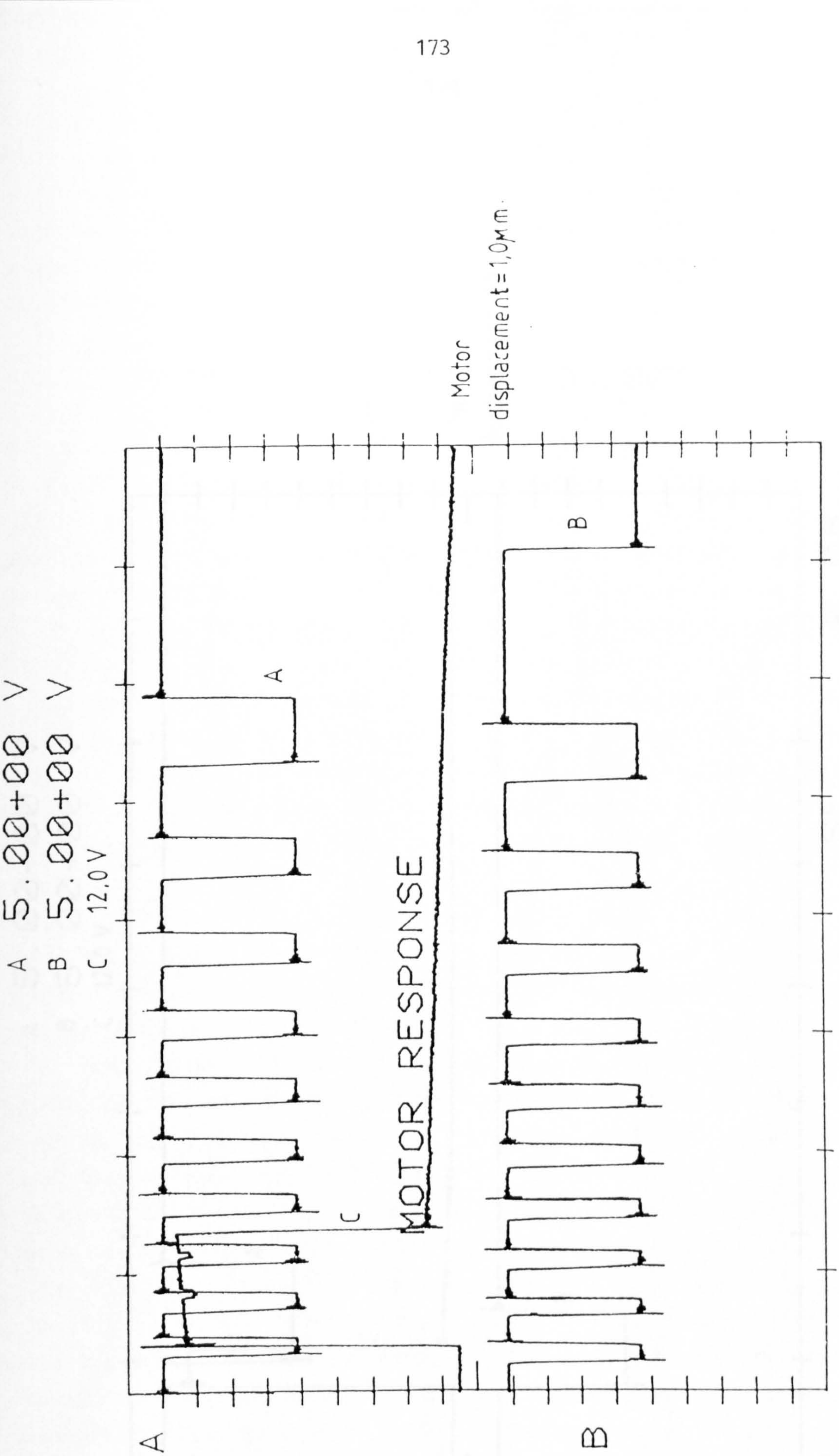

Fig,8,2,2 (a) Encoder signals A & B produced by motor

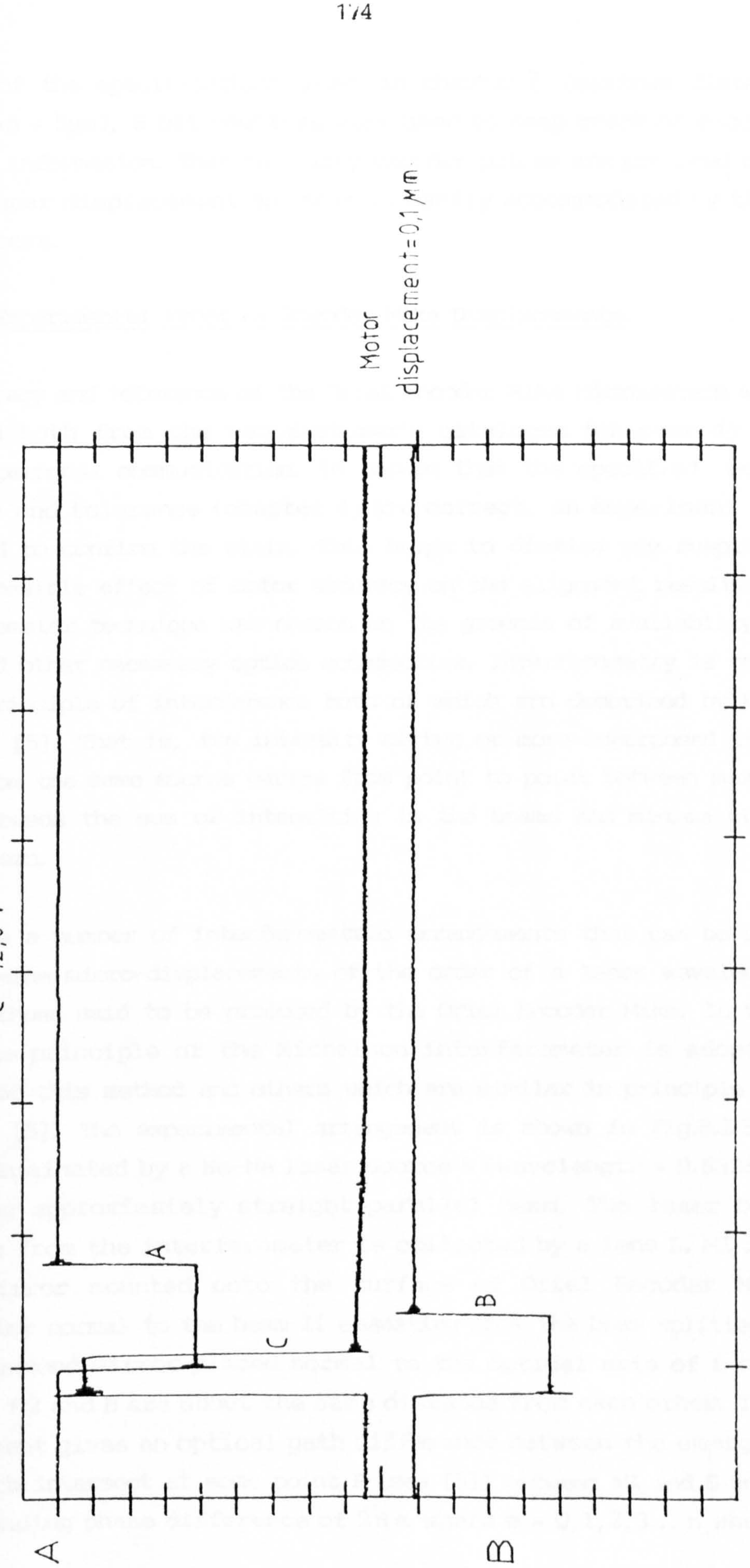

Fig. 8,2,2(b) Encoder Signals A & B produced by motor drive signal C

Because of the specifications given in chapter 2 (maximum distance traversed = 5μm), 8 bit counters were used to keep track of encoder position information. That is, fifty encoder pulses are produced over a 5μm linear displacement and this is easily accommodated by the 8 bit counters.

8.2.3 Experimental Proof of Encoder Mike Displacements.

The accuracy and tolerance of the Oriel Encoder Mike Micrometers were obtained both from the manufacturer's catalogue (chapter 4) and through personal communication. To ensure that the specified motor accuracy and tolerance (chapter 4) are correct, an experiment was conducted to confirm the claim. This helps to dismiss any suspicion of the possible effect of motor accuracy on the alignment results. An interferometer technique was chosen on the grounds of availabilty of laser and other necessary optics accessories. Interferometry is based on the principle of interference both of which are described by Born and Wolf [5]. That is, the intensity of two or more superposed light beams from the same source varies from point to point between maxima which exceeds the sum of intensities in the beams and minima which may be zero.

There are a number of interferometric arrangements that can be used to determine micro-displacements of the order of a laser wavelength such as those said to be produced by the Oriel Encoder Mike. In this test, the principle of the Michelson interferometer is adopted. Details of this method and others which are similar in principle are given in [5]. The experimental arrangement is shown in Fig.8.2.3(a). It is illuminated by a He-Ne laser source S (wavelength = 0.6328μm) producing approximately straight parallel beam. The laser beam emerging from the interferometer is collected by a lens L. M1 is a plane mirror mounted onto the surface of Oriel Encoder Mike manipulator normal to the beam I1 emanating from the beam splitter B. M2 is a second mirror placed normal to the optical axis of L such that M1, M2 and B are about the same distance from each other. This arrangement gives an optical path difference between the emergent rays which intersect at some point P (see [5]) between M1 and B and a corresponding phase difference of $2\pi m$ where $m = 0,1,2,3\ldots n$ when a

bright fringe is formed and m = 0.5,1.5,2.5,... n/2 for a dark fringe. It is stated [5] that due to a departure from monochromatism of the source, the fringes are visible only if the optical paths from the two arms are approximately equal. Details of this method are discussed in [5].

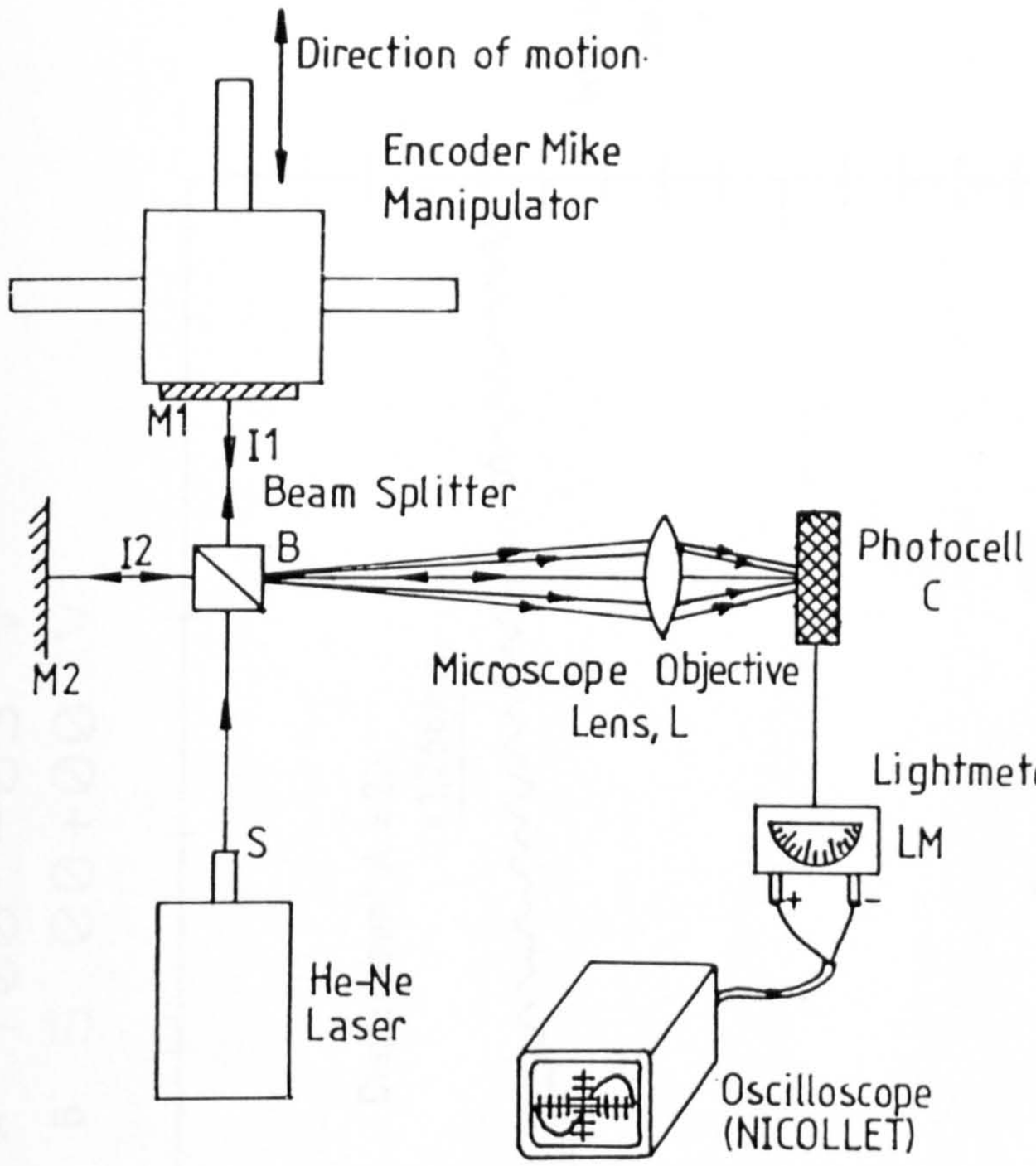

Fig,8,2,3(a) Interferometer arrangement for determining Encoder Mike response to step drive pulses.

The microscope objective L focusses the laser onto a photocell C connected to a light meter (LM). The meter is in turn connected to an oscilloscope (NICOLET). When the Encoder Mike manipulator moves in the given direction (Fig.8.2.3(a)), the fringe pattern on the photocell changes. This in turn produces a sinusoidal wave which is captured by the NICOLET when triggered. Each peak of the wave corresponds to a bright fringe while the trough corresponds to a dark fringe. The distance from peak to peak or trough to trough is the wavelength of the laser used. The total number of waves n produced is

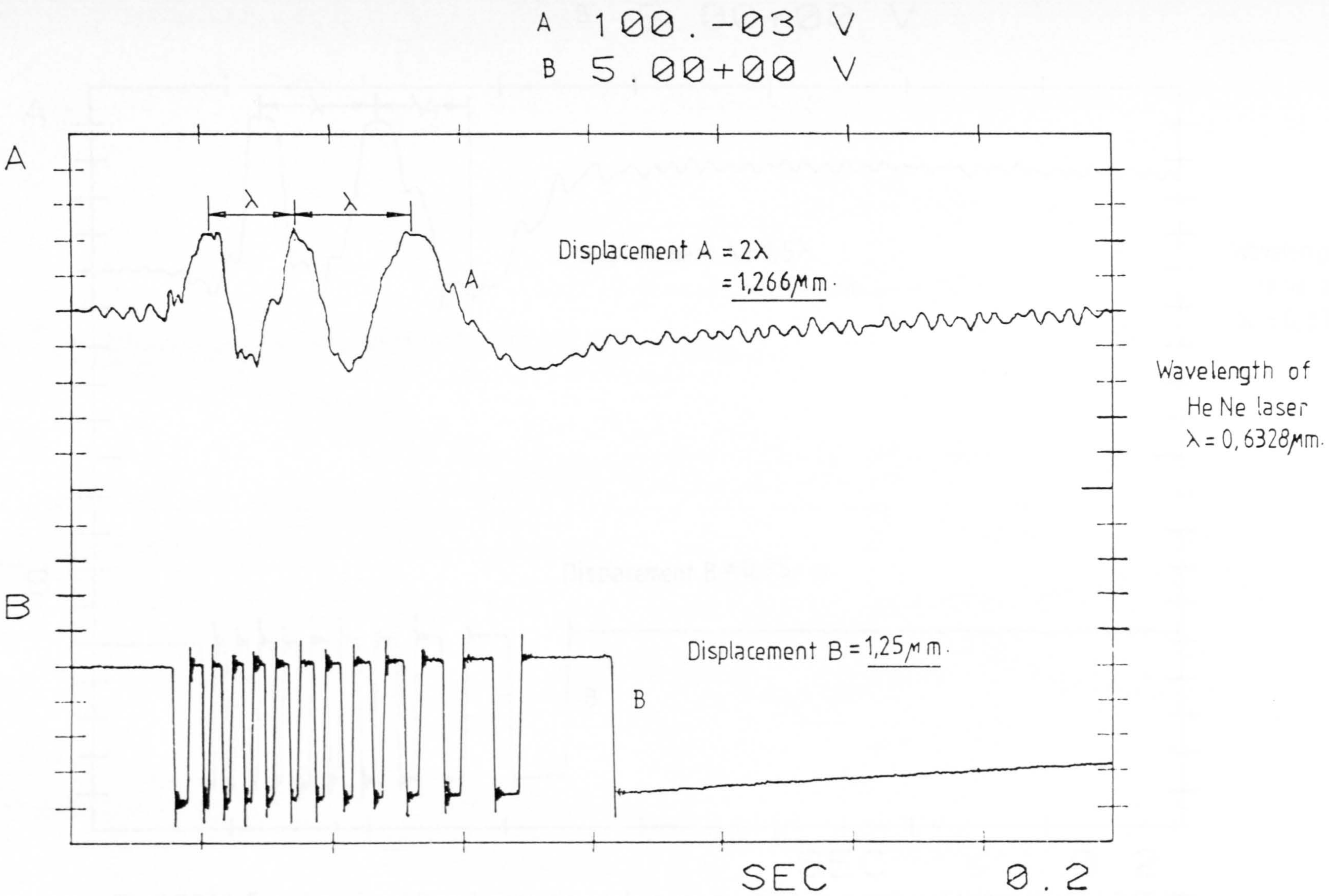

Fig, 8,2,3 (b) Encoder signal B and laser response A compared for motor displacement of 1,25μm.

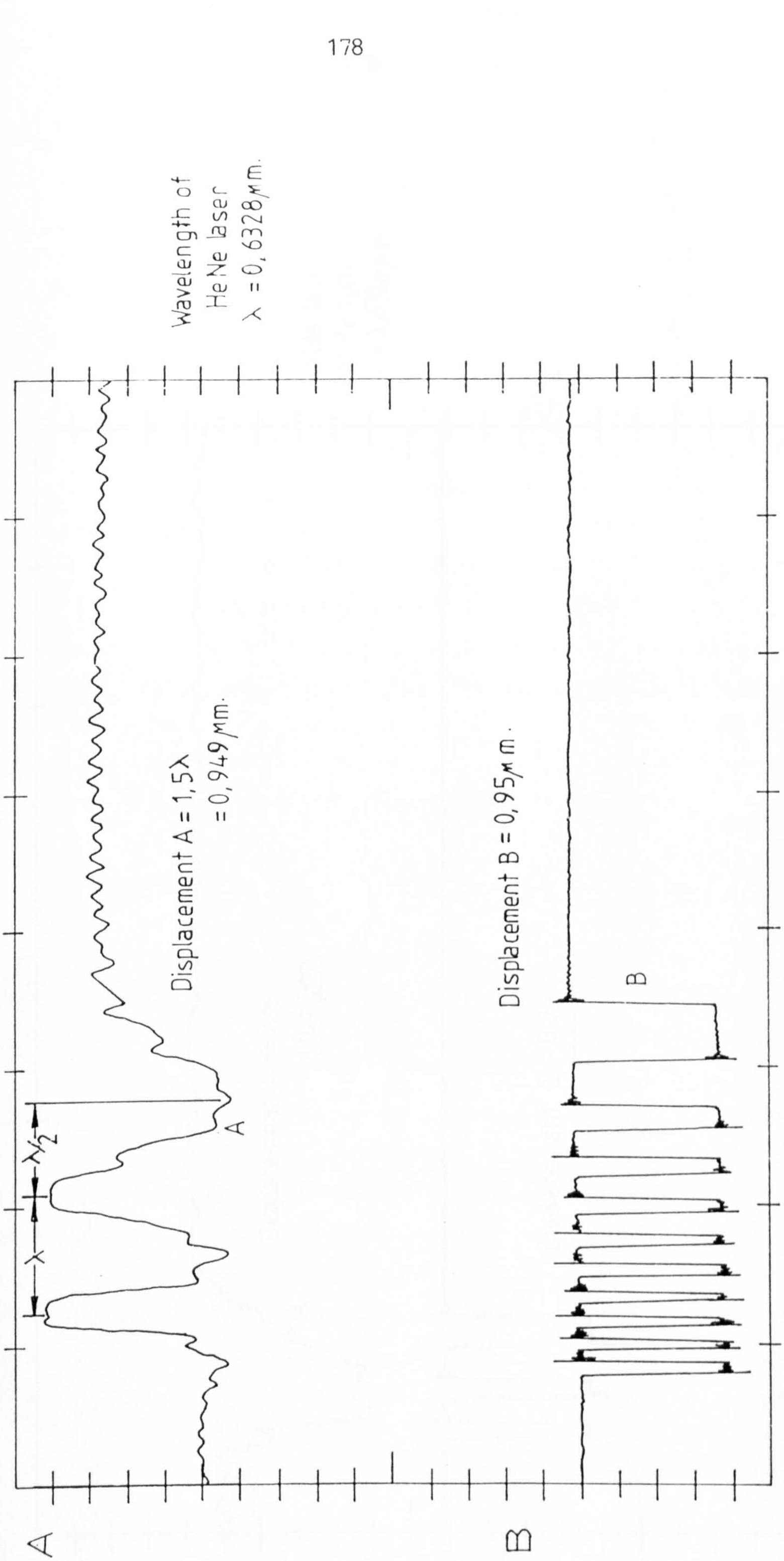

Fig, 8,2,3 (c) Encoder signal B and laser signal A corresponding to a motor displacement of 0,95μm.

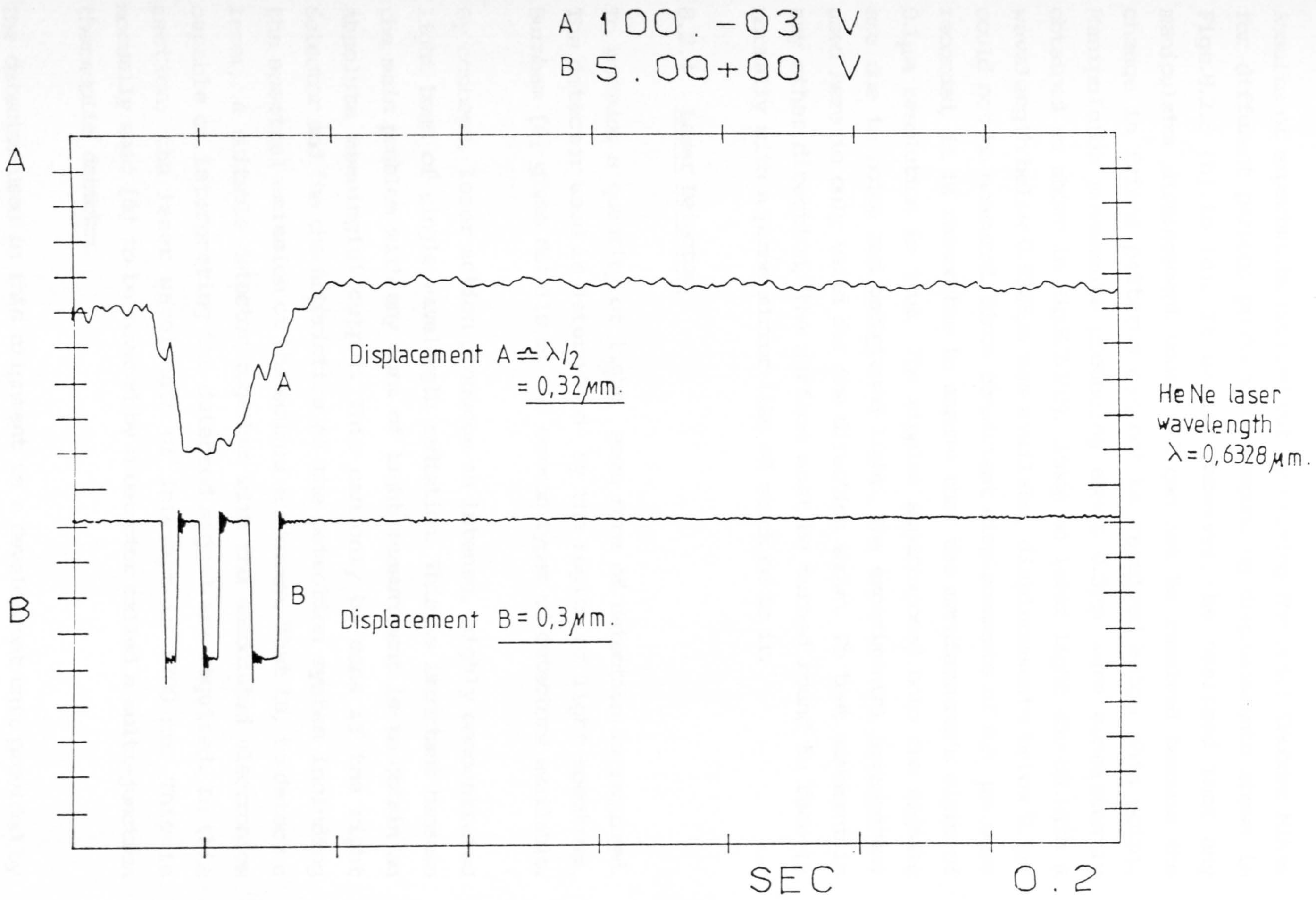

Fig,8,2,3 (d) Encoder signal B and laser signal A corresponding to a motor displacement of 0,3 μm.

equivalent to the manipulator displacement (nλ) where λ is the laser wavelength.

Results of experiments carried out by driving the Oriel Encoder Mikes for different periods produced corresponding displacements shown in Figs.8.2.3 (b) to (d). It should ,however, be realised that any manipulator displacement under λ/2 can not be resolved because the change in fringe patterns can not be resolved below this point. Manipulator movements producing about 0.3μm were consistently obtained as shown in Fig.8.2.3(d). Since no laser light source with a wavelength below 0.6328μm was availabe, displacements below 0.3μm could not be measured. Since consistent displacements of 0.3 μm were recorded, it is reasonable to assume that the manufacturer's claim of 0.1μm resolution is true. The ripples superimposed onto the signals are due to noise and background light. The experimental arrangement used here is only valid for the direction shown. To test movement in any other direction, the surface must be turned round to face I1 normally with a plane mirror like M1 stuck on to it.

8.2.4 Laser Detector.

To measure a quantity of light, some form of detection is required. The detector used is determined by the region of light spectrum. Burnham [6] gives details of the common types of detectors available.

By concept, laser action produces an intense, highly concentrated light beam of single wavelength radiation. This is important because the main problem with any form of light measurement is to obtain an absolute meaningful output. This can only be done if the right detector and the characteristics of the detection system including the spectral emission of the source are known. That is, to detect a laser, a suitable detector together with the associated electronics capable of interpreting the detected signal are required. In this section, the laser wavelength of interest is 1300 nm. This is normally said [6] to be covered by a detector called a multi-junction thermopile detector.

The detector used in this alignment is a development unit provided by STC. For this reason, details of the circuit were not provided. The

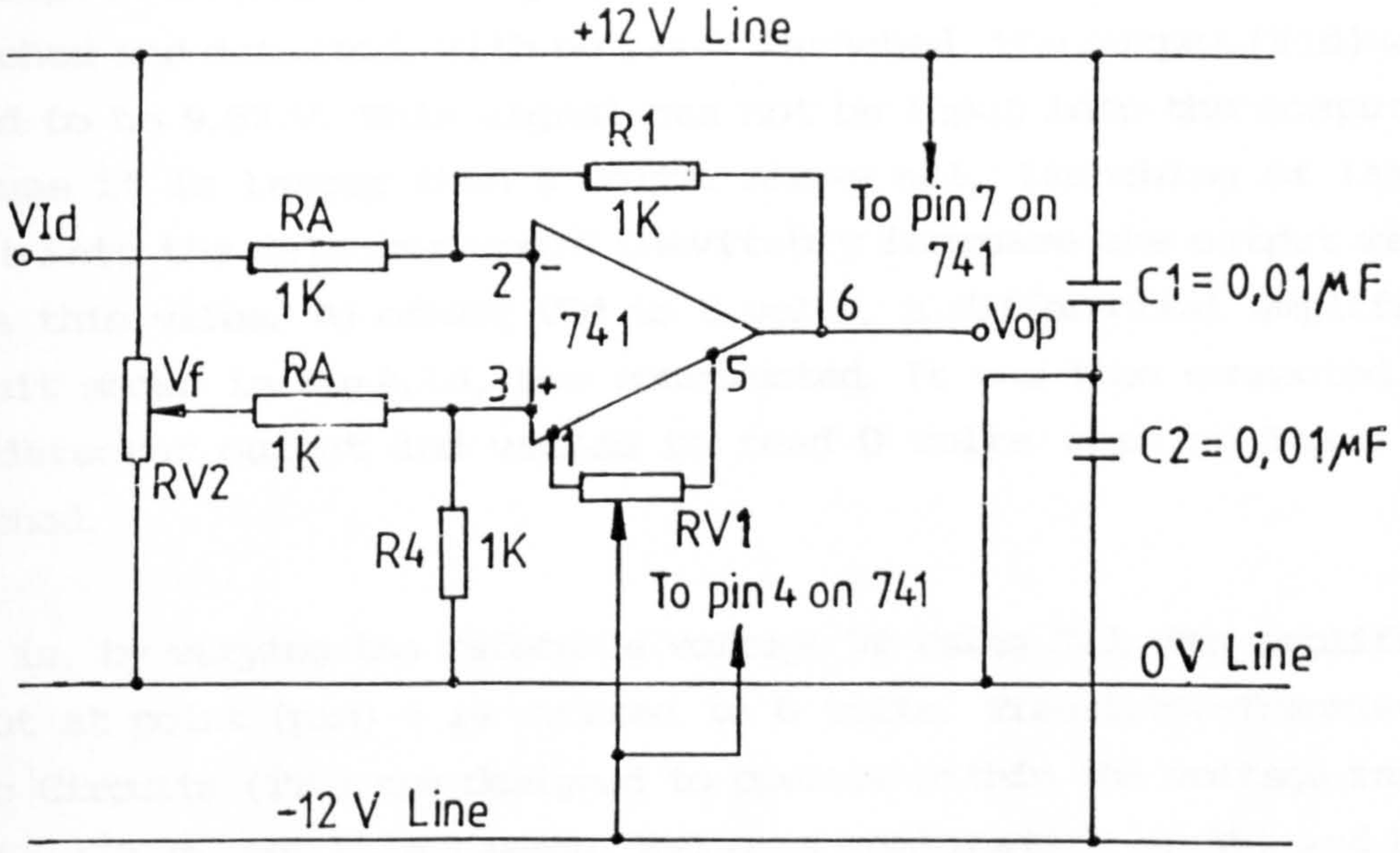

Fig,8,2,4 Differential Amplier Circuit.

VId = 9,52 V (Detector (circuit) output voltage)

Vf = Reference signal voltage (9,56 V).

Vop = 0,08 V (Amplifier output voltage at balance)

Amplifier gain $Av = \frac{R1}{R2}$ where R2 = source resistance + RA $\triangleq$ 1K.

PIN No.	FUNCTION
1	OFFSET
2	INVERTER
3	NON INVERTER
4	-ve SUPPLY
5	OFFSET
6	OUTPUT
7	+ve SUPPLY
8	UNCONNECTED

skeletal details given shows that it is fundamentally an FET-photodetector operated device which is spectrally matched to the detected 1300 nm laser. The output of the detector circuit does not read laser power directly. The laser signal is transformed so that the ouput records a voltage proportional to the amount of laser launched and detected. With no laser launched, the output (VId) was found to be 9.52 V. This signal can not be input into the computer because it is larger than 5 volts. Above all, launching of laser light into the detector would inevitably increase the output well above this value. To offset VId to 0 volts, a differential amplifier circuit shown in Fig.8.2.4, was constructed. It was then connected to the detector output and varied to read 0 volts when no laser is launched.

That is, by varying the reference voltage Vf using RV2, the amplifier output at point (pin) 6 is reduced to 0 volts. Transistor-Transistor Logic Circuits (TTL) are designed to operate within the voltage range $0 \leqslant V_{TL} \leqslant 5.25$. For this reason, RV1 or a combination of RV1 and RV2 are used to offset the output to 80 mV in order to maintain it constantly above 0 volts. Adjustment of Vf to 9.56 volts when VId is 9.52 volts produces an output Vop of 80 mV with no laser launched. When the laser is fired and launched into the detector, Vop varies proportionately with it. For zero power, Vop = 80 mV and at peak power, it records 5 volts. This construction is used in Chapter 9 to test the alignment program.

8.2.5 Effect of Temperature on Laser Operation.

The semiconductor laser diode is fired from a constant D.C. current source. The output power varies proportionately with the amount of drive current supplied (Fig.2.1.4(b)). STC laser diodes are fired with currents varying from 0 to 500 mA [7]. Many electronic devices exhibit temperature dependent parameters and semiconductor laser diodes are no exception. In general, this is caused by heat dissipation which in turn depends on the amount of current flow through the components.

According to STC [7] the life expectancy of a 1300 nm wavelength laser is in excess of 100,000 hours at $25^{o}C$ to 50% increase in

threshold current under suitably controlled conditions. Its lasing threshold current and wavelength are both said [7] to be temperature dependent (2 to 3% $^{o}C^{-1}$ over a range of 25 to 50 ^{o}C and 0.35 nm $^{o}C^{-1}$ respectively). It is therefore recommended that this device be operated such that the chip is maintained at a constant temperature of 25^{o}C and the case at about 65^{o}C. Storage and usage should be limited to a maximum temperature of 50^{o}C or 65^{o}C depending on the laser type otherwise its life is reduced. Laser output rises with reduction in temperature and damage to the laser below ambient (25^{o}C) can be avoided by reduced drive current and/or by heating the laser submount.

In order to cool the device, a separate circuit with the help of a heat sink needs to be incorporated. A peltier drive is normally used. This is a heat pumping device which extracts heat from the cold side and deposits it on the hot side of the module. This heat is then conducted away by another body called a heat sink otherwise the surface gets progressively hotter. Fundamentally, a heat sink must be maintained at a temperature higher than ambient so that heat can be transferred from its surface into the surrounding air. Thus, the surface of the heat sink must be highly conductive. The higher this temperature difference, the more heat can be transferred from the heat sink. Obviously there is a limit to this. Literature on the peltier drive suggests that as the temperature difference across the peltier becomes excessively large, the heat pumping capacity drops. Details of the peltier circuit applied to semiconductor laser diode cooling is presented in the next section.

8.2.6 The Peltier Drive Circuit.

The peltier cooling circuit shown in Fig.8.2.6 is provided by STC. The 334Z is a constant current source device that provides a fixed current. The READ/SET switch SW1(A) which is also connected to SW1(B) shown dotted in the diagram, is first opened and by varying RV1 (the 10 KΩ resistor), the thermistor voltage VRTH across pins 11 and 12 is set to 1 volt. SW1(A) is then closed and the output of the operational amplifier (1) is then set to 0 volts by varying RV2 (the 20 KΩ resistor).

PIN	DESCRIPTION
1	PELTIER HEAT PUMP ANODE (+ve) (for cooling)
14	PELTIER HEAT PUMP CATHODE (-ve)
11	THERMISTOR
12	THERMISTOR
334Z	IS AN ADJUSTABLE CURRENT SOURCE
R.V.	IS A VARIABLE RESISTOR

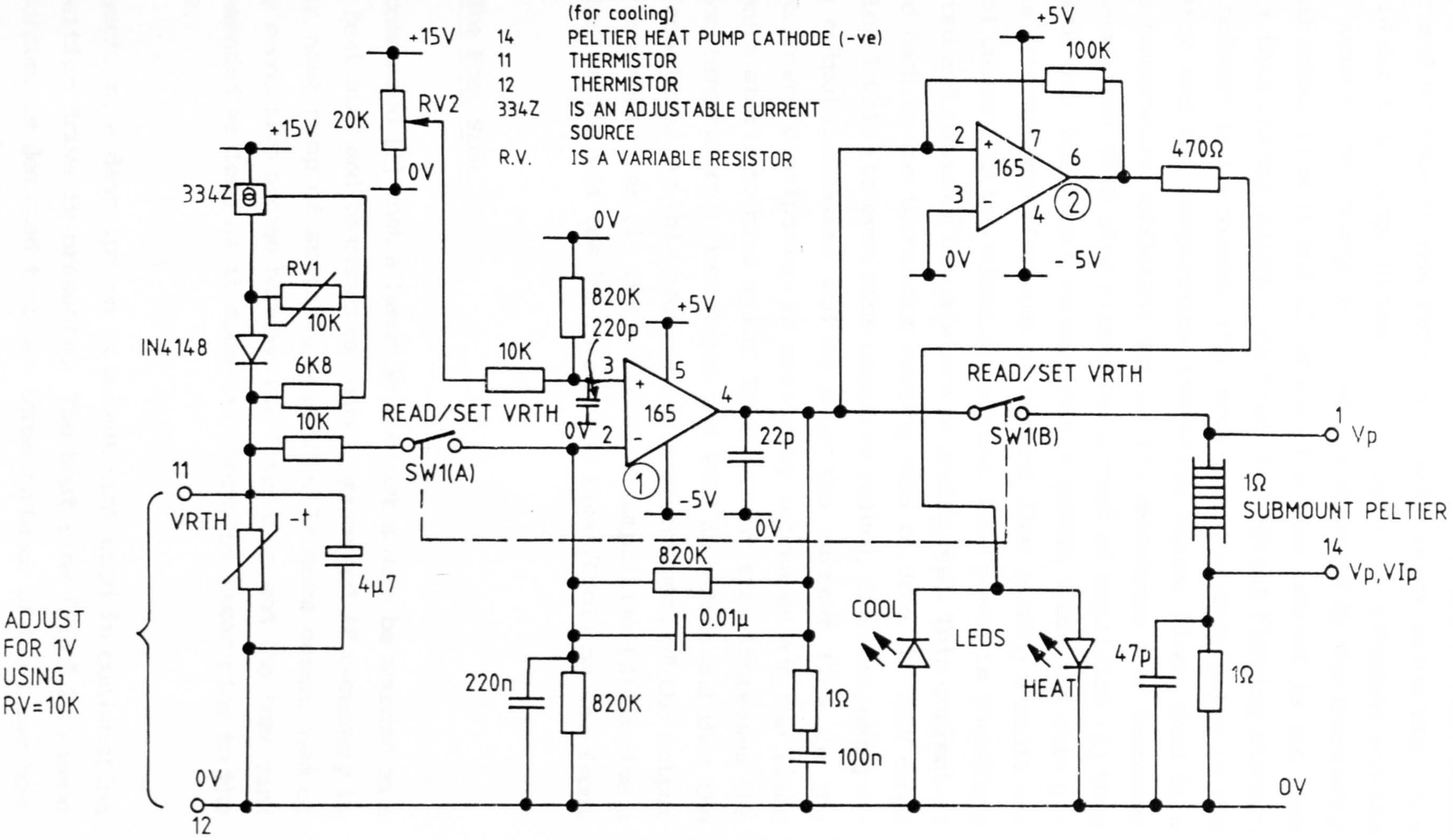

FIG.8.2.6 SUBMOUNT TEMPERATURE CONTROL.- THE PELTIER DRIVE CIRCUIT

The laser is then fired when the setting is completed. The voltage Vp across the peltier drives current through the submount which causes heating and voltage change from Vp to some other value VIp. This change is due to a change in the resistance of the submount and the flow of current. This change in current is detected by the thermistor connected across pins 11 and 12 because the same current is fed back to it. If this change occurs such that the current flowing through the thermistor is increased, then more power is dissipated in the thermistor and the temperature therefore rises. Since this is a positive temperature cofficient device, its resistance also increases which means that VRTH also rises. The output of amplifier (1) then drops. Note that its output voltage Vout = gxVRTH where the gain g = -82. This reverses the direction of current flow leaving a small net amount of current in the submount peltier. Less power is therefore dissipated and so laser temperature is stabilised. This current is again fed back to the thermistor causing VRTH to drop. If VRTH drops well below 1 volt (to even some negative value), then because g = -82, the output increases and so does the current flow in the submount. Power dissipation is similarly increased and the laser temperature starts to rise again. This current rise increases the thermistor temperature , resistance and VRTH as before and thus the process continues. As this process takes place, part of the output signal from amplifier (1) is used to drive amplifier (2) to give a status indication via the bi-colour LED (Heat/Cool) on the front panel.

8.2.7 The Heat Sink.

It is recommended [7] that a laser device must always be mounted on a metallic heat sink and temperature control augmented if necessary by a peltier heat pump of suitable capacity. In some cases, use of thermally conductive grease between the laser case and the heat sink is recommended as long as it does not short the laser pins to the heat sink.

In this section, a description of a heat sink used in conjunction with a peltier drive is presented. The heat sink (Fig.8.2.7) made from aluminium, is designed to cover three surfaces of the laser box. The laser box has 14 pins which are inserted and gripped by 14 slots

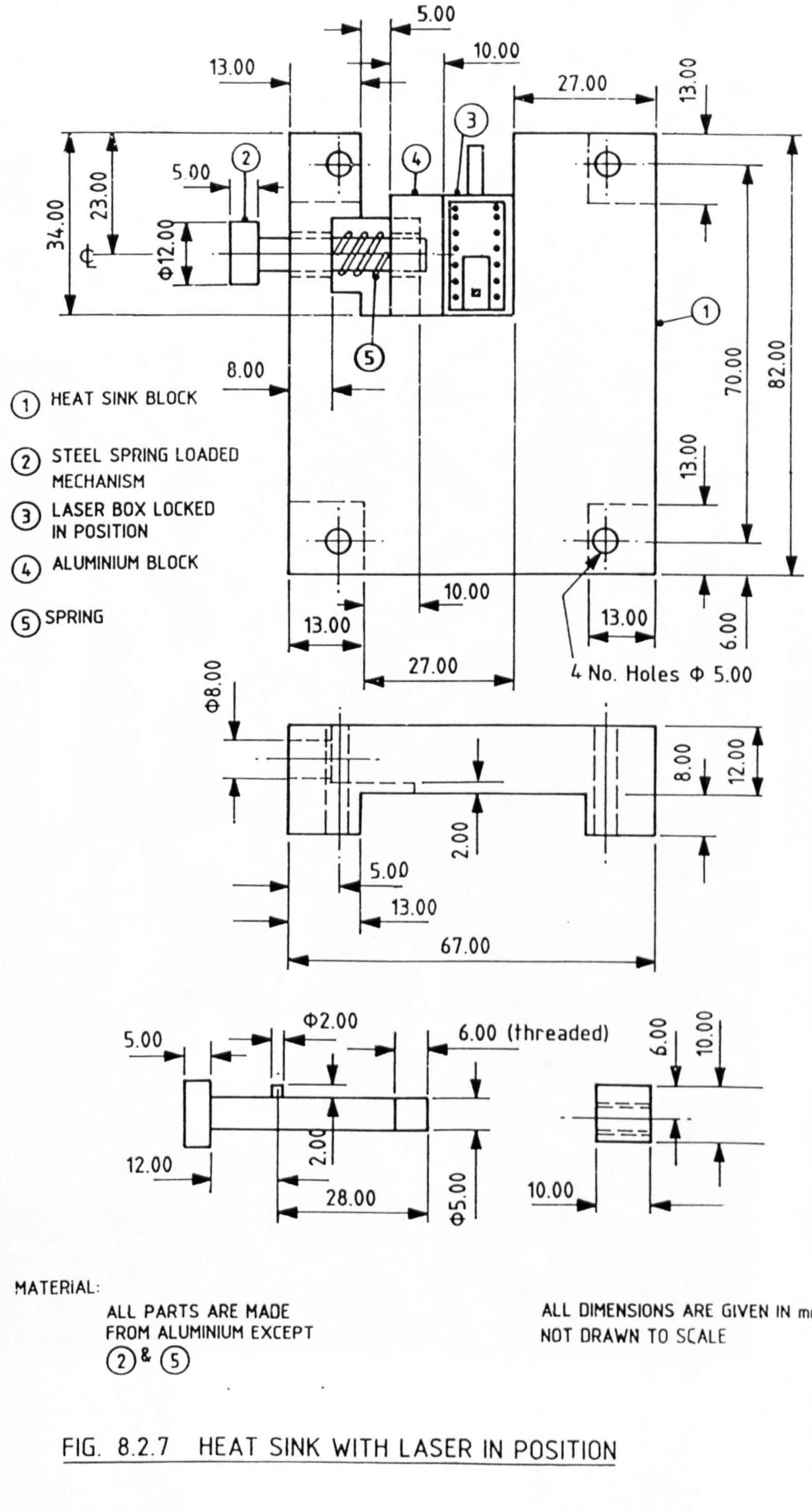

MATERIAL:

ALL PARTS ARE MADE FROM ALUMINIUM EXCEPT ② & ⑤

ALL DIMENSIONS ARE GIVEN IN mm
NOT DRAWN TO SCALE

FIG. 8.2.7 HEAT SINK WITH LASER IN POSITION

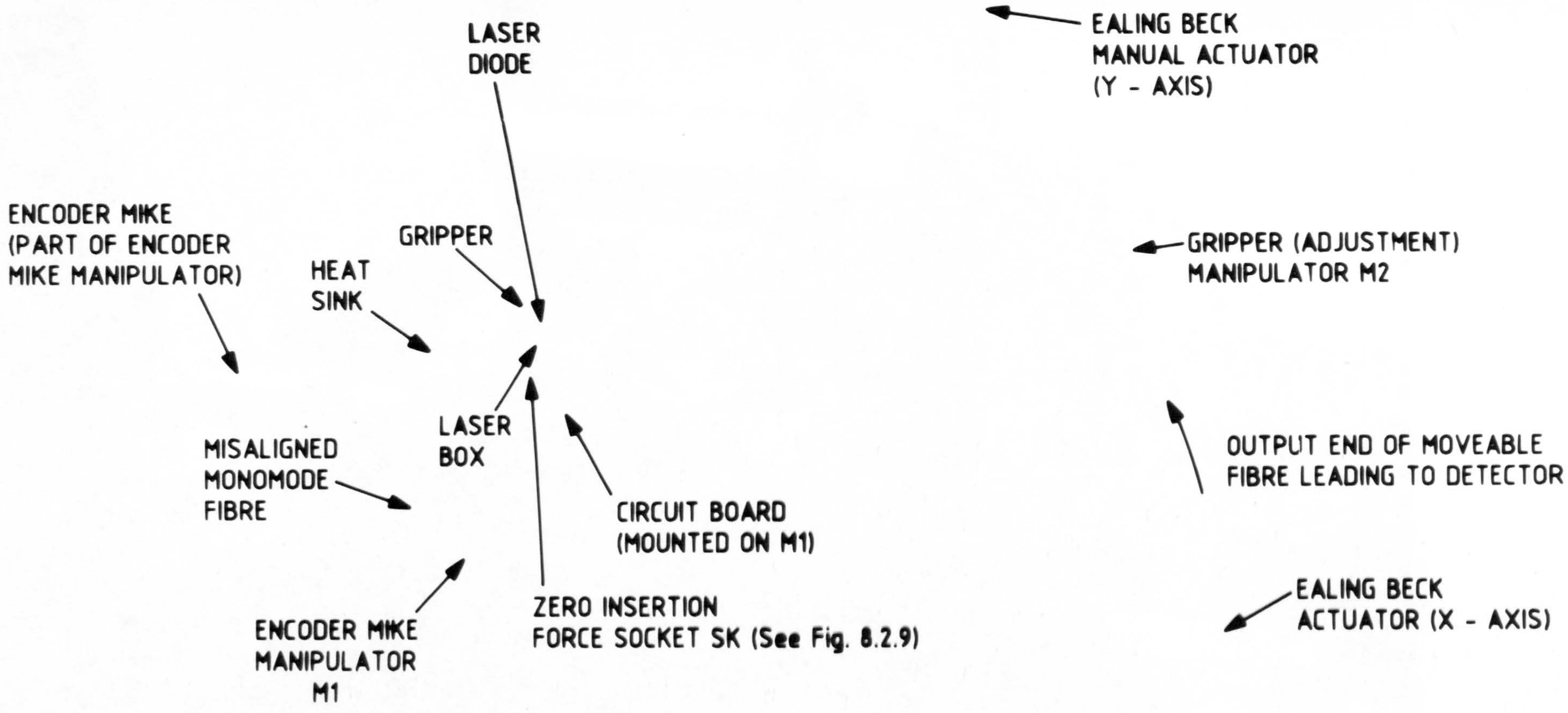

PLATE 8.2.7: LASER-FIBRE ALIGNMENT

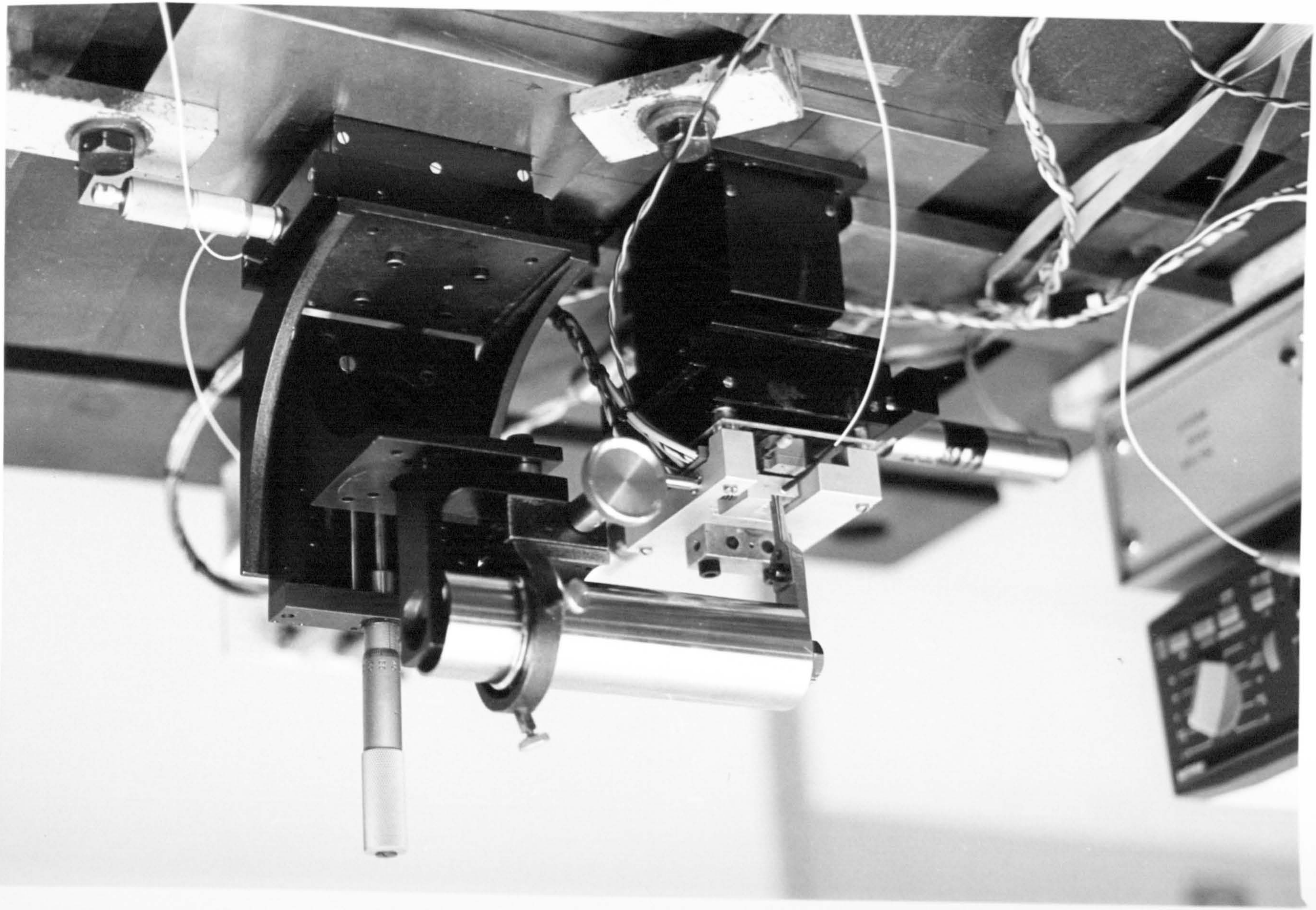

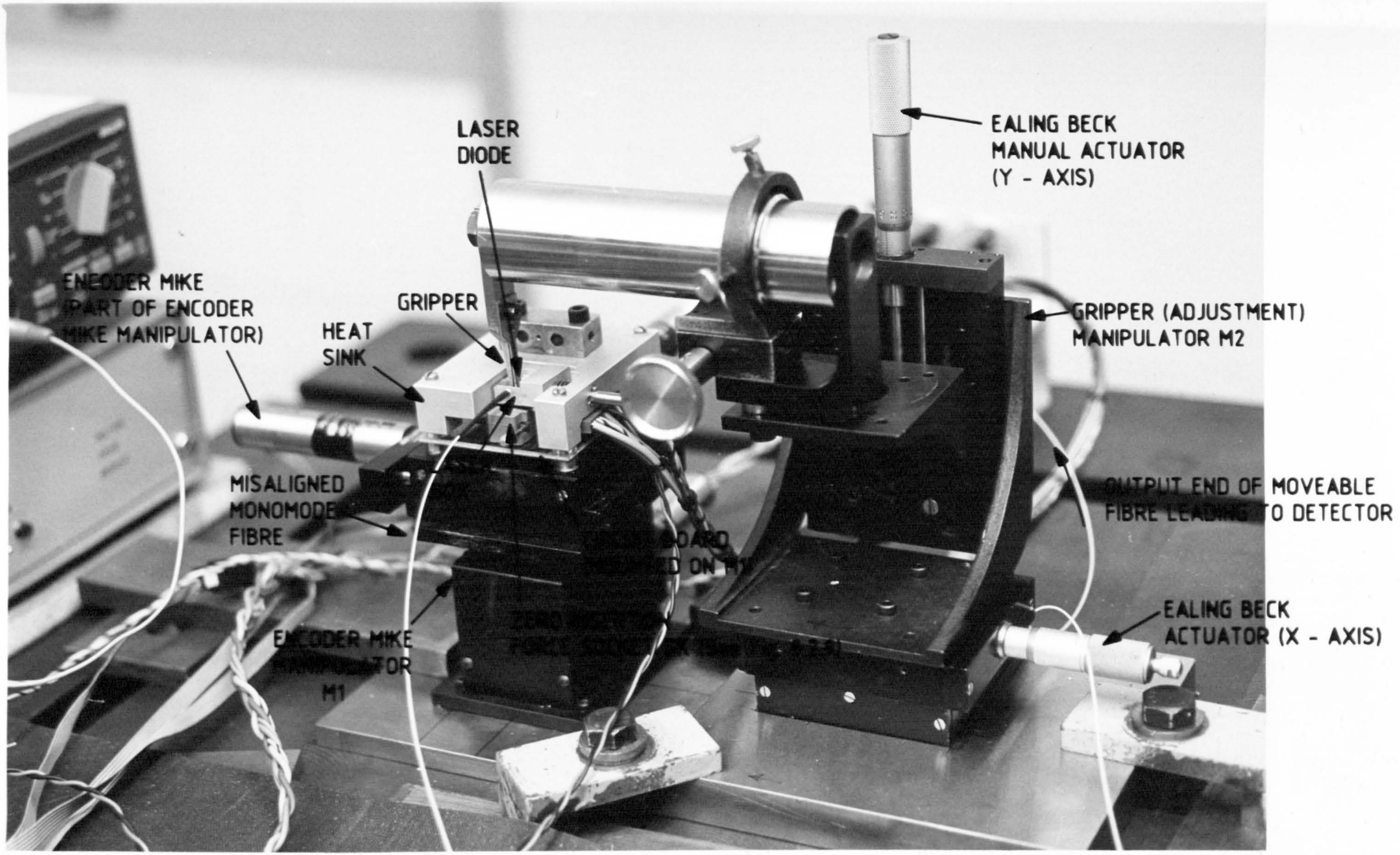

PLATE 8.2.7: LASER-FIBRE ALIGNMENT

(each containing moveable metallic inserts) specially moulded on top of a zero force insertion plastic socket SK (8.2.9) whose corresponding pins (14) are soldered on to a circuit board. The board is in turn mounted on top of the manipulator (PLATE 8.2.7). Since the laser box sits on top of SK, the heat sink was designed to cover the laser box from the top of the socket (8 mm from the surface of the circuit board) up to the top of the laser box (20 mm from the surface of the circuit board). The laser box inserted into SK was then set up so that it rests firmly against two surfaces of the heat sink while the third surface is closed in by means of a spring releasing mechanism (Fig.8.2.7) when the laser is inserted into the slots.

8.2.8 The Optical Fibre Gripper

In the manual alignment procedure (2.4), a fibre is threaded into an open box housing the laser diode and manipulated manually by means of a pair of tweesers without the need for a gripper. In an automated alignment procedure where a semiconductor laser diode is manipulated for aligning its beam with the fibre, one of the components (fibre or laser) needs to be held firmly in one position. Since this facility was not provided, one needed to be designed and made. In this section, the description of such a fibre gripper is presented.

Although the input terminations (tips) of the fibres used for this alignment are strengthened with brass sleeves, they are still flexible and are liable to permanent bending during alignmnet. This is particularly true when the fibre is moved hard against the inner walls of the tube through which it is threaded (Fig.8.2.8(b)). This could result in a false alignment as well as introducing strains in the fibre. In order to avoid this problem, the gripper needs to be designed to fit the limited space (7.8 mm x 6.0 mm) inside the laser box (Fig. 8.2.8(b)). In addition, the gripper must not come into contact with the pins inside the box thus causing a short circuit which destroys the laser and can damage the power supply. This gripper is shown in Fig. 8.2.8(a). Part 1 is ordinary sprung steel 30 mm long , 5 mm wide and 1 mm thick which is firmly screwed onto another piece 2 also made of steel. The latter is purposely made thin at the tip (2 mm x 5 mm) to fit inside the box and give allowance for manipulation but gets progressively wider at the top to provide for

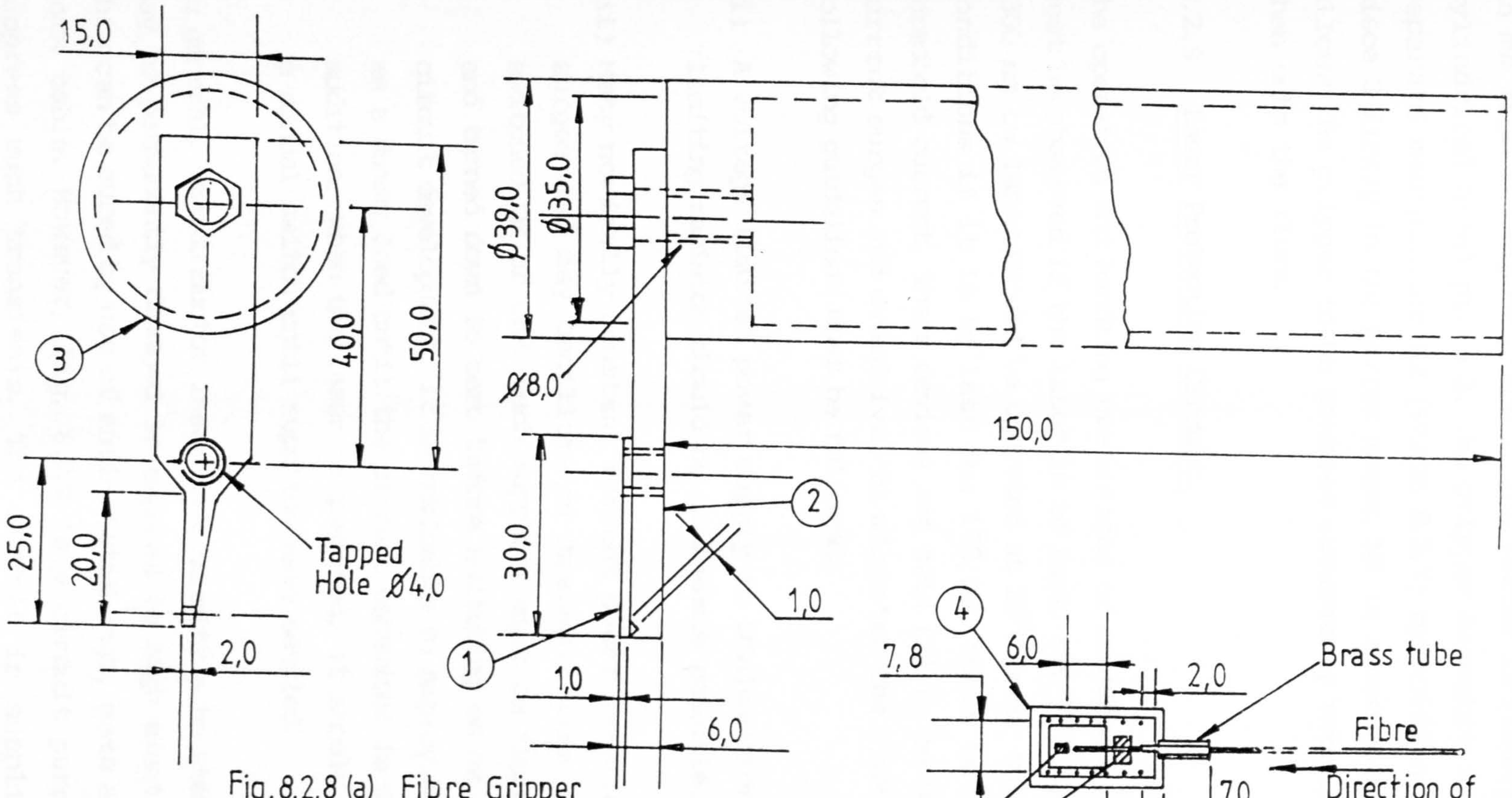

Fig, 8,2,8 (a) Fibre Gripper

ALL DIMENSIONS IN mm

① ORDINARY SPRUNG STEEL SCREWED ONTO ②

② STEEL COMPONENT WITH A V-GROOVE

③ CYLINDRICAL STEEL BLOCK (MADE TO FIT INTO A MIRROR MOUNT)

Fig, 8,2,8 LASER/FIBRE PACKAGE (b)

④ LASER BOX

rigidity. A right angled V-groove is made at the tip to fit the fibre brass terminations 1mm in diameter. A fibre can only be threaded into the V-groove if 1 is pushed out of position. This is done by means of a rigid slender pin inserted into a hole 2.5 mm in diameter drilled 15 mm from the tip of piece 2. The latter is firmly screwed onto a cylindrical steel piece 3. The gripper assembly is mounted onto a separate manipulator M2 (PLATE 8.2.7) by holding the cylindrical piece 3 firmly in the mirror mount. M2 is a manual manipulator which allows the gripper to be lowered accurately into the laser box and then onto the fibre.

8.2.9 Laser Protection Circuit.

The operation and handling precautions of continuous wave (cw) lasers must be observed if the laser is to last. STC [7] recommends that a 1300 nm cw laser should be operated at 25^{o}C under suitably controlled conditions if it is to last for 100,000 hours to 50% increase in threshold current. These devices are said [7] to be easily damaged by current surges and overdrive. To minimise the risk of damage, the following guidelines must be followed.

(i) A voltage limited power supply in conjunction with a 10 ohm limiting resistor should be used where possible.

(ii) Many nominally constant current power supplies give current surges and may oscillate or transmit line transients when switched ON or OFF. Such supplies must be transient suppressed and turned down to zero before switching on or off. Thus during circuit development, it is advisable to employ a 10 ohm resistor as a dummy load until the circuit behaviour is under control. In addition, when the laser is inserted, it should be shunted with a manual switch until supplies have settled.

In general, semiconductor lasers are sensitive to static voltages and may be permanently damaged if exposed to high electrostatic fields. This can be cured by use of anti-static bags, mats and earthing the work table. However, Fig. 8.2.9 is a circuit purposely built to suppress such transients. The circuit is supplied by STC and comprises of beads FB, inductors L1, L2, capacitors C1, C2 and a

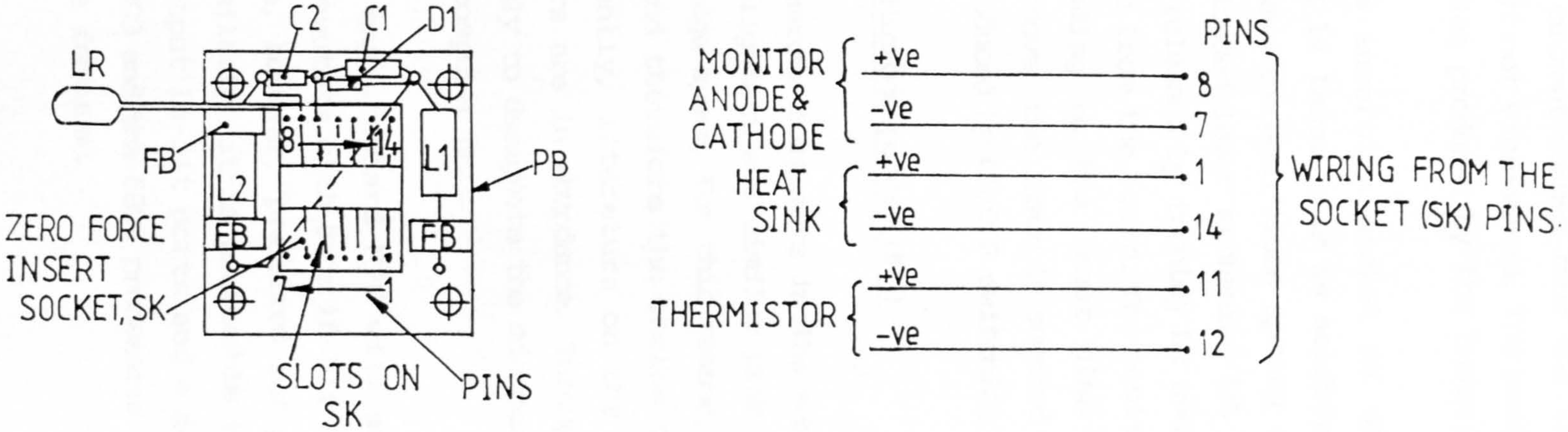

Fig, 8,2,9 LASER PROTECTION CIRCUIT

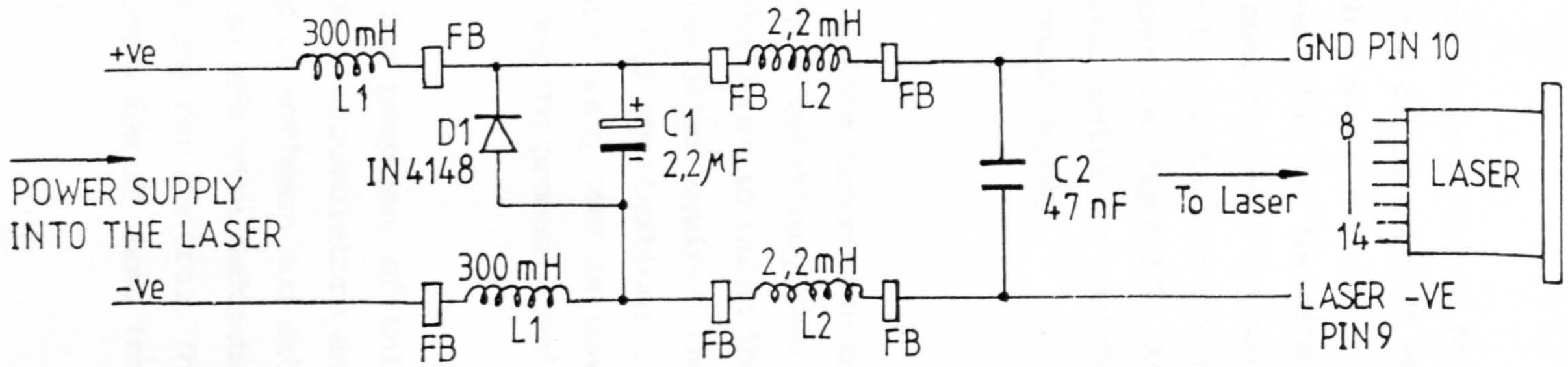

diode D1. This laser is a negatively operated device. Thus its anode and ground (pin 10) are connected together but the cathode (pin 9) is separate. Power is supplied to these pins from a Hewlett Packard constant current power pack via this circuit. D1 conducts any transient or current surges from the laser cathode line to the anode and ground but not vice-versa. The beads, capacitors and inductors suppress ripples produced by the transients.

A zero force insertion socket SK with provisions (slots) for accomodating 14 laser pins is soldered onto the circuit board PB (Fig.8.2.9). These are open/close spring adjustable slots controlled by a spring loaded lever mechanism LR. The laser pins can therefore be locked or released by turning LR when the laser is being mounted to or removed from the board. The positions of the slotted holes on SK corresponding to the laser pins are shown in Fig.8.2.9. As recommended above, the laser is shunted by a manual switch to isolate transients produced by ON/OFF switching of the power supply.

8.2.10 The Microcomputer-(MPU)

There are numerous computers in the market today. The automation of laser-fibre alignment and similar problems require relatively small computer storage space. For this reason, it is difficult to weigh the advantages and therefore the choice of one computer against the other. Currently, literature on the theory and applications of microcomputers are in abundance. Throughout this work, MPU is used interchangeably to designate the microcomputer and the processor unit or the microcomputer unit.

In general, any standard MPU will suffice for purposes of this research. Computers with 8 or 16-bit data buses, accumulators and registers are, however, preferred for purposes of software and data handling. Similarly, it is preferable to have an MPU with dedicated input and output 16-bit ports and a separate one for control. The 8080/8085, 6800 and the 6809 processors are among a few of those that possess these features.

The Transam microcomputer is based upon the Intel 8080 processor. It will accept the use of BASIC, 8080/8085 and the Z-80 assembly

language programming. The use of BASIC and any of the assembly languages interchangeably makes it relatively easy to program this machine. It also has four 8-bit input/output ports, three independent 16 bit programmable event timers or counters, eight 0 to 5 volt A/D channels with 8 bit resolution and similarly for D/A. In addition, it has 8 bit data bus, 8 bit accumulators and registers and a 64 K memory. The decision to choose this computer was based mainly on availability.

8.2.11 Analogue to Digital Converter-(ADC).

This type of conversion involves transformation of numerical information contained in an analogue signal into a digital coded word. This is the opposite of digital to analogue conversion. Kuo [8] recognises that ADC conversion is a more complex process and is generally more expensive with a slower response time for the same conversion accuracy than DAC. The input signal to the ADC converter can be in form of a voltage or current. Different types of the ADC circuits, details of its working procedure, the associated conversion errors as well as the range of typical conversion periods are given in [8] and books on ADC programming and control.

For greater resolution, an increase in the number of bits in the output signal is recommended [8]. This increases circuit complexity and a possible total conversion time which is liable to affect stability of closed loop control systems. The I/03 card of the Transam computer discussed in 8.2.10, contains eight 0 to 5 volt analogue to digital channels with 8 bit resolution. Its coversion time is 13.5 or 18 μs depending on whether a 4 MHz or 2 MHz clock is used. It has a conversion accuracy of ±0.4% Fs ± 1 bit and a settling time of 4 μs. It is set in a unipolar mode so that 0 volts input gives a value of 00 hex when read and 5 volts input corresponds to FF hex in full scale. Details of the unipolar logic coding relating the analogue input value to the output code (binary) can be obtained from the Transam I/03 catalogue available from the Transam microsystems Manufacturers.

8.3 Interfacing Control Circuits to the MPU.

The three motor control axes are connected to the MPU through two interface cards. The motor drive circuit (8.2.1) interfaces the motors directly to the I/O3 card in the MPU while the encoder board interfaces the encoders to the I/O3 via a multiplexer (Fig.8.2). Accessing the encoders (motor positions) is done through the 8-bit data buses. The encoder interface circuit is discussed in section 8.3.1 below.

8.3.1 The Encoder-MPU Interface Board.

The encoders attached to the Encoder Mike motor shafts are of the optical incremental types. This means that the board must possess some latching features, a means of counting the pulses and if necessary, a direction sensing capability. This circuit is shown in Fig.8.3.1(a).

The circuit accepts two identical signals (lines A and B) phase shifted by 90^{o} via dil switch S1 RS-337526 and converts them into two outputs UP or DOWN depending on whether the shaft is rotating clockwise or anti-clockwise. The first pair of inverters (U1) convert high data to low while a combination of the 270Ωresistors and the 0.01μF capacitors form low pass filters which absorb ripples from the signals. The second pair of inverters reconvert the low data signals to high (1's). At this juncture, the signals are differentiated for direction sensing.

Fig.8.3.1(b) shows two signals phase shifted 90^{o}. The location of the peaks, troughs, falling and rising edges of signal A relative to B are used to detect the direction of rotation of the motor shaft. Detection of these peaks, troughs, falling and rising edges are accomplished by means of inverters or monostables or both (U1 & U2). Resultant signal C indicates clockwise rotation of the shaft if it is read from left to right and anti-clockwise if read from the opposite direction. For clockwise rotation, the signal is read as:
$A\uparrow.\overline{B} + A.B\uparrow + A\downarrow.B + B\downarrow.\overline{A}$ and for anticlockwise rotation, it is read as $\overline{A}.B\uparrow + A\uparrow.B + A.B\downarrow + A\downarrow.\overline{B}$ in that order.

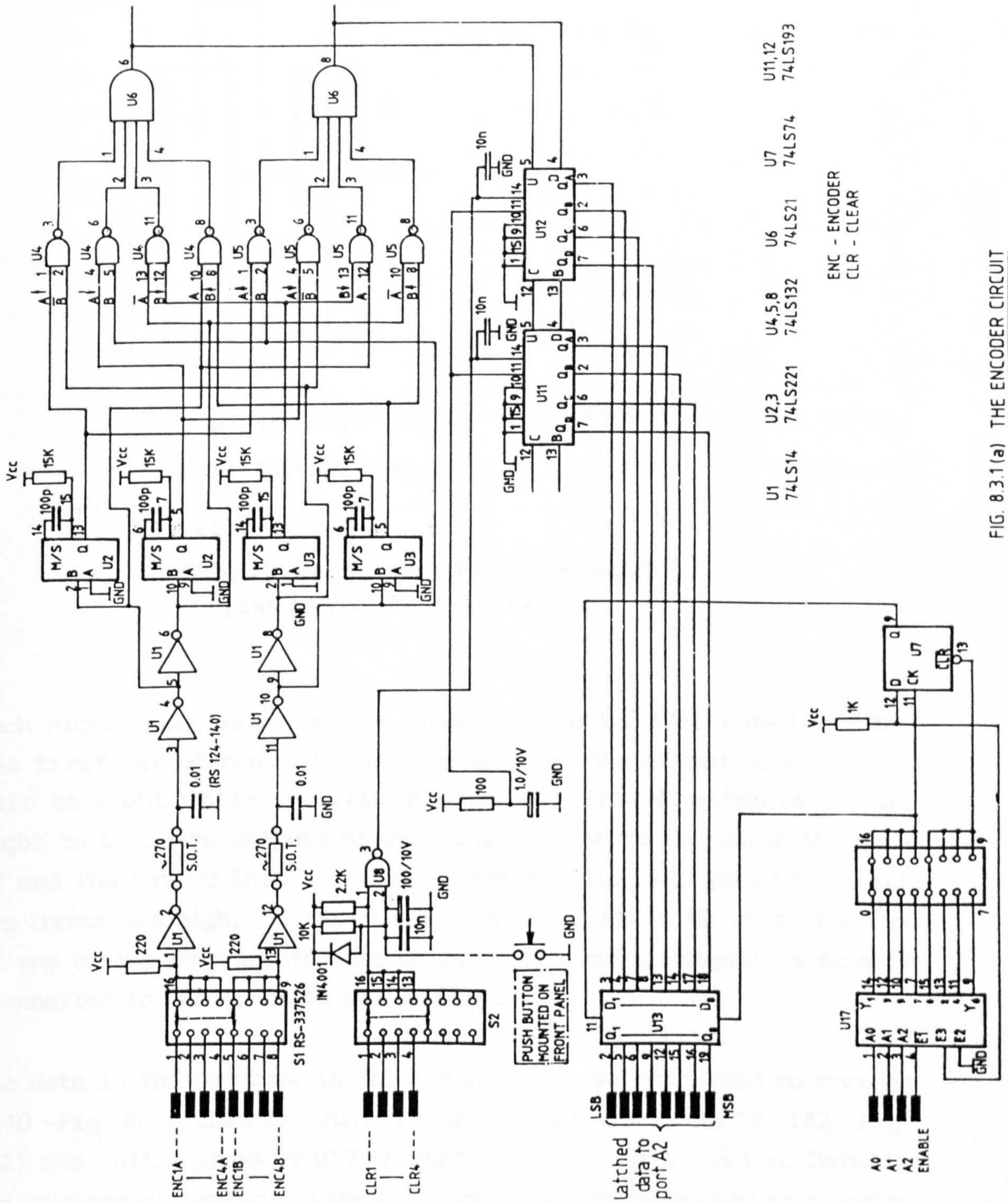

FIG. 8.3.1(a) THE ENCODER CIRCUIT

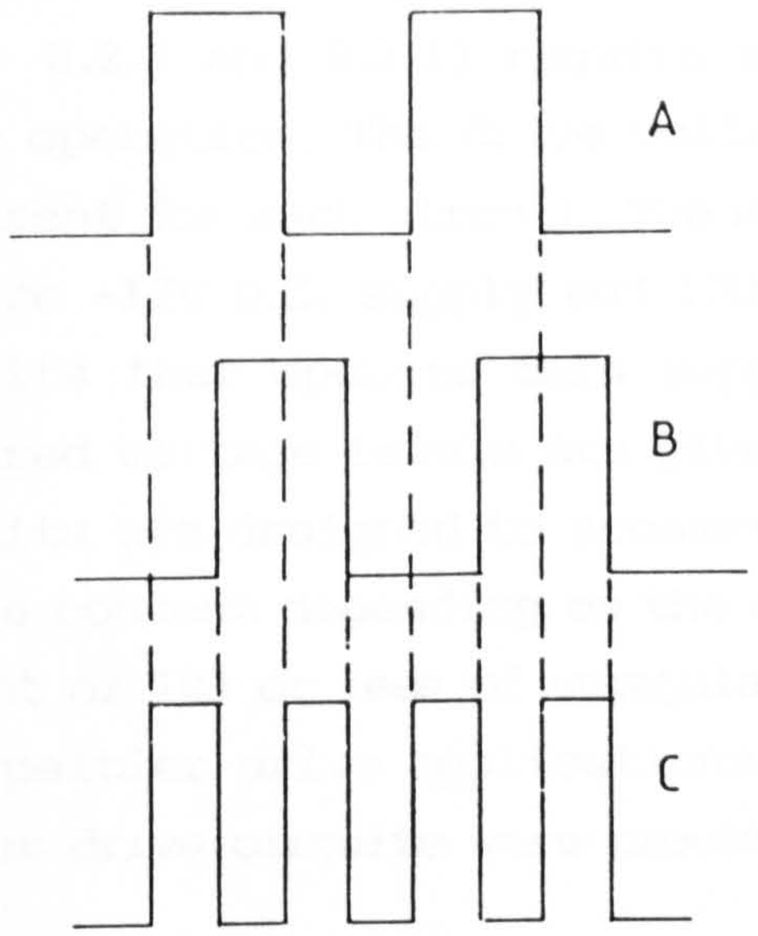

Fig, 8,3,1(b)

$A\uparrow\bar{B} + A\cdot B\downarrow + A\downarrow\cdot B + \bar{A}\cdot B\downarrow + \cdots\cdots\longrightarrow$ CLOCKWISE (CW)

$\longleftarrow\cdots\cdots + A\downarrow\cdot\bar{B} + A\cdot B\uparrow + A\uparrow\cdot B + \bar{A}\cdot B\uparrow$

COUNTER
CLOCKWISE (CCW)

ENCODER SIGNALS (A&B 90° OUT OF PHASE)
-A MEANS OF DIRECTION SENSING·

Each signal pair above is then channelled to the NAND gate U4 or U5. The first set of four (U4) NAND gates read the output signal from left to right while the remaining four (U5) NAND gates read from right to left. The outputs of U4 are channelled to the first AND gate U6 and the latter into a similar corresponding AND gate U6. If all the inputs are high, a high pulsed data is output by U6 otherwise low if any of the four inputs into U6 is 0. This output signal is finally channelled to the counters U11 and U12.

The data in the counters is latched into U13 and then read to port A2 (140 -Fig. 8.2). This latching is controlled from port C2 (142 -Fig. 8.2) and multiplexed by U17 to control the three circuits. Details for the use of control lines to latch data are discussed in chapter 9.

8.4 The Power Supply Unit

All the various component control circuits already discussed (8.2.1, 8.2.4, 8.2.5 and 8.3.1) require a separate D.C. power supply for their operation. The drive voltage and current signal levels are different for each circuit. The motor drive circiuts, for example, require +12V D.C. supply and 100 mA to drive the motor. The logic circuits that operate this supply requires +5V D.C. supply. The required voltage levels are given in the respective circuits. The circuits are designed to accommodate a certain minimum level of ripple content depending on the application. For example, a ripple content of 10% or less of unregulated D.C. supply is satisfactory for most peltier drive applications. Specifications for detector and peltier drive circuits were provided by STC.

Rectification of the mains supply is the most economical method of providing D.C. power. This is a means of obtaining D.C. signal (below 240V through a step down transformer) from the mains A.C. supply via a special diode circuit. Although the required voltage levels as well as the ripple contents of the component circuits are different, the principle of rectification is the same. A description of one power supply circuit shown in Fig.8.4 is therefore sufficient.

The diode circuit arrangement shown in Fig.8.4 producing +5 V D.C and -5 V D.C respectively is called a full wave rectification bridge circuit. Details of full wave and half wave rectification are discussed by Millman and Halkias [9]. The D.C. output voltage depends mainly on the A.C output voltage of the step down transformer. The 5V D.C output obtained can be explained by the relation:

$$Vdc = \frac{2Vm}{\pi} - IdcRf \text{ given in [9]}$$

where Vdc = 5V, Vm = 12V, Idc = D.C (load) current flowing in the circuit and Rf = load resistor. Assuming Rf = 0, Vdc = 7.6 volts. Thus, since there is capacitative load and obviously Idc flowing, Vdc must be less than 7.6 V. Based upon this relationship, different voltage levels can be obtained depending on the transformer output.

A ripple voltage is defined [9] as the deviation of the load voltage

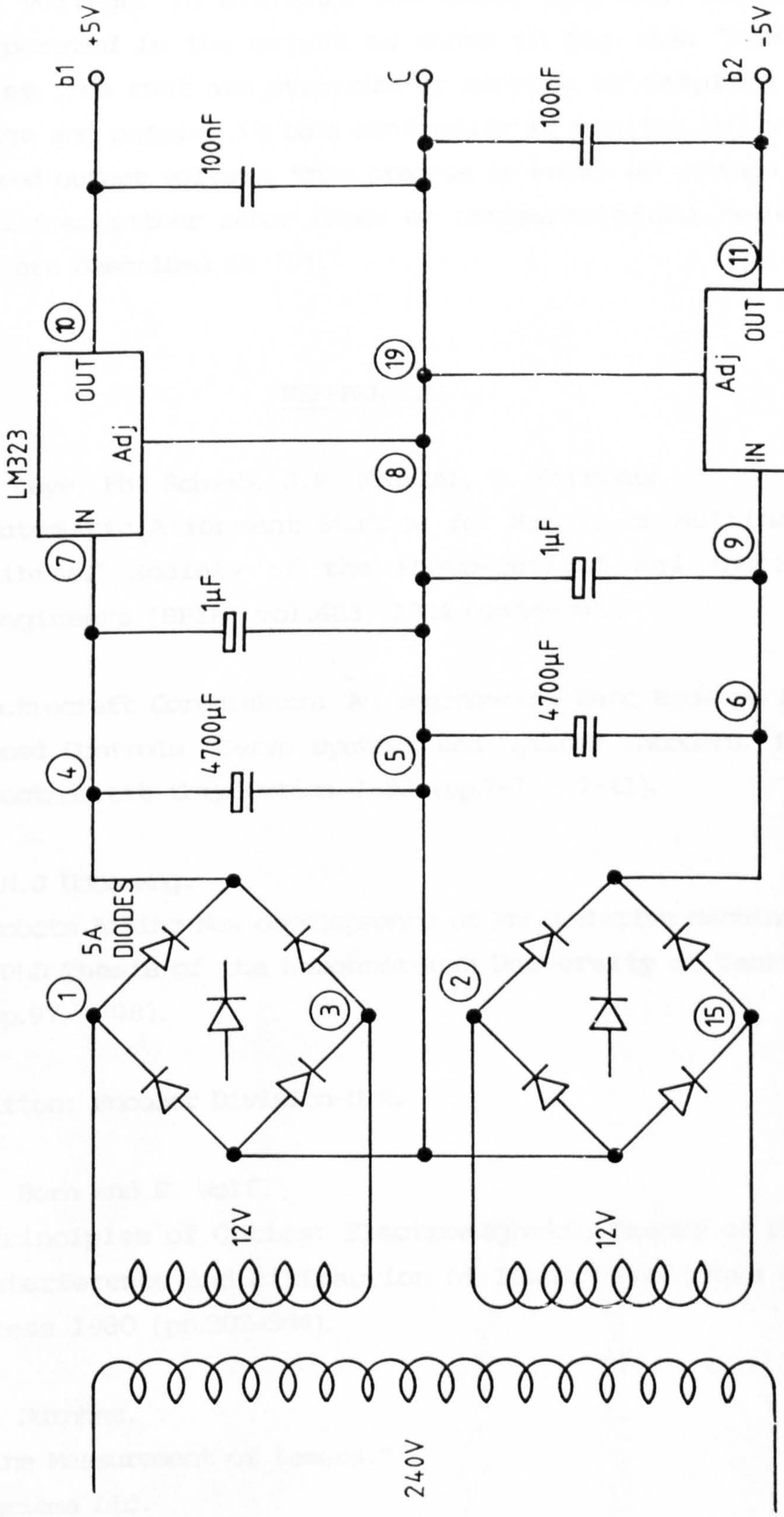

FIG.8.4 ±5V POWER SUPPLY (BRIDGE RECTIFIER) CIRCUIT LM323, LM345, ARE VOLTAGE REGULATORS

from its average or D.C value. This occurs because the output voltage of a rectified circuit is not constant and depends on the waveform (full or half wave rectification), variation of load current and the input voltage. To overcome the first problem, filters must be incorporated in the output as shown in Fig. 8.4. This minimises ripples. The rest are overcome by sensing or sampling the output voltage and passing it to a controller to monitor and maintain the required output voltage. This process is known as voltage regulation. It utilises either zener diode or series/switching methods both of which are described in [9].

REFERENCES.

1. T. Edye, Ph. Schwab, J.P. Roussel, O. Parriaux.
   "Automatic Alignment Station for Single or Multimode Optical fibres." Society of the Photo-optical and Instrumentation Engineers (SPIE) vol.483, 1984 (pp.65-69).

2. Electrocraft Corporation: An Engineering Hand Book on D.C Motors, Speed Controls, Servo systems and Optical Encoders. Published by Electrocraft Corporation 1980 (pp.7-1 - 7-11).

3. N.H.J Udoakang.
   "Robots Aiding New developments of Manipulative Machinery."
   A PhD Thesis of the Loughborough University of Technology 1983 (pp.97 - 98).

4. Litton: Encoder Division-U.K.

5. M. Born and E. Wolf.
   "Principles of Optics: Electromagnetic Theory of Propagation, Interference and Diffraction of light." Published by Pergamon Press 1980 (pp.302-304).

6. D. Burnham.
   "The Measurement of Lasers."
   Auriema Ltd.
   Personal Communication 1984.

7. Provisional Data on Continuous Wave Lasers (CW - 1300 nm Single Mode Fibres)." Personal Communication with STC 1985.

8. B.C. Kuo.
"Digital Control Systems."
Holt-Saunders 1980 (pp.33-40).

9. J. Millman and C.C. Halkias.
"Integrated Electronics." McGraw-Hill 1972 (pp.103-109).

CHAPTER 9

SOFTWARE DEVELOPMENT

CHAPTER OVERVIEW

This chapter examines the development of software based on a hill climbing technique to control the motion of a three degree of freedom manipulator for purposes of aligning a laser diode with a monomode fibre. Due to pre-alignment difficulties discussed in section 9.4, this arrangement was substituted by the fibre-fibre alignment. The alignment principle and therefore the program developed for the latter arrangement is equally applicable to the former because the laser beam emanating from the fibre is approximately Gaussian as stated in section 2.2.1. The objective is not only to automate the alignment process but also to try and achieve it in about three minutes as specified in section 2.5.

The reasons for using a three degree of freedom manipulator for this alignment are outlined in section 9.1 followed by the discussion of the hill climbing technique in section 9.2. The different aspects of the software design are presented in section 9.3. The alignment results and the associated experimental test procedure are presented in section 9.4. Finally, conclusions pertaining to the alignment objectives are then outlined in section 9.5.

9.0 Introduction.

Alignment of a monomode fibre with a laser beam or fibre with another fibre needs to be done quickly and accurately. Such a process can be achieved by automation. Automation helps to improve both the speed and quality of the alignment and consequently save on the time spent during the alignment process and wastage of components due to manual alignment inconsistency (2.4). Based on the desired alignment specifications outlined in section 2.5, the results of the search reported in Chapter 4 revealed that there were very few companies capable of supplying satisfactory positioning systems to solve this problem. This was the position in 1984 when the Department first initiated this research.

Methods that have already been tested (2.3) include the butt-joint, selfoc lens, hemipherical and cylindrical lens. Their major deficiencies are either due to low coupling efficiencies or difficulties in handling the different component parts during the coupling process or both. In the last two years, a few positioning systems have sprung up. Andrews et al [1], for example, produced an automatic fibre splicer capable of application in the field. Its optimisation procedure is said [1] to utilise a hill climbing method called the 'simplex' technique. Not much is known about this system but the 'simplex' method is said* to be incapable of finding the global maximum. This means that the system assumes that there is only one peak to arrive at which is not true in the case of laser beams having spikes. Centronic [2] has quite recently (summer 1986) produced an automatic alignment system called the Polytrope 1000. It is claimed [2] to be driven by a high resolution mechanical positioner and that it resolves 0.1 μm with a capability of aligning two discrete components with automatic signal optimisation. It is also said [2] to handle a wide wavelength range of 800-1800 nm and that it completes the laser/fibre alignment in under one minute. Apart from its current price of £26,000.0 excluding VAT, details of the system capability are still unknown. The same company also produces a piezoelectric fully manual alignment system which incorporates a TV monitor and costs £4,000.0 excluding VAT. Assuming that it conforms with the above specifications, the former is still considered expensive for this type of work and the latter, unsuitable because of its totally manual features.

Edye et al [3] also describes an alignment closed loop system but not much is known about its practicality. Others like Newport's PM500 [4] said to be accurate to 0.1 μm resolution and completely microprocessor controllable capabble of driving up to 5 axes and Walmore's AS-85M [5] manufactured by Cabloptic are some of the latest to come into the market. Very little is still known of them in terms of capability and price. The same applies to positioning systems produced by Photon Control [6].

There is no doubt that these systems are being built but until they flood the market and satisfy demand, highly accurate systems built for easy programming are likely to remain expensive. Above all, there

---

* T H Davies, Dept of Mechanical Engineering, LUT - personal communication

is no guarantee that they will be suited to the current STC (or other company) product designs.

9.1 Reasons for selecting a 3-degree of freedom manipulator.

Ideally, an automatic laser/fibre coupling device requires five axes of movement if the alignment is to be carried out successfully. That is, three linear displacements along X, Y and Z-axes and two angular rotations about the X and Y-axes respectively when both the fibre and laser diode emitting face are set along the Z-axis as shown in Fig. 9.1. Analysis of the optimum configuration of these axes (e.g. mounting the fibre on three linear axes and the laser on two rotary axes etc.) is not considered in this work.

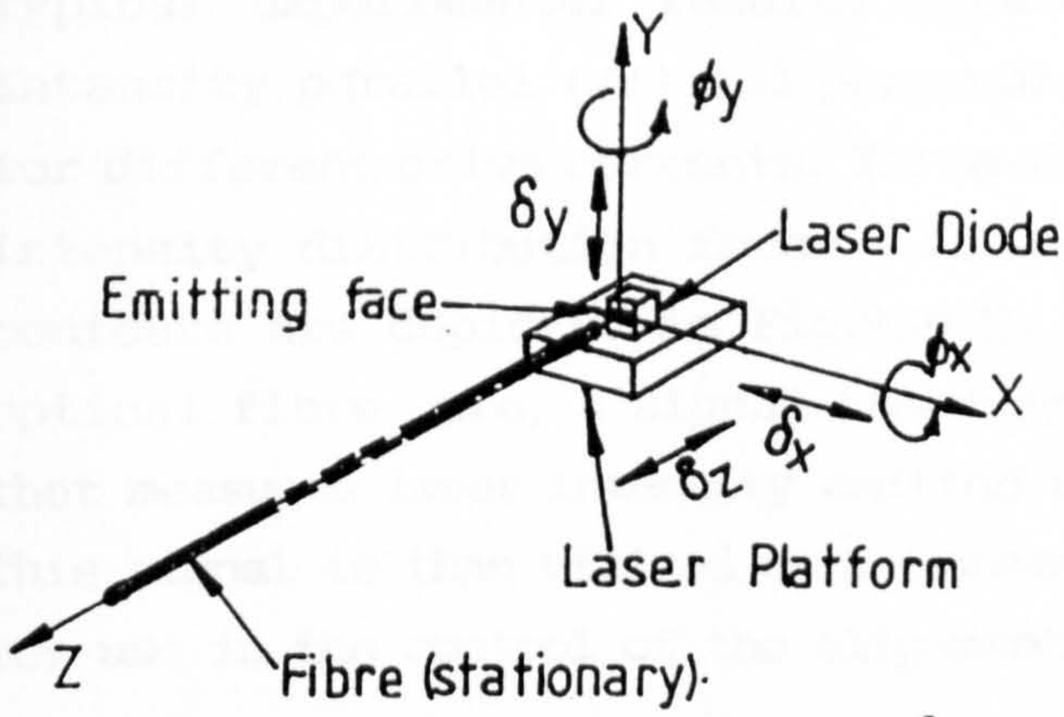

Fig.9.1 LASER/FIBRE ALIGNMENT SHOWING 5 d·o·f MOTION OF LASER.

d·o·f = Degree of Freedom.

ϕ_x = Angular rotation about X-axis.

ϕ_y = Angular rotation about Y-axis.

δ_x = Linear Laser Displacement along X-axis.

δ_y = Linear Laser Displacement along Y-axis.

δ_z = Linear Laser Displacement along Z-axis.

LEDs in general produce light with larger divergence angles than lasers (2.1.3). Contrary to this, the results surveyed in section 7.0 reveal that an angular shift of the fibre axis with respect to the LED surface of about 10^{o} produces a loss increase of only about 0.25dB. Since laser beams have smaller divergence angles than light produced by LEDs, it can be safely deduced that angular misalignment has even less significant effect on laser/fibre coupling efficiency. In addition, the cost price of each actuator (linear or rotary) can

vary from as low as £400.00 (Oriel Encoder Mikes -price in 1984) to nearly £800.00 (Oriel Stepper Mikes -price in 1984) or more. This suggests that a 3-degree of freedom manipulator is not only adequate for such an alignment but it is also much cheaper than a 5-degree of freedom manipulator (7.4.4). These were the major reasons for selecting this type of manipulator for alignment tests carried out in this Chapter. However, since a 5-degree of freedom manipulator is a viable possibility, a flow chart predicting an alignment control method for both manipulators is given in section 9.3.

9.2 The Approach to the Maximum (Hill Climbing).

The laser beam intensity emitted by the semiconductor laser diode is very closely Gaussian in shape (2.2.2). Figs.9.2(a) and (b) show typical experimental results obtained by STC depicting laser intensity parallel (//) and perpendicular ($\perp$) to the junction plane for different drive currents. Three-dimensionally, the laser beam intensity distribution forms a hill as shown in Fig.9.2(c) whose contours are depicted in Fig.9.2(d). To align the beam with the optical fibre core, a signal (feedback) is obtained from a sensor that measures laser intensity emitted from the far end of the fibre. This signal is then utlised as a measure of the accuracy of alignment for use in the control of the alignment actuators.

The problem is that of the transverse alignment of an optical waveguide to be excited with a light source (Fig. 9.2(c)) that can be the output of a laser diode or another fibre . The optical components to be aligned are not in contact. The approach used to get to the top of the hill assumes that at least some light is initially launched into the fibre and that all or part of the guided power can be measured. That is, since the two components are not in contact, the fibre position in the gripper in relation to the laser diode (8.2.8) must ensure that the initial laser power is non-zero. Mechanical contact between the components could result in the destruction of the laser diode emitting face and the microlens inserted into the fibre face. This type of approach would not interfere with the alignment mechanics to be described but would certainly damage the components themselves.

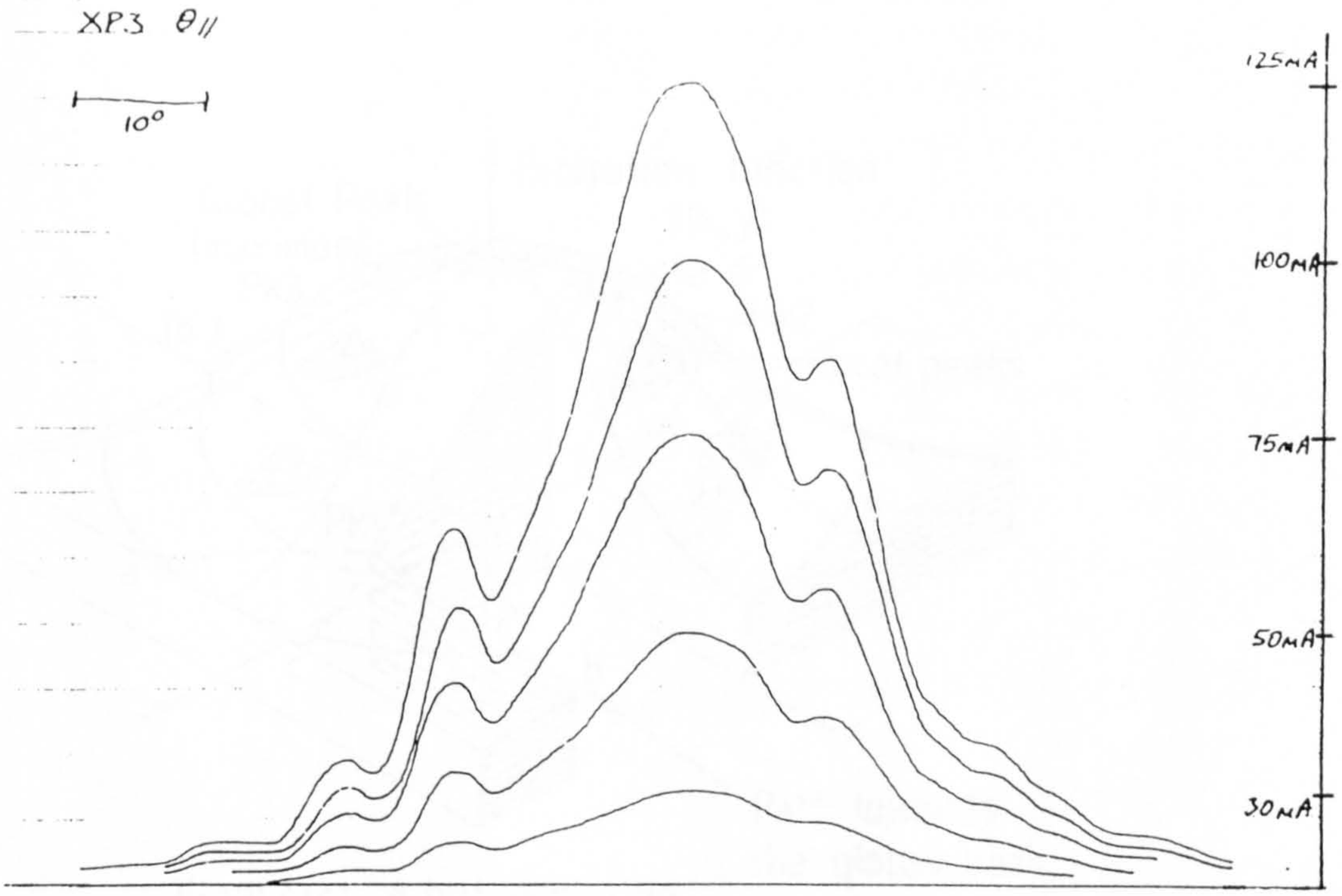

(a) Parallel to junction plane.

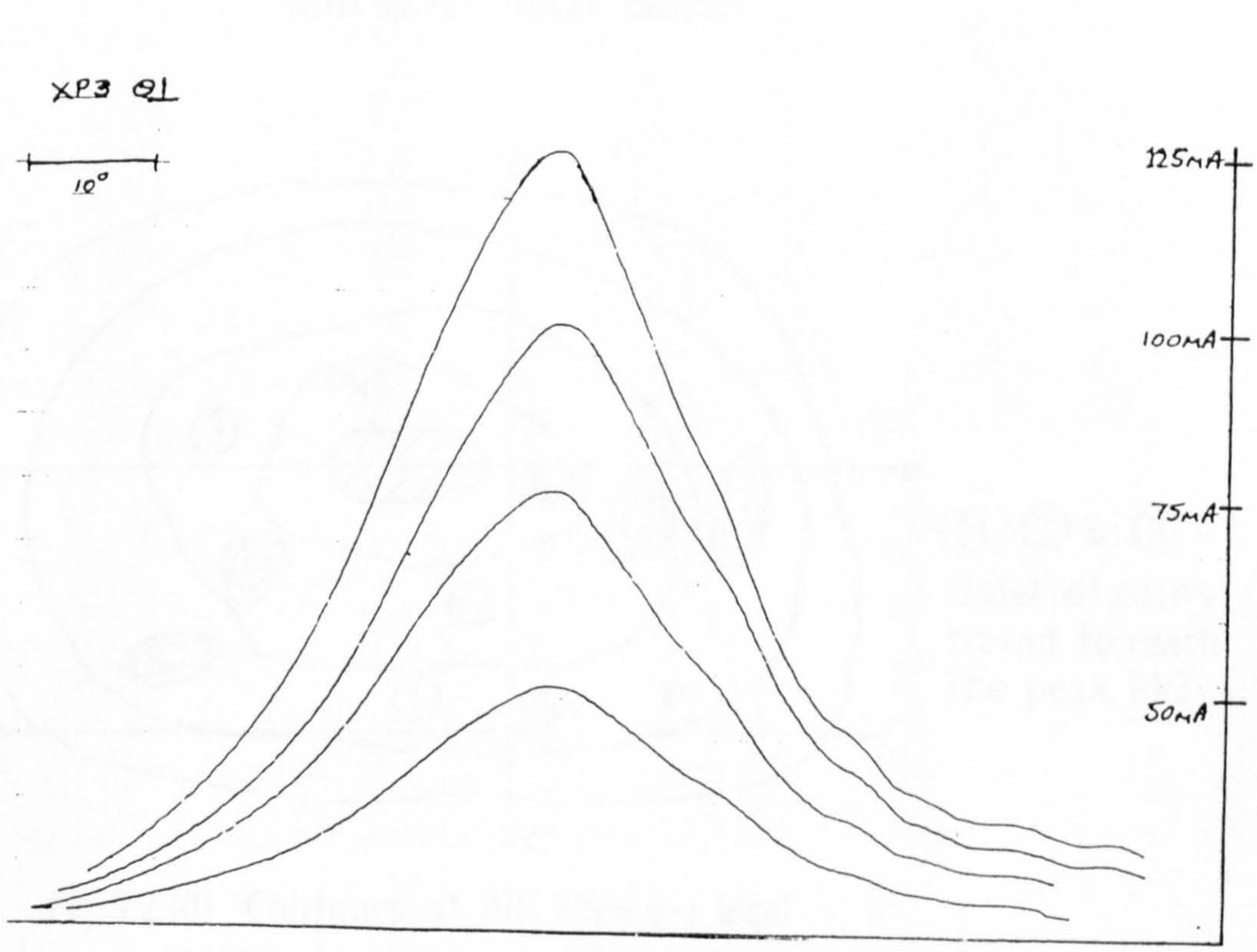

(b) Perpendicular to junction.

Figs, 9, 2 (a) and (b) SHOW TYPICAL LASER POWER DISTRIBUTION FOR DIFFERENT DRIVE CURRENTS (OBTAINED BY STC).

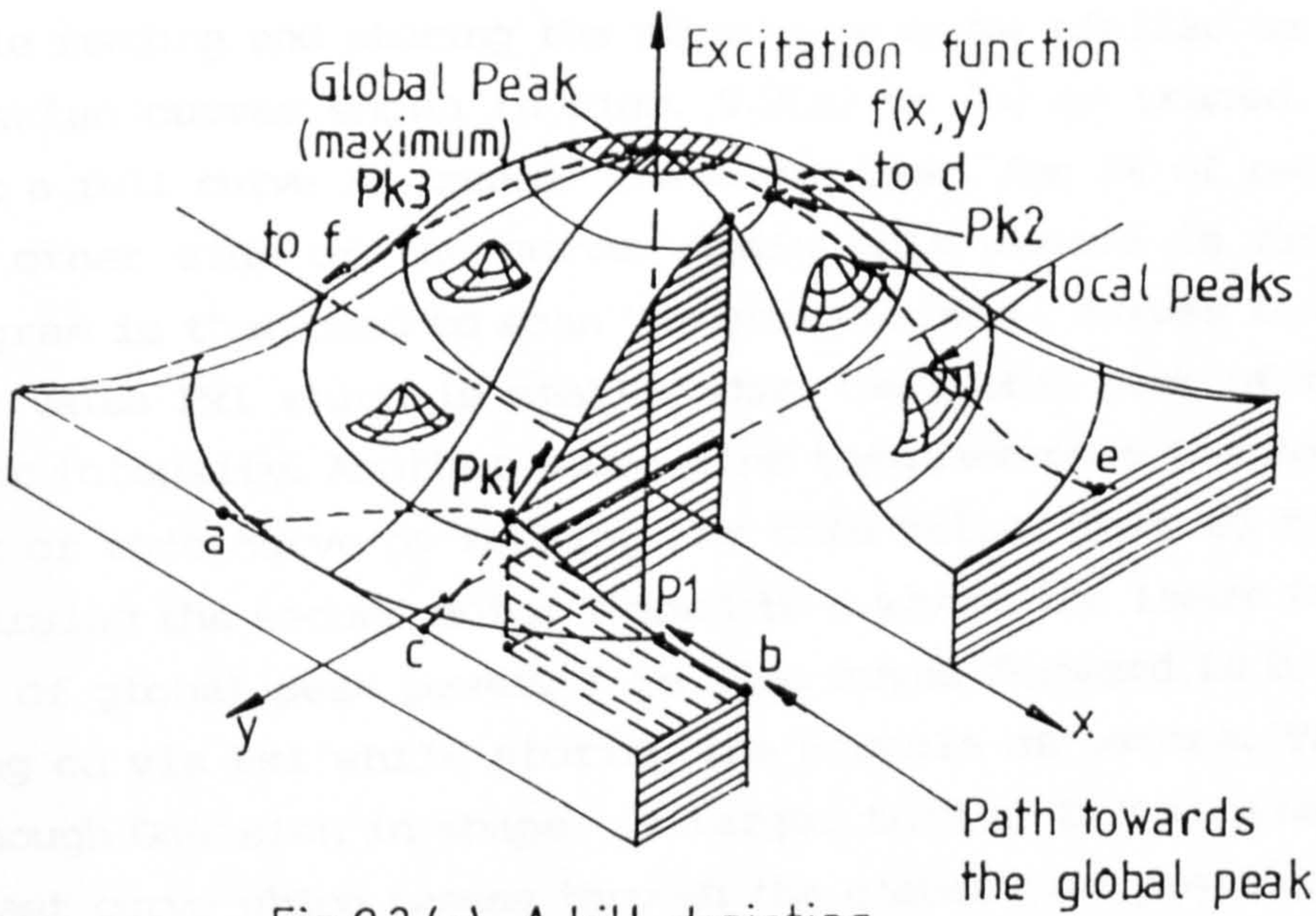

Fig,9,2 (c) A hill depicting typical laser distribution with spikes (local peaks).

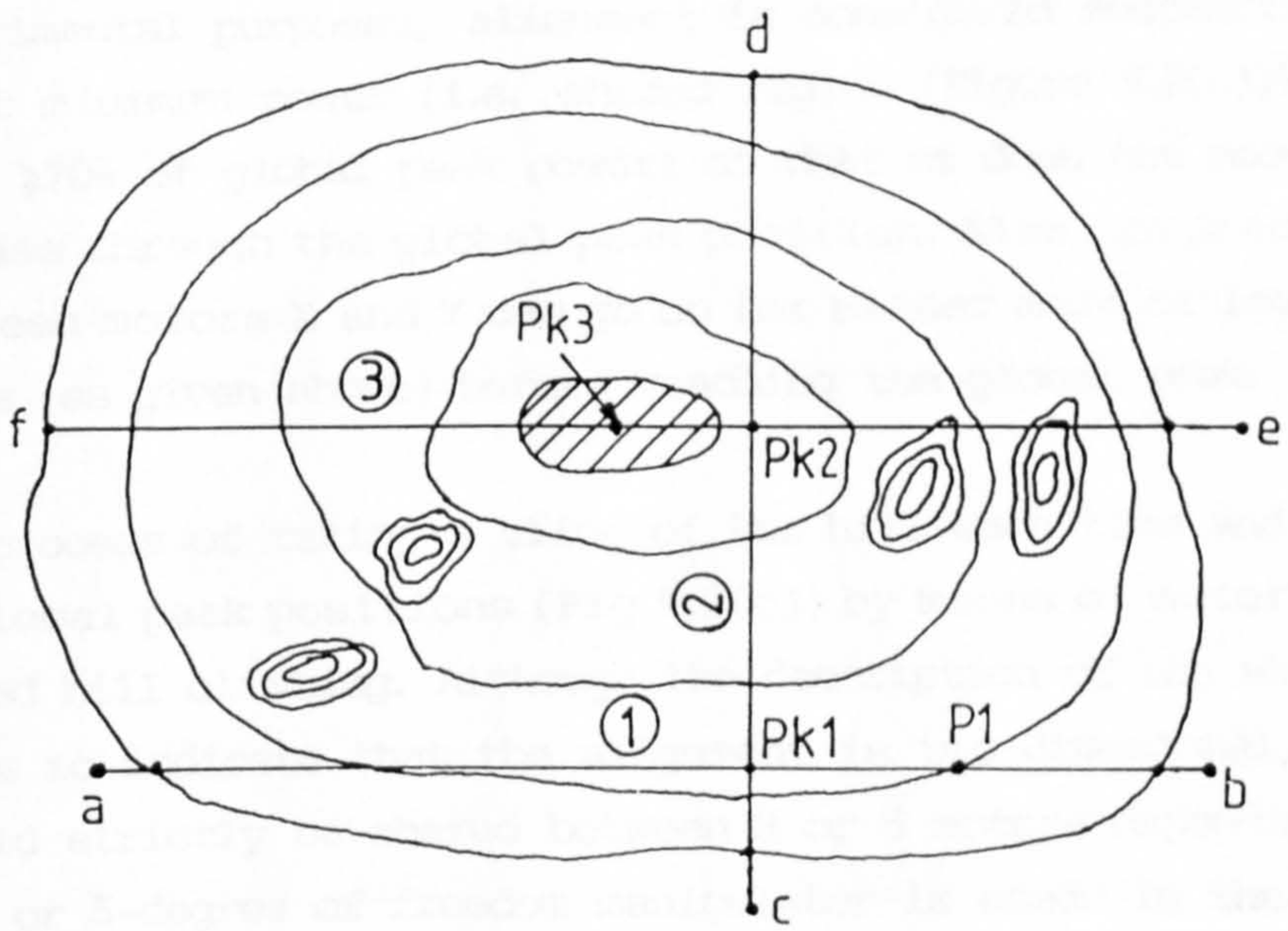

①, ② & ③ = Order of paths traced to reach the peak Pk3.

Fig, 9,2 (d) Contours of hill showing local peaks and the path to the maximum.

In this approach, the move to the maximum (Fig.9.2(c)) is based on a hill climbing technique. That is, some laser light (≥3.5% of peak power in this case) is first picked up at some position P1 (Fig.9.2(d)). The choice of 3.5% being completely arbitrary. By moving motor X one step (0.1 μm) at a time parallel to the X-axis (line ab) while reading and storing the signals, a curve similar to one of the Gaussian curves shown in Figs. 9.2(a) or (b) is traced. To ensure that a full curve is traced, the motor looks for 2% of peak power on the other side of the curve. Again this choice is arbitrary. A program is then used to scan the stored signal values to obtain the peak value Pk1 which is smaller than the global peak of the overall laser intensity. Another subroutine then reverses the motor to the peak of this curve by looking for this value. This is followed by reversing the second motor Y down to c where the laser intensity < 3.5% of global peak power. Y is then moved forward in 0.1 μm steps along cd via Pk1 while storing the signals as before. This curve, although Gaussian in shape, is larger than ab but smaller than the largest curve which passes through the global peak position. Its peak Pk2 is again located and motor Y reversed to it in the same manner as X. Finally, by changing to motor X and repeating the same procedure as before, the largest curve ef is traced with its peak position at Pk3 which is also the global peak. Curve ef is also Gaussian. For experimental purposes, alignment is considered successful as long as a set minimum power (i.e. shaded region (Figure 9.2(c))) is achieved (e.g. ≥70% of global peak power) so that ef does not necessarily have to pass through the global peak position. Also, in practice, a swop between motors X and Y can go on for either more or less than three times (as given above) before reaching the global peak.

The process of taking a slice of the hill each time and homing on to the local peak positions (Fig.9.2(c)) by means of motor movement is called hill climbing. Although the description of the above procedure seems to indicate that the alignment is two-dimesional, change over should strictly be shared between 3 or 5 motors depending on whether a 3- or 5-degree of freedom manipulator is used. In the case of a 3-degree of freedom manipulator, motor Z which is responsible for alignment in the fibre axis (Figure 9.1) is first moved and set in a suitable position within a range of ,say, 40 to 100 μm from the laser diode face before X-Y alignment commences. This stops the fibre from

hitting and possibly destroying the laser diode face. That is, the position of the fibre in relation to the semiconductor laser diode along the Z-axis determines whether or not the above procedure achieves the desired peak power (Fig.7(b)) and therefore making it a 3-dimesional problem.

9.3 Software Design

In this section and the accompanying subsections, the software developed for the control of a 3-degree of freedom manipulator (Oriel Encoder Mike manipulator (4.4.3)) is described. In such an application, the computer is working in real time or on line controlling both the electrical and mechanical hardware via the control circuit described in Chapter 8.

Writing and optimising the software can take a long time. At this stage, not only is it necessary to have a thorough understanding of the language used but also the handling of input/output data and the general working of the computer. The Digital Research CP/M Operating Manual [7], L.A. Leventhal [8] and similar books on the Assembly Language Programming cover this area sufficiently well.

Details of the software design for this alignment is directly linked to the hill climbing technique described in section 9.2. The control programme for the 3-degree of freedom manipulator is wholly written in the 8080/8085 Assembly Language Programming. A general purpose flow chart summarising the control of both a 3- and 5-degree of freedom manipulator is given in section 9.3.4.

9.3.1 Encoder Counts.

As outlined in section 8.2.2, the Encoder Mike has a pair of light emitting diodes (LEDs) and phototransistor detectors used with a shutter to generate quadrature signals in synchronisation with motor operation. The shutter has 10 equally spaced openings (one every 36^{o}) that provide 10 quadrature cycles (signals) per motor revolution (8.2.2). That is, one complete revolution is equivalent to 1μm of linear motion so that each signal represents 0.1 μm of linear displacement (Figures 8.2.2(a) and (b)). Unfortunately, the encoders

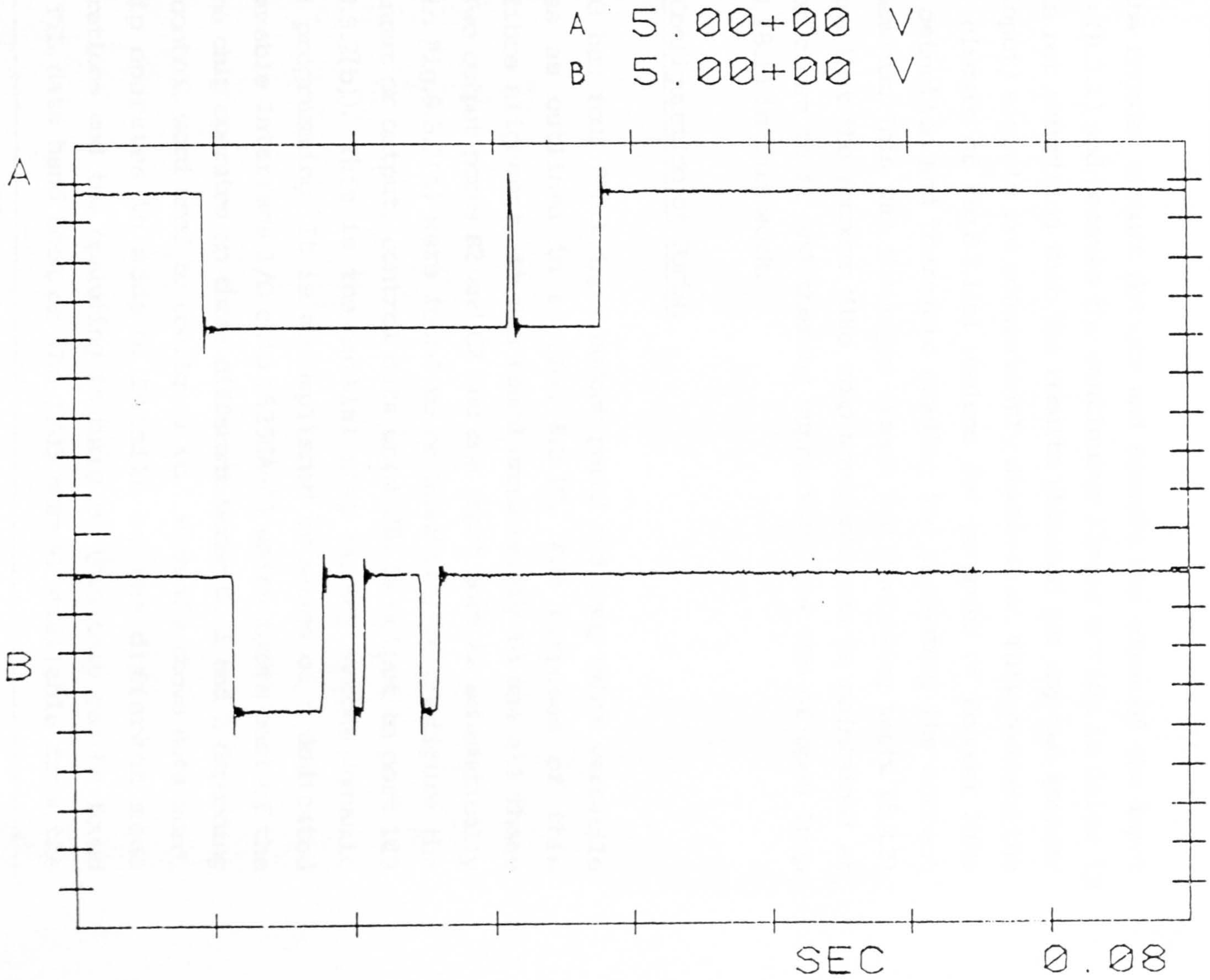

Fig,9,3,1

SIGNALS A, B AT THE OUT-PUT GATES U6 OF FIG,8,3,1(a) (PRODUCED BY PASSING SIGNALS OF FIG, 8,2,2 (b) THROUGH THE CIRCUIT OF FIG, 8,3,1(a)).

produce signals of unequal widths for any continuous linear motion below 3 μm[23†]. Oriel estimates this stabilising point to be in the range of 3 to 5 μm and recommends that Encoder Mikes should be tested individually in order to establish these points. Thus, an attempt to channel the signals (Fig. 8.2.2(a)) to the Encoder circuit (Fig. 8.3.1(a)) and tapping it from the output points of the two AND gates U6 of the Encoder circuit produced many results similar to those given in Fig.9.3.1. These are in complete contrast to those shown in Fig.8.3.1(b) which represent the standard output gate signals obtained when quadrature signals of equal widths are channelled into the Encoder circuit.

Since the Encoder circuit detects and records the edges of the input signals (8.3.1) and because the continuous linear motion is below 1μ m, it is not surprising that the results obtained for any two Encoder Mike (input) signals are consistently dissimilar. This renders the Encoder circuit of Fig.8.3.1(a) useless for purposes of Encoder Mike signal detection and therefore reading and recording its correct displacements. This was the major reason for conducting tests (8.2.3) to ensure that the Encoder Mike step movements can be maintained at 0.1μm or close to it and thereby supporting the use of open loop control (8.1) in this work.

9.3.2 Configuration of Ports.

The I/O3 has four 8-bit input/output ports and many other versatile features as outlined in section 8.2.10. For purposes of this laser/fibre alignment, it was found unnecessary to use all these ports. Two output ports B2 and C2 and one input port A2 schematically shown in Fig.9.3.2(a) were found to be adequate. To configure the ports input or output, control data word 90H is output to port 143 (Fig. 9.3.2(b)). This is the initial step in any system dynamic control programming. It is accomplished by means of a dedicated Programmable Interface I/O chip (8255A-5) which forms part of the I/O3. The chip operates in three different modes 0, 1 and 2 depending on the control word used to configure it. With the above data word, the chip operates in mode 0. Details of the different mode configurations and the operating features of this chip can be found in the TTL data hand book or the I/O3 manual available from the

---

23†. See reference 23, Chapter 4.

Transam system Manufacturers.

x	ENCz	ENCy	ENCx	Mz (S/ST3)	My (S/ST2)	Mx (S/ST1)	F/R
7	6	5	4	3	2	1	0

PORT B2
(141)-OUTPUT

x= 1 or 0

x	x	x	x	SELECT C(A_2)	SELECT B(A_1)	SELECT A(A_0)	INPUT ENABLE G
7	6	5	4	3	2	1	0

x = 1 or 0

PORT C2
(142)-OUTPUT

7	6	5	4	3	2	1	0

PORT A2
(140)-INPUT

ALL INPUT POSITIONS (TO BE PEAKED FOR ENCODER DATA)

MOTORS (Mx, My, Mz)
ENCODERS (ENCx, ENCy, ENCz)
ENCODER DATA LATCH SELECTS (A, B, C or A_0, A_1, A_2)
FORWARD/REVERSE CONTROL LINE (F/R)
ON/OFF MOTOR CONTROL LINES (S/STn): n = 1, 2, 3.

Fig.9.3.2 (a) PORTS A, B & C SHOWING WIRING OF MOTORS AND ENCODERS OR THE ENCODER DATA LATCH SELECTS.

After port configuration, any of the three motors Mx, My and Mz can be selected and moved forward or reversed. For example, to move Mx forward, a 1 is sent to bit 0 and 0's to the rest of the bits of port B2(Fig.9.3.2(a)). This data (01H) selects direction (forward), deselects all the motors and resets all the encoders (ENCx ,ENCy and ENCz). Secondly, a 1 is sent to bits 0, 1, 4, 5 and 6 of the same port. This data (73H) selects motor Mx and drives it forward keeping all the encoder positions high. The motor is then stopped by sending 71H to port B2 (i.e a 0 to bit position 1). The time lapse between 73H and 71H determines the motor drive pulse width and subsequently, the distance traversed by the motor. Mx is reversed by sending 72H to port B2 (i.e a 0 to bit 0). A similar procedure applies to the movement of My and Mz. It is, however, possible to move all three

PORT 143 SHOWING MODE DEFINITION AND
CONFIGURATION OF PORTS A, B & C.

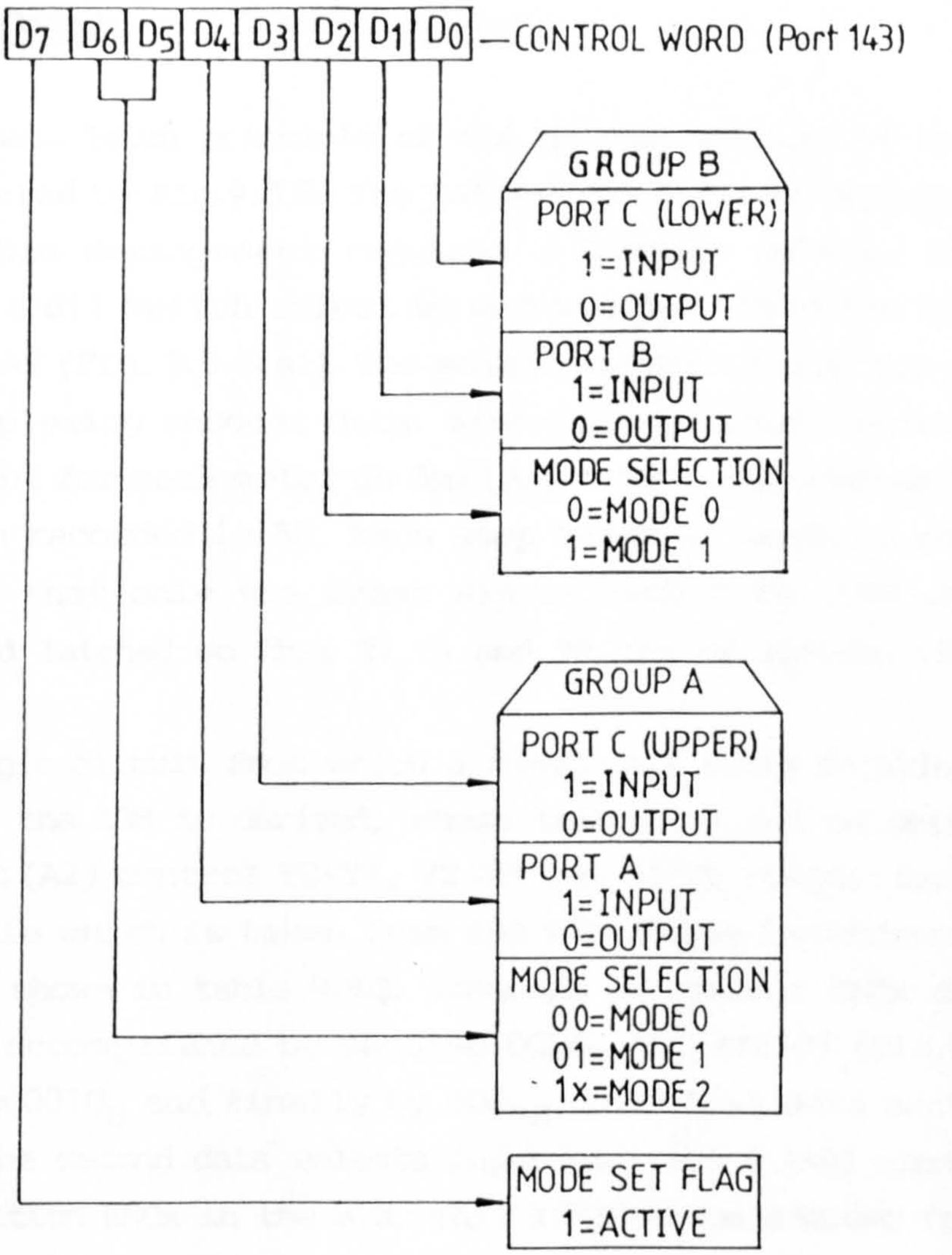

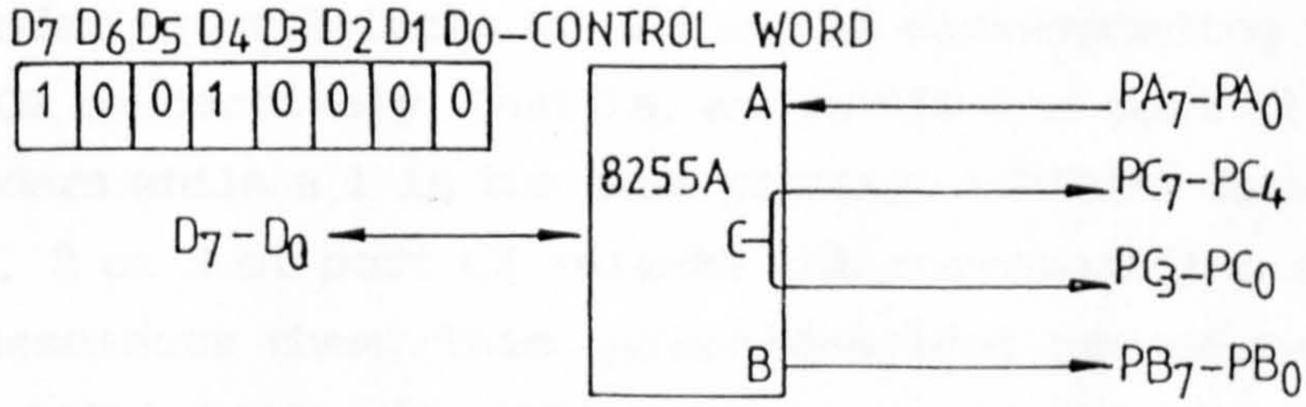

Fig, 9, 3, 2 (b)

motors at the same time by sending 1's to bits 1, 2 and 3 (i.e 7FH or 7EH to port B2) but this makes it extremely difficult to control the manipulator motion. This is why each motor must be selected and controlled individually (9.3.4). The control circuitry featuring each motor drive has been discussed (8.2.1).

9.3.3 The Control and Latching of Data.

The basic data latch principle of the encoder circuit of Fig.8.3.1(a) is illustrated by Fig.9.3.3. The latter is the lower portion of Fig. 8.3.1(a). This arrangement requires a decoder select, an enable select and a dil switch select to enroute data from the 373 to the input port A2 (Fig. 9.3.2(a)). The enable select is used for purposes of demultiplexing encoder data. Since the maximum overall linear displacement for each motor is 5μm (2.5), the total number of steps that can be recorded is 50. Each step being 0.1μm (8.2.2 and 8.2.3). This means that only the least significant byte (LSB data) are recorded and latched so that Y1,Y3 and Y5 can be ignored (Fig.9.3.3).

A simple logic circuit from which a functional table relating to the working of the 138 is derived, shows that the input selects A (A0), B (A1) and C (A2) control Y0-Y1, Y2-Y3 and Y4-Y5 respectively. Part of this table which is taken from the TTL (Texas Instruments) data Handbook is shown in table 9.3.3. Latching of encoder ENCx data into the 373 is accomplished by sending 0000_B to port C2 (Fig.9.3.2(a)) followed by 0010_B and finally by 0001_B. The first data enables the 138 while the second data selects input position A (A0) connected to encoder position ENCx in the 373. This latches the encoder (position) data to the 373. The last data select disables the 138 and deselects all the encoder input selects A0, A1 and A3 corresponding to ENCx, ENCy and ENCz respectively. That is, a 0 in bit 0 of port C2 enables all the encoders while a 1 in the same position inhibits data flow. A 1 in bits 1, 2 or 3 of port C2 selects the corresponding encoders while a 0 deselects them. This select/deselect procedure simply latches the LSB ignoring the MSB. A similar procedure is followed when latching ENCy and ENCz data. Since the most significant byte (MSB) is ignored, only three different sets of selections corresponding to the three encoders are made.

TABLE 9.3.3.

FUNCTIONAL TABLE RELATING TO THE WORKING OF CHIP 138.

CONTROL WORD (A0-A2 + ENABLE)				INPUT SELECTION
Enable	A0	A1	A2	
0	0	0	0	Y0
0	0	0	1	Y1
0	0	1	0	Y2
0	0	1	1	Y3
0	1	0	0	Y4
0	1	0	1	Y5
0	1	1	0	Y6
0	1	1	1	Y7

The data latch mechanism is effected by means of a clock CK. Data is cleared by sending a signal through the clear line CLR on U7. Details of the various data latching and selection codes can be found in TTL (Texas Instruments) data Handbook.

Due to variation in encoder signal widths produced by the Oriel Encoder Mike motion (9.3.1), the encoder circuit of Fig. 8.3.1(a) is useless for purposes of closed loop control and subsequently for use in this work. However, should the circuit be modified to accomodate signals with unequal widths such as these, the data latch mechanism outlined above would still apply. That is, the discussion of the latch mechanism is primarily intended for a future alignment work featuring closed loop control which is more desirable when applied to

D.C motors than using the open loop type control (8.1) for the same type of motors. The latter is best for the control of stepper motors.

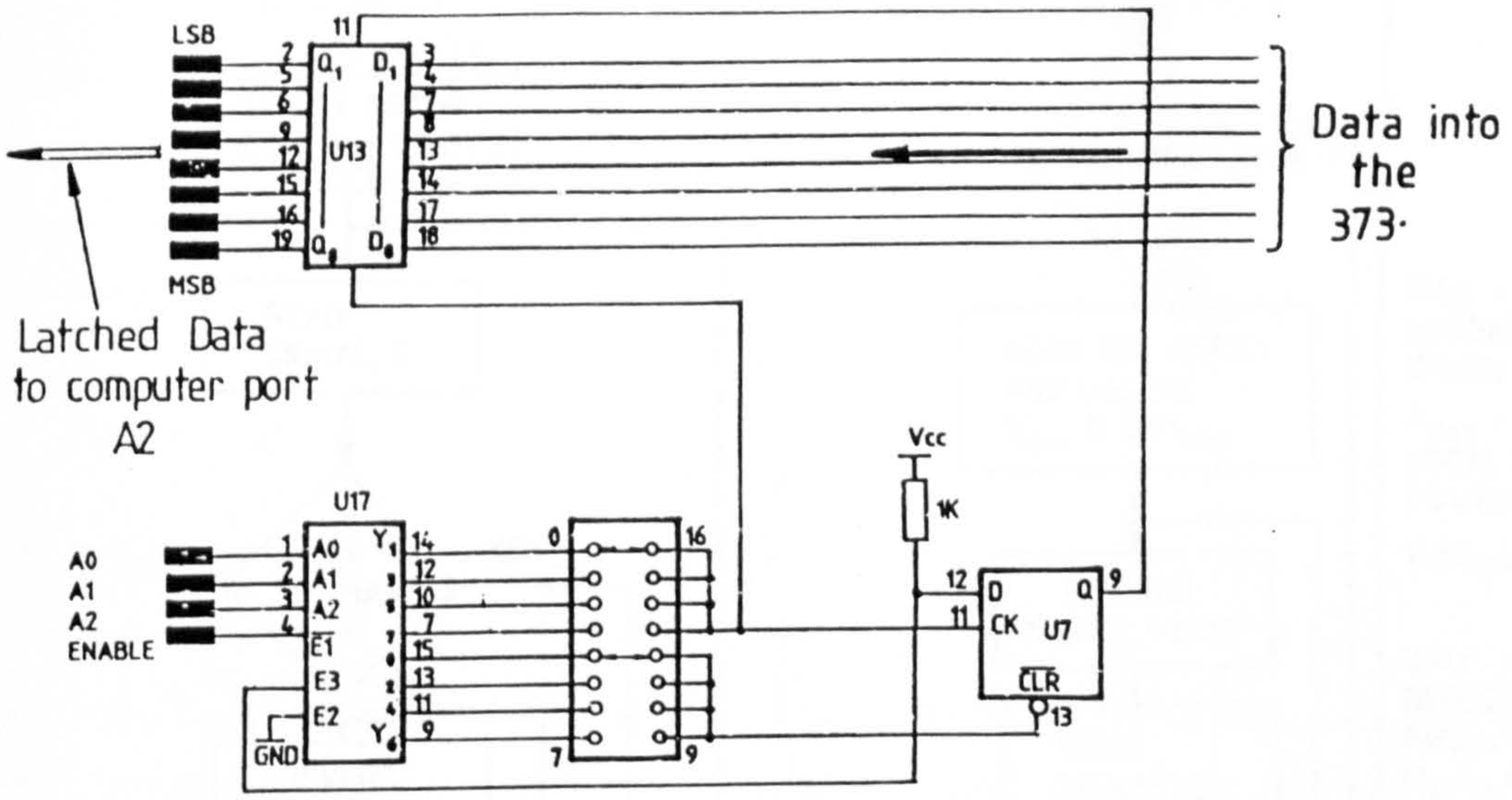

Fig,9,3,3 PART OF THE ENCODER CIRCUIT (Fig,8,3,1(a)) SHOWING DIL SWITCH SETTINGS, U13 & U17·

U13 74LS373 U17 74LS138 U7 74LS74

CK – CLOCK
$\overline{CLR}$ – CLEAR

9.3.4 The Programme.

The alignment programme outlined in Apppendix E is written in the 8080/8085 Assembly Language programming and tested on a 3-degree of freedom manipulator. The flow chart shown in Fig. 9.3.4 can be used for the control of both the 3- and 5-degree of freedom manipulators. The required motor is selected from the motor select box immediately after START.

The programme written for control of the 3-degree of freedom manipulator is based on the hill climbing technique described in section 9.2. Although motor z is not included in the programme, the alignment in the z-axis is arranged by manually moving the fibre

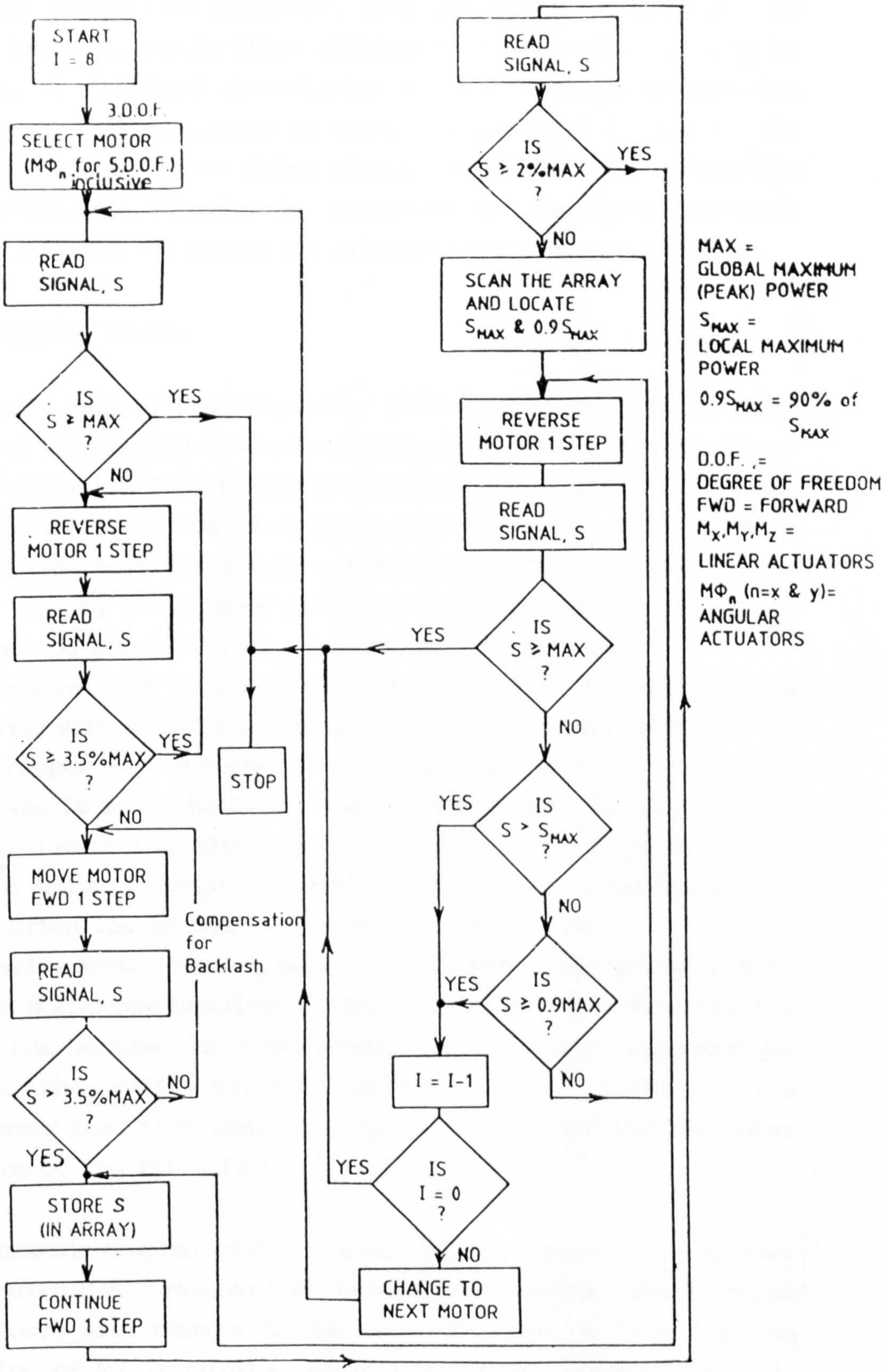

Fig,9,3,4 FLOW CHART FOR CONTROL OF 3- AND 5-D·O·F MANIPULATORS·

towards the laser source and fixing it in position inorder to maintain a constant gap between the two components (9.2). In the experimental fibre-fibre alignment, this gap can be as large as 3 mm while for laser/monomode fibre alignment it is as small as 40μm or less (2.5). A detailed description of the various stages and procedures in the programme is given in Appendix F. Due to the incapability of the motor drive circuitry (Fig. 8.2.1) to hold the motors when power is switched ON, a program that deselects and holds the motors is first run before the alignment programme commences.

9.4 Experimental Tests.

To carry out a laser/fibre alignment, a monomode fibre obtained from STC is first threaded into the laser box (plate 8.2.7) and a gripper (Fig.8.2.8(a)) manipulated manually using manipulator M2 is then lowered into the laser box in order to grip the fibre. This gripping process was unsuccessful because the brass strengthened fibre tip was physically bent by the gripper each time an attempt was made to grip it. This can be attributed to a number of reasons namely:

(a) the groove that holds the fibre was milled locally in the workshop with an old relatively imprecise milling machine;

(b) the gripper was sprayed with vycoat PVC coating inorder to insulate it from the laser box and the associated pins (8.2.8) to avoid shorting. This partially blocked the edges of the v-groove and an attempt to remove this material from the groove edges often led to flaking leaving a bare surface;

(c) the series manual (Ealing Beck) micrometers assembled to form M2 (plate 8.2.7) are unsuitable for positioning the fibre in the laser box because their tolerances are worse than 5 μm. And yet this is the ovality between the inner surface of the hole (in the laser box) into which the fibre is threaded and the outer surface of the fibre (2.5).

All these reasons coupled with the inaccuracy of mounting the gripper on to manipulator M2 (causing both angular and lateral misalignments of the v-groove with respect to the laser box) and the fact that the manipulation of M2 is purely manual, makes the laser-fibre pre-alignment exercise extremely difficult. In particular, it is difficult to estimate the gap between the fibre input end and the

NOTE: (See p.217, parag.1, line 6)

In optical fibre communication systems, fibre to fibre alignment is very important in the field [1]. This is because fibre defects usually occur along the communication lines and these can cause fibre breakage. Thus, inorder to bring the fibres back together again, fibre - fibre alignment must be used.

laser face to 40μm (2.5). Even if this was possible, if motor Z (Fig. 9.1) changed position once this exercise is completed, then the fibre input end could hit and possibly destroy the laser emitting face. Thus since the laser beam power distribution emanating from a fibre output end is very closely Gaussian (2.2.1), laser/fibre alignment is essentially the same as fibre-fibre alignment. For this reason and those outlined above, the alignment algorithm is tested for the alignment of two fibres (8 - 10 μm core diameter) obtained from STC.

Inorder to carry out the fibre-fibre alignment tests, a fully coupled laser/fibre package from STC producing over 95% of coupled laser power was mounted as shown in plate 9.4. The output end of the same fibre was then inserted into a tight fitting cylindrical hole drilled in a metal block B which is in turn mounted on top of the heat sink. A second fibre gripped in position by adjusting M2 then picks up (receives) the laser beam and channels it to the detector. The amount of laser launched into the receiving fibre depends on the extent to which the two fibres are misaligned.

When all the control units (Chapter 8) are connected up, the peltier drive is turned on and the laser is then fired. Proper laser handling and firing precautionary measures must be followed otherwise the laser could either be destroyed by overheating (8.2.5) or killed by static electricity (8.2.9). The gripped fibre which receives (picks up) the laser is then manually moved sideways (X-axis), up and down (Y-axis) (see Fig. 9.1) in order to locate the smallest possible laser power distribution curve from which to start the automatic alignment. This is done by adjusting M2 and observing the change in the detected power output which can be read directly in volts from a voltmeter connected to the detector output (8.2.4). The starting point on the curve must not be less than 3.5% of the peak power because the program is constructed to pick up an initial laser power at or above this value (9.2).

Once the small curve is established (the two fibres are misaligned), the program is run. The alignment results produced by running the program achieves over 90% of the peak power. This is well above the 70% specification given in section 2.5. This value (over 90%) was consistently obtained every time a deliberate misalignment between

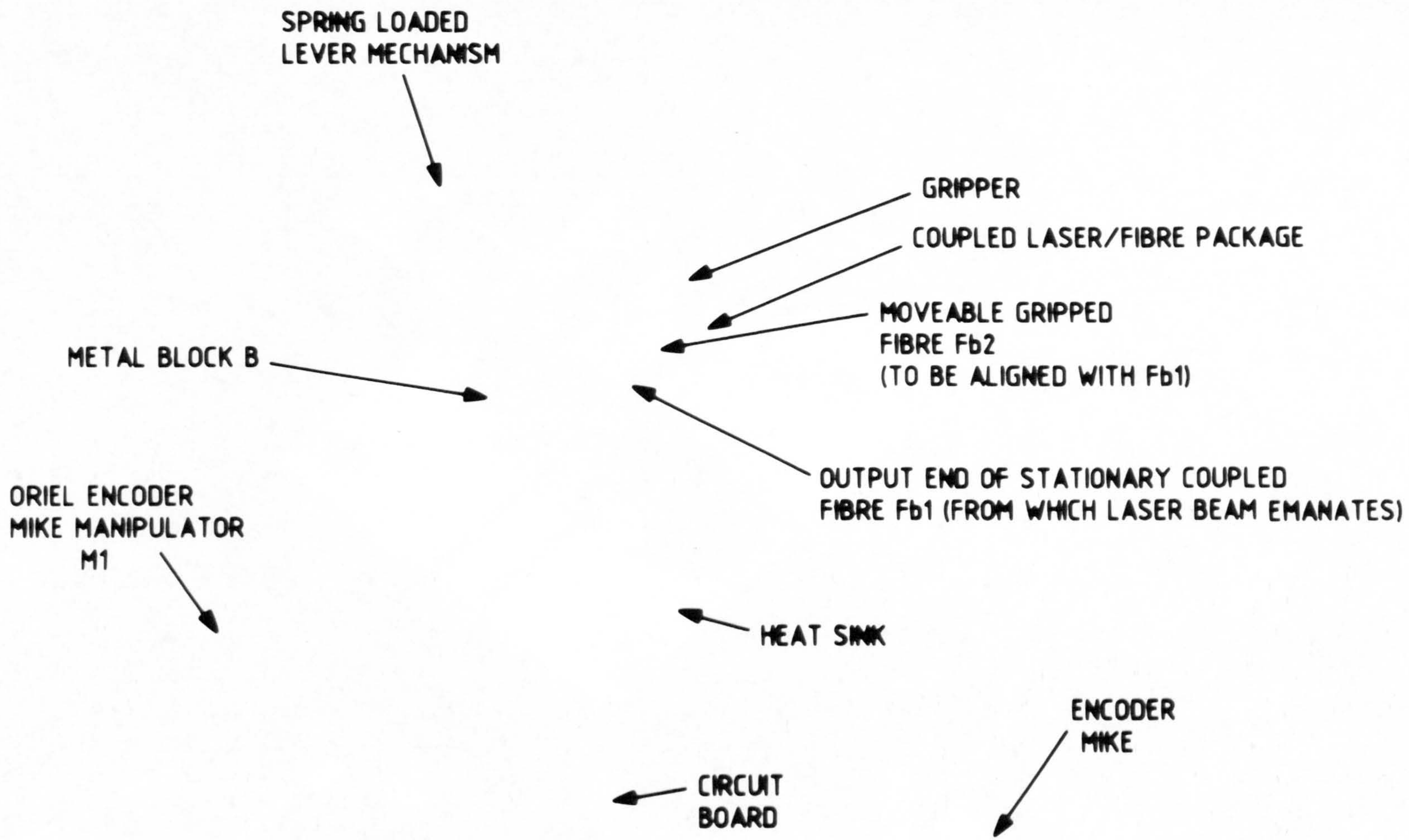

PLATE 9.4: FIBRE - FIBRE ALIGNMENT

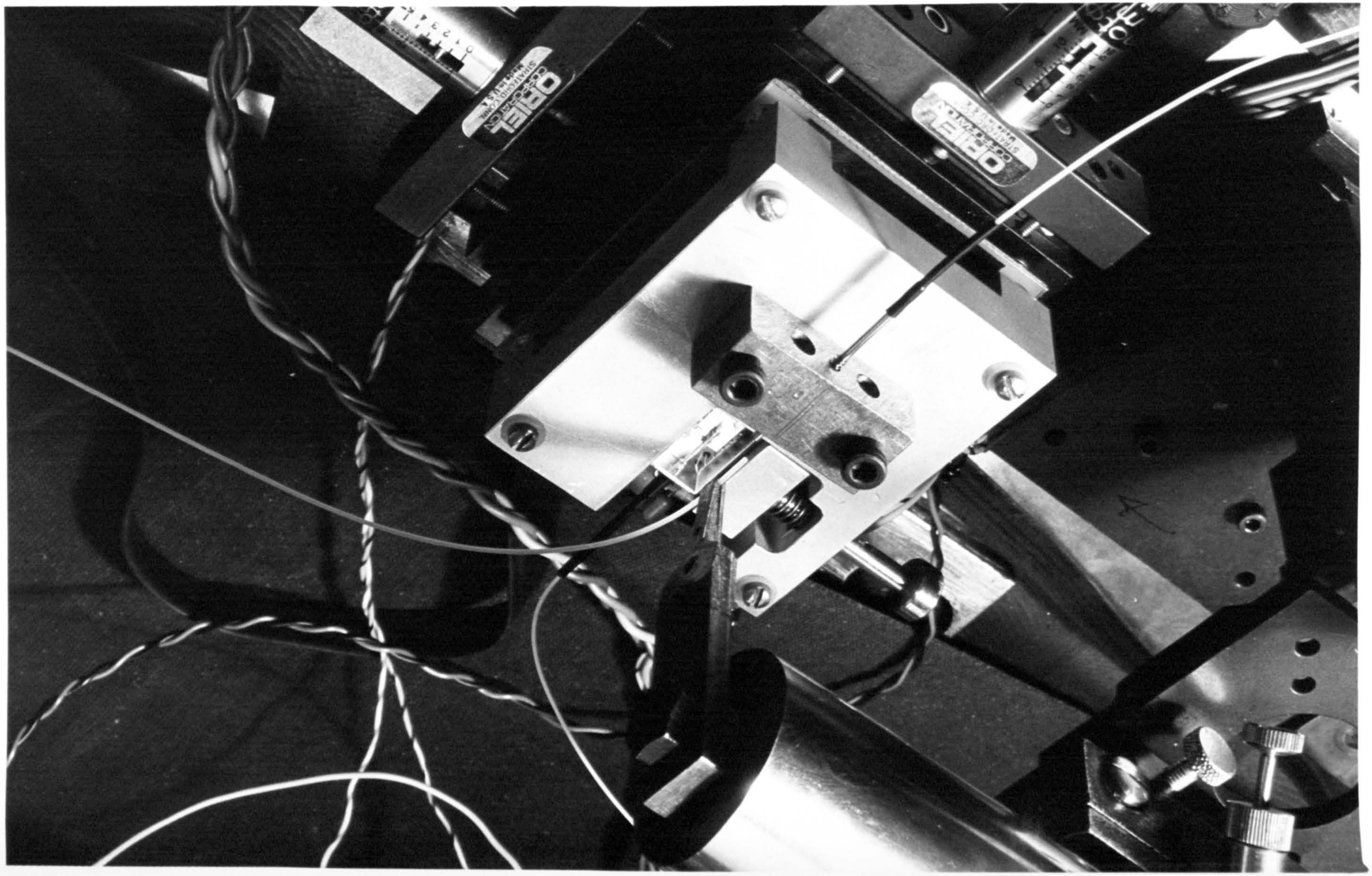
OPTICAL
OPTICAL

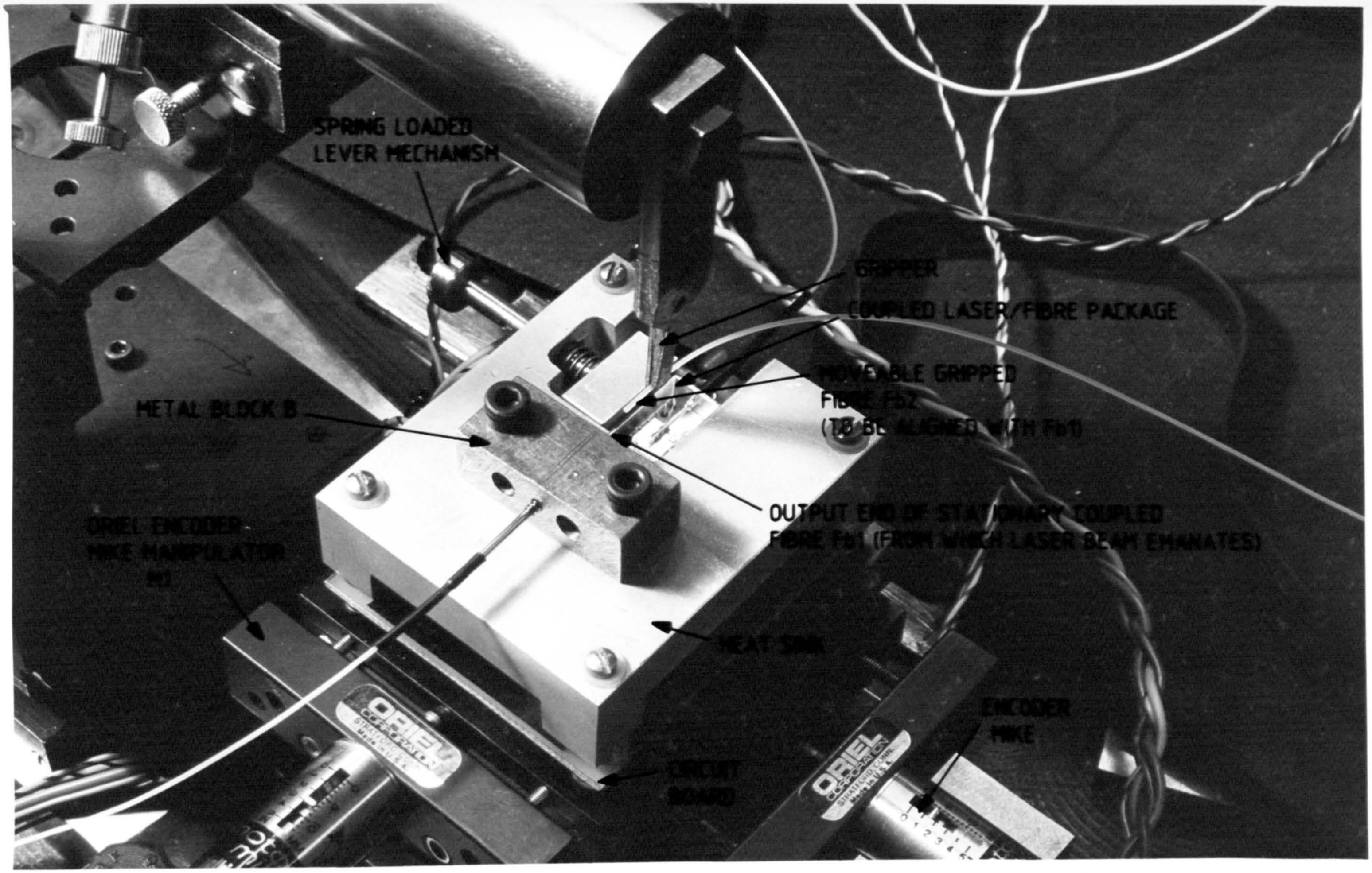

PLATE 9.4: FIBRE - FIBRE ALIGNMENT

the two fibres was made and the experiment repeated. Results of coupled laser power obtained by running the program with fibre-fibre axial gap distance of about 1 mm are presented in table 9.4. These results are then converted from hexadecimal to decimal by means of a conversion routine before plotting the curves. The intial small curve traced by motor Y is plotted in Fig.9.4(a) while the larger curve traced by motor X is plotted in Fig.9.4(b). By increasing the gap distance manually, it was found that the coupled laser power starts to drop very slightly (4.88 V to 4.87 V) when the fibre faces are 3 mm apart. With further increase, the power falls raipdly down to 50% at a gap distance of 4.5 mm. Figs.9.4(c) and (d) show similar curves at a gap distance of about 2.5 mm. The contrast between Figs.9.4(b) and (d) can be attributed to the nature of the beam emanating from the fibre[126] and the motor accuracy (8.1).

The fibre/fibre alignment process takes less than one minute. This is a successful result considering that the alignment specification time is 3 minutes and the minimum required coupled power is 70% (2.5). Since the dimensions of the laser diode, monomode fibre and the neck of the emitted laser beam are extremely small (Chapter 2), it is quite possible that laser/fibre alignment could even take less time.

9.5 Conclusions.

Due to the prealignment difficulties discussed above, the major objective of the thesis (laser-fibre alignment) has not been met. However, since fibre-fibre alignment is essentially the same as laser-fibre alignment, the principle of the alignment objective has been successfully demonstrated as shown above. The consistently large output power obtained from this alignment exercise could be due to the fact that the extremely tight ovality clearence of $\pm 2.5\ \mu m$ (2.5) is absent in fibre-fibre alignment. This power output is achieved in a considerably short time despite compounded inaccuracies such as the use of open loop type control to drive the D.C motors (Oriel Encoder Mikes), misalignment errors incurred by mounting the gripper onto M2 and the manual manipulation of M2.

---

126. See reference 12 of Chapter 2

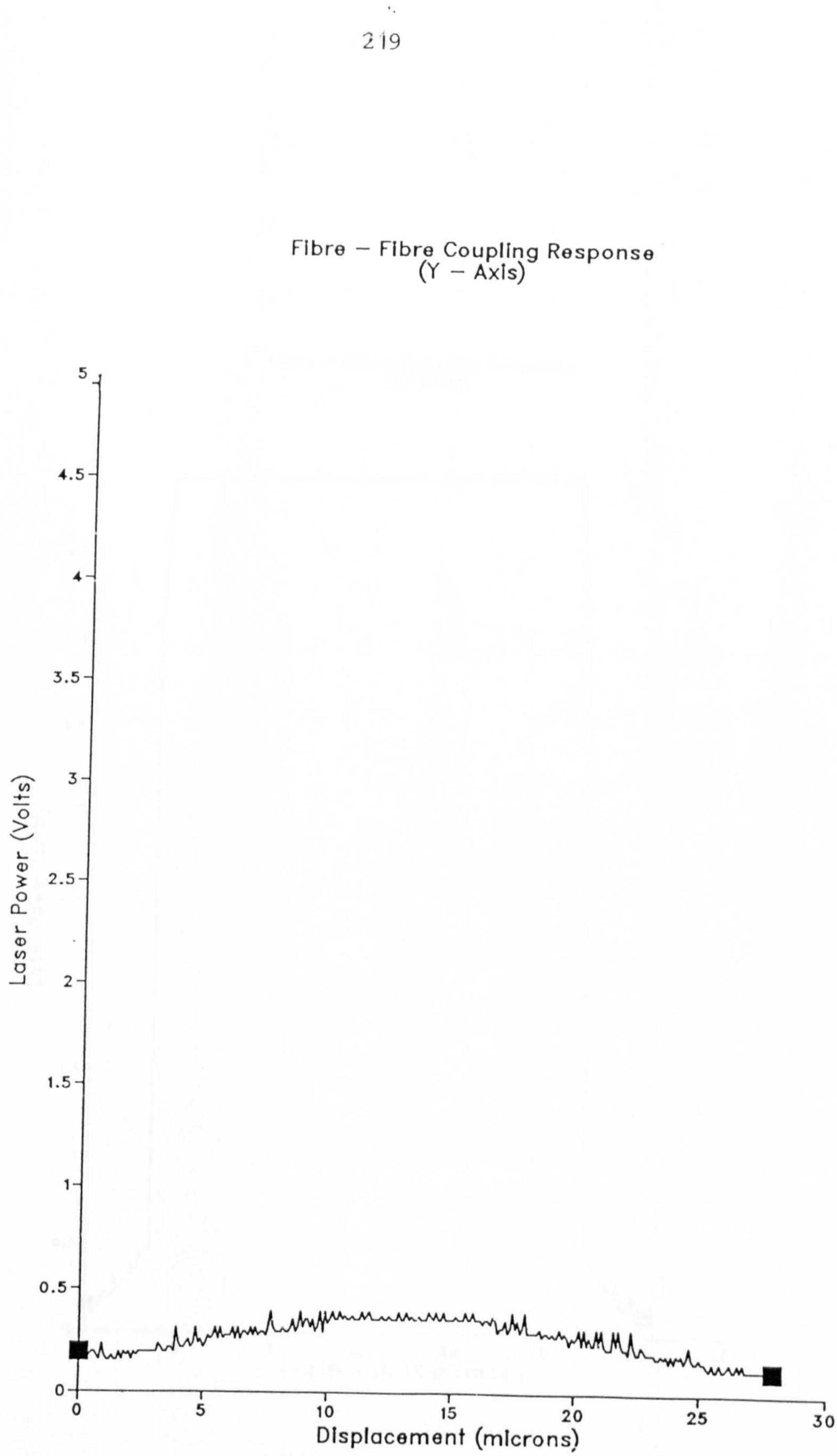
Fibre – Fibre Coupling Response
(Y – Axis)
Laser Power (Volts)
5
4.5
4
3.5
3
2.5
2
1.5
1
0.5
0
0
5
10
15
20
25
30
Displacement (microns)

Fig, 9,4 (a)

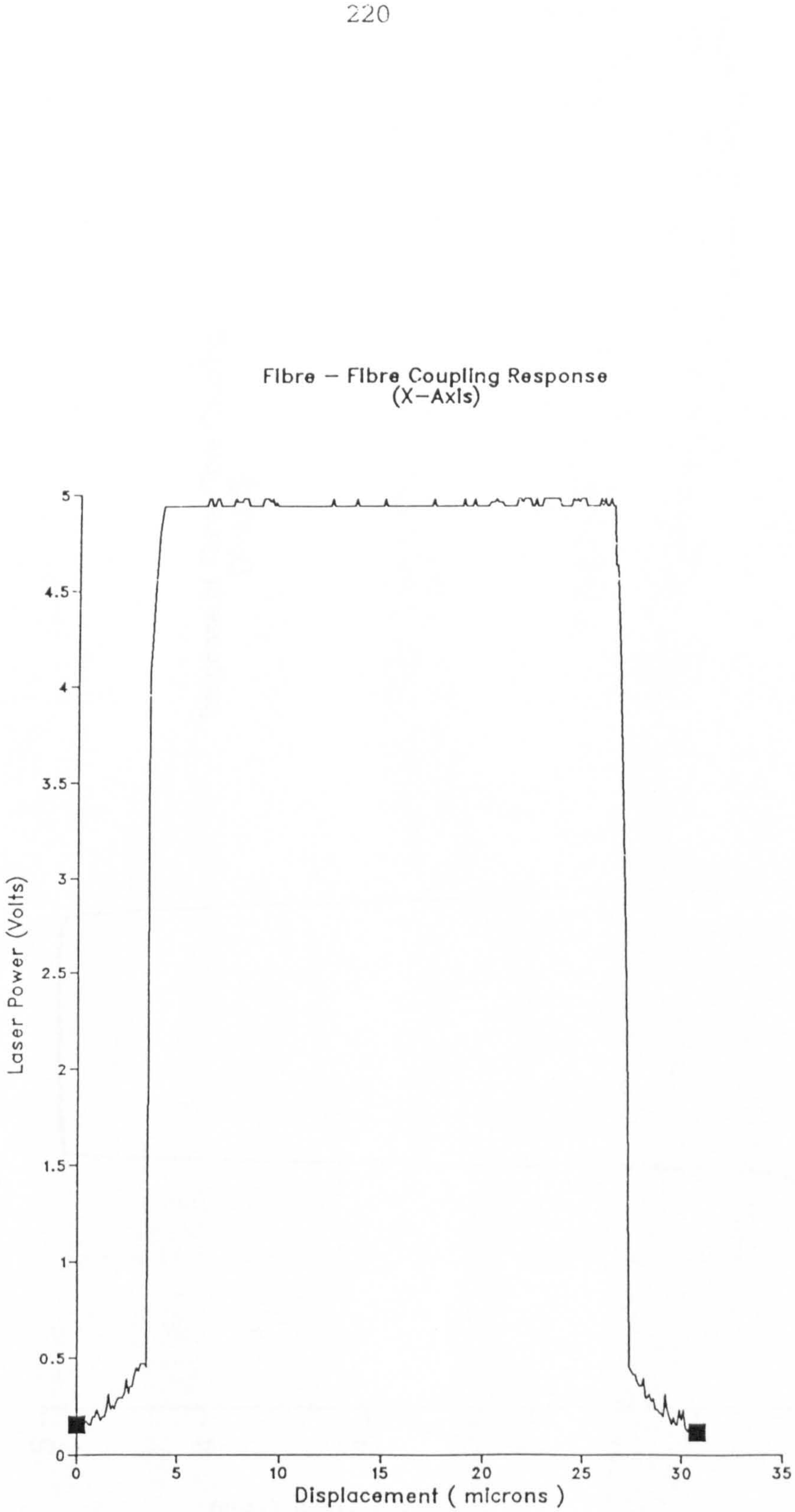
Fibre – Fibre Coupling Response
(X–Axis)
Laser Power (Volts)
5
4.5
4
3.5
3
2.5
2
1.5
1
0.5
0
0
5
10
15
20
25
30
35
Displacement (microns)

Fig,9,4 (b)

Response of Fibre-Fibre Coupling
(Y-AXIS)

Fig, 9,4 (c)

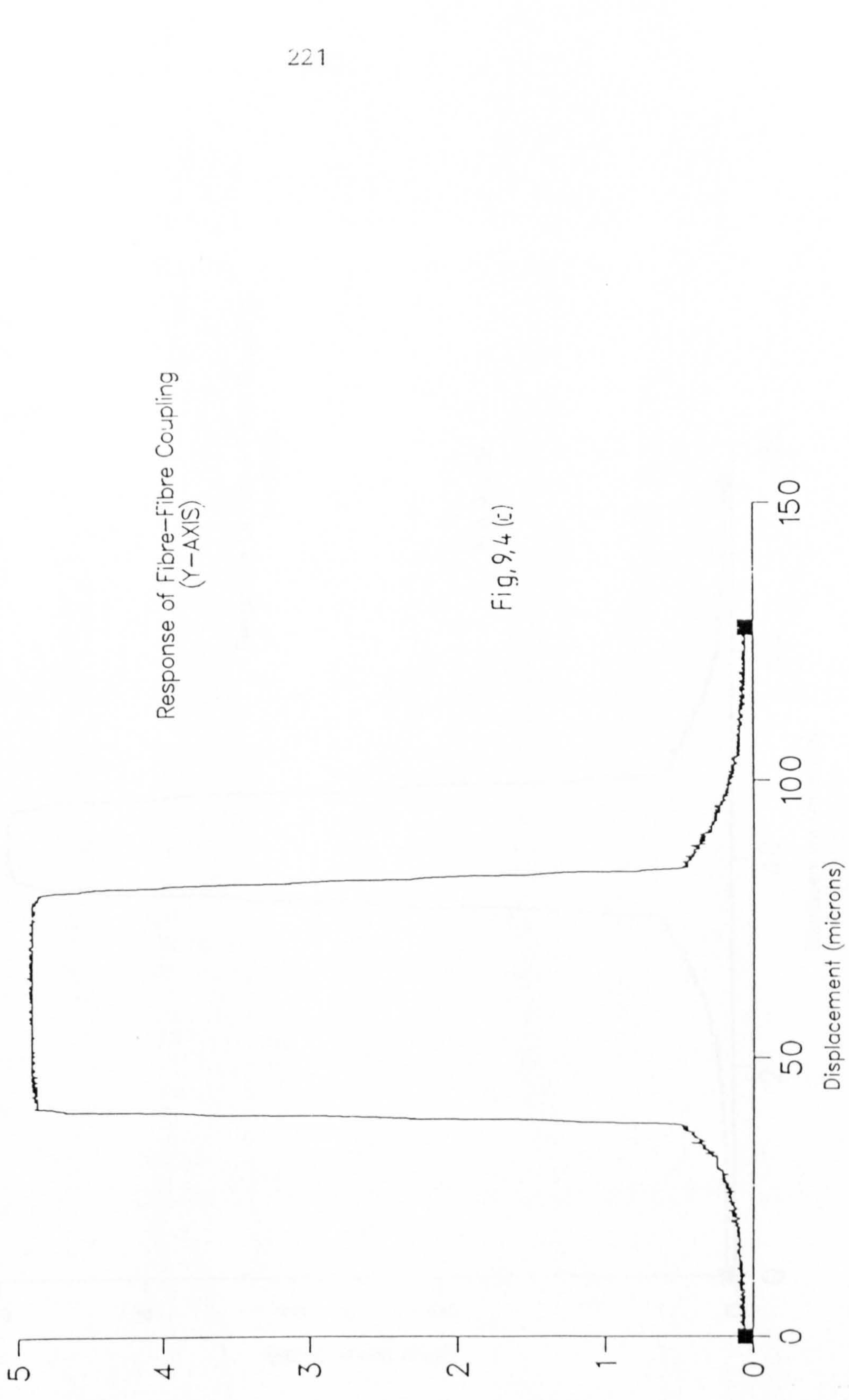

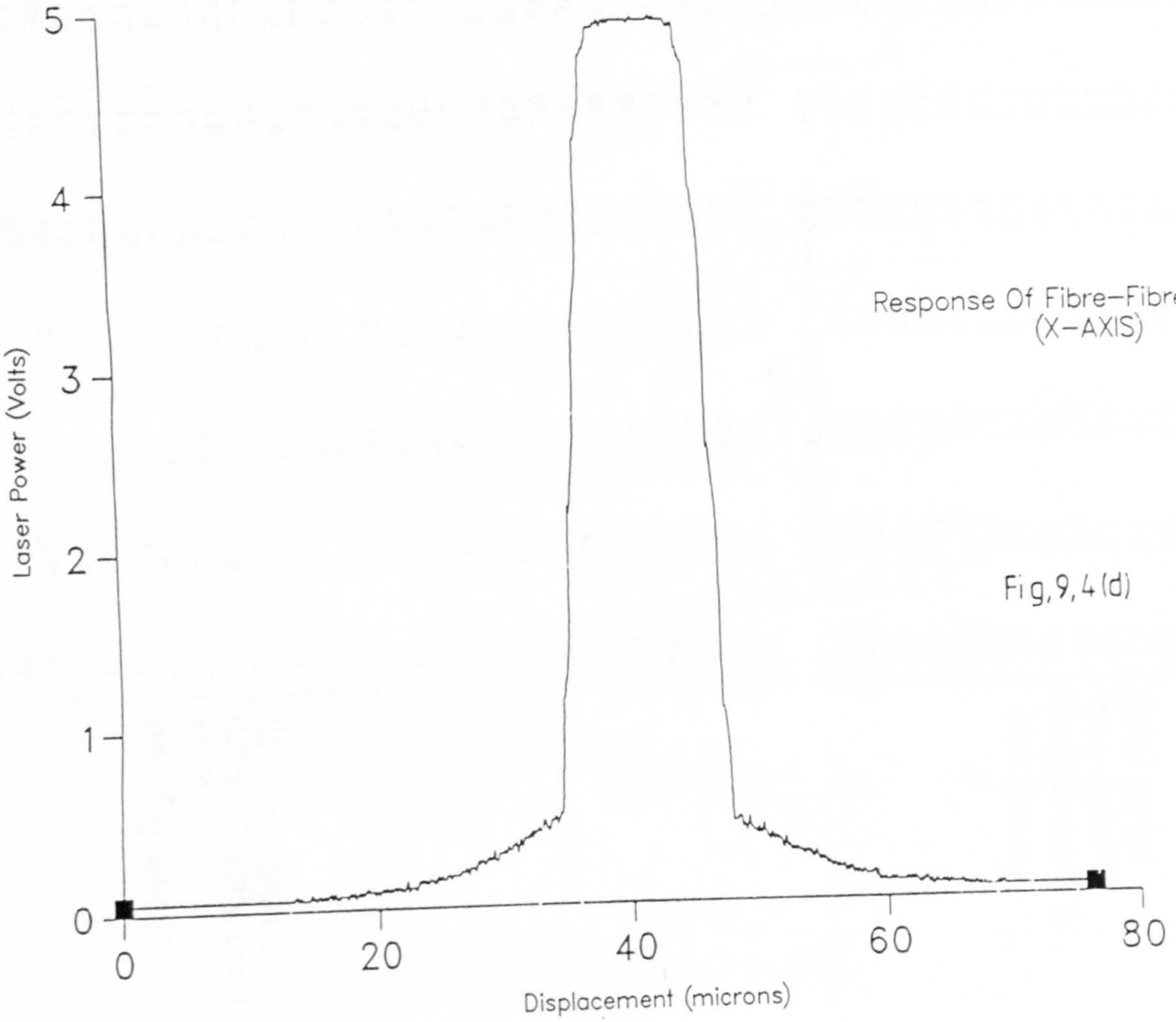

Response Of Fibre–Fibre Coupling
(X–AXIS)

Fig, 9, 4 (d)

TABLE 9,4: Fibre-Fibre alignment test results.

0A	0A	09	0A	09	0A	09
0A	0A	0C	0B	0A	0A	0A
0B	0B	10	0C	0B	0B	0C
0B	0E	0E	10	0D	0F	0E
0D	0F	0E	0F	10	0E	0F
10	12	12	10	11	0F	12
12	12	12	12	12	12	12
12	12	14	12	12	14	13
13	12	12	13	13	13	13
14	13	12	14	13	12	14
13	13	12	13	13	13	13
12	14	12	12	14	12	12
12	11	12	12	11	12	10
0F	0F	10	14	0F	0F	10
0F	10	0E	0E	0E	0E	10
0E	10	0C	0E	0B	0C	10
0E	10	0C	0B	0B	0B	10
0A	0A	0A	0C	0B	0A	0A
0B	09	08 ← (motor reverses to 08H)				

Data output from motor Y (Reverse down to 09H or less)

0A						
08	0A	08	09	0A	0A	09
08	0C	09	08	08	09	08
08	0A	08	0A	09	0A	08
0A	09	0A	0A	0A	0A	0A
0A	0A	0A	0C	0B	0A	0A
0B	0B	0A	10	0C	0B	0B
0A	0A	0A	0C	0B	0A	0A
0B	0B	0A	10	0C	0B	0B
0C	0D	0B	0C	10	0C	0D
0B	0C	0E	0D	0E	10	0D
10	0D	0E	0E	0E	10	0D
10	0D	0F	0F	0E	10	0E
10	0E	0F	0F	0E	10	14
10	0F	0F	0F	10	0F	0F
10	12	0F	10	14	10	12
12	10	12	0F	10	14	0F
14	11	12	14	12	12	14
12	13	12	12	13	12	12
12	14	12	13	14	12	12
12	12	13	12	12	13	12
12	12	14	12	12	14	12
13	12	12	13	12	12	13
14	13	12	14	12	12	14
12	12	12	12	13	12	12
12	14	12	12	14	12	12
12	11	12	12	11	13	12
0F	10	10	12	0F	10	14
10	12	0F	10	14	0F	0F
0F	0F	0F	10	0E	0F	0F
0E	0F	0E	0E	10	0E	0F
0E	0C	0E	0D	0E	10	0C
10	0C	0E	0C	0C	10	0C
10	0C	0B	0B	0B	10	0C
10	0C	0B	0B	0A	10	0C
0A	0A	0C	0B	0A	0A	0A
0A	09	09	0A	09	0A	08
0A	08	0A	09	0A	08	09
0C	09	08	08	09	08	08
07	06	08	06	06	08	06

Motor Y Forward motion (Storing down to 05H). (see Fig. 9,4(a))

TABLE 9,4 (contd).

06	07	08	06	06	08	06 } Last part of motor Y
08	06	06	06	06	06	06 } forward motion.
06	06	06	07	06	06	07 }
04						
01 } Total data stored during						
18 } Y-forward motion (=0118H).						
14 ← Local peak (S_{max})						
12 ← 0,9 Smax						
05	06	04	05	06	06	06
06	06	06	07	06	06	06
06	08	06	06	08	08	07
08	08	0C	08	08	08	09
08	08	09	0C	08	08	08 } Reverse motor Y
08	08	08	0A	09	0A	09 } to 0,9 MAX or better
0A	09	0B	0A	0A	0B	0A
0C	0A	0A	0C	0A	0B	0C
0B	0B	0B	0B	0B	0C	0B
0B	0C	10	0C	0E	0D	0C
10	0E	0F	0E	0E	0F	0E
0E	10	0F	10	0F	10	0F
10	0F	12 ← (Y reverses to 0,9 Smax)				
11	12	0F	10	14	12	12
12	22	27	34	43	5F	81
B9	FB	FB	FB	FB	FB	FB
FB	FB	FB	FB	FB	FB	FB
FB	FC	FB	FB	FC	FC	FC
FB	FB	FB	FC	FC	FC	FC
FC	FC	FC	FD	FC	FC	FC
FB	FB	FB	FB	FB	FB	FB
FB	FC	FC	FB	FB	FC	FB
FB	FB	FB	FB	FB	FB	FB
FB	FC	FB	FB	FB	FB	FB
FB	FB	FB	FB	FB	FB	FB
FB	FC	FC	FB	FC	FB	FB · Change to motor X
FB	FB	FB	FB	FB	FB	FB } and reverse down to
FC	FC	FC	FC	FC	FC	FC } 09H or less
FB	FC	FC	FB	FC	FC	FB
FD	FD	FD	FD	FC	FD	FD
FC	FD	FD	FC	FD	FD	FD
FD	FE	FD	FD	FE	FE	FE
FD	FD	FD	FD	FD	FD	FD
FD	FE	FD	FD	FE	FD	FD
FD	FD	FD	FD	FD	FD	FD
FE	FD	FD	FE	FD	FD	FD
FC	FB	FB	FB	FB	FB	FB
F8	16	15	16	16	14	13
14	0F	0F	10	0E	0F	0E
0C	0B	0A	0A	0A	0A	0C
0A	08 ← (X reverses to 08H)					

TABLE 9,4 (contd)

08						
08	08	09	08	08	09	08
08	0A	0A	0C	0B	09	0A
0A	0C	10	0C	0D	0C	0E
0F	0F	0F	10	14	10	12
12	15	17	16	18	18	18
17	D0	D9	E4	ED	F5	F9
FC	FC	FC	FC	FC	FC	FC
FC	FC	FC	FC	FC	FC	FC
FC	FC	FC	FC	FC	FC	FC
FC	FE	FE	FC	FC	FE	FE
FC	FC	FC	FC	FC	FC	FC
FE	FD	FD	FD	FE	FE	FE
FC	FC	FC	FC	FC	FC	FC
FE	FE	FE	FD	FE	FC	FD
FC	FC	FC	FC	FC	FC	FC
FC	FC	FC	FC	FC	FC	FC
FC	FC	FC	FC	FC	FC	FC
FC	FC	FC	FC	FC	FC	FE
FC	FC	FC	FC	FC	FC	FC
FC	FC	FC	FC	FE	FC	FC
FC	FC	FC	FC	FC	FC	FC
FC	FC	FC	FC	FE	FC	FC
FC	FC	FC	FC	FC	FC	FC
FC	FC	FC	FC	FC	FC	FC
FE	FC	FC	FC	FC	FC	FC
FC	FC	FC	FC	FC	FC	FC
FC	FE	FC	FC	FC	FC	FE
FC	FC	FC	FC	FC	FC	FC
FD	FD	FD	FE	FD	FD	FD
FC	FC	FC	FC	FC	FC	FC
FE	FE	FD	FE	FE	FE	FE
FC	FC	FE	FC	FC	FC	FE
FE	FE	FE	FE	FE	FE	FE
FE	FC	FC	FC	FC	FC	FC
FE	FD	FE	FD	FE	FE	FD
FC	FC	FC	FC	FC	FC	FC
FE	FC	FE	FC	FC	FE	FC
FC	EC	EC	DE	CE	B4	95
5E	17	16	15	15	13	12
12	14	0F	0F	10	0E	0F
0C	0C	0B	0B	0A	10	0C
0A	08	0A	08	08	0C	09
0C	07	06	08	07	06	06
06	04					

Move motor X forward storing signals down to 05H) (see Fig,9,4(b))

01, 35 } Total data stored during X-forward motion(=0135H).

FE ← Local Peak (Smax = MAX)

E4 ← 0,9Smax (=0,9MAX)

06	05	06	05	05	06	06
06	06	06	06	07	06	06
07	0C	07	08	08	0A	08
0A	0B	0C	0D	0B	0C	0E
0D	14	11	12	12	12	13
13	48	48	54	67	82	A6
DE	FB					

Reverse motor X to 0,9MAX or better.

FB ← X reverses to peak position (FB > 0,9MAX)

REFERENCES.

1. P.V. Andrews, R.Grigsby,R.J. Hazelden, M.T. McDonough, S. Saha.
"A portable self-aligning Fusion Splicer for Single-Mode fibres."
The International Wire and Cable Symposium/Nov.1984 (Nevada-USA).

2. Centronic Sales.
"Fibre Optic News."
Opto and Laser Products Vol.3 No.3 1986 (pp.45) and personal communication.

3. T. Edye, Ph. Schwab, J.P. Roussel, O. Parriaux.
"Automatic Assembly Station for guided Optic components."
Society of the Photo-Optical and Instrumentation Engineers (SPIE) vol.483, 1984 (pp. 70-75).

4. Newport Corporation -USA.
"Newport's PM500 Linear Motion System."
The British Electro-Optics Journal March 1987 (pp.1).

5. Walmore Advanced Components -U.K.
"The AS-85M Optical Fibre Alignment System."
(Manufactured by Cabloptic -Switzerland).
The British Electro-Optics Journal March 1987 (pp.3).

6. "Opto-mechanical and Micropositioning Equipment."
Photon Control -U.K. Personal Communication.

7. CP/M Operating System Manual.
Published by Digital Research 1976 - 1979 and 1982.

8. Lance A. Leventhal.
"8080A-8085 Assembly Language Programming."
Published by Osborne/Mcgraw-Hill 1978.

CHAPTER 10

CONCLUSIONS AND RECOMMENDATIONS FOR FURTHER WORK.

Although the laser/fibre alignment configuration was substituted by the fibre-fibre configuration because of prealignment problems (9.4) experienced during the experiment, the main objectives of this work have been achieved. The reasons for close similarity between the two configurations (9.4) justify this substitution. The alignment control rig (system) described in Chapter 8 successfully demonstrated a hill climbing concept applied to the fibre-fibre alignment.

10.0 Conclusions.

In the course of this research, conclusions based on the theoretical and experimental studies of laser/fibre or fibre-fibre alignment have emerged. These are outlined as follows:

1- The replacement of the human operator coupling method by an automatic assembly process would certainly produce significant improvements in the speed and quality of the laser diode to optical fibre or fibre-fibre alignment.

2- The assembly process ideally requires a 5 degree of freedom manipulator in order to align a laser diode with an optical fibre or fibre to fibre efficiently. However, in Chapter 9, it has been demonstrated experimentally that a 3 degree of freedom manipulator is adequate for fibre/fibre alignment. Since angular misalignments are insensitive to power coupling, it is envisaged that this manipulator will also suffice for laser/fibre alignment and above all, it is cheaper than the 5-degree of freedom manipulator.

3- The laser diode/fibre prealignment problems (9.4) can only be solved by either purchasing or making a more accurate gripper than the one used in this work and mounting it horizontally on to the manual manipulator (plate 8.2.7).

4- Ideally, the Oriel Encoder Mike actuators are designed for

continuous motion and not for very minute stepping motion for which it is applied in this work. As a result, the encoder circuit (8.3.1) designed to track the position of the Encoder Mike actuators for extremely small equal step (0.1 μm) motion was rendered useless (9.3.1) because the encoder signals produced were of unequal widths. However, for a continuous linear motion of 3 to 5μm the Encoder Mikes are said[23*] to produce signals of equal widths. Also, when Oriel controllers are used, the resolution attained is of the order of 0.02 μm but stopping the motor in the reverse direction causes the spindle to overshoot by 15μm and then slowly returns to the end point (4.4.3). This is in conflict with the clearance specification given in Chapter 2. This means that if the Oriel Encoder Mikes are to be used, a better circuit capable of accounting for the encoder pulse differences must be designed. This will allow the use of a closed loop type control for the alignment positioning system which is more desirable than the open loop.

5- The technique employed in Chapter 7 for the analysis of the manipulator characteristics has been recently developed[2†] in the Department. Its success in this respect means that it can be applied to evaluate the characteristics of other manipulators in general. However, the theoretical results of the characteristics of the 3- and 4- degree of freedom manipulators presented in that Chapter must be greatly improved upon if they are to be utilised to formulate a laser/fibre or fibre-fibre alignment algorithm (compare with the balancing algorithm used for laser/screen alignment in Chapter 6). In addition, the manipulators analysed in Chapter 7 need to be made to an extremely high accuracy because laser/fibre or fibre/fibre alignment calls for very stringent accuracy and tolerance demands (Chapter 2).

10.1 Recommendations for further work.

During the course of this research, some important and interesting areas of the work have been found to deserve closer investigation. It is therefore suggested that the following actions should be taken:

1- Currently, alignment in the axial direction (9.1) is accomplished

23* Ref 23, Chapter 4, personal communication with Oriel Corporation
2† Ref 2, Chapter 7

NOTE: (See p.229, parag.1, lines 10 - 21)

Firstly, it is important to specify the accuracy tolerance to which the 40 μm gap should be obtained. This means that the sum of the final positioning tolerances of the laser diode, fibre and the accuracy tolerance of the switch used must fall within this specification. If the latter can not be achieved, then a direct visual method involving the use of a powerful microscope such as that employed by STC should be adopted.

manually by adjusting the fibre and fixing it some distance away from the laser diode face. In order to fully automate the 3-axis laser/fibre or fibre-fibre alignment procedure, it is recommended that all the three motors in the X-, Y- and Z-directions should be computer controlled. This will reduce the manual alignment time in the Z-direction and increase the alignment reliability. That is, the final resting position of the fibre (input end) in the axial direction should be consistent. To avoid damaging the laser diode face and the fibre input lens, the gap between the laser and fibre lens must be maintained at 40 μm or a little less. This can be done by positioning an accurate switch along the axial direction such that X, Y, and Z alignment can commence at a gap distance of over 100μm axially and carries on closing the gap down to 40 μm or less when motor Z trips the switch. That is, by utilising the hill climbing technique (9.2) and selecting each of the three motors in turn, the alignment is completed at a point 40 μm or less from the laser diode face. There is a chance that at this point, the required coupled power level might not have been attained yet. In this case, motor Z is stopped while the hill climbing alignment procedure (9.2) continues only between motors X and Y until the required power is coupled.

2- Although theoretically, a 5-axis positioning device was found to account for all linear and the relevant angular misalignments, the actual configuration of the axes has not yet been studied. There are quite a number of possibilities based on the decision of whether or not to have either the laser diode stationary or the optical fibre stationary and hence avail all the five axes of movement to the moveable component. The other alternative is to split the five axes between the two components and give both a movement capability. If a 5 degree of freedom manipulator is to be used, it is suggested that such configurations should be fully analysed to see if some have better performance than others.

3- As already stated (2.5), some crucial alignment tolerance specifcations were given only after the Oriel Encoder Mike manipulator was already purchased. One slight drawback of this manipulator is that the actuators overshoot by 15 μm in the reverse direction (10.0). This can be overcome by approaching a

given point from the forward direction only. However, in future other types of actuators with suitable tolerances with no overshoot and unidirectional approach problems should be considered. In this respect, stepper drives offer better features for the control of laser/fibre or fibre-fibre alignment as long as they have a suitable resolution (0.1μm or less) and their price is within reach.

4- As part of a total alignment automation, it is recommended that a detailed investigation of fibre welding onto the laser platform (2.4) should be carried out. Essentialy, fibre welding forms the second part of this work. Currently, STC has not yet found a suitable automatic welding method which maintains consistency of the welding forces produced during the welding operation and also takes account of the welding stresses and creep. These factors are responsible for the degradation of coupled power at a later stage as the weld sets (2.4) and pulls the fibre away from the aligned position.

5- In order to avoid some unnecessary alignment and prealignment difficulties, there is a need to completely redesign the laser box. The height of the laser pins inside the box, for example, could be shortened to avoid short circuiting during alignment manipulation and the design of the hole through which the optical fibre is threaded (2.4) could be totally changed to avoid bending of the fibre.

APPENDIX TO CHAPTER 3

(Appendix A)

Application of Screws in Alignment

This appendix gives a summary of Bottema's [8] analysis of the screw displacements needed to superpose rigid bodies, line segments and lines in that order. Details of all the mathematical description and analyses of the axes and rotational angles of screws discussed here can be found in [8]. As already defined (3.5), a screw displacement is the rotation of a body about a given axis and a translation along the same axis. In contrast to the analyses presented in chapter 3, this method investigates the mathematical description of all the necessary screw displacements required for the different alignments.

A.1 Superposition of two congruent figures.

The position of a body in space is transformed into a second position by a screw displacement [8]. Since the body is moved to occupy a new positon in space, the second position can be regarded as another congruent figure. It is therefore equivalent to superposing two congruent bodies. For the displacement of such a rigid body in which the rotation angle γ_{ij}, translation distance d_{ij} and the screw axis s_{ij} are fully determined, the screw is unique.

A.2 Alignment of line segments.

Consider two skew lines l_1, l_2 with a row of points A1B1...on l_1 and a congruent row A2B2... on l_2 (Figure A.2). These lines are chosen so that they form equal angles α with the Z-axis. Bottema [8] quotes others who define the line m (Figure A.2) as the locus of the midpoints of the joins of homologous points on l_1 and l_2 such that the projections of A1A2, B1B2.... on it all have the same length. A frame (origin O) is then introduced [8] with m as the Y axis and W as the OXY plane so that A1 and A2 are the points (a, -d, 0) and (-a, d, 0) respectively. It would appear that m should be the Z-axis but if B1 is above W on l_1 and B2 is below W on l_2 then this is possible.

Let the complete set of screws that transforms l_1 into l_2 be Γ. Out

of this set, a few screws are identified [8] as follows:

(a) So ($\in\Gamma$) acts along line m with a rotation angle of 180^{o} and a translation 2d. This displacement is the basis for determining others mathematically.

Fig, A,2 Aligment of two skew line segments l_1 and l_2.

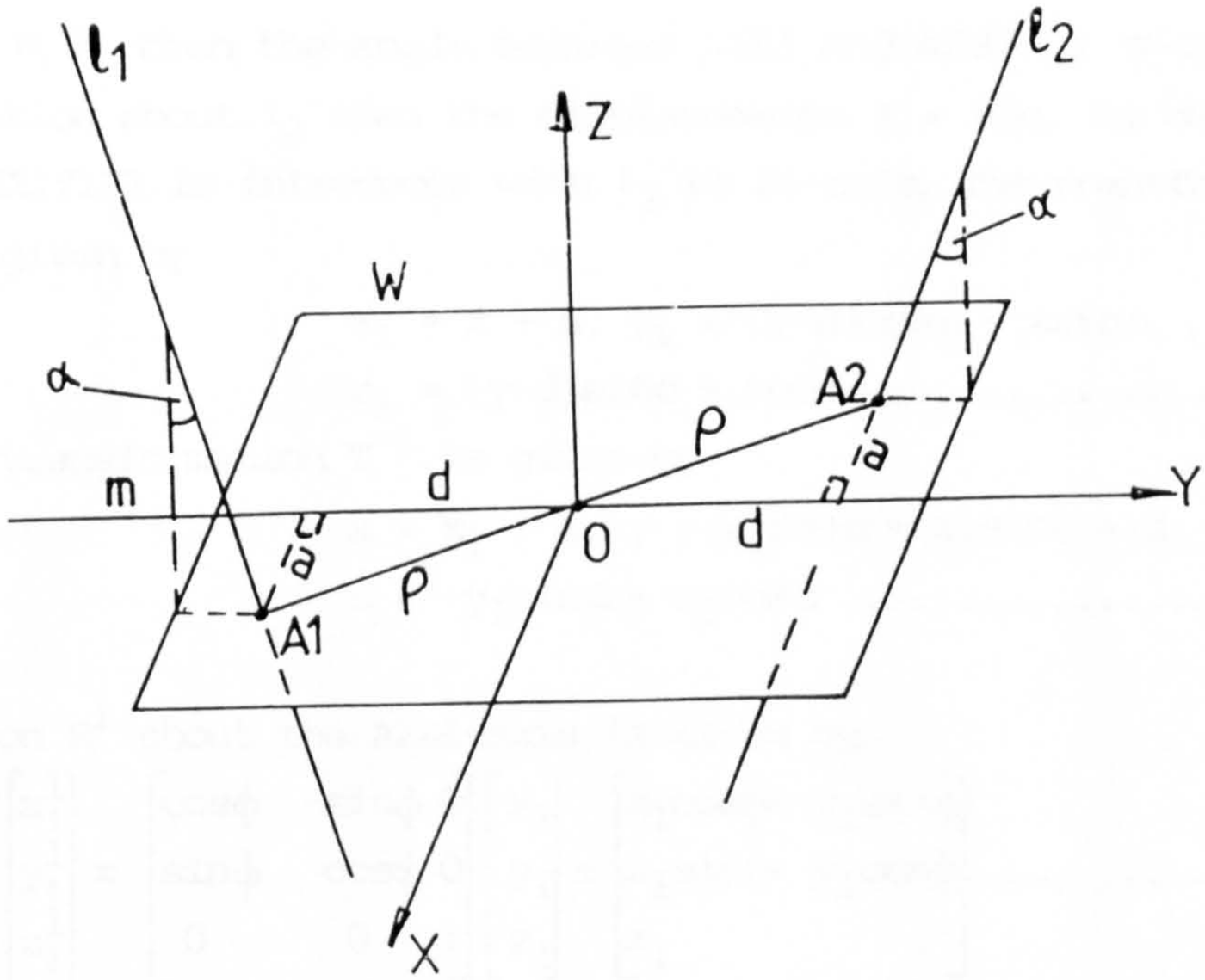

(b) S_t ($\in\Gamma$) is another screw displacement with its axis along A1A2 (Figure A.2) which has the largest translation component 2ρ. Its rotation angle γ is given by $\tan\gamma/2 = \rho/a\tan\alpha$.

(c) Sr ($\in\Gamma$) is the only single screw with a pure rotation. Its rotational axis is given by $ax - dy = 0$, $z = d\tan\alpha$ which is orthogonal to the line A1A2 ($dx + ay = z = 0$) and intersects the Z axis at $P_o(0,0,d\tan\alpha)$. Thus the rotational angle is $<A1P_oA2$ given by $\tan\gamma/2 = \rho/d\tan\alpha$.

(d) Lastly, Smin ($\in\Gamma$) is a screw with the smallest rotational angle $\gamma = 180^{o}-2\alpha$ (angle between the oriented lines $l1$ and $l2$). Its axis is given by $y = 0$, $z = d\tan\alpha$ and the translation part is $2a$.

It is reported [8] that there are altogether oo^1 displacements transforming the row on l_1 into a congruent row on l_2. The preceeding steps summarise the analysis leading to the mathematical description of the displacements.

S_o is the displacement $x^1 = -x,\ y^1 = y + 2d,\ z^1 = -z$ ..... A2.1.
Equations of l_1 and l_2 are given respectively by

$$x = a,\ y + d = -z\tan\alpha \quad \text{..... A2.2.}$$

$$\text{and } x = -a,\ y - d = z\tan\alpha \quad \text{..... A2.3.}$$

If $0<\alpha< \pi/2$, then the angle between A1B1 and A2B2 is $\pi-2\alpha$. If R is any rotation about l_2 then the displacements $\Gamma = RS_o$. To obtain R, a frame A2X1Y1Z1 is introduced with l_2 as Z1-axis. The transformation T is then given by

$$x_1 = x + a,\ y_1 = (y-d)\cos\alpha - z\sin\alpha,$$

$$z_1 = (y-d)\sin\alpha + z\cos\alpha \quad \text{..... A2.4.}$$

Inverse transformation T^{-1} is given by

$$x = x_1 - a,\ y = y_1\cos\alpha + z_1\sin\alpha + d,$$

$$z = -y_1\sin\alpha + z_1\cos\alpha \quad \text{..... A2.5.}$$

A rotation R^1 about the A2Z1-axis is given by

$$\begin{bmatrix} x_1^1 \\ y_1^1 \\ z_1^1 \end{bmatrix} = \begin{bmatrix} \cos\phi & -\sin\phi & 0 \\ \sin\phi & \cos\phi & 0 \\ 0 & 0 & 1 \end{bmatrix} \begin{bmatrix} x_1 \\ y_1 \\ z_1 \end{bmatrix} = \begin{bmatrix} x_1\cos\phi - y_1\sin\phi \\ x_1\sin\phi + y_1\cos\phi \\ z_1 \end{bmatrix} \quad \text{..... A2.6.}$$

where ϕ is the rotation angle. Thus $R = T^{-1}R^1T$ and the set $\Gamma = RS_o$[8].

Calculation of $T^{-1}R^1TS_o$:

(i) TS_o: Link A2.4 and A2.1 by replacing x, y, z with x^1, y^1, z^1.

i.e. $x_1 = x^1+a = -x + a,\ y_1 = (y^1-d)\cos\alpha - z^1\sin\alpha$

$$=(y+2d-d)\cos\alpha-(-z\sin\alpha).$$

Similarly, $z_1 = (y+d)\sin\alpha - z\cos\alpha$

(ii) R^1TS_o: Link A2.6 to the results of (i).

$x_1^1 = x_1\cos\phi - y_1\sin\phi = (-x+a)\cos\phi-\{(y+d)\cos\alpha + z\sin\alpha\}\sin\phi.$

$y_1^1 = x_1\sin\phi + y_1\cos\phi = (-x+a)\sin\phi+\{(y+d)\cos\alpha + z\sin\alpha\}\cos\phi.$

Similarly, $z_1^1 = z_1 = (y+d)\sin\alpha - z\cos\alpha.$

(iii) $T^{-1}R^1TSo$: Link A2.5 to the results of (ii).

$$x^1 = x_1^1 - a = -x\cos\phi - y\cos a\sin\phi - z\sin a\sin\phi - a(1-\cos\phi) - d\cos a\sin\phi.$$

$$y^1 = y_1^1\cos a + z_1^1\sin a + d$$

$$= \{(-x+a)\sin\phi + (y+d)\cos a\cos\phi + z\sin a\cos\phi\}\cos a$$

$$+ (y+d)\sin^2 a - z\cos a\sin a + d.$$

$$= -x\cos a\sin\phi + y\{1-\cos^2 a(1-\cos\phi)\} - z\sin a\cos a(1-\cos\phi)$$

$$+ d\{2-\cos^2 a(1-\cos\phi)\}.$$

$$z^1 = -y_1^1\sin a + z_1^1\cos a$$

$$= \{(x-a)\sin\phi - (y+d)\cos a\cos\phi - z\sin a\cos\phi\}\sin a + (y+d)\sin a\cos a$$

$$- z\cos^2 a.$$

$$= -x\sin a\sin\phi + y\sin a\cos a(1-\cos\phi) - z\{1-\sin^2 a(1-\cos\phi)\}$$

$$- a\sin a\sin\phi + d\sin a\cos a(1-\cos\phi) \quad \ldots\ldots \text{A2.7.}$$

Equations A2.7 are the complete set of screw displacements transforming l_1 into the homologous line l_2. Taking it further, it is found [8] that the locus of the axes of these screw displacements is a cylindroid. The screw Smin is its second generator through P_o while S_l is the second generator through the origin O. A generator is a line that forms part of the surface of the cylindroid. The first generator is the axis of the screw S_o. Mathematical details leading to the determination of the cylindroid from A2.7 as well as its generators (screws already identified above) can be found in [8].

A.3 Indirect Displacements.

The above procedure (A.2) that transforms l_1 into l_2 is described as direct (method I). A similar but indirect method that transforms a space into a symmetric one is also described [8]. The coefficients of its linear terms are the elements of an orthogonal matrix whose eigenvalue is -1. It differs from the direct one because the rotation R^1 (section A.2) used to obtain the complete set of displacements transforming l_1 into l_2 is replaced by a reflection U^1 in any plane through A2Z1. S_o and T are the same as before and the detailed mathematical analysis follows exactly the same trend as in method I. Inorder to avoid labouring essentially the same points here, the matter is referred to [8]. Following the same procedure as for direct displacements, but replacing the rotation angle ϕ (A.2) with the angle of reflection θ, it is found [8] that the locus of the screw

axes of the indirect displacements transforming l_1 into the homologous line l_2 is a paraboloid regulus.

A.4 Screw displacements for two oriented lines.

This section describes displacements transforming two skew infinite lines A and B without specified point rows on them. Line A is fixed and lies along the X-axis as shown in Fig. A.4. Line B is moveable and skew to A. Let line segments l_1 and l_2 lie on A and B respectively. Thus l_1 and l_2 are also skew. In order to align (or superpose) l_1 with l_2, the procedure described in section A.2 is followed. Such a transformation is satisfied by ∞^1 complete screw displacements (A.2). l_1 and l_2 can traverse the overall lengths of lines A and B respectively if the line segments are moved along them. If these movements are made by shifting l_1 and l_2 along A and B in predetermined steps, then for each of the shifts made, it requires ∞^1 screw displacements to superpose l_1 on to l_2. Since A and B are both infinitely long, it means that ∞^1 shifts are needed to cover the lengths. It therefore follows that $(\infty^1).(\infty^1)$ or ∞^2 complete screw displacements are required to align A with B. This result is also reported in [8].

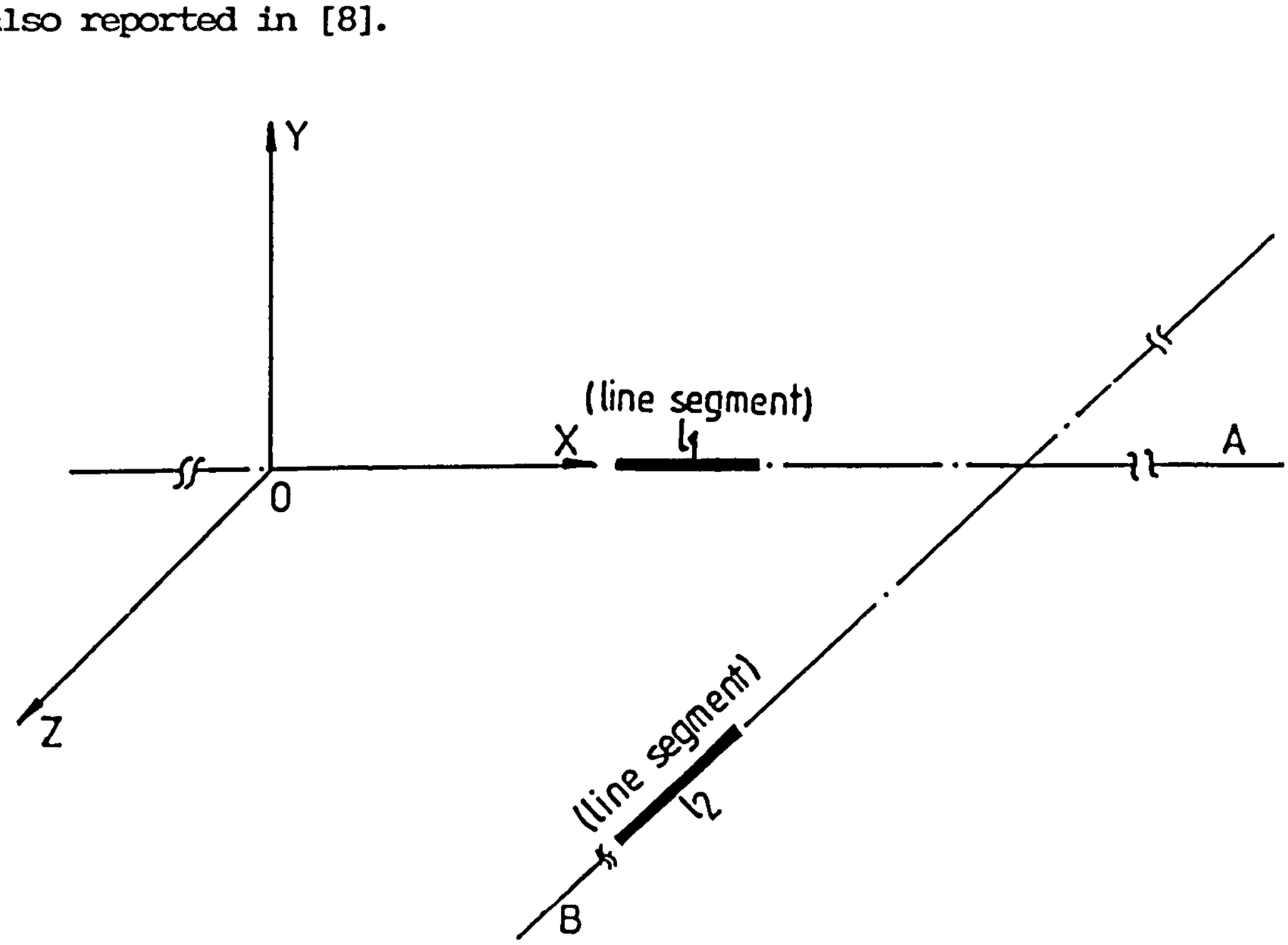

Fig A.4 Alignment of two skew lines A and B by screw method.

APPENDIX TO CHAPTER 4

(Appendix B)
Motorised Actuators

This Appendix presents a summary of the survey of some actuators thought to be suited to laser/fibre alignment. The sequence of sub-section numbering follows from the main chapter inorder to maintain consistency for purposes of references made to this Appendix from other areas of the thesis or vice versa.

4.4.1 Ealing Motorised Actuators

a) ACTUATOR: Ealing Stepper Motor Stage.
(SPECIFICATIONS FROM EALING OPTICS CATALOG [21])

Manufacturer: Ealing (Mass.-USA).

Range: 0 - 12 mm (6 mm).
(Travel is limited by microswitches).

Load Capacity: 10 kg - at max. speed of 2,000 microns/s.
(Stage Horizontal)

Load Capacity: 7 kg - off-set by a max. of 20 mm at a max. speed of 2,000 microns/s. (Stage Vertical)

Movement corresponding
to one step of motor: 1 micron

Half-step movement: 0.5 micron.

Step Range: 0.5 - 2,000 microns/s.

Accuracy:

i) Positioning accuracy: 1 micron.
(One direction of travel)

ii) Tracking accuracy: 1 micron
(Over full range of travel)

Moving Stage dimensions: 160 x 160 mm.

Manufacturer's Description and Comments

These stages can be cross-stacked to form a manipulator (section 6.1-Fig. 6.1(a)). It is designed for carrying out fine adjustments in the

vertical plane and because it covers only a short length of travel, 6mm either side of centre, speeds are restricted to 2,000 microns/s. It is quite possible to use the stage horizontally if required.

The stage has a 90 mm clear aperture through the centre which is maintained throughout the 12 mm range of travel. This aperture is normally used for mounting a range of different accessories.

Conclusion

Although Ealing also makes other stepper motor stages with various range of travel namely 50 mm, 100 mm, 300 mm, and 600 mm, the 12 mm range has far better accuracy than others. Its only major drawbacks for use in the alignment project are the extremely slow maximum speed of 2,000 microns/s and the the extremely large load capacity compared with the maximum load of 40 gm outlined in the alignment specification (2.5).

The 50 mm range is faster with a maximum speed of 10,000 microns/s horizontally and shares exactly the same accuracy with the 12 mm range. However, it has such an excessively large travel range and load capacity (25 kg horizontally and 6 kg vertically) that it would be an overkill to utilise for a solution in this work.

b) ACTUATOR: Ealing D.C. Motor Stage.
(SPECIFICATIONS FROM EALING OPTICS CATALOG [21]).
Manufacturer: Ealing (Mass.-USA).
Range: 0 to 25 mm.
Load capacity: 10kg.
Accuracy:
i) Positioning accuracy: The micrometer reads directly to 0.01 mm and can be estimated to better than 0.005 mm.
ii) Tracking accuracy: 2 microns (over the entire range).
Speed: Maximum achievable speed is 16 mm/min.
Moving Stage Dimension: 80x144.6 mm. (Unit thickness= 26 mm).

Manufacturer's Description and Comments

The stage provides a precision linear movement of 25 mm in a single plane. The moving stage rides on two rows of captured precision spherical ball bearings pre-loaded in ground and hardened V-grooves. The base is anodised aluminium.

A 15 mm diameter aperture in the moving stage and a 15 mm diameter by a 40 mm long slot in the stationary base ensures a 15 mm clear aperture at all points of the 25 mm travel. This can be used for mounting a wide variety of accessories.

Conclusion

The available literature suggests that the smallest D.C. motor stage currently manufactured by Ealing is the 25 mm range. There are other stages with various range of travel namely 50 mm and 100 mm. These are, however, far less accurate than the 25 mm range and are also designed to support unnecessarily heavier loads than are required for laser/fibre alignment.

It should be noted that a load capacity of 10 kg, a 25 mm range of travel and an inferior accuracy values of this actuator all weigh heavily against its possible application to this project.

4.4.2 Microcontrole Motorised Actuator

ACTUATOR : Model UT50-20.
(ALL SPECIFICATIONS FROM MICROCONTROLE CATALOG [22]).
Manufacturer: Microcontrole (Evry Cedex, FRANCE).
Range: 0 to 20 mm.
Load: Working load is 2 kg.
Accuracy:
i) Average Accuracy: 1 micron.
ii) Resolution:
a) DC motor driven: 1 micron.
b) Stepping motor driven: 0.1 micron.

Speed: The nominal speed of this actuator when D.C. motor driven is 1 mm/s but another option of the same model offers a speed of 0.1 mm/s.

Manufacturer's Description and Comments

This stage is a translation unit with ball bearing guidance. It is equipped with a choice of the following drive units:

i) differential manual drive, direct drive or dual sensitivity;
ii) DC motor or Stepping motor.

The travel range of 20 mm is limited by positive mechanical stops. In motorised systems, these stops are augmented by limit switches. The system can include one or more of the following options: incremental encoder, origin search device and a linear potentiometer.

Conclusion

Microcontrole manufactures quite a wide variety of both manually operated and programmable motorised actuators. Out of all these, only the manually operated MR-models and the motorised UT-models seem to match the specifications of the alignment problem. However, the major drawback of the MR-model is the fact that it is manually operated. On the other hand the UT-models are extremely slow and therefore not worth considering.

The MT160 series have high speeds, some at 60 mm/s, and fairly good resolutions but excessively large working load capacity measured in tens and hundreds of deca-newtons (daN).

Most of these specifications, particularly load capacity, disqualify all the Microcontrole models for use in this alignment problem.

4.4.3 Oriel Motorised Actuators

a) ACTUATOR: Oriel Stepper Mike.
(ALL SPECIFICATIONS FROM ORIEL CORPORATION CATALOG [23]).
Manufacturer: Oriel Corporation - Connecticut, USA.
i) Operation of stepper mike in full-step mode:
Range: 0 - 13 mm.

Load: The maximum loading (centred) of the Oriel Stepper Mike over the 13 mm range is 11 kg (horizontally) and 5 kg (vertically).

Accuracy and Tolerance: The motors operate in discrete steps of 2 microns per step in full-mode. The unidirectional repeatability is 1 micron while bidirectionally, it is 3 micron at the end of each full step or completed half step. For each completed half step add 0.5 micron. Accuracy of the motor being 5 microns.

Speed: The maximum step rate for full mode is 500 steps per second and the maximum spindle speed is 1.0 mm/s.

Spindle Force: The maximum spindle force is 7 kg. This gives an indication of how much load can be safely handled by the motor.

ii) Operation of Stepper Mike in half-step mode:

Range: 0 to 13 mm.

Load: Loading is the same as above.

Tolerance and Accuracy: When the Oriel controllers are used, the resolution as well as the step size of these translators (vertical or horizontal) is 1 micron. The straightness of travel is 1 micron per 10 mm measured horizontally at centre of stage.

Speed: The maximum step rate is 1000 steps per second and the maximum linear speed is 1.0 mm per second.

Spindle Force: This is the same as for full mode.

Manufacturer's Description and Comments

Two models of the stepper mikes are available; one with a 12.7 mm range and the other with a 25.4 mm range of travel. Both of them have exactly the same accuracy, load capacity and speed. Although compactly packaged, it is larger than the D.C. motor drives.

When the motor coils are energised in a designated sequence, the stepping motor shaft rotates a fraction of a 360^{o} turn, usually expressed as 1.8^{o} , 7.5^{o} , or 15^{o} per step. This is geared down and converted to linear motion with a lead screw. The non-rotating

spindle, itself a precision ball bearing translator, not only prevents frictional side loading of the driven device but also allows direct mounting of small components at the end of the spindle.

The stepping motor takes a single discrete step for each voltage pulse sequence it receives. The rate of movement depends on the frequency of the drive pulses. This step by step movement produces a number of inherent advantages. Digital position read out is readily obtained by counting pulses bidirectionally.

A given movement can be obtained precisely by preselecting the number of steps thus allowing precise point by point analysis. Scanning at constant speed can be done at any speed or any load up to the maximum specified.

Conclusion

As described above, the stepper mikes seem to have very high accuracy standards suited for use in this alignment.

However, some major drawbacks of these drives include extremely low maximum speeds, fairly lower step and linear resolutions (especially in the double mode) and they are generally larger in size and more expensive than the Oriel Encoder Mikes (next section). For these reasons, the stepper mikes do not quite offer the best option.

(b) ACTUATOR: Oriel Encoder Mike.

(ALL SPECIFICATIONS FROM ORIEL MOTORISED PRECISION MOTION CATALOG [23]).

Manufacturer: Oriel Corporation - Connecticut, USA.

Ranges: 0 to 12.7 mm, 0 to 25.4 mm, and 0 to 50.8 mm.

Load Capacity: The loading of an Oriel translator over 25 mm range of travel is between 1 to 2 kg with a varying speed of 12 mm/min down to 11 mm/min. This is not significantly different for the other two ranges of travel.

Backlash: 6 microns typical (unidirectionally). To eliminate it, the target must be approached from forward direction only [23].

Accuracy and Tolerance: When Oriel controllers are used, the resolution attained is of the order of 0.02 microns. The unidirectional repeatability is 1 micron. However, when stopping in the reverse direction, the spindle automatically overshoots 15 μm and slowly returns to the end point. The controller reduces velocity automatically before reaching the point. Since the maximum distance traversed is only 5μm (chapter 1), it means that the controller can not be used for this alignment.

Speed: Maximum linear speed is 12.5 mm/min at very low loads under 1kg and the minimum linear speed is 0.03 mm/min at a maximum load of approximately 10kg.

Size of table top: 76x89 mm for a motor drive range of 0 to 12.5 mm but 127x127 mm for a motor drive range of 0 to 25 mm.

Manufacturer's Description and Comments

Encoder Mike micrometers incorporate a miniature D.C. motor with integral gear head to produce continuously variable speed over a wide range. A fine pitch screw running in a precision threaded nut combined with a 485:1 gear reduction contribute towards the attainment of 0.02 micron resolution when Oriel controllers are used. The design of the Oriel Encoder Mike micrometers therefore allows for very high resolution positioning.

Precise performance is achieved by operating the motor at slow speeds or by jogging it to its set point. When operated with an axial load greater than 0.45kg, a backlash of 6 microns is typical. Using the read out display on the controllers, the unidirectional repeatability is 1 micron.

Conclusion

The optical shaft encoder that provides position information is not

the only advantage that this simple D.C. motor has over others. It is also small in size (Figure 4.4.3) and is said [23] to provide a smooth vibration free, high resolution positioning. Since position feedback is the key to computer control, the encoder provides a means of computer communication.

However, D.C. motors with or without optical encoders do exhibit a backlash. This backlash, encountered only unidirectionally in Encoder Mikes, can only be compensated for by means of computer control. The maximum speculated mass of the semiconductor laser diode package to be manipulated is 40 gm (2.5). The maximum speed that can possibly be attained with this load is 12.5 mm/min.

Encoder Mike Micrometer

ALL DIMENSIONS IN MM

Fig,4,4,3

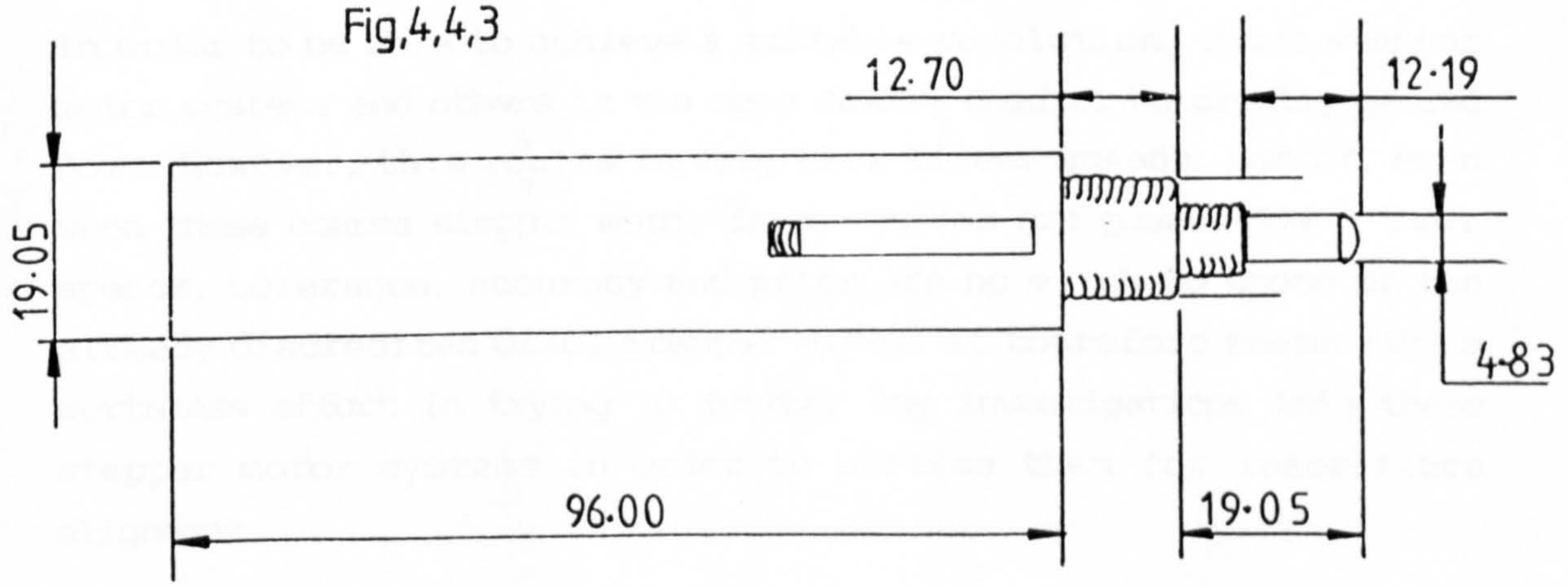

Although the overall speculated manipulation time involved if this actuator was used to solve the problem would be prolonged by its fairly slow speed, the overall performance of this actuator is far superior to all its current competitors. Its high repeatability and resolution, the available means of computer communication, the comparatively low backlash compensatable by means of a computer program and its comparatively competitive speed are some of the major unrivalled features that make it a suitable choice for the laser-

monomode fibre alignment. Figure 4.4.3 shows a typical full size Oriel Encoder Mike micrometer drive having a 12.7 mm range of travel.

However, a sixth manipulator that would very closely rival the Oriel Encoder Mike if it was not for its totally manual features is the F-915 precision fibre coupler manufactured by Newport Corporation-USA. Some other fine models include the F-916 and the F-917. In all these three models, fine translation is obtained without changing the angular orientation of the focussed laser beam on the fibre-end face (see [24] for further details). Other motorised systems together with their associated algorithms are cited in Chapter 9.

4.4.4 Other Stepper Motors

In addition to the stepper motor systems already surveyed and presented, there are quite a few other systems of similar sizes produced by a number of manufacturers. Digitran [25] and Sigma [26] are two such systems cited for purposes of clarification.

In order to be able to achieve a suitable resolution, these stepper motor systems and others in the same family need to be greatly geared down. However, this results in very slow linear speeds. Infact, even when these coarse stepper motor drive systems are geared down, their speeds, tolerance, accuracy and price are no match to those of the already discredited Oriel Stepper Mikes. It therefore seems like a worthless effort in trying to further any investigations into these stepper motor systems in order to utilise them for laser-fibre alignment.

APPENDIX TO CHAPTER 7
(APPENDIX C)

Analysis of Force and Velocity Motor Subspace

Matters related to the spatial analyses of the 3- and 4-degree of freedom manipulators (Section 7.1) are relegated to this appendix in order to avoid going through a strenuous procedure of transforming the velocity vectors in the main pages. The major points of interest are picked up directly from Davies [2] to illustrate how the spatial velocity transformation matrix $[M_v]$ is obtained. However, a general summary of all the spatial and planar transformation matrices for both the velocity and force motors are also presented. For further details of the transformation matrices that are simply stated here, the reader is referred to [2].

VMS and FMS are used in the appendix to mean velocity motor subspace and force motor subspace respectively. All references that appear in curly brackets { } in this appendix are stated in [2] specifically for the benefit of that work. The sub-headings in the appendix are numbered differently from those presented in [2] because of the omissions of the detailed derivations of some matrix transformations.

1. VMS and FMS in Local Coordinates

Any coupling can be characterised by a VMS or an FMS. One or the other is sufficient because, once one is known the other can be found using the reciprocity condition.

We begin by utilising local axes. These are chosen in such a way that the subspaces are in their simplest, one might say canonical form. We will avoid the use of Greek symbols that previously {1-4} have been liberally used, if only for the sake of the typist. It is helpful to use some specific examples. We start with an f = 1 coupling, the H (helical) pair shown in Figure 1.

We first need to identify a frame of 3 local axes (i.e. for use exclusively with this coupling). The axes are labelled x_1^a, x_2^a, x_3^a. The superscript identifies the coupling as coupling A in circumstances where there are several couplings and therefore several

sets of local axes. It is clearly convenient to align one of the three axes with the screw axis but there is no evidence to suggest which one. Here the $x_3{}^a$ axis has been chosen arbitrarily. The origin 0^a can be located anywhere on the axis and the other two axes can have any orientation provided they are perpendicular to the screw axis and to each other although, if we knew the orientation of the global axes this might influence our decision. The velocity motor subspace (VMS) of a coupling has up to 5 components (if 6 were present it would not be a proper coupling since it could not transmit a force). Associated with any coupling must be a sense and in this case we will say that it is body j with respect to (wrt) body i. This is indicated by the sense of an arrow on the network graph.

A VMS for j wrt i if they were uncoupled would comprise the angular velocity components V_1, V_2, V_3 of j wrt i about the three local axes respectively and the translational velocity components V_4, V_5, V_6 wrt i of the point in j that is instantaneously located at the local origin. If the bodies are coupled by a cylindrical (C) pair with its axis coincident with the $X_3{}^a$ axis then the VMS is constrained to be

$$V_\ell{}^a = \{0,\ 0,\ V_3{}^a,\ 0,\ 0,\ V_6{}^a\},$$

where the subscript ℓ is a reminder that we are using a local frame. For an H-pair the two non-zero components are related by

$$V_6{}^a = hV_3{}^a$$

where h is the ratio translational velocity/rotational velocity and has the units length/radian. It is related to the pitch p of the screw by

$$2\pi h = p$$

Thus for this H-pair the VMS can be written in terms of one component, as must be the case for any f = 1 coupling.

$$V^{\,a} = \{0,\ 0,\ V_3{}^a,\ 0,\ 0,\ hV_3{}^a\}$$

Normally it is necessary to use the superscript a to identify the coupling associated with the components. However, while discussing individual couplings this is not necesary and the superscript can be implied unless a network is examined, although the superscript a is essential for the local axes to distinguish them from the global axes.

The local FMS F_ℓ has components that can be found by using the reciprocity condition

$$V_\ell \cdot F_\ell = 0$$

Thus, if j and i were integral, all six components of force could be transmitted and the FMS would be

$$F_\ell = \{F_1, F_2, F_3, F_4, F_5, F_6\}$$

where F_1, F_2, F_3 are components of moments about the local axes respectively and F_4, F_5, F_6 are the components of force along these axes. The reciprocity condition requires that

$$[0, 0, V_3, 0, 0, hV_3] \begin{bmatrix} F_1 \\ F_2 \\ F_3 \\ F_4 \\ F_5 \\ F_6 \end{bmatrix} = [0]$$

because there is only one degree of freedom, and so

$$V_3 F_3 + hV_3 F_6 = 0$$

and $$F_3 = -hF_6$$

while the four other components remain undetermined and can therefore take any value,

thus $$F_\ell = \{F_1, F_2, -hF_6, F_4, F_5, F_6\}$$

It may be helpful in understanding the two subspaces to consider Figure 2. Here a closed loop has been formed from members i and j so that they are integral one with the other. Assuming there to be no friction in the H-pair then if there is to be any force built into the circuit with a component F_6 along the $x_3{}^a$ axis then there must also be a moment $-hF_6$ about this same axis. Such a force and moment would arise, for example, because of a differential expansion caused by a temperature change in the limb labelled X relative to the male part of the screw. The reciprocity condition we have used is essentially the application of the transpose of the KCL law to this circuit {4}: the row vector $V_\ell{}^a$ being the freedom matrix.

We could equally well derive the VMS from the FMS. The difference is that there are five reprocity conditions to be met instead of one because the coupling imposes five constraints.

$$\begin{bmatrix} F_1 & 0 & 0 & 0 & 0 & 0 \\ 0 & F_2 & 0 & 0 & 0 & 0 \\ 0 & 0 & 0 & F_4 & 0 & 0 \\ 0 & 0 & 0 & 0 & F_5 & 0 \\ 0 & 0 & -hF_6 & 0 & 0 & F_6 \end{bmatrix} \begin{bmatrix} V_1 \\ V_2 \\ V_3 \\ V_4 \\ V_5 \\ V_6 \end{bmatrix} = \begin{bmatrix} 0 \\ 0 \\ 0 \\ 0 \\ 0 \\ 0 \end{bmatrix}$$

whence since $F_1 \neq 0$, $V_1 = 0$, and likewise $V_2 = V_4 = V_5 = 0$

and $$-hF_6\, V_3 + F_6\, V_6 = 0$$

hence $$V_6 = hV_3$$

It is not difficult to see that the local subspaces for a cylindrical pair B are

$$V_\ell{}^b = \{0,\ 0,\ V_3{}^b,\ 0,\ 0,\ V_6{}^b\}$$

$$F_\ell{}^b = \{F_1{}^b,\ F_2{}^b,\ 0,\ F_4{}^b,\ F_5{}^b,\ 0\}$$

provided that the cylinder axis coincides with the $x_3{}^b$ axis. If the procedure explained in {1} had been used this coupling would have been dissociated into two joints, which could be equivalent to an R-pair and a P-pair in series labelled B_1 and B_2 and the velocity components would have been written as Lagrangian velocities $\dot{\psi}_{b1}$ and $\dot{\psi}_{b2}$.

2. The Velocity Transformation

We now seek the matrix M_v that will transform the components of any VMS from a local frame to one referred to a global frame having origin O and axes x_1, x_2, x_3. The local VMS, $V_\ell{}^a$ for a coupling A, becomes V^a without the subscript ℓ. The components of V^a are the 3 angular velocities of j wrt i about the global axes and the velocities of the point O in j wrt i. We begin with the general spatial case and then extract the submatrices that are sufficient for planar transformations.

2.1 Spatial transformations

The transformation can be performed in two stages and there are good reasons for doing this, one being that sometimes only one of the two transformations is required. The first transformation causes the VMS to be restated wrt a frame having the same origin O^a as the local frame but with axes parallel to the global axis as shown by dotted lines in Figure 2.1 . This rotation of axes is followed by a second transformation that restates the VMS wrt the global frame. The two transformations can each be expressed by 6 x 6 matrices R and T_v whereby

$$V^a = T_v \, R \, V_l{}^a$$

where $R = \begin{bmatrix} C & O \\ O & C \end{bmatrix}$ and $T_v = \begin{bmatrix} I & O \\ S & I \end{bmatrix}$

These expressions are similar to those used by Woo and Freudenstein {6, p 434, equation 3.1} with one minor departure that is now

explained in the following discussion of the 3 x 3 submatrices **I**, **C** and S. **I** is a 3 x 3 unit matrix. The submatrix **C** is **A** in {6} where "**A** is the rotation matrix, sometimes called the (3 x 3) orthogonal matrix". The components of **C** are not provided in {6} but they are by Jaeger {7. p 9, equation 1.12} who uses the symbol λ, and calls it the direction cosine matrix. As explained earlier we shall avoid Greek symbols where possible, and here we use **C** where

$$\mathbf{C} = \begin{bmatrix} c_{11} & c_{12} & c_{13} \\ c_{21} & c_{22} & c_{23} \\ c_{31} & c_{32} & c_{33} \end{bmatrix}$$

A clear understanding of the meaning of these elements is vital. c_{ij} is the cosine of the angle between the i^{th} axis of the global frame and j^{th} axis of the local frame. The nine elements **C** are not independent: there are six relationships between them provided by Jaeger {7, p 15, equation 2.5} as follows:

$$\begin{aligned} c_{11}^2 + c_{12}^2 + c_{13}^2 &= 1 \\ c_{21}^2 + c_{22}^2 + c_{23}^2 &= 1 \\ c_{31}^2 + c_{32}^2 + c_{33}^2 &= 1 \\ c_{11}c_{21} + c_{12}c_{22} + c_{13}c_{23} &= 0 \\ c_{21}c_{31} + c_{22}c_{32} + c_{23}c_{33} &= 0 \\ c_{31}c_{11} + c_{32}c_{12} + c_{33}c_{13} &= 0 \end{aligned}$$

The first three are called normalisation conditions and express the fact that the elements of **C** are direction cosines not direction ratios. The last three are called orthogonality conditions and express the fact that the axes of the frames are mutually perpendicular.

The (3 x 3) submatrix **S** is provided by Woo and Freudenstein {6, p 435, equation 3.4}:

$$\mathbf{S} = \begin{bmatrix} 0 & -z & y \\ z & 0 & -x \\ -y & x & 0 \end{bmatrix}$$

where x, y, z are the coordinates of O^a in the global frame.

We can now write the product

$$M_V = T_V R = \begin{bmatrix} C & 0 \\ SC & C \end{bmatrix}$$

where $SC = \begin{bmatrix} -zc_{21} + yc_{31} & -zc_{22} + yc_{32} & -zc_{23} + yc_{33} \\ zc_{11} - xc_{31} & zc_{12} - xc_{32} & zc_{13} - xc_{33} \\ -yc_{11} + xc_{21} & -yc_{12} + xc_{22} & -yc_{13} + xc_{23} \end{bmatrix}$

3. A Summary of Transformations for Motors and their Subspaces

Velocity motors and VMS

SPATIAL

$$T_V = \begin{bmatrix} I & 0 \\ S & I \end{bmatrix}$$

$$M_V = T_V R = \begin{bmatrix} C & 0 \\ SC & C \end{bmatrix}$$

PLANAR

$$M_{PV} = T_{PV} R_P = \begin{bmatrix} 1 & 0 & 0 \\ y & c_{11} & c_{12} \\ -x & c_{21} & c_{22} \end{bmatrix}$$

Force motors and FMS

SPATIAL

$$T_F = \begin{bmatrix} I & S \\ 0 & I \end{bmatrix}$$

$$M_F = T_F R$$

$$= \begin{bmatrix} I & S \\ 0 & I \end{bmatrix} \begin{bmatrix} C & 0 \\ 0 & C \end{bmatrix} = \begin{bmatrix} C & SC \\ 0 & C \end{bmatrix}$$

PLANAR

$$T_{PF} = \begin{bmatrix} 1 & -y & x \\ 0 & 1 & 0 \\ 0 & 0 & 1 \end{bmatrix}$$

$$T_{PV} = \begin{bmatrix} 1 & 0 & 0 \\ y & 1 & 0 \\ -x & 0 & 1 \end{bmatrix}$$

$$M_{PF} = \begin{bmatrix} 1 & -y & x & 1 & 0 & 0 \\ 0 & 1 & 0 & 0 & c_{11} & c_{12} \\ 0 & 0 & 1 & 0 & c_{21} & c_{22} \\ 1 & -yc_{11}+ & xc_{21} & -yc_{12}+ & xc_{22} & \\ 0 & c_{11} & & c_{12} & & \\ 0 & c_{21} & & c_{22} & & \end{bmatrix}$$

COMMON

$$R = \begin{bmatrix} C & 0 \\ & \\ 0 & C \end{bmatrix} \qquad SC = \begin{bmatrix} -zc_{21} + yc_{31} & -zc_{22} + yc_{32} & -zc_{23}+ yc_{33} \\ zc_{11} - xc_{31} & zc_{12} - xc_{32} & zc_{13} - xc_{33} \\ -yc_{11} + xc_{21} & -yc_{12} + xc_{22} & -yc_{13} + xc_{23} \end{bmatrix}$$

$$c_{11}^2 + c_{12}^2 + c_{13}^2 = 1$$
$$c_{21}^2 + c_{22}^2 + c_{23}^2 = 1$$
$$c_{31}^2 + c_{32}^2 + c_{33}^2 = 1$$
$$c_{11}c_{21} + c_{12}c_{22} + c_{13}c_{23} = 0$$
$$c_{21}c_{31} + c_{22}c_{32} + c_{23}c_{33} = 0$$
$$c_{31}c_{11} + c_{32}c_{12} + c_{33}c_{13} = 0$$

$$R_p = \begin{bmatrix} 1 & 0 & 0 \\ 0 & c_{11} & c_{12} \\ 0 & c_{21} & c_{22} \end{bmatrix} \qquad S = \begin{bmatrix} 0 & -z & y \\ z & 0 & -x \\ -y & x & 0 \end{bmatrix} \qquad C = \begin{bmatrix} c_{11} & c_{12} & c_{13} \\ c_{21} & c_{22} & c_{23} \\ c_{31} & c_{32} & c_{33} \end{bmatrix}$$

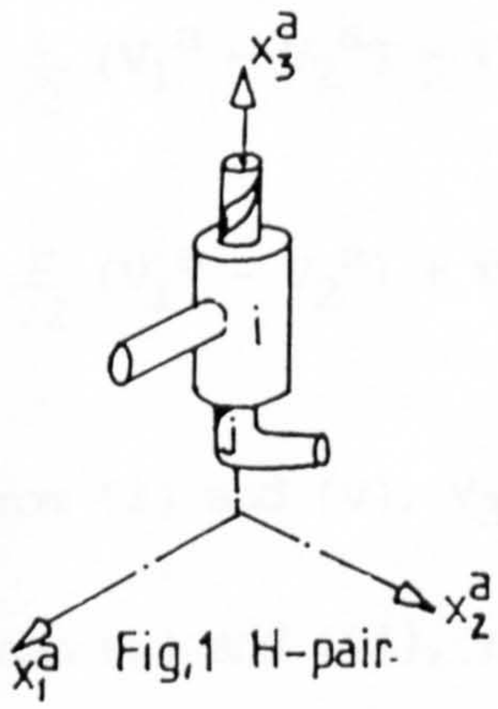

Fig,1 H-pair

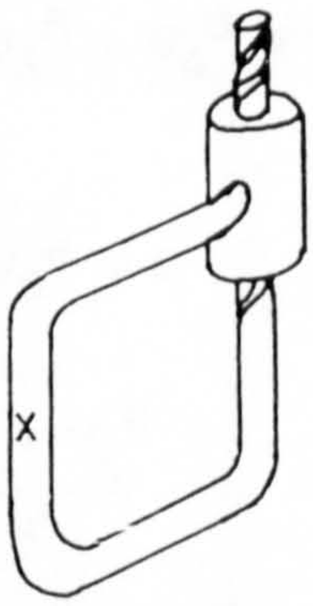

Fig,2 Closed Loop formed in H-pair

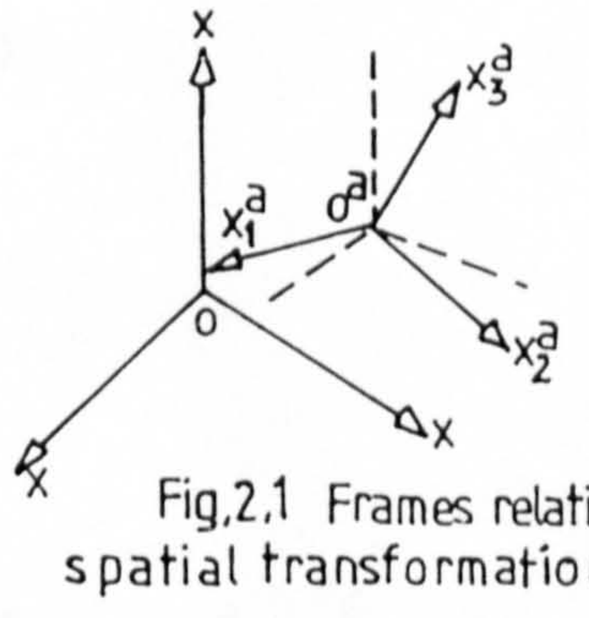

Fig,2.1 Frames relating spatial transformations

APPENDIX TO CHAPTER 7
(APPENDIX D)

SOLUTIONS TO THE ANALYSIS OF THE 3-DEGREE OF FREEDOM MANIPULATOR (METHOD I)

This appendix presents the detailed working procedure of the solutions to the 12 equations of circuits 1 and 2 (Section 7.1.1) derived by the application of Kirchoff's Laws [3]. The figures mentioned here relate directly to those in the main chapter.

1. Solutions to the 12 equations derived from the two circuits of Figure 7.1.1(b)

Circuit (1) (Figs.7.1.1 (a) and (b))

i) $$\frac{V_1^a - V_2^a}{\sqrt{2}} - V_2^d = 0$$

ii) $$\frac{V_1^a + V_2^a}{\sqrt{2}} + V_1^d = 0$$

iii) $$V_3^a + V_3^d = 0$$

iv) $$\frac{-\ell}{\sqrt{2}} (V_1^a + V_2^a) - \ell V_1^d - r V_3^a + V_5^c = 0$$

v) $$\frac{\ell}{\sqrt{2}} (V_1^a - V_2^a) - \ell V_2^d - r V_3^d + V_4^d + V_5^b = 0$$

vi) $$\frac{r}{\sqrt{2}} (V_1^a - V_2^a) + r.V_1^d + V_6^a = 0$$

a) From (i) and (v), $V_3^d = \dfrac{V_4^d + V_5^b}{r}$

b) From (i) and (vi), $r V_2^d + r V_1^d + V_6^a = 0 \rightarrow V_1^d = -(V_2^d + \dfrac{V_6^a}{r})$

c) From (ii) and (iv), $V_3^a = \dfrac{V_5^c}{r}$

d) From (i) and (ii), (i) + (ii) yields $V_1{}^a = \frac{V_2{}^d - V_1{}^d}{\sqrt{2}}$; and

(ii) - (i) gives $V_2{}^a = -\frac{(V_1{}^d + V_2{}^d)}{\sqrt{2}}$

Circuit (2) (Figs.7.1.1(a) and (b)):

i) $V_2{}^d = V_2{}^e$

ii) $V_1{}^d = V_1{}^e$

iii) $V_3{}^d = V_3{}^e$

iv) $\ell V_1{}^d + \ell V_1{}^e - V_3{}^e . \frac{\lambda e}{\sqrt{2}} - V_5{}^c + \frac{V_5{}^f}{\sqrt{2}} = 0$

v) $\ell V_2{}^d + \ell V_2{}^e + rV_3{}^d - V_3{}^e \frac{\lambda e}{\sqrt{2}} - V_4{}^d - \frac{V_5^f}{\sqrt{2}} = 0$

vi) $\frac{\lambda e}{\sqrt{2}} V_1{}^e - rV_1{}^d - \frac{\lambda e}{\sqrt{2}} V_2{}^e + V_6{}^e = 0$

From (ii) and (iv)

$$V_1{}^d = V_1{}^e = \frac{1}{2\ell} (V_3{}^e \frac{\lambda e}{\sqrt{2}} + V_5{}^c - \frac{V_5{}^f}{\sqrt{2}}) \qquad (a)$$

From (i), (iii) and (v)

$$V_2{}^d = V_2{}^e = \frac{1}{2\ell} [V_3{}^d (\frac{\lambda e}{\sqrt{2}} - r) + V_4{}^d + \frac{V_5{}^f}{\sqrt{2}}]$$

or $$V_2{}^d = V_2{}^e = \frac{1}{2\ell} [V_3{}^e (\frac{\lambda e}{\sqrt{2}} - r) + V_4{}^d + \frac{V_5{}^f}{\sqrt{2}}] \qquad (b)$$

From (ii) and (vi)

$$V_1{}^d = V_1{}^e = \frac{\{V_2{}^e \frac{\lambda e}{\sqrt{2}} - V_6{}^e\}}{(\frac{\lambda e}{\sqrt{2}} - r)} \qquad (c)$$

SOLUTIONS

From circuits (1) (iii) and (c) and 2(iii)

$$V_3{}^a = - V_3{}^d = - V_3{}^e = \frac{V_5{}^c}{r} \qquad [A]$$

From circuit 1(a) and [A] above,

$$V_4^d = -(V_5^b + V_5^c) \qquad [B]$$

From circuit 2(a) and [A] above,

$$V_1^d = V_1^e = \frac{1}{2\ell}\{V_5^c\,(1 - \frac{\lambda e}{r\sqrt{2}}) - \frac{V_5^f}{\sqrt{2}}\} \qquad [C]$$

From circuit 2(b) and [A] and [B] above,

$$V_2^d = V_2^e = \frac{1}{2\ell}[V_5^c\,(1 - \frac{\lambda e}{r\sqrt{2}}) - V_5^b - V_5^c + \frac{V_5^f}{\sqrt{2}}]$$

$$= \frac{1}{2\ell}[\frac{V_5^f}{\sqrt{2}} - V_5^b - \frac{\lambda e}{r\sqrt{2}}\,V_5^c] \qquad [D]$$

From circuit (1)(d) and [C] and [D] above,

$$V_1^a = \frac{V_2^d - V_1^d}{\sqrt{2}} = \frac{1}{2\ell}\cdot\frac{1}{\sqrt{2}}\{2\,\frac{V_5^f}{\sqrt{2}} - V_5^b - V_5^c\}$$

$$= \frac{1}{\ell\sqrt{2}}\{\frac{V_5^f}{\sqrt{2}} - (\frac{V_5^b + V_5^c}{2})\} \qquad [E]$$

and $$V_2^a = -\frac{(V_2^d + V_1^d)}{\sqrt{2}} = -\frac{1}{2\sqrt{2}}\,\frac{1}{\ell}\,(V_5^c\,(1 - \frac{2\lambda e}{r\sqrt{2}}) - V_5^b)$$

$$= -\frac{\sqrt{2}}{4\ell}\{V_5^c\,(1 - \frac{2\lambda e}{r\sqrt{2}}) - V_5^b\} \qquad [F]$$

From circuit (2)(c) and [C] and [D] above,

$$V_1^d = V_1^e = \frac{\{V_2^e\cdot\frac{\lambda e}{\sqrt{2}} - V_6^e\}}{(\frac{\lambda e}{\sqrt{2}} - r)}$$

or $$V_6^e = -V_1^d\,(\frac{\lambda e}{\sqrt{2}} - r) + V_2^e\,\frac{\lambda e}{\sqrt{2}}$$

$$= \frac{1}{2\ell}\,(r - \frac{\lambda e}{\sqrt{2}})(V_5^c\,(1 - \frac{\lambda e}{r\sqrt{2}}) - \frac{V_5^f}{\sqrt{2}}) + \frac{\lambda e}{\sqrt{2}}\,(\frac{V_5^f}{\sqrt{2}} - V_5^b - \frac{\lambda e}{r\sqrt{2}}\,V_5^c)\,\frac{1}{2\ell}$$

$$= \frac{1}{2\ell}\,[V_5^c\{r(1 - \frac{\lambda e}{r\sqrt{2}})^2 - \frac{\lambda_e^2}{r(\sqrt{2})^2}\} + V_5^f\{\frac{\lambda e}{2} - \frac{1}{\sqrt{2}}\,(r - \frac{\lambda e}{\sqrt{2}})\} - V_5^b\,\frac{\lambda e}{\sqrt{2}}]$$

$$= \frac{1}{2\ell}\left[V_5^{c}\{r-\lambda e\sqrt{2} + \frac{\lambda^2 e}{2r} - \frac{\lambda^2 e}{2r}\} + V_5^{f}\{\frac{\lambda e}{2} + \frac{\lambda e}{2} - \frac{r}{\sqrt{2}}\} - \frac{V_5^{b}\cdot\lambda_e}{}\right]$$

$$= \frac{1}{2\ell}\left[V_5^{c}\{r - \lambda e\sqrt{2}\} + V_5^{f}\,(\lambda_e - \frac{r}{\sqrt{2}}) - V_5^{b}\,\frac{\lambda_e}{\sqrt{2}}\right]$$

From circuit (1)(b) and [C] and [D] above,

$$V_6^{a} = -r\,(V_1^{d} + V_2^{d}) = \frac{-r}{2\ell}\,(V_5^{c}\,\{1 - \frac{2\lambda e}{r\sqrt{2}}\} - V_5^{b})$$

$$= \frac{r}{2\ell}\,\{V_5^{b} - V_5^{c}\,(1 - \frac{2\lambda e}{r\sqrt{2}})\}$$

2. <u>Selection of a path from body 1 to 3 and summation of velocity vectors:</u>

$$\{V^a\} + \{V^b\} = \begin{bmatrix} V_1^{a} \\ V_2^{a} \\ V_3^{a} \\ -(\ell V_2^{a} + V_3^{a}.r\cos\theta) + V_5^{b}\sin\theta \\ (\ell V_1^{a} + V_3^{a}.r\sin\theta) + V_5^{b}\cos\theta \\ (V_1^{a}\,r\cos\theta - V_2^{a}\,r\sin\theta + V_6^{a}) \end{bmatrix}$$

$$= \begin{bmatrix} \frac{1}{\ell\sqrt{2}}\{\frac{V_5^{f}}{\sqrt{2}} - \frac{V_5^{b}+V_5^{c}}{2}\} \\ -\frac{1}{2\sqrt{2}\ell}\{V_5^{c}\,(1 - \frac{2\lambda e}{r\sqrt{2}}) - V_5^{b}\} \\ \frac{V_5^{c}}{r} \\ -\{(-\frac{1}{2\sqrt{2}}(V_5^{c}(1-\frac{2\lambda e}{r\sqrt{2}}) - V_5^{b}) + \frac{V_5^{c}r}{r\sqrt{2}}\} + \frac{V_5^{b}}{\sqrt{2}} \\ \frac{1}{\sqrt{2}}\{\frac{V_5^{f}}{\sqrt{2}} - \frac{(V_5^{b}+V_5^{c}}{2}\} + \frac{V_5^{c}}{r}\frac{r}{\sqrt{2}} + \frac{V_5^{b}}{\sqrt{2}} \\ [\frac{r}{2\ell}\{\frac{V_5^{f}}{\sqrt{2}} - \frac{(V_5^{b}+V_5^{c}}{2}\} + \frac{r}{4\ell}\{V_5^{c}(1-\frac{2\lambda e}{r\sqrt{2}}) - V_5^{b}\} \\ + \frac{r}{2\ell}\{V_5^{b} - V_5^{c}\,(1 - \frac{2\lambda e}{r\sqrt{2}})\}] \end{bmatrix}$$

$$\begin{bmatrix} \frac{V_5^{f}\sqrt{2}-(V_5^{b}+V_5^{c})}{2\sqrt{2}\ell} \\ \frac{1}{2\sqrt{2}\ell}\{V_5^{b}-V_5^{c}(1-\frac{2\lambda e}{r\sqrt{2}})\} \\ V_5^{c}/r \\ \frac{1+\sqrt{2}}{\sqrt{2}}V_5^{b}+\frac{(3r-\sqrt{2}\lambda e)}{2\sqrt{2}r}V_5^{c} \\ \frac{V_5^{b}}{2\sqrt{2}}+V_5^{c}/2\sqrt{2}+V_5^{f}/2\sqrt{2} \\ V_5^{c}\{\frac{\lambda e}{2\sqrt{2}\ell}-\frac{r}{2\ell}\} \end{bmatrix} = \begin{bmatrix} \frac{V_5^{f}\sqrt{2}-(V_5^{b}+V_5^{c})}{2\sqrt{2}\ell} \\ \frac{1}{2\sqrt{2}\ell}\{V_5^{b}-V_5^{c}(1-\frac{2\lambda e}{r\sqrt{2}})r\} \\ V_5^{c}/r \\ \frac{(1+\sqrt{2})}{\sqrt{2}}V_5^{b}+\frac{(3r-\sqrt{2}\lambda e)}{2\sqrt{2}r}V_5^{c} \\ (V_5^{b}+V_5^{c}+V_5^{f})/2\sqrt{2} \\ V_5^{c}\{\frac{\lambda e-r\sqrt{2}}{2\sqrt{2}\ell}\} \end{bmatrix}$$

The final solutions to these equations are presented at the end of Section 7.1.1.

APPENDIX TO CHAPTER 7
(APPENDIX E)
THE ANALYSIS OF A 4-DEGREE OF FREEDOM MANIPULATOR
(METHOD I)

The analysis of the small displacements of point O located on the surface of this manipulator (Figure 7.1.2(a)) is presented in stages as outlined below. The sequence of figure numbering in this Appendix relate directly to those in the main chapter (section 7.1.2).

1. Selection of the position of global frame with origin at O on the surface of body 3 is given in Figure 7.1.2(a)
2. Setting of local frames and the corresponding velocity components.

i) Coupling A:(Fig.7.1.2(c))

This coupling has five degrees of freedom and hence five velocity components. The local frame is set with $X_2{}^a$ along the common normal and O^a at the point of contact between bodies 1 and 2.

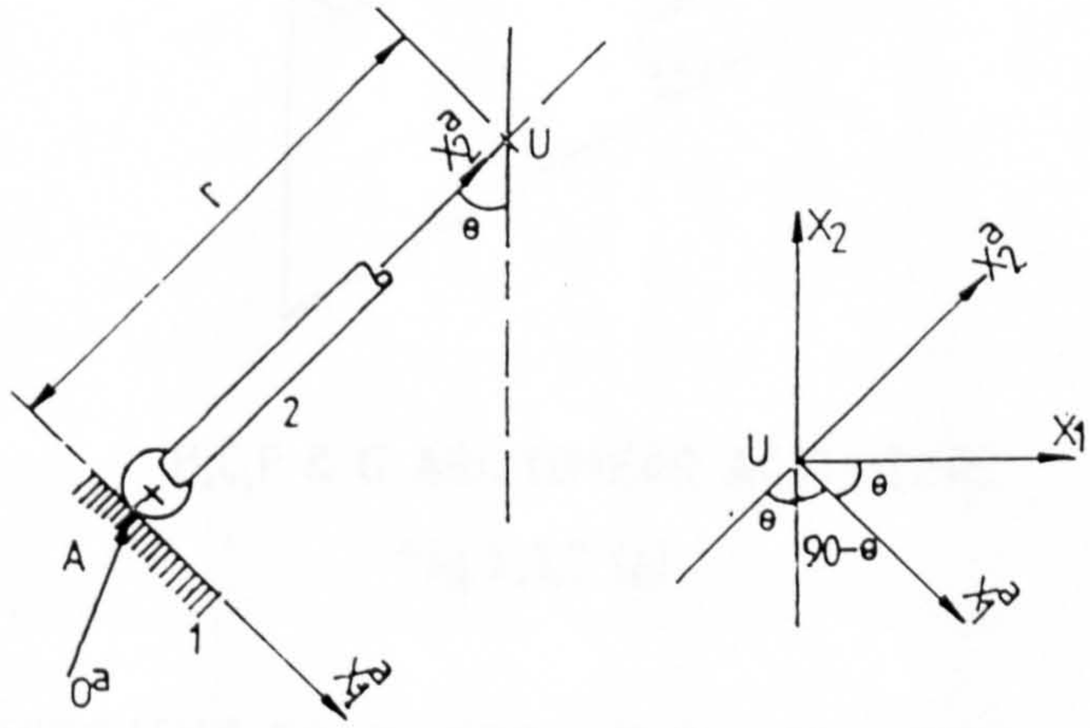

Fig.7.1.2 (c)

The local velocity vector is given by $\{V_\ell^a\} =$

$$\begin{bmatrix} V_1{}^a \\ V_2{}^a \\ V_3{}^a \\ V_4{}^a \\ 0 \\ V_6{}^a \end{bmatrix}$$

	$x_1{}^a$	$x_2{}^a$	$x_3{}^a$
x_1	θ	$90^o-\theta$	90^o
x^2	$90^o+\theta$	θ	90^o
x_3	90^o	90^o	0^o

Table of angles between the local and global frames.

SUPPORT OF A 4-DEGREE OF FREEDOM MANIPULATOR (E&H EACH MAKES 2 POINT CONTACTS AND A&D EACH MAKES 1 POINT CONTACT)

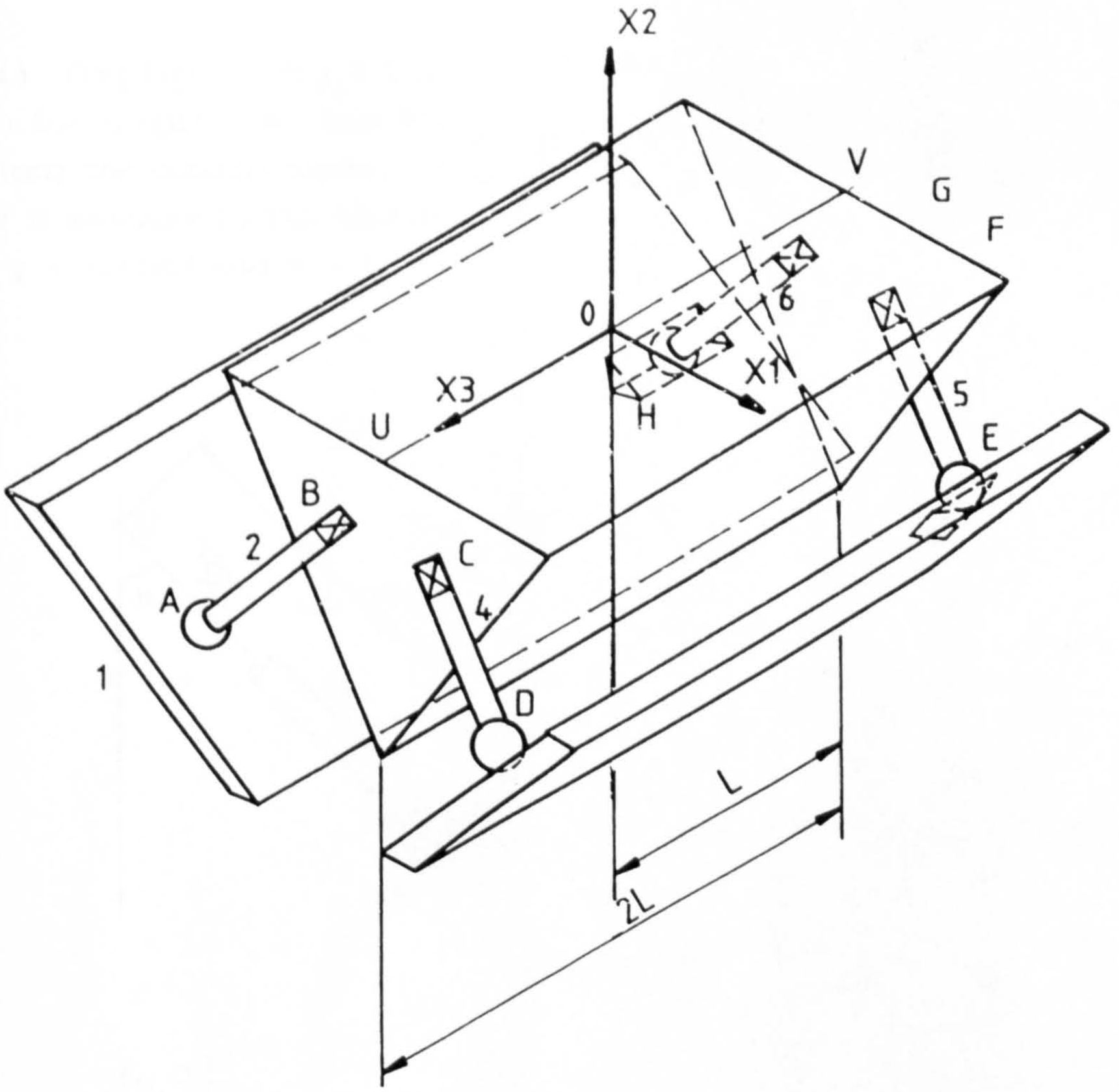

B,C,F & G ARE LINEAR ACTUATORS

Fig, 7 ,1,2 (a)

CONSTRAINT GRAPH FOR THE MANIPULATOR (ABOVE)

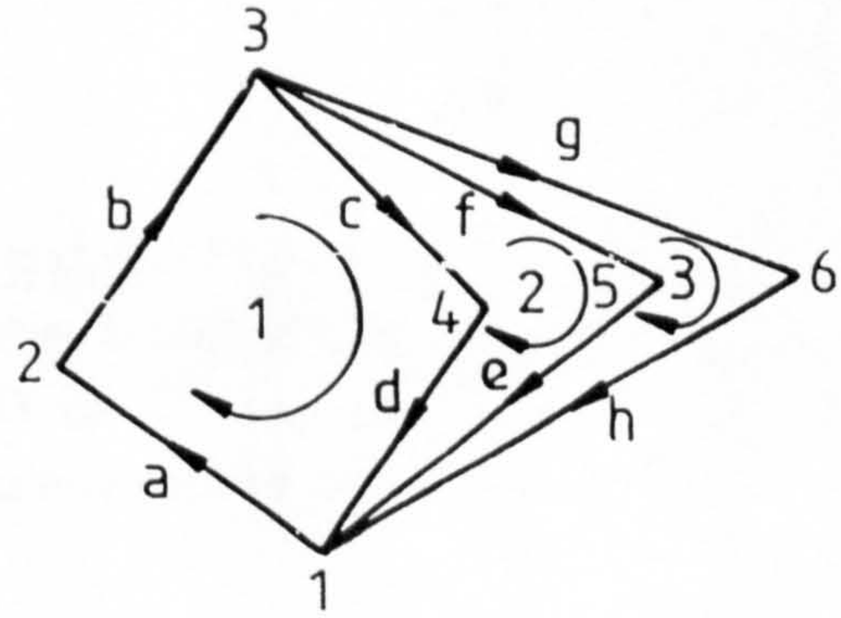

Fig, 7 ,1,2 (b)

Position of O^a measured with respect to the global frame is given by $x = -r\sin\theta$, $y = -r\cos\theta$ and $z = \ell$.

ii) Coupling D:(Fig.7.1.2(d))
As for coupling A, this coupling has five velocity components. $X_2{}^d$ is along the common normal while O^d is at the point of contact. Position of D measured with respect to the global frame is given by $x = r\sin\theta$ $y = -r\cos\theta$ and $z = \ell$.

Fig.7.1.2 (d)

$$\{V_\ell{}^d\} = \begin{bmatrix} V_1{}^d \\ V_2{}^d \\ V_3{}^d \\ V_4{}^d \\ 0 \\ V_6{}^d \end{bmatrix}$$

	$X_1{}^d$	$X_2{}^d$	$X_3{}^d$
X_1	θ	$90^o+\theta$	90^o
X_2	$90^o-\theta$	θ	90^o
X_3	90^o	90^o	0^o

Table of angles between the local and global frames.

iii) Couplings B and C:(Figs.7.1.2(e) and (f))
For coupling B, the local frame can be set at either point U (no translation needed) or O^b (translation required) but both yield the same result when transformed to global frame.

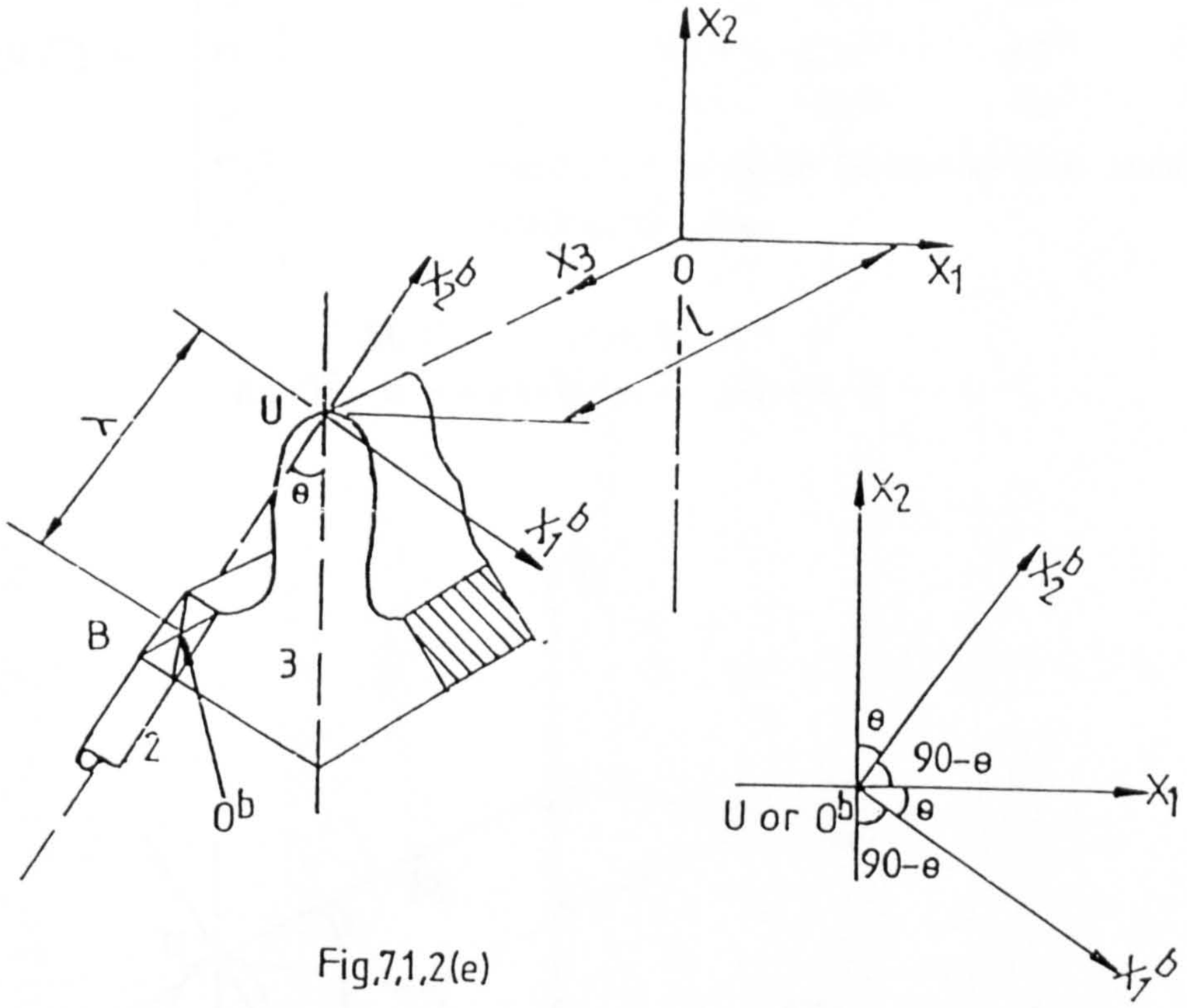

Fig.7.1.2(e)

At U, x = y = 0 and z = ℓ

At O^b, x = $-\lambda\sin\theta$, y = $-\lambda\cos\theta$, z = ℓ

$$\{V_\ell{}^b\} = \begin{bmatrix} 0 \\ 0 \\ 0 \\ 0 \\ V_5{}^b \\ 0 \end{bmatrix}$$

	$X_1{}^b$	$X_2{}^b$	$X_3{}^b$
X_1	θ	$90^o-\theta$	90^o
X_2	$90^o+\theta$	θ	90^o
X_3	90^o	90^o	0^o

Table of angles between the local and global frames.

Like in coupling B, the local frame for actuator C can be set either at U (in which case only rotation is required) or at O^C where both rotation and translation are needed but both will give the same result.

$$\{V_\ell{}^C\} = \begin{bmatrix} 0 \\ 0 \\ 0 \\ 0 \\ V_5{}^C \\ 0 \end{bmatrix}$$

	$X_1{}^C$	$X_2{}^C$	$X_3{}^C$
X_1	$180^O - \theta$	$90^O - \theta$	90^O
X_2	$90^O + \theta$	$180^O - \theta$	90^O
X_3	90^O	90^O	0^O

Table of angles between the local and global frames.

At U, $x = y = 0$, $z = \ell$

At O^C, $x = \lambda \sin\theta$, $y = -\lambda\cos\theta$, $z = \ell$

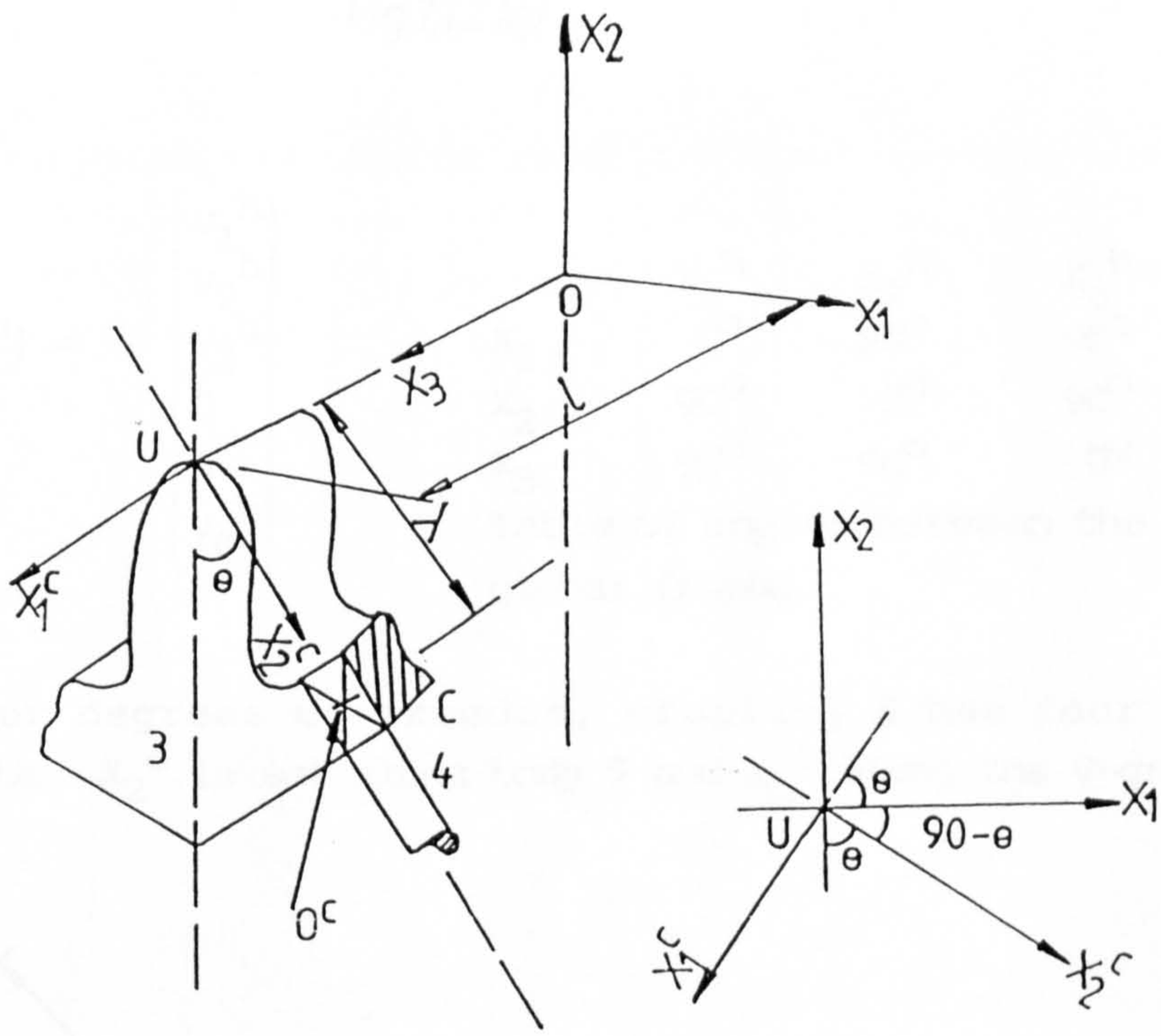

Fig. 7.1.2(f)

iv) Couplings E and H: (Figs. 7.1.2(g) and (h))

The local frame for coupling H is set (at O^h) parallel to the global frame so that only translation is required. Position of O^h with respect to the global frame is given by $x = -r\sin\theta$, $y = -r\cos\theta$, $z = -\ell$.

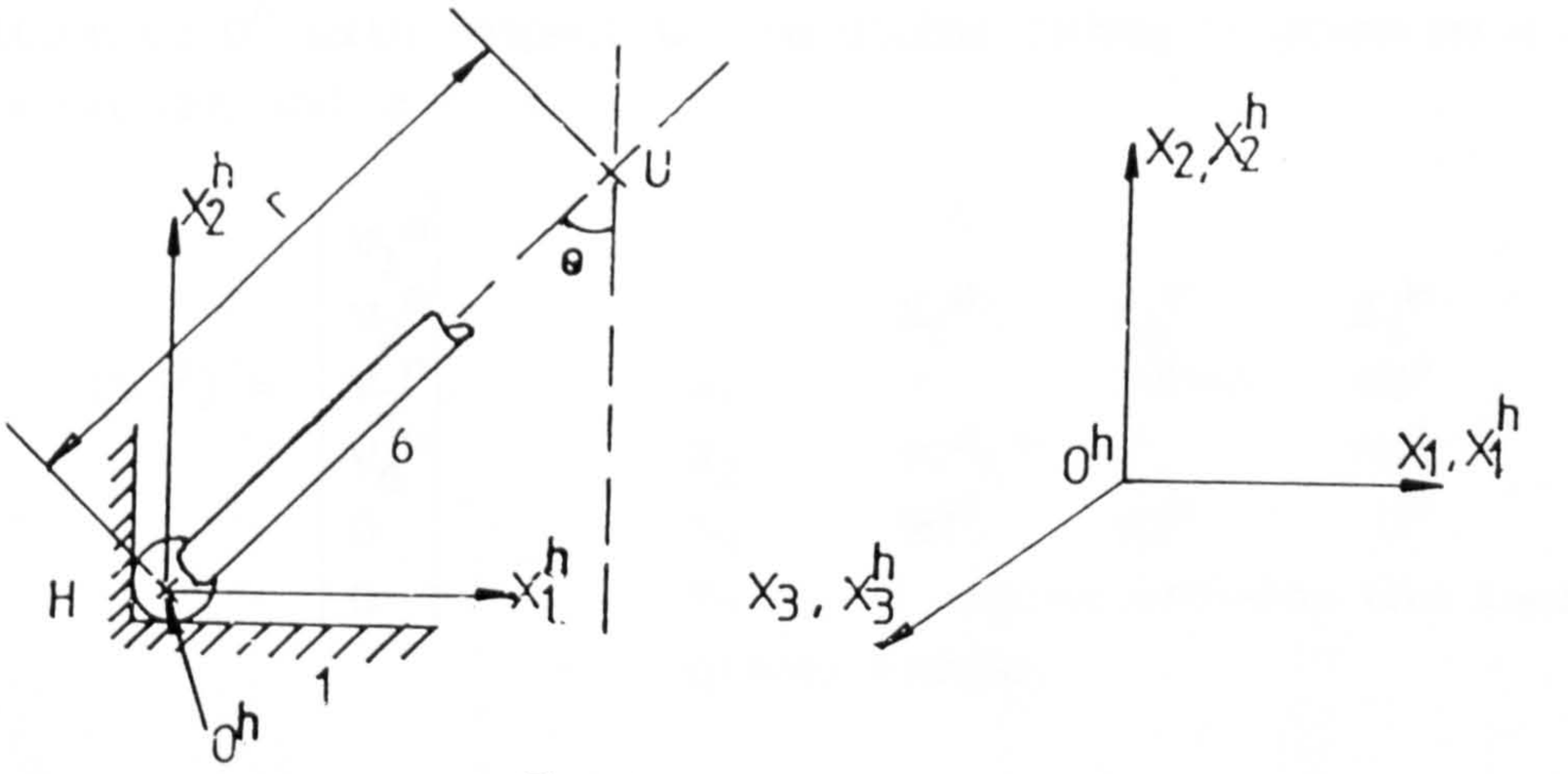

Fig,7,1,2 (g)

$$\{V_\ell{}^h\} = \begin{Bmatrix} V_1{}^h \\ V_2{}^h \\ V_3{}^h \\ 0 \\ 0 \\ V_6{}^h \end{Bmatrix}$$

	$X_1{}^h$	$X_2{}^h$	$X_3{}^h$
X_1	0^o	90^o	90^o
X_2	90^o	0^o	90^o
X_3	90^o	90^o	0^o

Table of angles between the local and global frames.

With four degrees of freedom, coupling E has four velocity components. $X_2{}^e$ is set along body 5 and $X_1{}^e$ along the V-groove.

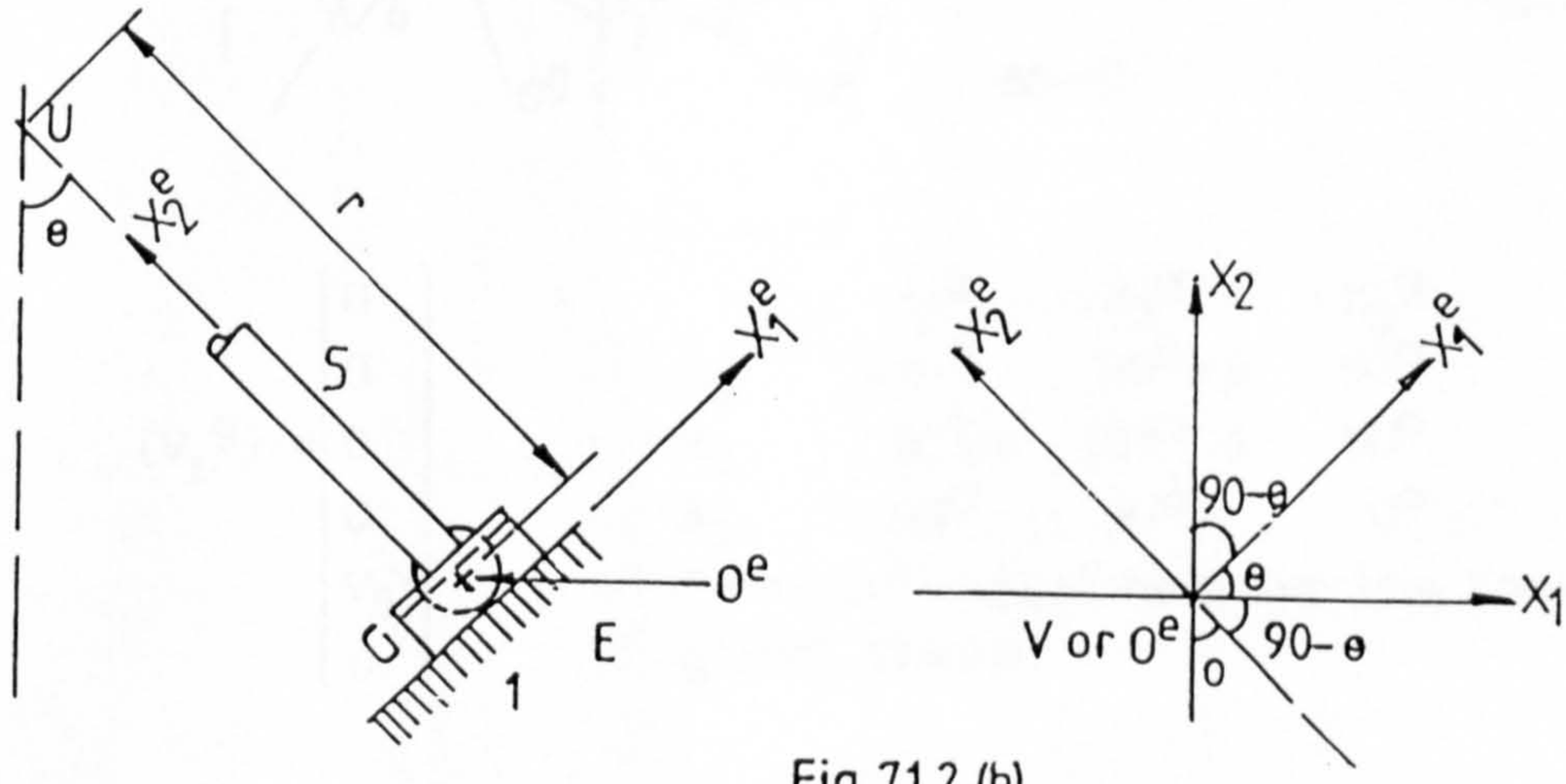

Fig, 7,1,2 (h)

Position of O^e with respect to the global frame is given by $x = r\sin\theta$
$y = -r\cos\theta$, and $z = -\ell$.

$$\{V_\ell{}^e\} = \begin{Bmatrix} V_1{}^e \\ V_2{}^e \\ V_3{}^e \\ V_4{}^e \\ 0 \\ 0 \end{Bmatrix}$$

	$X_1{}^e$	$X_2{}^e$	$X_3{}^e$
X_1	θ	$90^o+\theta$	90^o
X_2	$90^o-\theta$	θ	90^o
X_3	90^o	90^o	0^o

Table of angles between the local and global frames.

V) Couplings F and G:(Figs.7.1.2(i) and (j))

Like in B, the local frame for G can be set at either O^g or V but the final result of transformation to the global frame will be the same.
Position of O^g with respect to the global frame is given by $x = -\lambda\sin\theta$
$y = -\lambda\cos\theta$ and $z = -\ell$.

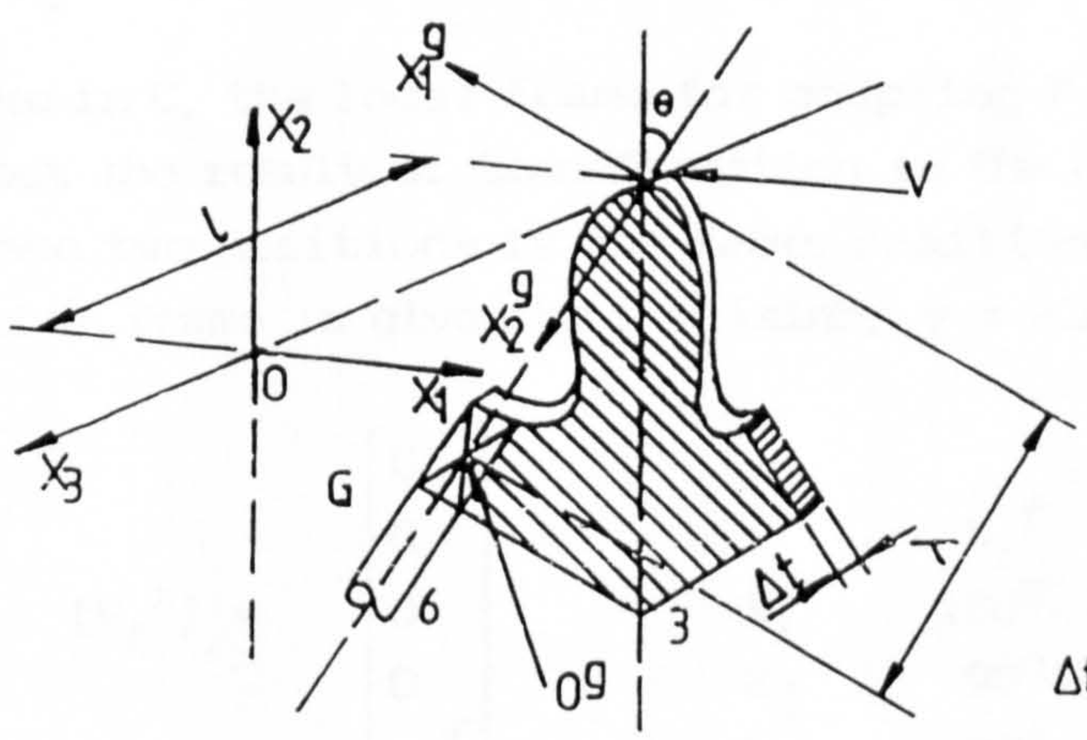

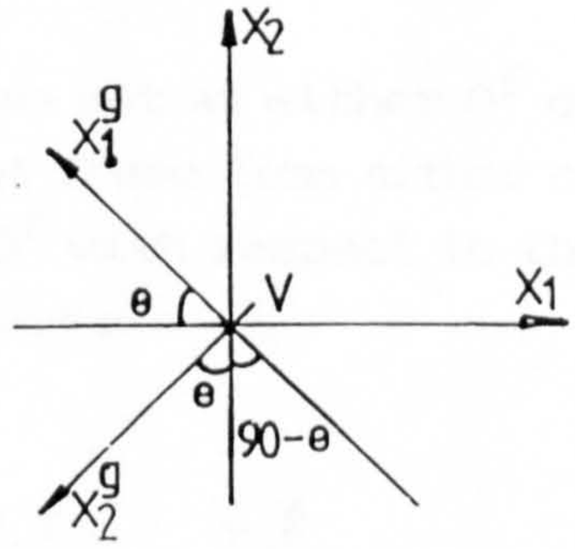

Fig.7.1.2 (i)

$$\{V_\ell{}^g\} = \begin{Bmatrix} 0 \\ 0 \\ 0 \\ 0 \\ V_5{}^g \\ 0 \end{Bmatrix}$$

	$X_1{}^g$	$X_2{}^g$	$X_3{}^g$
X_1	$180^o-\theta$	$90^o+\theta$	90^o
X_2	$90^o-\theta$	$180^o-\theta$	90^o
X_3	90^o	90^o	0^o

Table of angles between the local and global frames.

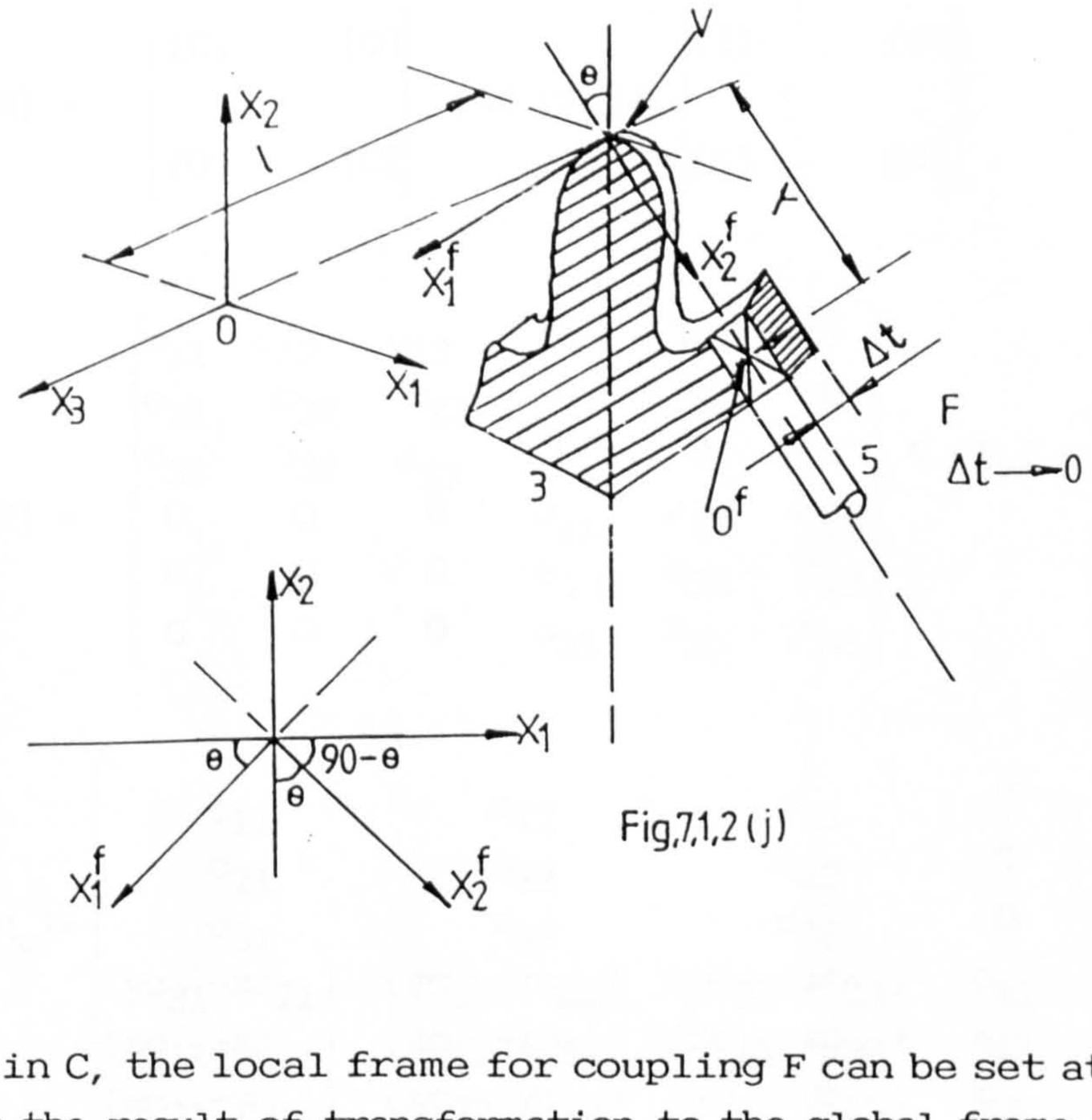

Fig,7,1,2 (j)

Like in C, the local frame for coupling F can be set at either 0^f or V but the result of transformation to the global frame from either of these two positions is the same. Position of 0^f with respect to the global frame is given by $x = \lambda\sin\theta$, $y = -\lambda\cos\theta$ and $z = -\ell$.

$$\{V_\ell{}^f\} = \begin{bmatrix} 0 \\ 0 \\ 0 \\ 0 \\ V_5{}^f \\ 0 \end{bmatrix}$$

	$X_1{}^f$	$X_2{}^f$	$X_3{}^f$
X_1	$180^o - \theta$	$90^o - \theta$	90^o
X_2	$90^o + \theta$	$180^o - \theta$	90^o
X_3	90^o	90^o	0^o

Table of angles between the local and global frames.

3. Transformation of Vectors to the Global Frame

$[M_V]$ is a matrix that transforms the components of any velocity motor subspace (VMS) from a local to global frame. $[M_V]$ and the accompanying matrices below are obtained from Appendix C.

$$\{V_a\} = [M_v]\{V_\ell^a\}, \qquad [M_v] = [T_v][R]$$

$$[R] = \begin{bmatrix} [C] & [O] \\ [O] & [C] \end{bmatrix} \text{ and } [T_v] = \begin{bmatrix} [I] & [O] \\ [S] & [I] \end{bmatrix}$$

$$\therefore [R] = \begin{bmatrix} c_{11} & c_{12} & c_{13} & 0 & 0 & 0 \\ c_{21} & c_{22} & c_{23} & 0 & 0 & 0 \\ c_{31} & c_{32} & c_{33} & 0 & 0 & 0 \\ 0 & 0 & 0 & c_{11} & c_{12} & c_{13} \\ 0 & 0 & 0 & c_{21} & c_{22} & c_{23} \\ 0 & 0 & 0 & c_{31} & c_{32} & c_{33} \end{bmatrix} \text{ \& } [T_v] = \begin{bmatrix} 1 & 0 & 0 & 0 & 0 & 0 \\ 0 & 1 & 0 & 0 & 0 & 0 \\ 0 & 0 & 1 & 0 & 0 & 0 \\ 0 & -z & y & 1 & 0 & 0 \\ z & 0 & -x & 0 & 1 & 0 \\ -y & x & 0 & 0 & 0 & 1 \end{bmatrix}$$

$$\therefore [M_v] = \begin{bmatrix} c_{11} & c_{12} & c_{13} & 0 & 0 & 0 \\ c_{21} & c_{22} & c_{23} & 0 & 0 & 0 \\ c_{31} & c_{32} & c_{33} & 0 & 0 & 0 \\ (yc_{31}-zc_{21}) & (yc_{32}-zc_{22}) & (yc_{33}-zc_{23}) & c_{11} & c_{12} & c_{13} \\ (zc_{11}-xc_{31}) & (zc_{12}-xc_{32}) & (zc_{13}-xc_{33}) & c_{21} & c_{22} & c_{23} \\ (xc_{21}-yc_{11}) & (xc_{22}-yc_{12}) & (xc_{23}-yc_{13}) & c_{31} & c_{32} & c_{33} \end{bmatrix}$$

i) <u>Couplings A and D</u>

For coupling A:

$$[M_v^a] = \begin{bmatrix} \cos\theta & \sin\theta & 0 & 0 & 0 & 0 \\ -\sin\theta & \cos\theta & 0 & 0 & 0 & 0 \\ 0 & 0 & 1 & 0 & 0 & 0 \\ z\sin\theta & -z\cos\theta & y & \cos\theta & \sin\theta & 0 \\ z\cos\theta & z\sin\theta & -x & -\sin\theta & \cos\theta & 0 \\ -(x\sin\theta+y\cos\theta) & (x\cos\theta-y\sin\theta) & 0 & 0 & 0 & 1 \end{bmatrix}$$

Now:

$$\{V^a\} = [M_v^a]\{V_\ell^a\} = \begin{bmatrix} (V_1^a\cos\theta + V_2^a\sin\theta) \\ (V_2^a\cos\theta - V_1^a\sin\theta) \\ V_3^a \\ (V_1^a z\sin\theta - V_2^a z\cos\theta + yV_3^a + V_4^a\cos\theta) \\ (z(V_1^a\cos\theta + V_2^a\sin\theta) - xV_3^a - V_4^a\sin\theta) \\ V_2^a(x\cos\theta - y\sin\theta) - V_1^a(x\sin\theta + y\cos\theta) + V_6^a \end{bmatrix}$$

But $z = \ell$, $x = -r\sin\theta$, $y = -r\cos\theta$.

$$\therefore \quad \{V^a\} = \begin{bmatrix} V_1{}^a\cos\theta+V_2{}^a\sin\theta \\ V_2{}^a\cos\theta-V_1{}^a\sin\theta \\ V_3{}^a \\ \ell(V_1{}^a\sin\theta-V_2{}^a\cos\theta)-V_3{}^a r\cos\theta+V_4{}^a\cos\theta \\ \ell(V_1{}^a\cos\theta+V_2{}^a\sin\theta)+V_3{}^a r\sin\theta-V_4{}^a\sin\theta \\ r.V_1{}^a+V_6{}^a \end{bmatrix}$$

For coupling D:

$$[M_v{}^d] = \begin{bmatrix} \cos\theta & -\sin\theta & 0 & 0 & 0 & 0 \\ \sin\theta & \cos\theta & 0 & 0 & 0 & 0 \\ 0 & 0 & 1 & 0 & 0 & 0 \\ -\ell\sin\theta & -\ell\cos\theta & -r\cos\theta & \cos\theta & -\sin\theta & 0 \\ \ell\cos\theta & -\ell\sin\theta & -r\sin\theta & \sin\theta & \cos\theta & 0 \\ r & 0 & 0 & 0 & 0 & 1 \end{bmatrix}$$

$$\{V^d\}=[M_v{}^d]\{V_\ell{}^d\} = \begin{bmatrix} V_1{}^d\cos\theta-V_2{}^d\sin\theta \\ V_1{}^d\sin\theta+V_2{}^d\cos\theta \\ V_3{}^d \\ -\ell(V_1{}^d\sin\theta+V_2{}^d\cos\theta)-V_3{}^d r\cos\theta+V_4{}^d\cos\theta \\ \ell(V_1{}^d\cos\theta-V_2{}^d\sin\theta)-V_3{}^d r\sin\theta+V_4{}^d\sin\theta \\ V_1{}^d r + V_6{}^d \end{bmatrix}$$

ii) Couplings B and C

For coupling B:

$$[M_v{}^b] = \begin{bmatrix} \cos\theta & \sin\theta & 0 & 0 & 0 & 0 \\ -\sin\theta & \cos\theta & 0 & 0 & 0 & 0 \\ 0 & 0 & 1 & 0 & 0 & 0 \\ z\sin\theta & -z\cos\theta & y & \cos\theta & \sin\theta & 0 \\ z\cos\theta & z\sin\theta & -x & -\sin\theta & \cos\theta & 0 \\ -(xs\theta+yc\theta) & (xc\theta-ys\theta) & 0 & 0 & 0 & 1 \end{bmatrix}$$

where $x = -\lambda\sin\theta$, $y = -\lambda\cos\theta$, $z = \ell$, $c\theta = \cos\theta$ and $s\theta = \sin\theta$.

$$\therefore \quad \{V^b\} = [M_v{}^b]\{V_\ell{}^b\} = \begin{bmatrix} 0 \\ 0 \\ 0 \\ V_5{}^b\sin\theta \\ V_5{}^b\cos\theta \\ 0 \end{bmatrix}$$

For coupling C:

$$[M_V^C] = \begin{bmatrix} -\cos\theta & \sin\theta & 0 & 0 & 0 & 0 \\ -\sin\theta & -\cos\theta & 0 & 0 & 0 & 0 \\ 0 & 0 & 1 & 0 & 0 & 0 \\ z\sin\theta & z\cos\theta & y & -\cos\theta & \sin\theta & 0 \\ -z\cos\theta & z\sin\theta & -x & -\sin\theta & -\cos\theta & 0 \\ (y\cos\theta - x\sin\theta) & (y\sin\theta - x\cos\theta) & 0 & 0 & 0 & 1 \end{bmatrix}$$

where $x = \lambda\sin\theta$, $y = -\lambda\cos\theta$ and $z = \ell$.

$$\therefore \quad \{V^C\} = [M_V^C]\{V_\ell^C\} = \begin{bmatrix} 0 \\ 0 \\ 0 \\ V_5^C\sin\theta \\ -V_5^C\cos\theta \\ 0 \end{bmatrix}$$

The results clearly indicate that in both cases, only rotation is required and it is therefore immaterial where the local frame is fixed.

iii) Couplings E and H

For coupling E:

$$[M_V^e] = \begin{bmatrix} \cos\theta & -\sin\theta & 0 & 0 & 0 & 0 \\ \sin\theta & \cos\theta & 0 & 0 & 0 & 0 \\ 0 & 0 & 1 & 0 & 0 & 0 \\ -z\sin\theta & -z\cos\theta & y & \cos\theta & -\sin\theta & 0 \\ z\cos\theta & -z\sin\theta & -x & \sin\theta & \cos\theta & 0 \\ (x\sin\theta - y\cos\theta) & (x\cos\theta + y\sin\theta) & 0 & 0 & 0 & 1 \end{bmatrix}$$

where $x = r\sin\theta$, $y = -r\cos\theta$, $z = -\ell$.

$$\therefore \quad \{V^e\} = [M_V^e]\{V_\ell^e\} = \begin{bmatrix} V_1^e\cos\theta - V_2^e\sin\theta \\ V_1^e\sin\theta + V_2^e\cos\theta \\ V_3^e \\ \ell(V_1^e\sin\theta + V_2^e\cos\theta) - r.V_3^e\cos\theta + V_4^e\cos\theta \\ \ell(V_2^e\sin\theta - V_1^e\cos\theta) - V_3^e.r\sin\theta + V_4^e\sin\theta \\ V_1^e.r \end{bmatrix}$$

For coupling H:

$$[M_v^h] = \begin{bmatrix} 1 & 0 & 0 & 0 & 0 & 0 \\ 0 & 1 & 0 & 0 & 0 & 0 \\ 0 & 0 & 1 & 0 & 0 & 0 \\ 0 & -z & y & 1 & 0 & 0 \\ z & 0 & -x & 0 & 1 & 0 \\ -y & x & 0 & 0 & 0 & 1 \end{bmatrix} \quad (x=r\sin\theta,\ y=-r\cos\theta \text{ and } z=-\ell)$$

because the local frame has been chosen such that $[R] = [I]_{6,6}$ i.e. a 6x6 unit matrix.

$$\therefore \quad \{V^h\} = [M_v^h]\{V_\ell^h\} = \begin{bmatrix} v_1^h \\ v_2^h \\ v_3^h \\ \ell v_2^h - v_3^h . r\cos\theta \\ v_3^h . r\sin\theta - \ell . v_1^h \\ v_1^h . r\cos\theta - v_2^h . r\sin\theta + v_6^h \end{bmatrix}$$

iv) Couplings F and G

For coupling F:

$$[M_v^f] = \begin{bmatrix} -\cos\theta & \sin\theta & 0 & 0 & 0 & 0 \\ -\sin\theta & -\cos\theta & 0 & 0 & 0 & 0 \\ 0 & 0 & 1 & 0 & 0 & 0 \\ z\sin\theta & z\cos\theta & y & -\cos\theta & \sin\theta & 0 \\ -z\cos\theta & z\sin\theta & -x & -\sin\theta & -\cos\theta & 0 \\ (y\cos\theta - x\sin\theta) & -(x\cos\theta + y\sin\theta) & 0 & 0 & 0 & 1 \end{bmatrix}$$

$$\therefore \quad \{V^f\} = [M_v^f]\{V_\ell^f\} = \begin{bmatrix} 0 \\ 0 \\ 0 \\ v_5^f \sin\theta \\ -v_5^f \cos\theta \\ 0 \end{bmatrix}$$

For coupling G:

$$[M_v^g] = \begin{bmatrix} -\cos\theta & -\sin\theta & 0 & 0 & 0 & 0 \\ \sin\theta & -\cos\theta & 0 & 0 & 0 & 0 \\ 0 & 0 & 1 & 0 & 0 & 0 \\ -z\sin\theta & z\cos\theta & y & -\cos\theta & -\sin\theta & 0 \\ -z\cos\theta & -z\sin\theta & -x & \sin\theta & -\cos\theta & 0 \\ (x\sin\theta+y\cos\theta) & (y\sin\theta-x\cos\theta) & 0 & 0 & 0 & 1 \end{bmatrix}$$

$$\{v^g\} = [M_v^g]\{v_\ell^g\} = \begin{bmatrix} 0 \\ 0 \\ 0 \\ -v_5^g\sin\theta \\ -v_5^g\cos\theta \\ 0 \end{bmatrix}$$

4. Applying Kirchoff's Circulation law [3] to the three circuits of Figure 7.1.2(b) and noting that there are six equations for a single circuit:

   a) For Circuit 1 (involving couplings A, B, C and D),

$$\{v^a\} + \{v^b\} + \{v^c\} + \{v^d\} = \{0\}$$

$$\begin{bmatrix} \cos\theta & \cos\theta & \sin\theta & -\sin\theta & 0 & 0 & 0 & 0 & 0 & 0 & 0 & 0 \\ -\sin\theta & \sin\theta & \cos\theta & \cos\theta & 0 & 0 & 0 & 0 & 0 & 0 & 0 & 0 \\ 0 & 0 & 0 & 0 & 1 & 1 & 0 & 0 & 0 & 0 & 0 & 0 \\ \ell\sin\theta & -\ell\sin\theta & -\ell\cos\theta & -\ell\cos\theta & -r\cos\theta & -r\cos\theta & \cos\theta & \cos\theta & \sin\theta & \sin\theta & 0 & 0 \\ \ell\cos\theta & \ell\cos\theta & \ell\sin\theta & -\ell\sin\theta & r\sin\theta & -r\sin\theta & -\sin\theta & \sin\theta & \cos\theta & -\cos\theta & 0 & 0 \\ r & r & 0 & 0 & 0 & 0 & 0 & 0 & 0 & 0 & 1 & 1 \end{bmatrix} \begin{bmatrix} v_1^a \\ v_1^d \\ v_2^a \\ v_2^d \\ v_3^a \\ v_3^d \\ v_4^a \\ v_4^d \\ v_5^b \\ v_5^c \\ v_6^a \\ v_6^d \end{bmatrix} = \{0\}$$

$\theta = 45^o$, and so the constant matrix becomes

$$\begin{array}{cccccccccccc}
1/\sqrt{2} & 1/\sqrt{2} & 1/\sqrt{2} & -1/\sqrt{2} & 0 & 0 & 0 & 0 & 0 & 0 & 0 & 0 \\
-1/\sqrt{2} & 1/\sqrt{2} & 1/\sqrt{2} & 1/\sqrt{2} & 0 & 0 & 0 & 0 & 0 & 0 & 0 & 0 \\
0 & 0 & 0 & 0 & 1 & 1 & 0 & 0 & 0 & 0 & 0 & 0 \\
\ell/\sqrt{2} & -\ell/\sqrt{2} & -\ell/\sqrt{2} & -\ell/\sqrt{2} & -r/\sqrt{2} & -r/\sqrt{2} & 1/\sqrt{2} & 1/\sqrt{2} & 1/\sqrt{2} & 1/\sqrt{2} & 0 & 0 \\
\ell/\sqrt{2} & \ell/\sqrt{2} & \ell/\sqrt{2} & -\ell/\sqrt{2} & r/\sqrt{2} & -r/\sqrt{2} & -1/\sqrt{2} & 1/\sqrt{2} & 1/\sqrt{2} & 1/\sqrt{2} & 0 & 0 \\
r & r & 0 & 0 & 0 & 0 & 0 & 0 & 0 & 0 & 1 & 1
\end{array}$$

or

$$\begin{array}{ll}
\frac{\sqrt{2}}{2}\{(1)-(2)\}\rightarrow(1) & \\
\frac{\sqrt{2}}{2}\{(1)+(2)\}\rightarrow(2) & \\
(3) \rightarrow (3) & \\
\frac{\sqrt{2}}{2}\{(4)-(5)\}\rightarrow(4) & \\
\frac{\sqrt{2}}{2}\{(4)+(5)\}\rightarrow(5) & \\
(6) \rightarrow (6) &
\end{array}
\begin{bmatrix}
1 & 0 & 0 & -1 & 0 & 0 & 0 & 0 & 0 & 0 & 0 & 0 \\
0 & 1 & 1 & 0 & 0 & 0 & 0 & 0 & 0 & 0 & 0 & 0 \\
0 & 0 & 0 & 0 & 1 & 1 & 0 & 0 & 0 & 0 & 0 & 0 \\
0 & -\ell & -\ell & 0 & -r & 0 & 1 & 0 & 0 & 1 & 0 & 0 \\
\ell & 0 & 0 & -\ell & 0 & -r & 0 & 1 & 1 & 0 & 0 & 0 \\
r & r & 0 & 0 & 0 & 0 & 0 & 0 & 0 & 0 & 1 & 1
\end{bmatrix}$$

Hence:

i) $V_1^a = V_2^d$

ii) $V_1^d = -V_2^a$

iii) $V_3^a = -V_3^d$

iv) $-\ell V_1^d - \ell V_2^a - rV_3^a + V_4^a + V_5^c = 0$

v) $\ell V_1^a - \ell V_2^d - rV_3^d + V_4^d + V_5^b = 0$

vi) $rV_1^a + rV_1^d + V_6^a + V_6^d = 0$

b) Circuit (2) (involving couplings C, D, E and F),

$$\{V^f\} + \{V^e\} - \{V^d\} - \{V^c\} = \{0\}$$

Thus in matrix form:

$$\begin{bmatrix}
-\cos\theta & \cos\theta & \sin\theta & -\sin\theta & 0 & 0 & 0 & 0 & 0 & 0 & 0 \\
-\sin\theta & \sin\theta & -\cos\theta & \cos\theta & 0 & 0 & 0 & 0 & 0 & 0 & 0 \\
0 & 0 & 0 & 0 & -1 & 1 & 0 & 0 & 0 & 0 & 0 \\
\ell\sin\theta & \ell\sin\theta & \ell\cos\theta & \ell\cos\theta & r\cos\theta & -r\cos\theta & -\cos\theta & \cos\theta & -\sin\theta & \sin\theta & 0 \\
-\ell\cos\theta & -\ell\cos\theta & \ell\sin\theta & \ell\sin\theta & r\sin\theta & -r\sin\theta & -\sin\theta & \sin\theta & \cos\theta & -\cos\theta & 0 \\
-r & r & 0 & 0 & 0 & 0 & 0 & 0 & 0 & 0 & -1
\end{bmatrix}
\begin{bmatrix}
V_1^d \\ V_1^e \\ V_2^d \\ V_2^e \\ V_3^d \\ V_3^e \\ V_4^d \\ V_4^e \\ V_5^c \\ V_5^f \\ V_6^d
\end{bmatrix} = \{0\}$$

Since $\theta = 45^{o}$, the constant matrix becomes:

$$\begin{bmatrix}
-1/\sqrt{2} & 1/\sqrt{2} & 1/\sqrt{2} & -1/\sqrt{2} & 0 & 0 & 0 & 0 & 0 & 0 & 0 \\
-1/\sqrt{2} & 1/\sqrt{2} & -1/\sqrt{2} & 1/\sqrt{2} & 0 & 0 & 0 & 0 & 0 & 0 & 0 \\
0 & 0 & 0 & 0 & -1 & 1 & 0 & 0 & 0 & 0 & 0 \\
\ell/\sqrt{2} & \ell/\sqrt{2} & \ell/\sqrt{2} & \ell/\sqrt{2} & r/\sqrt{2} & -r/\sqrt{2} & -1/\sqrt{2} & 1/\sqrt{2} & -1/\sqrt{2} & 1/\sqrt{2} & 0 \\
-\ell/\sqrt{2} & -\ell/\sqrt{2} & \ell/\sqrt{2} & \ell/\sqrt{2} & r/\sqrt{2} & -r/\sqrt{2} & -1/\sqrt{2} & 1/\sqrt{2} & 1/\sqrt{2} & -1/\sqrt{2} & 0 \\
-r & r & 0 & 0 & 0 & 0 & 0 & 0 & 0 & 0 & -1
\end{bmatrix}$$

or

$$\begin{array}{ll}
\frac{\sqrt{2}}{2}\{(1)+(2)\}\rightarrow(1) & \\
\frac{\sqrt{2}}{2}\{(1)-(2)\}\rightarrow(2) & \\
\frac{\sqrt{2}}{2}\quad (3) \rightarrow (3) & \\
\frac{\sqrt{2}}{2}\{(4)+(5)\}\rightarrow(4) & \\
\frac{\sqrt{2}}{2}\{(4)-(5)\}\rightarrow(5) & \\
\frac{\sqrt{2}}{2}\quad (6) \rightarrow (6) &
\end{array}
\begin{bmatrix}
-1 & 1 & 0 & 0 & 0 & 0 & 0 & 0 & 0 & 0 & 0 \\
0 & 0 & 1 & -1 & 0 & 0 & 0 & 0 & 0 & 0 & 0 \\
0 & 0 & 0 & 0 & -1 & 1 & 0 & 0 & 0 & 0 & 0 \\
0 & 0 & \ell & \ell & r & -r & -1 & 1 & 0 & 0 & 0 \\
\ell & \ell & 0 & 0 & 0 & 0 & 0 & 0 & -1 & 1 & 0 \\
-r & r & 0 & 0 & 0 & 0 & 0 & 0 & 0 & 0 & -1
\end{bmatrix}$$

Hence:

i) $V_1^{e} = V_1^{d}$

ii) $V_2^{d} = V_2^{e}$

iii) $V_3^{d} = V_3^{e}$

iv) $\ell V_2^{d} + \ell V_2^{e} + rV_3^{d} - rV_3^{e} - V_4^{d} + V_4^{e} = 0$

Therefore $V_2^{d} = V_2^{e} = \dfrac{V_4^{d} - V_4^{e}}{2\ell}$

v) $\ell V_1^{d} + \ell V_1^{e} - V_5^{c} + V_5^{f} = 0$

Therefore $V_1^{d} = V_1^{e} = \dfrac{V_5^{c} - V_5^{f}}{2\ell}$

vi) $V_1^{e}.r - V_1^{d}.r - V_6^{d} = 0 \rightarrow V_6^{d} = 0.$

c) For Circuit 3 (involving couplings E,F,G and H):

$$\{V^{g}\} + \{V^{h}\} - \{V^{e}\} - \{V^{f}\} = \{0\}$$

Thus in matrix form:

$$\begin{bmatrix} -\cos\theta & \sin\theta & 1 & 0 & 0 & 0 & 0 & 0 & 0 & 0 \\ -\sin\theta & -\cos\theta & 0 & 0 & 1 & 0 & 0 & 0 & 0 & 0 \\ 0 & 0 & 0 & 0 & -i & 1 & 0 & 0 & 0 & 0 \\ -\ell\sin\theta & -\ell\cos\theta & 0 & \ell & r\cos\theta & -r\cos\theta & -\cos\theta & -\sin\theta & -\sin\theta & 0 \\ \ell\cos\theta & -\ell\sin\theta & -\ell & 0 & r\sin\theta & r\sin\theta & -\sin\theta & \cos\theta & -\cos\theta & 0 \\ -r & 0 & r\cos\theta & -r\sin\theta & 0 & 0 & 0 & 0 & 0 & 1 \end{bmatrix} \begin{bmatrix} v_1^e \\ v_2^e \\ v_1^h \\ v_2^h \\ v_3^e \\ v_3^h \\ v_4^e \\ v_5^f \\ v_5^g \\ v_6^h \end{bmatrix} = \{0\}$$

Since $\theta = 45^o$, and so the constant matrix becomes:

$$\begin{bmatrix} -1/\sqrt{2} & 1/\sqrt{2} & 1 & 0 & 0 & 0 & 0 & 0 & 0 & 0 \\ -1/\sqrt{2} & -1/\sqrt{2} & 0 & 1 & 0 & 0 & 0 & 0 & 0 & 0 \\ 0 & 0 & 0 & 0 & -1 & 1 & 0 & 0 & 0 & 0 \\ -\ell/\sqrt{2} & -\ell/\sqrt{2} & 0 & \ell & r/\sqrt{2} & -r/\sqrt{2} & -1/\sqrt{2} & -1/\sqrt{2} & -1/\sqrt{2} & 0 \\ \ell/\sqrt{2} & -\ell/\sqrt{2} & -\ell & 0 & r/\sqrt{2} & r/\sqrt{2} & -1/\sqrt{2} & 1/\sqrt{2} & -1/\sqrt{2} & 0 \\ -r & 0 & r/\sqrt{2} & -r/\sqrt{2} & 0 & 0 & 0 & 0 & 0 & 1 \end{bmatrix}$$

or

$$\begin{array}{ll} \frac{\sqrt{2}}{2}\{(1)+(2)\}\rightarrow(1) & \\ \frac{\sqrt{2}}{2}\{(1)-(2)\}\rightarrow(2) & \\ \frac{\sqrt{2}}{2} \quad (3) \rightarrow (3) & \\ \frac{\sqrt{2}}{2}\{(4)+(5)\}\rightarrow(4) & \\ \frac{\sqrt{2}}{2}\{(4)-(5)\}\rightarrow(5) & \\ \frac{\sqrt{2}}{2} \quad (6) \rightarrow (6) & \end{array} \begin{bmatrix} -1 & 0 & \sqrt{2}/2 & \sqrt{2}/2 & 0 & 0 & 0 & 0 & 0 & 0 \\ 0 & 1 & \sqrt{2}/2 & -\sqrt{2}/2 & 0 & 0 & 0 & 0 & 0 & 0 \\ 0 & 0 & 0 & 0 & -1 & 1 & 0 & 0 & 0 & 0 \\ 0 & -\ell & -\ell/\sqrt{2} & \ell/\sqrt{2} & r & 0 & -1 & 0 & -1 & 0 \\ -\ell & 0 & \ell/\sqrt{2} & \ell/\sqrt{2} & 0 & -r & 0 & -1 & 0 & 0 \\ -r & 0 & r/\sqrt{2} & -r/\sqrt{2} & 0 & 0 & 0 & 0 & 0 & 1 \end{bmatrix}$$

Hence:

i) $-v_1^e + \frac{v_1^h}{\sqrt{2}} + \frac{v_2^h}{\sqrt{2}} = 0$

ii) $v_2^e + \frac{v_1^h}{\sqrt{2}} - \frac{v_2^h}{\sqrt{2}} = 0$

iii) $v_3^h = v_3^e$

iv) $-\ell V_2^e - \frac{\ell}{\sqrt{2}} V_1^h + \frac{\ell}{\sqrt{2}} V_2^h + rV_3^e - V_4^e - V_5^g = 0$

v) $-\ell V_1^e + \frac{\ell}{\sqrt{2}} V_1^h + \frac{\ell}{\sqrt{2}} V_2^h - rV_3^h - V_5^f = 0$

vi) $-rV_1^e + \frac{r}{\sqrt{2}} V_1^h - \frac{r}{\sqrt{2}} V_2^h + V_6^h = 0$

5. Solutions of the 18 equations derived from consideration of the three circuits:

Circuit 1:

Substituting (ii) into (iv) $\rightarrow V_4^a - rV_3^a + V_5^c = 0$ (a)

Substituting (i) into (v) $\rightarrow V_4^d - rV_3^d + V_5^b = 0$ (b)

Substituting (iii) into (a) $\rightarrow V_4^a + rV_3^d + V_5^c = 0$ (c)

(b) + (c) gives $V_4^a + V_4^d + V_5^b + V_5^c = 0$ (d)

Therefore $(V_4^a + V_4^d) = -(V_5^b + V_5^c)$

Circuit 2:

Substituting (ii) and (iii) into (iv) $\rightarrow V_2^d = V_2^e = \frac{V_4^d - V_4^e}{2\ell}$ (a)

Substituting (i) into (v) $\rightarrow V_1^d = V_1^e = \frac{V_5^c - V_5^f}{2\ell}$ (b)

Substituting (i) into (vi) $\rightarrow V_6^d = 0$ (c)

Circuit 3:

From (i) and (ii):

$V_1^h = \frac{1}{\sqrt{2}} (V_1^e - V_2^e)$; $V_2^h = \frac{(V_1^e + V_2^e)}{\sqrt{2}}$

Substitute V_1^h and V_2^h into (iv) $\rightarrow rV_3^e - V_4^e = V_5^g$ (a)

Substitute (iii) and V_1^h and V_2^h into (v) $\rightarrow -rV_3^e = V_5^f$

or $V_3^e = V_3^h = -\frac{V_5^f}{r}$ (b)

Substitute for V_1^h and V_2^h into (vi) $\rightarrow V_6^h = r(V_1^e + V_2^e)$ (c)

From circuit (2) (iii) and circuit 3 (b) $\rightarrow V_3^d = V_3^e = V_3^h = -\frac{V_5^f}{r}$

$= -\frac{V_5^f}{r} = -V_3^a$

[A]

So substituting these results into circuit (1) (b) $\rightarrow V_4^d = -(V_5^f + V_5^b)$ [B]

and circuit (1) (a) $\rightarrow (V_4^a = V_5^f - V_5^c)$ [C]

From circuit 3(a) and [A] above,

$$\rightarrow V_4^e = rV_3^e - V_5^g = -(V_5^f + V_5^g) \qquad [D]$$

and $V_4^h = 0$ (see Figure 7.1.2(b))

From circuit (2) (b), $V_1^d = V_1^e = \frac{V_5^c - V_5^f}{2\ell}$ [E]

From circuit (2) (a) and ([B] and [D]) above,

$$V_2^d = V_2^e = \frac{V_4^d - V_4^e}{2\ell}$$

$$= \frac{-(V_5^f + V_5^b) + (V_5^f + V_5^g)}{2\ell}$$

$$= \frac{V_5^g - V_5^b}{2\ell} \qquad [F]$$

Now, from circuit (1) {(i) and (ii)},

$$V_1^a = V_2^d, \text{ and } V_2^a = -V_1^d$$

Therefore $V_1^a = \frac{V_5^g - V_5^b}{2\ell}$ (see [F] above) [G]

and $V_2^a = \frac{V_5^f - V_5^c}{2\ell}$ (see [E] above) [H]

From circuit (3) {(i) and (ii)} and {[E] and [F]},

$$V_1^h = \frac{1}{\sqrt{2}}(V_1^e - V_2^e) = \frac{1}{\sqrt{2}}\left(\frac{V_5^c - V_5^f - V_5^g + V_5^b}{2\ell}\right) = \frac{1}{2\sqrt{2}\ell}(V_5^c - V_5^f - V_5^g + V_5^b)$$

and $V_2^h = \frac{1}{\sqrt{2}}(V_1^e + V_2^e) = \frac{1}{\sqrt{2}}\frac{(V_5^c - V_5^f + V_5^g - V_5^b)}{2\ell} = \frac{1}{2\sqrt{2}\ell}(V_5^c - V_5^f + V_5^g - V_5^b)$ [I]

From Figure 7.1.2(h), $V_6^e = 0$; from circuit 2(c), $V_6^d = 0$

Therefore from circuit (1) $(V_i) \rightarrow V_6{}^a = -r(V_1{}^a + V_1{}^d)$ and from [G] and [E] above, $V_6{}^a = \frac{-r}{2\ell}(V_5{}^g - V_5{}^b + V_5{}^c - V_5{}^f)$

From circuit 3 (c), $V_6{}^h = r(V_1{}^e + V_2{}^e) \rightarrow V_6{}^h = r(\frac{V_5{}^c - V_5{}^f + V_5{}^g - V_5{}^b}{2\ell})$

The final solutions to these equations are presented in Section *7.1.2 in the main chapter.*

APPENDIX TO CHAPTER 9
(APPENDIX F)

THE ALIGNMENT PROGRAM

```
DELAY   EQU     010         ;Tune for >13.5 ms I/03 delay.
SWOP    EQU     08          ;Tune no. of motor changeovers.
BDOS    EQU     5           ;Entry point to BDOS.
LIST    EQU     5           ;Sends data to listing device
CONOUT  EQU     2           ;Console output.
CR      EQU     13          ;Fixed ASCII value for carriage return.
LF      EQU     10          ;ASCII value for line feed.
ATOD    EQU     82H         ;Port 130 takes data to start A-D conversion.
SIGNAL  EQU     83H         ;Port 131 on I/03 contains coverted signal.
PULSE   EQU     8DH         ;Port 141 on I/03-selects motor & direction.
CONFIG  EQU     8FH         ;Port 143 on I/03-configures ports as I/P
                            ;or O/P.
COUNT1  EQU     500         ;Tune motor delay time.
TIMER   EQU     0001
START                       ;Begin program.
        ORG     100H
        LXI     H,0
        DAD     SP
        SHLD    OLDSP
        LXI      SP,STKTOP      ;Specify stack to avoid later
                                ;encroachment.
        MVI     A,90H
        OUT      CONFIG    ;Configure other ports I/P &/or O/P by
                           ;placing 144D into port 143.
        XRA     A
        STA     BYTCNT     ;Initialise no. of characters/line.
;*************************************************************
;*THIS PORTION OF THE PROGRAM READS AND PRINTS SIGNALS BEFORE MOTOR*
;*IS MOVED. THE SIGNAL IS THEN COMPARED WITH THE DESIRED VALUE (90%*
;*OF FFH). IF VALUE OBTAINED>=90%FFH, THEN PROGRAM REBOOTS.       *
;*************************************************************
        CALL    READ        ;Read signal before executing motion.
        CPI     231         ;Compare accumulator with 90%FFH.
```

```
        JC      PROCDE    ;Branch if accumulator<E7H.
        CALL    CHECK     ;Ensures that 7 characters are printed on one
                          ;line.
        CALL    REBOOT    ;Go to reboot system.
;*****************************************************************
;*THIS PART OF THE PROGRAM REVERSES MOTOR1 ONE STEP. IT THEN READS *
;*SIGNAL AND COMPARES WITH 20% OF FFH. IF SIGNAL>=20%FFH MOTOR CON-*
;*TINUES STEP MOVEMENTS IN THIS DIRECTION TILL SIGNAL<20%FFH.      *
;*****************************************************************
PROCDE  MVI     D,SWOP    ;Set no. of motor changeovers incase 0E7H
                          ;(90%FFH) or more is NOT FOUND.
CYCLE   PUSH    D
REPEAT1 MVI     A,0H
        OUT     PULSE     ;Selects direction from port 141.
        MVI     A,70H
        OUT     PULSE     ;Selects motor1 for reverse motion.
        MVI     A,72H
        OUT     PULSE     ;Starts reversing motor1.
        CALL    WAIT      ;Tune pulse duration.
        MVI     A,70H
        OUT     PULSE     ;Stop motor1 but keep it ready to move.
        CALL    READ      ;Read new signal.
        CPI     09        ;Compare new signal with 3.5% of FFH.
        JNC     REPEAT1   ;Branch if A>=3.5%FFH.
        STA     ADDR      ;Otherwise store in ADDR.
        CALL    CHECK     ;Ensures that 7 characters are printed on one
                          ;line.
;*****************************************************************
;*THIS PART OF THE PROGRAM COMPENSATES FOR MOTOR1 BACKLASH. MOTOR1*
;*IS MOVED IN FORWARD DIRECTION COMPARING NEW SIGNALS WITH ADDRESS*
;*(ADDR) CONTENTS PASS THE 51D (20%FFH) POINT TILL 20% OF FFH IS  *
;*OBTAINED ON THE OTHER SIDE OF THE GAUSSIAN CURVE (BEAM).        *
;*****************************************************************
BACKLASH1 ;Move motor1 forward and compensate for backlash.
        MVI     A,01H
        OUT     PULSE     ;Select direction from port 141.
        MVI     A,71H
        OUT     PULSE     ;Select motor1 for forward motion.
        MVI     A,73H
```

```
        OUT     PULSE     ;Starts motor1 in forward direction.
        CALL    WAIT      ;Tune pulse duration.
        MVI     A,71H
        OUT     PULSE     ;Stop motor.
        CALL    READ      ;Read up signal.
        LXI     H,ADDR
        CMP     M         ;Compare accumulator with ADDR contents.
        JNC     CONTINE   ;Continue forward if A>=(ADDR) contents.
        JMP     BACKLASH1         ;Otherwise jump BACK to BACKLASH1.
CONTINE CALL    CHECK
        CALL    FORWARD1 ;Move motor1 forward storing signals.
        CALL    MAXIMUM  ;Find maximum signal stored in the above
                         ;array.
        CALL    NINTYPC  ;Find 90% of max signal.
        CALL    REVERSE1 ;Reverse motor to peak position.
        CALL    DATRESET ;Reset array data.
        CALL    MOTOR2   ;Change to motor2 & repeat procedure.
        CALL    FORWARD2
        CALL    MAXIMUM
        CALL    NINTYPC
        CALL    REVERSE2 -
        CALL    DATRESET ;Go to reset array.
        POP     D        ;Retrieve no. of motor cycle change overs.
        DCR     D
        JNZ     CYCLE    ;Swop motors 8 times as long as location 90%
                         ;of FFH or higher is NOT FOUND.
        CALL    REBOOT   ;Reboot system.
CHECK   ;*************************************************
        ;*SUBROUTINE THAT ENSURES CARRIAGE IS RETURNED AFTER PRINTING*
        ;*A BLOCK OF DATA OR CHARACTERS (7 in this case)OBTAINED FROM*
        ;*A GIVEN SUBROUTINE etc.                                   *
        ;*************************************************
        ;*************************************************
MORCHR  LDA     BYTCNT
        MVI     D,0H
        ORA     D
        JZ      FINISH
        CALL    SPACE     ;Create double spacing before next character.
        CALL    LNFEED    ;Check if 7 characters (exclude spaces) are
                          ;printed then carriage return.
```

```
        JMP     MORCHR   ;Otherwise print more characters.
FINISH  RET
;*************************************************
;*THIS SUBROUTINE DETERMINES MOTOR PULSE DURATION.*
;*************************************************
WAIT    ;Delay routine.
        LXI     D,COUNT1 ;Load delay data into reg. pair DE.
AGAIN   DCX     D        ;Decrement regs. DE.
        MOV     A,D      ;To test for 0 mov D into A.
        ORA     E        ;Then logical OR A with E.
        JNZ     AGAIN    ;Branch if result <>0.
        RET
;*************************************************************
;*THIS PART OF THE PROGRAM MOVES MOTOR1 FORWARD STORING ALL SIGNALS*
;*IN INDEXED ADDRESS (ARRAY,X) using autopostincrement addressiong.*
;*ALL PROGRAM STATEMENTS INVOLVING (PULSE) ARE DEFINED IN backlash1*
;*routine ABOVE.                                                  *
;*************************************************************
FORWARD1         ;Move motor1 forward storing all signals.
        LXI     H,ARRAY  ;Start of array.
        SHLD    BASE     ;Store location array in BASE.
        LDA     ADDR     ;Load up first data into accumulator.
        CALL    BNHEX1   ;Print it out.
        LXI     B,TIMER  ;Start count to determineno. of signals
                          ;stored.
;*************************************************
;*Autopostincrementing adrress and storing accumulator. *
;*************************************************
LOOP    LHLD    BASE
        MOV     M,A
        INX     H
        SHLD    BASE
        INX     B
        PUSH    B
        MVI     A,01H
        OUT     PULSE
        MVI     A,71H
        OUT     PULSE
        MVI     A,73H
```

```
        OUT     PULSE
        CALL    WAIT
        MVI     A,71H
        OUT     PULSE
        CALL    READ        ;Read up new data in I/o3.
        POP     B
        CPI     05          ;Compare subsequent data with 05.
        JNC     LOOP        ;Move & read again if new data>=ADDR
                            ;contents.
        DCX     B           ;Decreasecounter toaccountfor last
                            ;unstored data.
        MOV     H,B         ;Store register pair B,C direct into COUNTER.
        MOV     L,C
        SHLD    COUNTER
        CALL    CHECK
        RET
;*************************************************************
;*THIS SUBROUTINE CONVERTS ANALOGUE TO DIGITAL SIGNAL AND READS IT*
;*INTO ACCUMULATOR.                                            *
;*************************************************************
READ    MVI     A,0FFH
        OUT     ATOD        ;All channels disabled.
        MVI     A,0F0H
        OUT     ATOD        ;Enable multiplexer - select channel 0.
        MVI     A,0D0H
        OUT     ATOD        ;Issue start conversion.
        MVI     A,0F0H
        OUT     ATOD        ;Repeat as above.
        MVI     A,DELAY     ;Tune waiting time to 13.5ms or more fora
                            ;4MHz clock to allow for conversion time.
BACK    DCR     A
        JNZ     BACK
        IN      SIGNAL      ;Read port 83H to obtain converted signal.
        STA     POT
        CALL    BNHEX1      ;Print it out.
        LDA     POT
        RET
```

```
;*************************************************************
;*THIS SUBROUTINE PRINTS DATA FROM ACCUMULATOR ONTO SCREEN &*
;*PRINTER.                                                   *
;*************************************************************
BNHEX1  ;Convert Hi-nibble to ASCII.
        STA     POT
        ANI     0F0H        ;Get hi-nibble.
        RRC
        RRC
        RRC
        RRC
        CALL    NASCII      ;Convert hi-nibble to ASCII.
        CALL    PRINT       ;Go to print MSB.
        CALL    BNHEX2      ;Go to Lo-nibble conversion routine.
        CALL    SPACE       ;Give double spacing.
        CALL    LNFEED      ;Go to print space and carriage ret
        LDA     POT
        RET                 ;RETURN.
BNHEX2  ;Convert Lo-nibble to ASCII.
        LDA     POT
        ANI     0FH         ;Get lo-nibble.
        CALL    NASCII      ;Convert lo-nibble to ASCII & return it in L.
        CALL    PRINT       ;Go to print LSB.
        RET                 ;Return to main program.
NASCII  CPI     10          ;Compare reg-A with 10.
        JC      NASCI1      ;Jump if hi-nibble<10.
        ADI     7           ;Otherwise add 7 so that after adding
                            ;'0' character will be in 'A'.....'F'.
NASCI1  ADI     '0'         ;Add ASCII 0 to make a character.
        RET                 ;Return to main program.
PRINT   STA     PTR         ;Store data in temporary location
                            ;ready for printing.
        MVI     C,CONOUT
        MOV     E,A
        CALL    BDOS
        LDA     PTR
        MVI     C,LIST
        MOV     E,A
```

```
        JMP     BDOS
;*****************************************************************
;*THIS SUBROUTINE SIMPLY GIVES DOUBLE SPACING BETWEEN ONE PRINTED*
;*DATA OUTPUT AND THE NEXT ON THE SAME LINE.                      *
;*****************************************************************
SPACE   MVI     A,20H
        CALL    PRINT       ;Give one space for next data.
        LDA     PTR
        CALL    PRINT       ;Give second space for next data.
        RET
;*****************************************************************
;*THIS SUBROUTINE CREATES SPACE AND ENSURES THAT THE CORRECT No. OF*
;*DATA O/P IS PRINTED ON A SINGLE LINE BEFORE CARRIAGE RETURN.    *
;*****************************************************************
LNFEED  CALL    SPACE       ;Create double spacing before next character.
        LDA     BYTCNT      ;Retrieve no. of characters already printed.
        INR     A
        STA     BYTCNT
        CPI     7           ;Are printed characters = 7?
        RNZ                 ;NO. RETURN.
        XRA     A           ;If yes then clear no. of counts in BYTCNT.
        STA     BYTCNT      ;START AGAIN
        MVI     A,CR
        CALL    PRINT       ;Send carriage return ASCII.
        MVI     A,LF
        CALL    PRINT       ;Start print on next line.
        RET
;*****************************************************************
;*THIS SUBROUTINE DETERMINES THE LARGEST LOCAL SIGNAL RECORDED IN*
;*AN ARRAY BY COMPARING ONE AGAINST THE OTHER.                    *
;*****************************************************************
MAXIMUM                     ;Determine largest signal recorded.
        LHLD    COUNTER
        MOV     A,H         ;Get MSB of no. of counts & print.
        CALL    BNHEX1
        CALL    CHECK       ;Print high byte on a single line.
        LHLD    COUNTER     ;Retrieve data counts & put in H,L.
        MOV     A,L         ;Get LSB of no. of counts & print.
        CALL    BNHEX1
```

```
        CALL    CHECK       ;Print low byte in the next line.
        LHLD    COUNTER
        MOV     B,H         ;Load register pair BC with counts.
        MOV     C,L
        LXI     H,ARRAY     ;Point to start address of data array.
        MOV     A,M
        STA     MAX
NEXTEL  LDA     MAX
        INX     H           ;Next address.
        CMP     M           ;Is next element> MAXIMUM?
        JNC     DECRT       ;If it is, jump to DECREASE.
        MOV     A,M         ;If greater or equal, replace.
DECRT   STA     MAX
        DCX     B           ;Decrease no. of counts by 1.
        MOV     A,B
        ORA     C           ;Then OR A with C
        JNZ     NEXTEL      ;If counter<>0, go to increase H.
        LDA     MAX
        CALL    BNHEX1      ;Print out MAXIMUM.
        CALL    CHECK
        RET
NINTYPC ;*************************************************************
        ;*THIS SUBROUTINE CALCULATES 90% OF MAXIMUM SIGNAL RECORDED *
        ;*BY TACKLING ODD AND EVEN DATA SEPARATELY AND STORES RESULT*
        ;*IN ADDRESS CALLED PERCNT.                                 *
        ;*************************************************************
DIVISION        ;Calculate 10's digit (i.e.10% of MAXIMUM).
                ;Divide data by 10D.
                ;M = Quotient.
                ;A = Remainder.
        ;PROGRAM BEGINS HERE.
        MVI     B,0H
        LDA     MAX         ;Load accumulator with contents of MAX
                            ;i.e. maximum recorded signal.
DIVLOOP                     ;Work out 90% of MAXIMUM.
        INR     B           ;Add 1 to quotient.
        MOV     M,B
        SUI     00AH        ;Subtract 10D from A.
        JNC     DIVLOOP     ;Branch if A>10D.
```

```
        MVI     D,00AH
        ADD     D
        MVI     D,0H        ;Test if A is 0.
        ORA     D
        JNZ     ODDNMB      ;Branch if A<>0.
        MOV     A,M
        LXI     H,MAX
        DCR     A
        CMA                 ;Negate A.
        JMP     RIBO
ODDNMB  MOV     A,M
        LXI     H,MAX
        CMA                 ;Negate accumulator.
RIBO    INR     A
        ADD     M           ;Form -A + reg M
        STA     PERCNT      ;Store difference (90%) in address PERCNT.
        CALL    BNHEX1      ;Print 90% of MAXIMUM signal.
        CALL    CHECK
        RET
;*****************************************************************
;*THIS PART OF THE PROGRAM REVERSES MOTOR Y TO PEAK POSITION*
;*DETERMINED BY THE maximum OR nintypc SUBROUTINES ABOVE.    *
;*****************************************************************
REVERSE1  ;Reverse motor1 to peak position found in MAXIMUM or
          ;NINTYPC above. All program statements involving PULSE
          ;are already defined at the beginning of the program
          ;starting at label statement REPEAT1.
        LHLD    COUNTER  ;Get no. of counts from (COUNTER).
        MOV     B,H
        MOV     C,L
REPEAT  PUSH    B        ;Save it in B,C reg. pair.
        MVI     A,0H
        OUT     PULSE
        MVI     A,70H
        OUT     PULSE
        MVI     A,72H
        OUT     PULSE
        CALL    WAIT
        MVI     A,70H
```

```
        OUT     PULSE
        CALL    READ
        POP     B           ;Retrieve counts.
        CPI     231         ;Compare signal with 90%FFH.
        JC      TRY1        ;Branch if A<231.
        CALL    CHECK
        CALL    DATRESET    ;Reset ARRAY to zero.
        CALL    REBOOT      ;Go to reboot system.
TRY1    LXI     H,MAX
        CMP     M           ;Otherwise compare with maximum signal
                            ;(contents of MAX).
        JNC     GOBAK       ;Return if A>=contents of MAX.
        LXI     H,PERCNT
        CMP     M           ;Otherwise compare signal with 90% of
                            ;maximum signal.
        JNC     GOBAK       ;Return if A>=contents of PERCNT (90% MAX).
        DCX     B           ;Decrease reg. pair BC (counter).
        MOV     A,B
        ORA     C
        JNZ     REPEAT      ;Go to scan the next signal if B,C<>0.
GOBAK   CALL    CHECK
        RET
MOTOR2                      ;Changeover to motor2 and reverse.
        MVI     A,0H
        OUT     PULSE       ;Selects direction of motion from port 141.
        MVI     A,70H
        OUT     PULSE       ;Selects motor2.
        MVI     A,74H
        OUT     PULSE       ;Starts motion in reverse direction.
        CALL    WAIT        ;Tune motor pulse duration.
        MVI     A,70H
        OUT     PULSE       ;Stop motor motion.
        CALL    READ
        CPI     09          ;Compare new signal with 09.
        JNC     MOTOR2      ;Branch if A>=3.5%FFH.
        STA     ADDR2       ;Otherwise store in ADDR2 before backlash
                            ;correction and forward motion.
        CALL    CHECK
BACKLASH2 ;Move motor2 forward till signal(A)>=ADDR2 contents.
```

```
        MVI     A,01H
        OUT     PULSE     ;Selects motor direction.
        MVI     A,71H
        OUT     PULSE     ;Selects motor2 for forward motion.
        MVI     A,75H
        OUT     PULSE     ;Motor starts motion in forward direction.
        CALL    WAIT      ;Tune motor pulse duration.
        MVI     A,71H
        OUT     PULSE     ;Stop motor motion.
        CALL    READ      ;Read signal.
        LXI     H,ADDR2
        CMP     M         ;Compare signal(A) with contents of ADDR2.
        JNC     PROCEED   ;Return if A>=(ADDR2) contents.
        JMP     BACKLASH2         ;Otherwise jump back to BACKLASH2.
PROCEED CALL    CHECK
        RET
;*****************************************************************
;*THIS PART OF THE PROGRAM MOVES MOTOR2 FORWARD STORING ALL   *
;*SIGNALS IN INDEXED ADDRESSING (ARRAY2,X) using autopostincr-*
;*ment addressing. ALL PROGRAM STATEMENTS INVOLVING (PULSE)   *
;*ARE DEFINED IN backlash2 routine ABOVE.                     *
;*****************************************************************
FORWARD2  ;Move motor2 forward storing all signals.
        LXI     H,ARRAY   ;Start of array.
        SHLD    BASE      ;Store location of array in BASE.
        LDA     ADDR2     ;Load up first data from ADDR2.
        CALL    BNHEX1
        LXI     B,TIMER   ;Start up count.
LOOP2   ;Autopostincrement address and store accumulator.
        LHLD    BASE
        MOV     M,A
        INX     H
        SHLD    BASE
        INX     B
        PUSH    B
        MVI     A,01H
        OUT     PULSE
        MVI     A,71H
        OUT     PULSE
```

```
        MVI     A,75H
        OUT     PULSE
        CALL    WAIT
        MVI     A,71H
        OUT     PULSE
        CALL    READ
        POP     B           ;Retrieve no. of counts.
        CPI     05          ;Compare subsequent data with 05.
        JNC     LOOP2       ;Move & store data if new data >= (ADDR2)
                            ;contents.
        DCX     B           ;Decrese counter to account for last unstored
                            ; data.
        MOV     H,B         ;Move total no. of counts into HL reg. pair.
        MOV     L,C
        SHLD    COUNTER     ;Store HL reg. pair direct into COUNTER.
        CALL    CHECK
        RET
;*****************************************************
;*THIS PART OF THE PROGRAM REVERSES MOTOR2 TO PEAK POSITION*
;*OBTAINED FROM THE maximum OR  nintypc SUBROUTINES ABOVE. *
;*ALL PROGRAM STATEMENTS INVOLVING (PULSE) ARE DEFINED IN  *
;*motor2 routine ABOVE.                                    *
;*****************************************************
REVERSE2                    ;Reverse motor2 to peak (MAX) position.
        LHLD    COUNTER     ;Move no. of counts into reg. pair B,C.
        MOV     B,H
        MOV     C,L
COUNTS  PUSH    B           ;Save no. of counts obtained from FORWARD2.
        MVI     A,0H
        OUT     PULSE
        MVI     A,70H
        OUT     PULSE
        MVI     A,74H
        OUT     PULSE
        CALL    WAIT
        MVI     A,70H
        OUT     PULSE
        CALL    READ
        POP     B           ;Retrieve counts.
```

```
        CPI     231         ;Compare signal with 90%FFH.
        JC      TRY2
        CALL     CHECK
        CALL    DATRESET ;Reset ARRAY data.
        CALL    REBOOT
TRY2    LXI     H,MAX
        CMP     M           ;Otherwise compare it with (MAX) contents.
        JNC     BACK2       ;Branch to motrorl if A>=(MAX) contents.
        LXI     H,PERCNT
        CMP     M           ;Compare signal with 90% of (MAX) contents.
        JNC     BACK2       ;Branch to motorl if A>=(PERCNT) contents.
        DCX     B
        MOV     A,B
        ORA     C
        JNZ     COUNTS      ;Go back to COUNTS if B<>0
BACK2   CALL    CHECK
        RET
;*********************************************
;*THIS PART OF THE PROGRAM REBOOTS THE SYSTEM*
;*********************************************
REBOOT  LHLD    OLDSP       ;Load H&L registers direct.
        SPHL                ;Load stack pointer from H&L registers.
        RET
;*********************************************
;*THIS PART OF THE PROGRAM RESETS ARRAY DATA*
;*********************************************
DATRESET         ;Reset all array data to zero.
        LHLD    COUNTER     ;Retrieve total no. of data stored.
        MOV     B,H
        MOV     C,L         ;Place hi and lo in reg. pair BC.
        INX     B           ;Increase B to ensure next ARRAY data<MAX.
        LXI     H,ARRAY     ;Point to ARRAY.
MLOOP   MVI     A,0H        ;Fill reg. M with 0.
        MOV     M,A
        INX     H           ;Increase H.
        DCX     B           ;Decrease BC.
        MOV     A,B
        ORA     C
        JNZ     MLOOP
```

```
        MVI     H,0H
        MVI     L,0H
        SHLD    COUNTER  ;Reset contents of COUNTER.
        RET
;*****************************************************************
;*THIS PART OF THE PROGRAM ALLOCATES BYTES TO ADDRESS LABELS *
;*AND DEFINES SPACES FOR STACK AND DATA STORED DURING FORWARD*
;*MOTION.                                                       *
;*****************************************************************
ADDR    DS      2       ;Allocate bytes to all the address
                        ;labels.
POT     DS      2
BASE    DS      2
COUNTER DS      2
MAX     DS      2
ARRAY   DS      1800    ;Sets up space for data array.
PERCNT  DS      2
ADDR2   DS      2
PTR     DS      2
BYTCNT  DS      2
OLDSP   DS      2
        DS      50              ;Sets up stack space.
STKTOP  EQU     $
        END
```